SCYR 2020

April, 2020
Košice, Slovakia

Nonconference Proceedings of Young Researchers

Faculty of Electrical Engineering and Informatics
Technical University of Košice

Co-Organizers

SCYR 2020
Nonconference Proceedings of Young Researchers

Published: Faculty of Electrical Engineering and Informatics
Technical University of Košice
Edition I, 212 pages, number of CD Proceedings: 50 pieces

Editors: prof. Ing. Alena Pietriková, CSc.
Ing. Emília Pietriková, PhD.

ISBN 978-80-553-3538-4

Program Committee of SCYR 2020

General chair:	Prof. Ing. Liberios Vokorokos, PhD.
Editorial board chairman:	Prof. Ing. Alena Pietriková, CSc.
Proceedings reviewers:	Prof. Ing. Roman Cimbala, PhD. Prof. Ing. Ján Paralič, PhD. Prof. Ing. Daniela Perduková, PhD. Prof. Ing. Alena Pietriková, CSc. assoc. Prof. Ing. František Babič, PhD. assoc. Prof. Ing. Ján Gamec, CSc. assoc. Prof. Ing. Ján Genči, PhD. assoc. Prof. Ing. Kristína Machová, PhD. assoc. Prof. Ing. Ján Papaj, PhD. assoc. Prof. Ing. Jaroslav Porubän, PhD.

Organization Committee of SCYR 2020

Members:	Prof. Ing. Alena Pietriková, CSc. Ing. Ivana Olšiaková Ing. Juraj Biľanský Ing. Anton Buday Ing. Daniel Dzivý Ing. Branislav Fecko Ing. Matej Gazda Ing. Peter Havran Ing. Jana Horniaková Ing. Lukáš Hruška Ing. Marianna Koctúrová Ing. Viera Maslej Krešňáková Ing. Emília Pietriková, PhD. Ing. Marek Ružička Ing. Martin Sivý
Contact address:	Faculty of Electrical Engineering and Informatics Technical University of Košice Letná 9 042 00 Košice Slovak Republic

Foreword

Dear Colleagues,

SCYR is a Scientific Event focused on exchange of information among young scientists from Faculty of Electrical Engineering and Informatics at the Technical University of Košice – series of annual events that was founded in 2000. Since 2000, the conference has been hosted by FEI TUKE with rising technical level and unique multicultural atmosphere. Due to **COVID-19** lockdown, **SCYR 2020** skipped the event and was published as **Nonconference Proceedings of Young Researchers**. The primary aim, to provide a forum for dissemination of information and scientific results relating to research and development activities at the Faculty of Electrical Engineering and Informatics, has been achieved. Approx. 73 participants, mostly by doctoral categories, were active this year.

Faculty of Electrical Engineering and Informatics has a long tradition of students participating in skilled labor where they have to apply their theoretical knowledge. SCYR is opportunities for doctoral and graduating students use this event to train their scientific knowledge exchange. Nevertheless, the original goal is still to represent a forum for the exchange of information between young scientists from academic communities on topics related to their experimental and theoretical works in the very wide spread field of a wide spectrum of scientific disciplines like informatics sciences and computer networks, cybernetics and intelligent systems, electrical and electric power engineering and electronics.

Traditionally, contributions can be divided in 2 categories:

- Electrical & Electronics Engineering
- Information Technologies

with approx. 73 technical papers dealing with research results obtained mainly in university environment. The results presented in papers demonstrated that the investigations being conducted by young scientists are making a valuable contribution to the fulfillment of the tasks set for science and technology at the Faculty of Electrical Engineering and Informatics at the Technical University of Košice. Although we could not meet in person this year, we already look forward to next year's interesting scientific discussions among the junior researchers and graduate students, and the representatives of the Faculty of Electrical Engineering and Informatics. This Scientific Network usually includes various research problems and education, communication between young scientists and students, between students and professors.

We want to thank all authors for contributing to these proceedings with their high quality manuscripts. We hope this proceedings constitutes a platform for a continual dialogue among young scientists.

It is our pleasure and honor to express our gratitude to our co-organizers and to all friends, colleagues and committee members who contributed with their ideas, discussions, and sedulous hard work. We also want to thank all our reviewers.

Liberios VOKOROKOS
Dean of FEI TUKE

April 2020, Košice

Contents

A final look back at the qualitative theory of differential and difference equations

[1]*Irena JADLOVSKÁ (4^{th} year)*
[2]*Supervisor: Blanka BACULÍKOVÁ*

Dept. of Mathematics and Theoretical Informatics, FEI TU of Košice, Slovak Republic

[1]irena.jadlovska@tuke.sk, [2]blanka.baculikova@tuke.sk

***Abstract*—The purpose of this paper is to briefly sum up our contributions to the qualitative theory of functional differential and difference equations.**

***Keywords*—qualitative theory, differential equation, difference equation, deviating argument.**

I. Introduction

Qualitative theory of differential and difference equations developed as a result of a significant demand coming from various sciences, which had found the equations as an accurate language to determine and to further advance their knowledge. Since diverse problems, sometimes originating in quite distinct fields, may be described by identical mathematical expressions, the study of differential (or difference) equations as a subject of mathematical theory does not aim to provide a concrete physical interpretation, rather offer an unifying principle behind diverse phenomena.

The aim of the qualitative theory is to gain as detailed information as possible about the qualitative properties of solutions such as oscillation, periodicity, convergence to zero, boundedness, zeros distribution, etc., without requiring knowledge about solutions themselves. For a brief description of the essential concepts in theory, we refer the reader to [1].

In our work, we have been mostly interested in the qualitative behavior of so-called *functional differential and difference equations* (FDEs), which are deemed to be more adequate tools in modeling than ordinary equations, because of their ability of taking advantage of the past or the most probable future, instead of the initial state only. Our research has been mainly motivated by the fact that, inspite of the intense research in the area, mathematical models of real processes involving FDEs still cannot explain at detail various qualitative phenomena caused by the response delay, due to the less developed mathematical framework, mostly generalizing ideas existing for ordinary equations. This primarily causes that in subsequent analysis, the delay effect (or let us generally say the effect of the functional argument) starts to be, at least partially, inadvertently neglected. Secondary, various assumptions on the deviating argument (such as a boundedness by a constant from above, a monotone growth, etc.) have to be posed.

As a result, the primary aim of this research has been to develop new computational-based techniques for investigation of qualitative properties of FDEs, which are applicable in cases when the existing methods fail or provide a weaker result in some sense.

II. Research Contributions

The progress made which is to be summarized within this section mainly reflects the open problems formulated in [2], closely following the results achieved, some of them already mentioned in [2, 3]. Here, we will try to comprehensibly divide the achieved results into three groups based on the order of the studied functional differential or difference equations, namely, first-order, second-order, and higher-order equations.

In case of first-order equations, we have payed our attention to the simplest linear differential and difference equations with general delay or advanced arguments, which are included as benchmark models in population dynamics and disease transmission models. From the mathematical point of view, such equations are of special importance, since their properties are widely used in investigating of differential equations of higher order. In summary, our contribution to the subject has been described in the following publications [4–12].

The most important part of the research focuses on second-order functional differential equations, which enjoy the longest history, from both theoretical or applicational perspective. Our results concern so-called half-linear functional differential equations, which form an imaginary borderline between linear and nonlinear equations, see [13–24]. The author is most proud of recent contributions [18, 19, 23], as they offer unimprovable results for a large class of equations investigated in hundreds of works for more than 40 years.

Last, the works [25–39] illustrate the progress gained in the field of differential equations of higher order. On the one hand, we generalized some of the obtained results for second-order equations [25, 27–29, 33, 34, 37, 39] and on the other hand, we got new results for several-terms equations, for which the consistent theory has been missing [30–32, 35, 36, 38, 40, 41].

The basis of the newly-developed techniques lies in constructing suitable a priori estimates for nonoscillatory solutions, based on the iterative application of functional inequalities and the subsequent use of standard methods of functional and mathematical analysis. The key factor in evaluating the sequences of estimates and, in particular cases, constructing the limit one, is the use of computational tools, which recently proved to be efficient in computer-assisted proofs. We have performed these computations using the algorithms implemented in the MATLAB environment.

III. Further research directions

There is a lot of work to do. In our recent works, we have employed various techniques which are extremely useful for lower-order equations; but they have no alternative nor in the higher-order case nor in the discrete case. Currently, we are working on generalizing them to be applicable on a general measure chain.

References

[1] I. Jadlovská, "Fundamental concepts in the theory of oscillation," in *Scientific Conference of Young Researchers FEI TU of Kosice*, 2017.

[2] ——, "Contributions to the qualitative theory of differential and difference equations," in *Scientific Conference of Young Researchers FEI TU of Kosice*, 2018.

[3] ——, "Further thoughts and results in the qualitative theory of differential and difference equations," in *Scientific Conference of Young Researchers FEI TU of Kosice*, 2019.

[4] G. E. Chatzarakis and I. Jadlovská, "Improved iterative oscillation tests for first-order deviating difference equations," *Int. J. Diff. Equ*, vol. 12, no. 2, pp. 185–210, 2017.

[5] ——, "Oscillations in deviating difference equations using an iterative technique," *Journal of Inequalities and Applications*, vol. 2017, no. 1, p. 173, 2017.

[6] ——, "Difference equations with several non-monotone deviating arguments: Iterative oscillation tests," *Dynamic Systems and Applications*, vol. 27, no. 2, pp. 271–298, 2018.

[7] ——, "Improved iterative oscillation tests for first-order deviating differential equations," *Opuscula Mathematica*, vol. 38, no. 3, 2018.

[8] G. E. Chatzarakis and I. Jadlovska, "Oscillations in difference equations with several arguments using an iterative method," *Filomat*, vol. 32, no. 1, 2018.

[9] G. E. Chatzarakis and I. Jadlovská, "Explicit criteria for the oscillation of differential equations with several arguments," *Dynamic Systems and Applications*, vol. 28, no. 2, pp. 217–242, 2019.

[10] ——, "Oscillation in deviating differential equations using an iterative method," *Communications in Mathematics*, vol. 27, no. 2, pp. 143–169, 2019.

[11] ——, "Oscillations of deviating difference equations using an iterative method," *Mediterranean Journal of Mathematics*, vol. 16, no. 1, p. 16, 2019.

[12] G. E. Chatzarakis, J. Džurina, and I. Jadlovská, "A remark on oscillatory results for neutral differential equations," *Applied Mathematics Letters*, vol. 90, pp. 124–130, 2019.

[13] G. E. Chatzarakis and I. Jadlovská, "Improved oscillation results for second-order half-linear delay differential equations," *Hacettepe Journal of Mathematics and Statistics*, vol. 48, no. 1, pp. 170–179, 2019.

[14] G. Chatzarakis, J. Džurina, and I. Jadlovská, "New oscillation criteria for second-order half-linear advanced differential equations," *Applied Mathematics and Computation*, vol. 347, pp. 404–416, 2019.

[15] J. Džurina and I. Jadlovská, "A note on oscillation of second-order delay differential equations," *Applied Mathematics Letters*, vol. 69, pp. 126–132, 2017.

[16] J. Dzurina, I. Jadlovská, and I. P. Stavroulakis, "Oscillatory results for second-order noncanonical delay differential equations," *Opuscula Mathematica*, vol. 39, no. 4, 2019.

[17] J. Dzurina, I. Jadlovská, and T. Li, "Oscillation criteria for second-order nonlinear delay differential equations with a sublinear neutral term," *Mathematische Nachrichten*, 2020, in press.

[18] J. Dzurina and I. Jadlovská, "Kneser type oscillation criteria for second-order half-linear differential equations," *Applied Mathematics and Computation*, 2020, accepted.

[19] ——, "A sharp oscillation result for second-order half-linear noncanonical delay differential equations," *Electronic Journal of Qualitative Theory of Differential Equations*, 2020, in press.

[20] S. R. Grace and I. Jadlovská, "Oscillation criteria for second-order neutral damped differential equations with delay argument," *Dynamical Systems–Analytical and Computational Techniques, INTECH*, pp. 31–53, 2017.

[21] S. R. Grace, J. Džurina, I. Jadlovská, and T. Li, "An improved approach for studying oscillation of second-order neutral delay differential equations," *Journal of inequalities and applications*, vol. 2018, no. 1, pp. 1–13, 2018.

[22] I. Jadlovska, "Iterative oscillation results for second-order differential equations with advanced argument," *Electronic Journal of Differential Equations*, vol. 2017, no. 162, pp. 1–11, 2017.

[23] I. Jadlovská, "Oscillation criteria of kneser type for second-order advanced half-linear differential equations," *Applied Mathematics Letters*, submitted.

[24] S. Grace, I. Jadlovská, and A. Zafer, "On oscillation of second-order delay differential equations with a sublinear neutral term," *Mediterranean Journal of Mathematics*, 2020, in press.

[25] B. Baculíková, J. Dzurina, and I. Jadlovská, "On asymptotic properties of solutions to third-order delay differential equations," *Electron. J. Qual. Theory Differ. Equ.*, vol. 2019, no. 7, pp. 1–11, 2019.

[26] ——, "Properties of the third order trinomial functional differential equations," *Electronic Journal of Qualitative Theory of Differential Equations*, vol. 2015, no. 34, pp. 1–13, 2015.

[27] M. Bohner, S. R. Grace, and I. Jadlovská, "Asymptotic behavior of solutions of forced third-order dynamic equations," *Analysis*, 2019.

[28] G. E. Chatzarakis, S. R. Grace, and I. Jadlovská, "Oscillation criteria for third-order delay differential equations," *Advances in Difference Equations*, vol. 2017, no. 1, pp. 1–11, 2017.

[29] G. Chatzarakis, J. Džurina, and I. Jadlovská, "Oscillatory and asymptotic properties of third-order quasilinear delay differential equations," *Journal of Inequalities and Applications*, vol. 2019, no. 1, p. 23, 2019.

[30] J. Džurina, B. Baculíková, and I. Jadlovská, "New oscillation results to fourth-order delay differential equations with damping," *Electronic Journal of Qualitative Theory of Differential Equations*, vol. 2016, no. 7, pp. 1–15, 2016.

[31] J. Džurina and I. Jadlovská, "Asymptotic behavior of third-order functional differential equations with a negative middle term," *Advances in Difference Equations*, vol. 2017, no. 1, pp. 1–15, 2017.

[32] ——, "Oscillation theorems for fourth-order delay differential equations with a negative middle term," *Mathematical Methods in the Applied Sciences*, 2017.

[33] ——, "Oscillation of third-order differential equations with non-canonical operators," *Applied Mathematics and Computation*, vol. 336, pp. 394–402, 2018.

[34] J. Džurina, S. Grace, and I. Jadlovská, "On nonexistence of kneser solutions of third-order neutral delay differential equations," *Applied Mathematics Letters*, vol. 88, pp. 193–200, 2019.

[35] J. Dzurina, B. Baculikova, and I. Jadlovska, "Oscillation of solutions to fourth-order trinomial delay differential equations," *Electronic Journal of Differential Equations*, vol. 2015, no. 70, pp. 1–10, 2015.

[36] S. R. Grace and I. Jadlovska, "Oscillatory behavior of odd-order nonlinear differential equations with a nonpositive neutral term," *Dynamic Systems and Applications*, vol. 27, no. 1, pp. 125–136, 2018.

[37] S. R. Grace, J. Džurina, I. Jadlovská, and T. Li, "On the oscillation of fourth-order delay differential equations," *Advances in Difference Equations*, vol. 2019, no. 1, pp. 1–15, 2019.

[38] S. Grace, I. Jadlovská, and A. Zafer, "Oscillatory behavior of n-th order nonlinear delay differential equations with a nonpositive neutral term," *Hacettepe Journal of Mathematics and Statistics*, pp. 1–11, 2019.

[39] Y.-C. Qiu, I. Jadlovská, D. Lassoued, and T. Li, "Nonoscillatory solutions to higher-order nonlinear neutral dynamic equations," *Symmetry*, vol. 11, no. 3, p. 302, 2019.

[40] M. Bohner, S. R. Grace, and I. Jadlovska, "Oscillation criteria for third-order functional differential equations with damping," *Electronic Journal of Differential Equations*, vol. 2016, no. 215, pp. 1–15, 2016.

[41] B. Baculíková, J. Dzurina, and I. Jadlovská, "Oscillatory solutions of fourth order advanced trinomial differential equations," *Mathematische Nachrichten*, 2020, in press.

ASIC Filters for M-Sequence UWB Radars

[1]*Martin PEČOVSKÝ (4rd year)*
Supervisor: [2]Pavol GALAJDA

[1,2]Dept. of Electronics and Multimedia Communications, FEI TU of Košice, Slovak Republic

[1]martin.pecovsky@tuke.sk, [2]pavol.galajda@tuke.sk

***Abstract*—This paper gives a brief overview of the ongoing research in the field of application-specific integrated circuits for M-sequence UWB radars. In the first section, motivation and background of the research is discussed. The second part provides a short description of the two most important blocks designed for the M-sequence system on chip recently– the integrated active low pass filter and an ECC band pass filter. Together with the exploited design approaches, basic prototype measurement results are provided.**

***Keywords*—ASIC, M-sequence, active filters, ECC.**

I. Introduction

The development of the M-sequence ultra-wideband (UWB) radars has long tradition at our department. In cooperation with TU Ilmenau, we have been a part of exciting research in areas of data processing software as well as ultra-wideband hardware, enabling the M-sequence technology to become one of the standards for short-range sensing, often outperforming earlier UWB approaches. With the continuous research and consequential technological improvements, new applications of the M-sequence radars are emerging. Some of them require not only the high performance offered by the M-sequence technology, but their dimensions and production costs have to be minimized as well. Examples of such applications are ground penetrating radar, industrial and medical sensors as well as the M-sequence radar applications in automotive and wearables. The strict dimensional and economical requirements of other applications may be fulfilled by the integration of the whole M-sequence radar into a monolithic system on chip (SoC) [1]. However, integration of the whole device brings technological challenges which have to be solved.

All devices radiating electromagnetic energy have to comply with regulations to avoid interference with other radio services. The regulations are expressed in the form of spectral masks issued by local regulatory authorities and may differ among them. The most common restrictions for UWB radars are those issued by the FCC (US) [2] and ECC (Europe) [3] committees. In this paper, we decided to design a filter for the ECC UWB band whose spectral mask is shown in Fig. 1 [1].

From the Fig. 1 it is clear that the main ECC UWB band is relatively narrow (compared to FCC band) starting at 6 GHz with the upper cutoff frequency reaching 8.5 GHz. The other frequency ranges are more than 25 dB below the maximum main band EIRP, therefore they are less important for practical UWB sensing. From the spectral mask, it is obvious that designing the integrated filter for the ECC band will not be a trivial task.

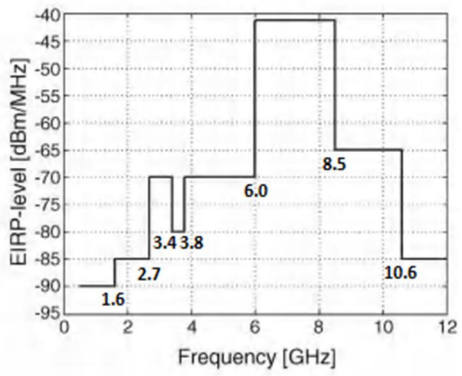

Fig. 1. European (ECC) regulation spectral mask for UWB radars.

II. Novel M-Sequence Radar ASICs

A. 1 GHz Low Pass Filter

One of the options to achieve ECC compliant (main ECC band spreads from 6 to 8.5 GHz) M-sequence UWB radiation is to truncate the frequency spectrum of the M-sequence at a cutoff frequency of about 1 GHz and mix the resulting signal with a carrier generated by a local oscillator (LO) at 7.25 GHz. Thus, considering two sidebands, we obtain a signal with frequency components reaching from 6.25 to 8.25 GHz, therefore compliant with the ECC spectral mask with protection bands of 250 MHz at both sides of the frequency range. A similar scheme can be used at the input of the M-sequence radar receiver.

To design the low pass filter with 1 GHz cutoff frequency, a common Sallen-Key architecture [4] of the active low pass filter was adopted as shown in Fig. 2. Several modifications and tradeoffs had to be made in contrast to the original Sallen-Key topology which assumes ideal components.

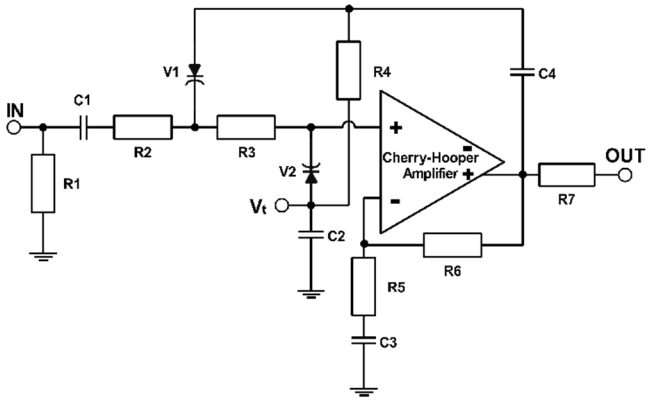

Fig. 2. Schematic diagram of the integrated Sallen-Key lowpass filter

The conventional active filter design assumes the gain bandwidth product (GBWP) of the operational amplifier to be

equal or more than a centuplicate of the cutoff frequency for Sallen-Key filters [5]. Such operational amplifiers are not available in the chosen IC technology. Instead of an operational amplifier, the Cherry-Hooper amplifier described in details in previous publications of our department [6][7] was used with certain modifications. Although the resulting amplifier block hardly imitates the properties of an ideal operational amplifier which are assumed by Sallen-Key filter topology, it is the best available tradeoff between the required parameters, manufacturing costs of the IC and technological compatibility with other ASICs for M-sequence radars.

Instead of ordinary capacitors, varactors V1 and V2 are used in the filter topology shown in Fig. 2. Their main role is to enable the compensation of filter characteristics deviation caused by process variations across the wafer. They also give an option to fine-tune the filter by external control voltage V_t if required by the application of the radar. Capacitors C1 to C4 are responsible for DC isolation of amplifier ports whose DC levels are not compatible. Resistors R1 and R7 ensure wideband matching of the filter circuit to 50 Ω impedance at the input as well as at the output port.

The prototype of the integrated low pass filter was measured at the probe station by placing the microprobes directly at the die pads. S-parameters of the circuit were examined by a vector network analyzer.

The forward transmission coefficient of the proposed filter prototype is shown in Fig. 9 as a function of frequency with the tuning voltage V_t as a parameter. The filter 3 dB cutoff can be tuned approximately between 750 MHz and 1900 MHz for the tuning voltage in the range from -0.8 to -1.6 V referred to ground.

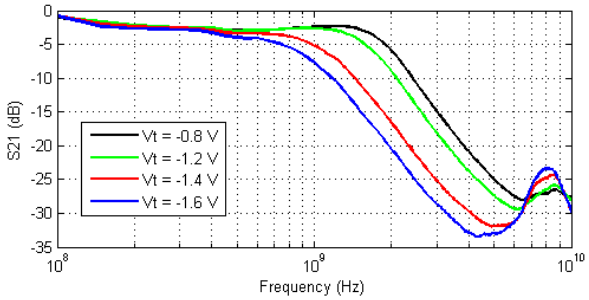

Fig. 3. Probe station measurement results for the proposed integrated lowpass filter forward transmission coefficient S21

B. Integrated ECC Band Pass Filter

In [8] we proposed a simple structure of an UWB ECC band pass filter based on a low noise amplifier with frequency selective negative feedback. Although it is not possible to design a filter with fixed frequency without dependence on process tolerances by this approach, the proposed filter is able to compensate the process deviations by external tuning. The proposed circuit is aimed rather as a proof of concept of a simple active RC filter in a low-cost ASIC technology than as a final market-ready device. However, the simulation results published previously in [8] promise that it can improve the performance of current UWB radars and offer sufficient parameters for some applications, as well as it can be easily integrated into the M-sequence SoC radar and eliminate the need for another external component.

In the recent months, the filter chip prototype has been delivered from the foundry and tested at the probe station. The forward transmission coefficient of the filter measured by the VNA is shown in Fig. 4. The tuning voltage applied to one of the control inputs is used as the measurement parameter. Only slight changes in the pass band center frequency can be observed in the measurement results. The main cause for that was that it was impossible to apply appropriate control voltages to all three control inputs in the probe station measurement setup. However, the pass band of the proposed filter shown in Fig. 4 matches almost exactly the frequencies of the main ECC band from 6 to 8. GHz.

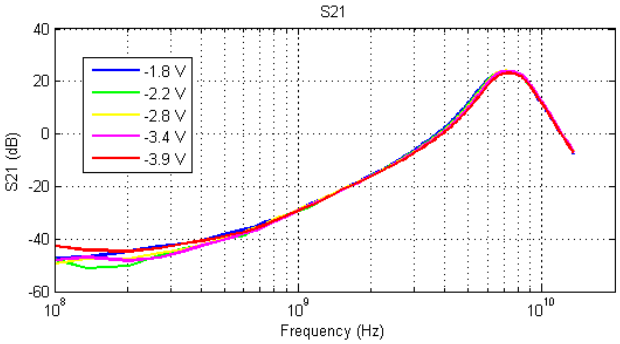

Fig. 4. Probe station measurement results for the proposed integrated bandpass filter forward transmission coefficient S21

III. Conclusion

The research results presented in this paper show that the design of the application-specific integrated circuits of UWB M-sequence radars is an up-to-date research task. The results achieved by the first prototypes prove the feasibility of the proposed concepts. We believe the presented circuits may be further improved in the future research and open the way to the integration of tunable filters into the M-sequence UWB radar system on chip, as they are considered as one of the last subcircuits which could not be implemented in the low-cost IC technology for the given frequency band so far. Except for the research mentioned above, additional promising results have been achieved during the previous period. However, they still cannot be published as the patent application process is ongoing now.

References

[1] J. Sachs, Handbook of Ultra-Wideband Short-Range Sensing. Weinheim: Wiley-VCH, 2012.

[2] Revision of Part 15 of the Commission's Rules Regarding Ultra Wideband Transmission Systems", *Federal Communications Commission Washington DC ET Docket 98–153*, 2002.

[3] "Harmonisation Of The Radio Spectrum For Equipment Using Ultra-Wideband Technology In A Harmonised Manner In The Community", *EU Commission Decision of 21 February 2007*, 2007.

[4] "Application note 1762: A Beginner's Guide to Filter Topologies", Maxim Integrated Products, 2003, available online: http://www.maximintegrated.com/an1762

[5] Baker, B. C. (2003). Select the Right Operational Amplifier for your Filtering Circuits-Analog Design Note ADN003. *Microchip Technology Inc*, 1-2.

[6] Sokol, M., Galajda, P., Slovák, S., & Pečovský, M. (2018, June). Modified Cherry-Hooper Amplifier for UWB Applications in 0.35 µm SiGe BiCMOS Technology. In 2018 19th International Radar Symposium (IRS) (pp. 1-7). IEEE.

[7] Pecovsky, M., Sokol, M., Slovak, S., Galajda, P., & Drutarovsky, M. (2019, April). Integrated Differential Amplifier for Ultra-Wideband Electrically Short Antennas. In 2019 IEEE Radar Conference (RadarConf) (pp. 1-5). IEEE.

[8] M. Pečovský, et al., "Integrated Active Filter for M-Sequence UWB Radar," Radioelektronika 2019, Pardubice, submitted for publication

Adaptive ε-greedy Exploration in Reinforcement Learning

[1]*Ján MAGYAR (3rd year),*
Supervisor: [2]*Peter SINČÁK*

[1,2]Department of Cybernetics and Artificial Intelligence, FEI TU of Košice, Slovak Republic

[1]jan.magyar@tuke.sk, [2]peter.sincak@tuke.sk

***Abstract*—Reinforcement learning is a method of artificial intelligence finding ever more application. However, there are still problems inherent to this paradigm of machine learning, among them finding a balance between exploration and exploitation. In this paper we compare simple Q-learning with methods using adaptive exploration rate and introduce our own adaptive method, heuristic ε-decay. Our tests show some advantages of the proposed method, such as faster learning, computational simplicity, and better overall performance of the trained agent.**

***Keywords*—adaptive reinforcement learning, directed exploration, ε-greedy, reinforcement learning**

I. Introduction

Reinforcement learning (RL) is a general method of artificial intelligence that bases its learning process on an interaction between an agent and an environment [1]. The environment has a defined set of states, and the agent can carry out pre-defined actions at each time step to which the environment reacts by changing its state. Based on this change, the agent obtains a reward signal that informs it about the appropriateness of the action taken: the higher the reward, the more fitting the action. The agent then acts in a way that maximizes the accumulated reward – or value.

Although reinforcement learning has been successfully used in a number of use cases, it has its limitations. In every RL application, the reward function is critical to the success of training, as a poorly designed function can lead to unwanted behavior from the agent. Infinite or continuous state spaces constituted another obstacle in the widespread use of RL algorithms, and were addressed with deep reinforcement learning [2]. One of the still prevailing major drawbacks of reinforcement learning is its relatively long training time. Since the agent learns based on trials and errors, it might take an unnecessarily long time for it to find an optimal behavior. This is especially problematic when a badly selected action can hinder the success of the interaction between the agent and the environment, such as human–computer interaction where there is no room for the agent learning from mistakes and it is near impossible to run a large number of simulations to pre-train the agent [3].

In this paper we look at methods developed in the past that try to shorten the training time of RL agents and make their learning process more effective (Section II). We also introduce our own heuristic ε-greedy method (Section III) and compare its performance to various already existing algorithms on a benchmark environment in Section IV.

II. Theoretical Background

Most methods aimed at minimizing the training time for RL algorithms use directed exploration during the learning process. Exploration is used to describe random action selection with the hope of finding a more rewarding behavior. In most algorithms, exploration is implemented using a constant, ε, that represents the probability of random action selection. By adjusting this constant, we can define a more exploring behavior for the agent in the early stages of learning, while the agent can rely on its past experience more in later stages.

Counter-based adaptive exploration methods direct the exploration of the agent by memorizing knowledge about the learning process itself and directing the exploration towards less frequently visited states. For each state s, a counter $c(s)$ counts how often this state was visited during training. Actions are then selected by a linear combination of an exploitation term and an exploration term [4]:

$$eval_c(a) = \alpha \cdot f(a) + \frac{c(s)}{E[c|s,a]} \tag{1}$$

where α is a constant weighting exploitation over exploration, $f(a)$ represents the utility of action a, and $E[c|s,a]$ denotes the expected counter value of the state obtained by selection action a in state s. During action selection, all available actions are evaluated using equation 1, and the action with the highest $eval_c$ is chosen deterministically.

Another method of adaptive exploration was presented in [5]. The authors of this paper introduced a value-difference based exploration (VDBE) that adjusted the exploration rate based on simple heuristics: if there is a high discrepancy between the expected utility of an action and the observed reward, the exploration rate should increase, since the agent does not have reliable knowledge of the state. On the other hand, if the expected utilities are accurate, the exploration rate should decrease, and the agent should rely on past knowledge. Each state has its own exploration rate which is updated the following way[5]:

$$\varepsilon_{t+1}(s) = \delta \cdot \frac{1 - e^{\frac{-|\alpha \cdot TD-error|}{\sigma}}}{1 + e^{\frac{-|\alpha \cdot TD-error|}{\sigma}}} + (1-\delta) \cdot \varepsilon_t(s) \tag{2}$$

where σ is a positive constant called inverse sensitivity and δ determines the influence of action selection on the exploration rate; $\alpha \cdot TD-error$ is the change in the expected utility and the observed utility.

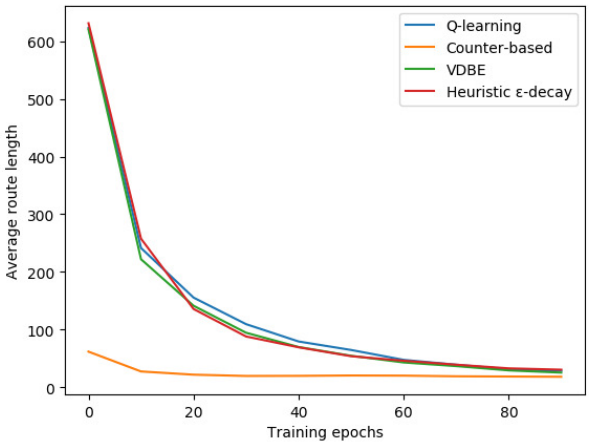

Fig. 1: Training process of various RL methods (first 100 epochs)

III. Methodology

VDBE can successfully adapt the exploration rate for each state, but it is a computationally expensive method. Therefore, we propose an alternative method that uses an ε-decay constant δ (=0.95 in our experiments) to adjust the exploration rate for a given state. We also remember the last TD-error for each state for further reference. Then we update the exploration rate as follows:

$$\varepsilon_{t+1}(s) = \begin{cases} \delta \cdot \varepsilon_t & \text{if } TD - err_t < TD - err_{t-1} \\ min(1, \varepsilon_t/\delta) & \text{otherwise} \end{cases}$$

For comparing different methods of increasing the speed and effectiveness of RL algorithms, we used the gridworld benchmark. A gridworld is a two-dimensional space in which the agent can move in four directions (north, east, south, and west). Each gridworld has one goal position, and the agent's task is to find a path to this goal position. A sparse reward function was defined for each algorithm (to prevent unexpected side-effects on the behavior) as follows:

1) 1 for reaching the goal position
2) 0 for any other valid move
3) -1 for any invalid move (hitting the edge of the world).

The algorithms were tested on 100 20×10 gridworlds with a single goal position which was generated randomly for each test run. Each test run consisted of 3,000 training epochs, where one epoch constituted a single navigation from a randomly generated starting position to the goal position.

During training, we observed the average number of steps it took the agent to get to the goal position from 50 randomly generated position after every tenth training epoch. These values were then plotted to a learning curve where a steeper learning curve suggested a more efficient training method. We also considered the average number of steps over the last 300 epochs, and the average training time for one epoch.

IV. Results

Figure 1 shows the learning curves of the tested RL methods over the first one hundred epochs of training. Epoch 0 represents the behavior of an untrained agent. At the beginning of training, the counter-based method performed already better; this is due to the fact the the algorithm prefers not-yet visited states and is therefore more suited for solving any problem where the entire state space needs to be explored.

Algorithm	Average steps after training	Training time per epoch (s)
Q-learning	13.26	1.52
Counter-based	14.65	4.84
VDBE	11.80	1.47
Heuristic ε-decay	11.20	1.36

TABLE I: Comparison of selected methods

All tested methods were quick to converge, although the convergence of Q-learning slowed down considerably already after the first ten training epochs. The proposed heuristic ε-decay method showed a slightly more random behavior at the beginning of training, but it already performed better than VDBE after 20 epochs and continued to perform at a comparable level later on during training.

We further compared the best policies the tested methods found by calculating the average length of paths at the end of training, the results of this comparison are shown in Table I. Despite having the best performance at the beginning of training, the counter-based adaptive method found policies for which the average length of paths leading to the goal position was 14.65. The average length of paths for Q-learning was 13.26. VDBE and heuristic ε-decay performed at a near-equal level, with heuristic ε-decay finding a slightly better policy.

Finally, we ranked the algorithms based on their training speed (see Table I). The counter-based adaptive method was found to be the slowest (4.84 s/epoch), while all other methods performed at a comparable speed with heuristic ε-decay being the fastest (1.36 s/epoch).

V. Conclusion

In this paper we looked at the problem of adaptive exploration in reinforcement learning with the aim to speed up the training process. We tested Q-learning, counter-based Q-learning, VDBE, and heuristic ε-decay proposed by us on a gridworld scenario. Our experiments showed that VDBE and heuristic ε-decay found the best policies, with the latter performing slightly better and at a slightly faster pace due to fewer calculations needed during the training process. Future research involves further testing of the proposed method and evaluating it in different scenarios.

Acknowledgment

This research work was supported by APVV project 015-0730 "Cloud Based Human Robot Interaction" and FEI grant "Increasing Server Performance for Deep Learning".

References

[1] R. S. Sutton, A. G. Barto *et al.*, *Introduction to reinforcement learning*. MIT press Cambridge, 1998, vol. 135.
[2] V. Mnih, K. Kavukcuoglu, D. Silver, A. Graves, I. Antonoglou, D. Wierstra, and M. Riedmiller, "Playing atari with deep reinforcement learning," *arXiv preprint arXiv:1312.5602*, 2013.
[3] J. Magyar, M. Kobayashi, S. Nishio, P. Sinčák, and H. Ishiguro, "Autonomous robotic dialogue system with reinforcement learning for elderlies with dementia," in *2019 IEEE International Conference on Systems, Man and Cybernetics (SMC)*. IEEE, 2019, pp. 3416–3421.
[4] S. B. Thrun, "Efficient exploration in reinforcement learning," 1992.
[5] M. Tokic, "Adaptive ε-greedy exploration in reinforcement learning based on value differences," in *Annual Conference on Artificial Intelligence*. Springer, 2010, pp. 203–210.

Advantages of simulation models in the MS Excel and general recommendations for serial and parallel connection of DC/DC converters

[1]*Dávid SCHWEINER (4th year)*
Supervisor: [2]Dobroslav KOVÁČ

[1,2]Dept. of Theoretical and Industrial Electrical Engineering, FEI TU of Košice, Slovak Republic

[1]david.schweiner@tuke.sk, [2]dobroslav.kovac@tuke.sk

***Abstract*—The paper describes advantages of the simulation models created in Excel, which is part of the MS Office package. These simulation models are newly designed and created, while they can simulate serial and parallel topologies of two DC/DC converters connected together. The paper also contains general recommendations for serial and parallel connections of more DC/DC converters, which are based on many simulations and measurement. The recommendations are presented in form of flowchart.**

***Keywords*—DC/DC converter, PC simulation, flowchart, transient analysis, Excel**

I. Introduction

While searching the best solution for parallel and serial (cascade) connection of more DC/DC converters, there were designed and created new simulation models. These simulation models were created on basis of mathematical model, specifically with help of transient analysis of buck DC/DC converter switching. For the transient analysis was used method of Laplace-Carson transformation. Calculations of the transient analysis were published in journal JIEE [1], [2]. Final simulation models were created in Excel, which is part of well-known Microsoft Office package. Design and creation of these models was also published in the journal JIEE [3], [4], [5]. This article describes advantages of the new simulation models and also brings recommendations for parallel and cascade connections of more DC/DC converters. These recommendations are summarized in the flowchart, which represents some kind of a manual for a user.

II. Advantages of the new simulation models

Simulation models in Excel were created based on the results of a transient analysis of a standard DC/DC converter. In other words, simulation models were created using theoretical knowledge in electrical engineering and mathematics. This means that simulation results from these models can be applied in general to a wider range of DC/DC converters, so the use of these models is not limited to a particular component. The results of simulations performed using these models may be slightly less accurate compared to simulation results obtained with specialized tools (eg PSpice) for specific parts (library models should accurately reflect the real types). However, the created simulation models provide a fairly accurate picture of the operation of the converter (or their series-parallel connections). In addition, the accuracy can be changed by the parameter Δt, which represents the calculation step. The smaller the calculation step, the more accurate the simulation, but the smaller calculation step requires more calculations (rows in Excel), which increases the data volume in the simulation model and also slightly increases the duration of the simulation calculations.

The great advantage of Excel simulation models is their modifiability and the ability to customize and extend these models with new features. From a simple simulation model for a single DC/DC converter, which had no advanced macro functions, models were created to simulate parallel topologies and cascades, and can calculate and display the maximum ripple of the output voltage, amplitude of the converter inductor current and ripple period of the output voltage. Later, the models were modified to allow simulation and response to dynamic changes in the resistance load at the output.

Another significant (if not the most significant) benefit is the speed of the simulation and the ability to observe the effect of inverter parameter changes in real time. If one of the inverter parameters is changed (eg inductance or capacitance), the simulation takes only a few seconds, and the change is then graphically reflected. The most significant difference between the two simulation tools, in terms of simulation speed, is observed when two converters are connected in cascade connection. Specifically, when changing the inductance of the second converter from 100µH to 150µH, the simulation in the Excel model (cascade) takes approximately 12 seconds. The simulation of the same change in cascade connection using the PSpice program, takes approximately 1 minute and 35 seconds. Simulation times may, of course, vary from device to device, but it is very likely that the simulation in Excel will always be significantly faster compared to PSpice, but most often with more complex connections (parallel topologies and especially a cascade). Thanks to the simulation speed and the way of rendering the graphical progress (continuous change in real time), the created models enable better observation of the effects caused by changing any of the parameters.

The created simulation models in Excel thus represent an innovative approach to the research of possibilities of serial and parallel cooperation of DC/DC converters, while they brings some appreciable advantages.

III. General recommendations

The flowchart, which contains recommendations for parallel and cascade connections is separated into two parts, and can be seen in the figures 1 and 2.

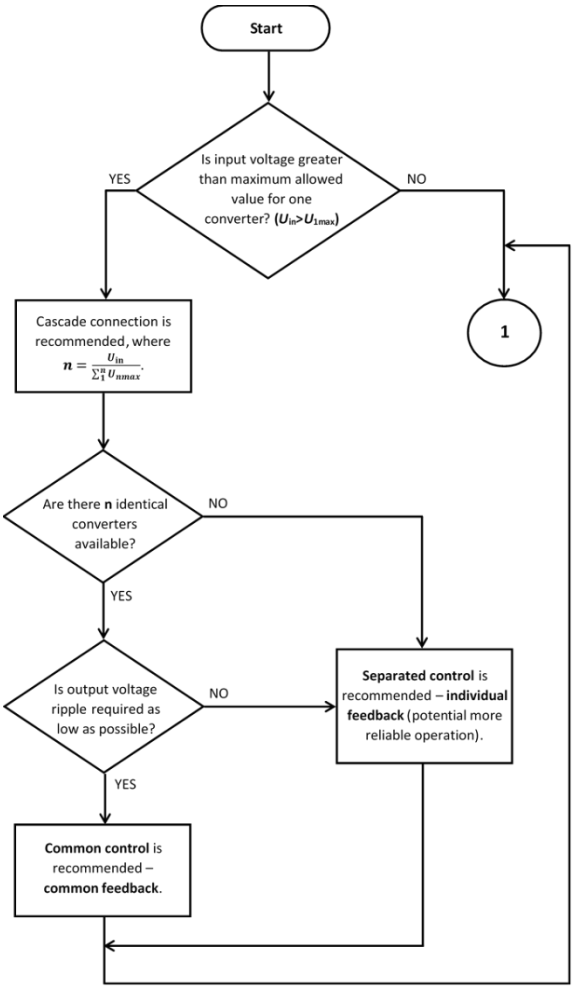

Fig. 1. The first part of the flowchart of recommendations

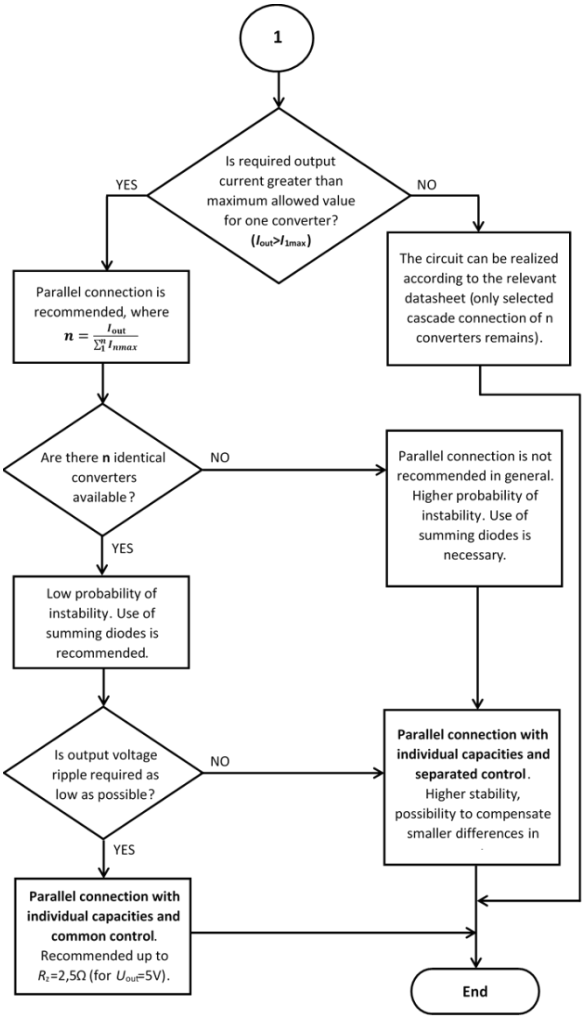

Fig. 2. The second part of the flowchart of recommendations

IV. Conclusion

The created simulation models allowed to obtain enough data to compile a flowchart that contains recommendations for designing circuits using serial and parallel topologies. This flowchart can serve as a universal guide for the user with respect to his requirements.

Acknowledgment

The paper has been prepared under support of grant project FEI-2020-61.

References

[1] D. Schweiner, D. Kováč, "Výpočet prechodného deja pri spínaní znižovacieho DC/DC meniča pre aperiodický priebeh veličín," *JIEE Časopis priemyselnej elektrotechniky*. Roč. 2, č. 1, 2018. ISSN 2454-0900.

[2] D. Schweiner, D. Kováč, "Výpočet prechodného deja pri spínaní znižovacieho DC/DC meniča pre kvazistacionárny priebeh veličín," *JIEE Časopis priemyselnej elektrotechniky*. Roč. 2, č. 2, 2018. ISSN 2454-0900.

[3] D. Schweiner, D. Kováč, "Vytvorenie modelu DC/DC meniča v programe Excel," *JIEE Časopis priemyselnej elektrotechniky*. Roč. 2, č. 4, 2018. ISSN 2454-0900.

[4] D. Schweiner, D. Kováč, "A simulation model for parallel buck DC/DC converters with mutual capacity created in MS Excel," *JIEE Časopis priemyselnej elektrotechniky*. Roč. 3, č. 2, 2019. ISSN 2454-0900.

[5] D. Schweiner, D. Kováč, "A simulation model for parallel buck DC/DC converters with separate capacities created in MS Excel," *JIEE Časopis priemyselnej elektrotechniky*. Roč. 3, č. 3, 2019. ISSN 2454-0900.

An Example of Prediction RSSI Parameter for Hybrid FSO/RF Line

[1]*Renát HALUŠKA (3rd year)*
Supervisor: [2]Ľuboš OVSENÍK

[1,2]Dept. of Electronics and Multimedia Communications, FEI TU of Košice, Slovak Republic

[1]renat.haluska@tuke.sk, [2]lubos.ovsenik@tuke.sk

***Abstract*— This article discusses the problem of optical space free communication (FSO), its use, and the conditions that affect it. Because of the vulnerability of the FSO transmission channel to weather conditions, such as fog, it is necessary to predict the Received Signal Strength Indicator (RSSI), and thus switch to a back-up RF (Radio Frequency) link using the decision tree method.**

***Keywords*— FSO, hybrid system, machine learning, radio communication**

I. Introduction

Optical fiber is the first most visible way of addressing the lack of bandwidth. Fiber is undoubtedly the most reliable means of optical communication, but digging, fiber storage costs and time to market are the most serious disadvantages of optical fiber. The second option is communication via radio frequency (RF) [1]. This technology is advanced and often deployed today. Radio-based networks require huge investments to obtain spectrum licenses, but they cannot be compared to fiber-optic transmission capacity. The third alternative is Free Space Optics (FSO) communication. FSO is the optimal solution in terms of technology, bandwidth scalability, deployment speed and cost-effectiveness [2].

Hybrid wireless communication based on FSO and radio frequency (RF) communication is a way to ensure reliable communication for critical real-time traffic in the outdoor environment, as fog weather affects FSO much more than RF connections. The main condition for running fiber-optical systems are seamlessly visible between two communication points, as FSO systems use light to communicate and can not pass through rigid obstacles such as walls, buildings, trees and others [3].

II. Hybrid FSO/RF System

Free Space Optics (FSO) communication involves the transmission, absorption and scattering of light through the Earth's atmosphere. The atmosphere interacts with light due to the composition of the atmosphere, which normally consists of molecules of various gases and small suspended particles called aerosols

Hybrid Wireless Free Space Communication (FSO) and Radio Frequency Communication (RF) (Fig. 1) is a way to ensure reliable communication for critical real-time outdoor traffic as weather like fog affects FSO much more than RF connections [4]. The main condition for using the FSO is that the receiver must be in line of sight with the transmitter [5].

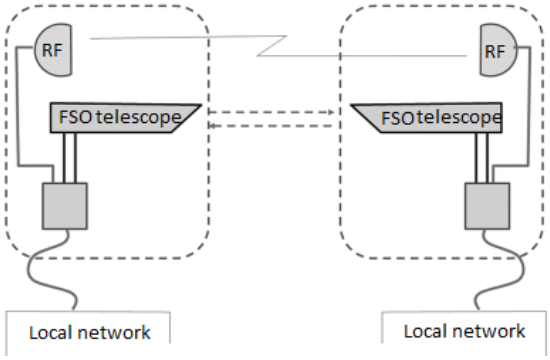

Fig. 1 Hybrid FSO / RF line

Hybrid FSO / RF provides a great application in ad-hoc mobile networks (MANET) [6]. The reconfigurable network environment can be created in the MANET combination of Wireless Sensor Network (WSN) technology and mobile robotics. However, the performance of this network is limited to node performance that provides RF-based communication. Therefore, the combination of RF and FSO provides a huge increase in MANETs transmission per node. The RF wireless network represents a strong capacity and performance limitation due to the growing development of communications technologies [7].

III. Prediction of RSSI Parameter

Machine learning techniques are widely used today for many other tasks. Different types of data related to different methods. The role of machine learning in FSO / RF hybrid systems is to predict the Received Signal Strength Indicator (RSSI) for which they have weather conditions [8]. To maximize the accuracy of the predictions, a form of machine learning and a transition to a decision tree that is designed to practice more complex methods is suggested. The transition enhancement is useful for predictive models that analyze organized data and categorical data. Decision trees are used to predict RSSI classification.

The decision tree is the classifier expressed as a recursive part of the instance space. The decision tree consists of nodes that form a rooted tree, meaning it is a routed tree with a node called a "root" that has no incoming edges. All other nodes have exactly one incoming edge. A node with outgoing edges is referred to as the "internal" or "test" node [9].

In the classification problem, use different metrics as a criterion for tree splitting. One option is an index that expresses the measure of total variance between classes *K*. When creating a decision tree, the input and training set is divided into smaller subsets, which gradually characterize the values of the output variables. The recursive division process is performed until the termination condition is met. In the process of atmospheric channel analysis for the FSO/RF system, a relatively extensive system of cases of input variables *X* with the corresponding mute output stages was designed. variables *y*. The output variable y is RSSI in this case. The general training set of cases has the following structure.

$$P = \begin{bmatrix} x_{11} & x_{12} & \dots & x_{1k} & y_1 \\ x_{21} & x_{22} & \dots & x_{2k} & y_2 \\ \dots & \dots & \dots & \dots & \dots \\ x_{n1} & x_{n2} & \dots & x_{nk} & y_n \end{bmatrix} \quad (1)$$

The input and training set is split to create a decision tree smaller subsets that gradually characterize the values of the output variables. The training matrix of the input variables for the FSO/RF system has the following structure:

$$P = \begin{bmatrix} P_1 & T_1 & G_1 & V_n & H_n & \cdots & W_1 \\ P_2 & T_2 & G_2 & V_n & H_n & \cdots & W_2 \\ \dots & \dots & \dots & \dots & \dots & \dots & \dots \\ P_n & T_n & G_n & V_n & H_n & \cdots & W_n \end{bmatrix} \quad (2)$$

where P is barometric pressure (hPa), H represents ambient humidity (%), T is air temperature (°C), wind speed W (m/s), G represents concentration Airborne particulate matter (mg/m3) and visibility (m). The matrix of the output variable *y* (target), which represents the received optical power of RSSI, is interpreted as follows:

$$y = [y_{RSSI.1} \quad y_{RSSI.2} \quad \cdots \quad y_{RSSI.n}]^T \quad (3)$$

To create a prediction *w* using a node in a tree that contains a set of instances, the weight of the instance in the current tree is predicted:

$$MSE(a, X) \quad = \frac{1}{l}\sum_{i=1}^{l}[a(x)_i - (y_i)]^2 \quad (4)$$

Determination coefficient or score determines the probability of how well the learning model will predict future samples of the output variable *y*. The best achievable score value is 1. The max depth parameter is selected based on optimum MSE and score values. For the selected algorithm, the max depth parameter was gradually tested from value 5 with step 1 to value 300. Fig. 2 shows the development of the MSE and score depending on the max depth. The cyclic training model showed that the optimal value of the parameter max depth for MSE = 0.94.

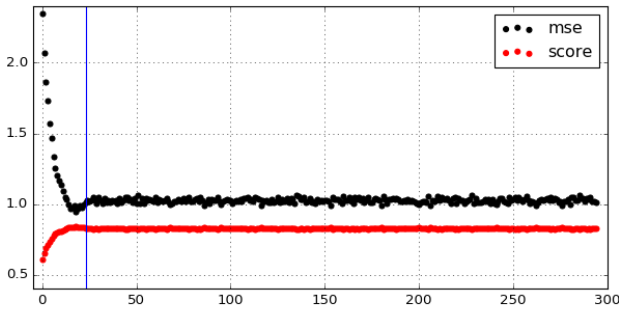

Fig. 2 Max depth parameter

The comparison of predicted and real RSSI values is shown in Fig. 3.

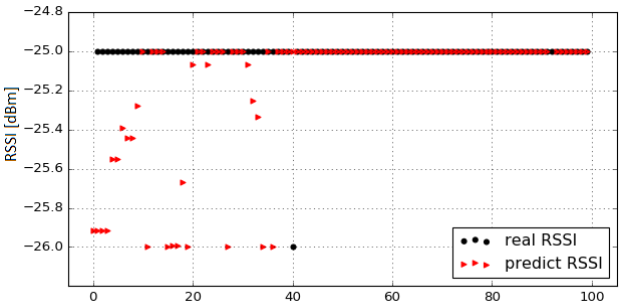

Fig. 3 measured and predicted data from the input matrix

IV. Conclusion

Due to the high impact of weather on FSO transmission, a backup RF line is required, which is less prone to, but much slower. For this reason, a hybrid FSO/RF line is required, which can be switched to the hard or soft switching principle. To create such a system, it is necessary to analyze the conditions and thus obtain the characteristics of the variables that affect the transmission channel. Appropriate RSSI prediction, using machine learning methods, makes it possible to quickly switch over communications over the RF line and back to a faster FSO line. In this way, it is possible to increase the efficiency of communication via the hybrid FSO/RF system.

Acknowledgment

This work was supported by Cultural and Educational Grant Agency (KEGA) of the Ministry of Education, Science, Research and Sport of the Slovak Republic under, the project No. 023TUKE-4/2017 and by the Slovak Research and Development Agency under the contract no. "APVV-17-0208 - Resilient mobile networks for content delivery".

References

[1] V. Brazda, O. Fiser, and J. Svoboda, "FSO and radio link attenuation: meteorological models verified by experiment," in *Free-Space and Atmospheric Laser Communications XI*, A. K. Majumdar and C. C. Davis, Eds. SPIE-Intl Soc Optical Eng, sep 2011.

[2] P. Singal, S. Rai, R. Punia, and D. Kashyap, "Comparison of different transmitters using 1550nm and 10000nm in FSO communication systems," *International Journal of Computer Science and Information Technology*, vol. 7, no. 3, pp. 107–113, jun 2015

[3] R. Gupta and P. Singh, "Hybrid fso - rf system: A solution to atmospheric turbulences in long haul communication," *International Journal of Scientific Engineering Research*, vol. 5, no. 11, nov 2014.

[4] J. Tóth, "High availability and reliability in wireless optics using data analytics techniques" - 2017.In: *SCYR 2017*. - Košice : TU, 2017 S. 118-119. - ISBN 978-80-553-3162-1

[5] T. Hastie and J. M. Chambers. "Statistical models." *Statistical Models in S*. Routledge, 2017. 13-44.

[6] H. Gavin. *Mastering Machine Learning with scikit-learn*. Packt Publishing Ltd, 2017.

[7] H. Gavin. *Mastering Machine Learning with scikit-learn*. Packt Publishing Ltd, 2017.

[8] M. Brzoska, "Modellierung zwischen „overfitting' und „underfitting'," *Rationale Entscheidungen unter Unsicherheit*, pp. 152–156, 2018.

[9] H. Hamsa, S. Indiradevi, and J. J. Kizhakkethottam, "Student Academic Performance Prediction Model Using Decision Tree and Fuzzy Genetic Algorithm," *Procedia Technology*, vol. 25, pp. 326–332, 2016.

An Overview on Generative Adversarial Networks

[1]*Marek RUŽIČKA (1st year),*
Supervisor: [2]*Juraj GAZDA*

[1,2]Dept. of Computers and Informatics, FEI TU of Košice, Slovak Republic

[1]marek.ruzicka@tuke.sk, [2]juraj.gazda@tuke.sk

***Abstract*—Generative adversarial networks (GANs) are from it's first appearance in 2014 widely discussed and investigated field. This work describes the concept of GAN, summarizes state-of-the-art knowledge and proposes a possible use of GANs in field of mobility.**

***Keywords*—generative adversarial networks, mobility, prediction**

I. Introduction

In 2014, Goodfellow et al. proposed a novel method of generating fake images via machine learning [1]. This model was called generative adversarial network (GAN) and has achieved wide interest in a short time. Main concept of GANs is based on two competing neural networks, where one of them is discriminator (D) and second is generator (G). Job of the G network is to learn how to produce fake data, such as synthetic faces. On the other hand, D is here to determine, if the produced output looks realistic, thus giving G network feedback. GAN can be used for a huge number of applications, from which several will be discussed throughout this paper. The most common usage for GANs is generating fake images, indistinguishable from reality. Synthesizing human voice is another possible use. Generating video sequences and real time applications were tested already. Transforming one type of data into another without knowledge about transformation function is an interesting application with wide possible usage. We will take a fast look at how GAN works and will go through several applications with perspective in real life use.

II. Generative adversarial network

As mentioned, GAN is a network which consist of two competing neural networks, D and G. We can imagine G network as a counterfeiter, trying to create perfect fake samples. On the other hand, D network is a cop trying to distinguish fake and real samples. These two networks are playing a min-max game, where both of them are getting better on what they do. D network is good if it determines all the correct samples as real and most of fake samples as fake. As G network is getting better, its output is close to the real and should be indistinguishable from real samples. D is then unable to tell if the output is real. A diagram of GAN is at figure 1

The above basic description of GAN network can be extended to a mathematical description. G distribution is defined $p_g = G(z, \theta_g)$, where z represents noise vector and θ_g are parameters of multilayer perceptron represented by differentiable function G. D network is also a multilayer perceptron represented as $D(x, \theta_d)$, which outputs a probability that the sample is real, coming from distribution x, or generated, coming from p_g. Both networks are trained simultaneously, where D is trying to maximize the probability of asserting correct label for $log(D(X))$. G is trying to minimize the probability $log(1 - D(G(z)))$. Together, optimization of the network is described by value function

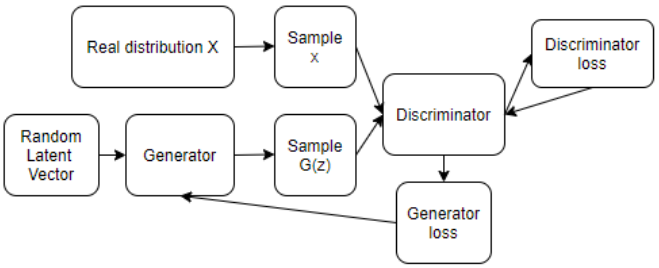

Fig. 1. Basic model of GAN network.

$$\min_G \max_D V(D,G) = \mathbb{E}_{x\sim p_{data}(x)}[\log D(x)] + \\ + \mathbb{E}_{x\sim p_z(z)}[\log(1 - D(G(z)))]. \quad (1)$$

The iterative algorithm of training a GAN network is described in algorithm 1.

Algorithm 1 Minibatch stochastic gradient descent training of GAN. The hyperparameter k denotes the number of steps applying the discriminator and equals $k = 1$.

1: **for** *iterations* **do**
2: **for** k steps **do**
3: Sample minibatch of m noise samples $z^{(1)}, ..., z^{(1)}$ from noise prior $p_g(z)$
4: Sample minibatch of m real samples $x^{(1)}, ..., x^{(1)}$
5: Update the D by ascending its stochastic gradient.

$$\nabla_{\theta_g} \frac{1}{m} \sum_{i=1}^{m} [\log D(x^{(i)}) + \log(1 - D(G(z^{(i)})))] \quad (2)$$

6: Sample minibatch of m noise samples $z^{(1)}, ..., z^{(1)}$ from noise prior $p_g(z)$
7: Update the G by descending its stochastic gradient.

$$\nabla_{\theta_g} \frac{1}{m} \sum_{i=1}^{m} \log(1 - D(G(z^{(i)}))). \quad (3)$$

A. General knowledge

Due to a large scale of applications, generalisation of knowledge in the field of GANs is limited. Many use-cases

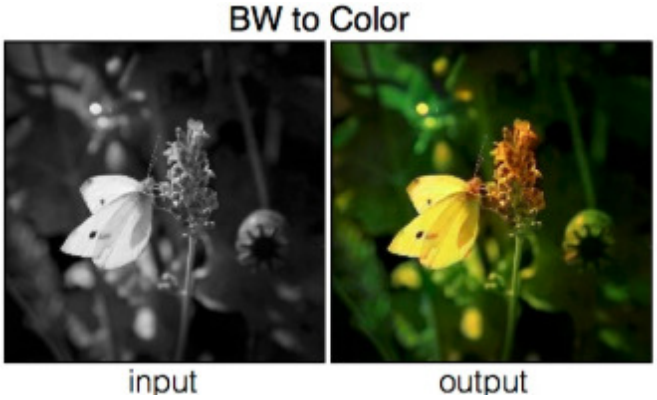

Fig. 2. Black and white image translated to colorized via pix2pix GAN [4]

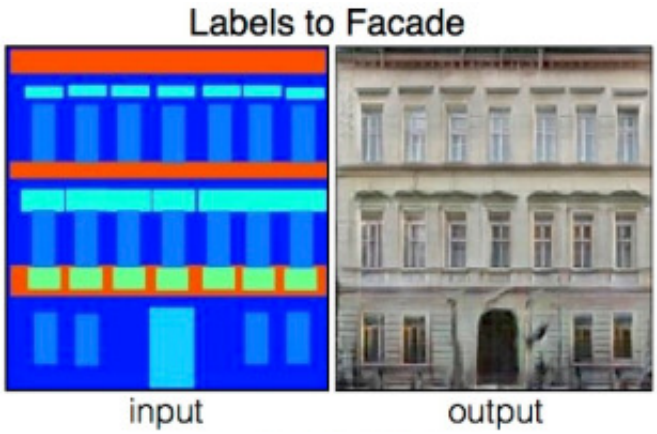

Fig. 3. Labels map image translated to facade via pix2pix GAN [4]

have its own needs and thus can't be generalized. Some of ideas, however, have general use in GANs.

Two times update rule (TTUR) was introduced by Heusel et al. [2]. D trains very fast in comparison to G, which causes troubles for G to train from start. In original paper, Goodfellow et al. proposed a method for proper training G as optimization of problem $log(1-D(G(z)))$ instead of $log(D(G(z)))$. TTUR extends this optimization by introducing two different learning rates for D and G. It was estimated that learning rate should be four times greater for D than for G.

For most implementations, binary cross entropy (BCE) is used as loss measure [3]. BCE itself is interpreted as logarithmic loss function and is defined as

$$H_p(q) = -\frac{1}{N}\sum_{i=1}^{N}[y_i * \log\left(p(y_i)\right) + \log\left(1-p(y_i)\right) * (1-y_i)], \tag{4}$$

where y is the label (1 for true and 0 for false) and $p(y)$ is the predicted probability of the point being true for all N points. Intuitively, the worse the prediction is, the higher is the loss. In case of GAN, two loss functions are defined, separately for *D* and for *G*. In case of *D*, the BCE value for generated samples should be close to one $BCE(D(G(z)), 1) \longrightarrow 1$. On the other hand, for *G*, BCE returned for *D* should be close to 0 $BCE(D(G(z)), 1) \longrightarrow 0$, as G is truing to fool D. In practice, good guiding point of correct GAN training is that the logarithmic loss should drop close to 0 for *D* and rise for *G*.

For more advanced GANs, where transformation is involved such as correcting blurry images or adding features to data, more advanced loss function is needed. In paper Image-to-Image Translation with Conditional Adversarial Networks [4], Isola et al. proposed a pix2pix GAN, which takes a conditional image as input and outputs a conditioned output. Such translated images can be seen at figures 2 and 3. Loss function is extended to use L1 or L2 losses along with BCE.

Conditional GAN learns a mapping from observed image x and random noise vector z to y, $G : x, z \rightarrow y$. Randomness is replaced by dropout layers, thus is still present, but partial data information is saved throughout the process. Objective function is defined as

$$\begin{aligned}\mathcal{L}_{cGAN}(G,D) =& \mathbb{E}_{x,y}[\log D(x,y)] + \\ &+ \mathbb{E}_{x,z}[\log(1-D(x,G(x,z)))].\end{aligned} \tag{5}$$

Distribution y is target distribution, a final data that should be generated from condition distribution x. Since this GAN has a condition in input, we know how the final output should look during training. Thanks to this, the objective function can be expanded by L1 distance (mean squared errors method), which is defined as

$$\mathcal{L}_{L1}(G) = \mathbb{E}_{x,y,z}[||y - G(x,z)||_1]. \tag{6}$$

Final objective for GAN is then

$$\arg\min_G \max_D \mathcal{L}_{cGAN}(G,D) + \lambda\mathcal{L}_{L1}(G). \tag{7}$$

Alternatively, a translation can be needed from domain X to domain Y where data pairs are unavailable. CycleGAN was introduced for this purpose by Zhu et al. [5]. This type of GAN network is able to translate a real data to alternative data, for example in figure 4, image of zebras is translated into image of horses. Examples for such translations are photos to paintings, summer to winter landscape etc. The objective in this case is to find a function for such translation. Instead of having final distribution, this GAN works in cycles. Translation from domain A to domain B takes place, and expecting it is reversible process, translated data are translated back to A. It is possible to train a cycleGAN, not only in a way from A to B but as well reverted. Objective function of this GAN and it's exact characteristics are out of the scope of this paper.

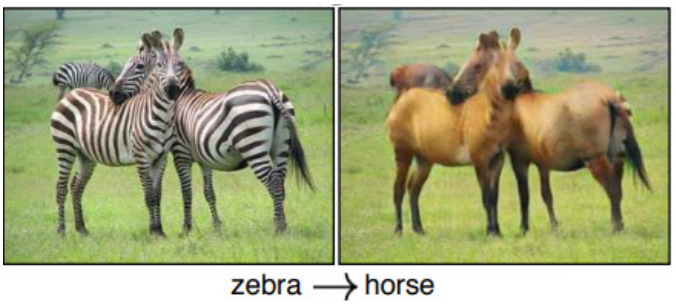

Fig. 4. Translating images of zebras into images of horses [5].

B. Use cases

Many different use cases have been published for the GAN networks. We will mention some of them throughout this section.

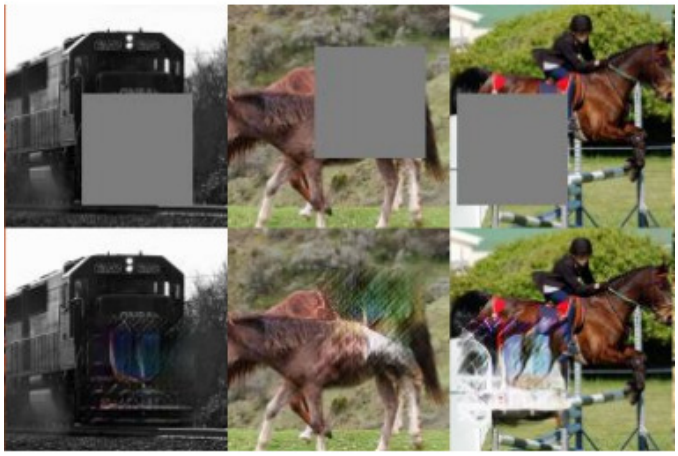

Fig. 5. Repairing masked images by CC-GAN [9]

Most common usage is to generate realistic images. Many Types of GANs were developed for this purpose. Odena et al. proposed auxiliary conditional GAN (AC-GAN) in 2017 [6], coming from conditional GANs [7]. AC-GANs generate samples along with its corresponding class label c p_c. The generated distribution is defined as $X_{fake} = G(c, z)$, so the output is a combination of noise vector and class label. The D network evaluates probability distribution over class label and over sources as well. D is defined as $D(x) = P(S|X), P(C|X)$. Objective function in this case contains two parts, log likehood of correct source L_s and likehood of correct class L_c. D is then trying to maximize $L_c + L_s$, while G is minimizing $L_c - L_s$.

Bidirectional Generative Adversarial Networks (BiGANs) are GANs, where not only G network is trained, but additionally an encoder $E : \Omega_X \rightarrow \Omega_Z$ [8]. Distribution $p_E(z|x) = \delta(z - E(x))$ is included within encoder, mapping data points x into the latent feature space of the generative model. D network is also modified. It takes input from latent space, predicting $P_D(Y|x, z)$. Y=1 if x is real or 0 if x is generated. BiGANs are specially useful for learning feature representation for auxiliary supervised discrimination tasks.

For problems like in-painting, context-conditional GAN (CC-GAN) was proposed [9]. In-painting is a method, when part of an image is missing or corrupt and needs to be recovered. A basic principle of CC-GAN is that G networks doesn't take latent vector alone, but also a corrupt image. This corrupt image is then recovered by generator and output is tested by discriminator. An example of in-panted images by CC-GAN can be seen at fig. 5.

For processing N-dimensional data, often convolutional neural network (CNN) is used [10]. The convolution process can be described as mapping a tuple of sequences of end user positions into a sequence of tuples. In most cases, CNN is used with images. Convolution looks for common features in multi-dimensional data via filters, which makes it possible to find eyes, nose, trees, etc. in images. Obviously, CNN is widely used within GAN networks. In [11], deep convolutional GAN (DCGAN) was proposed and achieved wide interest since. For example, Cui et al. used 1D convolution for processing errorous signals [12]. Very good results with 2D convolution was achieved by Ledig et al. [13]. The DCGAN they proposed was called super resolution GAN (SRGAN). With multiple convolutional layers, images were translated from low resolution to high resolution with high success. At figure 6 is presented a comparison of output of SRGAN and the real image.

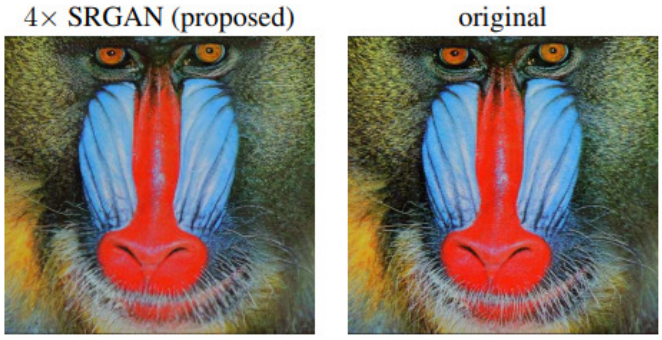

Fig. 6. Output of SRGAN vs. real image [13]

3D data generation is possible as well using this approach, e.g. gifs or videos. For example, Gupta et al. proposed a GAN, which predicts future socially acceptable trajectories of pedestrians from video [14]. Same approach was used for generating videos in [15], which output is presented at figure 7.

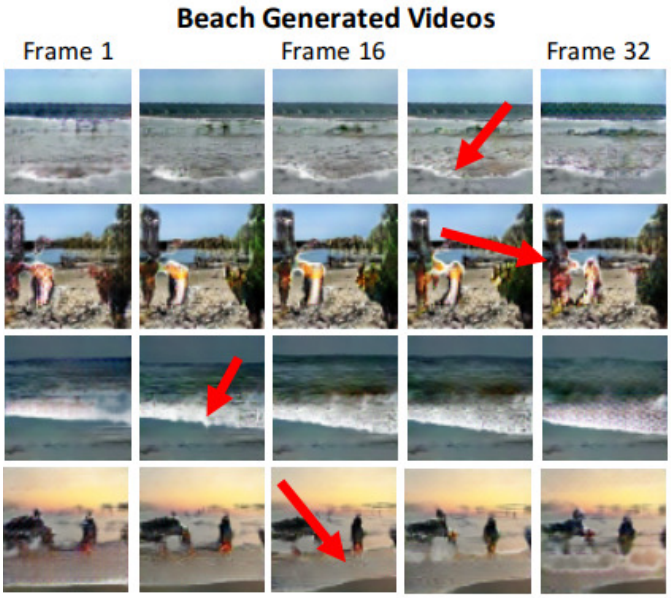

Fig. 7. Predicted video frames by GAN network, red arrows indicate movement [14]

Long Short Term Memory (LSTM) is used in GANs, that aim to generate not a file but a sequence of a data with time characteristics. It is better to generate sequential data not as whole file, but one by one data point with correlation with previous data points. This can be applied in computer-generated music [16], automated video captioning [17], or simulating trajectories of pedestrians or cars [18].

From various types of GAN implementations, not all can be mentioned within this search. We picked several more interesting implementations we have not mentioned yet. Zhang et al. achieved impressing results in rain removal from image and video frames [19]. An example de-rained image can be seen in fig. 8. Various GANs were used to find the best result. Similarly, multiple GAN types were used in research published by Brock at al., where a GAN created high resolution natural

images [20]. Many GANs were developed to generated human faces. An interesting application for human faces is rotation, which has been achieved by GAN in [21]. Similarly, rotating human pose is comparable application, as can be seen in [22].

Fig. 8. Sample image shot while raining and de-rained result by a GAN network [19]

III. Conclusion and discussion

As we could see throughout this search, generative adversarial networks have reached a wide attention since its first release in 2014. A wide range of different GAN architectures have been published in recent years, such as BiGAN, CC-GAN, SRGAN, cycleGAN and many more. Along with architectures, a large number of use-cases was published as well. Most of these implementations are image or video oriented. Since GAN networks are not limited to visual data, many implementations are yet to explore.

The end-user mobility patterns play a key role in the process of 5G network design. Massive increase of the RAN infrastructure complexity creates additional requirements on precise network planning and overall orchestration of the network as such. The possible solution to enhance the statistics feeding the network planning process is to generate massive dataset of the end-user mobility patterns. A future research is needed for developing a GAN network able to produce realistic samples of user trajectories.

Many existing mobility datasets have faulty data. Errors such as signal loss, corruptions while saving the data or invalid data submitted are common in user-tracking systems. With properly designed GAN network, we can feed a generator the whole tracked trajectory and errorous data could be replaced. A future work is to be done on creating such GAN.

Acknowledgment

This work was supported by the Slovak Research and Development Agency, project number APVV-18-0214 and by the Scientific Grant Agency of the Ministry of Education, science, research and sport of the Slovak Republic under the contract: 1/0268/19.

References

[1] I. Goodfellow, J. Pouget-Abadie, M. Mirza, B. Xu, D. Warde-Farley, S. Ozair, A. Courville, and Y. Bengio, "Generative adversarial nets," in *Advances in neural information processing systems*, 2014, pp. 2672–2680.

[2] M. Heusel, H. Ramsauer, T. Unterthiner, B. Nessler, and S. Hochreiter, "Gans trained by a two time-scale update rule converge to a local nash equilibrium," in *Advances in neural information processing systems*, 2017, pp. 6626–6637.

[3] L. Jost, "Entropy and diversity," *Oikos*, vol. 113, no. 2, pp. 363–375, 2006.

[4] P. Isola, J.-Y. Zhu, T. Zhou, and A. A. Efros, "Image-to-image translation with conditional adversarial networks," in *Proceedings of the IEEE conference on computer vision and pattern recognition*, 2017, pp. 1125–1134.

[5] J.-Y. Zhu, T. Park, P. Isola, and A. A. Efros, "Unpaired image-to-image translation using cycle-consistent adversarial networks," in *Proceedings of the IEEE international conference on computer vision*, 2017, pp. 2223–2232.

[6] A. Odena, C. Olah, and J. Shlens, "Conditional image synthesis with auxiliary classifier gans," in *Proceedings of the 34th International Conference on Machine Learning-Volume 70*. JMLR. org, 2017, pp. 2642–2651.

[7] M. Mirza and S. Osindero, "Conditional generative adversarial nets," *arXiv preprint arXiv:1411.1784*, 2014.

[8] J. Donahue, P. Krähenbühl, and T. Darrell, "Adversarial feature learning," *arXiv preprint arXiv:1605.09782*, 2016.

[9] E. Denton, S. Gross, and R. Fergus, "Semi-supervised learning with context-conditional generative adversarial networks," *arXiv preprint arXiv:1611.06430*, 2016.

[10] S. Lawrence, C. L. Giles, A. C. Tsoi, and A. D. Back, "Face recognition: A convolutional neural-network approach," *IEEE transactions on neural networks*, vol. 8, no. 1, pp. 98–113, 1997.

[11] A. Radford, L. Metz, and S. Chintala, "Unsupervised representation learning with deep convolutional generative adversarial networks," *arXiv preprint arXiv:1511.06434*, 2015.

[12] L. Cui, P. Zhao, K. Wang, J. Yang, and X. Bu, "A kind of arbitrary signal generator based on 1d generative adversarial network," in *2019 IEEE 8th Data Driven Control and Learning Systems Conference (DDCLS)*. IEEE, 2019, pp. 1324–1328.

[13] C. Ledig, L. Theis, F. Huszár, J. Caballero, A. Cunningham, A. Acosta, A. Aitken, A. Tejani, J. Totz, Z. Wang *et al.*, "Photo-realistic single image super-resolution using a generative adversarial network," in *Proceedings of the IEEE conference on computer vision and pattern recognition*, 2017, pp. 4681–4690.

[14] A. Gupta, J. Johnson, L. Fei-Fei, S. Savarese, and A. Alahi, "Social gan: Socially acceptable trajectories with generative adversarial networks," in *Proceedings of the IEEE Conference on Computer Vision and Pattern Recognition*, 2018, pp. 2255–2264.

[15] C. Vondrick, H. Pirsiavash, and A. Torralba, "Generating videos with scene dynamics," in *Advances in neural information processing systems*, 2016, pp. 613–621.

[16] O. Mogren, "C-rnn-gan: Continuous recurrent neural networks with adversarial training," *arXiv preprint arXiv:1611.09904*, 2016.

[17] Y. Yang, J. Zhou, J. Ai, Y. Bin, A. Hanjalic, H. T. Shen, and Y. Ji, "Video captioning by adversarial lstm," *IEEE Transactions on Image Processing*, vol. 27, no. 11, pp. 5600–5611, 2018.

[18] J. Amirian, W. Van Toll, J.-B. Hayet, and J. Pettré, "Data-driven crowd simulation with generative adversarial networks," in *Proceedings of the 32nd International Conference on Computer Animation and Social Agents*, 2019, pp. 7–10.

[19] H. Zhang, V. Sindagi, and V. M. Patel, "Image de-raining using a conditional generative adversarial network," *IEEE transactions on circuits and systems for video technology*, 2019.

[20] A. Brock, J. Donahue, and K. Simonyan, "Large scale gan training for high fidelity natural image synthesis," *arXiv preprint arXiv:1809.11096*, 2018.

[21] R. Huang, S. Zhang, T. Li, and R. He, "Beyond face rotation: Global and local perception gan for photorealistic and identity preserving frontal view synthesis," in *Proceedings of the IEEE International Conference on Computer Vision*, 2017, pp. 2439–2448.

[22] L. Ma, X. Jia, Q. Sun, B. Schiele, T. Tuytelaars, and L. Van Gool, "Pose guided person image generation," in *Advances in Neural Information Processing Systems*, 2017, pp. 406–416.

Application of ensemble methods on a severely imbalanced data - bankruptcy prediction

[1]*Peter GNIP (2nd year),*
Supervisor: [2]*Peter DROTÁR*

[1,2]Dept. of Computers and Informatics, FEI TU of Košice, Slovak Republic

[1]peter.gnip@tuke.sk, [2]peter.drotar@tuke.sk

***Abstract*—Detection of rare events and unusual behaviour is extremely challenging task in the field of machine learning. Imbalanced learning is a vivid research area that is drawing attention by many practitioners and academics. In this paper we provide some initial experiments to combat issue of bankruptcy prediction based on a severely imbalanced dataset consisting of thousands of annual reports of small and medium sized companies operating in different business areas in the Slovak Republic. Two different machine learning approaches were used: methods based on outlier detection and ensemble methods. The most accurate results for all business areas were achieved via RUSBoost algorithm with geometric mean scores from 78,7% to almost 100%. Ensemble methods based on sampling technique (Easy Ensemble and Balanced Random Forest) showed comparable results to RUSBoost algorithm. Application of outlier detection methods yielded competitive results, particularly Isolation Forest algorithm with prediction accuracy between 68,2% - 97,6%.**

***Keywords*—Anomaly detection, bankruptcy prediction, imbalanced learning, ensemble methods.**

I. Introduction

Unfavourable financial situation or inappropriate economic activities can lead into bankruptcy of the company. Early information about upcoming risky situation can be an extremely useful tool in decision making process. Importance of the bankruptcy prediction issue is demonstrated by many publications and methods summarized in the most recent review papers [1], [2]. In practise, the number of solvent companies is significantly higher than number of financially distressed enterprises that represents a severely imbalanced dataset. One of the most popular approaches to combat this issue is to use imbalanced learning techniques. The review paper [3] summarizes the most popular approaches for overcoming imbalanced scenarios. The most promising techniques are sampling, outlier detection and ensemble learning.

II. Dataset

In this study we worked with dataset that consisted of thousands of annual reports of SMEs companies from different business areas operating in the Slovak Republic. Each annual report was constituted of 20 financial attributes. Detailed characteristic of used financial attributes is provided in our previous publication [4]. The datasets are available for four different evaluation years: 2013, 2014, 2015 and 2016. As evaluation year we consider a year, in which company is evaluated as solvent (non-bankrupt) or insolvent (bankrupt). In this study we used data one year prior the evaluation year since these showed the most promising results in previous experiments [4]. Distribution of bankrupt and non-bankrupt samples for all used business areas is depicted in Table I. More detailed characteristic of each dataset is provided in [5].

TABLE I
Distribution of bankrupt and non-bankrupt samples

	2013	2014	2015	2016
agriculture	6/1442	6/1622	8/1882	8/1991
retails	11/5195	11/6107	7/6327	4/6263
construction	25/1709	30/2165	20/2726	14/3114

Visualization of data structure for evaluation year 2015 and 2016 is depicted in Figure 1. The t-SNE [6] (*t-distributed Stochastic Neighbor Embedding*) dimensionality reduction technique was used to convert similarities of high-dimensional data into 2D space.

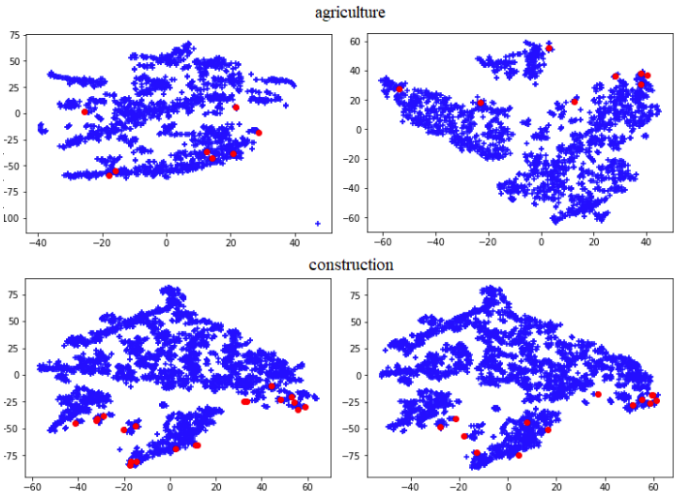

Fig. 1. Visualization of dataset to 2-dimensional space

III. Methodology

One of the most frequent approaches to deal with strongly imbalanced scenarios is ensemble learning technique. The main principle of ensemble methods is to combine multiple base learners (classifiers) in order to produce model with better prediction performance. In this paper we comparatively analyzed five ensemble methods - two standard ensemble methods: AdaBoost - AB [7], Random Forest - RF [8] and three ensemble methods based on sampling techniques:

Balanced Random Forest - BRF [9], Easy Ensemble - EE [10] and RUSBoost - RUSB [11]. Furthermore, two anomaly detection approaches were used, namely One-class Support Vector Machines - OCS [12] and Isolation Forest - IF [13].

Before applying machine learning algorithms it was necessary to process the dataset. Missing financial attributes were imputed with the mean value of the particular attribute. The dataset was also standardized by removing mean value of particular attribute and scaled to unit variance. In each iteration the dataset was randomly split into training (80%) and testing (20%) part with stratified sampling. Different approach was used with anomaly detection methods. Only 80% of non-bankrupt samples were used in training phase. The rest of majority class samples and the whole minority class were used for testing purposes. For better prediction performance hyperparameter tuning technique was included in training process. All experiments were repeated 100 times and achieved results were averaged.

The performance of trained prediction models was evaluated by geometric mean (GM) score. This metric is considered as one of the most suitable metrics to evaluate performance of models trained on imbalanced data [14]. GM is expressed as square root of the product of sensitivity (SEN) and specificity (SPE) and can by defined as follows

$$GM = \sqrt{sensitivity * specificity}. \quad (1)$$

IV. Experimental results

The GM scores of the best prediction models trained on data from annual reports from agriculture business area are depicted in Table II. The best results were achieved using data from evaluation year 2015 and 2016. The highest GM scores were from 88.7% to almost 100%. Similar results were observed using ensemble methods (EE, BRF and RUSB) on data from evaluation year 2014 with GM scores from 93.3% to 94.4%. The application of standard ensemble methods (AB, RF) resulted in poor model's performance across all evaluation years. According to balanced results on data from each evaluation year the RUSB algorithm was evaluated as the best one in the agriculture business area.

TABLE II
G-MEAN SCORES (%) FOR ALL METHODS USED IN EXPERIMENTAL STUDY ON AGRICULTURE DATASET

	Metric	2013	2014	2015	2016
AB	GM	40±49	70±46	88.7±26	100±1
	SEN	99.8±1	99.9±1	99.9±1	100±1
	SPE	40±49	70±46	77.5±29	100±0
RF	GM	18±39	26±44	92.8±16	100±1
	SEN	100±1	100±1	100±1	99.9±1
	SPE	18±39	26±44	85.5±22	100±0
OCS	GM	57.9±9	61±3	95±1	94.8±1
	SEN	58.5±4	75.2±3	90.2±2	89.9±2
	SPE	58.7±17	49.5±3	100±0	100±0
IF	GM	68.2±3	64.6±5	94.5±2	97.6±1
	SEN	70.4±4	59.8±4	89.9±2	95.3±2
	SPE	66.2±3	70.2±11	99.5±3	100±0
EE	GM	77.5±29	93.3±2	99.6±1	99.9±1
	SEN	78.1±6	87.1±3	99.1±1	99.9±1
	SPE	88±33	100±0	100±0	100±0
BRF	GM	74.4±28	92.9±2	94.2±11	98.3±1
	SEN	72.4±11	86.4±3	97.6±2	96.7±2
	SPE	88±33	100±0	92±19	100±0
RUSB	GM	78.7±21	94.4±2	99.5±1	99.9±1
	SEN	70.7±7	90.9±2	98.9±1	99.8±1
	SPE	94±24	99±10	100±0	100±0

The comparable results were achieved using annual reports from construction and retails busines areas. Bankruptcy prediction models with the best GM scores are provided in our previous paper [15]. The most balanced results for all business areas were achieved by RUSBoost algorithm with GM scores from 78.7% to almost 100%.

V. Conclusion and future work

In this study we have comparatively analyzed two different imbalanced learning approaches to combat issues represented by severely imbalanced dataset consisting of financial data of the SMEs companies operating in different business areas in the Slovak Republic. Five ensemble methods (AB, RF, EE, BRF, RUSB) and three anomaly detection methods (IF, OCS, LSAD). The most balanced results for all business areas were achieved by RUSBoost algorithm with GM scores from 78.7% to almost 100%.

The future work will be focused on proposing new machine learning methods for combating issue of a severely imbalanced data based on principle of ensemble methods that showed promising results. The efficiency of introduced methods will be tested on real and also synthetically generated data. Testing of different ratios between majority and minority samples will be also included in experimental study.

Acknowledgment

This work was supported by the Slovak Research and Development Agency under contact No. APVV-16-0211.

References

[1] H. A. Alaka, L. O. Oyedele, H. A. Owolabi, V. Kumar, S. O. Ajayi, O. O. Akinade, and M. Bilal, "Systematic review of bankruptcy prediction models: Towards a framework for tool selection," *Expert Systems with Applications*, vol. 94, pp. 164–184, 2018.

[2] F. Barboza, H. Kimura, and E. Altman, "Machine learning models and bankruptcy prediction," *Expert Systems with Applications*, vol. 83, pp. 405–417, 2017.

[3] G. Haixiang, L. Yijing, J. Shang, G. Mingyun, H. Yuanyue, and G. Bing, "Learning from class-imbalanced data: Review of methods and applications," *Expert Systems with Applications*, vol. 73, pp. 220–239, 2017.

[4] M. Zoričák, P. Gnip, P. Drotár, and V. Gazda, "Bankruptcy prediction for small-and medium-sized companies using severely imbalanced datasets," *Economic Modelling*, vol. 84, pp. 165–176, 2020.

[5] P. Drotár, P. Gnip, M. Zoričak, and V. Gazda, "Small-and medium-enterprises bankruptcy dataset," *Data in brief*, vol. 25, 2019.

[6] J. Tang, J. Liu, M. Zhang, and Q. Mei, "Visualizing large-scale and high-dimensional data," in *Proceedings of the 25th international conference on world wide web*, 2016, pp. 287–297.

[7] H.-J. Xing and W.-T. Liu, "Robust adaboost based ensemble of one-class support vector machines," *Information Fusion*, vol. 55, pp. 45–58, 2020.

[8] L. Breiman, "Random forests," *Machine learning*, vol. 45, no. 1, pp. 5–32, 2001.

[9] C. Chen, A. Liaw, and L. Breiman, "Using random forest to learn imbalanced data, dept. statistics," *Univ. California, Berkeley, CA, Tech. Rep*, vol. 666, 2004.

[10] X.-Y. Liu, J. Wu, and Z.-H. Zhou, "Exploratory undersampling for class-imbalance learning," *IEEE Transactions on Systems, Man, and Cybernetics, Part B (Cybernetics)*, vol. 39, no. 2, pp. 539–550, 2008.

[11] C. Seiffert, T. M. Khoshgoftaar, J. Van Hulse, and A. Napolitano, "Rusboost: A hybrid approach to alleviating class imbalance," *IEEE Transactions on Systems, Man, and Cybernetics-Part A: Systems and Humans*, vol. 40, no. 1, pp. 185–197, 2009.

[12] B. Schölkopf, J. C. Platt, J. Shawe-Taylor, A. J. Smola, and R. C. Williamson, "Estimating the support of a high-dimensional distribution," *Neural computation*, vol. 13, no. 7, pp. 1443–1471, 2001.

[13] F. T. Liu, K. M. Ting, and Z.-H. Zhou, "Isolation-based anomaly detection," *ACM Transactions on Knowledge Discovery from Data (TKDD)*, vol. 6, no. 1, pp. 1–39, 2012.

[14] M. Al Helal, M. S. Haydar, and S. A. M. Mostafa, "Algorithms efficiency measurement on imbalanced data using geometric mean and cross validation," in *2016 International Workshop on Computational Intelligence (IWCI)*. IEEE, 2016, pp. 110–114.

[15] P. Gnip and P. Drotár, "Ensemble methods for strongly imbalanced data: bankruptcy prediction," in *2019 IEEE International Symposium on Intelligent Systems and Informatics*, Subotica, Serbia, 2019.

Battery Storage Implementation to Improve Power Flow in Residential Smart Grid

[1]*Dávid MARTINKO (3rd year)*
Supervisor: [2]Michal Kolcun

[1,2]Dept. of Electric Power Engineering, FEI TU of Košice, Slovak Republic

[1]david.martinko@student.tuke.sk, [2]michal.kolcun@tuke.sk

***Abstract*— Battery storage can provide multiple services to power grids. The ongoing research is to consider and model effective use of battery storage units and photovoltaic systems in local low voltage distribution network with data based on real load profiles and collected by smart electricity meters and investigate the option of single private household energy storage versus community energy storage.**

***Keywords*— Smart Grid, Microgrid, Battery storage, Power flow, Photovoltaics, Mutual storage**

I. INTRODUCTION

Residential grid is low voltage local distribution network with group of loads and energy resources, such as wind and photovoltaic generators. Microgrid or smart grid, by definition, includes energy management system for monitoring and managing power flow and integrating distributed generation and storage devices [1],[2]. Fig. 1 illustrates smart residential grid or microgrid.

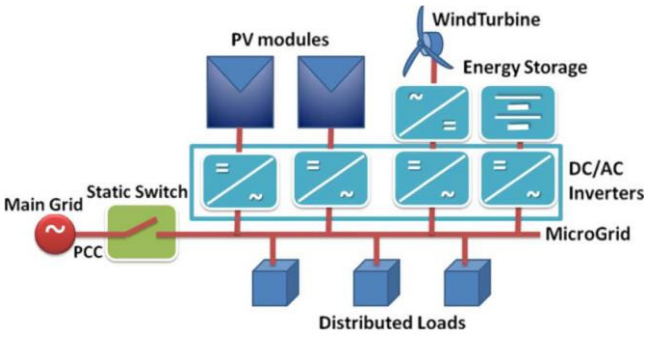

Fig. 1. Smart Grid [2]

Microgrids advantage is that energy is generated near loads, stored locally and can reduce power lines overlong losses.

Market penetration of electric in recent years rise rapidly all around the world. Distribution network is optimized for charging this vehicles at public charging stations and home random charging bring negative consequences to local distribution grid [3-4].

Battery storage units and photovoltaics energy sources could relieve overvoltage and overload issues. Smart regulation could defer grid changes, upgrades and investments, allow higher amount of installed photovoltaics panels.

II. METHODOLOGY

The proposed model is based on three phase 230/400V grid with rural topology in East Slovakia region. Schematic diagram of this type of grid topology is figured in Fig. 2.

Local electricity distributor operating in area of Eastern Slovakia has nearly 700k electricity meters which included more than 80k smart meters, what corresponding to a 12,3 % penetration level.

The level of use of photovoltaic panels on the territory of Eastern Slovakia is close to zero, therefore will be simulated existence of solar power plants on the roofs of individual houses randomly in the range of 10 to 30%. Only one single electricity generation profile of photovoltaic panels is used, because of correlation between photovoltaic panels installed profiles of houses in similar location and similar intensity of solar radiation [5]. The maximum installed capacity of local

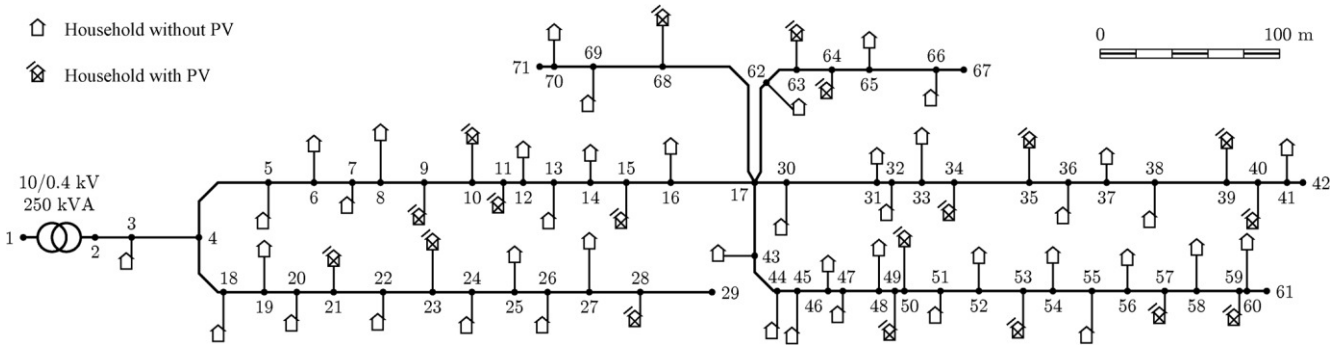

Fig. 2. Schematic diagram of rural grid

source can be 10kW due to connecting restrictions of distribution system operator [6].

Day long load flow for every household (Fig. 3) is divided into 96 equal time slots. Time slot duration is 15 minutes. For each time slot is calculated voltages and load flow for every household without or battery storage and photovoltaics and with them.

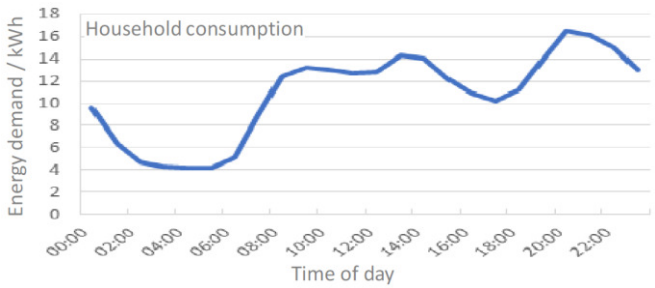

Fig. 3. Exemplary load profile for household consumption [7]

The battery storage unit is connected to the DC bus of a inverter, capable of providing active and reactive power in four quadrants for each phase individually. This functionality requires three single-phase inverters with a common dc-bus, or one three-phase four-wire inverter [8]. Battery charging time can be divided into same load flow time slots [9].

TABLE I
BATTERY PARAMETERS

	Li-ion	Lead acid	
Cycle life	3000	400	(-)
Cycle life exponent	-1,825	-1,607	(-)
Charge efficiency	88,2	78,4	(%)
Discharge efficiency	98	98	(%)
Charge power-to-energy ratio	1	1/3	(h^{-1})
Discharge power-to-energy ratio	4	1	(h^{-1})
Nominal energy specific cost	1000	250	(€/kWh)
Nominal power specific cost	270	0	(€/kWh)

The battery parameters for the simulation are listed in Table I. Set of parameters is from commercially available products. Two available technologies are considered:

1. **Lead-acid**: Each cell of a lead-acid battery comprises a positive electrode of lead dioxide and a negative electrode of sponge lead, separated by a micro-porous material and immersed in an aqueous sulfuric acid electrolyte. Lead acid batteries are a preferred solution for renewal energy systems (RES) which has power rating of approximately 100 kW. Better facilitate the connection and operation of generators of all sizes and technologies.
2. **Lithium-ion (Li-ion):** Lithiated metal oxide is used in the cathodes and graphitic carbon with a layer structure used for the anode. Having high energy density and high efficiency, this battery is suitable for many RES applications [10].

In contrast to individual storage, energy storage can be also introduced as community energy storage shared in close proximity. In some conclusions, community energy storage has lot of advantages over private storage including, decreasing the total amount of storage deployed, decreasing surplus PV generation which must be exported to the wider network and subsequently increasing the self-sufficiency of local smart energy communities [11] or significant cost reduction for similar performance by single household battery units [7].

An example for mutual storage and energy grid is further project in Alkimos Beach, Australia, by company Synergy [12]. A mutual LiIon battery with capacity of 1100 kWh connects 100 houses, which are equipped with PV systems. The aim is to investigate, how to integrate PV systems in existing power grids. The project runs from 2014 to 2020. As an intermediate result, the inhabitants can save up to 40 Australian Dollars per year due to the mutual storage.

III. NEXT STEPS

Investigative potential of using battery storage units with optimization method between voltage regulation, peak power reduction, battery degradation, annual cost based on real residential load flow. Load flow method for three phase unbalanced grid to be implemented in Matlab. Some of the major challenges will be battery degradation and battery degradation cost and power loss cost of the distribution network with charging and discharging cost.

REFERENCES

[1] J. C.Vasquez, J.M. Guerrero, J.Miret,M. Castilla, L.G. deVicuña, "Hierarchical control of intelligent microgrids," IEEE Ind. Electron. Mag., 2010
[2] Y. Levron, J.M.Guerrero, Y. Beck, "Optimal Power Flow in Microgrids With Energy Storage", 2013
[3] Q. Gong, S. Midlam-Mohler, V. Marano, G. Rizzoni, "Study of PEV charging on residential distribution transformer life," IEEE Trans. Smart Grid, 2012
[4] E. Veldman , R. A. Verzijlbergh, "Distribution grid impacts of smart electric vehicle charging from different perspectives," IEEE Trans. Power Syst., 2015
[5] J. Tant, F. Geth, D. Six, P. Tant, J. Driesen, "Multiobjective Battery Storage to Improve PV Integration in Residential Distribution Grids", IEEE Trans. On sustainable energy, 2013
[6] "Connection of Local Source, A notice for electricity producers", [Online], Available at https://www.vsds.sk
[7] E .Waffenschmidt, T. Paulzen, A. Stankiewicz, "Common battery storage for an area with residential houses", Atlantis Highlights in Engineering, volume 4, 2019
[8] M. Aredes, J. Hafner, and K. Heumann, "Three-phase four-wire shunt active filter control strategies," IEEE Trans. Power Electron., 1997
[9] Y. Huang, "A Day-Ahead Optimal Control of PEV Battery Storage Devices Taking into Account the Voltage Regulation of the Residential Power Grid", IEEE Transactions on Power Systems, accepted for publication in a future issue
[10] S. Tsianikasa, J.Zhoua, N. Yousefia, D. W. Coita "Battery selection for optimal grid-outage resilient photovoltaic and battery systems", IISE Annual Conference, 2019
[11] E. Barboura, D. Parrab, Z. Awwadc, M. C. Gonzáleza, "Community energy storage: A smart choice for the smart grid?", Applied Energy, 2018
[12] "Solar and Storage Trial at Alkimos Beach Residential Development", Australian Renewable Energy Agency, [Online] Available at: https://arena.gov.au/assets/2017/02/alkimos-beach-energy-storage-trial-customer-insights-research-2019.pdf

Communication architectures in the Internet of Things environment

[1]*Rastislav PETIJA (2nd year),*
Supervisor: [2]*František JAKAB*

[1,2]Dept. of Computers and Informatics, FEI TU of Košice, Slovak Republic

[1]rastislav.petija@tuke.sk, [2]frantisek.jakab@tuke.sk

***Abstract*—One of the challenges of the modern Internet of Things infrastructure is to support a communication model with the ability to adapt to situations such as congestion, component failure or anomaly in a network environment. This work provides an overview of anomaly detection in the Internet of Things environment. Attention is paid to the TinyIPFIX protocol. The mechanisms such as the process of mediation between IPFIX and TinyIPFIX and the use of the template concept allows existing infrastructure to be easily expanded through protocols to the Internet of Things environment, where the guarantee of transmission quality is crucial. This work aims to design an architecture model for monitoring and identifying anomalies in IoT infrastructures using TinyIPFIX protocol as transport protocol and machine learning as tool for evaluation of IPFIX data.**

***Keywords*—Internet of Things, Anomaly detection, TinyIPFIX, network monitoring**

I. Introduction

The Internet of Things is an ecosystem of interconnected devices that have unique identifiers and can transmit data over the network. Smart devices have built-in processors, hardware that is used to collect and send data and sensors that extract data from the environment. Current research is mainly concerned with data transmission in the Internet of Things environment. Little attention is paid to identifying anomalies in the Internet of Things environment. Anomalies include for example the detection of interference in the environment, the malfunction of sensors or some devices. The aim of this work is to create a communication architecture that would enable identification of anomalies in the Internet of Things environment by measuring the quality parameters of network infrastructure. Based on previous research in common network infrastructures, protocols such as NetFlow or IPFIX are most often used for monitoring and transfer of quality parameters. For the limited Internet of Things environment, it is possible to use the optimized version of the IPFIX protocol, namely the TinyIPFIX protocol. By creating such an architecture, it would be possible to verify the reliability and condition of the Internet of Things environment in a non-invasive way, where statistical data on actual data transfers (data flows) would be used for evaluation purposes. Each data flow can be described by five tuples that consist of source and destination IP address, source and destination port number and protocol number.

II. Current state of anomaly detection

The detection process is preceded by the phase of data collection from the observed environment. The more data can be collected, the better and more accurate their processing can be. The set of data collected represents a data set that is subsequently processed. In this work, the observed environment will be the Internet of Things environment and partially common network environment. The type of data that can be collected is classic sensor data [1], IPFIX statistics, or any organization defined data. Data flow processing can be divided into three main steps:

1) Obtaining data flow information from monitored devices or a monitored location on a network
2) Preprocessing and filtering the obtained data into a suitable form for subsequent processing by detection algorithms
3) Use detection algorithms to detect anomalies or network attacks

Detection algorithms can be divided into the following categories based on their function:

- Algorithms based on the detection of limit values set by the administrator for the observed data flow
- Algorithms based on classification rules learned from training data consisting of marked normal data flow and data flow showing anomalies
- Algorithms looking for the similarity between the observed data flow and the learned standard profile

Different types of information can be transmitted through a computer network. It may be relevant data, but a computer network resources may also be used for other purposes, such as attacks or other unwanted actions. All of these data flows that do not fall within the standard profile can be considered as anomalies that can be detected by comparing samples of transmitted data. For network administrators, it is very important that they can detect such anomalies and ideally to avoid them in the future. Several publications have been devoted to the detection of various types of anomalies. One of them was the detection of cryptocurrency mining. The authors in the publications [2] used machine learning to detect cryptomining using statistical data obtained by the NetFlow and IPFIX protocols as input. The quality evaluation of the transmission depends on measuring the following parameters related to the data flow: Delay, Jitter, Packet Loss and Bandwidth. With this mentioned approach, they were able to streamline the detection method for cryptocurrency mining. The previous approaches used were checking IP addresses or DNS records. This approach is already inadequate, as attackers can easily change these addresses. Another method used was based on

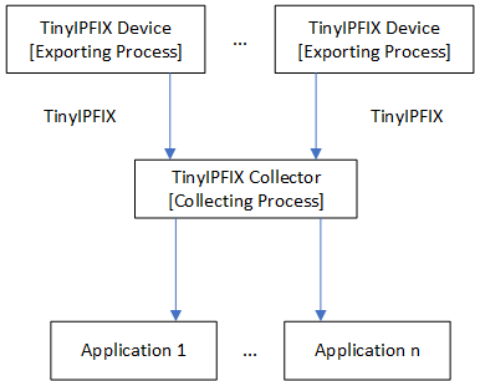

Fig. 1. Architecture of TinyIPFIX protocol [5]

an in-depth analysis of the transmitted data. This approach, in turn, is lengthy and inefficient, either in terms of time or computing resources.

III. Anomaly Detection Architecture

The proposed architecture for the detection of anomalies in the Internet of Things environment will have the task of linking the limited IoT environment to the classical network environment. TinyIPFIX protocol in IoT area and IPFIX protocol in common network will be used for transmission of quality parameters. As source [3] indicates, TinyIPFIX is suitable for transmitting both sensor and statistical data in a limited IoT environment. TinyIPFIX and IPFIX protocols were chosen because they are open standards. As source [4] says, there is a problem with standardization in the Internet of Things environment because the created solutions are often proprietary and do not cooperate with other systems.

The tasks that have been worked on over the past year can be divided into two main parts. The first task was related to the TinyIPFIX protocol, where, for experimental verification, this protocol was implemented on the Arduino and Raspberry Pi platforms. It was necessary to write libraries in C++ for Arduino and Python in Raspberry Pi. The architecture of TinyIPFIX is illustrated in Fig. 1. Based on the architecture shown, it was necessary to implement two processes. Exporting process on the Arduino or Raspberry Pi side, where the captured sensor data is encapsulated in the TinyIPFIX protocol and then sent to the server where the collecting process is running. Communication between the exporting and collecting process is based on the principle of sending templates and data. Fig. 2 shows an example of a template set and data set messages. We are currently working on a mediation mechanism that encapsulates data received by TinyIPFIX into IPFIX.

The second task on which we are currently working on is related to IPFIX collector and evaluation of collected IPFIX data. The open source IPFIXCOL2 tool, which is a combination of NetFlow and IPFIX collector, was used as a collector. This tool is tested on the internet service provider's production infrastructure. ELK tools, which stands for Elasticsearch, Logstash and Kibana, have been deployed to work with received data.

- Elasticsearch is a real-time search engine that supports multitenancy
- Logstash is a tool for managing events and logs

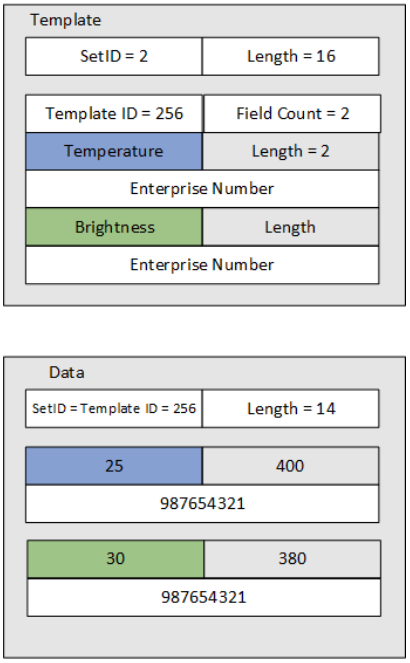

Fig. 2. Example of Template and Data set

- Kibana is a browser-based analytics and search interface for Elasticsearch that is used primarily to view Logstash event data

The last task we started to work on is to evaluate colected IPFIX data using neural networks. For this purpose, the Tensorflow platform with combination of Elasticsearch and Kibana was launched. Tensorflow is an open source library and API for machine learning and machine intelligence originated by Google.

IV. Conclusion

Based on the analysis, future work will be focused on identifying anomalies in the Internet of Things environment based on quality parameters of the observed environment. The work can be divided into these main steps:

1) Implement a mediation mechanism between IPFIX and TinyIPFIX protocol to enable data transfer from a limited Internet of things environment to traditional network environments
2) Design an algorithm for evaluating data received on the IPFIX collector in order to detect anomalies
3) Experimental verification of TinyIPFIX protocol as a tool for collection and transfer of transport parameters

References

[1] C. Schmitt, L. Braun, T. Kothmayr, and G. Carle, "Collecting sensor data using compressed IPFIX," in *Proceedings of the 9th ACM/IEEE International Conference on Information Processing in Sensor Networks - IPSN 10*. ACM Press, 2010.

[2] J. Z. i Munoz, J. Suarez-Varela, and P. Barlet-Ros, "Detecting cryptocurrency miners with NetFlow/IPFIX network measurements," in *2019 IEEE International Symposium on Measurements & Networking (M&N)*. IEEE, jul 2019.

[3] C. Schmitt, T. Kothmayr, B. Ertl, W. Hu, L. Braun, and G. Carle, "TinyIPFIX: An efficient application protocol for data exchange in cyber physical systems," *Computer Communications*, vol. 74, pp. 63–76, jan 2016.

[4] M. Noura, M. Atiquzzaman, and M. Gaedke, "Interoperability in internet of things: Taxonomies and open challenges," *Mobile Networks and Applications*, vol. 24, no. 3, pp. 796–809, jul 2018.

[5] C. Schmitt, B. Stiller, and B. Trammell, "TinyIPFIX for smart meters in constrained networks," Tech. Rep., nov 2017.

Computational models of systems biology and molecular programming

[1]*Pavol Korinek (1st year),*
Supervisor: [2]*Martin Tomášek*

[1,2]Dept. of Computers and Informatics, FEI TU of Košice, Slovak Republic

[1]pavol.korinek@tuke.sk, [2]martin.tomasek@tuke.sk

***Abstract*—Today's Systems Biology is wide science discipline having large scale of connections related to the many other science disciplines. Our focus is to see connections, and understand living organism using a knowledge of bioinformatics. We consider between biology inspired models and computations based on mathematics and logic in informatics. In Systems Biology and Bioinformatics we slightly shift from this consideration, and we try to see connections between how things work in living organisms and abstract models on the bases of mathematics and logic. In opposite, having certain view, of how living organisms, and their system works, we could see explanations of those principles by defining, or knowing similar models.**

***Keywords*—Process Algebra, Process Calculus, Logic Model, Computational Model, Natural Computing**

I. Introduction

Process calculus is used to describe processes, or components which processes are built from, using mathematics, combinatorics and logic. In certain level, formalism can be used to describe specification, or implementation, and implementation can be seen again as a specification for a different level of abstraction. Process calculus allows variations to their operators and so produce more suitable calculus with respect to studied or designed system. One could imagine that allow processes to be mobile, or allow processes to add, or remove communication channels [1], could be suitable formalism to describe living organisms.

II. Biologically inspired models

Computational models, like Artificial neural network, are inspired by biology. Lot of biology processes has been described by computational models and theories of informatics, mathematics and logic. The most exciting area is human brain and a way how we think. There are a numerous models, by which we try to explain people thinking the best. One of approaches is that our mind is not really something what we could touch. Probably it is something abstract, or better, it is emergent as a higher function of our brain [2].

A. Biology as numerical computation

We keep rather one idea in our mind. We got trouble to keep more ideas at one time, more troubles to deduce something in parallel without keeping focus somehow from the top of things. Respectively, there are processes inside our brain we can not really have on mind, so are somewhere in the background. Respectively, there are processes, or whole systems in our body, which are not interconnected at all. Anyway, the way how we think, can be put onto paper, and ideas can be written down in chronological order. When we are doing this, and we are using language of logic to describe such process, we see that there are more processes in parallel. When we come into a conclusion of a problem we solve, we used to guess what is the solution. Some problems is possible to solve straightforward way. Once that does not work, then we usually "start to think", and return to the rigorous reasoning [3].

B. Efective algoritms

To understand biological model, or process model, since we see cognition as a process, or for example how plants grow, we can observe a process behind that. We can study how it is realised, what are cells to build a process, or algorithm in terms of informatics. We know, that parallel systems, or multi-agent systems, or even Bayesian networks, or other models of Artificial Intelligence (AI), really behaves intelligently according to a function or a purpose they had been made. In nature we can see a small organisms adopted to an environment they live in. Semi-intelligent slime effectively searches for a food, and by that solves Traveler salesman's problem [4]. Repetitive concurrent process inside of a slime, pulsing inside of a slime, can deliver any information from one cell to any other cell in the organism. One could start to think about adoption of known algorithms related to this problem, which are based on approximation technic, but also algorithms which are only potentially related to this problem, like to design parallel version of cheapest ways in graph represented by vertexes and edges, by putting smaller parts into bigger ones, like we used to do in dynamic programming. For sure it is not that straightforward. We might see that combining with AI approach could lead to some approximation of a problem solution. Nature has its advantages here. There is an evolution behind the organism we study. We can see living cells and structures as building cells of an organism. Such building cells are already optimal from a point of their functionality. They were iteratively updating genetic information in a very long time of evolution. To unhide any aspects of their functionality we need to take all possible environment conditions and combinations into account, what is very complicated task.

C. Living

Principles how organisms live, respective biology systems work, could be crucial to answer how higher functions are

proceed and what's behind them. Organism cells need source of an energy to operate, and to keep alive. Whole process starts and ends with a supply of an energy, and ends when energy is not anymore supplied. Supply of the energy is necessary for living. It is also necessary for well functioning of an organism, communication, which is present at the level of living multi cell organisms, and regulation, which makes organism functions robust. Communication is present at the level of biology processes and their character is vectorial [5].

III. Computability

Solution of predefined problem, depends on, if we are able to get from one form of a process, or its property representation, to another one, just by making equivalent substitutions, and order forms as equivalent, so equivalency would be kept, and process equivalency, or its property verified. Generalisation of such system in symbol representation is called semi-Thue system and problem is known as Word problem (WP). The word problem of semi-Thue systems over $\Sigma = \{a, b\}$ is unsolvable [6]. Problem of algorithmically solvability is usually reduced, if possible, to other known problem, which is already proven as unsolvable. Method is called reduction method [7]. Hard problems are usually solved algorithmically by approximations, since we do not have deterministic algorithm solution for every problem. In opposite, we can build solvability and provability on a completeness of axioms of functional calculus in mathematical logic [8]. Valuable bricks for algorithms can be taken also from Graph Theory. Control structure of an algorithm is oriented graph. Graph also defines vector space upon its vertexes, edges, or cycles [9]. Theorems of Graph theory, which are related to graph topology, can be used to cut search of state space. Significant importance has theoretical arithmetic, algebra, and especially group theory, which tells us, for example, which is the smallest subgroup of a group G generated by a set X denoted as $[X]$. Intersection of all subgroups H of a group G containing X is a subgroup [10].

$$[X] = \cap\{H; X \subseteq H, (H; *) \subseteq (G; *)\}$$

Group theory is a base of an Equational logic, which allows rigorous reasoning [11].

IV. Transition Systems

There are many relations between transition systems and matrix representation of computational models. It can be shown, that there is a connection between matrix representation of a Finite Automaton (FA) and algebra of Semigroups. Exactly, that these two models are equal [12]. Looking for a more connections with interest into models by matrix representation, we can find, that there is also connection to a probabilistic models, or Markov chain model, what we can see as a form of FA definition [13]. Next connection is not really about power of a computational model, but more about logic upon it. It is a problem formulation to find synchronising word of predefined FA. Matrix representation of Deterministic Finite Automaton (DFA) is used here again. A word w of letters on edges of underlying graph Γ of DFA is called synchronising if w sends all states of the automaton to a unique state [14]. That is related to error handling mechanism, and recovery from an error state. The whole discipline, like fuzzy matrices and fuzzy automata, can be found for representations of automata and matrixes [15]. Yet another connection between transition diagram and matrix operations is when you would like to model relations, actions and consequences combining probabilistic theory [16]. Nice connection between matrix and automaton representation can be also seen regarding 1D cellular automaton [17]. We should know, that DFA can not be used only to recognise language, but also idea to use DFA as a tool for specification and compression of data is present [18]. There are much more connections to find between automaton, and its associated graph represented by relation matrix. There is a connection between matrix product factorisations of states and operators, and complex weighted finite state automata [19]. There is a straightforward connection of relation matrix to language accepted by DFA. It can be computed as a reflexive and transitive closure of relation matrix [20].

$$M^* = I + M + M^2 + M^3 + ... = I + \sum_{i=1}^{\infty} M^i = \sum_{i=0}^{\infty} M^i$$

V. Process Algebra

Process can be described, or defined by algebra equations. It is not trivial to see differences between FA and a process. Both can be modelled by transition graph made of states, transition function for FA, and actions for process. Since transitions of FA depends only of external input, in a case of a process, we consider between external and internal actions. When we think about nondeterminism of FA, it makes nondeterministic choice based on the input. This is idea of backtracking computation on the input. Simply we argue, that FA finds out which trace to choose, or good fairy tells advice which trace to choose. Process, in an opposite, can make choice itself, and it is not kind of backtracking, but it is one trace, which process chooses in runtime. As it usually is, process chooses trace which we do not want. That can be error case, or random case, or choice can be affected by environment. We talk about external and internal nondeterminism for a processes. It can be shown, that there is an axiomatic deduction system, which can be used to prove that two process equations are equal. This deduction system can be extended also for a communicating processes [21]. According to R. Milner [22]: to compare equality of two FAs it is enough to compare each traces for the same input. When we need to compare equivalency of a processes, it is a bit more complicated. We need to focus on a cases, when two processes can behave different way, cause of their internal activity. What needs to be considered here, is so called preemptive power of a silent action. Silent action can be internal and hides internal communication of subprocesses. We can not observe such process activities, so we can not guaranty equivalency of a processes without any restrictions. Important connection to group theory and so called many sorted algebras or free algebras results also to important consideration between initial algebras and final algebras [11] and theories which is possible to build on it.

VI. Bioinformatics

Applications of informatics helps biology research. First it is a big databases of data collected from scientific research. Analyse of Deoxyribonucleic acid (DNA) and Ribonucleic acid (RNA) means to store a huge amount of data. Sequences of DNA are being analysed and decoded. More and more it is not just about analytical data, but whole theories and models are being built, designed, and studied. DNA does not

store informations which are only responsible as a carrier of genetic information from a parent to a child, but stores also informations about all processes of living organisms. Basic building bricks for such processes are proteins. Proteins forms several levels dimension structures. Interest is to predict next level structure, or to see similarities between proteins, which are also determined by evolution. Comparing the sequences and structures of different domains are preferred instead of comparing whole protein. Domain is mainly composed of secondary level of a protein structures [23].

"One of aims of bioinformatics is to predict and analyse the structures of protein and the relationship to the structure to the function. (...) How a protein chain of a given sequence folds up are not yet understood and it is impossible to predict the folded structure of a protein de novo from its amino acid sequence alone. Helping to solve this problem is one of challenges facing bioinformatics. (...) The general goal of theoretical systems biology is to develop computer models that predict the properties of the large, adaptive, interconnected network that are found in living things" [23].

A. Systems biology

There are several goals which are studied by systems biology: signal processing, regulations, brain emergent properties, hierarchy and network of interacting proteins, topology and protein visualisation [23].

"The higher-order properties and functions that arise from the interaction of the parts of a system are called ***emergent properties****. For example, the human brain, capable of thought, dependents on practically all the cells in the brain and their interconnections. But a single brain cell is incapable of the property of thought; therefore thought is emergent of a complex system"* [23].

"Role of computational systems biology in drug development has already begun to shift from "potential" to "actively contributing". In many cases contributions are still modest, but they do suggest the growing contribution of systems biology should be expected to play as increasingly important role in exploring the choice of target (ligand, receptor, complex), or the need to account for diffusion and transport (within tumors, through membranes, across the blood-brain barrier, etc.)" [24].

As stated by L. Cardelli [25]: functional architecture of systems biology can be divided into four abstract machines. It is protein machine, gene machine, membrane machine, and glycan machine. Abstract machines of biochemistry are biochemical networks, gene regulation networks, and transport networks. Functions related to proteins are: regulation, degradation, metabolism, movement, assembly, transport, structure, and signalling. Interaction of proteins can be denoted using molecular interaction maps. There is a language, Systems biology markup language (SBML), to note and view protein interactions. There are several notations used for research of proteins: Stochastic π Calculus, Petri Nets (PNs), Stochastic PNs, or Pathway Logic, BioCham [25], BioSPi, PEPA, k-calculus, Kohn Diagrams and Kitano Diagrams [26]. Gene machine is central dogma of molecular biology. Regulatory system can be described by Gene Regulatory Networks. A lot of known approaches, which apply at protein machine can be used here, but model is different. There are specific techniques used here: Hybrid PNs, gene regulation diagrams, or mix of protein and gene networks [25]. Process behind the protein regulation is called polymerase. Inputs for this process is DNA, and RNA, and product is protein. Each RNA is responsible of creation of each protein, or group of proteins [23]. Membrane machine is very complex from point of its building cells and interactions. Membrane algorithms requires deep understanding of biology and medicine. There are few notations used here: "Snapshot diagrams", P-systems, BioAmbients, and Brane calculi [25]. Rarely used example to describe membrane algorithm is infection of a cell by virus. Virus can go thru a membrane cell and change cell structure from the inside.

B. Computational models

There are few articles regarding systems biology and available tools, what necessary gives links to recent research.

"The resulting models are executable, their computations can be seen as in silico experiments from which deducing information about the modelled biological entity, and possibly driving wet-lab experiments to confirm and refine these findings" [27].

One of a principles which is used for validation is Model Checking. That is used in many tools. Some of models used for such tools are: Ordinary differential equations (ODE), stochastic, discrete, boolean, or reactive modules, continuous-time Markov chain (CTMC) and others. Some logics used together with model checkers are: Computational tree logic (CTL), Linear temporal logic (LTC), or their variants and others [28]. It is possible to define properties on processes by certain logic and verify them by process run, or process verification techniques. By logic property composition we can define properties like: Safety, or Liveness, or their weak versions. Modal logic can be extended to make variant of CTL [1]. Similar way we can verify properties of processes by rewriting of process definitions, or their formal specifications using axiomatic system, and verify strong, or weak equivalence, between two processes [21], or between specification, and process [22]. According to L. Cardelli [26]: brief list of model construction, and validation techniques is: stochastic simulation, static analysis, model checking, and formal reasoning. Stochastic simulation can be done using Stochastic π calculus, which is based on π calculus introduced by R. Milner. Using few restrictions, that parallel composition of processes can be used only in an outer equation of a process definition, process model is forming so called Interacting Automata (IA). Stochastic IA model can be used to model biochemical reactions. There can be shown, that stochastic IA model can be used to model basic boolean circuits and functions like XOR [29]. There exist an equivalent labeled Petri Net for IA [30] and also there exist a translation from PNs to process algebra notation [31]. There are disadvantages to practically use PNs in case of realistic biochemical reaction simulations. One reason, for example, is exponential size of states, which need to be represented in the model [32]. There are advantages to use Stochastic π calculus instead. It allows, for example, the biological components to be modelled separately [32].

VII. Next Steps

There are many computational models, which are currently used as a tool of systems biology. Computational model have its grammar or automaton representation in theory of Formal Languages, or is described as an algorithm, or can be described by specification. Basic classes of formal languages are described by Chomsky hierarchy of languages. Automaton, machine, or computational model, from FA to Turing Machine (TM), is sequential, and can be used to prove properties of formal language, formalise algorithmic construction, or formulate decision problem according to a studied computational model. There is a framework for studying grammars [33]. There are also parallel models in the Theory of Parallel Computations. It can be shown that combining with parallel computation, grammars of Chomsky hierarchy can be moved from their class of languages. Sometimes parallel grammar systems are too complex to even imagine, what such systems do, but parallel models have their place in natural computing. Even if basic parallel models are very complex to describe formally or mathematically, we can design new models, ruled by logic, or meaning can be denoted by semantics. Word, form, which evolve as a grammar system, can be seen as a living organism (L-system, Aristid Lindenmayer, 1968). In term of algebra of processes we can see word, which evolve by grammar system, as a term, as a process, which evolve by change, by term rewriting. Term rewriting is used in Pathway Logic [25]. Using a term rewriting, or logic rewriting, it is possible to develop a symbolic systems biology. Regular grammar can evolve into repeating actions, so can be representation of a loop, or repeating process, or simple recursive process. Context-free grammar can evolve into tree structure, and also allows loops, so can be seen as a recursive process, or rather as recursive schema. Context-sensitive grammar evolution can also be seen as a recursive process, but also communication, or synchronisation between sub-processes, or cells is possible. There is a connection to Synchronised Alternating Finite Automata (SAFA), which has the same class of accepted languages, and that is context-sensitive languages [34]. According to a model of IA [29] and connection to PNs [30], we see possible connection of IA to SAFA, or Parallel Communicating Grammar System (PCGS). There are more models proposed for validation, or simulation as natural computing and also for modelling of processes of systems biology. Stochastic π calculus seems to be suitable for simulation of biochemical reactions [32]. PNs were proposed for modelling of pathways, and Stochastic PNs to simulate natural processes [25]. Matrix grammars, or graph grammars are kind of generalisation, or specialisation of a grammar classes, also combinations of more models, like Grammars Controlled by PNs are studied to support natural computing [35]. Next potential of models of systems biology can be in probabilistic, and quantum machines, or models of Formal Languages, and Theory of Parallel Computations. Further research of computational models of system biology is strongly connected to Process Algebra, Process calculus, π-calculus, and PNs, CTL, LTC, CTMC models and Model Checking as an automation validation tool. Our research of computational models, and connections to mentioned above, are steps which help Systems Biology to reach its goals.

References

[1] C. Stirling, *Modal and Temporal Properties of Processes*. Springer-Verlag, 2001.

[2] I. Farkaš, "Konceptuálne východiska pre model stelesnenej mysle," in *Modely mysle*, V. Kvasnička, V. Kelemen, and J. Pospichal, Eds. Európa, 2008, pp. 35–64.

[3] J. Šefránek, "Modely usudzovania," in *Modely mysle*, V. Kvasnička, V. Kelemen, and J. Pospichal, Eds. Európa, 2008, pp. 200–214.

[4] H. Barnett, "What humans can learn from semi-intelligent slime." [Online]. Available: https://www.ted.com/talks/heather_barnett_what_humans_can_learn_from_semi_intelligent_slime

[5] L. Kováč, "Princípy molekulárnej kognície." *Kognice a umělý život VI*, pp. 215–222, 2006.

[6] Z. Manna, *Mathematical Theory of Computation*. Dover (2003) unabridged republication of the edition published by McGraw-Hill, New York, 1974, 2003.

[7] J. Hromkovič, *Theoretical Computer Science*. Springer-Verlag, 1998.

[8] K. Godel, *ÚPLNOSŤ A NEÚPLNOSŤ*. OPS and Vydavatelství Západočeské univerzity v Plzni, 2015.

[9] R. Diestel, *Graph Theory*. Springer-Verlag, 2010.

[10] T. Katriňák, M. Gavalec, E. Gedeonová, and J. Smítal, *algebra a teoretická aritmetika(1)*. ALFA Bratislava, SNTL Praha, 1985.

[11] I. Van Horebeek and J. Lewi, *Algebraic Specification in Software Engineering*. Springer-Verlag, 1989.

[12] J.-É. Pin, "Finite semigroups and recognisable languages," 2002. [Online]. Available: https://www.irif.fr/~jep/PDF/York.pdf

[13] R. Pinch, "Automata, methods of specification." [Online]. Available: https://www.encyclopediaofmath.org/index.php/Automata,_methods_of_specification_of

[14] A. N. Trahtman, "Matrix approach to synchronising automata," 2019. [Online]. Available: https://www.researchgate.net/publication/327981267_Matrix_approach_to_synchronizing_automata

[15] A. Stamenković, M. Ćirić, and B. M., "Ranks of fuzzy matrices. applications in state reduction of fuzzy automata," *Fuzzy Sets and Systems*, pp. 124–139, 2018.

[16] M. J. Sterling, "How to create a matrix from a transition diagram." [Online]. Available: https://www.dummies.com/education/math/create-matrix-transition-diagram

[17] "Cellular automata/decision problems." [Online]. Available: https://en.wikibooks.org/wiki/Cellular_Automata/Decision_Problems#Regular_language_of_Garden_of_Eden_configurations_for_1D_CA

[18] M. Mindek and M. Hynar, "Finite state automata as a data storage," *Phys. Rev. A 78, 012356 (2008)*, 2005.

[19] G. M. Crosswhite and D. Bacon, "Finite automata for caching in matrix product algorithms," *APS Phisics*, 2008.

[20] D. J. Lehmann, "Algebraic structures for transitive closure," *Theoretical Computer Science*, vol. 4, no. 1, pp. 59 – 76, 1977.

[21] M. Hennessy, *Algebraic Theory of Processes*. The MIT Press, 1988.

[22] R. Milner, *Communication and Concurrency*. Prentice Hall Europe, 1989.

[23] M. J. Zvelebil and J. O. Baum, *understanding bioinformatics*. Garland Science, Taylor & Francis Group, 2008.

[24] E. O. Voit, *A FIRST COURSE IN SYSTEM BIOLOGY*. Garland Science, Taylor & Francis Group, 2013.

[25] L. Cardelli, "Languages & notations for system biology." Pisa. [Online]. Available: http://lucacardelli.name/Talks/2004-12-14LanguagesforSysBio(Pisa).pdf

[26] ——, "Abstract machines of systems biology," *Transactions on Computational Systems Biology*, vol. 3737, pp. 145–168, 2005.

[27] A. Bernini, L. Brodo, P. Degano, M. Falaschi, and D. Hermith, "Process calculi for biological processes," *Natural Computing*, pp. 345–373, 2018.

[28] M. Carrillo, P. A. Góngora, and D. A. Rosenblueth, "An overview of existing modelling tools making use of model checking in the analysis of biochemical networks," *Frontiers in Plant Science*, vol. 3, p. 155, 2012.

[29] L. Cardelli, "Artificial biochemistry," 2009. [Online]. Available: http://lucacardelli.name/Papers/ArtificialBiochemistry.pdf

[30] I. A. Lomazova, "Communities of interacting automata," 2003. [Online]. Available: https://www.researchgate.net/publication/273948933_Communities_of_Interacting_Automata

[31] S. Šimoňák and M. Tomášek, "Acp semantics for petri nets," *Computing and Informatics*, vol. 37, pp. 1464–1484, 2018.

[32] L. Cardelli and O. Kahramanogullari, "An intuitive modelling interface for systems biology," *International Journal of Software and Informatics*, 2013.

[33] B. Rovan, "A framework for studying grammars," in *Mathematical Foundations of Computer Science 1981. MFCS 1981. Lecture Notes in Computer Science*, C. M. Gruska J., Ed. Springer, Berlin, Heidelberg, 1981, vol. 118.

[34] A. Slobodová, "One-way globally deterministic synchronised alternating finite automata recognise exactly deterministic context-sensitive languages," *Information Processing Letters*, vol. 36, pp. 69–72, 1990.

[35] J. Dassow, G. Mavlankulov, M. Othman, S. Turaev, M. Selamat, and R. Stiebe, "Grammars controlled by petri nets," *Petri Nets - Manufacturing and Computer Science, Pawel Pawlewski, IntechOpen*, 2012.

Convolutional neural networks and data augmentation

[1]*Viera Maslej Krešňáková (2st year),*
Supervisor: [2]*Peter Butka*

[1,2]Dept. of Cybernetics and Artificial Intelligence, FEI TU of Košice, Slovak Republic

[1]viera.maslej.kresnakova@tuke.sk, [2]peter.butka@tuke.sk

***Abstract*—This paper presents an overview of open problems in deep learning and a possible solution to the robustness of neural network models. It deals with the process of data augmentation parameterized in the learning process neural networks. It also brings achieved results and future work ideas.**

***Keywords*—deep learning, convolutional neural networks, open problems, data augmentation**

I. Introduction

Deep learning allows computational models that are composed of multiple processing layers to learn representations of data with multiple levels of abstraction. These methods have dramatically improved state-of-the-art speech recognition, visual object recognition, object detection, and many other domains such as drug discovery and genomics. Deep learning discovers intricate structure in large data sets by using the backpropagation algorithm to indicate how a model should change its internal parameters that are used to compute the representation in each layer from the representation in the previous layer. The convolutional neural networks have brought in recent years breakthrough improvements in the processing of images, video, speech, and audio. In contrast, recurrent neural network models showed improved results on sequential data such as text and speech [1].

The most discussed open problems in deep learning are:

1) **Explainability**
   This is one of the main concerns the community is currently facing. A considerable amount of criticism is in fact that neural network models are often used as a Black Box model. In general, neural networks are a model in which it is difficult to explain the relationship between input and output. It is necessary to "open" these Black Boxes and provide a deeper understanding of its functions [2]. Many areas require an explanation of what information the model extracted in the learning process, which makes it disadvantageous. DARPA [3] has initiated a new program to look into this particular issue.
2) **Robust neural models**
   The neural network is as good as the data you give it. The stronger the abstraction you want to extract from the data, the more parameters you need to tune. More parameters = more data.
3) **Training a universal model**:
   Once learned, deep neural networks provide an effective and accurate solution to a particular problem. Currently, however, neural network architectures are highly specialized in specific areas of application. Designing a good model for a new application requires iteration, and iteration requires an additional time-consuming learning process.

We need a lot of labeled data to be able to train our neural network to extract suitable abstraction. My thesis deals with data augmentation, which is directly related to the second open problem.

We study the usage of deep learning methods in support of decision making processes in different domains using data augmentation. The main goal of the PhD. thesis is to improve the robustness of learning by appropriate parametrization of data augmentation methods in convolutional neural networks. We are working on the development of a new layer for the convolutional neural network that will parameterize the process of data augmentation directly during the learning phase. We want to develop such a layer first for image data processing; then, we will add augmentation for sequences. Our goal is to bring the domain-independent solution as much as possible, but with the possibility to remove some augmentation techniques (by data scientist or domain-specific rules) if they can produce irrelevant data. Experiments within selected domains will be used not only to test this solution but also to provide some manual or methodology for application in individual domains. The first areas we started to explore for this purpose are astronomy, text processing, and medicine. The first results in these areas will be described in the following chapters.

II. Data augmentation

Data augmentation is an artificial enlargement of a training set by creating the modified versions of the original data and leads to a better ability of the model to generalize what it has learned on input data [4]. Although the problem of robust learning prevails in other machine learning areas, a direct transfer of solutions from other areas is complicated.

Augmentation techniques for image processing include flip, zoom, rotation (Figure 1), or shift (Figure 2), but also adjusting brightness or contrast. Of course, data augmentation can also be used for sequences. If we add a small amount of white noise to a data point and feed it to a trained model, the neural network will get easily fooled. This problem is famously called as an adversarial example. We can also generate synthetic data based on the mathematical or physical rules of analyzed phenomena.

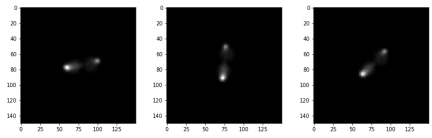

Fig. 1. Rotation – radio galaxy

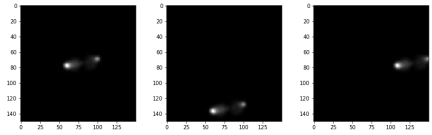

Fig. 2. Shift – radio galaxy

Our research group is also involved in natural language processing. There are other open problems in this area, namely sarcasm, irony, or metaphors, which are hard for detection by current algorithms.

We intend to extend our layer to include augmentation techniques used in the processing of text documents such as synonyms replacement, random insertion, random swap, random deletion [5].

III. Our preliminary results

A. Astronomy

Our first experiments were based on international collaboration with South African Radio Astronomy Observatory researchers. It was a classification of radio galaxies. The first experiments based on convolutional neural networks and transfer learning were published in [6]. Other experiments were based on data augmentation in the preprocessing phase, like moving the object in the image and adjusting the brightness and contrast of the original images. We were able to improve the accuracy of 99.6% (training time: 00: 08: 36.75). The results were tested on images obtained from various astronomical catalogs.

	Precision	**Recall**	**F1 score**	**support**
Results in [7]				
COMPT	0.98	0.98	0.98	1000
BENT	0.96	0.98	0.97	1000
FRI	0.98	1.00	0.99	1000
FRII	0.96	0.93	0.95	1000
	0.97	**0.97**	**0.97**	**4000**
Our results				
COMPT	1.00	1.00	1.00	392
BENT	0.99	1.00	0.99	454
FRI	0.99	0.99	0.99	393
FRII	1.00	0.99	1.00	395
	0.995	**0.995**	**0.995**	**1634**

TABLE I
COMPARISON OF OUR RESULTS AND STATE-OF-THE-ART RESULTS IN RADIO GALAXY CLASSIFICATION

The results showed us a solid ground for the development of the proposed data augmentation layer.

B. Text processing

Our work presented in [8] aimed at the usage of deep learning techniques to tackle the problem of the detection of fake news from the text. We trained different neural network models (feedforward, convolutional, and LSTM) on data containing the full text of the analyzed articles as well as only on their titles. The models were trained using a labeled dataset of fake and real news, and such models proved to be effective in this task. When comparing the evaluation metrics, most of the models gained consistent performance. However, convolutional and LSTM models proved to be the most effective. When comparing the evaluation metrics on the full-text data to only titles, the models still managed to perform on a similar level. On the other hand, the effect of using just titles for training proved to be effective during the training phase. This could be significant in real-world tasks, when using much larger training data or when the deployed models have to be updated frequently due to incoming documents from some data streams.

While the first experiments analyzed English documents, our goal is to detect fake news in the Slovak online space. In order to have suitable data, we are preparing an annotation project that will provide us with the annotated database of Slovak documents..

IV. Conclusion

The variability of data affects the robustness of learning and the quality of models. One method to increase model robustness is data augmentation. The aim is to design procedures for improving the robustness of learning by means of a new layer of the convolutional neural network, which parameterizes the process of augmentation of input data during the learning phase. We will focus on the generalization of image data augmentation procedures in astrophysics and medicine. Convolutional neural networks have also been successfully applied in the analysis of text documents. Nowadays, the global Internet is an environment that poses problems known as anti-social behavior. Therefore, another goal is to propose a model using a 1-D convolutional neural network, which will improve the detection of anti-social behavior in the Slovak online space.

Acknowledgment

This work was supported by Slovak Research and Development Agency projects APVV-16-0213 and APVV-17-026.

References

[1] Y. Lecun, Y. Bengio, and G. Hinton, “Deep learning,” 2015.
[2] W. Samek, T. Wiegand, and K. Müller, “Explainable artificial intelligence: Understanding, visualizing and interpreting deep learning models,” *CoRR*, vol. abs/1708.08296, 2017. [Online]. Available: http://arxiv.org/abs/1708.08296
[3] D. Gunning, “Explainable artificial intelligence (xai).”
[4] D. A. van Dyk and X.-L. Meng, “The art of data augmentation,” *Journal of Computational and Graphical Statistics*, vol. 10, no. 1, pp. 1–50, 2001.
[5] W. W. Jason and K. Zou, “EDA: easy data augmentation techniques for boosting performance on text classification tasks,” *CoRR*, vol. abs/1901.11196, 2019. [Online]. Available: http://arxiv.org/abs/1901.11196
[6] V. Maslej Kresnakova, K. H. Le Thanh, E. Pizur, and P. Butka, “Klasifikacia radiovych galaxii metodami hlbokeho ucenia,” *Data a Znalosti WIKT 2019*, pp. 35–38, 2019.
[7] W. Alhassan, A. R. Taylor, and M. Vaccari, “The FIRST Classifier: Compact and extended radio galaxy classification using deep Convolutional Neural Networks,” *Monthly Notices of the Royal Astronomical Society*, 2018.
[8] V. Maslej Kresnakova, M. Sarnovsky, and P. Butka, “Deep learning methods for fake news detection,” *2019 IEEE 19th International Symposium on Computational Intelligence and Informatics and 7th IEEE International Conference on Recent Achievements in Mechatronics, Automation, Computer Sciences and Robotics (CINTI-MACRo)*, pp. 143–148, 2019.

Data storing of electrical appliances

[1]*Aleš DEÁK (4th year)*
Supervisor: [2]František JAKAB

[1,2]Dept. of Computers and Informatics, FEI TU of Košice, Slovak Republic

[1]ales.deak@cnl.sk, [2]frantisek.jakab@cnl.sk

***Abstract*—The purpose of this article is to suggest data storage for measured values. This section explains what is a smart meter and why you need to use it. The second part clarifies the communication model and shows the structure of the measured values. The last part defines the SQL and NoSQL databases and describes the differences between them. This section also contains practical information using both types of databases in our solution, examples and a conclusion.**

***Keywords*—Smart meter, SQL, NoSQL.**

I. Introduction

The amount of used electricity is growing proportionally with the growing number of household appliances. Electric meters currently used for measurement remain inadequate. This problem creates the need of more and more energy in power plants. This solution also has an effect on the nature. Today we need to focus on quality and individually analyzing consumption instead of buildingg new sources of electricity. Currently used electric meters do not support the use of ecological energy sources, eg. solar panels or home wind generators.

For these reasons it is it is important to replace old, outdated electricity meters with new smart grids. The idea of using smart power meters is to transfer electricity to where it is needed. Communication between the server (in the power plant) and the client (Smart Grid) is essential to increase system and transportation efficiency [1]. Real-time and long-term consumption indicator statistics are stored, which can affect the amount of energy made in different places.

II. Communication Model

The basic communication model consists of an intelligent electricity meter, an intelligent device, a concentrator and a server. The smart meter measures energy consumption. The intelligent gadget acquires the readings from the electrometer; and sends them wirelessly to the concentrator. The concentrator connects many smart networks to the server over an internet connection. The server collects data in the database.

This solution can connect large geographic areas without the need of internet connection for each smart network. The server communicates with smart networks via DLMS / COSEM. The communication model is shown in the figure below.

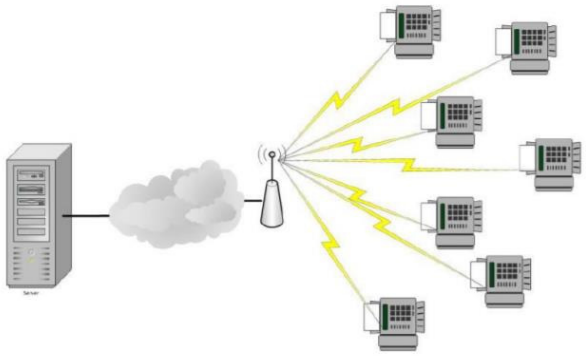

Figure 1 Communication model

III. Measurement of Power Usage

Electrical equipment extracts electricity from the transmission system. Generally, force consists of multiplication electric current in amperes and electric potential or voltage in volts. The electrical power used is changed to the active power in appliance. Electrical equipment connected to alternating current work on the principle of induction.

These appliances obtain electricity from the transmission system, which is necessary to create a magnetic field. This special energy is called reactive power [2]. Smart grids can measure active and reactive power. All of the measured values are sent to the server. These data and the consumption curve may be used for deduction of appliances switched on. Every intelligent grid sends energy consumption data to a server where they are processed. The curved line is created based on these values and the measured power is displayed in watts. An example of a curve is shown at image below. Green line shows active power and the blue line shows reactive power.

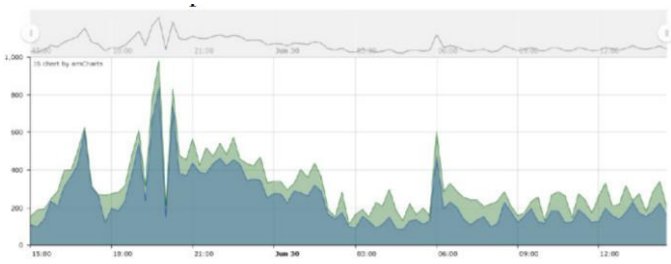

Figure 2 Consumption curve

IV. Database Models

The SQL database provides a repository of related data tables. A well built database model is also easy to read for the unskilled users. Each column is strictly determined by the data type and size. The number of columns is also permanently defined. for For example, you cannot use the same table for different information or enter characters if a number is expected. Each row in SQL is a different record. The SQL scheme must be determined before the data are entered and before the evelopment of business application logic. Small changes are possible, but large edits can cause complications. SQL tables create a strict data template, making it difficult to make mistakes. The integrity of the SQL database is guaranteed by foreign key restrictions. The user cannot edit or delete records related to other records.

NoSQL databases are different. Data is stored in JSON-like forms without data or type constraints, so they are more flexible as SQL [3]. This characteristic behavior can cause inconsistencies. NoSQL databases consist of documents and similar documents are stored in collections. The scheme is free, there is no need to first determine the design of the document. Adding new record types is easy. In the NoSQL database structures are composed of other structures. Data integrity is is not guaranteed.

V. Our Solution

The NoSQL database model is a JSON-like document. Data is the same as in the SQL database. An example of a NoSQL document is shown below.

```
{Users:
  [{ First name: "name1",
     Surname: "surname1",
     Identification: "ident",
     Houses:
       [{Name: "house1",
         Address: "Letna 9, Kosice",
         Appliances:
          [{ Name: "Appliance1",
             Type: "Type1",
             Brand: "Brand1",
             Model: "Model1",
             Location: "Location1",
             Consumptions:
              [{ Timestamp: 00000000,
                 Active power: 0.1Wh
                 Reactive power: 0.2VAr
              },],
          },],
       },],
  },]
}
```

Figure 3 NoSQL Document

The SQL database model is a bit easier to read and rules record keeping is clearly defined. On the other hand, changing the database model is more challenging. A NoSQL database is preferable because of the 2 major reasons. The first is speed. Many calculations, comparisons and database requests are needed display all appliances in one table. The user cannot wait a long time for a curve. Another reason is adding a new functionality. This project is still in a developing state of change and adding new behavior is possible. So our option is the NoSQL database.

VI. Conclusion

Using smart networks to determine when devices are turned on has many advantages. Users don't have to buy many expensive smart sockets that are not accurate devices. An integral part should be the prediction of abnormal behavior in every intelligent building. This would increase the security of users in relation to accident prevention, in particular in the case of older generation of people.

Another important area is automated discovery of appliances in an intelligent house. An app can notify you of forgotten irons or others dangerous appliances. If it's a large community that uses our application, an extensive database of devices will be created. Then the user enters only the name, model, device type and power consumption are automatically assigned without measurement.

Acknowledgment

This publication is the result of the Project implementation: University Science Park TECHNICOM for Innovation Applications Supported by Knowledge Technology, Phase II., ITMS: 313011D232, supported by the Research & Inovation Operational Programme funded by the ERDF. We support research activities in Slovakia/This project is being cofinanced by the European Union.

References

[1] Kheaksong, A. – Lee, W.: Packet transfer of DLMSúCOSEM standards for smart grid, In proceedings of Communications (APCC), pp. 2391 - 396, 2014.

[2] IEEE 100: the authoritative dictionary of IEEE standards terms-7th edition. ISBN 0-7381-2601-2, page 13.

[3] Leavitt, N.: Will NoSQL Databases Live Up to Their Promise?, Computer, ISSN: 0018-9162, pp. 12-14, 2010.

Deep learning based segmentation of volumetric ultrasound images

[1]*Ladislav POMŠÁR (1st year),*
Supervisor: [2]*IVETA ZOLOTOVÁ*

[1,2]Dept. of Cybernetics and Artificial Inteligence, FEI TU of Košice, Slovak Republic

[1]ladislav.pomsar@tuke.sk, [2]iveta.zolotova@tuke.sk

***Abstract*—Over the decades, medical ultrasound has become increasingly popular modality in the area of medical imaging. It is used for diagnosis in several areas such as cardiology, gynecology, emergency medicine, or pulmonology. With the increasing popularity of deep learning, there is an increasing demand for artificial intelligence systems of various uses for medical ultrasound. In this review, we review methods, that utilize both intraslice and interslice features, used in 3D ultrasound image segmentation. As there are quite a few such systems in medical ultrasound, we also review other medical imaging modalities.**

***Keywords*—convolutional neural networks, 3D Ultrasound, segmentation, artificial intelligence**

I. Introduction

Since it's creation in the 1950s, medical ultrasound has quickly become one of the most used diagnostic modality in medicine. While some regard medical ultrasound as 'a stethoscope of the 21st century' [1], it has also found many applications outside the field of cardiology. These applications include, for example, the fields of gynecology, anesthesiology, emergency medicine, neonatology, or pulmonology. Among the most significant advantages of ultrasound compared to other modalities are the ability to scan the patient in real-time, it's low price and the fact it doesn't utilize any form of ionizing radiation.

Ultrasound can capture both 2D, 3D (volumetric) images, 3D (2D + time) clips, and 4D (3D + time) clips. While 2D is the most common scanning mode of ultrasound, 3D is becoming increasingly important over time. The usages of 3D include fetal diagnosis, real-time 3D echocardiography, surgical guidance, musculoskeletal tissue examination, or diagnosis of carotid atherosclerosis via evaluation of arterial wall motion [2].

Segmentation of ultrasound images is necessary for further evaluation and analysis of the anatomy. Once anatomy is segmented, we can calculate the different qualitative and quantitative measurements necessary for clinical practice. The area of segmentation in ultrasound is also impacted by the deep learning boom. In the last years, there were many systems [3] [4] [5] designed for the segmentation of volumetric ultrasound images, mostly utilizing 3D convolutional neural networks (CNN) with different architectures. However, there are several notable downsides of 3D CNNs, including their long training time, lack of pre-trained models, and VRAM memory requirements. We would like to tackle this problem via the utilization of 2D CNN for intra-slice feature extraction from 3D image slices and recurrent neural networks (RNN) for inter-slice feature extraction. We believe that this emerging approach has significant potential and isn't well explored, especially in ultrasound.

II. Review of the current state

In this section, we talk about different systems designed for the segmentation of volumetric ultrasound images. The problem of volumetric ultrasound image segmentation is currently solved using several different approaches. Those approaches are mentioned in subsection II-C. In the rest of this section, we focus on the combination of CNN and RNN in medical ultrasound and other modalities for anatomy segmentation. As U-Net is the most common CNN in the area of medical image segmentation and most of the systems are using some modification of LSTM, we also provide a brief overview of these networks.

A. U-Net

U-Net [6] is a fully convolutional neural network (FCN) proposed by Ronnenberg, Fischer, and Brox for biomedical image segmentation in 2015. This network features contracting and expanding path on different levels, effectively creating U shaped architecture. Both contracting and expanding path consist of 4 blocks. Opposite blocks are connected in a fashion that feature map from contraction block is cropped and passed to a corresponding expansion block. The contraction blocks are build from 2 convolutional layers, followed by activation and max-pooling that effectively downsamples an image. Each of these blocks features upsampling procedure, "up-convolution", concatenation with feature map from opposite block in the contracting path, and 2 convolutions followed by rectified linear unit activation. At the top level of expanding path, there is one final 1x1 convolution layer used to map feature vector to desired classes. This architecture is visible in Figure 1. Inspired by this approach, Milletari, Navab and Ahmadi created V-Net [7] for the segmentation of 3D biomedical images.

B. LSTM

Long short-term memory (LSTM) [8] is an RNN introduced by Hochreiter and Schmidhuber in 1997. They aimed to tackle the problem of lacking long term memory and related problems of vanishing/exploding gradient of RNNs. The authors introduced the input gate unit and the output gate unit. Gates are designed to protect current memory from irrelevant inputs

in case of an input gate and other units in case of an output gate. Later, forget gate was added to allow LSTM to forget outdated information, and it was even further extended with the addition of peephole connections [9]. Architecture is visible on Figure 2.

During forward pass, we first calculate cell input. Then, the input squashing function is applied. The result of squashing is multiplied by the output of the input gate. This result is input to all cells of the current memory block, where it is summed with the previous state multiplied by activation of forget gate. The cell output is calculated as the multiplication of cell state and activation of the output gate. With the inclusion of peephole connections, activations of the gates are also dependant on the current state of cells.

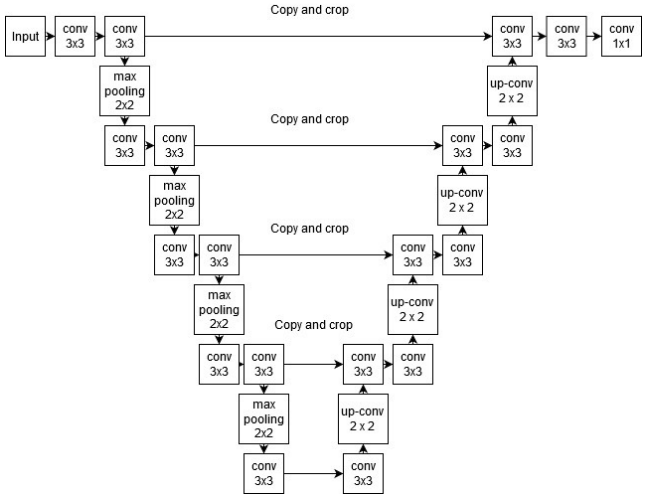

Fig. 1. Architecture of U-Net [6]

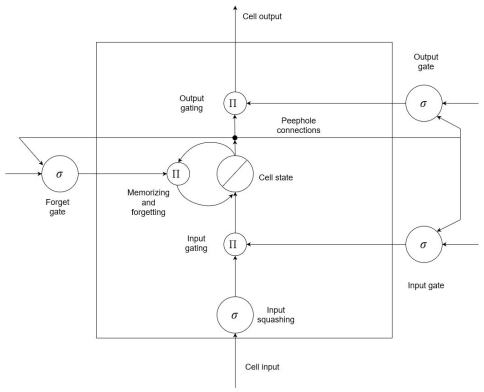

Fig. 2. Architecture of LSTM as described by [9]

C. Methods commonly used in ultrasound

There are several reviews of segmentation techniques in ultrasound based on used mode [10], or clinical application [11] [12] [13] [14]. While providing information about the used method is important, the comprehensive review of all the different approaches is beyond the scope of this paper.

We have therefore selected one high-quality review [10] and followed the list of approaches mentioned in the review:

1) Active contours - based on parametric or geometric deformable models
2) Shape priors - based on the fact that the shape of the anatomical structure is well known
3) Superpixel or patch-based and classification - based on dividing the structure into superpixels/patches labeled as the object or background
4) Texture and classification - based on finding the feature of underlying texture and usage of classifier
5) Pixel intensity and/or local statistics based - based on the fact that an image has different objects with different intensity distributions. This approach includes methods based on thresholding
6) Edge tracking - utilizes edge detectors, mostly used to get a more fine-grained solution in the second step
7) Optimization techniques - used after coarse segmentation methods to provide more fine-grained solutions
8) Transform-based - uses mathematical transformations (Hough transform) or modeling techniques (Markov random field)
9) Data-mining
10) Heuristics - gradually searches the image to find desired tissue
11) Neural networks and deep learning - include the usage of both classical feedforward neural networks, CNNs and RNNs

D. Ultrasound studies

Yang et al. [15] proposed Boundary Completion RNN (BCRNN) for automatic prostate segmentation in ultrasound images. The BCRNN is stacked into the cascade and consists of Bidirectional Long-Short Term Memories (BLSTM). At each level, BCRNNN serializes the static ultrasound image from several different perspectives and then conducts shape predictions for each of the perspectives. In the end, the predictions are merged via a multi-view fusion strategy. To refine the shape, a result of the last BCRNN concatenated with the test image is the input to the next BCRNN. They achieved the best performance with 2 BCRNN levels (0 and 1), competitive with at the time state-of-the-art results. The same team also used a similar approach for boundary delineation in ultrasound images of the fetal head and abdomen [16].

Yang et al. [17] worked towards the automatic segmentation of fetus in volumetric ultrasound. Their neural approach consisted of U-Net and BLSTMs combination. Firstly, the volumes were input to the 3D U-Net. Then, the probability volumes generated by U-Net concatenated with raw Ultrasound volumes were used as an input to BLSTMs. In this case, BLSTMs are extracting local contextual knowledge for better refinement of local boundaries. Their system is able to retrieve volumes of fetus, background, gestational sac, and placenta. They also introduced deep hierarchical supervision to tackle problems with vanishing gradient while training the system.

Anas, Mousavi, and Abolmaesumi [18] proposed an approach for real-time prostate segmentation in a freehand ultrasound-guided biopsy. While this is not directly dealing with a volumetric image, but sequence comparable to video, it brings some interesting ideas. Their approach was based on modified U-Net architecture, where authors introduced

residual convolutional gated recurrent unit blocks in-between the expanding and contracting branch in the last two levels of U-Net. The input to the network was the sequence of the last three images. However, they also experimented with another branch incorporating t-4 and t-8 images (image t is current).

E. Other modalities

Chen et al. [19] observed the fact that 'when human experts label the ground truth for biomedical images, they tend first to zoom out the image to figure out where are the target objects and then zoom in to label the accurate boundaries of those targets'. Inspired by this idea, they created a model called k-UNet that is simulating such human behavior by operating on different scales. They start with the largest region with the lowest resolution and slowly descent down towards the smallest region with the highest resolution. They also argued about the problem of the computational cost of 3D convolution and issues that arise when we try to substitute it by 2D convolution. To tackle this problem, they proposed the framework combining FCN for the extraction of intra-slice information and RNN for the extraction of inter-slice information from volumetric images. As an RNN for this framework, bi-directional convolutional LSTM (BCLSTM) was proposed. This BCLSTM consists of two layers of convolutional LSTMs (CLSTM) working in opposite directions. They claimed to achieve state-of-the-art performance on the 3D fungus dataset at the time.

Novikov et al. [20] used so-called Sensor3D network for segmentation of liver and vertebrae from volumetric CT images. This Sensor3D network consists of U-Net like architecture with BCLSTM integrated in-between the bottom-most contraction and expansion blocks and another one just before the final 1x1 convolution. The contraction and expansion blocks are wrapped in time-distributed wrapper, and the sequence's slices are therefore processed separately. The CLSTMs are used to capture the spatio-temporal features. With this approach, they looked to tackle the problem of other 3D segmentation algorithms - the necessity of whole 3D volume being present at the time and the computation costs. They claimed their solution to be among the best on the CSI 2014 and 3Dircadb datasets.

Jia, Yuan, and Peng [21] used a light-weight encoder-decoder network for automatic segmentation of brain tumors from multi-modal MRI volumes. Instead of application of recurrent network and 2D CNN, they opted for 3D CNN encoder-decoder architecture with so-called hierarchical separable convolution block that was incorporating view-wise separable convolution and group-wise separable convolution. This way, they were able to divide performance-intensive 3D convolutions into two complementary 2D convolutions. As their model was asymmetrical in view, they incorporated ensemble of such classifiers taking axial view, sagittal and coronal view as input. They managed to outperform all other methods on the BraTS 2017 dataset that consists of multi-modal images of volumes with a brain tumor. This work was included in this review despite not featuring the combination of CNN and RNN, as it tried to tackle the problem of computational costs of 3D CNNs.

Lu and Banerjee [22] from Siemens Healthcare GmbH try to patent the U-Net + CLSTM approach for segmentation in cardiac MRI. The LSTM was situated at the bottom level, in-between the contraction and expansion part of U-Net.

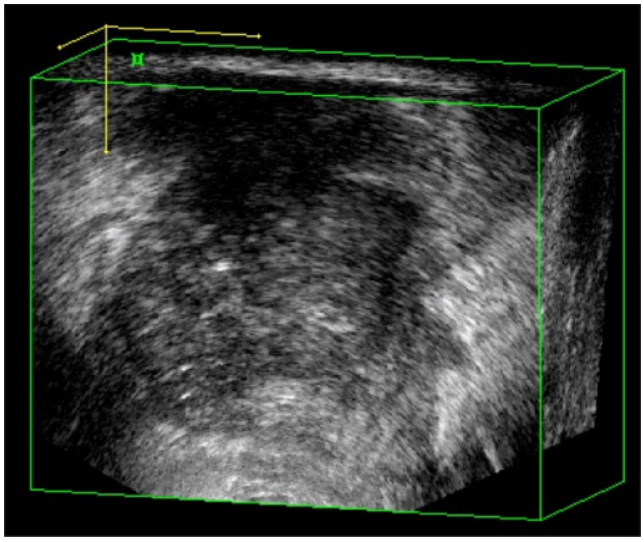

Fig. 3. Example of 3D ultrasound image from openI database [23]

Zhu et al. [24] utilized convolutional LSTMs for prostate cancer segmentation from volumetric MRI. Their proposed bidirectional convolutional LSTM (BCLSTM) layer is composed of two sets of CLSTMs. One set is streaming from the previous slice through the current to the next; the other is working in the opposite direction. The BCLSTM layer should extract both intraslice and interslice features out of this sequence. Authors formed U-Net like architecture, with both contraction and expansion path, from the said BCLSTM. Their input sequence to this network consists of 3 slices - previous, current, and next slice. With their solution called UR-Net, they claimed to outperform a fully connected neural network, both U-Net, V-Net, and also Modified FCN with BCLSTM layers.

Poudel, Lamata and Montana proposed recurrent FCN (RFCN) [25]. They used U-Net architecture and utilized GRU on the bottom-most connection between the contraction and expansion paths they name global feature component. Their methods were evaluated on MICCAI 2009 dataset and PRETERM dataset and achieved competitive results.

Bates et. al [26] used U-Net style architecture with BCLSTM. Every CLSTM layer used 20 units, and every stack (BCLSTM) was followed by a 1 x 1 convolution to reduce dimensionality. They have experimented with setup, where slices were firstly passed through U-Net and then through stacked CLSTMs. They have utilized two possible approaches - deep, where CLSTMs were shaped stacked in U-shaped configuration. In this configuration, the first BCLSTM is followed by the pooling layer, second by upsampling layer and third by 1 x 1 convolution and sigmoid. In Shallow configuration, only single BCLSM followed by 1 x 1 convolution was used. They were able to outperform 2D and 3D U-Net with both proposed architectures.

III. Challenges

As outlined in a review, the proposed approach is starting to gain traction in the area of medical image segmentation. It seems that utilizing RNN within CNN allows the network to extract improved inter slice context information compared to only using 3D CNN. While there is an ongoing development of such hybrid segmentation systems for CT and MR modalities, there seems to be little to no development of such systems in

the area of ultrasound. We would like to start with the design of such systems for ultrasound.

During the review, another question arose - Is it better to use 3D CNNs to create the segmented volumes and apply RNNs to refine the local boundaries such as [17] or should we try to emulate the approach of [19], where 2D CNN is utilized, and BCLSTMs are used to distill the 3D context from a sequence of 2D images? We think that detailed, experiment-based, comparison of those two ideas with the classic 3D CNN segmentation approach could be helpful for a selection of the most promising method. For experiments, we would like to obtain a 3D ultrasound dataset with the help of Siemens Healthineers. Datasets from other modalities could also be used such as one of the versions of BRATS [27] for MRI, LiTS [28] for CT or the Medical Segmentation Decathlon dataset [29] for both.

Afterwards, we would like to dive deeper into the area and try to improve the method. Improvements may include, but are not limited to, improving the U-Net's performance via the usage of nested, dense skip pathways [30] or multiscale dense connected schema [31], reducing the number of U-Net's parameters via the usage of inception modules [32], using different RNNs, or incorporating such a hybrid network into GAN. As seen in the review, only one of the systems [33] has utilized the combination of CNN and RNN in the GAN scheme. GANs are nowadays gaining traction in the area of deep learning in medical imaging. While they are mostly used for medical image reconstruction or synthesis, they can achieve state-of-the-art performance in segmentation [34].

These improvements should lead to even more accurate segmentation results and faster, less memory consuming models. While the first is important for accurate assessment and diagnosis of patients, performance is also an important question, as most of the medical devices aren't equipped to become computational intensive platforms. Therefore we also need to watch the development in the areas of CNNs and RNNs carefully as they are evolving rapidly and coming with new approaches almost daily.

Acknowledgment

This publication was supported by the grant VEGA - 1/0663/17 - Intelligent Cyber-Physical Systems in Heterogeneous Environment Supported by IoE and Cloud Services.

The publication is a result of cooperation between The Technical University of Kosice and Siemens Healthineers.

Image seen in Figure 3 was retrieved from openI databse. Licensed under CC BYNCND 3.0

References

[1] A. Genc, M. Ryk, M. Suwała, T. Żurakowska, and W. Kosiak, "Ultrasound imaging in the general practitioner's office–a literature review," *Journal of ultrasonography*, vol. 16, no. 64, p. 78, 2016.

[2] Q. Huang and Z. Zeng, "A review on real-time 3d ultrasound imaging technology," *BioMed research international*, vol. 2017, 2017.

[3] H. Williams, L. Cattani, W. Li, M. Tabassian, T. Vercauteren, J. Deprest, and J. Dhooge, "3d convolutional neural network for segmentation of the urethra in volumetric ultrasound of the pelvic floor," in *2019 IEEE International Ultrasonics Symposium (IUS)*. IEEE, 2019, pp. 1473–1476.

[4] J. J. Cerrolaza, M. Sinclair, Y. Li, A. Gomez, E. Ferrante, J. Matthew, C. Gupta, C. L. Knight, and D. Rueckert, "Deep learning with ultrasound physics for fetal skull segmentation," in *2018 IEEE 15th International Symposium on Biomedical Imaging (ISBI 2018)*. IEEE, 2018, pp. 564–567.

[5] H. Yang, C. Shan, A. F. Kolen, and P. H. de With, "Efficient catheter segmentation in 3d cardiac ultrasound using slice-based fcn with deep supervision and f-score loss," in *2019 IEEE International Conference on Image Processing (ICIP)*. IEEE, 2019, pp. 260–264.

[6] O. Ronneberger, P. Fischer, and T. Brox, "U-net: Convolutional networks for biomedical image segmentation," *CoRR*, vol. abs/1505.04597, 2015. [Online]. Available: http://arxiv.org/abs/1505.04597

[7] F. Milletari, N. Navab, and S. Ahmadi, "V-net: Fully convolutional neural networks for volumetric medical image segmentation," *CoRR*, vol. abs/1606.04797, 2016. [Online]. Available: http://arxiv.org/abs/1606.04797

[8] S. Hochreiter and J. Schmidhuber, "Long short-term memory," *Neural computation*, vol. 9, no. 8, pp. 1735–1780, 1997.

[9] F. A. Gers, N. N. Schraudolph, and J. Schmidhuber, "Learning precise timing with lstm recurrent networks," *Journal of machine learning research*, vol. 3, no. Aug, pp. 115–143, 2002.

[10] K. M. Meiburger, U. R. Acharya, and F. Molinari, "Automated localization and segmentation techniques for b-mode ultrasound images: A review," *Computers in biology and medicine*, vol. 92, pp. 210–235, 2018.

[11] J. A. Noble and D. Boukerroui, "Ultrasound image segmentation: a survey," *IEEE Transactions on Medical Imaging*, vol. 25, no. 8, pp. 987–1010, Aug 2006.

[12] C. P. Loizou, "A review of ultrasound common carotid artery image and video segmentation techniques," *Medical & biological engineering & computing*, vol. 52, no. 12, pp. 1073–1093, 2014.

[13] M. Deeparani, M. Kalamani, and M. Krishnamoorthi, "A survey on ultrasound image segmentation algorithm for detection of female pelvic masses," *International Journal of Recent Technology and Engineering*, vol. 7, no. 4.

[14] Q. Huang, Y. Luo, and Q. Zhang, "Breast ultrasound image segmentation: a survey," *International journal of computer assisted radiology and surgery*, vol. 12, no. 3, pp. 493–507, 2017.

[15] X. Yang, L. Yu, L. Wu, Y. Wang, D. Ni, J. Qin, and P. Heng, "Fine-grained recurrent neural networks for automatic prostate segmentation in ultrasound images," *CoRR*, vol. abs/1612.01655, 2016. [Online]. Available: http://arxiv.org/abs/1612.01655

[16] X. Yang, L. Yu, W. Lingyun, D. Ni, and P.-A. Heng, "Shape completion with recurrent memory," *ECCV 2016 workshop on Biological and Artificial Vision*, 10 2016.

[17] X. Yang, L. Yu, S. Li, X. Wang, N. Wang, J. Qin, D. Ni, and P.-A. Heng, "Towards automatic semantic segmentation in volumetric ultrasound," in *Medical Image Computing and Computer Assisted Intervention MICCAI 2017*, M. Descoteaux, L. Maier-Hein, A. Franz, P. Jannin, D. L. Collins, and S. Duchesne, Eds. Cham: Springer International Publishing, 2017, pp. 711–719.

[18] E. M. A. Anas, P. Mousavi, and P. Abolmaesumi, "A deep learning approach for real time prostate segmentation in freehand ultrasound guided biopsy," *Medical image analysis*, vol. 48, pp. 107–116, 2018.

[19] J. Chen, L. Yang, Y. Zhang, M. Alber, and D. Z. Chen, "Combining fully convolutional and recurrent neural networks for 3d biomedical image segmentation," in *Advances in neural information processing systems*, 2016, pp. 3036–3044.

[20] A. A. Novikov, D. Major, M. Wimmer, D. Lenis, and K. Bühler, "Deep sequential segmentation of organs in volumetric medical scans," *CoRR*, vol. abs/1807.02437, 2018. [Online]. Available: http://arxiv.org/abs/1807.02437

[21] Z. Jia, Z. Yuan, and J. Peng, "Multimodal brain tumor segmentation using encoder-decoder with hierarchical separable convolution," in *Multimodal Brain Image Analysis and Mathematical Foundations of Computational Anatomy*. Springer, 2019, pp. 130–138.

[22] X. Lu and M. Banerjee, "Machine learning-based segmentation for cardiac medical imaging," Jul. 25 2019, uS Patent App. 15/879,486.

[23] J. F. Tyloch and A. P. Wieczorek, "The standards of an ultrasound examination of the prostate gland. part 2," *Journal of ultrasonography*, vol. 17, no. 68, p. 43, 2017.

[24] Q. Zhu, B. Du, B. Turkbey, P. Choyke, and P. Yan, "Exploiting interslice correlation for mri prostate image segmentation, from recursive neural networks aspect," *Complexity*, vol. 2018, 2018.

[25] R. P. Poudel, P. Lamata, and G. Montana, "Recurrent fully convolutional neural networks for multi-slice mri cardiac segmentation," in *Reconstruction, segmentation, and analysis of medical images*. Springer, 2016, pp. 83–94.

[26] R. Bates, B. Irving, B. Markelc, J. Kaeppler, R. J. Muschel, V. Grau, and J. A. Schnabel, "Extracting 3d vascular structures from microscopy images using convolutional recurrent networks," *CoRR*, vol. abs/1705.09597, 2017. [Online]. Available: http://arxiv.org/abs/1705.09597

[27] B. H. Menze, A. Jakab, S. Bauer, J. Kalpathy-Cramer, K. Farahani, J. Kirby, Y. Burren, N. Porz, J. Slotboom, R. Wiest *et al.*, "The multimodal brain tumor image segmentation benchmark (brats)," *IEEE transactions on medical imaging*, vol. 34, no. 10, pp. 1993–2024, 2014.

[28] P. Bilic, P. F. Christ, E. Vorontsov, G. Chlebus, H. Chen, Q. Dou, C. Fu, X. Han, P. Heng, J. Hesser, S. Kadoury, T. K. Konopczynski, M. Le, C. Li, X. Li, J. Lipková, J. S. Lowengrub, H. Meine, J. H. Moltz, C. Pal, M. Piraud, X. Qi, J. Qi, M. Rempfler, K. Roth, A. Schenk, A. Sekuboyina, P. Zhou, C. Hülsemeyer, M. Beetz, F. Ettlinger, F. Grün, G. Kaissis, F. Lohöfer, R. Braren, J. Holch, F. Hofmann, W. H. Sommer, V. Heinemann, C. Jacobs, G. E. H. Mamani, B. van Ginneken, G. Chartrand, A. Tang, M. Drozdzal, A. Ben-Cohen, E. Klang, M. M. Amitai, E. Konen, H. Greenspan, J. Moreau, A. Hostettler, L. Soler, R. Vivanti, A. Szeskin, N. Lev-Cohain, J. Sosna, L. Joskowicz, and B. H. Menze, "The liver tumor segmentation benchmark (lits)," *CoRR*, vol. abs/1901.04056, 2019. [Online]. Available: http://arxiv.org/abs/1901.04056

[29] A. L. Simpson, M. Antonelli, S. Bakas, M. Bilello, K. Farahani, B. van Ginneken, A. Kopp-Schneider, B. A. Landman, G. J. S. Litjens, B. H. Menze, O. Ronneberger, R. M. Summers, P. Bilic, P. F. Christ, R. K. G. Do, M. Gollub, J. Golia-Pernicka, S. Heckers, W. R. Jarnagin, M. McHugo, S. Napel, E. Vorontsov, L. Maier-Hein, and M. J. Cardoso, "A large annotated medical image dataset for the development and evaluation of segmentation algorithms," *CoRR*, vol. abs/1902.09063, 2019. [Online]. Available: http://arxiv.org/abs/1902.09063

[30] Z. Zhou, M. M. R. Siddiquee, N. Tajbakhsh, and J. Liang, "Unet++: Redesigning skip connections to exploit multiscale features in image segmentation," *IEEE Transactions on Medical Imaging*, 2019.

[31] J. Zhang, Y. Jin, J. Xu, X. Xu, and Y. Zhang, "Mdu-net: Multi-scale densely connected u-net for biomedical image segmentation," *arXiv preprint arXiv:1812.00352*, 2018.

[32] H. Zhao and N. Sun, "Improved u-net model for nerve segmentation," in *International Conference on Image and Graphics*. Springer, 2017, pp. 496–504.

[33] M. Rezaei, H. Yang, and C. Meinel, "Recurrent generative adversarial network for learning imbalanced medical image semantic segmentation," *Multimedia Tools and Applications*, pp. 1–20, 2019.

[34] X. Yi, E. Walia, and P. Babyn, "Generative adversarial network in medical imaging: A review," *Medical image analysis*, p. 101552, 2019.

Deep neural networks for speech-to-text systems

[1]*Slavomír GEREG (1st year)*
Supervisor: [2]Jozef JUHÁR

[1,2]Dept. of Electronics and Multimedia Communications, FEI TU of Košice, Slovak Republic

[1]slavomir.gereg@tuke.sk, [2]jozef.juhar@tuke.sk

***Abstract*—The topic of this article is automatic speech recognition. The main part of the article is a description of the principle of automatic recognition and some of the best-known approaches to this problem. Furthermore, there are briefly described modern methods used in automatic speech recognition. Also, a brief description of the Kaldi system used for speech recognition in my previous research is provided. In conclusion there are briefly outlined topics. I would like to deal with in my dissertation.**

***Keywords*—automatic speech recognition, deep neural networks, Kaldi toolkit**

I. Introduction

Automatic speech recognition is the process of converting a speech signal into the corresponding text form. Automatic speech recognition algorithms can be implemented on different devices, computers, or servers. Systems for automatic speech recognition have been under research for more than 60 years. Currently, there are many commercial products using automatic speech recognition. One of the most common uses of automatic speech recognition for the general user is the use of user interfaces and voice control. Historically, automatic speech recognition has been used in a variety of applications such as voice dialing, interactive voice dialogue, call routing, text dictation, voice control, gaming industry, official document transcription, voice search, and robotics. As computer technology grows and improves, even more sophisticated automatic speech recognition applications are becoming a reality. Examples include the extensive use of voice assistants in mobile phones (Google assistant, Siri, Cortana, ...), voice control in home gaming systems (Kinect), voice navigation and many other advanced applications that use automatic speech recognition [1], [2], [3], [4], [5], [6].

II. Automatic Speech Recognition

The principle of automatic speech recognition is based on the human speech recognition model shown in Figure 1.

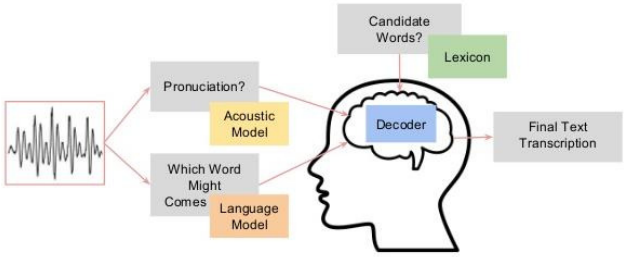

Figure 1 Human speech recognition scheme

In Figure 2 there is shown how computer speech recognition works.

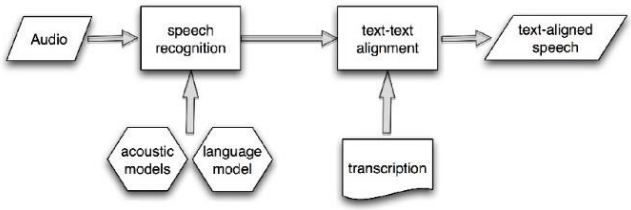

Figure 2 Computer speech recognition scheme

In the first step, the human speech is converted into an analog signal by a microphone. Then it is digitized in the analog-to-digital converter of the sound card. This is done by recording the sound intensity values at a certain sampling frequency moments. Thus, obtained digital data is then processed. Because it is a system with high computational demands, we cannot work with all the samples. To solve the computational complexity, we need to extract only important data from the samples. This transformed digitized signal in the form of vectors is called observation. Usually, FFT (Fast Fourier Transformation), MFCC (Mel Frequency Cepstral Coefficient), cepstrum (produced by applying an inverse Fourier transformation to the logarithm of the estimated signal spectrum) and their modifications are used to extract the observations. Based on the calculated observations, the system looks in the dictionary for the word that was most likely captured by the microphone. Thus, recognition consists of finding the closest similarity of the scanned word to the words in the dictionary.

Consequently, the wrong words may be removed in other layers according to the context, or the words may be composed into sentences [7].

In terms of usage, speech recognition methods using statistical decision making, the so-called statistical methods, are currently the most widely used. In this approach, speech variations are modeled statistically using training methods. The principle of speech recognition is currently based on statistical acoustics and language models. Language and acoustic models in automatic speech recognition systems for an unlimited domain need a large amount of acoustic and language data for parameter estimation. The processing of large amounts of training data is a key element in the development of an efficient automatic speech recognition system. These methods can be divided into three groups according to the technology they use:

- HMM (Hidden Markov Model)
- ANN (Artificial Neural Network)
- Hybrid methods - using both HMM and ANN

Individual words can be modeled as a whole word, which means we get one result model for each word in the dictionary. The second option which is being used is modeling using smaller acoustic units such as phoneme. Such a word model is obtained after the phoneme models are concatenated. We can also associate individual word models with a language model that provides additional information about the consecutive word occurrence statistics [8], [9], [10].

The language model allows for classifications to suppress those sequences of words whose frequency in the training text set was minimal.

III. Methods of automatic speech recognition using neural networks

When using neural networks in automatic speech recognition systems, their ability to classify elements of certain properties into classes is mainly used. The neural network is made up of elementary elements called neurons. These neurons are arranged in layers and interconnected in manner that each higher layer neuron is associated with each lower layer neuron. In to each neuron enters input signals, the inputs have different weights. If the sum of the signals multiplied by the weights exceeds a certain threshold, the neuron sends an output signal of 1, otherwise it sends 0 [11].

To recognize speech with neural network (Figure 3):

1. We will teach a neural network to assign a sound to a given word in a dictionary according to a set of observations
2. The calculated observations are given to the neuronal network inputs
3. The network will have several hidden layers and the network will have as many neurons as the phoneme in the output layer
4. The network will be trained so that the output is an active neuron corresponding to the phoneme
5. For a neural network to determine which dictionary word is associated with input observations, we must train the network. Training is done by bringing observations calculated from a known word to the neural network input and letting the network calculate the output. Since observations belong to a familiar word, we know which output neuron should be active. If this is not the case, we adjust the weights of the neurons throughout the network to approach the desired result [11].

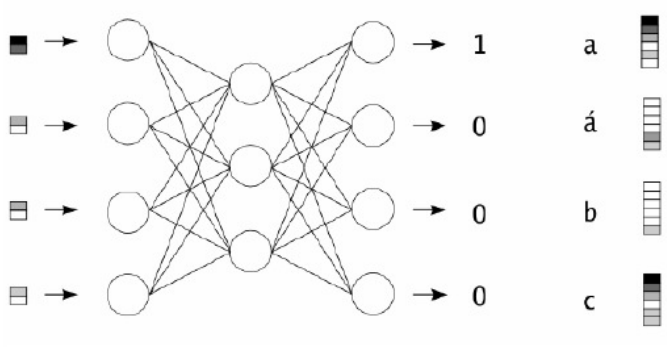

Figure 3 Speech recognition using ANN [11]

IV. DNN (Deep Neural Network)

Popular approach in modern speech recognition system is also usage-based on DNN. Deep neural networks are composed of neurons that are interconnected. The neurons are arranged in layers. The first layer is the input layer that corresponds to the data properties. The last layer is the output layer, which provides probabilities of classes or markings (classification task). The output of the y-th neuron is calculated as the non-linear weighted sum of its input. The input xi of the neuron may be either an input if the neuron belongs to the first layer or the output of another neuron [12].

Deep neural network is defined by three types of parameters:

1. The pattern of interconnection between different layers of neurons
2. Training process to update weights wi from the link
3. Activation function f that converts a weighted input of a neuron into its activation output (Figure 4)

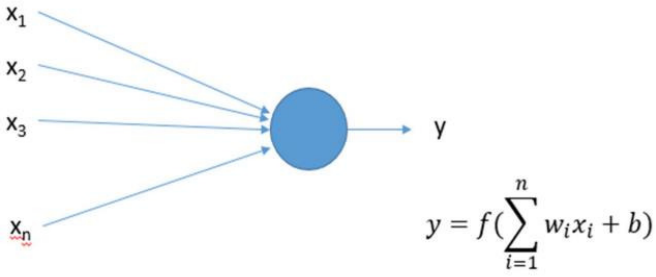

Figure 4 Example of one neuron and its connection [13]

The frequently used activation function is a non-linear weighted sum. By using only linear functions, neural networks can only separate linearly separable classes. Non-linear activation functions are therefore essential for real data [13].

The Kaldi system that I used in my work can be classified into a group of hybrid methods.

V. End-to-end speech recognition systems

To put it simply, end-to-end speech recognition systems consist of three main components:

1. Flag extraction that treats raw audio signals (e. g. from a .wav file) as inputs and generates a sequence of feature vectors with one feature vector

for a given audio input frame. Examples of symptom extraction phase outputs include slices of the raw waveform, spectrograms, as well as the popular Mel Frequency Cepstral Coefficients (MFCC).

2. An acoustic model that processes feature vector sequences as inputs and generates probabilities of character or sound sequences conditioned by feature vector input.
3. A decoder that processes two inputs - outputs of the acoustic model and the language model - and looks for the most likely transcript given by the sequences generated by the acoustic model, which is limited by the language rules encoded in the language model.

The block diagram of the end-to-end speech recognition system can be seen in Figure 5.

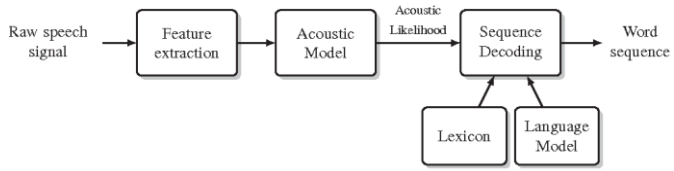

Figure 5 End-to-end speech recognition system block diagram

Systems for automatic speech recognition based on deep neural networks as well as end-to-end systems can now be classified as one of the most widely used and most promising systems for automatic speech recognition [14].

VI. Speech Recognition Toolkit Kaldi

Kaldi is an open-source toolkit for automatic speech recognition. It is written in C ++ and licensed under the Apache License v2.0. Kaldi's goal is modern, flexible and easily extensible code that is easy to understand and modify. Kaldi is available for download at SourceForge (Available at: http://kaldi.sf.net/). Kaldi can be compiled on commonly used Linux-based systems as well as on Microsoft Windows-based systems [15], [16], [17].

The Kaldi toolkit allows to use many specific requirements for automatic speech recognition systems, such as structure based on Finite-State Transducer (FST), extensive linear algebra support and non-limiting license [15], [18].

In Figure 6 we can see the basic block diagram of the Kaldi tool. It can be seen from the figure that the toolkit is dependent on two External Libraries, which are also freely available. The first is OpenFst for the finite-state machine and the other is the library of numerical algebra.

Library modules can be grouped into two different groups, each of these groups depends only on one of the external libraries. These two groups are bridged by the DecodableInterface module [15].

The modules shown in Figure 6 below are always dependent on one or more modules above them.

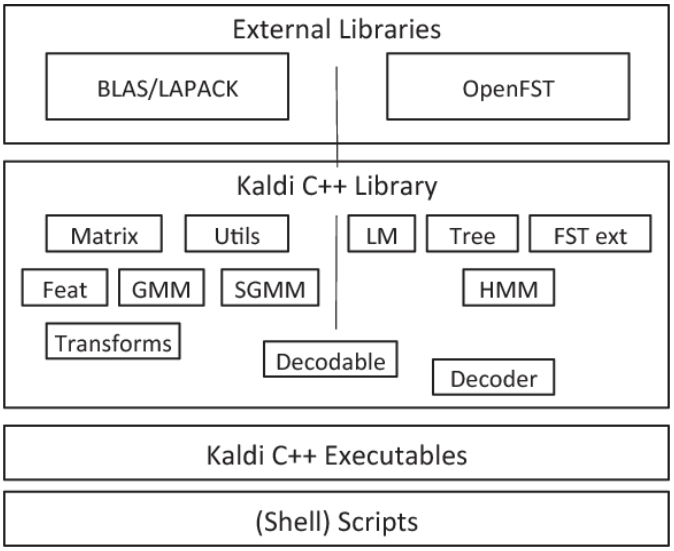

Figure 6 Basic block diagram for Kaldi automatic speech recognition [15]

VII. My Previous Research

As a part of my previous work, I have decided to create a test database for automatic speech recognition system. I have created this database from the acoustic data of the meeting audio recordings. The creation process of this test database consisted largely of manual annotation of acoustic data, and its modification into a form suitable for testing by the automatic speech recognition system Kaldi. I have also decided to experimentally investigate the impact of the training database on the success of automatic data recognition by the Kaldi system. I have chosen to compare the results of automatic speech recognition when training the Kaldi system with the LRMT KEMT TUKE laboratory database and when training with this database extended by the high volume of data (247 hours 31 minutes and 57 seconds) automatically recognized by SARRA (speech transcription system created in LRMT KEMT TUKE)[1]. I have based my hypothesis on the assumption that a higher volume of automatically recognized training data of the same type (data like test data - meeting audio, the same acoustic channel, ...) should result in a lower system error rate in automatic recognition speech. The block diagram of proposed system can be seen in Figure 7. The block marked in red is a set of data prepared and added by me to improve the system's success.

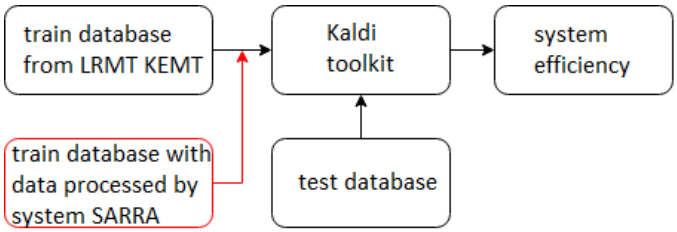

Figure 7 Block diagram of my system with added training data

VIII. Current State of Research

In my current work, I have started with a more thorough examination of the functionality of the Kaldi speech recognition tool. In addition to basic control of the Kaldi tool

[1] https://marhula.fei.tuke.sk/sarra/login

and running system testing, I have begun to get acquainted with the process of preparing data for processing by the Kaldi system and also with the process of training the acoustic models needed for speech recognition Kaldi system. In my previous work, I have managed to prove that adding a higher volume of automatically rewritten data to the Kaldi training process will help improve speech recognition success. However, I have found out during the experiment that from a certain point this improvement is minimal and ineffective in terms of increasing the calculation and time requirements of the system.

IX. Further research direction

In my next work, I would like to look more closely on the training process of the Kaldi Speech Recognition System. I would also like to examine more closely the impact of the volume of automatically rewritten data in the process of system training on speech recognition Kaldi. In this step I want to focus on the success of speech recognition but also the computational and time-consuming system training.

I would also like to explore the possibility of improving the robustness of the Kaldi speech recognition system by designing the correct training data database. A system trained in this way should not have any problem with input data with different properties. At present, many researches are concerned with systems that would also be able to recognize child speech by extracting the symptoms of child speech and then modifying the training database with these symptoms.

Acknowledgment

The research in this paper was supported by the Ministry of Education, Science, Research and Sport of the Slovak Republic under the project KEGA 009TUKE-4/2019 and by the Slovak Research and Development Agency under the projects APVV-15-0731 and APVV-15-0517.

References

[1] Deng, L., O'Shaughnessy, D., 2003. Speech Processing-A Dynamic and Optimization Oriented Approach. Marcel Dekker Inc., New York.

[2] Huang, X., Acero, A., Hon, H.W., 2001b. Spoken Language Processing. Prentice-Hall, Upper Saddle River, NJ.

[3] Baker. J.. Deng, L., Glass, J., Khudanpur, S., Lee, C.H, Morgan, N., et al., 2009a. Research developments and directions in speech recognition and understanding, Part I. IEEE Signal Process. Mag. 26 (3), 75-80.

[4] Davis, K.H., Biddulph, R, Balashek, S., 1952. Automatic recognition of spoken digits. J. Acoust. Soc. Am. 24 (6), 627-642.

[5] He, X., Deng, L., 2013. Speech-centric information processing: An optimization-oriented approach. Proc. IEEE 101 (5), 1116-1135.

[6] Li, J. & Deng, L. & Haeb-Umbach, Reinhold & Gong, Y.. (2015). Robust automatic speech recognition: A bridge to practical applications, ISBN 978-0-12-802398-3.

[7] Juhár, J. et al.: Rečové technológie v telekomunikačných a informačných systémoch. Košice: Equilibria, s.r.o., 2011. ISBN 978-80-89284-75-7.

[8] Juhár, J. et.al.: Development of Slovak GALAXY/VoiceXML Based Spoken Language Dialogue System to Retrieve Information from the Internet. In: Proceedings of 9th International Conference on Spoken Language Processing / Interspeech 2006, Pittsburgh, PA, USA 2006.

[9] E. Trentin and M. Gori, "A survey of hybrid ANN/HMM models for automatic speech recognition," Neurocomputing, vol. 37, Apr. 2001. DOI: 10.1016/S0925-2312(00)00308-8.

[10] Li L, Zhao Y, Jiang D, Zhang Y, Wang F, Gonzalez I, et al. Hybrid deep neural network–hidden Markov model (DNN-HMM) based speech emotion recognition. 2013 Humaine Association Conference on Affective Computing and Intelligent Interaction. 2013. pp. 312–317. https://doi.org/10.1109/ACII.2013. 58

[11] RYBANSKÝ, P.: Automatické rozpoznávanie informácie v zvukových dokumentoch, Žilina, 2006.

[12] Bundzel, M., Sincak, P.: Combining gradient and evolutionary approaches to the artificial neural networks training according to principles of Support Vector Machines. In: Proceedings of the IEEE International Joint Conference on Neural Network, Vancouver, Canada, July 16-21, 2006, DOI: 10.1109/IJCNN.2006.246976.

[13] Dominique Fohr, Odile Mella, Irina Illina. New Paradigm in Speech Recognition: Deep Neural Networks. IEEE International Conference on Information Systems and Economic Intelligence, Apr 2017, Marrakech, Morocco. 2017

[14] NDIRANGO, A., LEE, T. 2016. End-to-end speech recognition with Neon. [online]. [cit. 17.4.2019] Online: https://www.intel.ai/end-end-speech-recognition-neon/#gs.5ps57e

[15] Povey, D., Ghoshal A., et al.: The Kaldi Speech Recognition Toolkit. In: IEEE 2011 Workshop on Automatic Speech Recognition and Understanding, Hilton Waikoloa Village, Big Island, Hawaii, US, 2011. ISBN 978-1-4673-0366-8

[16] Peter Smit, Sami Virpioja, Mikko Kurimo. Improved Subword Modeling for WFST-Based Speech Recognition. In Annual Conference of the International Speech Communication Association (INTERSPEECH), Stockholm, pages 2551–2555, August 2017.

[17] Alyousefi, S. H.: Digital Automatic Speech Recognition using Kaldi. MSc. Thesis, Florida Institute of Technology, Melbourne, Florida, May 2018.

[18] Seppo Enarvi, Peter Smit, Sami Virpioja, Mikko Kurimo. Automatic Speech Recognition with Very Large Conversational Finnish and Estonian Vocabularies. IEEE/ACM Transactions on Audio, Speech, and Language Processing, volume 25, issue 11, pages 2085–2097, November 2017.

Design and Implementation of Distributed Control Systems and their Selected Applications

[1]*Milan TKÁČIK (1st year),*
Supervisor: [2]*Ján JADLOVSKÝ*

[1,2]Dept. of Cybernetics and Artificial Intelligence, FEEI TU of Košice, Slovak Republic

[1]milan.tkacik@tuke.sk, [2]jan.jadlovsky@tuke.sk

***Abstract*—The aim of this paper is to demonstrate how the same principles of distributed system operation could be shared between the applications in different areas. For the case study we selected two examples. The first describes a control system developed by our group for the Inner Tracking System of the ALICE experiment at CERN. The second case focuses on the application of the same principles of the distributed system operation in the field of mobile robotics.**

***Keywords*—Communication Interfaces, Detector Control System, Distributed Control System, Mobile Robotics**

I. Introduction

This paper deals with design and implementation of Distributed Control Systems (DiCS) in two different areas. Firstly, it describes basic concept and advantages of DiCS over Centralized Control Systems (CCS) [1]. The main focus of this paper is the overall upgrade of the ALICE experiment at CERN and brief description of newly developed hardware and software modules, including their integration within DiCS of the ALICE, that is called Detector Control System (DCS) [2]. Next it focuses on the implementation of several software modules for the DCS and their actual usage at ALICE, specifically for the Interlock system. Last but not least, the paper deals with DiCS implementation at the Center of Modern Control Techniques and Industrial Informatics (CMCT&II) at Department of Cybernetics and Artificial Intelligence (DCAI) with the focus on mobile robotics area, showing the similarity to the DCS at CERN.

II. Distributed Control System

The DiCS is computer based control system for complex processes, where individual controllers are distributed through the system with no central supervisory control node. Unlike CCS, individual controllers are positioned closer to the controlled processes, resulting in greater reliability and lower initial costs. At the same time, superior systems have the possibility to monitor and supervise individual subsystems, thanks to which they have a comprehensive overview of the state of controlled processes. Conceptually, the DiCS can be divided into several levels of control [1]:

Level of Sensors and Actuators: (Zero Level) includes various sensors and actuators. Individual sensors and actuators can be connected to a higher level by analog, digital or frequency inputs and outputs, or by various technological interfaces. This level also includes more complex models consisting of multiple sensors and actuators.

Technological Level of Control and Regulation: (First Level) ensures the control and regulation of individual parts of the lower level while ensuring communication with the second level of DiCS. Control and regulation at this level is ensured by PLCs, technological computers and single-chip microcomputers [3].

Level of SCADA/HMI: (Second Level) includes SCADA/HMI systems for supervisory control, data acquisition and archiving. It also involves various visualizations to present production process information to the operator. Connection with lower and higher levels are provided by network interfaces mostly using TCP/IP protocol with various extensions. This level also covers simulation models implemented mostly in MATLAB/Simulink environment [4].

Information Level of Control: (Third and Fourth Level) represents the level of Manufacturing Enterprise Systems (MES) for performing production management tasks such as production and inventory control, warehouse management, or operational planning of production. These systems are based on relational databases with client web applications. It also includes the level of Enterprise Resource Planning (ERP) and Manufacturing Resource Planning (MRP) systems. This level uses the same technological resources as the third level systems and provides mainly planning of production resources and processes

Management Level of Control: (Fifth Level) is implemented on the basis of multidimensional databases using OLAP (Online Analytical Processing) technology. This level provides the resources to support strategic planning of business direction.

III. Detector Control System of ALICE experiment

The European Organization for Nuclear Research (CERN) is the largest laboratory for basic and applied research in the field of particle physics in the world. It is located on the Swiss-French border and was founded in 1954 by the twelve founding states. The number of member states has gradually increased to 23 [5].

The CERN accelerator complex is based on several linear and circular accelerators, providing beams of particles, such as leptons (electron, positron) or hadrons (protons, atomic nuclei). The largest accelerator (the Large Hadron Collider, LHC) accelerates protons or heavy ions to ultrarelativistic energies [5]. The particle beams collide at the speed of

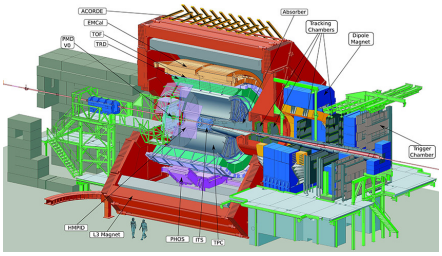

Fig. 1: The ALICE experiment and its subdetectors.

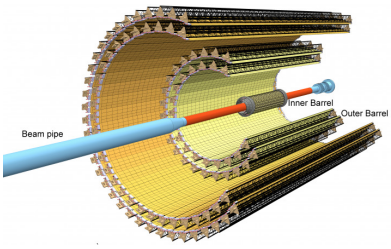

Fig. 2: Layered structure of the new ITS detector.

the light in four experimental areas, where the experiments ALICE, ATLAS, CMS and LHCb are installed. The LHC is the largest and most powerful circular accelerator in the world. It has circumference of 27 kilometers and allows the particles to accelerate to energy of 6.5 TeV with a total collision energy of 13 TeV [6].

The ALICE experiment consists of 18 detectors and is used to investigate quark-gluon plasma, which is produced by collisions of lead nuclei in LHC [6]. The properties of extremely hot plasma (200 000 times hotter than the centre of the stars) allow for a study of the processes in the early Universe, before the particles as we know them today were created. Looking into the collisions, the scientists get an deep insight into the formation of the matter and the nature of the forces that define its behavior. Main focus is on understanding of the main basic mysteries of the physics today: where does the mass come from and what is the Universe made off. The measurements suggest, that more than 70% of the Universe is made of a dark matter and dark energy that generates gravitational interactions but is not made of ordinary matter. The ALICE experiment and its subdetectors are shown in Fig. 1.

A. Upgrade of ALICE detectors for Run 3

At the end of 2018, Run 2 was finished, and thus the LHC accelerator, and all of its experiments are currently shut down for two years, with each experiment being able to upgrade their hardware and software resources [7]. After ten years of operation, the individual detectors of the ALICE experiment were removed from the underground cavern of the experiment for the purpose of maintenance and modernization.

After the upgrade, the LHC will provide by factor of 100 more collisions in ALICE compared to previous operations [8]. This will increase the data flow and ALICE will produce continuously 4TB/s of data. A new system (called O2) combines the functionality of online and offline in one place. A farm of 1600 servers equipped with GPUs will analyze the detector data as it arrives and will provide the compression based on the real time analysis of the data. This is a paradigm shift compared to the standard batch processing model, where physics data was first stored and then processed after all collisions data were collected.

To cope with these demanding requirements, the front-end electronics was completely redesigned. A common optical link (the GBT) will be used to transmit both the control and physical data. Dedicated chips (SCA, Slow Control Adapters) were deployed on the front-end cards. These allow for injection of controls data into the datastreams using dedicated bits in the data packets, hence without disturbing the physics data flow.

Our group (CMCT&II at DCAI) is directly involved in the developments of the control system for the Inner Tracking System (ITS) of the experiment. However, the developed tools became an ALICE standards and are being deployed to all upgraded ALICE subdetectors. The ITS detector is the pixel detector closest to the collision point of the beams and is used to track the trajectory of subatomic particles formed directly after collision of the beams. The original ITS detector used during Run 2 consisted of 6 layers of three different detector types - the Silicon Pixel Detector (SPD), the Silicon Drift Detector (SDD), and the Silicon Strip Detector (SSD) [9].

Unlike the original detector, the new ITS detector consist of seven layers of the Silicon Pixel Detectors, while each layer is built of the same type of sensors [10]. A schematic representation of layers of the new ITS detector can be seen in Fig. 2. The layers consist of Stave units, where each contains multiple ALPIDE chips for particle detection while providing cooling for the individual sensors. ALPIDE chips were developed by ALICE using the newest available technologies. They use a new generation of monolythic pixels, where the readout circuitry is implemented on the same chip as the pixels sensors registering the particles.

The ITS is a biggest pixel detector ever built, it could be compared to a 12 billion pixel camera with continuous readout. The new version of the detector is divided into two sections. Closer to the collision point, the Inner Barrel is made up of three layers of Half-Staves (48 in total) with 432 ALPIDE chips in total. The outer section is called Outer Barrel and consists of four layers of Staves (272 in total). A half layer of the Inner Barrel can be seen in Fig. 3.

Power supply of individual Staves is provided by Power-Boards developed by ALICE for the ITS detector. The pre-production version of the PowerBoard can be seen in Fig. 4a. One PowerBoard consists of two PowerUnits, where each PowerUnit containing 8 digital and 8 analog voltage regulators. The PowerBoard is powered by CAEN power supplies. Each PowerUnit is connected to ReadoutUnit via an I2C bus and one ReadoutUnit can handle two PowerUnits that can provide power to 8 Half-Staves or one Stave [11].

Control of the PowerBoard and the ALPIDE chips on Staves is provided by ReadoutUnit developed by ALICE for the ITS detector. ReadoutUnit is based on several FPGA chips and provides a large number of interfaces to connect detector electronics. Communication with the CRU (Common Readout

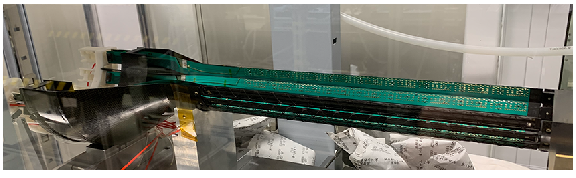

Fig. 3: Half layer of the Inner Barrel.

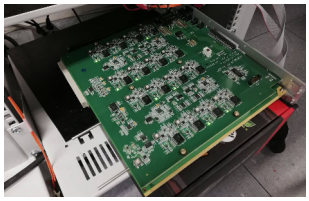

(a) PowerBoard

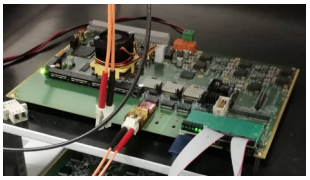

(b) ReadoutUnit

Fig. 4: New electronics for the ITS detector.

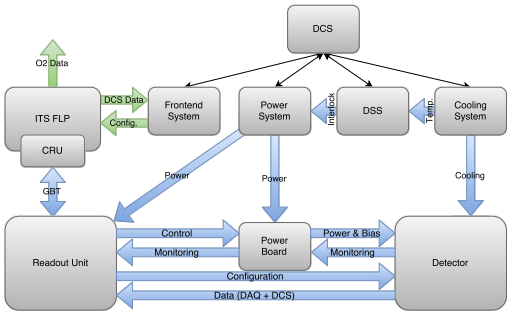

Fig. 5: New DCS system for the ITS detector.

Unit) cards is provided by two GBTx chips using the optical link [12]. The ReadoutUnit itself can be seen in Fig. 4b.

B. New structure for DCS of ALICE

The new DCS structure for the individual detectors of the ALICE experiment must ensure control of all systems critical to the operation and safety of the electronics of each detector. It must be also able to read both the DCS and the physical data that are later distributed, where the physical data are being passed to the O2 computer farms and the DCS data being sent to the higher levels of the distributed control system. The DCS must also provide continuous power supply to the individual parts of the detector as well as cooling of the electronics. In the event of critical situations such as overheating the detector parts, the DCS must be able to respond immediately and take the required action, e.g. turning off the power of corresponding part of the detector [2] .

Fig. 5 shows a schematic representation of the ITS detector crucial subsystems with their connection to the central DCS. At the highest level of control there are WinCC OA systems that ensure the archiving of received data for a offline processing and also provide the operator panels necessary for the smooth operation of the detector. Using the FSM structures, they provide an easy way to operate the detector and perform individual procedures without the need for a operator to know the physical connection of individual parts of the system. The communication between individual subsystems within the DCS is driven via the DIM network protocol [13].

FLP (First Level Processor) is a server computer that hosts multiple CRU cards. The CRU sends signals via the GBT optical link to the detector electronics and also ensures the reception and postprocess of the response. The commands sent by the CRU are used to set electronics parameters, to requests data acquisition or to upload data to the memory registers of the detector electronics. The DCS data is interleaved between the physical data within each GBT packet, whereby the FLP rips the DCS data from the stream and sends it to the front-end system. The rest of the data goes to O2 clusters for processing [14].

The most of the detectors use the SCA protocol to control their electronics, however some detectors need to communicate with the DCS system at a higher rate, so the concept of Single Word Transaction (SWT) has been introduced. The concept of SWT involves usage of whole GBT packet, not only a few bits as used with the SCA. This approach provides much higher data throughput than SCA messages. The SWT protocol is essential for the ITS detectors.

C. Implementation of the DCS

Essential part of the new DCS system is the ALFRED (ALICE Low-Level Front-End Device) architecture. The ALFRED system is independent from Readout systems and is used only by the DCS for control and monitoring of the detectors. It consists of three main modules - ALF, FRED and WinCC OA applications, while the development of the FRED module will be the main part of research activities during my PhD study.

In order to interface the CRU in a safe and efficient way, a software module ALF has been developed. The ALF is a detector independent software layer, maintained by O2, and is able to send and receive DCS data over the GBT. The communication between ALF and FRED is via DIM RPC, where FRED makes the request to ALF, and ALF publishes the response.

FRED is able to receive commands via published DIM Commands, and publish the responses from ALF via published DIM Services [15]. Commands can be complex sequences, configuration instructions, or even prompts to execute learned procedures. FRED is able to publish all response data to a supervisory control process, like the WinCC OA detector node. The FRED is able to handle multiple ALF servers in parallel and is fully customizable for detector requirements. The main idea behind the FRED is a software layer that is able to translate raw data acquired from detector electronics to real physical data and vice versa. It is also able to process error situations and determine actions that have to be done in order to recover the detector back to operational mode.

Up to now, multiple WinCC OA applications have been developed. The purpose of these detector specific nodes is to provide simple interface for human operator and execute complex tasks of detector operations in the background. One of the WinCC OA application that is currently in a commissioning phase is the Interlock system. The Interlock system takes care of safe detector operation, while monitoring connectivity and temperatures of PowerBoards and Staves of the ITS detector. It is divided into several sections monitoring individual parts of the ITS. If even one temperature sensor shows temperature out of specified limit or any ReadoutUnit stops responding, then the Interlock turns of power of all electronics in the section. The Interlock system is currently being tested by ITS experts and shows no major problems since its deployment.

IV. DiCS at CMCT&II at DCAI

The DiCS infrastructure at CMCT&II at DCAI can be seen in Fig. 6. Individual models of cyberphysical systems such as the Ball&Plate model, Inverted Pendulum model, Flexible Manufacturing System or individual mobile robots and robotic manipulators can be considered as Zero Level of DiCS.

On the First Level of DiCS there are PLCs and control computers of individual models, which are connected to a higher level by Ethernet or RS232 network interface. On the

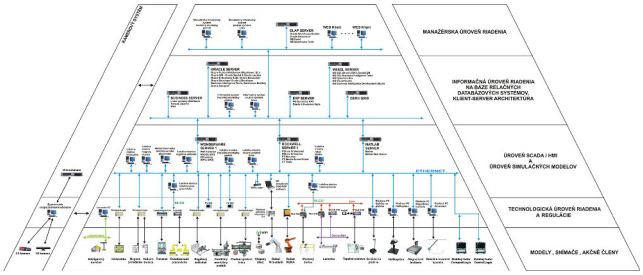

Fig. 6: Architecture of DiCS at CMCT&II at DCAI.

Second Level of DiCS are server computers with WonderWare, Rockwell and MATLAB software. Individual visualization and supervisory control is realized by local stations of models. The First and Second levels of DiCS are interconnected mostly via Ethernet interface, using communication protocols with the TCP/IP basis. In case of communication with PLC devices, the DDE or OPC protocols are used. In the application of robotic soccer, the ROS (Robot Operating System) system is used for communication between individual systems.

The Third and Fourth Levels include Oracle and MySql servers together with individual information systems implemented on ERP and Business servers. On the Fifth Level there is an OLAP server and Management Information Systems for individual models. There are also computers with client web applications for viewing the analysis. These levels are interconnected via Ethernet, using communication protocols used to access databases, such as the ODBC interface.

A. Mobile robotics

Development and research in area of mobile robotics is one of the focus areas of the CMCT&II [4]. The development of applications based on mobile robots within the DiCS will be also one part of the research within my PhD study. One of the mobile robotic platforms developed within CMCT&II is a robotic soccer player, which is a two-wheel differential mobile robot [1]. Although it's primary use is for robotic soccer applications, it can be used in various robotic applications when equipped with additional sensors.

The robotic soccer application also implements the concept of DiCS. It involves the three lowest levels of the DiCS architecture at CMCT&II at DCAI. A camera used for determining robots position and orientation implements the Zero Level of DiCS architecture. So do the sensors and actuators within the robot such as micromotors, encoders and additionally a gyroscope with an accelerometer.

On the First Level there are single-chip microcomputers on the robot control boards. These provide control of the movement of the robot at a lowest level, which includes controlling the speed of the robot and navigating the robot to the desired coordinates. At the same time, they provide communication with the supervisor computer via the Bluetooth interface.

The supervisor computer is located on the Second Level. It provides supervisory control of the movement of robots based on selected strategies using the ROS communication system [16]. The ROS system allows a remote control and visualization of connected robots, eventually it can be used for postprocessing and archiving of acquired data [17].

V. Conclusion

This paper presents an overview of Detector Control System of ALICE experiment at CERN and Distributed Control System at CMCT&II at DCAI. It shows that same principles are used in both system, what points to the versatility of Distributed Control System concept. The same principles include the multi-layer architecture of both system with usage of the similar network interfaces and protocols in both cases. Next it describes actual design and implementation of part of the DCS with emphasis on the Interlock system for ITS detector. Finally, it shows implementation of mobile robotic system into the DiCS concept.

Acknowledgment

This work has been supported by grant KEGA Implementation of research results in the area of modeling and simulation of cyber-physical systems into the teaching process - development of modern university textbooks – 072TUKE-4/2018 (100%).

References

[1] J. Jadlovský and M. Kopčík, "Distributed control system for mobile robots with differential drive," in *2016 Cybernetics & Informatics (K&I)*. IEEE, 2016, pp. 1–5.

[2] A. Augustinus, P. Chochula, L. Jirdén, M. Lechman, P. Rosinskỳ, O. Pinazza, G. De Cataldo, A. Kurepin, and A. Moreno, "Computing architecture of the alice detector control system," in *Proc. of Int. Conf. on Accelerator and Large Experimental Physics Control Systems*, 2011.

[3] H. Benítez-Pérez and F. García-Nocetti, *Reconfigurable distributed control*. Springer, 2005.

[4] J. Jadlovský *et al.*, "Research activities of the center of modern control techniques and industrial informatics," in *2016 IEEE 14th International Symposium on Applied Machine Intelligence and Informatics (SAMI)*. IEEE, 2016, pp. 279–285.

[5] E. Mobs, "The cern accelerator complex-august 2018," Tech. Rep., 2018.

[6] K. Aamodt, A. A. Quintana, R. Achenbach, S. Acounis, D. Adamová, C. Adler, M. Aggarwal, F. Agnese, G. A. Rinella, Z. Ahammed *et al.*, "The alice experiment at the cern lhc," *Journal of Instrumentation*, vol. 3, no. 08, p. S08002, 2008.

[7] M. Bernardini and K. Foraz, "Long shutdown 2@ lhc," *CERN Yellow Reports*, vol. 2, no. 00, p. 290, 2016.

[8] A. Collaboration, "Performance of the alice experiment at the cern lhc," *International Journal of Modern Physics A*, vol. 29, no. 24, p. 1430044, 2014.

[9] K. H. Wyllie, T. Grassi, V. O'Shea, P. Lamanna, M. Burns, S. D Segundo-Bello, V. Quiquempoix, K. C. Kloukinas, W. Snoeys, R. Dinapoli *et al.*, "A pixel readout chip for tracking at alice and particle identification at lhcb," 1999.

[10] S. Kushpil, A. collaboration *et al.*, "Upgrade of the alice inner tracking system," in *Journal of Physics: Conference Series*, vol. 675, no. 1. IOP Publishing, 2016, p. 012038.

[11] A. Szczepankiewicz, A. Collaboration *et al.*, "Readout of the upgraded alice-its," *Nuclear Instruments and Methods in Physics Research Section A: Accelerators, Spectrometers, Detectors and Associated Equipment*, vol. 824, pp. 465–469, 2016.

[12] J. Mitra, S. Khan, S. Mukherjee, and R. Paul, "Common readout unit (cru)-a new readout architecture for the alice experiment," *Journal of Instrumentation*, vol. 11, no. 03, p. C03021, 2016.

[13] C. Gaspar *et al.*, "Dim-a distributed information management system for the delphi experiment at cern," Tech. Rep., 1994.

[14] P. Buncic, M. Krzewicki, and P. Vande Vyvre, "Technical design report for the upgrade of the online-offline computing system," Tech. Rep., 2015.

[15] C. Gaspar, M. Dönszelmann, and P. Charpentier, "Dim, a portable, light weight package for information publishing, data transfer and inter-process communication," *Computer Physics Communications*, vol. 140, no. 1-2, pp. 102–109, 2001.

[16] J. M. Santos, D. Portugal, and R. P. Rocha, "An evaluation of 2d slam techniques available in robot operating system," in *2013 IEEE International Symposium on Safety, Security, and Rescue Robotics (SSRR)*. IEEE, 2013, pp. 1–6.

[17] M. Quigley, K. Conley, B. Gerkey, J. Faust, T. Foote, J. Leibs, R. Wheeler, and A. Y. Ng, "Ros: an open-source robot operating system," in *ICRA workshop on open source software*, vol. 3, no. 3.2. Kobe, Japan, 2009, p. 5.

Design of web platform for radiation models automation: Technology review

[1]*Daniel GECÁŠEK (1st year),*
Supervisor: [2]*Ján GENČI*

[1,2]Dept. of Computers and Informatics, FEI TU of Košice, Slovak Republic

[1]daniel.gecasek@tuke.sk, [2]jan.genci@tuke.sk

***Abstract*—This article introduces current technologies relevant to the creation of a web platform for simulation models automation. First, it introduces approaches to scientific computing more specific parallel architectures and distributed computing platforms. Then we describe technologies that may be used to create the web user interface. After that, we review existing platforms for scientific computing used in two different domains. Lastly, we analyze our findings and sketch out the next direction of the work.**

***Keywords*—data analysis, GUI, scientific computing, web interfaces**

I. Introduction

Methods of gaining scientific knowledge change over time. According to [1] we recognise four paradigms of science:

- Empirical science - characterized by observing the natural world.
- Theoretical science - characterized by models and generalizations in the form of laws and mathematical equations.
- Computational science - characterized by simulation of real-world phenomena based on models from the previous paradigm.
- Data-driven science - characterized by analysis of data created by computational science.

Notice that each paradigm uses approaches of the previous one and adds something on top of it. For example, we couldn't create generalizations about the world without first observing the world.

In this article, we are mainly interested in the last two paradigms. We will review techniques used in computational science and data-driven science, ways to use the web to make them accessible to wide and international scientific user base and existing systems that solve the problem for specific domains.

Besides using computers to create and analyze data it is also increasingly popular to provide and access them over web interfaces [2], [3], [4].

We want to implement a web platform for simulation of radiation near Earth and the Sun and interactive post-processing of the simulated data. There are existing implementations of models that solve these simulations and others are in development now. Our goal is to design a platform where users can input parameters for those simulations, get the data simulated and perform their analysis on them through a web interface.

II. Computational approaches used in scientific computing platforms

The scientific computing of today is largely done on a variety of hardware and is implemented in many architectural ways. This section introduces different approaches for scientific computing, their pros, and cons. Most of the approaches described here can be combined so usage of one of them does not exclude the other approaches.

A. General-purpose computing on graphics processing units

GPGPU (General-purpose computing on graphics processing units) is a concept where general-purpose computing is done on specialized graphics hardware instead of traditionally used CPUs (central processing units) [5]. The reason why this method of computation is attractive for scientists is that the GPU (graphics processing units) SIMD architecture is highly parallel and many problems in science are also highly parallelizable [6]. GPGPU methods usually do not exclude CPU processing and workloads are usually split between GPUs and CPUs in various ratios specific for each problem [7]. There are of course problems that don't fit the GPGPU paradigm because they are either not massively parallelizable, they are too irregular or they contain too many conditional statements. These are for example graph algorithms [8]. There are two mainstream options for GPGPU:

- CUDA (Compute Unified Device Architecture) - This is a proprietary solution by NVIDIA that only functions with NVIDIA GPUs [9].
- OpenCL (Open Computing Language) - This is a more open option from the Khronos group that is supported on hardware by multiple vendors and even supports heterogeneous architectures composed of GPUs, CPUs, and other microprocessor designs [10].

There is a split in the scientific community and none of the mentioned options are a universal solution [11], [12]. CUDA tends to be more optimized and performant on the other hand utilization of existing hardware and heterogeneous systems are attractive because of their lower price and flexibility.

B. Distributed computing

Distributed computing is computing done on a distributed system. One of the definitions for a distributed system is: "A distributed system is a collection of independent computers that appear to the users of the system as a single computer"

[13]. There are multiple options for distributed cluster management systems.

Popular systems for distributed computing cluster management include Slurm Workload Manager [14] and HTCondor [15].

Slurm Workload Manager is a cluster management job scheduling system. It has a server-client architecture where the client connects into a network controlled by a server. It manages resources of only one cluster. It has a simple scheduling algorithm based on the first in first out principle but this can be changed by using a plugin. Plugin in a SLURM sense is dynamically linked object that is loaded during runtime. Slurm Workload Manager plugin implements a well-defined API (application programming interface), for example, scheduling as previously mentioned.

HTCondor is a batch system where users can queue jobs. Its original mission was to unify idle computers belonging to one organization into a grid [16]. If a grid computer was being used (for example keypresses and mouse movements were detected) it would function as usual. On the other hand, when the system detected that the computer is idle, it would start utilizing it for computing of queued jobs. Now HTCondor can unify computers in a big geographical area into a computer grid.

HTCaaS (High-Throughput Computing as a Service) [17] is a distributed computing infrastructure created for the needs of Korean supercomputing infrastructure. It is specially designed to handle thousands to billions of tasks that have a large variance of execution time (from seconds to hours). It prides itself with a dynamic scheduler that is fair, adaptive, reliable and easy to use. Tasks are entered in an XML (Extensible Markup Language) format or GUI (graphical user interface) tool that generates the XML based on user input.

C. Volunteer computing

Volunteer computing is a type of distributed computing based on the utilization of free computational resources for scientific purposes when personal computers of volunteers are idle [18]. One of the most popular systems for volunteer computing is BOINC (Berkeley Open Infrastructure for Network Computing) [19]. In BOINC, volunteers provide resources for projects. Each volunteer can choose which project they want to contribute their resources to and set limits on resources provided. If a volunteer contributes their computing resources to multiple projects, they can choose the ratio of resources contributed to each project.

D. Possibility of usage of described computational approaches

If we want to use GPGPU, we need to purchase specific hardware (NVIDIA GPUs in case of CUDA) and rewrite the implementation of scientific models so they can be run on GPUs. Heliospheric models are well suitable for GPGPU implementation and were implemented in CUDA as part of this [20] thesis. Other models are implemented conventionally but if they are suitable for GPGPU implementation, they can be later converted. Our system should, for this reason, support both, CPU and GPU based tasks.

Distributed computing is a necessary technology for our purpose since physical models are well parallelizable and their runtime is in hours. In our case, we have long-lasting physical simulations but also comparatively short-lasting data analysis scripts that users will input through the web interface. In this case, using HTCaaS which prides itself with its scheduling algorithms that guarantee efficient computation of short tasks looks promising.

Volunteer computing may be a good option with a popular project. This approach is risky because if the project does not have enough volunteers, or it has no volunteers our project would not have have any computational resources available. For this reason, volunteer computing should not be our main strategy but might be a good supplementary strategy.

III. Options to implement web interface

Here we describe options for implementation of the website interface to the backend simulation system. There are two leading paradigms in web technologies, the older paradigm is called multiple-page application and the never one is called a single-page application. In both paradigms, the leading software creation pattern is model-view-controller which splits functionality into three interconnected elements [21].

A. Multiple-page application

This is the conventional approach to website rendering. The web browser communicates with the webserver with queries for whole pages. The server accepts the query, generates the output and sends it to the client. The advantage of this approach is mainly in the simplicity of initial development. In this approach, the model is usually communicating with the database system directly through SQL queries.

B. Single-page application

A single-page application is a web application that dynamically rewrites its content based on user queries. Thew client sends a query to the server, the server accepts the query and sends response. The client then parses the response and rewrites only the relevant part of a web application. In this approach, we need a separate model element that communicates with the database system and replies to the client with text-based responses holding the data. This approach has many advantages in comparison with the traditional approach:

- Faster load times - the first-page access can be slow because the browser downloads the whole page logic but after this, queries to the server tend to be lightweight and fast to download.
- Easier to develop complex GUIs, better user experience since the user can still interact with other parts of the GUI that are not being updated.

Both approaches can be mixed. A webpage can be implemented in a multi-page paradigm where parts of each page that need to be reloaded frequently are implemented using AJAX (Asynchronous JavaScript + XML) and similar technologies.

IV. Examples of web-based computing platforms

In this section, we present web platforms for the automation of simulations and result analysis. One of them, called SPENVIS (Space Environment Information System) [2], is in domain of our interest (radiation models automation) and another similar system specialized in the domain of biomedical analysis called Galaxy [3].

Fig. 1. Spenvis web user-interface after creating a project "TEST1" and opening it.

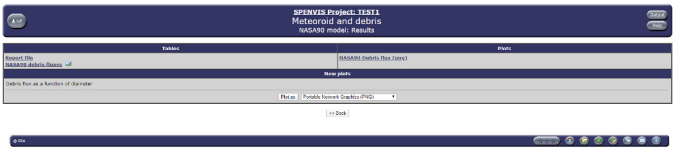

Fig. 2. SPENVIS web user-interface with report file generated by the simulation model and output plot that visualizes this result.

A. SPENVIS

SPENVIS is a system that offers access to models of the near-earth space environment through a web interface [2]. To use this system user first needs to create a user profile. After registration, the user will get an activation e-mail, without activating your account you can't fully utilize the system. After creating an account you need to create a project. Project as a concept is a collection of model inputs and outputs for a series of related runs [2].

In a project, you can choose from existing simulations and run them. Each simulation needs input. In figure 1 we can see a list of simulation topics, each topic can be clicked on and after that, it will expand and show models. Some topics have only one option and some topics have multiple model options. For example, coordinate generators can generate spacecraft trajectory coordinates or geographical coordinate grid.

The generation of coordinates is mandatory for each simulation topic. After generating data the user can generate plots in multiple image formats. In figure 2 we can see a link to the generated report file, link to generated plot and we can generate a new plot in the bottom of the GUI element. If we want to recalculate an existing simulation of a specific model in a project, existing results will be deleted.

SPENVIS differs from our proposed system in that, it can only analyze generated data with preexisting tools. Also, it divides simulation results into projects which separate them from each other. In our proposed system, results from each simulation would become a part of the dataset accessible by all users. Only analysis results would be bound to a specific user. There is also a problem with hard timeout of process execution if it exceeds the timeout period. This case is shown in figure 3.

B. Galaxy

Galaxy is a platform for interactive large-scale genome analysis. Users can perform analysis on data that is their own or query the data from domain-specific databases. Users can create workflows composed of nodes in a visual programming style. Workflows are exportable and can be shared in JSON (JavaScript Object Notation) [1] format.

[1]JSON syntax specification: https://www.json.org/json-en.html

Fig. 3. SPENVIS web user-interface showing error message about job abortion due to timeout.

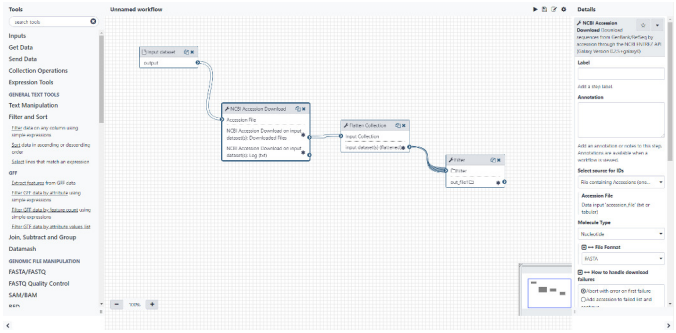

Fig. 4. Web user interface of Galaxy for creating workflows.

In figure 4 we can see an example of a Galaxy workflow. In the left panel, we can choose nodes that represent data sources, text operations, genomic file manipulation, common genomics tools and so on. In the middle panel, we can see a workflow pipeline composed of interconnected nodes. On the right pane, there are editing options for the currently selected node. After the user is done creating a workflow, he can save it and then run it. If any errors occur during runtime, the user is notified and can return to workflow designer and redesign it.

After data processing is finished, you can use Galaxy to further analyze and visualize them. There are two approaches to data visualization:

- Create visualizations - here you can choose one of the existing predefined visualization types.
- Interactive environments [22] - here you can interactively work youth your datasets with Python programming language using Jupyter notebook [23].

The more interesting option for us is the interactive environments. They were introduced in the 2018 update of the Galaxy system. They also plan to introduce RStudio [24] interactive environment so users can have more options when analyzing their data [22]. When the user chooses interactive analysis environments, they can choose which environment they want to use (right now only Jupyter option is present), Docker [25] image they want to use and dataset they want to perform analysis on.

After launch, user interface in figure 5 is displayed in browser. The user can then analyze the data as if they were on their local computer but without the need of downloading the data and installing the data analysis tools.

Using Docker image to run the Jupyter notebook script is beneficial mainly for security purposes. Docker images run in isolation from Operating System and can only use defined mounting points for data storage. After the Docker process is shut down, the data they worked with do not persist on the

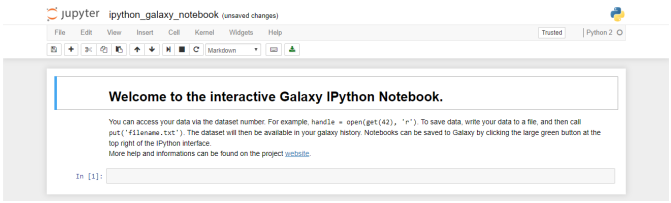

Fig. 5. Web user interface of Galaxy for Jupyter notebook data analysis and visualization.

hard drive only the data stored in defined mounting points are stored.

V. Summary

Existing high-performance computing technologies are suitable for radiation model implementation. Parallel models can be implemented conventionally on CPUs but if the problems fit the SIMD architecture, GPGPU implementations can be developed. Parallel models developed can be deployed on distributed computing architectures. We will later decide whether we will use SLURM or HTCondor or a combination of both as our base cluster management tool. Volunteer computing systems such as BOINC can be used as a supplementary strategy to harness resources of volunteer computers but their usage can be risky if the project does not get enough volunteers.

To implement the website interface a hybrid approach should be used. Most of the site can be implemented using a conventional multiple-page approach and critical parts where user experience is a priority such as data analysis that can be implemented using AJAX and similar technologies.

From a security perspective, Docker containers should be used for the implementation of custom user data analysis scripts. This approach is the one that Galaxy implemented.

SPENVIS is a good case study for our proposed system. It has a web interface and contains tools for simulation of the geomagnetic field and relevant phenomena. It also contains basic visualization tools. While it is a good system for a specific purpose it also lacks in few areas. It is missing a system for more thorough data analysis and only offers users already existing data analysis tools and no option to interactively analyze the data. It also separates data from individual users so there is a possibility for result duplication and it is not possible to access the databank as a whole and perform analysis on a big database of results.

Galaxy, on the other hand, gives users big flexibility with the creation of workflow pipelines and access to existing databases. It also offers a more complex post-analysis of results and interactive scripting options. The only disadvantage of Galaxy is that it is domain-specific. It should be modular and it is open source so it might be possible to tweak it to fit any domain.

Future research should focus on the feasibility of the implementation of the web platform using reviewed technologies.

References

[1] A. Agrawal and A. Choudhary, "Perspective: Materials informatics and big data: Realization of the "fourth paradigm" of science in materials science," *Apl Materials*, vol. 4, no. 5, p. 053208, 2016.

[2] D. Heynderickx, B. Quaghebeur, E. Speelman, and E. Daly, "Esa's space environment information system (spenvis)-a www interface to models of the space environment and its effects," in *38th Aerospace Sciences Meeting and Exhibit*, 2000, p. 371.

[3] B. Giardine, C. Riemer, R. C. Hardison, R. Burhans, L. Elnitski, P. Shah, Y. Zhang, D. Blankenberg, I. Albert, J. Taylor *et al.*, "Galaxy: a platform for interactive large-scale genome analysis," *Genome research*, vol. 15, no. 10, pp. 1451–1455, 2005.

[4] J. Byrne, C. Heavey, and P. J. Byrne, "A review of web-based simulation and supporting tools," *Simulation modelling practice and theory*, vol. 18, no. 3, pp. 253–276, 2010.

[5] J. D. Owens, D. Luebke, N. Govindaraju, M. Harris, J. Krüger, A. E. Lefohn, and T. J. Purcell, "A survey of general-purpose computation on graphics hardware," in *Computer graphics forum*, vol. 26, no. 1. Wiley Online Library, 2007, pp. 80–113.

[6] D. M. Chitty, "A data parallel approach to genetic programming using programmable graphics hardware," in *Proceedings of the 9th annual conference on Genetic and evolutionary computation*, 2007, pp. 1566–1573.

[7] S. Mittal and J. S. Vetter, "A survey of cpu-gpu heterogeneous computing techniques," *ACM Computing Surveys (CSUR)*, vol. 47, no. 4, pp. 1–35, 2015.

[8] F. Dehne and K. Yogaratnam, "Exploring the limits of gpus with parallel graph algorithms," *arXiv preprint arXiv:1002.4482*, 2010.

[9] NVIDIA. (2007, jun) Cuda. [Online]. Available: https://developer.nvidia.com/cuda-zone

[10] A. Munshi, "The opencl specification," in *2009 IEEE Hot Chips 21 Symposium (HCS)*. IEEE, 2009, pp. 1–314.

[11] K. Karimi, N. G. Dickson, and F. Hamze, "A performance comparison of cuda and opencl," *arXiv preprint arXiv:1005.2581*, 2010.

[12] J. Fang, A. L. Varbanescu, and H. Sips, "A comprehensive performance comparison of cuda and opencl," in *2011 International Conference on Parallel Processing*. IEEE, 2011, pp. 216–225.

[13] A. S. Tanenbaum and M. Van Steen, *Distributed systems: principles and paradigms*. Prentice-Hall, 2007.

[14] A. B. Yoo, M. A. Jette, and M. Grondona, "Slurm: Simple linux utility for resource management," in *Workshop on Job Scheduling Strategies for Parallel Processing*. Springer, 2003, pp. 44–60.

[15] D. Thain, T. Tannenbaum, and M. Livny, "Distributed computing in practice: the condor experience," *Concurrency and computation: practice and experience*, vol. 17, no. 2-4, pp. 323–356, 2005.

[16] M. J. Litzkow, "Remote unix: Turning idle workstations into cycle servers," in *Proceedings of the Summer USENIX Conference*, 1987, pp. 381–384.

[17] J.-S. Kim, S. Rho, S. Kim, S. Kim, S. Kim, and S. Hwang, "Htcaas: leveraging distributed supercomputing infrastructures for large-scale scientific computing," in *Proceedings of the 6th ACM Workshop on Many-Task Computing on Clouds, Grids, and Supercomputers (MTAGS'13) held with SC13*. Citeseer, 2013.

[18] L. F. G. Sarmenta, "Volunteer computing," Ph.D. dissertation, Massachusetts Institute of Technology, 2001.

[19] D. P. Anderson, "Boinc: A system for public-resource computing and storage," in *Fifth IEEE/ACM international workshop on grid computing*. IEEE, 2004, pp. 4–10.

[20] M. Solanik, "Prepis modelov distribúcie kozmického žiarenia v heliosfére do cuda jazyka," Bachelor's Thesis, Technical university of Košice, 2018.

[21] G. E. Krasner, S. T. Pope *et al.*, "A description of the model-view-controller user interface paradigm in the smalltalk-80 system," *Journal of object oriented programming*, vol. 1, no. 3, pp. 26–49, 1988.

[22] E. Afgan, D. Baker, B. Batut, M. Van Den Beek, D. Bouvier, M. Čech, J. Chilton, D. Clements, N. Coraor, B. A. Grüning *et al.*, "The galaxy platform for accessible, reproducible and collaborative biomedical analyses: 2018 update," *Nucleic acids research*, vol. 46, no. W1, pp. W537–W544, 2018.

[23] T. Kluyver, B. Ragan-Kelley, F. Pérez, B. E. Granger, M. Bussonnier, J. Frederic, K. Kelley, J. B. Hamrick, J. Grout, S. Corlay *et al.*, "Jupyter notebooks-a publishing format for reproducible computational workflows." in *ELPUB*, 2016, pp. 87–90.

[24] J. Allaire, "Rstudio: integrated development environment for r," *Boston, MA*, vol. 537, p. 538, 2012.

[25] D. Merkel, "Docker: lightweight linux containers for consistent development and deployment," *Linux journal*, vol. 2014, no. 239, p. 2, 2014.

Design, realization and implementation of ASIC for UWB sensor systems

[1]*Miroslav Sokol (3rd year),*
Supervisor: [2]*Pavol Galajda*

[1,2]Dept. of Electronics and Multimedia Communications, FEI TU of Košice, Slovak Republic

[1]miroslav.sokol@tuke.sk, [2]pavol.galajda@tuke.sk

***Abstract*—This article describes the design, realization and implementation Application Specific Integrated Circuit (ASIC) for Ultra-Wideband (UWB) sensor systems. Introduction is focused to overview of UWB systems and design development tools. The used semiconductor technologies and bonding to the package as well as the implementation into the UWB system via PCB are described.**

***Keywords*—UWB, Ultra-wideband, ASIC, QFN, Rogers, PCB**

I. Introduction

In the last two decades, a low-power ultra-wideband (UWB) sensor systems and high-speed communication have come to the fore. The main categories of the UWB sensors system are impulse radars [1], noise radars [2] and FMCW radars [3]. These radars and UWB sensors systems represent noninvasive measurement and they are perspective in many applications. From measured data, it can be possible to get information about materials, dimensions or location of objects or persons. UWB sensors are used in GPR radar [4], [5] and newer applications such as material reflectometer [6], through the wall radar [7] and radars for the medical [8] or automotive applications [9]. For all UWB systems, the semiconductor chips implementation are needed. Chip design starts in the computer design development tools, through manufacturing, bonding, to the measuring. The printed circuit board (PCB) caries have to be designed for further system implementation, as well.

II. Design development tools

For semiconductor chip design, the Electronic design automation (EDA) tools are used. Especially, for ASIC design, the Cadence® Custom IC / Analog / RF Design development tool is used as a member of Europractice [10]. In this EDA tool, the specific design packages are used. The Virtuoso® Custom Design Platform is a package for an integrated circuit (IC) design. It consists of Virtuoso Schematic Editor, Virtuoso Layout Suite and Analog Design Environment (ADE) simulation tool. Virtuoso Schematic Editor, Virtuoso Layout Suite is used for schematic and layout design or editing. Within ADE simulation tool the Spectre®, Ultrasim, APS and XPS Spectre RF simulation engines are used. This simulation engines also have the multi-threading support for time reduction of complex circuits simulations. For a specific design, the particular semiconductor technology or library is required. Thus the libraries from the target manufacturer have to be installed to the Cadence environment. The final design is generated to GDSII Gerber files and it is sent for manufacturing.

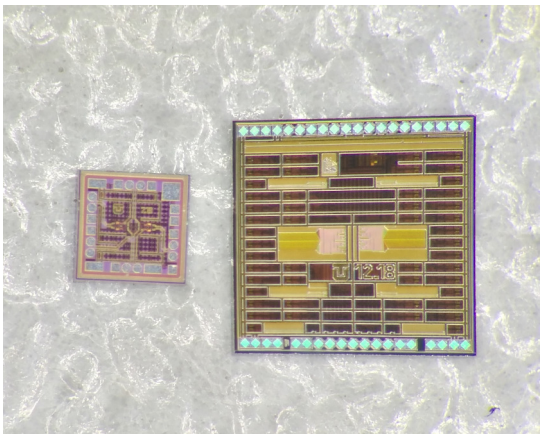

Fig. 1: On the left IHP 0.9x0.9mm die and on the right AMS 2x2mm die

III. Semiconductor technology

Today existing many semiconductor technologies differing in material and lithography size from hundreds of micrometers to the units of nanometers. However, not all are appropriate for RF and high-frequency design. For relatively low cost and fast prototyping is used multi-project wafer MPW. The MPW can be used under Europractice [11] or CMP [12] membership. Bring together multiple ASIC designs into one production run, significantly reduces the cost of prototypes. Europractice MPW offers a variety of technologies, the most famous are GLOBALFOUNDRIES, TSMC, AMS, IHP and many others[13]. For UWS sensor system design, the AMS 0.35 µm SiGe BiCMOS S35D4M5 [14] and IHP 0.25 µm SiGe BiCMOS SG25H3[15] technologies were chosen. These technologies were chosen for Bipolar Transistor (BJT) model support and relatively lower price in comparison to other semiconductor technologies. The AMS 2x2mm and IHP 0.9x0.9mm dies are shown in Fig. 1. AMS semiconductor technology support design up to 12 GHz with F_t= 65 GHz, while IHP support designs up to 30 GHz with F_t= 110 GHz.

IV. Assembling and PCB design

After manufacturing, the naked die tests are performed. The on-die measurements are performed by means of the probe station, but there is a limitation for more complex circuits. The on-die measurements are only for verification of basic functionality or power consumption. After on-die measurements, the die is assembled on PCB carrier for the

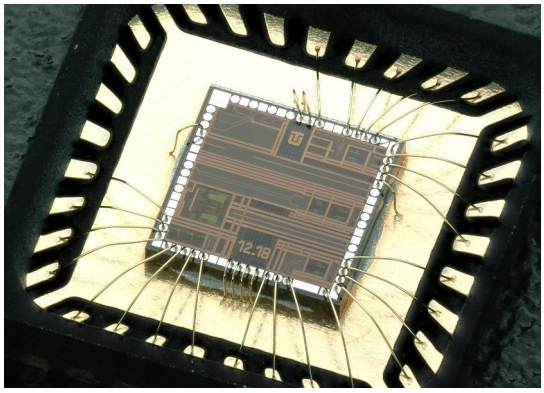

Fig. 2: Wire bonded the naked die in QFN with 32 leads

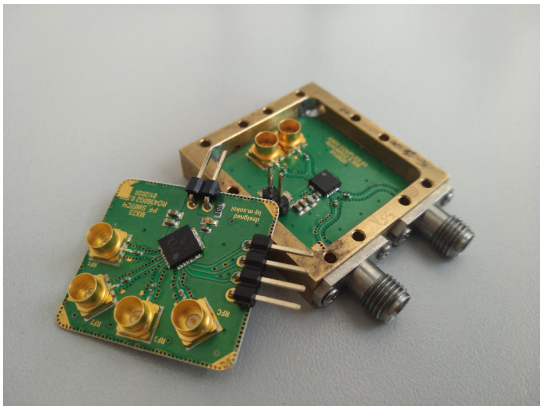

Fig. 4: Assembled UWB circuit on PCB

complex measurement and for simpler implementation to the UWB system. The most used method is wire bonding of the die to the IC package. Here the package of bonding method is selected [16]. Most commonly used packages for prototypes assembling are open-air cavity QFN packages [17]. Based on package and wire bonding method requirements the bonding diagram is created. The manufacturer uses the bonding diagram for die contacting to package. The contacted dies in QFN packages are shown in Fig. 2 and 3. Another very demanding process is the design and tuning as well as the match of the PCB board. Based on packages, maximum working frequency and used connectors the PCB substrate has to be chosen. Basic FR4 substrate supports frequencies up to 4 GHz and it has large dielectric losses. For higher frequencies are more appropriate substrates from Rogers [18]. The QFN packages have very small solder pads, with width 0.3 mm and gap 0.2 mm. The Rogers R4360G2 has dielectric constant Dk=6.15. Using the R4360G2 substrate with thickness 0.508mm is possible to design 50 Ω coplanar waveguide with path width 0.3 mm. This the straight path to QFN, without path width changes, reduce the signal reflection. Final assembled IC is shown in Fig.4.

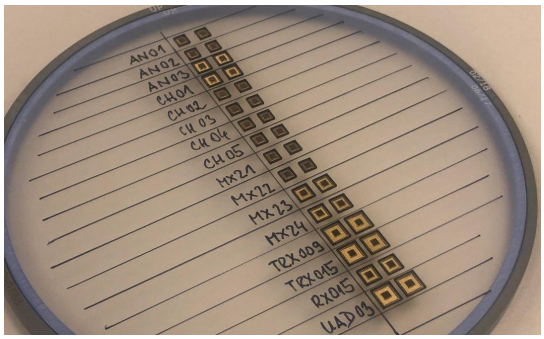

Fig. 3: Different kinds of front-end circuits for UWB systems, wire bonded to QFN packages.

V. Conclusion

The ASIC circuits for UWB sensor systems were designed and implemented. For the last three years, almost all front-end circuits were designed, namely the wideband amplifiers, directional couplers, 4-bit and 7-bit UWB ADC, frequency mixers and dividers and many others. Nowadays we focus to implement our UWB system for perspective UWB applications and measurements.

Acknowledgment

This work was supported by the Slovak Research and Development Agency under the Contract no. APVV-18-0373, Scientific Grant Agency (VEGA) under the contract No. 1/0584/20.

References

[1] J. C. Y. Lai, Y. Xu, E. Gunawan, E. C.-P. Chua, A. Maskooki, Y. L. Guan, K.-S. Low, C. B. Soh, and C.-L. Poh, "Wireless sensing of human respiratory parameters by low-power ultrawideband impulse radio radar," *IEEE Transactions on Instrumentation and Measurement*, vol. 60, no. 3, pp. 928–938, 2011.

[2] J. Sachs, "Handbook of Ultra-wideband Short-range Sensing," 2012.

[3] J. Gamec and M. Gamcova, "Experimental Frequency Modulated Continuous Wave radar," in *Radar Symposium (IRS), 2015 16th International*. IEEE, 2015, pp. 1010–1015.

[4] P. Galajda, M. Pecovsky, J. Gazda, and M. Drutarovsky, "Novel M-Sequence UWB Sensor for Ground Penetrating Radar Application," in *2018 IEEE Asia-Pacific Conference on Antennas and Propagation (APCAP)*. IEEE, 2018, pp. 110–111.

[5] J. Sachs, P. Peyerl, M. Roßberg, P. Rauschenbach, and J. Friedrich, "Ultra-wideband principles for surface penetrating radar," in *Ultra-Wideband, Short-Pulse Electromagnetics 5*. Springer, 2002, pp. 247–257.

[6] M. Kmec, M. Helbig, R. Herrmann, P. Rauschenbach, J. Sachs, and K. Schilling, "Toward integrated µNetwork analyzer," in *Ultra-Wideband, Short-Pulse Electromagnetics 10*. Springer, 2014, pp. 443–451.

[7] J. Rovnnakova and D. Kocur, "Experimental comparison of two uwb radar systems for through-wall tracking application," *Acta Electrotechnica et Informatica*, vol. 12, no. 2, p. 59, 2012.

[8] E. M. Staderini *et al.*, "UWB radars in medicine," *IEEE aerospace and electronic systems magazine*, vol. 17, no. 1, pp. 13–18, 2002.

[9] Z. Qian, T. Wang, and J. Chen, "Compatibility Studies of IMT System and Automotive Radar in the Frequency Range 24.5-25.5 GHz," in *2018 IEEE 18th International Conference on Communication Technology (ICCT)*. IEEE, 2018, pp. 505–508.

[10] EUROPRACTICE. (2019) Europractice university software program. [Online]. Available: https://www.cadence.com/ja_JP/home/company/cadence-academic-network/university-software-program.html

[11] ——. (2019) Europractice ic service. [Online]. Available: http://www.europractice-ic.com/

[12] ——. (2019) Circuits multi projets. [Online]. Available: https://mycmp.fr/

[13] ——. (2020) Europractice ic service. [Online]. Available: https://europractice-ic.com/mpw-prototyping/general/mpw-minisic/

[14] AMS. (2019) Multi project wafer reference. [Online]. Available: http://www.austriamicrosystems.com

[15] IHP. (2019) 0.25 µm technology with a set of npn-HBTs ranging from a higher RF performance. [Online]. Available: https://www.ihp-microelectronics.com/en/services/mpw-prototyping/sigec-bicmos-technologies.html

[16] G. G. Harman and G. G. Harman, *Wire bonding in microelectronics*. McGraw-Hill New York, 2010.

[17] QUIK-PAK. (2020) Air cavity qfn packages. [Online]. Available: http://www.icproto.com/cap-ic-open-cavity-qfn.html

[18] AMS. (2019) RO3000® Laminates,. [Online]. Available: https://rogerscorp.com/en/advanced-connectivity-solutions/ro4000-series-laminates

Designing Intelligent Systems to Refine Human Wellbeing

[1]*Dominika ČUPKOVÁ (2nd year),*
Supervisor: [2]*Iveta ZOLOTOVÁ*

[1,2]Department of Cybernetics and Artificial Intelligence, FEI TU of Košice, Slovak Republic

[1]dominika.cupkova@tuke.sk, [2]iveta.zolotova@tuke.sk

***Abstract*—Modern healthcare is facing several challenges. Among others, costs are increasingly growing while resources are shrinking, which demands our attention and should lead to new innovative solutions in this area. One of the possible approaches is an effort to prevent severe cases by precautionary methods, such as consideration of human wellbeing as an integral element of human health. Implementing artificial intelligence in this area could benefit people's health in unexpected ways. This paper explores a synergy between machine learning techniques and wellbeing based on the paradigms of wellbeing computing. The main area considered is quantifying humans and human wellbeing within intelligent spaces. Two of the fundamental questions are, "Are we able to define human wellbeing in a way that is understandable for machines participating in intelligent environments? What does it mean to be a human in an intelligent environment in general?"**

***Keywords*—intelligent systems, wellbeing computing, machine learning, wellbeing**

I. Introduction

Healthcare costs are growing globally and are at an unsustainable level in numerous western countries. People, authorities, and corporations carry the financial burden. At the same time, employers have become more conscious of the costs due to decreased productivity and the importance of employee wellbeing when measuring organizational performance. Employees that are coming to work while not healthy enough to adequately perform are estimated to cost employers as much as illness-related absences.

The previous decade of machine learning has produced self-driving cars, speech recognition systems, efficient web search, and robots playing video games. While artificial intelligence has been remarkable in delivering these specific tasks, this does not necessarily resemble the broader goal of improving human wellbeing. This research intends to connect the gap between technology and societal goals: What is the relationship between health and wellbeing, and how can we use AI to benefit this relationship?

II. Wellbeing Computing

By the term Wellbeing Computing (WBC), we understand a synergy between health & wellbeing sciences and artificial intelligence to support psychological wellbeing and maximize human potential. This term was first proposed in 2016 at the AAAI Spring Symposium: Well-being Computing: AI meets health and happiness science. The interest in the community around wellbeing computing can be divided into several areas.

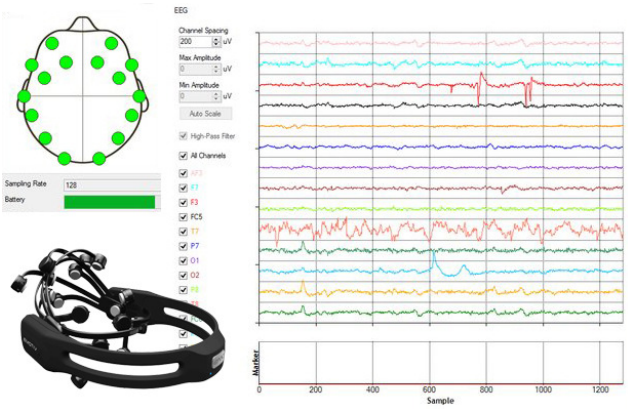

Fig. 1. EEG measurements from 14 channels using the emotiv EPOC headset

- **quantifying wellbeing** - sleep monitoring, diet monitoring, vital data, diabetes monitoring, sport monitoring, personal genome, self-tracking devices, health data collection, wearable devices and cognition, brain fitness and training, sleep, dreaming, relaxation, meditation, physiology, electrical stimulation
- **analyzing health and wellbeing data to discover new correlations**
  - **discovery informatics technologies** - deep learning, data mining and knowledge modeling for wellness, biomedical informatics
  - **cognitivne and biomedical modeling** - brain science, brain interface, physiological modeling, biomedical informatics, mathematical modeling, health and disease risk prediction
- **practices and methods for designing health and wellbeing spaces** - mood analysis, stress reduction, human-computer interaction, healthcare communication systems, personal behavior discovery, calming technology, Kansei engineering, assistive technologies, Ambient assistive living (AAL), medical recommender systems, care support systems for aging population, web services for personal wellness, lifelog applications, disease improvement, sleep improvement experiments

III. Quantifying Human Wellbeing

One of the fundamental problems in the area of wellbeing computing is the task of quantifying human data rationally and conveniently. Before we proceed with any further analysis,

TABLE I
COMPARISON OF RELATED WORK ON PSYCHOPHYSIOLOGICAL MEASURES STUDIES THAT IMPLEMENTS MACHINE LEARNING TECHNIQUES

Authors	**Psychophysiological measures**	**Machine learning methods**
Cavallo et al. [1]	ECG, EDA, Brain activity	SVM, Decision tree, k-nn
Subramaian et al. [2]	EEG,ECG,GSR	SVM, Naive Bayes
Al Machot et al. [3]	EDA	SVM-RBF, SVM-KNN
Wen et al. [4]	OXY, GSR, HR	Random forest
Zhuang et al. [5]	EEG	SVM
Moaiyed et al. [6]	ECG, EEG	SVM

it is necessary to find a reasonable way to quantify human psychophysiological processes.

A. Psychophysiological Measures for Inner States Detection

Psychophysiological measures are an essential apparatus in the process of quantifying users and their inner states in intelligent environments. Several research works are taking advantage of these measures as a tool of quantifying emotions, moods and attitudes. [1][2][3][4][5][6]

ASCERTAIN [2] claims to be the first database attaching personality characteristics and emotional states through physiological responses. MAHNOB-HCI [7] is a database that claims to be the first in having five precisely synchronized modalities – eye gaze data, video, audio, and peripheral and central nervous system physiological signals. It could be used to examine the relations between simultaneous emotion-related activity and behavior. Comparison of some works, usage of psychophysiological measures and machine learning algorithms are shown in TABLE I

B. Brain-Computer Communication

The possibilities of using electroencephalogram (EEG) for a variety of applications has widened thanks to the availability of profoundly sensitive low noise electrodes, the capability of fast multivariate signal processing, low-cost hardware options, and wireless communication. Applications are no longer limited to medical studies [8], but also the wellbeing of disabled patients is becoming in the greater interest of researchers. Brain-computer interface (BCI) transcribe brain waves into control commands [9], for instance, there are efforts to build effective and convenient BCI to help ALS or patients with spinal cord injuries to communicate easier by using BCI. [10]

IV. RESEARCH PLAN

Several articles were already published on these topics, namely on implementing an intelligent lighting system for mental wellbeing improvement [11] and applying AI methods for analysis at the edge of the networks [12]. The dissertation proposal on designing intelligent systems to refine human wellbeing was written, and the initial data acquisitions have started. The first EEG data were captured using the Emotiv EPOC helmet. An example of the output is shown in Figure 1. Understanding of how these data can be used is still work in progress.

For the next steps in the research plan, it is necessary to conduct broader research on the topic of psychophysiological measurements for the detection of inner states and brain-computer communication. These two topics are closely related, and the research could benefit from one another. A more concise overview of research articles will be done, resulting in a separate article.

It is necessary to get equipment for specific measures and to build the IoT network in which the user will participate doing numerous tasks so we can simulate different human states. We would like to measure ECG and brain activity during these tasks. It would be beneficial to obtain more sensors for data acquisition, for instance, sensors for galvanic skin response (GSR) and electrodermal activity (EDA). Another step is an analysis of the data we acquired, more specifically, looking for correlations and relationships. Then we would try to model a criterion function that will represent the digital wellbeing of a user.

ACKNOWLEDGMENT

This publication was supported by the grant KEGA – AICybS - Smart Industry/Architectures of Intelligent Information and Cybernetic Systems, 033TUKE-4/2018, 2018-2020 (50%) and VEGA – Intelligent cyber-physical systems in a heterogeneous environment with the support of IoE and cloud services, 1/0663/17 2017-2020 (50%).

REFERENCES

[1] F. Cavallo, F. Semeraro, G. Mancioppi, S. Betti, and L. Fiorini, "Mood classification through physiological parameters," *Journal of Ambient Intelligence and Humanized Computing*, pp. 1–14, 2019.

[2] R. Subramanian, J. Wache, M. K. Abadi, R. L. Vieriu, S. Winkler, and N. Sebe, "Ascertain: Emotion and personality recognition using commercial sensors," *IEEE Transactions on Affective Computing*, vol. 9, no. 2, pp. 147–160, 2016.

[3] F. Al Machot, M. Ali, S. Ranasinghe, A. H. Mosa, and K. Kyandoghere, "Improving subject-independent human emotion recognition using electrodermal activity sensors for active and assisted living," in *Proceedings of the 11th PErvasive Technologies Related to Assistive Environments Conference*, pp. 222–228, ACM, 2018.

[4] W. Wen, G. Liu, N. Cheng, J. Wei, P. Shangguan, and W. Huang, "Emotion recognition based on multi-variant correlation of physiological signals," *IEEE Transactions on Affective Computing*, vol. 5, no. 2, pp. 126–140, 2014.

[5] N. Zhuang, Y. Zeng, L. Tong, C. Zhang, H. Zhang, and B. Yan, "Emotion recognition from eeg signals using multidimensional information in emd domain," *BioMed research international*, vol. 2017, 2017.

[6] V. Moaiyed, M. Firoozabadi, and M. Khezri, "Recognition of music-induced emotions based on heart-brain connectivity," in *2017 24th National and 2nd International Iranian Conference on Biomedical Engineering (ICBME)*, pp. 330–333, IEEE.

[7] M. Soleymani, J. Lichtenauer, T. Pun, and M. Pantic, "A multimodal database for affect recognition and implicit tagging," *IEEE Transactions on Affective Computing*, vol. 3, no. 1, pp. 42–55, 2011.

[8] J. J. Shih, D. J. Krusienski, and J. R. Wolpaw, "Brain-computer interfaces in medicine," in *Mayo Clinic Proceedings*, vol. 87, pp. 268–279, Elsevier, 2012.

[9] K.-R. Muller and B. Blankertz, "Toward noninvasive brain-computer interfaces," *IEEE Signal Processing Magazine*, vol. 23, no. 5, pp. 128–126, 2006.

[10] G. Chakraborty and S. Horie, "Towards an efficient and convenient brain computer interface," in *2016 AAAI Spring Symposium Series*, 2016.

[11] D. Cupkova, E. Kajati, J. Mocnej, P. Papcun, J. Koziorek, and I. Zolotova, "Intelligent human-centric lighting for mental wellbeing improvement," *International Journal of Distributed Sensor Networks*, vol. 15, no. 9, p. 1550147719875878, 2019.

[12] D. Cupkova, E. Kajati, J. Vascak, and P. Papcun, "Smart/intelligent edge - artificial intelligence in data analysis at the edge of the network," *ATP Journal*, vol. 26, no. 3, pp. 54–55, 2019.

Determining the Colors of Detected Objects from Image Information

[1]*Martin Štancel (3rd year)*
Supervisor: [2]Liberios VOKOROKOS

[1,2]Dept. of Computers and Informatics, FEI TU of Košice, Slovak Republic

[1]martin.stancel@tuke.sk, [2]liberios.vokorokos@tuke.sk

***Abstract*—Detecting objects in computer vision have become very popular these days, especially in self-driving vehicles and autonomous cars. We are proposing a method to enhance this experience by detecting colors, which could also lead in the color perception by robotic systems in the future. First, there are described technologies used in the first part of the paper and then the method to determine the colors of detected objects is proposed with several conducted experiments.**

***Keywords*—color perception, clustering, object detection, YOLO.**

I. Introduction

We see colors as a reflection of light that comes from the surface of objects we observe. During the reflection, some of the light is absorbed, so what we see is the rest of the reflected part. Every person perceives colors subjectively, there are many shades, color perception disorders and factors that affect it and many errors can occur during the determination phase. For computers, the image information is a graphic file. It contains a sequence of numbers, each of which determines the color of each point. In determining the color of a computer, the human factor is eliminated. It can represent each color and its shades using a color model. However, if we want it to be transformed into what people describe colors, there is one limitation. Not every color shade has its own name, so in classification we determine the name of the color it most closely resembles. The motivation for this paper is to create a program that extends the functionality of current object detectors by adding an ability to perceive and determine colors. For each object found in the image, it also adds its color information to its name, which will help to better specify it.

The structure of the paper is as follows: *section II* describes the used technologies, *section III* deals with a proposal of the method, *section IV* shows the imperfections of the algorithm and there are several future improvements mentioned in *section V*.

II. Object Detection

The modern era of computer vision goes back to the 1960s. As reported by Andreopoulos [1], there have been various attempts to apply detection systems to automate processes and replace people. At that time, concepts such as detection, localization, recognition, classification, categorization, verification and identification began to emerge. Today, object detection is a combination of two tasks - image classification and object localization. The combination results in a system whose output is localized objects with a border and a category. These systems have a wide range of usability, thanks to which they have been used in the electronics, engineering, pharmaceutical, but also the food industry.

Recently, object detection has seen great progress due to new technologies, large companies that support research and development, the amount of data collected and an enormous capability of computing power. Several methods have been developed to detect text, faces, vehicles and moving people [2]. With the increasing number of algorithms, rules are needed to measure their performance. This can be achieved by comparing the output of the algorithm with the expected output. For us, two parameters of the quality of the algorithm, speed and accuracy are the most interesting. Before comparing selected algorithms, we explain the concept of a convolutional neural networks, which have been proven to be the best tool for image classification and object detection.

A. Convolutional Neural Networks

The idea of the convolutional neural network (CNN) architecture dates back to 1970s when it was inspired by neurophysiological knowledge [3]. The model was the organization of neurons in the visual cortex of animals. CNNs are a special type of multilayer neural networks and are trained by a back propagation algorithm [4]. Today, this architecture is widely used in computer vision, because it has a huge efficiency while analyzing an image information. More about the CNNs is for example here [5].

For the purpose of this paper, the YOLO [6] object detector was used.

B. YOLO Object Detector

There was used the third version of the You Only Look Once (YOLO) Detection Algorithm. The author of the algorithm. Redmon, in the documentation on his official webpage states, that it is state of the art in object detection and image classification, especially while detecting in real time.

Our initial tests of this detector were published in this paper [7].

In this paper, the mentioned algorithm was altered to be able to detect colors which is described further in the paper.

III. Prototype

Before we begin to solve the color determination itself, we have to detect objects first. After this phase the color determination occurs. Subsequently, we have the possibility to cut individual objects based on the boundaries and work with

them as separate images. To do so there was used modified version of YOLO that is supported along with OpenCV.

In determining the object's color, the task is to get all the colors and select the dominant colors of the image. One method that offers a solution is K-Means clustering. The aim of this algorithm is to find groups in data whose number is given by the number of clusters parameter. In this case, the data that need to be divided into groups are the individual pixels of the image. Each pixel is represented by three parameters R, G and B.

Another method that was used for this prototype is to have intervals of colors where every detected pixel of an image would be part of the given interval. Since we are detecting objects with background already removed, then we can easily detect color according to the most popular interval. The HSV scale was used as a color model. In the next table Table I you can see the mentioned intervals and how this method determines the dominant color.

TABLE I. INTERVALS FOR THE COLORS DETERMINATION

Color	**Interval**	
	from	***to***
red	0, 170, 150	10, 255, 255
	171, 170, 150	180, 255, 255
orange	11, 180, 150	20, 255, 255
yellow	21, 170, 150	32, 255, 255
green	33, 170, 150	85, 255, 255
blue	86, 170, 150	135, 255, 255
purple	136, 170, 150	135, 255, 255
white	0, 0, 170	180, 35, 255
black	0, 0, 0	180, 255, 75

There were conducted several experiments that compare the implemented methods from the time consuming and the result correct color determination point of views.

The interval method was customized for this experiment so it could measure the time according to the every x^{th} pixel. It is clear that the less pixels are measured; the less time is spent to determine the color of the object.

Correct results of the algorithm, see Fig. 1.

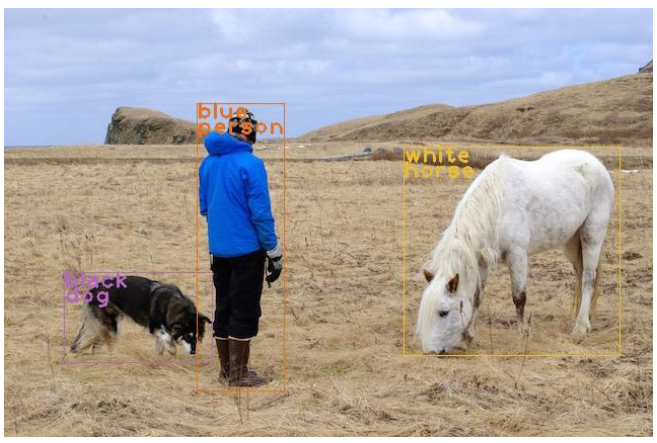

Fig. 1. Correctly determined colors of several detected objects

IV. ALGORITHM IMPERFECTIONS

This is an initial phase of our algorithm and of course it comes with some imperfections, too. In the next figure Fig .2 you can see correctly determined colors by the interval method and unknown result by the clustering method.

Clustering Interval Method

Fig. 2. Algorithm Imperfections

V. CONCLUSION

In this paper we proposed methods for color determination in object detector YOLO. Color perception is very important for humans as well as computers these days. Colors help us express our feelings and emotions. Nowadays the technology is everywhere around us and it's about the time for humanoid robots to rise and shine. This could be a start for robots to perceive colors in their every day's life through the real time object detection that would be embedded in their cameras.

The proposed method could be improved for determination of more colors or enhanced with histograms and another computer vision techniques.

ACKNOWLEDGMENT

This work was supported by the Faculty of Electrical Engineering and Informatics at the Technical University of Košice under contract No. FEI-2020-70: Behavioral model of component systems based on coalgebras and linear logic.

REFERENCES

[1] A. Andreopoulos and J. Tsotsos, "50 Years of object recognition: Directions forward," in: Computer Vision and Image Understanding. 2013, vol. 117, pp. 827–891, DOI: 10.1016/j.cviu.2013.04.005.

[2] V. Mariano, J. Min, J. Park, R. Kasturi, D. Mihalcik, H. Li, D. Doermann and T. Drayer, "Performance Evaluation of Object Detection Algorithms," 3rd ed., 2002, pp. 965–969, DOI: 10.1109/ICPR.2002.1048198.

[3] J. Schmidhuber, "Deep Learning," in Scholarpedia, vol. 10, iss. 11, pp. 32832, DOI: 10.4249/scholarpedia.32832. revision #184887.

[4] Y. Lecun and Y. Bengio, "The Handbook of Brain Theory and Neural Networks," in: ARBIB, Michael A. (ed.). Cambridge, MA, USA: MIT Press,1998, kap. Convolutional Networks for Images, Speech, and Time Series. pp. 255–258.

[5] A. Krizhevsky, I. Sutskever and G. Hinton, "ImageNet Classification with Deep Convolutional Neural Networks," in: Advances in Neural Information Processing Systems. 2012, vol. 25.

[6] J. Redmon and A. Farhadi, "YOLOv3: An Incremental Improvement," Tech Report. arXiv:1804.02767. 2018.

[7] M. Štancel and M. Hulič, "An Introduction to Image Classification and Object Detection using YOLO Detector," in: 15th International Conference on ICT in Education, Research, and Industrial Applications. Ukraine, 2019.

Dielectric breakdown in soft magnetic fluids on based transformer oil

[1]*Pavol BARTKO (1st year),*
Supervisor: [2]Juraj KURIMSKY

[1,2] Faculty of Electrical Engineering and Informatics, Technical University of Košice, Letná 9, 041 54 Košice, Slovakia

[1]pavol.bartko@tuke.sk, [2]juraj.kurimský@tuke.sk

Abstract — **This paper is devoted to a soft magnetic fluid based on transformer oil and iron oxide nanoparticles stabilized with oleic acid. The investigated magnetic fluid is characterized from magnetization and magnetic susceptibility point of view. Quasi linear increase in magnetization of saturation with increasing magnetic volume fraction (ranging from 0.05 to 0.35 vol%) has been found. The particle size distribution has been obtained by applying the superposition of Langevin fitting functions on the magnetization curve. Measurements of AC magnetic susceptibility revealed almost zero magnetic losses in a wide frequency range. Especially at 50 Hz the magnetic nanoparticles in the studied samples are well relaxed. This behavior makes the magnetic fluid suitable for electrical engineering applications, e. g. in power transformers. In this regard, the dielectric and insulating properties of the magnetic fluid must be also verified [1,2]. Herein, we focus on a dielectric breakdown in the transformer oil and three magnetic fluid samples. The breakdown tests are carried out in the needle-sphere electrode geometry with the high negative potential applied once to the needle and then to the sphere. The experiments revealed a remarkable polarity effect on the dielectric breakdown voltage of the magnetic fluids. A significant increase in the breakdown voltage was measured in the case with the negative high potential applied to the needle electrode, as compared with the high potential on the sphere at different voltage ramp rate.**

Keywords — **breakdown, DC voltage, ferrofluid, transformer oil.**

I. INTRODUCTION

Currently demand for electric energy is higher than ever before and because of this it is necessary to operate power transformer with higher performance [1]. Many researches of transformer oil were conducted, where breakdown strength of these oils was tested [2, 3].

Breakdown characteristics of transformer oil were mainly tested for secure operation of energy equipment [4, 5]. Breakdown of transformer oil is caused by spreading charged gaseous canals (streamers) under effect of electric field with high intensity [6]. It was found that positively charged streamers are initiated under lower voltage than, propagate faster and further than negative streamers [7, 8], what represents bigger hazard for insulation oils that are used in high voltage equipment. It was found that impulse positive breakdown of transformer oil depends on pre-breakdown and we can influence it by adding additives [9, 10]. Since it is necessary to operate transformers with higher voltage, it is necessary to consider alternatives to pure transformer oil [1]. As a potential replacement of pure oil, we could use ferrofluid [11]. In the last two decades, ferrofluids have received great attention because they have good insulation and thermal conduction properties [12, 13]. Preparation of ferrofluids consist of diffusion of nanoparticles in transformer oil. It was found out that addition of Fe_2O_3 nanoparticles can significantly increase breakdown voltage up to 82.6% [13].

In this article we measured breakdown voltage of three different concentration nanoparticles Fe_2O_3 in ferrofluid (0.05, 0.15 and 0.35vol%) and compared them with pure transformer oil. Electric breakdown voltage was tested using DC voltage with needle-sphere layout. Experiment shows us change in breakdown voltage of ferrofluids and pure transformer oil by changing the polarity of the electrodes and at different voltage ramp rate.

II. THEORETICAL BACKGROUND

Liquid insulators are more efficient and useful than gaseous or solid insulation materials. The main reason is the density of solid and liquid materials thousands of times higher than gaseous insulators. Liquid insulators or transformer oil is more effective than nitrogen or oxygen. Liquid insulators are mainly used as impregnation of substances in capacitors, high voltage cables or as filling of power transformers.

One of the most important insulating components of oil is breakdown voltage. Breakdown voltage of oil is voltage which oil has not been able to resist the passage of electricity, and the electricity will pass through it [14]. Molecular ionization of insulating medium which depends on electric field is the key mechanism for breakdown in transformer oil [15].

Through the ionization, oil molecules turn into fast electrons and slow positive ions, fast electrons are swept away to the positive electrode from the ionization zone because an area of net positive space charge quickly develops. Electric field distribution in the oil is modified during ionization such that the electric field at the ahead of the positive charge in the oil increases whereas at the positive electrode decreases. These electrodynamics processes cause a developing ionizing electric field wave that vaporize transformer oil and create a gas phase due to temperature raise. The result of oil vaporization is the formation of the low density streamer channel in oil [16].

In recent years, many studies on the impact of nanoparticles on the electrical and thermal characteristics of the transformer

oil have been done. Segal and colleagues [17] showed that the addition of magnetic nanoparticles to transformer oil has not had bad influence on insulation resistance of the oil and its AC breakdown voltage approximately is equal to the base oil (pure oil without nanoparticles).

Our results also showed that the impulse breakdown voltage of magnetic nanofluids based on transformer oil (called ferrofluid) for needle-sphere electrodes, when the needle is positive polarity, 30% improved compared to the base oil [18].

Kopcansky [19] showed that the DC dielectric breakdown voltage of magnetic nanofluids produced based on transformer oil with an average diameter of nanoparticles 8.6 nm and volume fraction of 0.01 is improved compared to transformer oil.

Kudelcik [20] dispersed magnetic nanoparticles with mean diameter of 10.6 nm in ITO 100 inhibited transformer oil, and showed that the humidity effects will be magnified within base oil without nanoparticles.

They also examined the change of breakdown voltage versus varying the gap distance between electrodes and aimed that increasing the distance between electrodes ascends the breakdown voltage. According to their results it was found that the optimum volume concentration of nanoparticles is approximately equal to 0.2% which leads to best results.

III. Materials and Methods

In this experiment we tested three concentrations of ferrofluids, which were prepared from commercial transformer oil MOGUL TRAFO CZ-A and nanoparticles Fe_2O_3 stabilized by oleic acid. Exact preparation of ferrofluids is described here [14]. Samples tested in this experiment were diluted from concentrated ferrofluid at 60 °C. As we mentioned before we diluted three different concentration of nanoparticles Fe_2O_3 at 0.05, 0.15 and 0.35vol%. We also tested pure transformer oil MOGUL TRAFO CZ-A from which were made other ferrofluids.

The breakdown voltage tests were conducted by direct voltage. All samples were tested according to international standard IEC 60897. After filling the testing vessel with the tested liquid, the vessel was evacuated in a desiccator by a vacuum pump in order to get rid of the unwanted gas bubbles that could have formed during the filling procedure. Then, the samples were investigated under ambient conditions (20 °C). The breakdown tests were performed in two ways.

First, with the negative high potential applied to the needle and then to the sphere. In both cases, the samples were tested with three voltage rise rates: 470 V/s, 750 V/s, and 1100 V/s, controlled by an external controller. The measured test voltage transients with linear fits are depicted in Fig. 1.

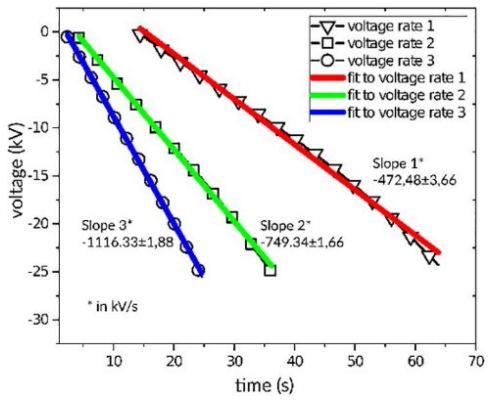

Fig. 1 Voltage rise rates used in the experimental study of the polarity effect.

For each sample, we measured 30 values of breakdown voltage to get a reproducible average value with an eliminated statistical error.

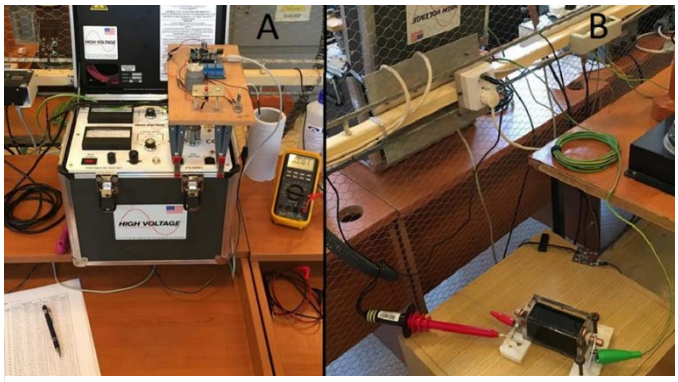

Fig. 2 The experimental setup employed in the breakdown voltage measurements. (A) – High voltage power supply with the output voltage rise rate control system. (B) – BDV test vessel filled with the ferrofluid.

Measurements of breakdown voltage were conducted by using DC power supply PTS – 37,5 (High Voltage, USA) and external controller of DC voltage rise rate. Besides that, our measuring workplace consists of digital multimeter Hexagon 720 (Beha Electronics, CN). High voltage power supply and digital multimeter are on Fig. 2 **A**. A high voltage probe HV 40 (Elma Instruments, DK) was used to record the breakdown voltage and was applied to the one of the electrodes while the other electrode was grounded. Testing vessel for breakdown voltage can be seen on Fig. 2 **B**. In the experiment we used the electrode arrangement needle-sphere, the distance between electrodes was 0.5 mm during the whole experiment. A detailed view of the test vessel is on Fig. 3. After pouring the liquid into test vessel, we first sucked off the unwanted bubbles using a vacuum pump and desiccator that could have formed during the pouring insulating liquid.

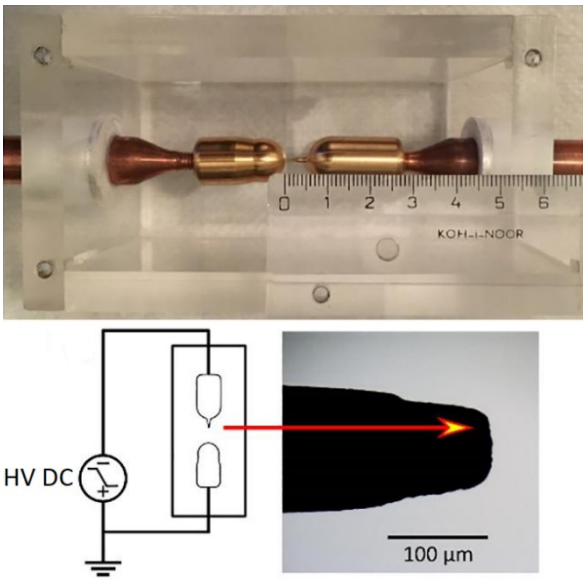

Fig. 3 A detailed view of the experimental setup for breakdown measurements.

IV. Results

Measured values of breakdown voltage were statistically and graphically processed for all concentrations ferrofluids and pure transformer oil. Measured results are shown on Fig. 4. It is apparent from the graphs that breakdown voltage of

ferrofluid have higher value than pure transformer oil. Furthermore, we observe that a higher concentration of nanoparticles has favorable effect on the breakdown voltage. Higher breakdown voltage values were recorded due to the increase of DC negative voltage. With sample MOGUL TRAFO CZ-A were recorded higher values od breakdown voltage due to an increase in the DC voltage rise rate by 2 kV. Ferrofluids with concentrations of nanoparticles 0.05 and 0.15vol% increase of breakdown voltage was 1 kV and concentration 0.35vol% increase was 0.6 kV.

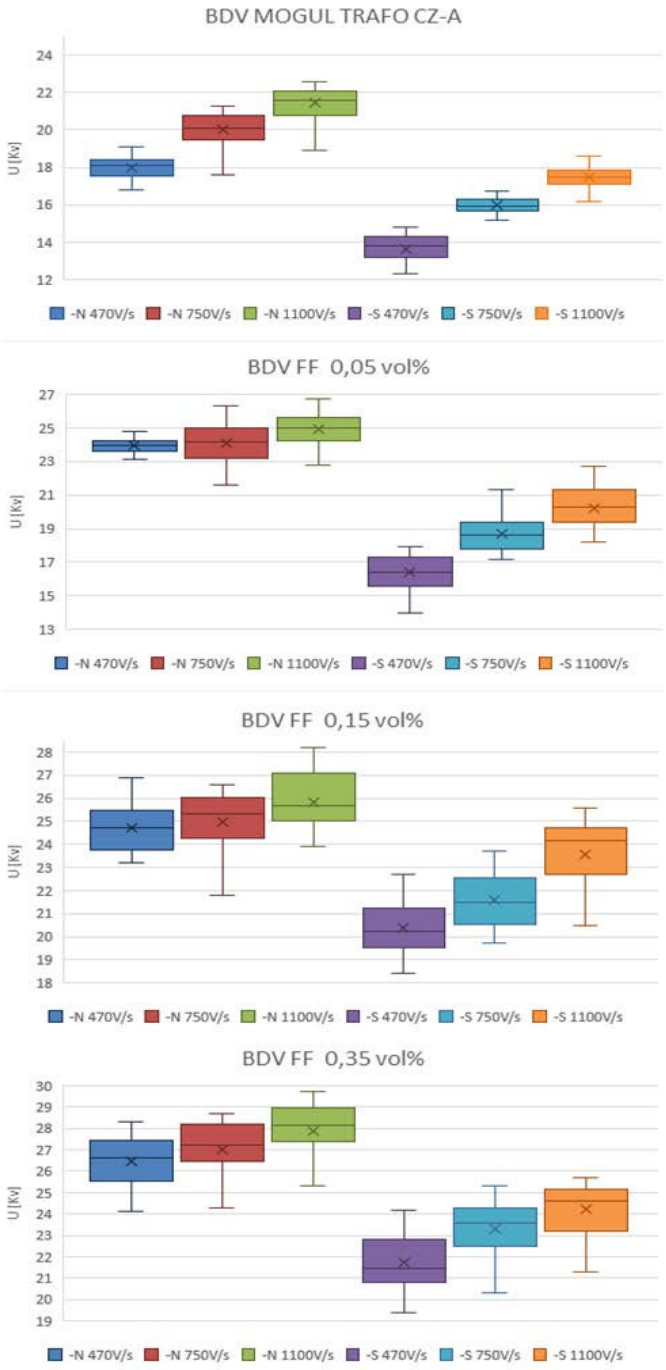

Fig. 4 Statistical interpretation of the needle polarity effect on BDV in clear transformer oil and magnetic fluids with nanoparticle concentration of 0.05 vol%, 0.15 vol%, and 0.35 vol%.

Every tested sample shows higher values of breakdown voltage when needle electrode has negative charge and sphere is grounded. This is also true when comparing the different DC negative voltage rise rates. Considering previous studies, this may result in different rates of spread of negative and positive streamers. Negative streamers spread slower than positive ones [22]. An effect of electrical polarity was observed for each sample. In sample MOGUL TRAFO CZ-A, due to a change of polarity of the electrodes breakdown voltage dropped by 3.5 kV for each DC negative rise rate. For ferrofluid 0.05vol% we also measured a decrease of 4.5 kV of breakdown voltage under the influence of exchange of the electrodes polarity at the DC voltage rise rate 470 V/s. This phenomenon has also shown with other samples of ferrofluid and with all DC negative voltage rise rates. Ferrofluid with concentration 0.15vol% decrease of breakdown voltage was 4 kV and ferrofluid with concentration 0.35vol% decrease of breakdown voltage was 5 kV.

Overall, the observed polarity effect is presented in Fig. 5 for each sample and each voltage rise rate. There, BDV constitutes the difference between the BDV values measured with negative and positive potential applied to the needle. The most pronounced polarity effect on BDV is found for the magnetic fluid with the lowest nanoparticle concentration (0.05 vol%) measured under the voltage rise rate of 470 V/s. In this case, the difference between the negative and positive BDV is 7.53 kV.

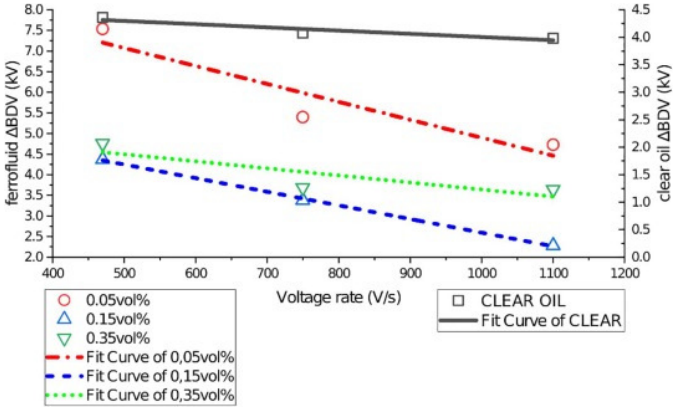

Fig. 5 The effect of the needle electrical polarity on the BDV in magnetic fluids measured at various voltage rise rates. The presented BDV values constitute the difference between the BDV with negative and positive needle

V. Conclusions

In this article we tested influence of electrode polarity on breakdown voltage of alternative insulation fluids. Tests were performed by DC voltage with three voltage rise rates. We tested three concentrations of ferrofluid and pure transformer oil. Ferrofluids were based on transformer oil MOGUL TRAFO CZ-A. After evaluation of measured results we confirmed influence of electrode polarity effect on breakdown voltage for all tested samples. In the case of a negatively charged needle, we measured higher values of breakdown voltage than opposite polarity of the electrodes. We also found that breakdown voltage is influenced by the rates of increase of DC voltage also by the concentration of nanoparticles in fluid. The findings may contribute to theoretical knowledge of breakdown in insulating fluids and, of course, research offers the opening of a more detailed investigation of the dielectric properties of magnetic fluids.

ACKNOWLEDGMENT

This work was supported by the Slovak Academy of Sciences and Ministry of Education in the framework of projects VEGA 2/0141/16, and 1/0340/18, Ministry of Education Agency for structural funds of EU: ITMS 26220220186 and ITMS 26220120055, COST CA15119 NANOUPTAKE, Slovak Research and Development Agency APVV-15-0438, APVV-17-0372 and APVV-18-0160.

REFERENCES

[1] C. Perrier, and A. Beroual, *IEEE Electr. Insul. Mag.* 25, 6–13 (2009). DOI: 10.1109/MEI.2009.5313705.

[2] Š. Hardoň, J. Kúdelčík, P. Bury, and M. Gutten, *Acta Phys. Pol. A* 133, 477–479 (2018). DOI: 10.12693/APhysPolA.133.477.

[3] Š. Hardoň, J. Kúdelčík, E. Jahoda, and M. Kúdelčíková, *Int. J. Thermophys*. 40, 24 (2019). DOI: 10.1007/s10765-019-2486-4.

[4] Wedin, P. *Electrical breakdown in dielectric liquids—A short overview. IEEE Electr. Insul. Mag.* 2014, 30, 20–25. DOI: 10.1109/MEI.2014.6943430.

[5] Devins, J.C. *Breakdown and prebreakdown phenomena in liquids. Jpn. J. Appl. Phys*. 1981, 52, 4531–4543. DOI: 10.1063/1.329327.

[6] Linhjell, D.; Lundgaard, L.; Berg, G. *Streamer propagation under impulse voltage in long point-plane oil gaps*. IEEE Trans. Dielectr. Electr. Insul. 1994, 1, 447–458. DOI: 10.1109/94.300288.

[7] Massala, G.; Lesaint, O. *A comparison of negative and positive streamers in mineral oil at large gaps*. J. Phys. D Appl. Phys. 2001, 34, 1525. DOI: 10.1088/0022-3727/34/10/312.

[8] Liu, Q.;Wang, Z.D. *Streamer characteristic and breakdown in synthetic and natural ester transformer liquids under standard lightning impulse voltage.* IEEE Trans. Dielectr. Electr. Insul. 2011, 18, 285–294. DOI: 10.1109/TDEI.2011.5704520.

[9] Dung, N.V.; Hoidalen, H.K.; Linhjell, D.; Lundgaard, L.E.; Unge, M. *Influence of Impurities and Additives on Positive Streamers in Paraffinic Model Oil*. IEEE Trans. Dielectr. Electr. Insul. 2012, 19, 1593–1603. DOI: 10.1109/TDEI.2012.6311505

[10] Lesaint, O.; Jung, M. *On the relationship between streamer branching and propagation in liquids: Influence of pyrene in cyclohexane*. J. Phys. D Appl. Phys. 2000, 33, 1360. DOI: 10.1088/0022-3727/33/11/315.

[11] I. Fernández, A. Ortiz, F. Delgado, C. Renedo, and S. Pérez, Electr. *Power Syst. Res*. 98, 58–69 (2013). DOI: 10.1016/j.epsr.2013.01.007.

[12] Lue, Y.-F.; Hung, Y.-H.; Li, F.-S.; Teng, T.-P.; Chen, S.-Y.;Wu, C.-H.; Ou, Y.-C. *Performance Assessment and Scooter Verification of Nano-Alumina Engine Oil.* Appl. Sci. 2016, 6, 258.

[13] Abhishek, R.; Hamouda, A.A. *Effect of Various Silica Nanofluids: Reduction of Fines Migrations and Surface Modification of Berea Sandstone*. Appl. Sci. 2017, 7, 1216.

[14] Y.-f Du, Y.-z Lv, F.-c Wang, X.-X. Li, C.-r Li, *Effect of TiO2 nanoparticles on the breakdown strength of transformer oil*, in: Proceedings of the Electrical Insulation (ISEI), Conference Record of the 2010 IEEE International Symposium, 2010, pp. 1–3.

[15] F. O'Sullivan, J.G. Hwang, M. Zahn, O. Hjortstam, L. Pettersson, R. Liu, P. Biller, A model for the initiation and propagation of positive streamers in transformer oil, Conference Record of the 2008 IEEE International Symposium on, 2008, pp. 210–214

[16] J.G. Hwang, M. Zahn, F.M. O'Sullivan, L.A. Pettersson, O. Hjortstam, R. Liu, *Electron scavenging by conductive nanoparticles in oil insulated power transformers*, in: Electronics Joint Conference, Boston 2009.

[17] V. Segal, A. Hjortsberg, A. Rabinovich, D. Nattrass, K. Raj, *AC (60 Hz) and impulse breakdown strength of a colloidal fluid based on transformer oil and magnetite nanoparticles*. In: Proceedings of Electrical Insulation, 1998. Conference Record of the 1998 IEEE International Symposium, 1998, pp. 619–622

[18] P. Bartko, R. Rajnak, R. Cimbala, K. Paulovicova, M. Timko, P. Kopcansky, J. Kurimsky, *Effect of electrical polarity on dielectric breakdown insoft magnetic fluid*, Journal of Magnetism and Magnetic Materials, Volume 497, 2020, DOI: 10.1016/j.jmmm.2019.166007

[19] P. Kopcansky, L. Tomco, K. Marton, M. Koneracká, M. Timko, I. Potočová, *The DC dielectric breakdown strength of magnetic fluids based on transformer oil*, J. Magn. Magn. Mater., 289 (2005), pp. 415-418.

[20] J. Kudelcik, P. Bury, P. Kopcansky, M. Timko, *Dielectric breakdown in mineral oil ITO 100 based magnetic fluid*, Phys. Proced., 9 (2010), pp. 78-81.

[21] M. Rajnak, J. Kurimsky, B. Dolnik, P. Kopcansky, N. Tomasovicova, E. A. Taculescu-Moaca, and M. Timko, Phys. Rev. E 90, (2014) . DOI: 10.1103/PhysRevE.90.032310.

[22] E. O. Forster, H. Yamashita, C. Mazzetti, M. Pompili, L. Caroli, and S. Patrissi, *IEEE Trans. Dielectr. Electr. Insul.* 1, 440–446 (1994). DOI: 10.1109/94.300287.

Dielectric spectroscopy and its use in analyzing changes in the electrophysical structure of insulating materials

[1]*Peter HAVRAN (1st year)*
Supervisor: [2]*Roman CIMBALA*

[1,2]Department of Electric Power Engineering, FEI TU of Košice, Slovak Republic

[1]peter.havran@tuke.sk, [2]roman.cimbala@tuke.sk

***Abstract*—This publication deals with the theoretical description of polarization phenomena and methods of dielectric spectroscopy for analyzing changes in the electrophysical structure of insulating materials. It also points to the direction of research in this field using DC and AC diagnostic methods.**

***Keywords*—dielectric spectroscopy, complex capacity, dissipation factor, polarization current.**

I. Introduction

The electrical equipment insulation system faces various electrical, mechanical, thermal and other degradation factors during its service life. These factors cause a reduction in insulation properties. Moisture, which accelerates the degradation of the insulating material, is also considered a negative product of aging. The available literature suggests that the main cause of electrical equipment failure is the deterioration of the insulating state. Therefore, it is necessary to study the dielectric properties of the insulation in detail to ensure a trouble-free operation of electrical equipment. Current time and frequency domain analyzes of dielectric spectroscopic data are currently being used as tools for a detailed evaluation of the isolation status. Measurement of polarization and depolarization current and IRC (Isothermal relaxation current analysis) is performed over time. In the frequency domain, various parameters such as complex capacity, dissipation factor, and complex permittivity are calculated as a function of frequency. Frequency domain measurement is preferred over time-domain measurement in terms of reliability and efficiency [1].

Dielectric spectroscopy is a modern investigation method that studies the material response at the molecular level at the applied field strength. The electric field intensity response is the electric current in the sample, which is measured as a function of the electric field frequency. Then, the resulting dielectric spectrum provides information on the state and behavior of the material under investigation in frequency ranges that are far from the mechanical analysis [5].

II. Polarization of Dielectrics

Dielectric polarization is a process in which the arrangement of electric charges is changed by applying an external electric field. This process leads to the formation of electrical dipoles in dielectrics [3]. The electric dipole comprises two electric charges having the same size but opposite polarity with a certain distance between them. All-electric dipoles have their electric dipole moment to characterize the magnitude of the electric dipole size [4].

Electric charges move out of their original equilibrium positions by the influence of external and internal force effects of the electric field. The applied electric field causes the induction of dipoles in the substance, which causes the opposite polarity shifts from the previous equilibrium positions. The measure of this process is electrical polarizability, which is a major physical property of dielectrics. The macroscopic parameter of electrical polarizability is the relative permittivity $\mathcal{E}_r$ and the dissipation factor *tan* δ, which shows the losses in dielectrics, the aging of the insulation and its lifetime [13].

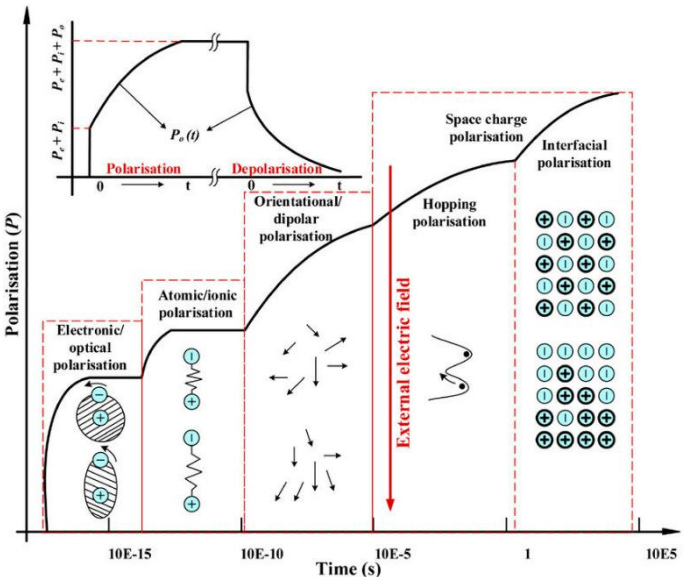

Fig. 1. Polarization types of normal dielectric materials under a step-function electric field [4]

By applying an external electric field, the coupling of bound electric charges is monitored through electric current (for direct measurements) or impedance (for alternating measurements) [14].

III. DIELECTRIC SPECTROSCOPY

Dielectric spectroscopy allows the investigation of dielectric relaxation processes in a wide range of characteristic times of 10^{-12} – 10^{6} s, thus filling a special place among many modern diagnostic methods for physical and chemical analysis of materials. By using dielectric spectroscopy, intermolecular interactions and various events are observed because they combine the properties of the individual components of the complex material [6][19].

The essence of this method is to monitor the response of the electric dipole in the dielectric under the influence of the external electric field. The polarization processes are investigated in both direct and alternating electric fields, therefore dielectric spectroscopy is performed in the frequency and time domain. The frequency domain is characterized by measuring the frequency dependence of the complex impedance of the material. In the time domain, the charging and discharging currents together with the recovered voltage of the capacitors are investigated, where the dielectric function is created by the studied material by applying a DC electric field [7][20].

Successful developments in the time domain and broadband dielectric spectroscopy (Fig. 2) have sharply changed the view of dielectric spectroscopy, which is an effective means of examining solid and liquid substances at the macroscopic and microscopic levels [6].

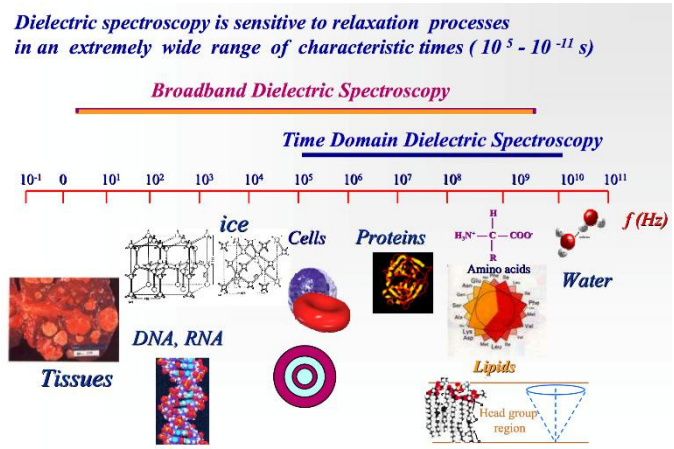

Fig. 2. The frequency band of dielectric spectroscopy [6]

A. Dielectric spectroscopy in the frequency domain

The analytical transformation from the time domain to the frequency domain can be realized using Laplace or Fourier transform [2]. Taking into account the ideal step response for the total current density of the dielectric response function *f(t)* together with the instantaneous polarization processes:

$$j(t) = \sigma_0 E(t) + \mathcal{E}_0 \frac{dE(t)}{dt} + \mathcal{E}_0 \frac{d}{dt}\int_0^t f(t-\tau)E(\tau)d\tau \qquad (1)$$

with

$$j(t) \Rightarrow j(p); E(t) \Rightarrow E(p);\ E'(t) \Rightarrow pE(p); f(t) \Rightarrow F(p);$$

and concerning the convolution of the last term in this equation we get, where *p* is a Laplace operation:

$$j(p) = \sigma_0 E(p) + \mathcal{E}_0 pE(p) + \mathcal{E}_0 pF(p)E(p) \qquad (2)$$

Since *p* is complex frequency $i\omega$, we reduce the equation to

$$j(\omega) = E(\omega)\left[\sigma_0 + i\omega\mathcal{E}_0\left(I + F(\omega)\right)\right] \qquad (3)$$

So $F(\omega)$ is the Fourier Transform of the dielectric response function $f(t)$ or the complex susceptibility:

$$\chi(\omega) = F(\omega) = \chi'(\omega) - i\chi''(\omega) = \int_0^\infty f(t)exp(-i\omega t)dt \qquad (4)$$

It may be noted that the frequency scale is now $0 \leq \omega \leq \infty$. Connections (3) and (4) show the total current density:

$$j(\omega) = \{\sigma_0 + \mathcal{E}_0\omega\chi''(\omega) + i\omega\mathcal{E}_0[1 + \chi'(\omega)]\}E(\omega) \qquad (5)$$

The source of the main part of this current is the complex electrical displacement $D(\omega)$, which corresponds to the complex dielectric permittivity $\mathcal{E}(\omega)$ as follows:

$$D(\omega) = \mathcal{E}_0\mathcal{E}(\omega)E(\omega) \qquad (6)$$

where:

$$\mathcal{E}(\omega) = \mathcal{E}'(\omega) - i\mathcal{E}''(\omega) = \left(1 + \chi'(\omega)\right) - i\chi''(\omega) \qquad (7)$$

It is difficult to make real measurements of this dielectric response in the frequency domain if the frequency range increases. Often only one "*C - tan δ*" measurement is made in the power industry, e.g. at the power frequency. However, sophisticated laboratory measuring instruments can also drive a wide frequency band [11]. It can be noted in formula (5) that such devices cannot discriminate between the benefits of "pure" DC conductivity σ_0 and the dielectric loss $\chi''(\omega)$. This indicates that there is a difference between the measured relative dielectric permittivity $\widetilde{\mathcal{E}_r}(\omega)$ and the relative permittivity $\mathcal{E}(\omega)$ that is in (6) and (7). Subsequently, the relative dielectric permittivity $\mathcal{E}(\omega)$ is measured as follows:

$$j(\omega) = i\omega\mathcal{E}_0\widetilde{\mathcal{E}_r}(\omega)E(\omega) \qquad (8)$$

Therefore:

$$\widetilde{\mathcal{E}_r}(\omega) = \mathcal{E}_r'(\omega) - i\mathcal{E}_r''(\omega) = \mathcal{E}'(\omega) - i[\mathcal{E}''(\omega) + \sigma_0/\mathcal{E}_0\omega] = 1 + \chi'(\omega) - i[\chi''(\omega) + \sigma_0/\mathcal{E}_0\omega] \qquad (9)$$

and the dielectric dissipation factor, $tan\,\delta(\omega)$,

$$tan\,\delta\,(\omega) = \frac{\mathcal{E}_r''(\omega)}{\mathcal{E}_r'(\omega)} = \frac{\mathcal{E}''(\omega)+\sigma_0/\mathcal{E}_0\omega}{\mathcal{E}_r'(\omega)} \qquad (10)$$

The real part (9) is the capacity of the test object (samples), and the imaginary part represents the losses. Both are frequency-dependent [9][10]. This does not apply if the measurement "*C - tan δ*" is only performed at one frequency. In quite different frequency ranges, aging processes will change these parameters, and new diagnostic tools will allow these changes to be monitored and investigated [12].

The relation between frequency and time domain is hidden in equation (4), where real and imaginary parts of complex susceptibility $\chi(\omega)$ can be converted to the function of dielectric response $f(t)$ and vice versa. In practice, only the measurement results will be available for each conversion, notwithstanding that both domains have expanded from zero to infinity. However, the possible conversion procedures are

not described in detail here, but some information may appear at the end of this article [9][15].

However, it should be understood that all-dielectric quantities are more or less temperature-dependent. This must be taken into account in any examination, comparison or measurement of these quantities [18].

The measurement in the frequency domain can be realized e.g. IDAX-300 (Fig. 3), where the meter system applies an alternating voltage to a sample of insulating material at a certain frequency. This voltage creates a current in the sample. By accurately measuring voltage and current, it is possible to calculate the total impedance, from which the capacitance and dissipation factor are further expressed.

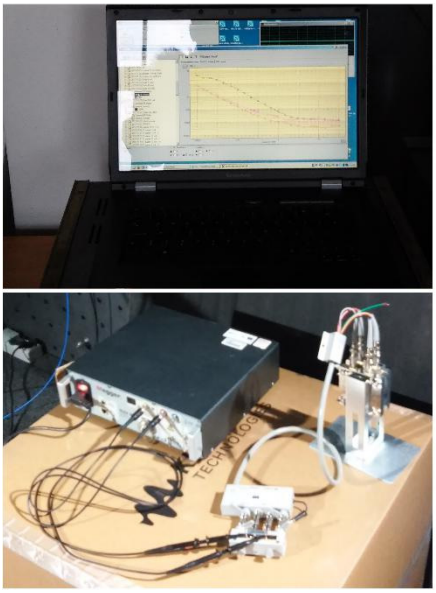

Fig. 3. Frequency domain measurement in practice

B. Dielectric spectroscopy in the time domain

Indirect observation of polarization of polarized or polarizable materials by a certain response to a certain change in the applied voltage pulse is the essence of the dielectric spectroscopy method. The time domain is focused on examining the polarizing (charging) and depolarizing (discharging) current flowing through the insulating material at the applied DC voltage, or in other words during the voltage step change, the course of the dielectric current is recorded [8].

The total dielectric polarization during charging (or discharging) and its time dependence is characterized by response function ϕ_t :

$$P(t) = \varepsilon_0(\varepsilon_\infty - 1)E + \varepsilon_0(\varepsilon_S - \varepsilon_\infty)E\phi(t) \quad (11)$$

where $\varepsilon_0 = 8{,}854 \cdot 10^{-12}$ F·m^{-1} is the permittivity of the vacuum, ε_∞ is the optical permittivity (relative permittivity at frequency $f(\varepsilon_\infty) \rightarrow 10^{14}$ Hz), ε_S represents the static permitivity, E denotes the electric field intensity and t is the time. The relationship between the charge/discharge currents time and polarization time dependence is explained in the following. The charge and discharge currents in the dielectric have exponentially increased and decreasing characteristics in the time zone. These facts are described in the case of a vacuum capacitor by exponential time functions. Using the function of decrease $\varphi(t)$ is described as the time dependence of the depolarization current density j_{depol} in dielectric:

$$j_{depol} = \varepsilon_0(\varepsilon_S - \varepsilon_\infty)E\varphi(t) \quad (12)$$

The sum of the two components describes the charge current (polarization) current density:

$$j_{pol}(t) = \frac{dP}{dt} + \gamma E \quad (13)$$

where γE is the conductivity in the dielectric (where γ is the specific electrical conductivity of the dielectric after applying DC voltage and subsequent dielectric charge dissipation). The density of the discharging (depolarizing) current has a conductive component of the current and therefore it is possible to write:

$$j_{depol}(t) = \frac{dP}{dt} \quad (14)$$

In Fig. 4 is a circuit diagram of an insulating system over time, followed by a response of the electrical current upon connection (charging current) and after disconnection of the electrical voltage (discharge current) [16].

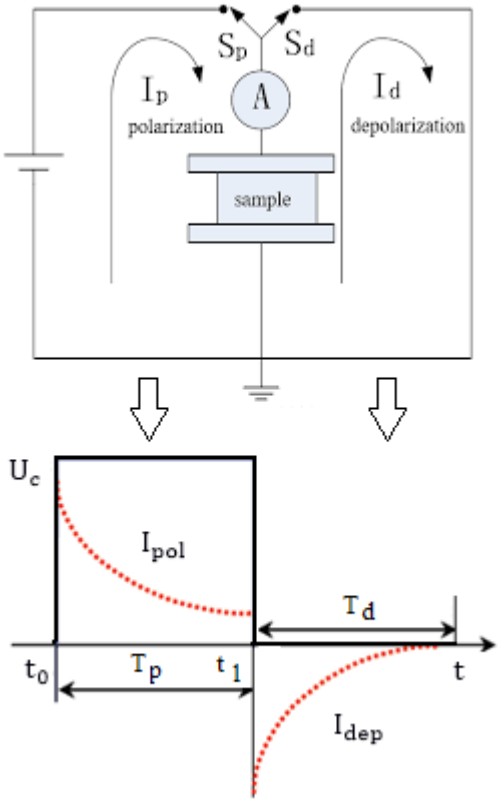

Fig. 4. The current response to the applied voltage pulse [16]

Dielectric relaxation mechanisms can be identified by studying dielectric spectra that correspond to the polarization mechanisms. The occurrence of different types of electrical dipoles, ions, or electrons tending to effect different movements due to the external electric field is detectable in such materials, causing an increase in the number of time-relaxation mechanisms [17].

The time domain measurement can be performed e.g. KEITHLEY 6517B (Fig. 5), where the meter system applies a DC voltage to a sample of insulating material at a certain charging time to measure the charging and discharging currents as a function of time.

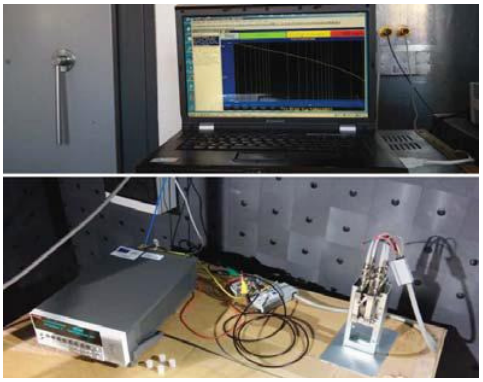

Fig. 5. Measurement in the time domain in practice

IV. Conclusion

My dissertation aims to measure, investigate and compare the behavior of dielectric parameters (at the level of polarization and conductivity processes) of selected insulating materials using the non-destructive method of dielectric respectively impedance spectroscopy.

Non-destructive dielectric spectroscopy methods, namely frequency domain dielectric spectroscopy and time domain dielectric spectroscopy, the nature of which is described in Chapter III, will be used for all investigated experiments. In the frequency domain, dielectric parameters such as complex impedance, complex permittivity and other derived parameters such as series-parallel capacitance, series-parallel resistance and dissipation factor will be measured and compared. In the time domain, the charging currents will be examined as a function of time.

The work will focus on the investigation of conventional transformer oils compared to the new Shell DIALA S4 ZX-1 insulating oil, their thermal characteristics when investigating insulation properties, the insulation properties at real operating temperatures of XLPE cables and the thermal characteristics of polypropylene film insulated capacitors, which in the near future are in demand as components in electric vehicles.

Acknowledgment

This work was supported by structural funds of EU in the frame of projects ITMS 313011T565, and Ministry of Education Agency for VEGA 1/0340/18, 2/0141/16 and APVV 15-0438, 17-0372, 18-0160.

References

[1] R. Cimbala, P. Semančík, "Tepelná degradácia kvapalných izolačných materiálov (Thermal degradation of liquid insulating materials)," Technical University of Košice, Letná 9, Košice. 2016, 147 p., ISBN 978-80-553-2545.

[2] J. Kudelcik, S. Hardon, L. Varacka, "Measurement of Complex Permittivity of Oil-Based Ferrofluid in Magnetic Field," Acta Physica Polonica A, Volume: 131, Issue: 4, pp. 931-933.

[3] A. Mikkelsen, J. Wojciechowski, M. Rajňák, J. Kurimský, K. Khobaib, A. Kertmen, Z. Rozynek, "Electric Field-Driven Assembly of Sulfonated Polystyrene Microspheres," Materials. 10 (2017) 329.

[4] Y. Feldman. Department of Applied Physics. The Physics Of Dielectrics 83887. Lecture 1. The Hebrew University of Jerusalem. Online: <http://aph.huji.ac.il/courses/2008_9/83887/index.html>.

[5] J. Kurimský, M. Fol'ta, Z. Čonka, S. Bucko: „Investigation of effects of non-ionizing electromagnetic fields interacting with biological systems"; In: 8th International Scientific Symposium on Electrical Power Engineering (ELEKTROENERGETIKA 2015) Pages: 564-567

[6] Y. Feldman, "Broad Band Dielectric spectroscopy in Time and Frequency Domain," The Hebrew University of Jerusalem, Online: < http://aph.huji.ac.il/people/Feldman/research.htm#>.

[7] J. Zbojovský, L. Kruželák, M. Pavlík, "Impedance Spectroscopy of Liquid Insulating Materials," 2018. In: Proceedings IEEE International Conference AND Workshop in Óbuda on Electrical and Power Engineering, s. 249-253 [USB-key]. - ISBN 978-1-7281-1153-7.

[8] B. A. Dhande, P. S. Swami, A. G. Thosar, "Analysis of Transformer Insulation Parameters Using Polarization and Depolarization Current Method and Frequency Domain Spectroscopy," INTERNATIONAL JOURNAL OF SCIENTIFIC & TECHNOLOGY RESEARCH, vol. 8, issue 09, 2019.

[9] I. Fofana, et al., "On the Frequency Domain Dielectric Response of Oil-paper Insulation at Low Temperatures," IEEE Transactions on Dielectrics and Electrical Insulation, vol. 17, no. 3, 2010.

[10] Y. Zhang, et al., "Feasibility of a Universal Approach for Temperature Correction in Frequency Domain Spectroscopy of Transformer Insulation," IEEE Transaction on Dielectrics and Electrical Insulation, vol. 25, no. 5, 2018.

[11] M. Malviya, H. C. Verma, A. Baral, S. Chakravorti, "Development of a Low Cost Portable Frequency Domain Spectroscopy Data Measurement Module for Oil-paper Insulation," 7th International Conference on Power Systems, 978-1-5386-1789-2/17, 2017.

[12] A. K. Pradhan, B. Chatterjee, S. Chakravorti, "Estimation of Paper Moisture Content based on Dielectric Dissipation Factor of Oil-paper Insulation under Non-Sinusoidal Excitations," IEEE Transaction on Dielectrics and Electrical Insulation, vol. 22, no. 2, 2015.

[13] X. Xu, T. Bengtsson, J. Blennow, S. M. Gubanski, "Arbitrary Waveform Impedance Spectroscopy for Accurate Contact-free Dielectric Characterization," International Conference on High Voltage Engineering and Application, 978-1-4673-4746-4/12, 2012.

[14] M. Váry, J. Packa, V. Ďurman, J. Lelák, V. Šály, "Polarization in cables with Current Load," Institute of Power and Applied Electrical Engineering, 978-1-5386-4612-0/18, 2018.

[15] A. K. Pradhan, B. Chatterjee, S. Chakravorti, "Estimation of Dielectric Dissipation Factor of Cellulosic Parts in Oil-paper Insulation by Frequency Domain Spectroscopy," IEEE Transaction on Dielectrics and Electrical Insulation, vol. 23, no. 5, 2016.

[16] S. K. Ojha, P. Purkait, S. Chakravorti, "Cole-Cole Representation of Transformer Oil-Paper Insulation Dielectric Response," 3rd International Conference on Condition Assessment Techniques in Electrical Systems, 978-1-5386-3138-6/17, 2017.

[17] Ch. Suo, Y. Sun, Z. Li, Y. Han, "Application of L1 Trend Filtering Technology on the Current Time Domain Spectroscopy of Dielectrics," DOI: 10.3390/electronics8091046, 2019.

[18] R. Färber, C. M. Franck, A. Nasef, "Online Dielectric Response Analysis Under Mixed-Frequency Medium-Voltage Stress," 21th International Symposium on High Voltage Engineering, 2020.

[19] H. Zhao, J. Tian, D. Zhang, X. Liu, "Research on Dielectric Properties about Different Curing Degree of Epoxy Glass Fiber," Condition Monitoring and Diagnostic, 2018.

[20] S. Chatterjee, S. Chakravorti, S. Dalai, B. Chatterjee, "Use of chirp excitations of frequency domain spectroscopy measurement of oil-paper insulation," IEEE Transactions on Dielectric and Electrical Insulation, vol. 25, no. 3, 2018.

Dynamic Emulation of Mechanical Loads - Overview

[1] *Jozef Ivan (1st year)*
Supervisor: [2]František Ďurovský

[1,2]Dept. of Electrical Engineering and Mechatronics, FEI TU of Košice, Slovak Republic

[1]jozef.ivan@tuke.sk, [2]frantisek.durovsky@tuke.sk

***Abstract*—This paper point out the problem of the emulation of mechanical loads (EML). In recent years there were published several articles discussing this problem with the impressive results. This article mentions the most used techniques of emulation and some types of loads that can be emulated. The paper should serve as a brief introduction to the EML.**

***Keywords*— Drive control, dynamic emulation, dynamometer, load emulation,**

I. Introduction

In modern companies, there is a constant request for shortening the period of time of the processes connected with the production, where every delay is costly. Also, in the stage of development and testing, it's desired to test and evaluate every possible issue that can encounter in the future process. In such cases, it's suitable to imitate a specific type of load which will be affecting the shaft of an electric machine in operating conditions.

As it would be very difficult and costly to equip the laboratory with all the equipment to simulate all kinds of mechanical load, simulating with a dynamometer is a satisfactory alternative. The conventional dynamometer is a device that can deliver a particular steady-state torque-speed relationship and is often equipped with devices for measuring the position and speed of the shaft. Mostly we use the second electric motor as a dynamometer, which is bounded to a tested motor with a shaft.

The dynamometer has been mostly used to perform a static load test of electrical machines in the past [1]. The current need for the industry is to simulate a wide range of torque behavior. Thus, a dynamometer in which mechanical parameters can be programmed or varied is used. This type of dynamometer is called an Emulator.

The basic structure of the emulator was shown in Fig. *1* where the system consists of a load machine and a drive machine connected with a common shaft. Drive machine produces torque T_e and dynamometer produces required torque T_L. The ω_r and φ_r are real speed and position common for both motors.

With an emulator, we can test a large variety of mechanical loads such as constant step, linear or quadratic incrementation or their various combinations. Another example of exploitation of this system is the verification testing of high precision gears and scalers. It allows replacing currently used loading arms and burdens. In conclusion, it allows complex dynamic systems to be emulated in a cost-effective, safe and repeatable way and it enables off-site testing and developing of control algorithms in laboratory conditions.

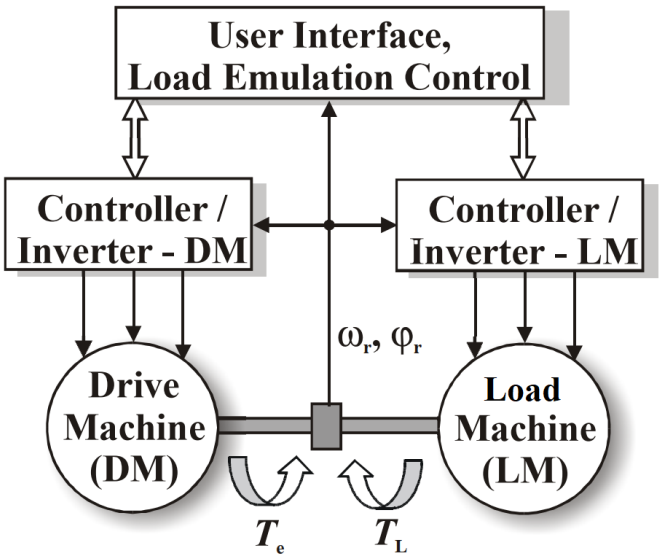

Fig. 1 Basic structure of emulation system [4]

It's possible to use any type of electric motor as a load motor. In [2] induction machine has been used as a load and also as a tested machine. In order to achieve the best performance, we need a motor with good speed-torque characteristics. Synchronous motor with permanent magnets (SMPM) is widely used in many demanding applications because of his good dynamic abilities and with the possibility of overloading. With this type of motor as a loading motor, we can emulate complicated types of dynamic loads. Thus it's a suitable option to use it as a load motor like in [6].

II. Techniques used for emulation

Since the first attempts to emulate a load, there have been invented strategies on how to achieve this goal. Every individual approach differs in used regulation structure. In [7], the open-loop structure was used, but in [2][4] the closed-loop structure was implemented. Other differences are an approach to neglecting of the mechanical friction of the system and bandwidth of the load that can be emulated.

The most basic approach was to use a simple dynamometer. They have mostly been used to perform static load tests of electrical machines. Another method was based on programming mechanical parameters of the dynamometer load with varying speed or position in order to simulate torque-speed characteristics. Although this static emulation is a sufficient

option for testing prime motor under steady-state or slowly changing conditions, it's not suitable for applications with transient and high dynamic behavior [5].

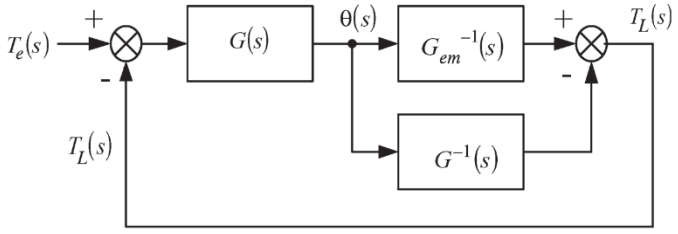

Fig. 2 Structure of IMD approach [3]

In [7], the effort was to imitate dynamic loads was based on the principle of the inverse mechanical dynamics (IMD). In this approach, it's required to measure the shaft speed or position which is then used to derive the torque for the dynamometer to achieve desired dynamics.

The basic principle of the IMD approach is presented in Fig. 2. The *G(s)* represents the dynamics of the testing Drive Machine – Load Machine (DM-LM) mechanism. The $G_{em}(s)$ represents the dynamics of the emulated load. The real position of the shaft is represented by θ. T_e is the applied electrical torque of the drive machine and the T_L is the applied load torque of the load machine. The open-loop transfer function of the DM-LM is presented in (1).

$$\frac{\theta(s)}{T_e(s)} = \frac{1}{Js^2 + Bs} = G(s) \tag{1}$$

J is inertia and *B* is the viscous friction coefficient of the DM-LM mechanism. Both these parameters correspond to the nominal parameters of the rig [3].

$$\frac{\theta(s)}{T_e(s)} = \frac{1}{J_{em}s^2 + B_{em}s} = G_{em}(s) \tag{2}$$

The transfer function of the desired dynamics can be represented by (2), where subscript *em* corresponds to emulated inertia and friction. The main objective is to design a control structure so that the relationship between the position θ and electrical driving torque T_e reaches the dynamics of $G_{em}(s)$ [3].

However, such a method has many disadvantages. In some cases, it's hard or even impossible to design an inverse dynamic model. This approach is effective in the continuous-time system but with the usage of computing technology such as PLC or DSP, sampling effects have to be considered. Due to the derivative terms in the transfer function, the output of the system can be very noisy in digital form and the emulation can become unstable. With using a digital filter on the output signal T_L we can achieve acceptable results with open-loop structure but the pole-zero structure is violated. Thus if this emulation would be used in the closed-loop structure, responses would be erroneous [2][4].

In many cases, this technique is not suitable for practical use, therefore, the new procedures had to be developed. A new approach was presented in [2][3], where the emulation is based on a speed-tracking control with the implicit feedforward of the inverse dynamics and compensation for the closed-loop tracking control dynamics. This type of emulation preserves the dynamics of the testing mechanism and can be discretized without affecting the zero-pole structure. The basic structure of EML with the feedforward dynamics can be observed in Fig. 3.

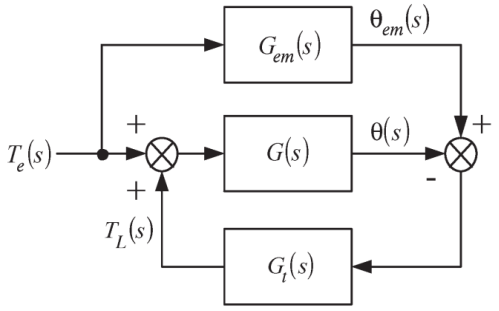

Fig. 3 EML using feedforward dynamics [3]

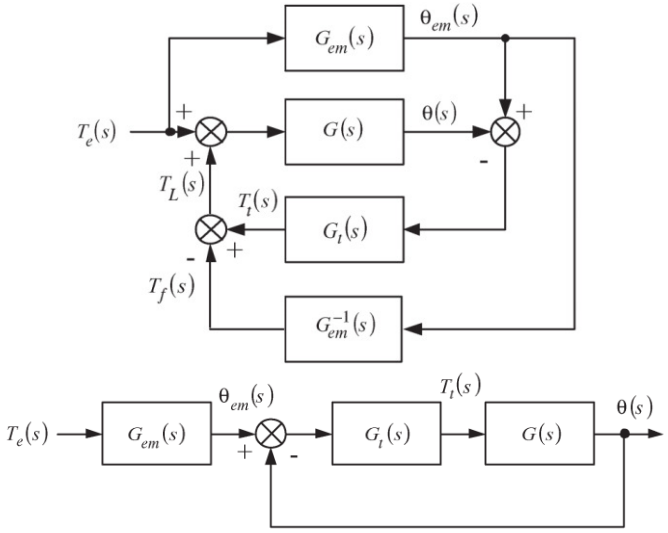

Fig. 4 EMD with feed-forward torque compensation with position tracking before and after Gem-1 cancelation

In this type of structure, the motor-drive torque T_e is fed to $G_{em}(s)$ outputting the desired position θ_{em}. This position is a demand for a position-tracking loop with the controller $G_t(s)$ which yields motor-load torque T_L. With reference to [3], the final relation between T_e and $\theta(s)$ is shown in (3) and $G_{comp}(s)$ is represented in (4).

$$\frac{\theta(s)}{T_e(s)} = G_{comp}(s)G_{em}(s)G_{comp}^{-1}(s) = G_{em}(s) \tag{3}$$

$$G_{comp}(s) = \frac{G_t(s) + (1/G_{em}(s))}{G_t(s) + (1/G(s))} \tag{4}$$

$$\frac{\theta(s)}{T_e(s)} = G_{em}(s)\frac{G(s)G_t(s)}{1 + G(s)G_t(s)} = G_{em}(s)G_{comp}^{-1}(s) \tag{5}$$

In the ideal case, $G_{comp}(s)$ should include only parameters of the real system in order to be independent of the emulation parameters. Thus according to [3], the new transfer function should be represented by (5) where $G_{comp}(s)$ is no longer a function of $G_{em}(s)$. The upgraded block scheme of the approach

is shown in Fig. 4. $G_{em}(s)$ is creating position demand θ_{em} that is compared with the real position of the shaft θ. After forward and inverse dynamics in the feed-forward path cancels each other, G_{em}^{-1} won't be implemented anymore and the scheme cancels T_e. The desired position θ_{em} is fed into the system via the load-machine feedback loop as shown in Fig. 4. The tracking controller can be PD, lead, or P controller [3].

This method presented very satisfactory results comparing simulation responses from ideal models with experimental data from the testing rig.

Nevertheless [4], refers that in this measurement the dynamic of the linear feedback controller was included in compensator, which can cause undesirable behavior such as time delays. This issue can occur in case the dynamics of the testing rig would be nonlinear.

Thus in [4], a new approach was presented. The author uses the inverse dynamics of the testing rig with input values of speed and acceleration calculated from a numerical model of the emulated system, combined with the feedback controller. This structure is modified structure from [2][3] and it presents a number of improvements such as the possibility to investigate the unmodelled dynamics of drive rig, using the emulation method and possibility to adjust criteria for selecting the bandwidth of the speed-tracking controller. Another advantage is that the feedforward structure allows compensation of the nonlinear friction effects for improving the performance of the structure, especially at low speed. Estimated values of the applied torque can be obtained by measurement of real load or by the suitable observer. In [5] the classical current model observer was implemented.

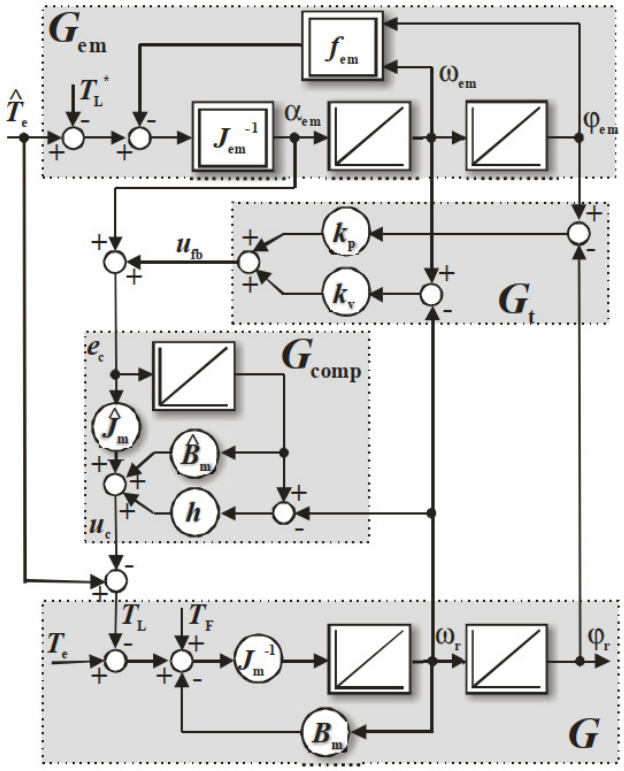

Fig. 5 EMDL approach using feedback with PI controller [5]

The structure of the approach using feedback with the PI controller is presented in Fig. 5. G presents a DM-LM mechanism, G_{em} emulated load model, G_{comp} the compensator and e_c represent compensator input. The electrical torque of the drive machine is denoted by T_e, load torque applied by load machine T_L, compensator output u_c. α_{em} is the acceleration of the emulated system, J_m is inertia and B_m is viscous friction of the DM-LM mechanism, J_{em} is inertia and B_{em} viscous friction of the emulated system. f_{em} presents the emulated model friction as well as impacts of any other contribution of the load like gravity, centrifugal forces, etc. T_L^* is an additional torque input applied to the emulated model, φ_{em} is the emulated mechanism position and ω_{em} emulated mechanism speed. T_F refers to the input of the unmodeled dynamics torque estimation error of the LM-DM mechanism. G_t is an additional feedback controller with output u_{fb} which is the compensation of unmodeled dynamics, parameter variations, and numerical errors and h which is the gain of this controller. Also, the estimated values are denoted by $\hat{}$ and the desired values are denoted by ^{d} [5].

III. Modeling the Specific Types of Emulations

After deciding which emulation approach is suitable for application there is a question on how to emulate a specific type of the desired load for testing. In recent years there has been a lot of paper published about this problem:

- Emulation of the wind turbine [9]
- Emulation of the vehicle brake system [10]
- Emulation of the mechanical impact during mining [11]
- Emulation of the elevator [12]
- Emulation of the tracked vehicle [13]

IV. Conclusion

In the field of the emulation of the mechanical loads, there are some open problems. The current approaches are investigated only with transfer functions, so the state-space representation approach would be advisable.

The performance of the emulator can be degraded if the emulator is implemented into the various systems, where different sampling times are used. Thus is desirable to use the discrete description to analyze this problem. Another problem is to examine the impact of the friction and find the options to eliminate it.

Also, there is a need to examine which specific types of load can be emulated by emulation approaches mentioned in this paper and their bandwidth.

The main problem is that the validation of the experimental results is made only by comparing it to a not accurate model. Comparing these results to the measured data from the real load would be more sufficient. This type of approach would make high requirements for laboratory equipment. Experimental results with such comparison have not been published yet.

References

[1] NEWTON, Robert Wendel; BETZ, Robert E.; PENFOLD, H. Bruce. Emulating dynamic load characteristics using a dynamic dynamometer. In: *Proceedings of 1995 International Conference on Power Electronics and Drive Systems. PEDS 95*. IEEE, 1995. p. 465-470.

[2] AKPOLAT, Z. Hakan; ASHER, Greg M.; CLARE, Jon C. Dynamic emulation of mechanical loads using a vector-controlled induction motor-generator set. *IEEE Transactions on industrial electronics*, 1999, 46.2: 370-379.

[3] ARELLANO-PADILLA, Jesus; ASHER, Greg M.; SUMNER, Mark. Control of an AC dynamometer for dynamic emulation of mechanical loads with stiff and flexible shafts. *IEEE Transactions on Industrial Electronics*, 2006, 53.4: 1250-1260.

[4] RODIČ, Miran; JEZERNIK, Karel; TRLEP, Mladen. Dynamic emulation of mechanical loads: an advanced approach. *IEE Proceedings-Electric Power Applications*, 2006, 153.2: 159-166.

[5] Rodič, Miran, Karel Jezernik, and Mladen Trlep. "Dynamic emulation of mechanical loads—position control approach." *Proceedings of 14th International Power Electronics and Motion Control Conference EPE-PEMC 2010*. IEEE, 2010.

[6] SUCHÝ, Ľuboš, KYSLAN, Karol, FERKOVÁ, Želmíra, ĎUROVSKÝ František, et al. Dynamic emulation of mechanical loads—Analysis and implementation into industrial drive. In: *2016 ELEKTRO*. IEEE, 2016. p. 238-242.

[7] SANDHOLDT, Per, et al. A dynamometer performing dynamical emulation of loads with nonlinear friction. In: *Proceedings of IEEE International Symposium on Industrial Electronics*. IEEE, 1996. p. 873-878.

[8] RODIC, Miran; JEZERNIK, Karel; TRLEP, Mladen. Use of dynamic emulation of mechanical loads in the testing of electrical vehicle driveline control algorithms. In: *2007 European Conference on Power Electronics and Applications*. IEEE, 2007. p. 1-10.

[9] DAMIAN, Iñaki Erazo; IACCHETTI, Matteo; APSLEY, Judith. Emulation of prime movers in wind turbine and diesel generator systems for laboratory use. In: *2019 21st European Conference on Power Electronics and Applications (EPE'19 ECCE Europe)*. IEEE, 2019. p. P. 1-P. 10.

[10] ZHANG, Zhongshi, et al. Study on requirements for load emulation of the vehicle with an electric braking system. *IEEE Transactions on Vehicular Technology*, 2017, 66.11: 9638-9653.

[11] BETZ, Robert Eric; MIRZAEVA, Galina; SUMMERS, Terrence J. A Dynamic dynamometer for testing of mining DC motors. In: *2010 IEEE Industry Applications Society Annual Meeting*. IEEE, 2010. p. 1-8.

[12] SAARAKKALA, Seppo, et al. Dynamic emulation of multi-mass mechanical loads in electric drives. In: *Proceedings of the 2011 14th European Conference on Power Electronics and Applications*. IEEE, 2011. p. 1-10.

[13] WANG, Zhe, et al. Design and modeling of a test bench for dual-motor electric drive tracked vehicles based on a dynamic load emulation method. *Sensors*, 2018, 18.7: 1993.

Dynamic Thermal Rating of Overhead Power Line Conductors

Anastázia MARGITOVÁ (3rd year)
Supervisor: Michal KOLCUN

Dept. of Electric Power Engineering, FEI TU of Košice, Slovak Republic

anastazia.margitova@tuke.sk, michal.kolcun@tuke.sk

***Abstract*—An overhead power line is a structure used in the electric power system to transmit electrical energy. The performance of overhead power lines depends on their parameters. An important parameter of the power line in the power system is its thermal limit. This article is focused on the research of steady-state and transient dynamic thermal rating (ampacity) of overhead power line ACSR conductors. This article deals with the thermal behavior of overhead power line conductors taking into account variations in weather conditions or current with time according to CIGRE Technical Brochure 601.**

***Keywords*—overhead power line, ACSR conductor, CIGRE Technical Brochure 601, dynamic thermal rating, ampacity.**

I. Introduction

One of the most important factors that affect power line operation, is the temperature of conductors [1]. If the heat generated by the current flowing exceeds the thermal limit, the conductor will be irreversibly damaged. To avoid power line conductors thermal damage, it is necessary to determine the maximum current that can flow through conductors [2]. Ampacity is the main parameter of the overhead power line design and operation, this value is the maximum amount of electrical current, that can flow through the power line (or conductor) without disturbing its mechanical and electrical properties [3]. Ampacity is determined by mechanical and electrical properties of the conductor, the ability of heat generation within a conductor and ambient conditions [4].

In some transmission power systems, different fixed and weather independent ampacity limits are used for the summer and winter seasons. The set current limits for the summer and winter seasons represent much lower values than the current values that can be loaded to power lines under the actual weather conditions [4]. Dynamic thermal rating (DTR) of transmission lines provides the actual ampacity of overhead lines based on real-time operating (weather/atmospheric) conditions. The main aim of DTR is to increase the ampacity of existing transmission lines, mitigate transmission line congestion, facilitate wind energy integration, enable economic benefits, and improve the reliability performance of power systems [5].

Several industrial standards deal with the calculation of the temperature and ampacity of overhead power line conductors. The most commonly used methods are described in the IEEE Standard for calculating the current-temperature relationship of bare overhead conductors [6], CIGRE Technical Brochure (TB) 207 [7] (2002) and its extended version CIGRE Technical Brochure (TB) 601 [8] (2014). According to Neil Schmidt [9], these methods provide similar results and they can be considered equivalent.

II. Thermal Balance Equations of Overhead Power Lines Calculation Methods

The thermal behavior of overhead power line conductors is based on the thermal balance between the gained and lost heat in the conductor due to the current load and environmental conditions [10]. There are two ways how to calculate the conductor temperature or dynamic thermal rating of overhead power lines [11].

Firstly, the basic thermal balance equation (model) used in steady-state conditions is represented by the quantities/powers on the left side causing the heating of the conductor. The right part of the equation is characterized by quantities/powers causing the cooling of the conductor [8], [12]:

$$P_j + P_s + P_m = P_c + P_r, \quad (1)$$

where

- P_j is the heating of the conductor by the current flowing (Joule heating, W/m),
- P_s is the heating of the conductor by the sunlight (solar heating, W/m),
- P_m is the heating of the conductor by the magnetic effect (magnetic heating, W/m),
- P_c is the cooling of the conductor by the convection (convective cooling, natural and forced convection, W/m),
- P_r is the cooling of the conductor by the radiation (radiative cooling, W/m).

Secondly, if the thermal inertia of the conductor is considered (both ambient conditions and the current load of the power line vary with time), the following transient thermal balance equation (model) is used [11]:

$$mc\frac{dT_s}{dt} = P_j + P_s + P_m - P_c - P_r, \quad (2)$$

where

- m is the mass per unit length of the conductor (kg/m),
- c is the specific heat capacity of the conductor (J/(kg·K)),
- dT_s/dt is the conductor temperature time change (°C).

Based on thermal balance equations (1) and (2) two problems can be solved using the steady-state or transient thermal model [12]:

- Calculation of the conductor temperature when the electrical current is known.
- Calculation of the current (steady-state and transient DTR) that yields a given maximum allowable conductor temperature.

III. Comparison of the Temperature Calculated by CIGRE TB 601 with Real Temperature Measurement on ACSR Conductors under Laboratory Conditions

Several temperature measurements were performed for two ACSR conductors (352-AL1/59-ST1A, 429-AL1/52-ST1A). Technical parameters of these ACSR conductors are shown in [12]. Temperature measurements were carried out in a laboratory using simulation without and with the presence of wind (speed 2 m/s at a 90° angle of attack). Ambient temperature was recorded at these measurements, assuming height above sea level of 208 m, intensity of solar radiation of 0 W/m^2. Measurements were carried out from the ambient conductor temperature to the steady-state conductor temperature at different steady-state RMS values of the current flowing through the conductor. One of these measurements for the conductor 352-AL1/59-ST1A and current of 600 A is shown in Fig. 1. In the first step, the conductor temperature was determined without considering the influence of wind. In the second step, the presence of wind was simulated for the same conductor and approximately the same current value [12].

Fig. 2 and Fig. 3 show temperature dependencies on the RMS current flowing through the conductor 352-AL1/59-ST1A at wind speed 0 m/s or 2 m/s, and intensity of solar radiation 0 W/m^2 (calculated according to TB 601 and TB 207). Fig. 2 and Fig. 3 also show the actual measured current and temperature values of the analyzed conductor. Differences between measured and calculated temperature values were also caused by considering only one (average) ambient temperature value (23 °C for no-wind simulation, 24 °C for considering wind influence). Temperature calculation according to TB 207 and TB 601 does not differ too much. The basic equations in these standards (TB) are the same, but TB 601 considers more precise equations for some of the variables needed to calculate the conductor temperature (see [12]).

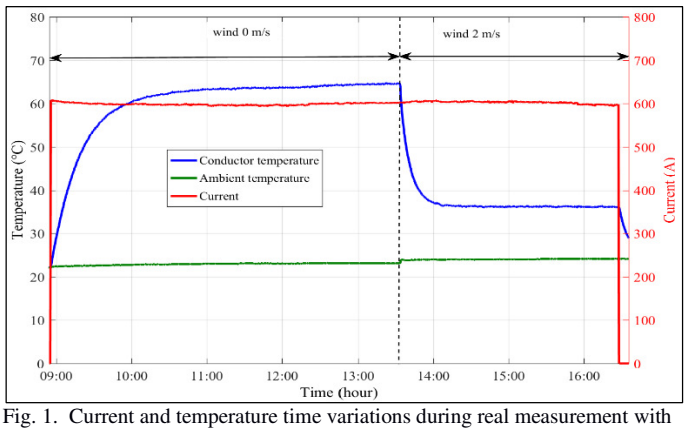

Fig. 1. Current and temperature time variations during real measurement with the conductor 352-AL1/59-ST1A [12].

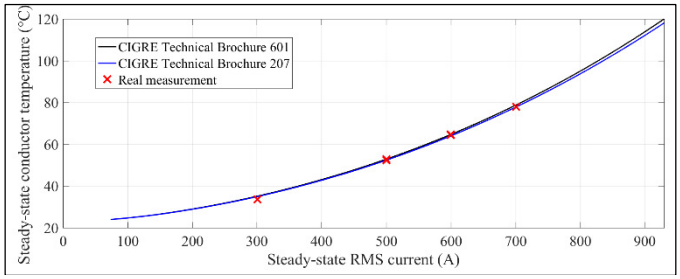

Fig. 2. Steady-state temperature dependence on the RMS current flowing through the conductor 352-AL1/59-ST1A at a wind speed 0 m/s, intensity of solar radiation 0 W/m^2, ambient temperature 23 °C [12].

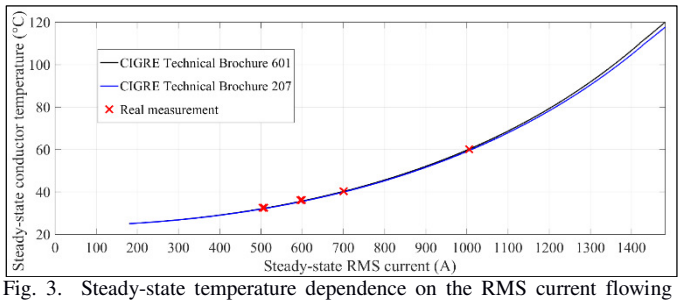

Fig. 3. Steady-state temperature dependence on the RMS current flowing through the conductor 352-AL1/59-ST1A at a wind speed 2 m/s (90° angle of attack), intensity of solar radiation 0 W/m^2, ambient temperature 24 °C [12].

IV. Conclusion

The mathematical description of the impact of climatic conditions on power line conductors (temperature/DTR) is stated in CIGRE TB 601. The main objective of recent research mentioned in this article was to analyze this standard (TB 601) and to determine the conductor steady-state DTR, taking into account actual climatic conditions. The main aim of future research is to examine the transient DTR of overhead power line conductors.

Acknowledgment

This work was supported by the Ministry of Education, Science, Research and Sport of the Slovak Republic and the Slovak Academy of Sciences under the contract No. VEGA 1/0372/18.

References

[1] S. Beryozkina, A. Sauhats, and E. Vanzovichs, "Climate conditions impact on the permissible load current of the transmission line," in *Proceedings of the IEEE Trondheim PowerTech*, Trondheim, Norway, 2011, pp. 1–6.

[2] Z. Yan, Y. Wang, and L. Liang, "Analysis on ampacity of overhead transmission lines being operated," in *Journal of Information Processing Systems*, vol. 13, 2017, pp. 1358–1371.

[3] J. Šnajdr, J. Sedláček, and Z. Vostracký, "Application of a line ampacity model and its use in transmission lines operations," In *Journal of Electrical Engineering*, vol. 65, 2014, pp. 221–227.

[4] M. Kanálik, A. Margitová, J. Urbanský, and Ľ. Beňa, „Temperature calculation of overhead power line conductors according to the CIGRE technical brochure 207," In *Proceedings of the 20th International Scientific Conference on Electric Power Engineering (EPE)*, Kouty nad Desnou, Czech Republic, 2019, pp. 24–8.

[5] S. Karimi, P. Musilek, and A. M. Knight, "Dynamic thermal rating of transmission lines: a review," in *Renewable and Sustainable Energy Reviews*, vol. 91, 2018, pp. 600–612.

[6] IEEE Standard for calculating the current-temperature relationship of bare overhead conductors, IEEE Std 738, 2012.

[7] CIGRE, Working Group 22.12, Thermal behaviour of overhead conductors, Technical Brochure 207, 2002.

[8] CIGRE, Working Group B2.43, Guide for thermal rating calculation of overhead lines, Technical Brochure 601, 2014.

[9] N. Schmidt, "Comparison between IEEE and CIGRE ampacity standards," In *IEEE Transactions on Power Delivery*, vol. 14, 1999, pp. 1555–1559.

[10] A. A. P. Silva and J. M. B. Bezerra, "Applicability and limitations of ampacity models for HTLS conductors," in *Electric Power Systems Research*, vol. 93, 2012, pp. 61–66.

[11] A. Arroyo, et al., "Comparison between IEEE and CIGRE thermal behaviour standards and measured temperature on a 132-kV overhead power line," In *Energies*, vol. 8, 2015, pp. 13660–13671.

[12] M. Kanálik, A. Margitová, and Ľ. Beňa, "Temperature calculation of overhead power line conductors based on CIGRE Technical Brochure 601 in Slovakia," In *Electrical Engineering*, vol. 101, 2019, pp. 921–933.

Dysgraphic handwriting processing for decision support systems

[1]*Zuzana HUDÁKOVÁ (4th year)*
Supervisor: [2]*Liberios VOKOROKOS*

[1,2]Dept. of Computer and Informatics, FEI TU of Košice, Slovak Republic

[1]zuzana.hudakova@tuke.sk, [2]liberios.vokorokos@tuke.sk

***Abstract*—The paper deals with the issue of the dysgraphic handwriting processing and recognition. The research applies several machine learning methods - random forest technique, support vector classification and adaptive boosting. To visualize handwriting attributes in 2D space, principal component analysis are used. 120 handwriting samples was collected. By segmentation technique, over 3000 data samples were obtained for testing.**

***Keywords*—classification, data mining, decision support system, dysgraphia, handwriting.**

I. INTRODUCTION

In todays world of modern technology, we often encounter writing disorders [1]. Our research is focused primarily on handwriting recognition using online handwriting, specifically for dysgraphia. This disorder manifests in childhood and it can cause various difficulties in adulthood. Timely diagnosis and provide preventive and remedial assistance are important.

Our goal is to process, compare and evaluate the handwriting samples using various classification models - random forest, support vector machine and adaptive boosting. For visualization, principal component analysis is used. 120 handwriting samples - 58 from dysgraphic subjects and 62 from healthy subjects are collected. Each sample was subjected to segmentation. 22 to 23 samples were obtained from each sample and over 3000 data samples were obtained for testing.

The paper is organized as follows. In the next section we describe the process of data acquisition. Then we provide briefly overview of used classification models in our research. At last, the experimental results are presented and further work is described.

II. DATA ACQUISITION

A. Data collection

Wacom Intuos Pro Large graphic tablet we used for data collection. We also created the template presented in previous research [2] and it was created based on the research [3][4].

B. Dataset

For approximately 18 months, we collected 192 samples. Unfortunately, not all samples were usable and some had to be discarded from the dataset. After that, we have 120 usable samples. Subjects aged 8 to 15 years participated in the testing. All tested subjects or their legal representatives signed informed consent to the testing and processing of the data collected for research purposes.

The resulting number of samples in terms of age, sex, dominant hand and divided of samples into healthy and pathological samples are shown in Table 1.

TABLE 1
SAMPLE GROUPS

Age	number of samples	Sex		Dominant hand		Samples	
		male	female	right-handed	left-handed	dysgraphic	healthy
8	8	6	2	7	1	3	5
9	10	7	3	10	0	5	5
10	14	9	5	13	1	7	7
11	12	8	4	7	5	6	6
12	22	15	7	19	3	6	16
13	18	12	6	14	4	10	8
14	17	10	7	16	1	9	8
15	19	13	6	17	2	12	7
Sum	**120**	**80**	**40**	**103**	**17**	**58**	**62**

C. Sample segmentation

We decided to segment the template into smaller parts to achieve more accurate results, better analyze the sample and also train a classifier. At first, we split each handwriting into 8 rows. Then, from each template row we segmented individual letters, syllables, words and sentence separately. In this way, from the original 120 handwriting samples, we obtained over 3000 data samples.

D. Handwriting samples analysis

To data analysis and processed every handwriting sample is used Python programming language with the scikit-learn library [5]. Parameters for each sample are computed separately. Then, the results of calculations are compared and preliminary result of the samples are determined.

III. CLASSIFICATION MODEL

A. Random Forest

Random forest is the most used algorithm based on decision trees [6]. It is used to classification and regression tasks. This algorithm is made up from multiple decision trees for more stable and accurate prediction. This adds randomness to the model. For our research, this method is used to prediction.

B. Support Vector Machine (SVM)

SVM is used to classification, regression and outliers detection [7]. The principle of SVM is to find an optimal linear hyperplane with the maximal margin in a dimensional space by splitting two classes of training data in that space and classifying data points. In our research, support vector classification (SVC) is also used to prediction.

C. Adaptive Boosting (AdaBoost)

AdaBoost algorithm is used to improve performance of any machine learning algorithm [8]. But is more often used to boost the performance of random forest method or decision trees on classification problems. In this research, AdaBoost is used to achieve better prediction.

D. Principal Component Analysis (PCA)

PCA is used for making predictive models and to data analysis [9]. Smaller datasets are easier to explore and visualize. So PCA is a statistical procedure used to reduce dimensionality of datasets into a smaller one, while preserving as much information as possible. For our research, this technique is used to project the data into a lower dimensionality space.

IV. EXPERIMENTAL RESULTS

Based on previous research [10] into the extraction of parameters from a dysgraphic handwriting, we continued to calculate the predictions. For that, we used three classification method - random forest, support vector classification and adaptive boosting. 3 fold stratified cross validation was used for calculation. The data were normalized on per feature basis to a zero mean a standard deviation equal to one. Comparing of the prediction results are shown in Table 2.

TABLE 2
PREDICTION RESULTS

Classification Method	Prediction Results
Random Forest	67,1 ± 3
SVC	66,1 ± 4
AdaBoost	64,1 ± 2

For better view of the data structure to project of the attributes, the PCA technique is used. Linear dimensionality reduction using Singular Value Decomposition (SVD) is used. The input data is centered but not scaled for each feature before applying the SVD. 2D visualization by the PCA method, with 133 on-surface movement features from each sample are shown in Fig. 1. It shows how healthy and dysgraphic subjects are distributed in 2D space and how their attributes are overlapping.

V. CONCLUSION

We collected handwriting samples by the Wacom digital tablet. 120 handwriting samples are used. A prediction by 3 fold stratified cross validation were calculated. Success rate for random forest method was 67,1 ± 3%, support vector classification method was 66,1 ± 4% and for adaptive boosting it was only 64,1 ± 2%. For the visualization into a 2D space of the extracted attributes, the principal component analysis technique was used.

Further work is intended to creating a system for processing and subsequent comparison of handwriting samples. The aim is to create a complex CDSS system with a simple user interface. This will include the possibility to enter patient data, process and evaluate of handwriting samples, propose treatment procedures, assist clinical decisions and, last but not least, have an informative character.

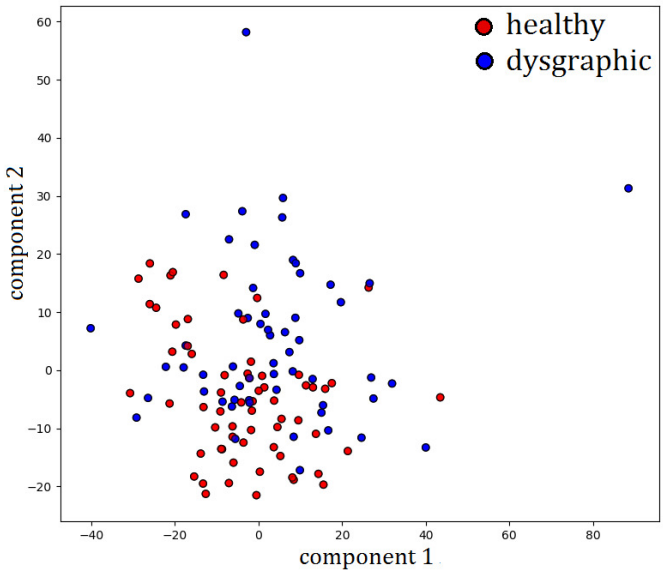

Fig. 1 2D visualization by PCA method

ACKNOWLEDGMENT

This work was supported by the Slovak Research and Development Agency under the contract No. APVV-16-0211.

REFERENCES

[1] J. Mekyska, M. Faundez-Zanuy, Z. Mzourek, Z. Galaz, Z. Smekal and S. Rosenblum, "Identification and Rating of Developmental Dysgraphia by Handwriting Analysis," IEEE Transactions on Human-Machine Systems, vol. 47, no. 2, pp. 235-248, 2017.

[2] Z. Dankovicova, "Handwriting pre-processing for clinical decision support systems," in SCYR 2018, Kosice: TU, pp. 117-119, 2018.

[3] P. Drotar, J. Mekyska, I. Rektorova, L. Masarova, Z. Smekal and M. Faundez-Zanuy, "Decision support framework for parkinsons disease based on novel handwriting markers," Neural Systems and Rehabilitation Engineering, IEEE Transactions on, vol. 23, no. 3, pp. 508-516, 2015.

[4] S. Rosenblum and G. Dror, "Identifying Developmental Dysgraphia Characteristics Utilizing Handwriting Classification Methods," IEEE Transactions on Human-Machine Systems, vol. 47, no. 2, pp. 293-298, 2017.

[5] F. Pedregosa, et al., "Scikit-learn: Machine Learning in Python," JMLR 12, pp. 2825-2830, 2011.

[6] L. Breiman, "Random forests, machine Learning," vol. 45, pp. 5-32, 2001.

[7] C. W. Hsu, C. C. Chang and C. J. Lin. "A practical guide to support vector classification." pp. 1396-1400, 2003.

[8] Y. Freund, R. Schapire, N. Abe, "A short introduction to boosting," in Journal-Japanase Society For Artificial Intelligence, vol. 14, pp. 771-780, 1999.

[9] I. Jolliffe, . "Principal component analysis," Springer berlin Haidelberg, 2011.

[10] Z. Dankovicova, M. Uchnar, "Extraction of parameters from dysgraphic handwriting for CDSS systems," in Acta Electrotechnica et Informatica, Kosice: TU, no, 19, vol. 1, pp. 48-54, 2019.

EEG based Speech detection

[1]*Marianna KOCTÚROVÁ (3rd year),*
Supervisor: [2]*Jozef JUHÁR*

[1,2]Dept. of Electronics and Multimedia Communications, FEI TU of Košice, Slovak Republic

[1]marianna.kocturova@tuke.sk, [2]jozef.juhar@tuke.sk

***Abstract*—BCI speech recognition systems are on the rise in scientific research. Speech detection from EEG signals can help create a better speech recognizer. The problem in speech recognition which is being recognized directly from the brain is the number of mixed signals that interfere with each other during recording. These signals mixture make it difficult to classify speech correctly. In this paper, we propose a framework for speech detection using EEG signals, which is intended to be a serious contribution to the field of BCI communication research.**

***Keywords*—BCI, Electroencephalography, Feed-forward neural network, Machine learning, Speech detection**

I. Introduction

The article describes an experiment that uses a neural network to create models for speech activity detection (SAD) in brain signals. The design of an EEG-based speech activity detector is a very important step towards analyzing brain and speech activity as well as creating an EEG-based speech recognizer [1].

Our SAD system is based on the time series recognition of brain electrical impulses that transfer information about speech between individual brain areas. SAD uses supervised machine learning techniques to create a model that will classify brain signals as speech or non-speech. SAD may help serve as one part of speech recognition frameworks based on brain signals [2].

In our research, it was necessary to process the recorded brain signal appropriately so that the speech signal information was not lost during processing. Then, end-to-end feed-forward artificial neural network models were trained in the experiment to classify speech activity in EEG signals using labeled EEG data.

II. Materials and methods

The SAD algorithm was performed in several steps schematically indicated in Figure 1. The EEG data of Slovak speaking participants were recorded in the first step. The participants were pronouncing the single words that were shown to them on the paper during EEG recording. For recording brain signals, the EEG device incorporated 16 channels that were placed over the scalp of the user according to the International 10-20 system[3]. The EEG data were processed in the Matlab environment. Signal processing consisted of filtering, signal decomposition, and signal framing. The additional audio signal was recorded for the time synchronization and labeling of spoken words. Binary labels were processed as an average of all label values in frame.

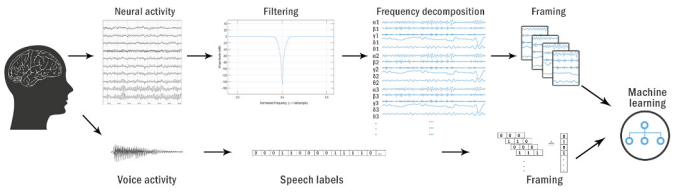

Fig. 1. EEG based speech activity detector's blocked diagram

A. Signal processing

The recorded EEG signals were manually browsed, to find excessive noise. Founded noise was mainly located at the start and ends of records. These parts have been removed from the EEG and the audio recording. A Butterworth filter was used for EEG signals to remove 50 Hz power line interference [4] [5]. Unlike the experiment [6], we used less filtering to keep as much speech information in the signal as possible.

The first experiment [7] was shown that the results of the speech recognition system reach higher accuracy with the decomposed signal into wave frequencies. Because the individual brain waves carry the type of information in a specific way [8], the decomposition of the signal into these waves was crucial in this experiment. We decomposed EEG signal for each channel into 5 separate signals oscillated with specific frequency band known as alpha ($8-13$ Hz), beta($14-26$ Hz), gamma(up to 30 Hz), delta($0.5-4$ Hz), and theta($4-7.5$ Hz) [9]. Separate waves were merged into a row matrix of shape (1, 80) which consists of 5 amplitudes per each wave type for all 16 recording channels. Figure 2 shows an example of an EEG signal from one channel distributed over five frequency ranges.

B. Speech labels annotation

Speech activity labels were annotated in the Transcriber tool. Transcriber exports a .stm file with timestamps of pronounced words which was later edited in the Matlab environment. The file includes the start and end times of each segment in seconds and its text annotation. Only speech activity was annotated in .stm files. Everything else was considered as silence.

The speech segment's timestamps were converted to a one-dimensional binary-valued matrix with a size of a discrete-time length of EEG recording, where 1 represents speech activity for specific timestep (250Hz sampling frequency [10]).

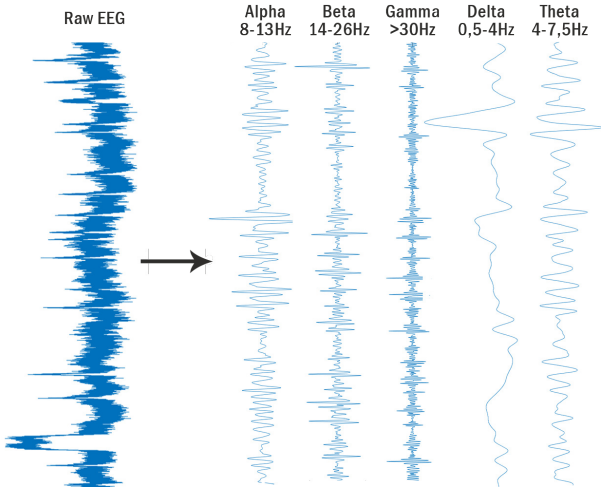

Fig. 2. Sample of EEG signal decomposition.

In the experiment, different frame sizes of EEG signals for neural network training were tested. The label matrix to match its length was adjusted.

III. Experiment

In the initiation experiment[6], we designed a SAD algorithm that was able to learn to detect the speech signal but searching for the non-speech signal was not successful. The proposed model also had problems with estimating silence in short pauses between words. We changed signal processing methods in the experiment as described in this paper.

A. Neural network training

EEG data in 2 layer feed-forward neural network in the experiment were tested.

The best results with 50 neurons in the first hidden layer. The input layer was row vector consist of 1x80 signal amplitudes per each timestep (0,004 seconds). This row vector was extended for various frame size setting. The second layer was the output layer with shape 1x1 with sigmoid activation. Output pseudo probabilities were thresholded with 0,5 decision boundary.

By decomposing the EEG signal into bandwidths alpha, beta, gamma, delta, and theta we got a larger input vector. On the other hand, the neural network may select values with the frequency range with the largest informative value from the input vector.

Input data was randomly split to 70% training, 15% validating and 15% testing parts.

B. Results

Figure 3 shows part of the results from the test set. Graphical representation in the figure shows values one and zero as labels of speech. A blue shape shows labels of speech and non-speech (ground truth) and red bullets indicate predicted values by our neural network. Table I shows results for testing in the Neural network for various settings of windows sizes. The neural network model trained with frequency decomposed EEG signals is more sensitive for short pauses between words. The best result of our experiment was about F1 = 0.76 (F-Speech).

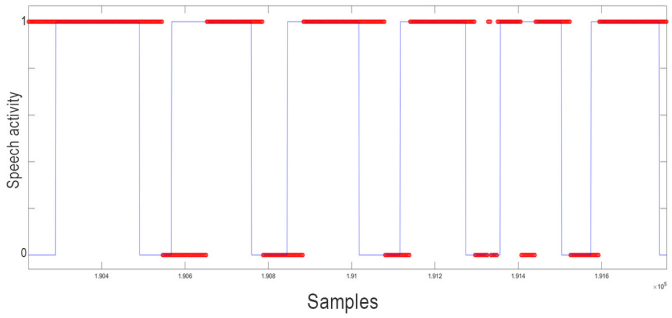

Fig. 3. Graphical representation of results. Speech and non-speech (ground truth) labels depicted as blue shape, predicted values depicted as red bullets

TABLE I
NEURAL NETWORK TRAINING RESULTS FOR VARIOUS LENGTH OF FRAME IN THE INPUT OF NETWORK. F1 SCORE VALUES WERE CALCULATED FROM PRECISION RECALL METRICS. TP = TRUE POSITIVE RATE, TN = TRUE NEGATIVE RATE

Size of frame in seconds	TP	TN	F1 score
0, 4	54,1%	13,7%	76.4
0, 3	44,8%	18,5%	71
0, 2	33,7%	33,8%	67,4
$No framing$	33%	36,1%	68

IV. Conclusion and Future Work

The proposed SAD algorithm can be tuned with different hyperparameters and also the movement of the decision threshold. In future work, it is we will use deep learning techniques such as recurrent and convolutional neural networks, which are expected to deliver better results in this field.

Acknowledgment

The research in this paper was supported by the Ministry of Education, Science, Research and Sport of the Slovak Republic under the project KEGA 009TUKE-4/2019 and by the Slovak Research and Development Agency under the projects APVV-15-0731 and APVV-15-0517.

References

[1] P. Kumar, R. Saini, P. P. Roy, P. K. Sahu, and D. P. Dogra, "Envisioned speech recognition using eeg sensors," *Personal and Ubiquitous Computing*, vol. 22, no. 1, pp. 185–199, 2018.

[2] J. S. Brumberg, A. Nieto-Castanon, P. R. Kennedy, and F. H. Guenther, "Brain–computer interfaces for speech communication," *Speech communication*, vol. 52, no. 4, pp. 367–379, 2010.

[3] V. Jurcak, D. Tsuzuki, and I. Dan, "10/20, 10/10, and 10/5 systems revisited: their validity as relative head-surface-based positioning systems," *Neuroimage*, vol. 34, no. 4, pp. 1600–1611, 2007.

[4] S. Leske and S. S. Dalal, "Reducing power line noise in eeg and meg data via spectrum interpolation," *NeuroImage*, vol. 189, pp. 763–776, 2019.

[5] R. M. Rangayyan, *Biomedical signal analysis*. John Wiley & Sons, 2015, vol. 33.

[6] M. Koctúrová and J. Juhár, "Speech activity detection from eeg using a feed-forward neural network," in *2019 10th IEEE International Conference on Cognitive Infocommunications (CogInfoCom)*. IEEE, 2019, pp. 000 147–000 151.

[7] M. Rosinová, M. Lojka, J. Staš, and J. Juhár, "Voice command recognition using eeg signals," in *2017 International Symposium ELMAR*. IEEE, 2017, pp. 153–156.

[8] S. Sanei and J. A. Chambers, *EEG signal processing*. John Wiley & Sons, 2013.

[9] S. Sanei, *Adaptive processing of brain signals*. John Wiley & Sons, 2013.

[10] O.-O. S. B. Tools, "Openbci.com. retrieved 24 february 2018," 2018.

Edge-enabled approach for Intelligent Human-System Interoperability

[1]*Erik KAJÁTI (4th year),*
Supervisor: [2]*Iveta ZOLOTOVÁ*

[1,2]Department of Cybernetics and Artificial Intelligence, FEI TU of Košice, Slovak Republic

[1]erik.kajati@tuke.sk, [2]iveta.zolotova@tuke.sk

***Abstract*—In recent years, the Industry 4.0 concept brings new demands and trends in different areas; one of them is distributing computational power to the cloud. The paper presents four studies. The first one aims to assess the efficiency of data communication in the Cloud-Based Cyber-Physical Systems (CB-CPS). The evaluation of the network properties of the communication protocols eligible for CB-CPS is presented. The results show that the intelligence on the edge of the network will play a significant role. The second study presents an augmented reality usage for Human-Machine Interaction (HMI) with the use of edge technology. The third study focuses on edge computing. Lastly, the fourth study describes indoor localization techniques.**

***Keywords*—Industry 4.0, Human-Machine interaction, Internet of Things, Edge-enabled computing**

I. Introduction

In recent years, the Industry 4.0 concept brings new demands and trends in different areas; one of them is distributing computational power to the cloud. Aiming to evaluate the efficiency of data communication in the CB-CPS. The evaluation of the network properties of the communication protocols eligible for CB-CPS is presented. The network properties to different cloud providers and data centers' locations have been measured and interpreted.

Industry 4.0 enables new types of interactions between humans and systems, interactions that will transform the workforce. With changing interactions, there is also a need to implement new technologies to support these changes. Advanced usage of new technologies can provide cognitive support for intelligent interactions. Operator 4.0 represents the "operator of the future", a smart and skilled operator who can utilize Industry 4.0 benefits [1].

II. The initial status

During past years the technologies and approaches that can support intelligent human-system interoperability driven by the present industrial revolution were presented. Architectures that depend solely on cloud technologies have a few problems. In recent years, ideas have arisen that have attempted to overcome these problems. Among the most well-known concepts is edge computing. The edge-enabled Bluetooth Low Energy sensorial network that can support better localization and identification of the objects thus can provide better support to the humans. During past years we have focused mainly on edge computing and indoor localization techniques as well as a combination of the mentioned. The goal should be a better understanding of the environment, thus better cognitive support for the people inside such an environment.

III. The tasks solved in the previous year

In the past year, we have worked on four main ideas. The first was the network evaluation study [2] [3]. The second case study focuses on the use of Augmented Reality (AR) technology, together with principles of edge computing, to provide modern Human-System Interaction [4]. The third case study focuses on edge-enabled computing [5]. The last study aims for evaluation and recommendations of indoor localization techniques (still in progress).

A. Network evaluation study

In this research, the following four communication protocols were selected:

- HTTP - Hypertext Transfer Protocol - commonly used protocol for communication between server and clients.
- WCF - Windows Communication Foundation service - a framework for building service-oriented applications.
- OPC UA - Open Platform Communication Unified Architecture - a machine to machine communication protocol for industrial automation.
- AMQP - Advanced Message Queuing Protocol - publish-subscribe-based messaging protocol, commonly used in IoT solutions.

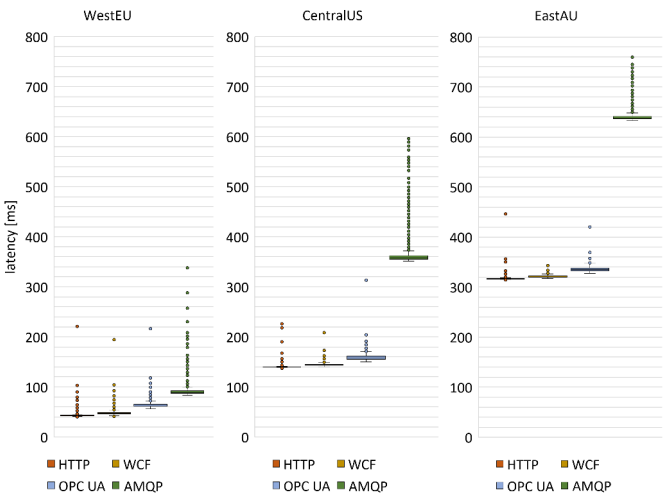

Fig. 1. Distribution of the latency values grouped by location [2].

From Fig. 1 can be seen that the results from HTTP, WCF, and OPC UA are less scattered than that from AMQP communication. Moreover, results from HTTP and WCF are very similar in all locations; OPC UA is just slightly slower than the two mentioned. On the contrary, AMQP communication is a lot slower compared to the other three; also, the dispersion of the values is a lot wider [2].

B. AR and Computer Vision for Human-System Interaction

In this study, we have proposed an AR environment for operators, where they can see a robots' planned path. They can add virtual obstacles and walls to the mobile robots' cyber-physical navigation view. These virtual obstacles and barriers can be used to determine restricted areas for mobile robots. This can be seen, for example, as safe areas for humans' and/or robots' stationary work. Finally, we introduce the system architecture supporting the proposed AR environment for humans-mobile robots' safe and productive interaction.

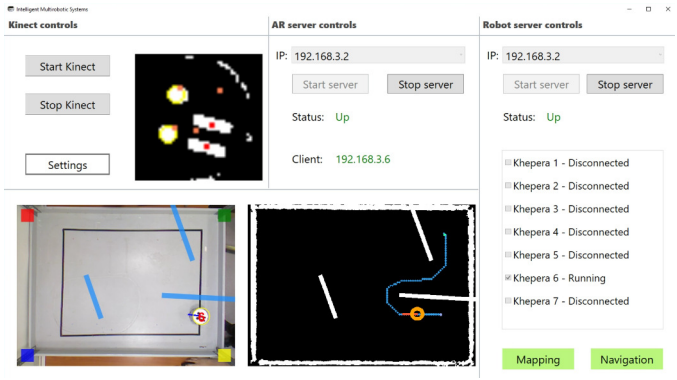

Fig. 2. The AR core app interface [4].

C. Edge-enabled Gateway

In [5], we have defined the general architecture for edge-enabled solutions, and we pointed out the importance of the IoT gateways in these solutions. From the scientific work carried out and the analysis of other scientific articles, a set of 14 criteria for edge-enabled architecture was chosen. These criteria fell into four main categories (device connectivity, data pre-processing, data analytics, and special hardware requirements).

We have also focused on the analysis of the edge-enabled gateway, mainly on the topics like principles of data processing on the edge of the network [6]; artificial intelligence in data analytics on the edge of a network [7]; distribution of the neural network models [8]; edge-enabled solutions criteria selection and evaluation [9]; hardware parameters of edge devices [10]; and more.

D. Indoor localization techniques

In this study, we are focusing on the evaluation of indoor localization techniques. Currently, we are testing the solution that aims to compare several technologies that can be used for indoor positioning. Technologies that we aim to compare can be divided into the following groups:

- Technologies that require placement of the additional modules into the environment:
  - Computer vision (stereo vision, ToF cameras)
  - Wireless (WiFi, Bluetooth beacons, RFID)
- Technologies that only require wearable device:
  - Pedestrian dead reckoning (accelerometer, gyroscope)
  - Augmented Reality (AR)

We expect to have results at the end of February. After that, we want to focus on the comparison of the fusion of mentioned technologies to provide faster, more accurate, and efficient ways of indoor localization. Soon, we also aim to incorporate the Ultra Wide Band (UWB) and Bluetooth 5.1 (providing Angle of Arrival and Angle of Departure) into our study.

IV. Conclusion

All of the mentioned studies should help with providing intelligent interaction between humans and the system. One of the main premises for the intelligent environment is understanding of such environment, thus gathering data and knowing what is where. AR, together with precise positioning of the objects, could help fulfill that objective. To offer faster responses and to efficiently transfer data, edge computing should be a vital part of the intelligent environment. Further research will be focused on implementing of the mentioned works to create one application that can support operators' work.

Acknowledgment

This publication was supported by the grant KEGA – AICybS - Smart Industry/Architectures of Intelligent Information and Cybernetic Systems, 033TUKE-4/2018, 2018-2020 (50%) and VEGA – Intelligent cyber-physical systems in a heterogeneous environment with the support of IoE and cloud services, 1/0663/17, 2017-2020 (50%).

References

[1] I. Zolotova, P. Papcun, E. Kajati, M. Miskuf, and J. Mocnej, "Smart and cognitive solutions for operator 4.0: Laboratory h-cpps case studies," *Computers & Industrial Engineering*, vol. 139, p. 105471, 2020.

[2] E. Kajati, P. Papcun, C. Liu, R. Y. Zhong, J. Koziorek, and I. Zolotova, "Cloud based cyber-physical systems: Network evaluation study," *Advanced Engineering Informatics*, vol. 42, p. 100988, 2019.

[3] P. Papcun, E. Kajati, , C. Liu, R. Y. Zhong, and I. Zolotova, "Cloud-based control of industrial cyber-physical systems," in *48th International Conference on Computers and Industrial Engineering (CIE48)*, pp. 1–14, 2018.

[4] P. Papcun, J. Cabadaj, E. Kajati, D. Romero, L. Landryova, J. Vascak, and I. Zolotova, "Augmented reality for humans-robots interaction in dynamic slotting "chaotic storage" smart warehouses," in *IFIP International Conference on Advances in Production Management Systems*, pp. 633–641, Springer, 2019.

[5] P. Papcun, E. Kajati, D. Cupkova, J. Mocnej, M. Miskuf, and I. Zolotova, "Edge-enabled iot gateway criteria selection and evaluation," *Concurrency and Computation: Practice and Experience*, p. e5219, 2019.

[6] M. Miskuf, E. Kajati, J. Mocnej, and P. Papcun, "Smart/intelligent edge - principy spracovania dat na hrane siete," *ATP Journal*, vol. 7, pp. 50–51, 2018.

[7] D. Cupkova, E. Kajati, J. Vascak, and P. Papcun, "Smart/intelligent edge - umela inteligencia v datovej analytike na hrane siete," *ATP Journal*, vol. 3, pp. 54–55, 2019.

[8] E. Kajati, D. Cupkova, P. Papcun, and I. Zolotova, "Smart/intelligent edge - sposoby distribucie modelov neuronovych sieti," *ATP Journal*, vol. 4, pp. 40–41, 2019.

[9] E. Kajati, P. Papcun, D. Cupkova, and I. Zolotova, "Smart/intelligent edge - kriteria vyberu a hodnotenia parametrov rieseni na hrane siete," *ATP Journal*, vol. 5, pp. 64–65, 2019.

[10] P. Papcun, E. Kajati, and J. Vascak, "Smart/intelligent edge - hardverové parametre zariadeni na hrane siete," *ATP Journal*, vol. 6, pp. 40–41, 2019.

Efficient algorithms for multi-view video encoding

[1]*Peter ŠUĽAJ (3rd year)*
Supervisor: [2]Stanislav MARCHEVSKÝ

[1,2]Dept. of Electronics and Multimedia Communications, FEI TU of Košice, Slovak Republic

[1]peter.sulaj@tuke.sk, [2]stanislav.marchevsky@tuke.sk

***Abstract*—This work deals with streaming and processing multi-track video streams from multiple drones. Existing communications and routing protocols, including ad hoc protocols, will be used. Work focuses on networking and video content routing in ad-hoc networks using multicast, focusing on the use of drones and the processing and routing of drones' video content, the analysis of drones communication applications, and the requirements for video streaming processing. The work describes the use of these technologies for the requirements of surveillance and monitoring, natural disasters, or streaming of multi-view video from social events.**

***Keywords*— UAV, drones, video streaming, multi-view video, routing protocols, AD-HOC network, multicast**

I. Introduction

This topic was chosen as a springboard for the analysis and experimental use of codecs for multi-view video and airborne images. Utilizing today's technology and technical progress, people open up different horizons in wide spectrum. One of these is also the use of a combination of virtual reality and flying people which can be drones, for example. Think about the possibility that these devices can to fully replace people who would have to risk their lives in any situation. An example use of simulated drone in virtual reality where we can see monuments, museums and other natural orders from our homes. As a good example, the Notre Dame is in Paris as it was a few weeks ago by fire. Creation of simulation and implementation of imaginary drone in this simulation into a virtual reality would be able to faithfully approach this monument. We cannot avoid solving this issue without technological advancements such as [1] [2] [3].

- Drones or other flying equipment, including controllers
- Sufficient graphically performance
- Any device for virtual reality

II. Information for Authors

The within the results achieved, an experimental network consisting of Tello drones, featuring a relatively low weight of only 80 grams and having a 1100mAh battery, was created. All control is provided by Tello application with clear user interface. Flawless and stable image transmission and drone instructions are provided by two powerful SmartSwitch 2 antennas. Tello is fully compatible with VR glasses. This drone achieves a maximum speed of 32km / h. According to the schedule, we devoted to the design of experimental network simulation and based on the results we proceeded to a real test using the drones mentioned above.

The simulations took place at the Department of KEMT, TUKE Košice. In the simulation, the server was configured to have sufficient hardware reserves to calculate the simulation even for 10,000 drones. The server parameters were as follows: two 16-core processors with 128 GB RAM, for testing the system we created three simulation profiles, which had available 4,8 and 16 cores with 16,32 and 64 GB RAM. The average time is shown in Figure 1. This is the time that elapsed between the request and the response to 1,000 drones.

With 8 connections, an 8-core processor is almost four times faster than a 4-core processor. With 10,000 connections, it's almost twice as fast. It should be noted that the proposed platform shows predictable enlargement behavior. Processing times increase linearly with the number of connections, and server performance results in significant performance gains.

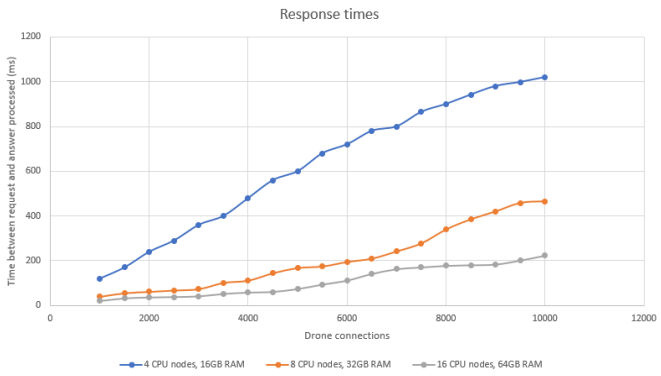

Figure 1Graph of simulation result

III. NS – 3 Software

According to the project schedule, we continued testing for various simulations that will determine the network throughput depending on the number of drones / nodes. We investigated the network parameters and how the communication behaves

in the increasing number of nodes, each node had a random movement with a speed of 8km / h. In this section we have not dealt with the trajectory and collision of several nodes yet [4] [5] [6].

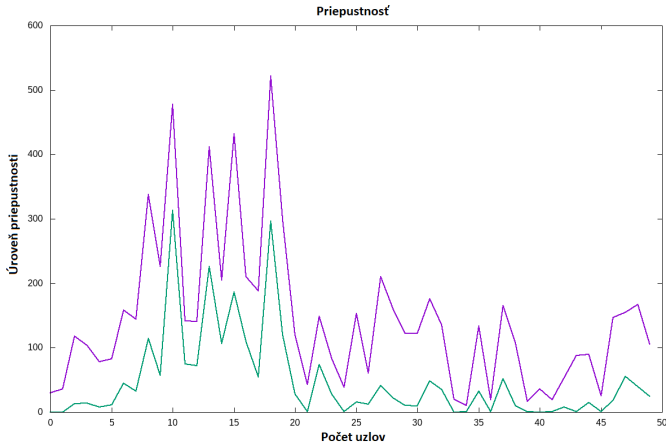

For the purpose of obtaining the simulation we use the simulation program NS-3. This program is a network simulator with discrete events. The NS-3 project is an open source project developing NS-3. In NS-3, the simulator is written exclusively in C ++, with optional Python bindings. This program uses a modular kernel that is easily extensible thanks to C ++ or Python support. This program is free of charge, which has saved us considerable resources for science and research. Its main advantage is the use of the simulator in the creation and testing of the analytical part of bachelor and master theses, by means of which students contribute to the partial objectives of the project. When teaching through NS-3, students can visually see the work of the network protocol and understand the effects of various environmental or other factors on the network and can also demonstrate the advantages and disadvantages of different strategies through comparison [7] [8] [9].

f) Simulation results can be reproduced and easily analyzed. On this platform, an experimenter can obtain an "ideal" network environment by configuring environment parameters and can monitor and record important information on the key node in real time to get first-hand information about evaluating network performance. In addition, certain special circumstances may be repeated at any time, which is difficult to do in the real network [10] [11] [12].

IV. Achieved results

Achieved results:

1. Proposed software tools in Python for programmed Tello drone control
2. Proposed software tools for Tello edu drone control
3. Designed software tools for joining drone video streams
4. Designed software tools for the simulation of an ad-hoc network based on nodes created by a network of flying sensors using the NS-3 simulator [13]
5. Designed software for multi-view imaging using a network of flying sensors with object recognition using artificial neural networks using a open-source program [14,15]

V. Conclusion

Goals for the future are summarized in these points:

- Design of algorithms and protocols for content delivery and data distribution from mobile devices.
- The architecture of content delivery and data distribution from mobile vehicles
- Design of algorithms for processing multiple video streams from a sensor flying network in a terrestrial component of flying sensor network based on a methodology for big data processing.

Acknowledgment

This work was supported by Cultural and Educational Grant Agency (KEGA) of the Ministry of Education, Science, Research and Sport of the Slovak Republic under the project No. 023TUKE-4/2017 and by the Slovak Research and Development Agency under the contract no “ APVV-17-0208-Resilient mobile networks for content delivery”.

References

[1] B. Bross, W.-J. Han, G. J. Sullivan, J.-R. Ohm, and T. Wiegand, High Efficiency Video Coding (HEVC) Text Specification Draft 9, document JCTVC-K1003, ITU-T/ISO/IEC Joint Collaborative Team on Video Coding (JCT-VC), Oct. 2012.

[2] Video Codec for Audiovisual Services at px64 kbit/s, ITU-T Rec. H.261, version 1: Nov. 1990, version 2: Mar. 1993.

[3] Video Coding for Low Bit Rate Communication, ITU-T Rec. H.263, Nov. 1995 (and subsequent editions).

[4] Coding of Moving Pictures and Associated Audio for Digital Storage Media at up to About 1.5 Mbit/s—Part 2: Video, ISO/IEC 11172-2 (MPEG-1), ISO/IEC JTC 1, 1993.

[5] Coding of Audio-Visual Objects—Part 2: Visual, ISO/IEC 14496-2 (MPEG-4 Visual version 1), ISO/IEC JTC 1, Apr. 1999 (and subsequent editions).

[6] Generic Coding of Moving Pictures and Associated Audio Information—Part 2: Video, ITU-T Rec. H.262 and ISO/IEC 13818-2 (MPEG 2 Video), ITU-T and ISO/IEC JTC 1, Nov. 1994.

[7] Advanced Video Coding for Generic Audio-Visual Services, ITU-T Rec. H.264 and ISO/IEC 14496-10 (AVC), ITU-T and ISO/IEC JTC 1, May 2003 (and subsequent editions).

[8] H. Samet, “The quadtree and related hierarchical data structures,” Comput. Survey, vol. 16, no. 2, pp. 187–260, Jun. 1984.

[9] T. Wiegand, G. J. Sullivan, G. Bjøntegaard, and A. Luthra, “Overview of the H.264/AVC video coding standard,” IEEE Trans. Circuits Syst. Video Technol., vol. 13, no. 7, pp. 560–576, Jul. 2003.

[10] S. Wenger, “H.264/AVC over IP,” IEEE Trans. Circuits Syst. Video Technol., vol. 13, no. 7, pp. 645–656, Jul. 2003.

[11] S.Hayat,E.Yanmaz,andR.Muzaffar,“Surveyonunmannedaerial vehicle networks for civil applications: a communications viewpoint,”

[12] Kemal Akkaya and Mohamed Younis. A survey on routing protocols for wireless sensor networks. Ad Hoc Networks, 3(3):325–349, 2005.

[13] Simon Morgenthaler, Torsten Braun, Zhongliang Zhao, Thomas Staub, and Markus Anwander. UAVNet: A mobile wireless mesh network using unmanned aerial vehicles. In Proc. IEEE GLOBECOM, 2012.

[14] Yu Ming Chen, Liang Dong, and Jun-Seok Oh. Real-time video relay for UAV traffic surveillance systems through available communication net- works. In Proc. IEEE WCNC, 2007

[15] Carlos Cambra Baseca, Juan R D´ıaz, and Jaime Lloret. Communication ad hoc protocol for intelligent video sensing using AR drones. In Proc. IEEE MSN, 2013.

End-to-end based speech recognition systems using deep neural networks

[1]*Anton BUDAY (1st year),*
Supervisor: [2]*Anton ČIŽMÁR*

[1,2]Dept. of Electronics and Multimedia Communications, FEI TU of Košice, Slovak Republic

[1]anton.buday@tuke.sk, [2]anton.cizmar@tuke.sk

***Abstract*—In this paper I introduce an overview on the state-of-the-art knowledge in automatic speech recognition systems (ASRs), I mainly focus on an end-to-end ASR. Here, I compare two main state-of-the-art approaches to ASR - hybrid HMM/DNN systems and quite new and not widely verified end-to-end ASR systems. Nowadays, many engineering groups try to develop and experiment with an end-to-end ASR. This paper summarizes both technologies in terms of advantages or disadvantages, differences etc. End-to-end approach can be either attention-based or CTC-based. Possibilities of future work with the utilization of end-to-end ESPnet or similar ASR framework are described in the final parts of this paper.**

***Keywords*—acoustic modeling, automatic speech recognition, deep neural networks, end-to-end speech recognition, language modeling**

I. Introduction

Automatic speech recognition (ASR) is the compartment of information and communication technologies whose potential reaches various areas of daily life, spanning from smart home, robotics to big data analysis and processing.

Conventional ASR phonetic-based (e.g. HMM, hybrid HMM/DNN models) approaches require separate components for acoustic, language and pronunciation modeling [1]. These approaches integrate ideas from many different domains, such as signal processing (e.g. MFCC - Mel-Frequency Cepstral Coefficients), natural language processing (n-gram language models), or even statistics (HMM - Hidden Markov Models). These components of an ASR are hugely optimized individually and isolated, so it negatively influences overall ASR system performance [2].

End-to-end approaches optimize components jointly, these use a single criterion. This reduces the need for experts to make every effort to find the best combination for several resources. For example, a n-gram language model is a must for all HMM-based systems. Moreover, a typical n-gram language model takes several gigabytes of memory making it impractical to deploy on mobile devices. State-of-the-art commercial ASR systems from brands like Google or Apple are deployed on the cloud systems, so mobile devices only require sufficient network connection opposing to local devices [3].

II. Current research status in ASR

A. Challenges in automatic speech recognition

Automatic speech recognition has recently achieved major breakthroughs and vastly improved its performance [4]. This allegation is proved by existence of speech-specific intelligent human-machine communication systems, e.g. Apple's Siri, Microsoft's Cortana, Amazon's Echo, etc. One of the main problems in ASR is the performance degradation due to ambient noise and reverberation, which contribute to corrupted speech received by microphones. Generally, noise can be divided into stationary (constant in time) or non-stationary (variable in time - e.g. speaker interference, transient sound events ...) [5]. Detection and reduction of non-stationary ambient noise together with non-stationary sound sources is still quite challenging in practise, proven by [6]. That is why new robust speech recognition challenges, such as REVERB and CHiME are currently showcased [7]. In recent years, *data-driven* approach which is based on supervised machine-learning, receives attention. These techniques emerged after arrival of deep neural networks "comeback" in 80's [8]. The goal of these approaches is to utilize large amounts of training data to either obtain cleaner signals and corresponding features from noisy speech recordings or even perform speech recognition of noisy speech. Deep learning, which is based on deep neural networks, has recently played important value in variety of fields, such as gaming [9], visual recognition, language translation [10] and others. These facts accelerate additional work on robustness of ASR technologies.

B. Principle of general speech recognition

General principle of speech recognition can be characterised by its fundamental equation [11]. Fundamental equation of speech recognition is expressed as

$$W' = arg\max_{W} P(W|O) \equiv arg\max_{W} p(O|W)P(W) \qquad (1)$$

It represents the search for the best sequence *W'* on an observation

$$X = \mathbf{x}_1, \mathbf{x}_2, \mathbf{x}_3, ..., \mathbf{x}_T. \qquad (2)$$

Variables as *P(W)* and likelihood *p(O|W)* represent any language model and any acoustic model, respectively. The mathematical meaning of Eq. 1 is minimization of

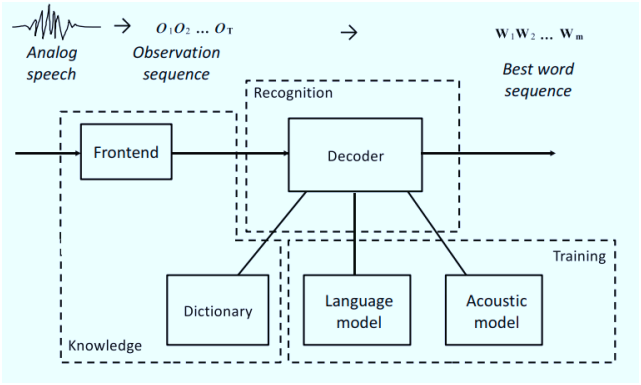

Fig. 1. Principle of conventional speech recognition system (ASR). Preprocessing (frontend) and lexicon are knowledge-based without any training. The acoustic model minimizes frame cross-entropy or any discriminative criterion. Language model should be less complicated and Viterbi's decoder aims to minimize SER metrics value, however evaluation is based on WER metrics [2].

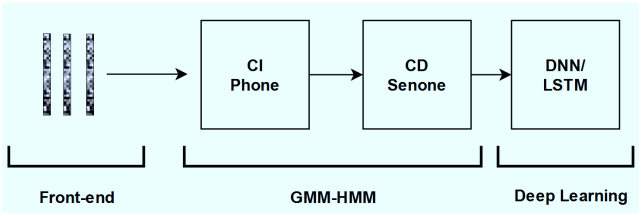

Fig. 2. Workflow of acoustic model preparation using deep learning for the state-of-the-art ASR system. Context-dependent subphonetic states (senones) are learned using chained GMM models to align and cluster data [2].

SER (i.e. sentence error rate), because it refers to word sequence *W'*. On the other hand, contemporary ASR systems use evaluation method called WER (word error rate). This metrics corresponds to the sequence $\{w_1, w_2, ...w_n\}$ of words that have the highest expectation to be correct individually (opposing to SER, which refers to whole sentence). Correlation between them is undeniable, as well as the fact that each compartment of the speech recognition system is optimized individually. This implies that creating a robust ASR system requires heuristics, know-how and knowledge from multiple research areas [2].

C. Disadvantages of conventional complex ASR systems

Even, if hybrid state-of-the-art automatic speech recognition system is built without any weakness, it may fall into local minima during optimization process for several reasons.

1) *Many training phases.* Hidden Markov model (HMM)/Gaussian mixture model (GMM) is in the beginning of a conventional ASR system. At first, pre-processing takes place and generates frame-level alignments of training data, commonly known as targets in neural network training. Deep learning model takes over after HMM/GMM model was built. Training HMM/GMM requires involvement of CI (context-independent) model and then CD (context-dependent) model, whereas senones represent HMM states. Each step is normally repeated several times. Moreover, discriminative training can be included, as well.
2) *Many resource types.* Conventional, e.g. hybrid (non-end-to-end) system requires dictionary and phonetic information preparation used in acoustic modeling. This adds to disadvantages for low-resource languages. Of course, preexisting alignments can be useful, but eventually it is hard to reproduce a training from the very beginning.
3) *Hyper-parameters tuning.* These parameters might be represented by the number of HMM states and the number of Gaussian components inside each state. Designation of these values relies on know-how.
4) *Various optimization functions.* Separate optimizations of various components contribute to disadvantages of conventional ASR. Feature representation and training of effective model are considered as separate problems in ASR community. For example, MFCC coefficients model the acoustic perception of human ear, however this feature extraction does not optimally fit acoustic models training. Inequality of optimization objectives can be demonstrated on the difference between HMM/GMM model and deep neural network (DNN) model. Purely HMM/GMM model uses maximum likelihood estimation (MLE), whereas DNN models use different discriminative criteria for optimization like cross-entropy (CE) criterion. Unfortunately, these criteria refer to frame classification rather than sequence classification of words. Language models tend to be simpler during decodings, so this does not correspond to the reduction of WER metrics.
5) *Model mismatch.* It is widely known that conventional HMM models do not match phone durations quite well [12]. Transitions between states for the most recent ASR systems are set to fixed values. To demonstrate, there is a non-continuous (sudden) jump in HMM phone states, this drawback is tempered with the utilization of subphonetic units. Moreover, gamma distribution is much more suitable for phone state transitions, but these transitions are ignored in the state-of-the-art ASR systems [2].

D. Transition to end-to-end (E2E) learning

Involvement of HMM/GMM represents significant obstacles, because implementation of whole complex conventional ASR system is dependent on it. Thus, direct inclusion of deep learning neural networks is preferred. The researchers suggest that conventional HMM/GMM ASR systems transit to non-HMM/DNN systems, e.g. DNN acoustic models with no dependence on the HMM/GMM. Such systems utilize uniform alignments (every state has equal duration). Additionally, this involves progressive updates (iterations) or in other words, alignment regeneration. In DNN approach, phonetic state tying is included in the space of hidden activations in trained network model. Other types of DNNs, e.g. in [13] use context-dependent state clustering. Eventually, previously mentioned systems inherit drawbacks from HMM-based systems. End-to-end systems try to alleviate disadvantages of HMM speech recognition systems [14].

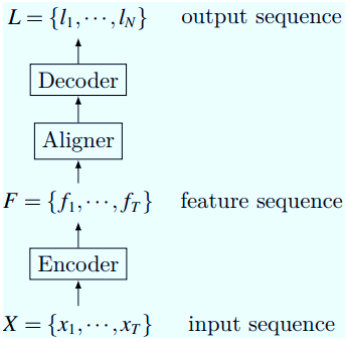

Fig. 3. Function structure of general end-to-end ASR model [16].

E. End-to-end (E2E) learning

Utilization of the end-to-end solutions is becoming widespread in several areas, such as image classification (Convolutional Neural Networks - abbrev. CNNs), object detection, face recognition, video classification, etc. Automatic speech recognition model incorporates mapping from speech feature vectors to a corresponding transcript (e.g., phones, characters, words), whereas both features and the transcript are in a sequence. It is possible to directly learn such a mapping, thus, there are no isolated acoustic and language models [2]. On the other hand, these models sometimes need to be separated to easily debug system workflow. Generally, the language model describes *what* is being said and the acoustic model expresses *how* it is being said. This breaches original end-to-end motivation to ASR. Nonetheless, CTC-based approach has been accepted as *end-to-end* by speech engineering community, because loss function is sequence-based [15].

Nowadays, two general end-to-end approaches exist. They are different in the way they align among observations and output symbols, or else how they order output symbol dependencies. The first category, CTC-based algorithms create explicit alignments and treat symbols as independent units. The latter, encoder-decoder models do not compute any alignments provided no attention mechanisms are used [2].

CTC-based ASR models

The very first attempt in an end-to-end ASR used CTC (i.e., Connectionist Temporal Classification) by Google DeepMind and University of Toronto in 2014 [3]. This model used RNN (i.e., recurrent neural networks) and CTC layer, whereas in this model the pronunciation and acoustic model were learned together. On the contrary, such neural model is unable to learn (incorporate) language because of conditional independence premises similar to HMM. Generally, CTC models map speech acoustics to language characters, but these models make many common spelling mistakes. Consequently, these models forcefully rely on separate language models to correct the transcripts.

Baidu, Chinese technology giant, expanded previous work with extremely large datasets and showcased commercial success with Mandarin and English language [4]. Similarly, Oxford's University LipNet (E2E sentence-level lip reading model) used spatiotemporal convolutions with combined RNN-CTC architecture in restricted grammar dataset [17]. In 2018, Google DeepMind struck back with six times better performance than human experts [18].

Neural networks, which require training targets for every segment in the input sequence, produce equally dense outputs. The ramifications of this fact are that training data have to be presegmented (to acquire targets) and also any dependency between some adjacent words has to be externally preprocessed, before it is chosen as a neural network input. The main goal of ASR is to mark the sequence states in data, not to segment data. Interestingly, CTC loss function, which is defined over target symbols, has special *blank* label, which can be predicted by network without biasing the output sequence. Moreover, this loss function presumes that neighboring symbols are independent of each other - then, we deal with *tokenization* of the input features [2]. CTC ASR systems usually use stacked layers of long short-term memory (abbrev. LSTM) neural network architectures [19]. There are some additional papers where researchers use simpler, basic recurrent neural networks (abbrev. RNNs) with e.g. rectified linear units (abbrev. ReLU) [20]. At present, there are purely end-to-end architectures of neural networks that use CTC method (at least one particular lexicon-free CTC ASR system) with roughly 10% WER [21].

Attention-based ASR models

The idea behind encoder-decoder paradigm is that the entire sequence is compressed into a single vector, which contains all the input information in one unit. This is realized with the utilization of encoder RNN to read the input sequence (one time step at a time). Conversely, a decoder RNN is applied to generate output sequence from previously create single vector entity. RNN decoder imitates language model, but it is based on the input sequence [2]. LSTM networks are widely used as a fundamental block in the encoder/decoder architecture. LSTMs manage to learn long-range associations from input neural network data [22]. This approach works decently on concatenated utterances without any obvious degradation, moreover it reduces monotonicity opposing to CTC approach. An encoder-decoder variant, called attention models were developed in [23].

For the first time, these models were developed at Carnegie Mellon University and Google Brain in 2016. The original LAS ("Listen, Attend and Spell") model *listens* to speech signal, pays *attention* to different parts of signal and *spells* out the one character at a time. Conversely, attention-based models do not have conditional-independence (abbrev. CI) premises and can directly learn all modules of speech recognition system, namely pronunciation, acoustic and language model. This implies that there is no need to have separate language model, so it is useful for memory limited applications. At the end of 2016, the attention-based models started to outperform the CTC models without any dependency on an external language model. Nevertheless, there have been recently various modifications of previously proposed models, like inclusion of sub-word units instead of language characters [2].

Fig. 4 displays the structure of an attention-based ASR system. Input speech waveform is converted to a

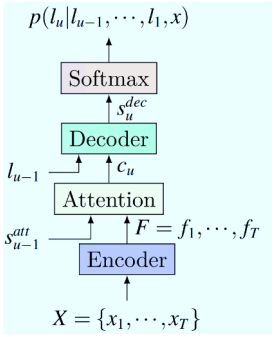

Fig. 4. Function structure of an attention-based (encoder-decoder) model [16].

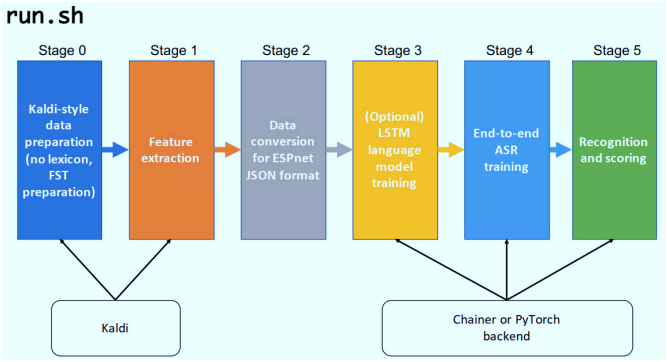

Fig. 5. Stages of ESPnet toolkit workflow. Stage 0 - Kaldi style data preparation without lexicon & with FST (Finite State Transducer), Stage 1 - Extract feautures, Stage 2 - Data2JSON conversion, Stage 3 - LSTM language model (LM) training, Stage 4 - E2E training, Stage 5 - Recognition and scoring [25].

sequence of d-dimensional feature vectors denoted as $x = (x_1, x_2, ..., x_T)$, where $x_T \in \mathbf{R}^d$. Set of graphemes is denoted by $\boldsymbol{l}$, and the output sequence by $\boldsymbol{l} = (l_1, l_2, ..., l_u)$. For an ASR, the number of output graphemes, u, is mostly much smaller than the number of acoustic frames, T. The decoder network in the Fig. 4 consists of a number of recurrent layers. Softmax layer's output represents the decoder output, which is based on the full sequence of previous predictions and the acoustics. This particular decoder model displayed on the Fig. 4 uses single decoder to produce a distribution over the labels conditioned on previously mentioned sequence. The state of the lowest layer of the decoder is denoted as $\mathbf{s}_{u-1}^{att}$ after prediction of the previous labels, $l_1, ..., l_{u-1}$ [16].

III. Future plans and actual state of work

A. Recent research state

As a postgraduate student at the Department of Electronics and Multimedia Telecommunications (abbr. KEMT) of Faculty of Electric Engineering and Informatics (abbr. FEI) at the Technical University of Košice (abbr. TUKE), I plan to focus on more in-depth study of state-of-the-art ASR principles as these are described in a quite complicated way in various recent research papers from broadly known companies like Mitshubishi Motors, Nvidia, Google, etc. The area of ASR closely relates to my master thesis about speech enhancement in a multi-array manner with the utilization of neural networks [24]. Speech enhancement improves the robustness of current-state ASR technologies, which slowly begin to employ multiple microphones, so it is much easier to enhance present ASR systems (in terms of input speech quality). Labouring from previous work, I plan to evaluate recently created end-to-end frameworks, while being notably interested in the framework called ESPnet [25] created by the Japanese ASR engineering group. Fig. 5 explains ESPnet's workflow.

B. Possibilities of future work

At the beginning of this research, prototype experiments can be performed on ESPnet toolkit or even Kaldi (chainer architecture) using already tested & verified (only on Kaldi) training data. Thus, theoretically, we might be able to compare conventional approach using Kaldi versus end-to-end approach using innovative ESPnet toolkit. We might try to verify the compatibility of original Kaldi data with ESPnet data formats and throughout the year to assess (possibly change the direction of) the future work. Since neural networks are data-driven approaches to ASR, we can create, format and apply completely different speech data in the following years. There are various types of speech data, such as child's speech (currently, there's a lack of such data and also decent ASR results), perturbated or somehow augmented speech data, etc.

Laboratory of Speech and Communications Technologies at KEMT has a working non-end-to-end hybrid ASR system based on Kaldi, Viterbi decoder, HMM, etc. The financed project APVV-15-0517 (2016-2018) helped to develop the system for automatic subtitling of audiovisual content, whose baseline comprises ASR system for Slovak language, optionally applicable for hearing-impaired people. A drawback for the transition from hybrid approach to E2E approach is the lack of annotated data, since neural-based ASR requires drastically more data.

To sum up, these are some interesting directions for future research.

Acknowledgment

The research in this paper was supported by the Ministry of Education, Science, Research and Sport of the Slovak Republic under the project KEGA 009TUKE-4/2019 and by the Slovak Research and Development Agency under the projects APVV-15-0731 and APVV-15-0517.

References

[1] D. Jurafsky and J. H. Martin, *Speech and Language Processing: An Introduction to Natural Language Processing, Computational Linguistics, and Speech Recognition*, 1st ed. USA: Prentice Hall PTR, 2009.

[2] S. Watanabe, M. Delcroix, and F. Metze, *New Era for Robust Speech Recognition: Exploiting Deep Learning*. Springer Publishing Company, Incorporated, 2018.

[3] A. Graves and N. Jaitly, "Towards end-to-end speech recognition with recurrent neural networks," in *Proceedings of the 31st International Conference on International Conference on Machine Learning - Volume 32*, ser. ICML'14. JMLR.org, 2014, p. II–1764–II–1772.

[4] D. Amodei *et al.*, "Deep speech 2: End-to-end speech recognition in english and mandarin," in *ICML*, 2015.

[5] Z. Zhang *et al.*, "Deep learning for environmentally robust speech recognition: An overview of recent developments," *ACM Trans. Intell. Syst. Technol.*, vol. 9, no. 5, Apr. 2018. [Online]. Available: https://doi.org/10.1145/3178115

[6] J. Barker, E. Vincent *et al.*, "The pascal "CHiME" speech separation and recognition challenge," *Computer Speech & Language*, vol. 27, p. 621–633, 05 2013.
[7] K. Kinoshita, M. Delcroix, S. Gannot, E. A. P. Habets *et al.*, "A summary of the "REVERB" challenge: state-of-the-art and remaining challenges in reverberant speech processing research," *EURASIP Journal on Advances in Signal Processing*, vol. 2016, no. 1, 2016.
[8] P. Werbos, "Backpropagation: Past and future," in *Neural Networks, 1988., IEEE International Conference On*, vol. I, 08 1988, pp. 343 – 353 vol.1.
[9] V. Mnih, Kavukcuoglu *et al.*, "Human-level control through deep reinforcement learning," *Nature*, vol. 518, no. 7540, p. 529–533, 2015.
[10] Y. Wu and e. a. Mike Schuster, "Google's neural machine translation system: Bridging the gap between human and machine translation," *CoRR*, vol. abs/1609.08144, 2016. [Online]. Available: http://arxiv.org/abs/1609.08144
[11] L. Bahl, F. Jelinek, and R. Mercer, "A maximum likelihood approach to continuous speech recognition," *Pattern Analysis and Machine Intelligence, IEEE Transactions on*, vol. PAMI-5, pp. 179 – 190, 04 1983.
[12] L. R. Rabiner, "A tutorial on hidden Markov models and selected applications in speech recognition," *Proceedings of the IEEE*, vol. 77, no. 2, pp. 257–286, Feb 1989.
[13] A. Senior, G. Heigold, M. Bacchiani, and H. Liao, ""GMM"-free "DNN" training," in *Proceedings of the International Conference on Acoustics, Speech and Signal Processing*, 01 2014.
[14] M. Bacchiani, A. W. Senior, and G. Heigold, "Asynchronous, online, "GMM"-free training of a context dependent acoustic model for speech recognition," in *INTERSPEECH*, 2014.
[15] A. Graves, S. Fernández *et al.*, "Connectionist temporal classification: Labelling unsegmented sequence data with recurrent neural networks," in *Proceedings of the 23rd International Conference on Machine Learning*, ser. ICML '06. New York, NY, USA: Association for Computing Machinery, 2006, p. 369–376. [Online]. Available: https://doi.org/10.1145/1143844.1143891
[16] D. Wang, X. Wang, and S. Lv, "An overview of end-to-end automatic speech recognition," *Symmetry*, vol. 11, p. 1018, 08 2019.
[17] Y. M. Assael *et al.*, "Lipnet: Sentence-level lipreading," *CoRR*, vol. abs/1611.01599, 2016. [Online]. Available: http://arxiv.org/abs/1611.01599
[18] B. Shillingford, Y. Assael *et al.*, "Large-Scale Visual Speech Recognition," *arXiv e-prints*, p. arXiv:1807.05162, July 2018.
[19] H. Sak, A. Senior, A. Graves *et al.*, "Learning acoustic frame labeling for speech recognition with recurrent neural networks," in *2015 IEEE International Conference on Acoustics, Speech and Signal Processing (ICASSP)*, 04 2015, pp. 4280–4284.
[20] A. L. Maas, A. Y. Hannun, D. Jurafsky, and A. Y. Ng, "First-pass large vocabulary continuous speech recognition using bi-directional recurrent "DNNs"," *CoRR*, vol. abs/1408.2873, 2014. [Online]. Available: http://arxiv.org/abs/1408.2873
[21] G. Zweig *et al.*, "Advances in all-neural speech recognition," *CoRR*, vol. abs/1609.05935, 2016. [Online]. Available: http://arxiv.org/abs/1609.05935
[22] A. Karpathy, J. Johnson, and F. Li, "Visualizing and understanding recurrent networks," *CoRR*, vol. abs/1506.02078, 2015. [Online]. Available: http://arxiv.org/abs/1506.02078
[23] D. Bahdanau, K. Cho, and Y. Bengio, "Neural machine translation by jointly learning to align and translate," *CoRR*, vol. abs/1409.0473, 2014.
[24] A. Buday, A. Čižmár, and J. Juhár, "Microphone array speech enhancement using "LSTM" neural network," in *ICETA 2019: 17th International Conference on Emerging eLearning Technologies and Application, Starý Smokovec (Slovakia)*, 11 2019, pp. 100–107.
[25] S. Watanabe, T. Hori, S. Karita, T. Hayashi *et al.*, ""ESPnet": End-to-end speech processing toolkit," *CoRR*, vol. abs/1804.00015, 2018. [Online]. Available: http://arxiv.org/abs/1804.00015

Evaluation of 1.6 Tbps CSRZ-DQPSK DWDM System

[1]*Tomáš HUSZANÍK (3rd year)*
Supervisor: [2]Ján TURÁN

[1,2]Dept. of Electronics and Multimedia Communications, FEI TU of Košice, Slovak Republic

[1]tomas.huszanik@tuke.sk, [2]jan.turan@tuke.sk

***Abstract*—This paper deals with the optical carrier suppression (OCS) over optical fiber dense wavelength division multiplexing (DWDM) system considering advanced optical modulation methods, such as optical differential quadrature phase shift keying. The method of suppressing the carrier within the modulation process is the useful method to mitigate fiber nonlinear effects and thus reach better overall performance. The quantitative simulation results validate that the carrier suppression could improve the resistance of fiber nonlinear effects in the high capacity DWDM system.**

***Keywords*—carrier suppression, DWDM, fiber optics**

I. Introduction

In order to minimize linear and nonlinear effects in high-capacity DWDM systems, optimal modulation format needs to be found. A narrow band modulation format can increase spectral efficiency and chromatic dispersion resistance. Conversely, a modulation format with constant optical performance may be less prone to SPM and XPM. A multilevel modulation format can contain more information than a binary signal, and due to the longer symbol duration, it reduces degradation due to chromatic and polarization dispersions. In addition, remote transmission is an important factor influencing the occurrence of non-linear phenomena, as well as the amplification of the optical signal often carried out by an Erbium Doped Fiber Amplifier (EDFA), which also introduces noise into the system and, under certain circumstances (depending on the length of erbium doped fiber) the non-linear SPM and XPM phenomena can build up in the optical fiber [1, 2].

The current generation of optical fiber networks relies mainly on the basic optical modulation techniques such as OOK (On-Off Keying) or OPM (Optical Phase Modulation). These modulation techniques are satisfactory for the majority of applications. However, with the ever-increasing demand of multimedia, high data rates and transmission distances these modulation techniques become inadequate. Due to the nature of the single-mode optical fiber, the optical nonlinear effects are dominant degradation mechanisms in high data rate and long-distance transmission [3-6].

II. Simulation Model

The performance of NRZ-DQPSK and CSRZ-DQPSK modulated 16-channel DWDM system with the data rate of 100 Gbps per channel was firstly analyzed over 15 optical segments. Each segment includes 50 km of HNFL, 10 km of DCF and two EDFAs. Block diagram of proposed DWDM is in Fig. 1. Fig. 2 shows the eye diagrams of received signals after 5 loops (250 km). The most important parameters of the eye diagram are the eye opening and the thickness of the lines. CSRZ-DQPSK modulated DWDM system shows better eye opening which indicates lower bit error rate (BER) and higher Q-factor. NRZ-DQPSK modulated DWDM system shows less opened eye diagram. Thicker the lines of the eye diagram, higher the bit rate. The thickness of the lines also indicates the OSNR (Optical Signal-to-Noise Ratio). In term of these results, the nonlinear effects can be mitigated by deployment of carrier suppressed optical modulation. Fig. 3 shows eye diagrams of the signals of the same DWDM system received after 550 km (11 loops).

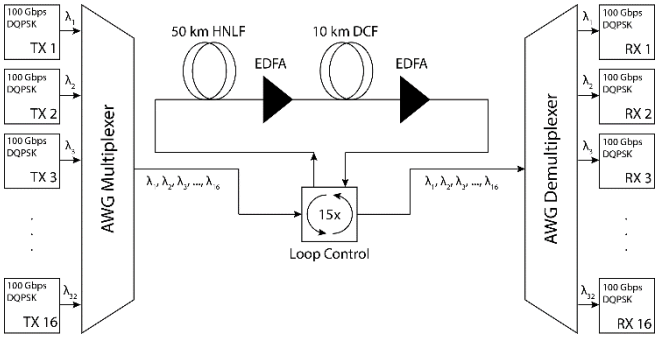

Fig. 1. 16-channel 100 Gbps DQPSK DWDM system.

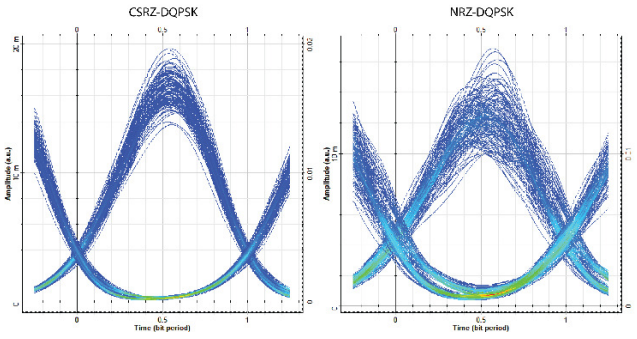

Fig. 2. Eye diagrams of received signals after 250 km.

The dependence between the length of the fiber optical transmission path and the modulation method used in DWDM is shown in Fig. 4.

In the next experiment, the effect of increased CW laser launch power on the creation of fiber nonlinear effects is analyzed. The transmission distance is set to 350 km

(7 loops). The CW laser launch power is linearly swept from 0 dBm to 10 dBm. This dependence is in Fig. 5.

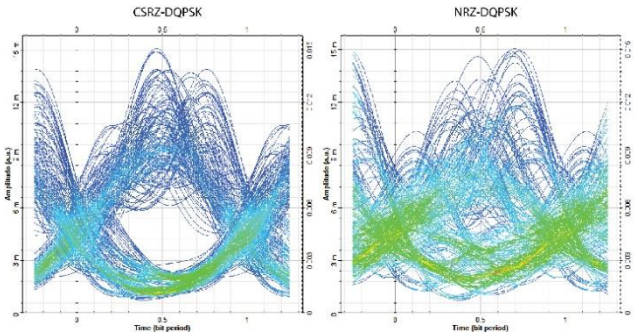

Fig. 3. Eye diagrams of received signals after 550 km.

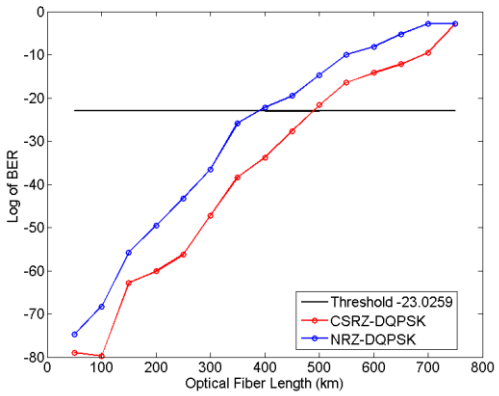

Fig. 4. Optical spectra of DQPSK modulated signal.

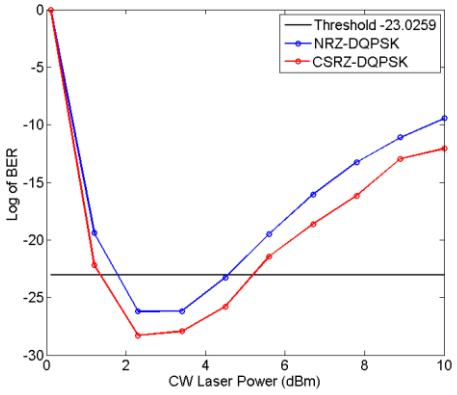

Fig. 5. Optical spectra of DQPSK modulated signal.

Our research of the influence of fiber nonlinear effect started by publishing the article [6]. In this article we investigated the influence of several intensity optical modulation techniques in 10 Gbps DWDM system on the impact of fiber nonlinear effects. We came to the conclusion, that the performance of the DWDM with the basic NRZ-OOK (Non-Return-to-Zero On-Off Keying) can be increased by simple modifications of the original transmitter - CSRZ-OOK (Carrier-Suppressed-Return-to-Zero On-Off Keying) showed the best resistance to fiber nonlinear effects [7-13].

III. Future Work

Our future work is defined by dissertation thesis:

1) Design of multichannel high-capacity Ultra-DWDM systems for the investigation of nonlinear effects (SPM, XPM and FWM) for transmission of signals in fully optical transmission networks.
2) Design of implementation of modified advanced optical modulation formats to reduce the impact of nonlinear phenomena suitable for multichannel high-capacity Ultra-DWDM optical transmission systems.
3) Optimization of optical link with the optical amplifier (EDFA, SOA and ROA) transmission paths in high-capacity Ultra-DWDM optical transmission systems.

Acknowledgment

This work was supported by following research grants: "APVV-17-0208 - Resilient mobile networks for content delivery".

References

[1] S. P. Singh and N. Singh, "Nonlinear Effects in Optical Fibers: Origin, Management and Applications," *Progress In Electromagnetics Research*, vol. 73, 249-275, 2007. DOI:10.2528/PIER07040201.

[2] H. Nain, U. Jadon, V. Mishra, "Performance investigation of Kerr effects on to WDM fiber optical networks," *IEEE International Conference on Recent Trends in Electronics, Information and Communication Technology*, 2016, pp. 2018-2022, DOI: 10.1109/RTEICT.2016.7808193.

[3] T. Huszaník, "Analytical Review of Erbium-Ytterbium Waveguide Amplifier for C-Band Allocated DWDM System," Poster 2019 : proceedings of the international student scientific conference, p. 1-4, 2019. ISBN 978-80-01-06581-5.

[4] T. Huszaník, J. Turán, Ľ. Ovseník, "Realization of a Long-haul Optical Link with Erbium Doped Fiber Amplifier," Carpathian Journal of Electronic and Computer Engineering. vol. 11, no. 2, p. 44-49, 2018. ISSN 1844-9689.

[5] T. Huszaník, "Influence of Co-directional EDFA on 16x40Gbps DWDM Communication System," POSTER 2018, p. 1-6, 2018. ISBN 978-80-01-06428-3.

[6] P. Ivaniga, T. Ivaniga, J. Turán, Ľ. Ovseník, M. Márton, D. Solus, J. Oravec, T. Huszaník, "The influence of FWM with AWG multiplexor in DWDM system," Przeglad Elektrotechniczny. vol. 94, no. 4, p. 113-117, 2018 ISSN 0033-2097.

[7] T. Huszaník, J. Turán, Ľ. Ovseník, "On Mitigation of Four-Wave Mixing in High Capacity Ultra-DWDM System," ICCC 2019: 20th International Carpathian Control Conference (ICCC), p. 1-4, 2019. ISBN 978-1-7281-0701-1.

[8] T. Huszaník, J. Turán, Ľ. Ovseník, "Mitigation of Fiber Nonlinear Effects in 1.28 Tbps DQPSK Modulated DWDM System," Electronics. - Banja Luka, vol. 23, no. 1, p. 3-10, 2019. ISSN 1450-5843.

[9] T. Huszaník, J. Turán, Ľ. Ovseník, "Comparative Analysis of Optical IQ Modulation in Four-channel DWDM System in the Presence of Fiber Nonlinearities," ICCC 2018: 19th International Carpathian Control Conference (ICCC)., p. 468-473, 2018. ISBN 978-1-5386-4761-5.

[10] T. Huszaník, J. Turán, Ľ. Ovseník, "On The Impact of Fiber Nonlinear Effects on The CP-DQPSK Modulated Ultra-DWDM System," Acta Electrotechnica et Informatica, vol. 19, no. 4, p. 21-28, 2019. ISSN 1335-8243.

[11] T. Huszaník, J. Turán, Ľ. Ovseník, "Evaluation of CP-DQPSK modulated DWDM system with highly nonlinear fiber in C band," Radioelektronika 2019 : 29th International conference. – Pardubice, p. 304-307. ISBN 978-1-5386-9321-6.

[12] T. Huszaník, J. Turán, Ľ. Ovseník, "On the Carrier Suppressed Optical Modulation Methods for High Capacity DWDM Systems," IEEE 15th International Scientific Conference on Informatics, p. 171-174, 2019. ISBN 978-1-7281-3178-8.

[13] T. Huszaník, J. Turán, Ľ. Ovseník, "Experimental Simulation of Coherent 40 GBPS 2-DPSK DWDM Long-haul Fiber Optical System with Counter-directional EDFA," Acta Technica Napocensis, vol. 59, no. 2, p. 5-8, 2018. ISSN 1221-6542.

Explainable Artificial Intelligence: A review

[1]*Ivan Čík (1st year),*
Supervisor: [2]*Marián MACH*

[1,2]Dept. Cybernetics and Artificial Intelligence, FEI TU of Košice, Slovak Republic

[1]ivan.cik@tuke.sk, [2]marian.mach@tuke.sk

***Abstract*—Nowadays, artificial intelligence is a trend that is used in every application field, e.g. in finance, healthcare, sport, music, military and many others. Advances in areas such as healthcare, law, government, finance, military or self-driving cars have also brought attention to trust-related problems. Lack of transparency and interpretability is the issue with many state-of-the-art models. This article describes the current approaches in explainable artificial intelligence.**

***Keywords*—explainable artificial intelligence (XAI), deep learning (DL), machine learning (ML)**

I. Introduction

The increase in computational power has allowed the emergence of a sub-area of artificial intelligence called deep learning and we also achieved super performance in many tasks that were previously thought to be computationally unattainable [1]. Improvements in artificial intelligence and deep learning were made possible by the rise of available information, hardware enhancements, new optimization algorithms, open-source libraries, datasets and etc. Advances in areas such as healthcare, law, government, finance, military or self-driving cars have also brought attention to trust-related problems. Deep learning approach has been criticized in [2], where the credibility of the results has been questioned, pointing to weaknesses in language and vision models. In [3] for visual recognition and in [4], [5] for language processing spoofability and biasedness have been demonstrated.

Until now there has been no robust solution to these problems. The current problem is that we do not see in-depth the algorithms of deep learning, so we do not understand why do we have the exact result. Lack of transparency and interpretability is the issue with many state-of-the-art models. In some cases it would be unbearable for us to know what is happening in these algorithms, such as medical diagnosis, where a confidence criterion is a basis for a model decision. The key solution would be to know why the algorithm output is as trustworthy as obtaining this information would not reduce the performance of the algorithm. Due to these problems, explainable artificial intelligence (XAI) has become an area of interest in the research community. This paper summarizes recent developments in this field.

II. Understanding Explainable Artificial Intelligence

A. Basic terms in Expliable Artificial Intelligence

By the term explainable AI (XAI) was first mentioned in 2004 by Van Lent *et al.* [6], where they tried to explain the behavior of AI-controlled entities during computer game simulations. However as the term is relatively new, we have encountered the problem of explainability earlier in the 1970s when research focused on the explanation of expert systems [7].

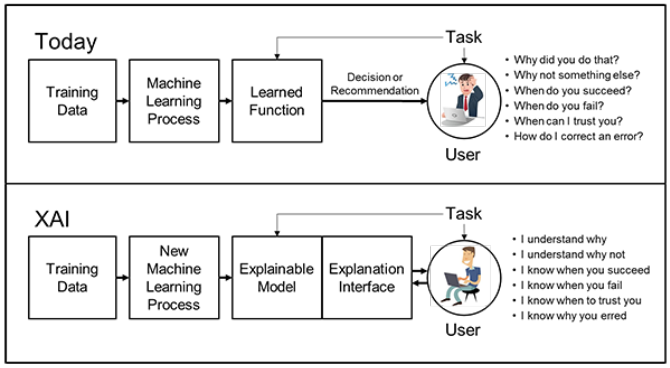

Fig. 1: Today's systems without XAI against today's systems with XAI [8]

Fig 1 shows the difference between XAI today and in the future based on [9]. Technically, there is no standard and generally accepted definition of explainable AI [10]. According to DARPA [8], the definition of XAI is "XAI will create a suite of machine learning techniques that enables human users to understand, appropriately trust, and effectively manage the emerging generation of artificially intelligent partner".

Trust is described in [11] as a psychological state in which an entity becomes willingly and securely vulnerable, or depends on, a trustee having taken into consideration the trustee's characteristics.

At the Fairness, Accountability, and Transparency in Machine Learning [12], the main goal of explainability in machine learning, " is to ensure that algorithmic decisions, as well as any data driving those decisions, can be explained to end-users and other stakeholders in non-technical terms".

As stated by FICO, the organizer of Explainable Machine Learning Challange [13], see XAI as "opening up the black-box of ML [14] " and " explanation of artificial intelligence [15]" in a specific domain- finance is defined.

textbfExplainability is similar to the concept of interpretability: interpretable systems are explainable if their operations can be understood by humans. In [16] interpretation is the mapping of abstract concepts into a domain that humans can make a sense of, while the explanation is the set of interpretable domain features that have helped to generate a decision for a given example. **An interpretable system** is a system in which the user understands how inputs are

mathematically mapped to outputs [17]. Sometimes terms "interpretability" and "explainability" are used synonymously [18], [19]. In industry [20] they prefer to use term "intelligible AI" , while some researchers use another terms such as "understandability" [21] or "comprehensibility" [22].

In science, computing, and engineering, a **black box** is a device, system or object that allows us to see the inputs and outputs but without any knowledge of its internal workings. The human brain, an engine or almost anything can be referred to as a black box. There are also terms like white box and gray box, these terms are used for describing the amount of the knowledge we have about its internal working [23]. In particular, a black box component does not disclose anything about its internal design, structure and implementation, contrariwise a white box component is completely understandable by its user. There is no specific definition for a grey box, which means there may exist different levels of the grey box depending upon how many details are available. The black-box problem is described by the difficulty to find an suitable explanation of how the system arrived at an answer. This problem is addressed in XAI research.

Responsible AI is an AI that considers societal values, moral and ethical considerations. Responsible AI has three main pillars: Accountability, Responsibility and Transparency. Together, these considerations form the A.R.T. (Accountability, Responsibility, and Transparency) principles for AI [24]:

- Accountability refers to the need for its owners, consumers and others with whom the program communicates to explain and justify its decisions and actions.
- Responsibility refers to the position of individuals themselves and the capacity of AI systems to react to their own decisions and recognize errors or unexpected results.
- Transparency refers to the need to describe, inspect and reproduce the mechanisms through which AI systems make decisions and learns to adapt to its environment, and to the governance of the data used created [12].In [25] transparency is one of the properties that can enable interpretability.

XAI focuses on the task of demystifying the black boxes, and also implies Responsible AI as it can help to create transparent models. This should happen without affecting the accuracy of the AI models, but there is a tradeoff between accuracy and interpretability in AI in general and in ML specifically. An obvious connection with the field of data science exists because accuracy is closely linked to the quality and quantity of the training data.

B. Why do we need XAI?

There are at least four reasons, based on the explored literature, that the need for explaining AI systems is needed, although it may appear that there is an overlap between there four reasons:

- Explain to justify - There were several controversies over AI / ML-powered systems that yielded biased or discriminatory results over the last several years [26], [27].
- Explain to control - Understanding system behavior provides greater visibility over unknown bugs and defects and helps identify and correct errors in low critical situations.
- Explain to improve - A model that can be clarified and understood is one that can be boosted easier.
- Explain to discover - Asking for answers is a valuable tool for learning new facts, gathering information and thus gaining knowledge.

However, not everyone agrees that the need for interpretability is necessary. Google research director Norvig looked at the fact that even people can not explain their decisions often. He claimed that the credibility of the AI system can be achieved by monitoring the outputs over time [28]. Explainability is an integral property, although it is not always a necessity. In reality, requiring each AI system to justify each decision could lead to less efficient systems, forced design choices and a bias towards explainable, but less capable and versatile outcomes. Furthermore, making AI systems explainable is computationally demanding. It is important to think about why do we need explanations, the need for explainability depends on:

- The degree of functional opacity caused by the complexity of AI algorithms (if it is low, no high level of interpretability is required)
- The degree of resistance of the application domain to errors (if it is high resistance, unexpected error are acceptable)

C. The technical challenge

Apparently, knowledge and demand for explanation are growing in different domains, hence the question as "why the use of XAI is not systematic?" or "why is XAI not being used in every AI system?".

It is currently a very difficult technical issue to add interpretability to AI systems. In some cases expert systems are explainable but inflexible and hard to use, sometimes we use Deep Neural Networks as a solution. The main advantage of these algorithms is that they are effective but on the other hand it is virtually impossible to see inside.

Advanced machine learning algorithms go to the opposite end of the spectrum, generating systems able to function solely from observations and construct their own world models on which to base their predictions. Nonetheless, the complexity which gives ML algorithms exceptional predictive abilities often makes the results that the algorithms generate difficult to understand. Nevertheless, because of their structure and how they operate, ML algorithms are difficult to interpret. Intrinsically, ML algorithms consider high-degree interactions between features of inputs which make it difficult to disaggregate such functions into humanly understandable forms. We take the most popular contemporary ML model, the DNN as an example. DNN has a common nonlinear multilayer structure consisting of many hidden layers and several neurons per layer, this architecture allows to generate high-level prediction by multiple levels of linear transformations and nonlinear activations. While a single linear transformation can be represented by looking at the weights from the input features to each of the output groups, multiple layers and non-linear correlations in each layer suggest that a super-complicated hierarchical structure is separated, which is a complex and theoretically problematic process[29].

III. Related Work

Considering the rapid expansion of the amount of research into interpretable and explainable AI, there are few research

articles in this field according to the literature. There are two inevitable position papers [25] and [30] which attempt to formalize the principle of explainability. Lipton's work provides a solid overview of what could be interpretability through the lens of the literature. The overview of Dhishi-Velez and Kim was attempting to define taxonomies and best practices for interpretability as a "rigorous science" and the main contribution of this paper is a taxonomy of assessment of interpretability. Authors shifted their focus to just one aspect of expendability - calculating it.

Based on 289 core papers and 12 412 citing papers, Abdul *et al.* in [31] examined a substantial literature of explainable research and built a citation network. This work focuses mainly on the human-computer interaction research agenda in explainability.

A review by Guidotti *et al.* [32] describes methods for understanding large scale black-box models including data mining and machine learning. They provided a comprehensive taxonomy of explainability methods depending on the type of problem confronted. A detailed technical analysis of the methods studied makes it difficult to get a simple understanding of the methods of description space.

A general overview of the topic has been proposed by Dosilovic *et al.* in [33]. Under the supervised learning paradigm they introduced the progress on explainability in machine learning models, with a particular focus on DNN.

IV. METHODS FOR INTERPRETABILITY AND EXPLAINABILITY

To make the AI system explainable, several methods and strategies have been presented in a relatively short time. In this section, we present a description of some interpretability methods. There are two types of interpretability and explainability approaches integrated (transparency-based) and post-hoc.

The first step towards the protection of rights in human-based institutions was transparency. It implies openness, accountability and communication. Analogically, it was translated into algorithms as a concept. Nevertheless, AI models are becoming much more complex than human-based organizations, so finding a meaningful explanation that users would understand becomes difficult. Human reasoning, including ours, is also not clear to us, and justifications in the form of explanations and interpretations that vary from the process of the actual decision. Therefore, predictive performance and transparency are competing priorities, and they must be traded-off in a model [34], [35]. It is not clear how transparent the AI system should be in the long run, although if the system is self-contained and robust enough it may not be necessary. If it is part of other systems, then transparency should be useful for good debuggability.

Post-hoc interpretability derives information from the model already learned and it does not rely specifically on how the model works. This method has the advantage that it does not affect the efficiency of the model that is treated as a black-box. This approach is similar to how people make justifications for their own choices, without fully knowing the real functioning of their decision-making mechanisms. However, we have to consider systems that generate plausible but misleading explanations.

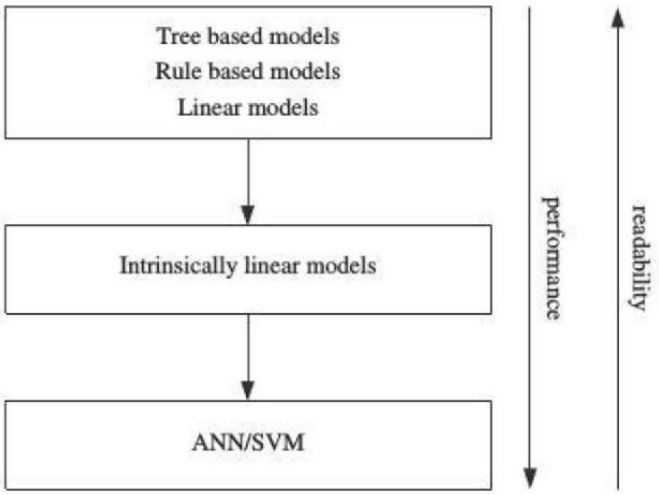

Fig. 2: Performance-transparency trade-off [36]

A. Integrated intepretability

The best explanation for a simple model is the model itself, it is clear and understandable [37]. This approach is limited to less complex model families, such as linear models, decision trees and rules. However, other model families like artificial neural networks (ANN) and support vector machines (SVM), random forests, and boosted trees are considered opaque. The complexity of these algorithms prevents users from finding logic behind predictions. Mostly they are considered as black-boxes and they are dealt with in a post-hoc manner. The tradeoff between these types of algorithms is shown in Fig 2. Models may be subject to various constraints to enhance their interpretability. Some of the constraints used in the literature are model size, sparsity and monotonicity freitas2004critical, martens2011performance. Transparent models are both interpretable and explainable. In [38] decision tables have been described as the easiest option for inexperienced users. The size of this model harms its interpretability, response time and credibility.

Two sub-approaches exist: pure transparent and hybrid.

We are limited to using model families that are considered transparent in pure transparent approaches. In [39], evolutionary programming was used to look for sets of interpretable rules for classification with a limited number of rules and conditions. Interpretable sets of decisions are composed of independent if-then rules. Since each rule can be implemented separately, interpretation is simple. The model is identified by optimizing objective which takes both accuracy and interpretability into consideration.

Hybrid strategies merge transparent model families with black-box methods to get an acceptable trade-off between the interpretability of the model and predictive results. To improve the accuracy of the initial interpretable model, the combination of logistic regression and SVMs was used for credit scoring in [40].

B. Post-hoc methods

Through hardware improvements and 'proved data access, the advantages of using sophisticated, opaque models for predictive analysis are enhanced. Interpretability and explainability are problems that need to be discussed properly, though. We start with qualified black-box predictors in these strategies and,

often, the data used for preparation. Many approaches deal with interpretability while others deal with explainability, as defined in section II-A. Techniques are model-agnostic when they only work with the BB model's inputs and outputs, and model-specific if they use any representation idiosyncrasies.

V. Conclusion

Nowadays machine learning and artificial intelligence solve various problems in different spheres like medicine, law, sports or everyday life. The way neural networks work is still a sort of black box for us. In the future, we would like to focus on various experiments in explainable artificial intelligence. XAI is interested in explaining how individual algorithms map inputs to their outputs. It will be necessary to explain some algorithms in the future in some questions. Experiments such as adding noise to images, cutting out a portion of an image, or following how the classifier is defined will be part of the experiments.

Acknowledgment

This research work was supported by APVV project 015-0730 "Cloud Based Human Robot Interaction" and FEI grant "Increasing Server Performance for Deep Learning" for the year 2020.

References

[1] Y. LeCun, Y. Bengio, and G. Hinton, "Deep learning," *nature*, vol. 521, no. 7553, pp. 436–444, 2015.

[2] G. Marcus, "Deep learning: A critical appraisal," *arXiv preprint arXiv:1801.00631*, 2018.

[3] C. Szegedy, W. Zaremba, I. Sutskever, J. Bruna, D. Erhan, I. Goodfellow, and R. Fergus, "Intriguing properties of neural networks," *arXiv preprint arXiv:1312.6199*, 2013.

[4] T. Bolukbasi, K.-W. Chang, J. Y. Zou, V. Saligrama, and A. T. Kalai, "Man is to computer programmer as woman is to homemaker? debiasing word embeddings," in *Advances in neural information processing systems*, 2016, pp. 4349–4357.

[5] M. J. Wolf, K. Miller, and F. S. Grodzinsky, "Why we should have seen that coming: comments on microsoft's tay" experiment," and wider implications," *ACM SIGCAS Computers and Society*, vol. 47, no. 3, pp. 54–64, 2017.

[6] M. Van Lent, W. Fisher, and M. Mancuso, "An explainable artificial intelligence system for small-unit tactical behavior," in *Proceedings of the national conference on artificial intelligence*. Menlo Park, CA; Cambridge, MA; London; AAAI Press; MIT Press; 1999, 2004, pp. 900–907.

[7] J. Moore and W. Swartout, "Explanation in expert systems: A survey," 01 1989.

[8] D. Gunning, "Explainable artificial intelligence (xai)," *Defense Advanced Research Projects Agency (DARPA), nd Web*, vol. 2, 2017.

[9] K. So, "Why explainable ai is exciting to vcs," Jan 2020. [Online]. Available: https://towardsdatascience.com/investor-view-explainable-ai-5ba66b31cd82

[10] A. Adadi and M. Berrada, "Peeking inside the black-box: A survey on explainable artificial intelligence (xai)," *IEEE Access*, vol. 6, pp. 52 138–52 160, 2018.

[11] B. W. Israelsen, "I can assure you... that it's going to be all right'–a definition, case for, and survey of algorithmic assurances in human-autonomy trust relationships," *ArXiv*, vol. 170800495, pp. 677–686, 2017.

[12] M. FAT, "Fairness, accountability, and transparency in machine learning," *Retrieved December*, vol. 24, p. 2018, 2018.

[13] [Online]. Available: https://community.fico.com/s/explainable-machine-learning-challenge

[14] "Explainable ai breaks out of the black box." [Online]. Available: https://www.fico.com/blogs/explainable-ai-breaks-out-black-box

[15] [Online]. Available: https://community.fico.com/s/explainable-machine-learning-challenge

[16] G. Montavon, W. Samek, and K.-R. Müller, "Methods for interpreting and understanding deep neural networks," *Digital Signal Processing*, vol. 73, pp. 1–15, 2018.

[17] D. Doran, S. Schulz, and T. R. Besold, "What does explainable ai really mean? a new conceptualization of perspectives," *arXiv preprint arXiv:1710.00794*, 2017.

[18] P. W. Koh and P. Liang, "Understanding black-box predictions via influence functions," in *Proceedings of the 34th International Conference on Machine Learning-Volume 70*. JMLR. org, 2017, pp. 1885–1894.

[19] M. Bojarski, P. Yeres, A. Choromanska, K. Choromanski, B. Firner, L. Jackel, and U. Muller, "Explaining how a deep neural network trained with end-to-end learning steers a car," *arXiv preprint arXiv:1704.07911*, 2017.

[20] D. S. Weld and G. Bansal, "The challenge of crafting intelligible intelligence," *Communications of the ACM*, vol. 62, no. 6, pp. 70–79, 2019.

[21] A. Andrzejak, F. Langner, and S. Zabala, "Interpretable models from distributed data via merging of decision trees," in *2013 IEEE Symposium on Computational Intelligence and Data Mining (CIDM)*. IEEE, 2013, pp. 1–9.

[22] M. Luštrek, M. Gams, S. Martinčić-Ipšić *et al.*, "What makes classification trees comprehensible?" *Expert Systems with Applications*, vol. 62, pp. 333–346, 2016.

[23] R. R. Suman, R. Mall, S. Sukumaran, and M. Satpathy, "Extracting state models for black-box software components." *Journal of Object Technology*, vol. 9, no. 3, pp. 79–103, 2010.

[24] K. J. Danjuma, "Performance evaluation of machine learning algorithms in post-operative life expectancy in the lung cancer patients," *arXiv preprint arXiv:1504.04646*, 2015.

[25] Z. C. Lipton, "The mythos of model interpretability," *Queue*, vol. 16, no. 3, pp. 31–57, 2018.

[26] R. Caruana, Y. Lou, J. Gehrke, P. Koch, M. Sturm, and N. Elhadad, "Intelligible models for healthcare: Predicting pneumonia risk and hospital 30-day readmission," in *Proceedings of the 21th ACM SIGKDD international conference on knowledge discovery and data mining*, 2015, pp. 1721–1730.

[27] A. Howard, C. Zhang, and E. Horvitz, "Addressing bias in machine learning algorithms: A pilot study on emotion recognition for intelligent systems," in *2017 IEEE Workshop on Advanced Robotics and its Social Impacts (ARSO)*. IEEE, 2017, pp. 1–7.

[28] S. J. Russell and P. Norvig, *Artificial intelligence: a modern approach*. Malaysia; Pearson Education Limited,, 2016.

[29] S. Tan, K. C. Sim, and M. Gales, "Improving the interpretability of deep neural networks with stimulated learning," in *2015 IEEE Workshop on Automatic Speech Recognition and Understanding (ASRU)*. IEEE, 2015, pp. 617–623.

[30] F. Doshi-Velez and B. Kim, "Towards a rigorous science of interpretable machine learning," *arXiv preprint arXiv:1702.08608*, 2017.

[31] A. Abdul, J. Vermeulen, D. Wang, B. Y. Lim, and M. Kankanhalli, "Trends and trajectories for explainable, accountable and intelligible systems: An hci research agenda," in *Proceedings of the 2018 CHI conference on human factors in computing systems*, 2018, pp. 1–18.

[32] R. Guidotti, A. Monreale, S. Ruggieri, F. Turini, F. Giannotti, and D. Pedreschi, "A survey of methods for explaining black box models," *ACM computing surveys (CSUR)*, vol. 51, no. 5, pp. 1–42, 2018.

[33] F. K. Došilović, M. Brčić, and N. Hlupić, "Explainable artificial intelligence: A survey," in *2018 41st International convention on information and communication technology, electronics and microelectronics (MIPRO)*. IEEE, 2018, pp. 0210–0215.

[34] A. A. Freitas, "A critical review of multi-objective optimization in data mining: a position paper," *ACM SIGKDD Explorations Newsletter*, vol. 6, no. 2, pp. 77–86, 2004.

[35] Y. Jin and B. Sendhoff, "Pareto-based multiobjective machine learning: An overview and case studies," *IEEE Transactions on Systems, Man, and Cybernetics, Part C (Applications and Reviews)*, vol. 38, no. 3, pp. 397–415, 2008.

[36] D. Martens, J. Vanthienen, W. Verbeke, and B. Baesens, "Performance of classification models from a user perspective," *Decision Support Systems*, vol. 51, no. 4, pp. 782–793, 2011.

[37] S. M. Lundberg and S.-I. Lee, "A unified approach to interpreting model predictions," in *Advances in neural information processing systems*, 2017, pp. 4765–4774.

[38] J. Huysmans, K. Dejaeger, C. Mues, J. Vanthienen, and B. Baesens, "An empirical evaluation of the comprehensibility of decision table, tree and rule based predictive models," *Decision Support Systems*, vol. 51, no. 1, pp. 141–154, 2011.

[39] A. Cano, A. Zafra, and S. Ventura, "An interpretable classification rule mining algorithm," *Information Sciences*, vol. 240, pp. 1–20, 2013.

[40] T. Van Gestel, B. Baesens, P. Van Dijcke, J. Suykens, J. Garcia, and T. Alderweireld, "Linear and nonlinear credit scoring by combining logistic regression and support vector machines," *Journal of credit Risk*, vol. 1, no. 4, 2005.

Extending the Formalization of Cellular Automata in Lean – Custom Boundary Conditions

[1]*František SILVÁŠI (4th year),*
Supervisor: [2]*Martin TOMÁŠEK*

[1,2]Dept. of Computers and Informatics, FEI TU of Košice, Slovak Republic

[1]frantisek.silvasi@tuke.sk, [2]martin.tomasek@tuke.sk

***Abstract*—We show how to extend our formalization of cellular automata to also allow for definitions of custom boundary conditions. We then define two most common situations – constant boundary and periodic (wrap–around) boundary. We show how to use the periodic boundary on Lengton's Ant cellular automaton.**

***Keywords*—cellular automata, formalization, Lean**

I. Introduction and context

This work is a continuation of our previous study [1] that formalized the theory of cellular automata in Lean. This paper outlines how to extend the mechanization to also allow us to define custom boundary conditions, which is an important step towards brining the formalization closer to its abstract mathematical counterpart. This is important because experts from the field of cellular automata are naturally used to having this possibility.

Not only do we extend the formalization to allow for this eventuality, we also define two very common boundary situations. The constant boundary condition simply behaves as though boundaries of lattices of cellular automata always contain a constant, pre–defined cell state. We do not explicitly formulate an example for this kind of boundary condition as it was the only possibility in our previous work and as such, one can simply confer it [1] to inspect various examples. The second boundary condition we formulate is periodic, which effectively turns our two–dimensional flat topology into a torus, thus creating the illusion of a space wrapping around itself. While the most common models that use this kind of boundary behaviour are traffic–modelling cellular automata [2][3], we use Lengton's Ant [4] instead to demonstrate the concept – for brevity.

II. Modifications and extension

Let us first show the altered definition of cellular automata, now with support for boundary conditions.

```
structure cautomaton (α : Type)
  [decidable_eq α] :=
  (g     : vec_grid₀ α)
  (empty : α)
  (neigh : point → list point)
  (bound : (bounding_box → bounding_box)
       ⊕ (α → vec_grid₀ α → point → α))
  (f     : α → list α → α)
```

The first component of a cellular automaton is a two dimensional lattice g. The field *empty* represents the empty cell state, *neigh* is a neighbourhood function and f is the automaton rule acting on local configurations. Originally, the member *bound* was called *ext* and represented an extension function that would shrink or expand the grid based the needs of the function *f*. Now we have added the possibility to either provide an extension function, or instead give a rule for boundary condition. If one opts into the latter, it is implicitly assumed that no extension of the underlying lattice happens. The boundary itself is a function $(notin : \alpha) \to (lattice : vec\_grid_0\ \alpha) \to (p : point) \to \alpha$. The idea behind it is that we allow for two kinds of behaviours, depending on whether $p \in lattice$. The first argument *notin* allows us to specify a default value, generally used when $p \notin lattice$.

We also define two commonly used boundary situations.

```
def bound_const {α : Type*}
  [grid α] (empty : carrier α)
  (g : α) (p : point) : carrier α :=
  if h : p ∈ g
  then abs_data g p
  else empty
```

This is the most straightforward boundary situation, in which every position outside of underlying lattice is defined to be some constant $empty$. The function $abs\_data\ g\ p$ simply returns a cell of lattice g on position p. Also, we use gbl and gtr to respectively represent bottom left and top right corners of grids – note that gtr can be easily computed from gbl and $rows\ g / cols\ g$. The rest of notation should be self–explanatory.

```
def bound_periodic {α : Type*}
  [grid α] (empty : carrier α)
  (g : α) (p : point) : carrier α :=
  if h : p ∈ g
  then abs_data g p
  else
  if b₁ : (gbl g).y ≤ p.y ∧
            p.y < (gtr g).y
  then
    if p₁ : p.x ≥ (gtr g).x
    then abs_data g P₁
    else abs_data g P₂
  else
  if b₂ : (gbl g).x ≤ p.x ∧
```

```
            p.x < (gtr g).x
  then
    if p₂ : p.y ≥ (gtr g).y
    then abs_data g P₃
    else abs_data g P₄
  else empty
```

Where

$P_1 = \langle$p.y, (gbl g).x + (p.x − (gbl g).x) % (cols g)$\rangle$
$P_2 = \langle$p.y, (gtr g).x − 1 − ((gbl g).x − p.x − 1) % (cols g)$\rangle$
$P_3 = \langle$(gbl g).y + (p.y − (gbl g).y) % (rows g), p.x$\rangle$
$P_4 = \langle$(gtr g).y − 1 − ((gbl g).y − p.y − 1) % (rows g), p.x$\rangle$

The function $abs\_data\ g\ p$ requires a proof of $p \in g$, which is just notation for $(gbl\ g).x < p.x \leq (gtr\ g).x \wedge (gbl\ g).y \leq p.y < (gtr\ g).y$. For brevity, we just note that it is relatively straightforward to show the necessary properties for all P_n. Said proofs are of course formalized in full and we invite the interested reader to inspect the enclosed formalization at https://github.com/frankSil/CAExtensions [5].

This boundary condition specifies periodic boundaries in the sense that "leaving" the lattice from one side has the effect of entering the lattice on the opposite side. This corresponds spatially with a torus.

Having modified the definition of cellular automaton itself, we also need to slightly alter the way we compute with them. The function $ext\_aut\ a$ that expands underlying lattices is changed in a way such that it acts as the identity function in case a boundary condition has been specified. Otherwise it uses the supplied extension function, i.e. the left part of $a.bound$. On the other hand, the function $next\_gen\ a$ that computes future generations of configurations checks if an extension function has been supplied. If so, it uses $bound\_const\ a.empty$. Otherwise we just utilize the provided boundary function, i.e. the second component of the sum $a.bound$.

These changes are fairly trivial and therefore do not warrant an inclusion in–full within the paper. Please do consult the enclosed git repository.

III. Lengton's Ant

Due to space constraints, it is difficult to show the definition. However, we can at the very least demonstrate the behaviour on an example.

Listing 1. Initial configuration

```
. . . . . .
. . . . . .
. . . . . .
. . . . . .
. . . . . .
. . . . . < .
. . . . . .
. . . . . .
. . . . . .
. . . . . .
. . . . . .
```

Now note how the ant fills up some space on the left side, by walking "past" the right side.

Listing 2. 48th generation

```
  . . . . . .
. . . . . .
. . . . . .
. . . . . .
X X . . . . . X X
< . X . . . . X . .
. . X . . . . X . .
. X . . . . . X .
X . . . . . . X
. . . . . .
. . . . . .
```

IV. Conclusions and future work

There was no way to specify custom boundary conditions in the original formalization. We have addressed the issue by providing a convenient way of specifying them by invalidating an automaton's extension function whenever a custom boundary function is present. This ensures that underlying lattices of automata never expand – as of course, only then can we actually reach a boundary. We show on a simple example that the periodic boundary works as intended.

There are many things that need to be added to the formalization still. We currently only support two–dimensional cellular automata and our notion of equality is computational rather than purely judgemental in the sense that equality of automata is defined in terms of equality of underlying cell configurations. Both of these issues can be addressed in a straightforward manner in our formalization. In addition, we also need to provide better support for handling neighbourhoods. We currently have to specify all neighbours exhaustively – a better way of doing it is to allow a user to define notion of closeness and have the automaton find cells that are "close enough". Also, we need to extend the general interface to better support purely judgemental reasoning, as many of our proofs rely heavily on computation. Note that this is of course not a negative as our design was meant to be computation–centric, but it is an important way forward. Finally, we need to make many performance improvements because in the current state, it takes several minutes to evaluate more than 500 generations of just about any automaton.

Acknowledgment

This work was supported by the Slovak Research and Development Agency under the contract No. APVV-15-0055. The paper was supported by project KEGA no. 079TUKE4/2017. This work was supported by FEI TUKE Grant no. FEI-2018-57.

References

[1] F. Silváši and M. Tomášek, "Lean Formalization of Bounded Grids and Computable Cellular Automata Defined Thereover," *Science of Computer Programming*, 2020, to appear in SCP.
[2] C. Applegate, S. Laycock, and A. Day, "Real-time traffic simulation using cellular automata." 01 2010, pp. 91–98.
[3] N. Wu and W. Brilon, "Cellular automata for highway traffic flow simulation," *Proceedings 14th International Symposium on Transportation and Traffic Theory (Abbreviated presentations)*, 01 1999.
[4] C. G. Langton, "Studying artificial life with cellular automata," *Physica D: Nonlinear Phenomena*, vol. 22, no. 1, pp. 120 – 149, 1986, proceedings of the Fifth Annual International Conference. [Online]. Available: http://www.sciencedirect.com/science/article/pii/016727898690237X
[5] F. Silváši and M. Tomášek, 2020, available at: https://github.com/frankSil/CAExtensions.

Extension of Web-based Collaborative Virtual Environments for Mixed Reality Interfaces

[1]*Marián HUDÁK(3rd year)*
Supervisor: [2]Branislav SOBOTA

[1,2]Dept. of Computers and Informatics, FEI TU of Košice, Slovak Republic

[1]marian.hudak.2@tuke.sk, [2]branislav.sobota@tuke.sk

***Abstract*— Web-based Collaborative Virtual Environments (CVEs) enhance user's experiences in solving a variety of collective tasks within one shared virtual environment. With respect to the web Virtual reality (VR), there is a rapid expansion of cross-platform support. However, the utilization of CVEs is facing Mixed Reality (MR) that requires modified visual output. This paper presents the Adaptive 3D Content Filtering (ACFI 3D) interface that is able to modify the content of a web-based CVE for MR usage. The resulting functionality and support can rapidly enhance virtual collaboration through different VR and MR technologies.**

***Keywords*— virtual reality, mixed reality, web-based, virtual environment, virtual collaboration.**

I. INTRODUCTION

In recent years, virtual collaboration has come into multi-purpose use. The utilization of Virtual Reality (VR) and web technologies enables people to interact in variety of shared Collaborative Virtual Environments (CVEs) [1]. In fact, the web-based CVEs are user-friendly considering their simplicity and accessibility through web-browsers. In contrast to standard VR applications, deployment of a web-based CVE is more efficient due to its adaptability on different platforms [2]. That is supported by a considerable minimization of code refactorization when a technology change occurs.

Deployment of web-based CVEs for Mixed Reality (MR) purposes brings Collaborative Mixed Reality Environments (CMREs) [3]. CVEs and CMREs focus on the same context, but through a different technology. Integrating them into a uniformed shared environment can raise their usability in various cases. However, rendering visual output for VR and MR purposes is facing different 3D contents. While VR displays the whole virtual environment, MR concerns only 3D objects on which the collaboration is focused. The filtering of 3D content can ensure proper visual output and optimize rendering performance. Otherwise, utilizing MR with non-filtered CVEs may be confusing and useless for users.

II. LIRKIS G-CVE

During the research, we implemented the LIRKIS G-CVE [4] (Global Collaborative Virtual Environments) a fully immersive web-based VR system that is also a testing platform for VR and MR interfaces. The LIRKIS G-CVE offers an effective approach to a multiuser connection for virtual collaboration in real-time. A variety of end-devices and platforms are supported without any restrictions on their functionality. The architecture of LIRKIS G-CVE includes an Entity-Component System (ECS) that provides high flexibility to deploy a variety of modules and extensions of the system's functionality. Like other web-based systems, the LIRKIS G-CVE utilizes client-server architecture as well.

A. Server-side Implementation

The server is responsible for communication and interaction among clients which concerns all the networking entities. The server side was implemented using three JavaScript frameworks including Node.js, Express.js, and Networked-Aframe (NAF), which support all backend services and handling. Usage of the Node.js manages parallel client connection and handles every asynchronous data stream between each client and a server. The Express.js provides a stable application layer built on the Node.js to perform HTTP requests from clients during connection. The NAF is responsible for each of the Networked-Aframe components (NAC) which consist of the networked scene, all its entities, and features of 3D interaction.

B. Client-side Implementation

In the stage of a client-side interface implementation, the web framework A-frame [5] was chosen. The A-frame is powerful for building virtual and mixed reality front-end applications that are running on clients' web browsers. The drawing of 3D contents is provided by the HTML <canvas> element and served by JavaScript [6]. Therefore, the client-side rendering (CRS) was used to produce visual output and interactions. Considering different 3D content for VR and MR, it was important to create adaptive functionality that is able to recognize type of device and then prepares corresponding visual output.

III. ADAPTIVE 3D CONTENT FILTERING

Taking the diversity between VR and MR technologies, there was implemented the Adaptive 3D Content Filtering Interface (ACFI 3D) as a component of the LIRKIS G-CVE. As shown in Fig.1, the entire component is integrated on the client-side, where the rendering is performed. The main role of the ACFI 3D is to filter the 3D content of the same virtual environment for different VR and MR platforms. The ACFI 3D provides two types of 3D contents of the same CVE.

The first type concerns *Common VR content (CVRC)* which relates to the utilization of VR devices. The visual output includes all parts of the CVE content which contains:

- Main objects, on which the collaboration is focused.
- All surrounding objects, the ambient environment.
- Virtual avatars, visual and haptic interaction.

The second type called *Adaptive MR content (AMRC)* prepares a visual output for MR devices. The 3D content of CVE is filtered into CMRE, which includes:

- Main objects, on which the collaboration is focused.
- Visual and gesture interaction.

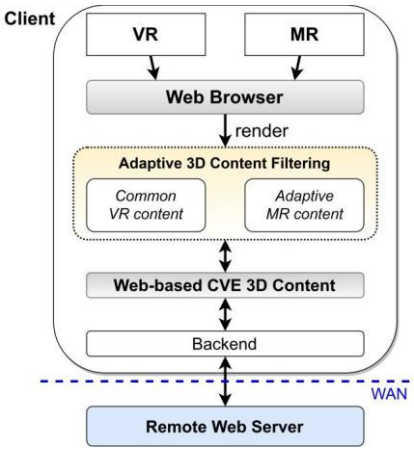

Fig. 1. Integration of Adaptive 3D Content Filtering Interface on the client-side.

IV. Deployment And Testing

The testing of ACFI 3D was held under two devices, the MS HoloLens 1st generation (MR) and Oculus Quest (VR). Both were tested in the same shared CVE containing 70 000 polygons. In the first experiment, it was necessary to find out how the ACFI 3D affects the rendering performance of MS HoloLens. Therefore, the measurements of the framerate in Frames Per Second (FPS) was performed. The first measurement was carried out using CVRC and second under AMRC. Both measurements lasted 300 seconds. The results shown in Fig.2 reflects differences of measured FPS. The average resulted FPS of the AMRC was 27 FPS while the CVRC has only 18 FPS. Unlike CVRC, the AMRC reduced the number of polygons to 50,000 which increases the framerate by filtering surrounding virtual objects.

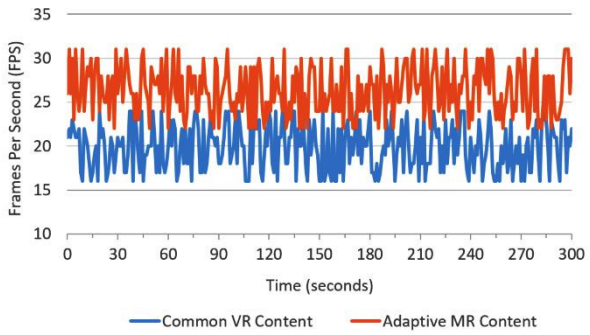

Fig. 2. The resulting comparison of measured FPS on MS HoloLens with utilizing filtered (AMRC) and non-filtered (CVRC) 3D content.

The second experiment was aimed on the visual output, where MS HoloLens utilizes AMRC and Oculus Quest CVRC. The corresponding visual outputs are visible in Fig.3. Two participants were required to work with three 3D objects in one shared virtual environment. On the MS HoloLens, the ACFI 3D modified visual output to only objects that were directly supposed for collaboration.

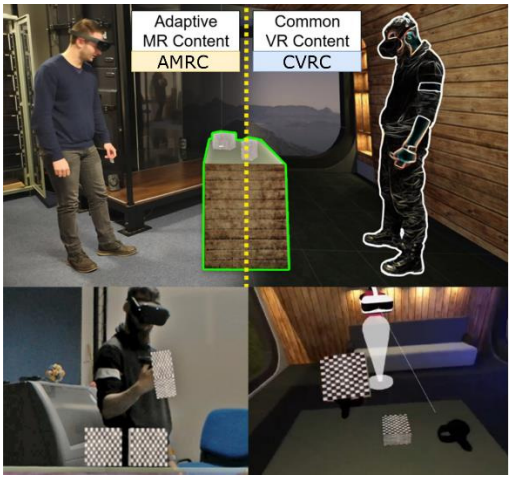

Fig. 3. Testing of ACFI 3D with MS Hololens on the left and Oculus Quest on the right. Both devices are connected to LIRKIS G-CVE.

V. Conclusion

Developing uniformed interfaces for MR and VR is effective for their deployment and use. In the previous research, we have focused on the implementation of LIRKIS G-CVE as a fully immersive and globally accessible VR system. During the research, we have enhanced the system cross-platform support and designed smart interfaces to simplify user interaction. In this paper, we have presented the uniformed interface ACFI 3D which positively affects the usage of VR and MR as one. In further research, we will focus on client rendering performance optimization under WebGL. Reaching this goal can be helpful for speed up performance on devices, that are not equipped with powerful graphics processors.

Acknowledgment

This work has been supported by the APVV grant no. APVV-16-0202 "Enhancing cognition and motor rehabilitation using mixed reality".

References

[1] E., Poppe, R., Brown, J., Recker & D., Johnson. Improving remote collaborative process modelling using embodiment in 3D virtual environments. In *Proceedings of the Ninth Asia-Pacific Conference on Conceptual Modelling-Volume 143*, 2013, pp. 51-60.

[2] W. S., El-Kassas, B. A., Abdullah, A. H., Yousef & A. M., Wahba. Taxonomy of cross-platform mobile applications development approaches. In: *Ain Shams Engineering Journal*, *8*(2), 2017, pp.163-190.

[3] M., Gonzalez-Franco, R., Pizarro, J., Cermeron, K., Li, J., Thorn, W., Hutabarat, P., Bermell-Garcia. Immersive mixed reality for manufacturing training. In Frontiers in Robotics and AI, 2017, no.4, pp.1-3.

[4] M., Hudák, M., Sivý.Web-based collaborative virtual environments to support cross-platform access, In: *Poster 2019 International student scientific conference*, Prague, 2019, pp.178-182.

[5] Aframe: A web framework for building virtual reality experiences homepage (2019), https://aframe.io/

[6] A., Muennoi, D., Hormdee. 3D Web-based HMI with WebGL Rendering Performance. In MATEC Web of Conferences, 2016, vol.77, p.090

External interleaved mode designing by the STM32F446RE microcontrollers

[1]*Patrik JACKO (4th year)*
Supervisor: [2]Dobroslav KOVÁČ

[1,2]Dept. of Theoretical and Industrial Electrical Engineering, FEI TU of Košice, Slovak Republic

[1]patrik.jacko.2@tuke.sk, [2]dobroslav.kovac@tuke.sk

***Abstract*—Speed of AD converters and its resolution are the most important factor for quality signal measuring. These parameters are established by manufacturer. Is it possible increase speed with the same components? In this topic we will talk about external interleaved mode designing with fast microcontrollers STM32F446RE.**

***Keywords*— STM32 microcontroller, STM32F746ZG, STM32F446RE, AD converters, Interleaved mode**

I. INTRODUCTION

The STM32 microcontrollers are strong tools for a various applications – communication with external and internal peripherals, devices controlling such as motors, smart houses, or signal processing by use AD converters. These microcontrollers are special designed for the digital signal processing. Their operating frequency is higher than the others microcontrollers at the same price.

The topic will be focus on the AD converters of STM32F4 microcontrollers. We know that microcontrollers offers fast mode of three ADC combination. Thanks it, ADC makes samples so much faster. This combination is designed by developer, but we want make the other combinations of ADC which name is external interleaved mode. [1]

II. INTERLEAVED MODE OF MICROCONTROLLER STM32F446RE

It is known, that STM32F446RE includes three AD converters operating to 45MHz frequency. The ADC converters work separate or in combination modes. The choice of AD converter combinations depends on the application. If it is necessary to perform samples at one time on several converters, we will use simultaneous mode. If samples need to be performed as quickly as possible, we will use interleaved mode. And interleaved mode is the main part of this article.

Interleaved mode is a fast tool that uses two or three AD converters with a time delay. In this mode, only one channel is used to which all converters are connected. The principle is based on a delayed triggering of individual converters. The ADC1 transducer starts on an external stimulus, while the other transducers start automatically at the selected delay. In this case, the delay is 6 ADC clock pulses. The minimum delay can be 5 ADCCLK (ADC clock cycles). This is to avoid a collision where two converters are sampled at the same time on the same channel. Since the minimum sampling time is 3 ADCCLK, this mode is provided by an additional 2 ADCCLK, after which ADC2 is started. That is, the resulting minimum delay time is 5 ADCCLK. Subsequently, after starting ADC2 and delaying at least 5 ADCCLK, it starts sampling ADC3, after which it resumes scanning ADC1. The trigger time delay between the A/D converters can be set from 5 to 20 ADCCLK. This setting can be made when configuring A/D converters. [2]

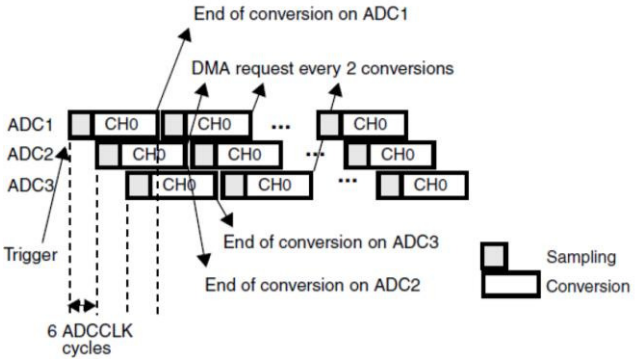

Fig. 1 The Interleaved mode of STM32F446RE microcontroller

III. EXTERNAL INTERLEAVED MODE DESIGN

Interleaved mode designed by the microcontroller manufacturer will be called internal interleaved mode. We know that AD converters of all microcontrollers operate at a frequency of 45MHz. This means that the factory-set internal interleaved mode will run converters at the fastest possible mode at 111.11ns intervals. As our goal is to shorten the sampling time, we have designed the concept of microcontroller involvement to create an external interleaved mode.

The principle of creating an external interleaved mode is based on triggering the converters on individual microcontrollers at precisely determined time intervals. We have stated that the internal interleaved mode requires adherence to the minimum set delay times when starting ADC2 and ADC3. The delay must only be observed within one microcontroller. By applying additional microcontrollers we can shorten this time. The principle is shown in the following figure. We will start from Fig.2, where the process of creating one sample is divided into a

part of sampling and converting to digital form. The above-mentioned rule (delay in triggering converters) applies only to the sampling phase and not to the conversion phase.

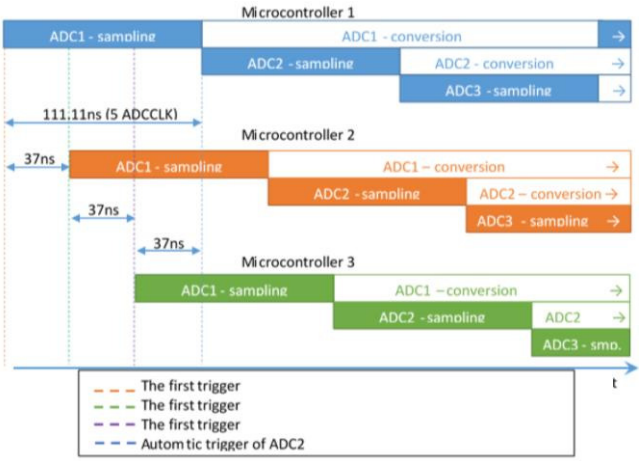

Fig. 2 External interleaved mode design of three microcontrollers

Thus, the external interleaved mode operates such that, within the trigger range of the first and second AD converters of microcontroller 1, we will start, with some time delay, the ADC1 converters on microcontrollers 2 and 3. In order to be able to synchronize the microcontrollers and trigger pulses to trigger the AD converters of the microcontrollers 2 and 3, it is necessary to create a synchronization part of the system. This will be one microcontroller that will control the clock synchronization while sending trigger pulses for microcontrollers 1, 2 and 3.

The design of external interleaved mode will be realized by three microcontrollers STM32F446RE (marked as Slave). The STM32F746ZG microcontroller (referred to as the Master) uses 3 pins - PF0, PF1 and PF2, which are individually connected to the start pins of the AD converters of the Slave microcontrollers (blue, red and orange). The master can send start pulses at specified time intervals to start the AD converters with a certain time delay. In this way we realize the external interleaved mode.

The wiring diagram for the described external interleaved modes is shown in Fig. 3.

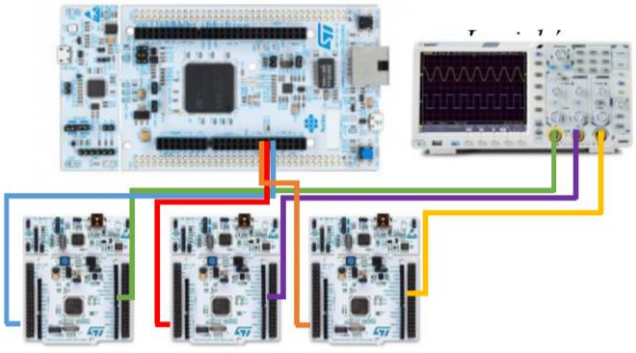

Fig. 3 Connection of trigger wires for AD converters

IV. External Interleaved Mode Testing

Connection and functional verification of the device was realized by logic analyzer Tektronix TLA6202. Three wires from each microcontroller lead to a logic analyzer. In total, 9 conductors are connected to the analyzer, each AD converter having its own conductor. Testing of the external interleaved mode was as follows:

Each microcontroller AD converter contains various status bits in the status register, which inform us about the converter status - conversion error, conversion end, start of conversion. In experimental verification of external interleaved mode functionality, we used conversion start and end conversion states. In these cases, the microcontroller will generate an interrupt that initiates a certain function. In our case, at the start of the conversion, log.1 is set to the pine corresponding to the AD converter, and log.0 is set to this pine at the end of the conversion. Experimental verification of external interleaved mode can be seen in the following figure.

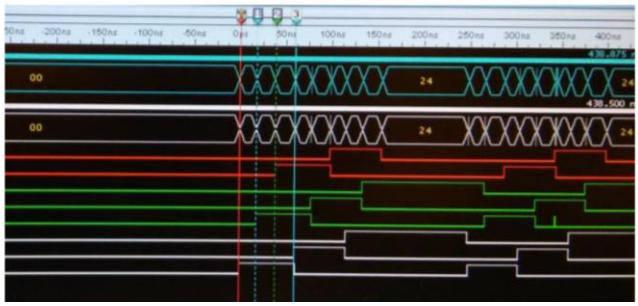

Fig. 4 Verification of external interleaved mode using logic analyzer

The three-color waveforms represent the three STM32F446RE microcontrollers. The waveforms shown in white represent ADC1, ADC2, and ADC3 of microcontroller 1, green waveforms belong to microcontroller 2 and red waveforms belong to microcontroller 3. We can see that the first AD converter was run on microcontroller 1. ADC1 and ADC2 (solid red vertical line and solid vertical blue line) were triggered at the same time intervals by the ADC1 converters of microcontroller 2 and 3. We conclude that the selected method of external interleaved mode is suitable for practical use. If using the internal inteleaved mode, we obtained 90 samples per 100kHz signal per period with 111.11ns sampling time, using the external interleaved mode it is possible to obtain up to 270 samples per 100 kHz signal period. Now is sample time 37ns.

V. Conclusion

Thanks External interleaved mode we can sampling signals with a greater accuracy. The testing was performed by three microcontrollers, but there is possible insert up to 15 microcontrollers, with 7.4 ns sampling time.

Acknowledgment

The paper has been prepared under support of Slovak grant project FEI-2020-61.

References

[1] STMicroelectronic, “STM32F446xC/E” (PDF), 2015
[2] STMicroelectronic, “RM0090 Reference manual” (PDF), 2016

Generalization of minimum redundancy maximum relevance feature selection

[1]*Peter BUGATA (2nd year),*
Supervisor: [2]*Peter DROTÁR*

[1,2]Dept. of Computers and Informatics, FEI TU of Košice, Slovak Republic

[1]peter.bugata@student.tuke.sk, [2]peter.drotar@tuke.sk

***Abstract*—The feature selection is an important challenge in many areas of machine learning. There are various approaches to the feature selection problem and methods based on the information theory comprise an important group. Here, the minimum redundancy maximum relevance (mRMR) feature selection is undoubtedly the most popular one with widespread application. In this paper, we present a form of equivalence of the mRMR method leading to its generalization.**

***Keywords*—dimensionality reduction, feature selection, high-dimensional data, minimum redundancy maximum relevance, mRMR**

I. Introduction

Recently, huge amounts of data have been generated by computer and internet applications in multiple domains. These data often have characteristics of high dimensions and their analysis is a challenge for researchers in the fields of machine learning and data mining. Feature selection (FS) is a dimensionality reduction technique that aims to select a subset of relevant features from the original feature set. Various FS approaches are described in survey papers such as [1], [2], [3].

Probably the most popular[1] from all available FS methods that have widespread application is minimum redundancy maximum relevance (mRMR) FS [4], [5]. It is widely used in many areas such as bioinformatics and multimedia processing [6]. The mRMR is a supervised filter method that iteratively extends the set of selected features by maximizing relevance toward the target variable and at the same time, minimizing the redundancy among the selected features. For calculation of dependency, mutual information is used.

This paper presents the generalization of the mRMR FS method. The rest of the paper is organized as follows: Section II explains the main idea of the mRMR algorithm. Section III discusses the question of mRMR equivalence and describes the generalization of the method. In Section IV the experimental results are shown and Section V presents our conclusion.

II. mRMR feature selection

Let $F = \{f_1, f_2, \ldots, f_k\}$ be a set of k explanatory variables or features and let $\boldsymbol{y}$ be a target variable. The FS aims to find the smaller subset $S \subset F$ that optimally characterizes the target variable $\boldsymbol{y}$. Under optimal characterization, we will understand the highest statistical dependency of the target $\boldsymbol{y}$ on the selected subset S. This criterion is known as a maximal dependency (*Max-Dependency*).

[1]There are more than 3400 Web of Science citations to the paper [4]

Utilizing mutual information (I) as a dependency measure, the *Max-Dependency* criterion can be approximated by a combination of two conditions: maximum relevance (*Max-Relevance*)

$$\max_S D(S,\boldsymbol{y}), \quad D = \frac{1}{|S|}\sum_{f_i \in S} I(f_i;\boldsymbol{y}) \tag{1}$$

and minimum redundancy (*Min-Redundancy*)

$$\min_S R(S), \quad R = \frac{1}{|S|^2}\sum_{f_i,f_j \in S} I(f_i;f_j). \tag{2}$$

The criterion that combines both conditions is the mRMR. The following function represents the simplest way to concurrently optimize relevance D and redundancy R:

$$\max_S \Phi(D(S,\boldsymbol{y}), R(S)), \quad \Phi = D(S,\boldsymbol{y}) - R(S). \tag{3}$$

First-order incremental search can be used to find the feature subset close to the optimal features obtained by maximizing the function Φ (3). In the first step, the feature with the largest relevance toward the target variable is selected. If S is a set of previously selected features, then the next feature is chosen from the others according to the following condition [5]:

$$\max_{f_i \notin S} \left[I(f_i;\boldsymbol{y}) - \frac{1}{|S|}\sum_{f_j \in S} I(f_i;f_j) \right]. \tag{4}$$

III. Equivalence and generalization of mRMR

Whereas the algorithm for *Max-Dependency* is computationally demanding especially in the case of continuous variables, the mRMR algorithm represents a computationally more feasible approach. Peng et al. [4] claims the equivalence of mRMR and *Max-Dependency*:

Theorem 1: For the first-order incremental search, mRMR is equivalent to Max-Dependency.

In [7], we showed that this theorem does not hold. Using a synthetically constructed discrete dataset, we demonstrated the shortcomings of the proof described in [4].

It can also be shown that the results of mRMR based on the definition (4) are different from the results obtained by the incremental algorithm for maximization of the function Φ (3).

To answer the question of mRMR equivalence, we introduced the objective function Φ' about which we proved by induction that the first-order incremental algorithm for its maximization selects the same subset of features as mRMR with the incremental definition (4) [7].

Lemma 1: Let the function Φ' be defined as follows:

$$\Phi'(S) = \frac{1}{|S|}\sum_{f_i \in S} I(f_i;\mathbf{y}) - \frac{1}{2\,|S|\,(|S|-1)}\sum_{\substack{f_i,f_j \in S,\\ i\neq j}} I(f_i;f_j).$$

For the first-order incremental search, mRMR is equivalent to the algorithm for maximization of the function Φ'.

The objective function Φ' is the difference between the average dependency of the explanatory variables on the target variable $\mathbf{y}$ and the average dependency between different variables in the set S to each other weighted by $\frac{1}{2}$. The function Φ' allows generalizing the mRMR algorithm by applying various weights $\lambda \in \mathbb{R}^+$ of the average redundancy.

Using the first-order incremental search, the generalized mRMR maximizes the function defined for $\lambda \in \mathbb{R}^+$ as follows:

$$\Phi'_\lambda(S) = \frac{1}{|S|}\sum_{f_i \in S} I(f_i;\mathbf{y}) - \frac{\lambda}{|S|\,(|S|-1)}\sum_{\substack{f_i,f_j \in S,\\ i\neq j}} I(f_i;f_j).$$

IV. Experimental Results

To examine the influence of the weight of the average redundancy λ on FS quality, we conducted experiments for eight high-dimensional real-world datasets stated in Table I precisely cited in [7]. They are publicly available DNA microarray datasets that constitute the binary classification tasks.

TABLE I
Characteristics of Datasets Used

Dataset (Abbr.)	Samples	Features	Class 0	Class 1
Alon (ALN)	62	2,000	40	22
Burczynski (BRC)	127	22,283	85	42
Chowdary (CHW)	104	22,283	62	42
Golub (GLB)	72	7,129	47	25
Gordon (GRD)	181	12,533	94	87
Pomeroy (PMR)	60	7,128	39	21
Singh (SNG)	102	12,600	52	50
Tian (TIA)	173	12,625	36	137

We used nine values of $\lambda = 0.00, 0.25, 0.50$ up to 2.00. If the weight is $\lambda = 0.00$, no redundancy is considered. For $\lambda = 0.50$, the average redundancy has half the weight of the average relevance and the optimization task is equivalent to the original mRMR (*Lemma* 1). As the maximum λ, we used the value of 2.00, where the weight of the average redundancy is twice as the weight of the average relevance.

For each value λ, we evaluated the prediction performance of four classifiers on given datasets after applying FS using the generalized mRMR. Fig. 1 shows ranks of maximum values of F_1 score obtained from the four classifiers – for each dataset, the best value gets the rank of 1, the second best rank 2, etc.

The experiments showed that the value of λ influences the quality of the FS. For all datasets, we obtained distinct feature subsets for all λ values. The optimal value of the weight λ depends on a particular dataset, e.g., in the case of the Pomeroy dataset, maximum F_1 score was achieved with $\lambda = 0.25$, whereas for the Singh dataset, it was for $\lambda = 1.75$.

The summary of the experimental results is in Table II, where we present the average ranking obtained on examined datasets and computed from maximum and average values of F_1 score for all four used classifiers. As the results show, too-small values of λ (0.00, 0.25) or too large values (2.00) yield suboptimal results. For the test datasets in general, the optimal values are in the range 0.75 to 1.50, which are higher weights of redundancy as in the standard mRMR ($\lambda = 0.50$).

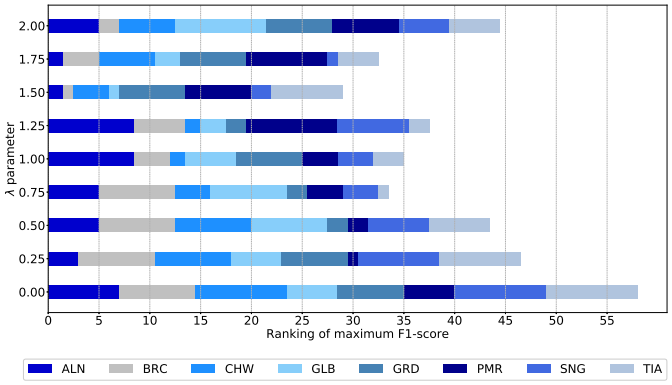

Fig. 1. Ranking of maximum F_1 score versus parameter λ.

TABLE II
Mean Ranks of Maximum and Average F_1 Score Versus λ

par. λ	0.00	0.25	0.50	0.75	1.00	1.25	1.50	1.75	2.00
max F_1	7.25	5.81	5.44	**4.19**	**4.38**	**4.69**	**3.63**	**4.06**	5.56
avg F_1	6.88	5.38	**4.50**	**3.81**	**4.06**	**3.94**	**4.69**	5.13	6.63

V. Conclusion

FS is one of the essential tools in machine learning which has a significant impact on the performance and interpretability of a predictive model. In this paper, we focused on the minimum redundancy maximum relevance (mRMR) method, which is the very popular FS method based on the information theory. We defined the objective function whose maximization is equivalent to mRMR and provided its generalization. In experimental results, we presented the optimal parameter values of the generalized mRMR for DNA microarray datasets.

Further research focuses not only on the analysis and generalization of known FS methods, but also on designing new FS methods in accordance with current challenges in this area [2].

Acknowledgment

This work was supported by the Slovak Research and Development Agency under the contract No. APVV-16-0211.

References

[1] J. C. Ang, A. Mirzal, H. Haron, and H. N. A. Hamed, "Supervised, unsupervised, and semi-supervised feature selection: A review on gene selection," *IEEE/ACM Transactions on Computational Biology and Bioinformatics*, vol. 13, no. 5, pp. 971–989, 09 2016.

[2] Y. Li, T. Li, and H. Liu, "Recent advances in feature selection and its applications," *Knowledge and Information Systems*, vol. 53, no. 3, pp. 551–577, 12 2017. [Online]. Available: https://doi.org/10.1007/s10115-017-1059-8

[3] J. Li, K. Cheng, S. Wang, F. Morstatter, R. P. Trevino, J. Tang, and H. Liu, "Feature selection: A data perspective," *ACM Comput. Surv.*, vol. 50, no. 6, 12 2017. [Online]. Available: https://doi.org/10.1145/3136625

[4] H. Peng, F. Long, and C. Ding, "Feature selection based on mutual information: Criteria of Max-Dependency, Max-Relevance, and Min-Redundancy," *IEEE Trans. on Pattern Analysis and Machine Intelligence*, vol. 27, no. 8, pp. 1226–1238, 2005. [Online]. Available: https://ieeexplore.ieee.org/document/1453511

[5] C. Ding and H. Peng, "Minimum redundancy feature selection from microarray gene expression data," *Journal of bioinformatics and computational biology*, vol. 3, no. 02, pp. 185–205, 2005.

[6] A. Toyoda, T. Ogawa, and M. Haseyama, "Favorite video estimation based on multiview feature integration via KMvLFDA," *IEEE Access*, vol. 6, pp. 63 833–63 842, 2018.

[7] P. Bugata and P. Drotár, "On some aspects of minimum redundancy maximum relevance feature selection," *Science China Information Sciences*, vol. 63, no. 1, p. 112103, 12 2019. [Online]. Available: https://doi.org/10.1007/s11432-019-2633-y

Geometry of domain wall in glass coated Fe-based microwires

[1]*Jana HORNIAKOVÁ (1st year)*
Supervisor: [2]*Jozef ONUFER*

[1,2]Dept. of Physics, FEI TU of Košice, Slovak Republic

[1]jana.horniakova@tuke.sk, [2]jozef.onufer@tuke.sk

***Abstract*—Most of microwires with positive magnetostriction have a rectangular hysteresis loop and exhibit a so-called bistable behavior. The reversal of the magnetization vector begins with the release of a single domain wall from the closure domains at the end of the microwire. Because of this, these microwires allow studying the dynamics of a single domain wall between axial domains that propagate along the microwire. A knowledge about the structure and geometry of the domain wall is necessary in order to understand mechanism of these processes. The paper describes new experimental set-up designed to provide information about changes in wall shape during its propagation along the microwire.**

***Keywords*— amorphous microwire, domain wall geometry, Sixtus-Tonks experiment**

I. Introduction

Amorphous ferromagnetic glass-coated microwires with positive magnetostriction attract attention from physical and application points of view caused by specific properties they exhibit [1-4]. Practical way of preparing glass-coated microwires is Taylor-Ulitovski method [4-6]. Result of this method is microwire in as quenched state with its characteristic stress distribution that causes the typical domain structure (Fig. 1). Amorphous glass-coated microwires with positive magnetostriction have axially magnetized core with radial domains in outer shell, while most of the volume is occupied by axially magnetized core [7]. Due to the stray fields the closure domains are created at microwire's ends.

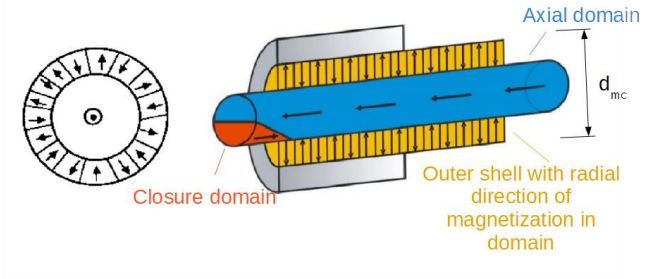

Fig. 1 Domain structure of glass-coated microwire with positive magnetostriction [7].

Usually in works dealing with the dynamics of a single domain wall in bistable magnetic microwires is domain wall considered as a solid object that does not change the shape with different applied fields, or to interpret the observed behavior are discussed possible changes in wall structure. Wall deformations or changes in the wall axial dimension can be expected if $L>>d_{mc}$, where L is axial dimension of the wall and d_{mc} is diameter of the metal core of the microwire [4].

The theory and experimental set-up of how changes of the shape of domain wall could be registered in the pick-up coils in modified Sixtus-Tonks experiment as well as their analysis is presented.

II. Theory

As already discussed in [8], relatively good agreement between the experimental and theoretical values of domain wall mobility can be obtained if the radius of the microwire is comparable with the axial wall dimension. On the other hand, the wide voltage peaks induced in the pick-up coils (inset of Fig. 2a during the Sixtus–Tonks experiment seems to be in contradiction with short axial dimension of the wall [4].

It is known [4] that with increasing applied axial magnetic field mobility of domain wall decreases (Fig. 2b) and with increasing applied axial magnetic field, from a comparison of theoretical and experimental voltage peaks, provides information about shortening of the axial dimension of the propagating domain wall. Theory of how the shape of induced voltage peaks with combination of measurement of domain wall velocity can give information about changes in the wall geometry presented in [4], shows that shape of induced voltage peaks are dependent on the radius of the pick-up coil as well as on the length of a domain wall.

As described in Fig. 2b the wall propagates with very high mobility at the low field. It means that the axial dimension of a static and moving wall at a very low field is very long.

It has been discussed in [4], that the shape of the signal is influenced by the presence of a stray field produced by moving wall as well as by the shape of the domain wall. Combination of theoretical prediction that eddy currents produced by propagating wall create an inhomogenous damping field which influences the wall shape, in [4] with experimental result predicts a shortening of the wall at higher velocity due to its deformation. Little disagreement between the theoretical and measured values of wall mobility may be caused by the fact that the model dependences of wall mobility for planar wall were calculated, which could be applicable for a domain wall in low fields [10]. In higher fields (above 100 A/m), different wall shape is possible compared to modeled planar wall. The fact that observed signals are not symmetrical supports this assumption [9].

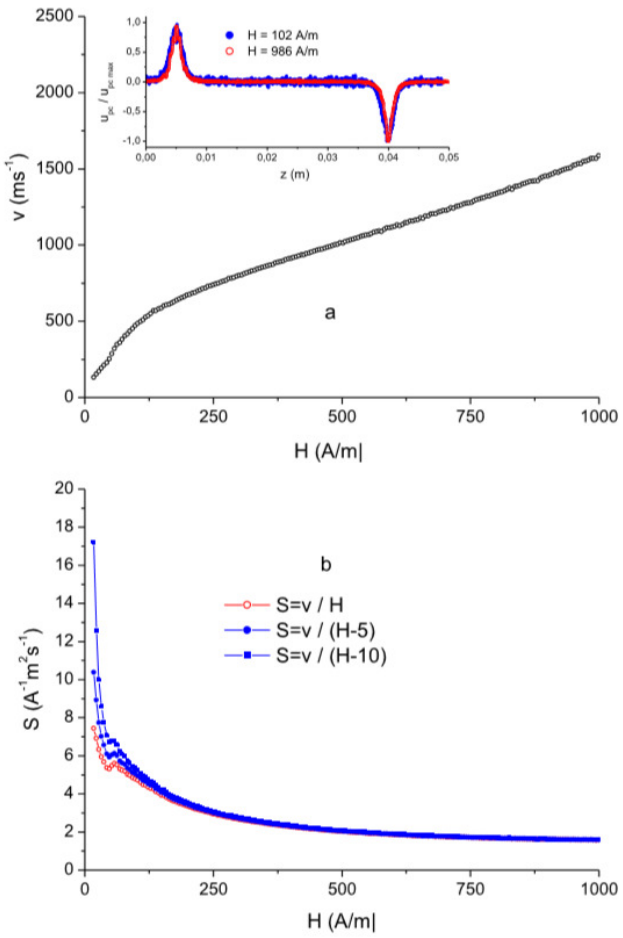

Fig. 2 Wall velocity versus applied magnetic field (a), wall mobility versus applied magnetic field for different H (b) [4].

An abrupt change of mobility (Fig 2b) at a certain field strength at low field region can be observed. It could be reasonable to expect that the shape of a moving wall in low field region is similar to that at the rest up to a certain field strength. In case of the planar wall the highest field created by eddy currents is in the central part of the wall which results in shortening of the wall since the damping force is highest in the central part as well. The abrupt change in mobility as a function of applied field can be caused by transformation of a wall shape. In Fig. 3 are schematically plotted two wall shapes that satisfy cylindrical symmetry. Both shapes respect damping force distribution mentioned above and wall curvature compensates the non-uniform damping forces on the wall [8]. Elongation of the wall caused by increasing of velocity in Fig. 3a can even lead to collapse of this type of the wall at some critical field strength [11, 12].

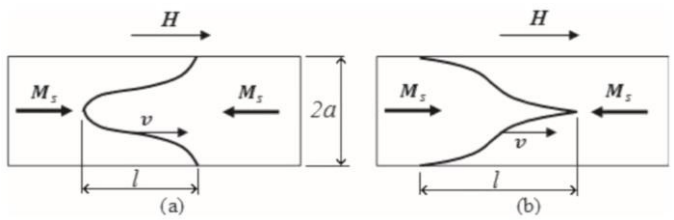

Fig. 3 Two types of possible domain wall shape with cylindrical symmetry. [8].

For the shape of the domain wall depicted in Fig. 3b magnetostatic energy can be notably minimized compared to the wall depicted in Fig. 3a and no possible collapse due to the shortening of the wall can be expected. A wall similar to the one depicted in Fig. 3b can propagate in a high field region. With increasing velocity its mobility decreases due to the shortening of the wall's axial dimension [8].

III. EXPERIMENTAL

The experimental set-up is schematically depicted in Fig. 5a. The system of coils consists of six coils, three magnetizing (Solenoid, C1, C2) and three pick-up coils (PuC1, PuC2, PuC3). Two co-axial pick-up coils PuC1 and PuC2 have the same center. The length of the pick-up coil PuC1 is l_1 (1 mm) with diameter 0,5mm and number of turns z_1= 25, the length of pick-up coil PuC2 is l_2 (20 mm) with diameter 0,2 mm and number of turns z_2= 2400 . Parameters of the pick-up coil PuC3 are identical with PuC1 and the distance between them is 36 mm. The geometry and number of turns of coils C1 and C2 are the same (diameter = 1 mm, length = 5 mm). Magnetizing coils (Solenoid, C1, C2) are used to release single domain wall from particular wire end. Detailed usage of magnetizing coils are described in [8].

To study the single domain wall dynamics in bistable microwires the wall propagates from one particular wire end. This experimental set-up is designed to no need to manipulate with a sample in order to measure both directions of possible propagation (possible depinning of domain wall from left as well as from right end of the microwire). With this set-up of coils it is even possible to measure hysteresis loops [8].

Using pick-up coils PuC1 and PuC3 it is possible to measure an average speed of a domain wall in the region between them. But more relevant to obtain information about domain wall geometry of propagating wall is to measure current velocity using pick-up coil PuC2 in the suggested way explained in next chapter.

IV. ANALYSIS OF INDUCED VOLTAGE PEAKS

In this chapter we propose how can be voltage peak induced in the pick-up coil analysed in modified Sixtus-Tonks experiment to obtain information about domain wall geometry changes.

We consider glass-coated microwire with positive magnetostriction. Such microwires exhibit so called bistable behaviour in an as quenched state and their hysteresis loop is perfectly rectangular (Fig. 4).

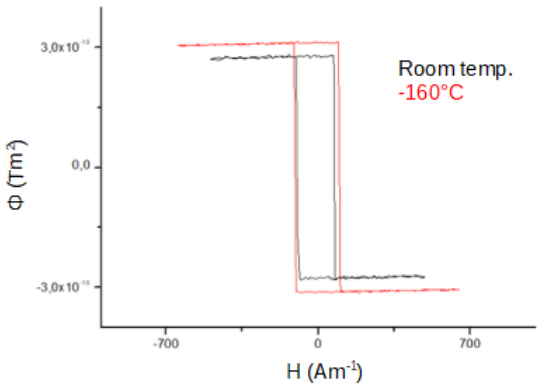

Fig. 4 Hysteresis loops at -160°C and room temperature of amorphous glass-coated FeSiB microwire with positive magnetostriction [7].

Single domain wall is depinned from microwire end at critical field strength and that is when the magnetization reversal starts. Sixtus-Tonks experiment is usually used to study domain wall dynamics during single wall propagation

along the microwire. In such experiment to measure time interval between voltage peaks induced in pick-up coils (inset of Fig. 2a) a pair of pick-up coils is used. An average wall velocity for a region of the microwire between pick-up coils can be determined using this experiment. But more information besides the value of average velocity can be obtained.

Let's first consider a single turn j of the pick-up coil. Using Faraday's law the voltage induced in this turn due to the wall propagation along x - axis can be expressed as follows:

$$u_i = -\frac{d\Phi_j}{dt} = -\frac{d\Phi_j}{dx}v, \tag{1}$$

where v is wall velocity and Φ_j is magnetic flux due to magnetization inside the microwire and also due to stray field around the wall. The pick-up coil signal reflects not only magnetic flux due to magnetization of domains in the microwire (i.e. exactly the wall length), but also any stray field of magnetic charge accumulated near the wall, which causes that the determination of the wall shape and its length become more complex [4].

For standard 180° domain wall the normal to the wall component of magnetization is equal to zero. In bistable microwires the situation is more complex and the so called head to head (or tail to tail) domain wall is a source of a stray field that is affecting parameters of induced voltage peaks [9].

It was shown in [10] that the stray field has to be taken into account when information about domain wall dimension is deduced from analysis of the signal induced in the pick-up coil.

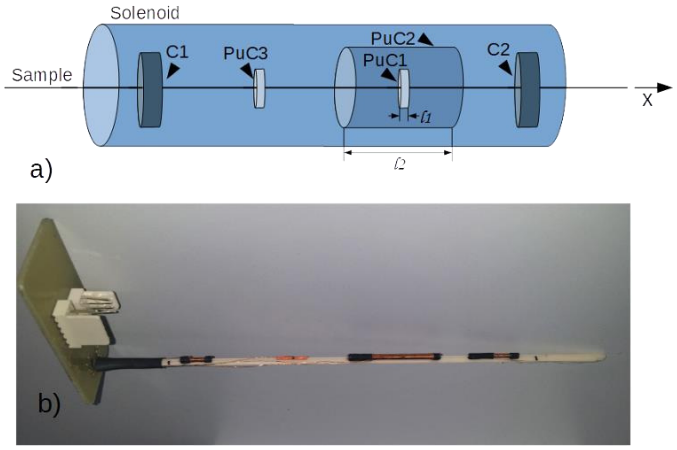

Fig. 5 Schematically depicted experimental set-up (a) and real picture of experimental set-up without solenoid.

The total voltage induced in all (n) turns of the pick-up coil can be obtained as

$$u = \sum_{j=1}^{n} u_j = -v\sum_{j=1}^{n}\frac{d\Phi_j}{dx}, \tag{2}$$

Now let us consider system of two coaxial pick-up coils PuC1 and PuC2 schematically depicted in Fig. 5a.

Well known fact that the peak width can be influenced by the wall length is shown in [4]. Based on the calculations presented there, we can conclude that in an experiment in which coil radius is much greater than microwire radius, it is very difficult to measure changes in the wall length as well as in the wall shape.

It is already known that the typical width of induced peaks is of few millimetres, depending on coil parameters (length, radius). In Sixtus-Tonks experiment a stray field produced by so-called head-to-head domain wall influences the shape of the voltage peaks induced in the pick-up coils. So as was mentioned above the pick-up coil parameters (radius and length) have to be considered if we want to obtain information about the wall geometry from the shape of these peaks [9]. Pick-up coils PuC1 and PuC2 in Fig. 5a fulfil the following conditions:

1. short pick-up coil PuC1 with z_1 turns and length l_1 is shorter than the dimension of region of inhomogeneous magnetic induction around the wall mentioned above,
2. long pick-up coil PuC2 with z_2 turns and length l_2 is much longer than the dimension of this region.

For these coils the induced voltage given by Eq. (2) can be expressed in different way.

Considering that elementary length dx of a coil contains dz_i turns voltage induced in this elementary length of the coil is given by

$$du_i = -v\frac{d\Phi_i}{dx}dz_i \tag{3}$$

Number of turns dz_i can be expressed as

$$dz_i = \frac{z_i}{l_i}dx,$$

so after substitution into Eq. (3) we have

$$du_i = -v\frac{z_i}{l_i}d\Phi_i \tag{4}$$

Integration over the whole length of the coil gives

$$u_i = -v\frac{z_i}{l_i}(\Phi_{iR} - \Phi_{iL}) = -v\frac{z_i}{l_i}\Delta\Phi_i, \tag{5}$$

where Φ_{iL} and Φ_{iR} are magnetic fluxes in the left and right ends of the coil, respectively.

It is useful to write Eq. (5) for short pick-up coil PuC1 in the form

$$\frac{u_1}{v} = -\frac{z_1}{l_1}\Delta\Phi_1 \tag{6}$$

It can be seen from this equation that the quantity on the left side plotted as a function of position provides information about changes in wall shape. The signal from short coil u_1 has to be measured along with the velocity of the wall moving inside short coil to obtain this quantity. This can be achieved in the following way. The stray field does not contribute to the change in magnetic flux $\Delta\Phi_2$ if wall position is far from the ends of long coil (PuC2) and it can be expressed as

$$\Delta\Phi_2 = 2\mu_0 M_s A, \tag{7}$$

where A is area of axial domain wall cross section and M_s is saturation magnetization. We can obtain this quantity by measurement of hysteresis loop or it can also be obtained by time integration of the signal induced in long pick-up coil PuC2. By integration of the voltage given by Eq. (5) we obtain

$$U_2 = \int_{-\infty}^{\infty} u_2 dt = -\frac{z_2}{l_2}\Delta\Phi_2\int_0^{l_2} dx = -z_2\Delta\Phi_2 \tag{8}$$

and so

$$\Delta\Phi_2 = -\frac{U_2}{z_2} \tag{9}$$

Finally the wall velocity of the wall moving inside short coil can be determined using formula

$$v = -\frac{l_2}{z_2}\frac{u_2}{\Delta\Phi_2} = l_2\,\frac{u_2}{U_2} \tag{10}$$

Wall position can be calculated using equation

$$x = -\frac{l_2}{U_2}\int_0^t u_2 dt \tag{11}$$

From Eqs. (6) and (10) we can obtain

$$\frac{\Delta\Phi_1}{l_1} = -\frac{U_2}{l_2 z_1}\,\frac{u_1}{u_2} \tag{12}$$

Parameters l_1, l_2, z_2 are constants. Induced voltage u_1, u_2 in pick-up coils PuC1 and PuC2 can be measured. Integration of u_2 can be done. And the quantity of Eq. (12) should be plotted as a function of position given by Eq. (11) to analyse domain wall changes during its propagation.

V. Conclusion

Presented way to obtain information about domain wall geometry is unique and should bring useful knowledge about changes in domain wall shape during its propagation along the so-called bistable microwires at various values of velocities. Till now the theory and experimental set-up is done.

References

[1] M. Vazquez, H. Kronmuller, S. Parkin (Eds.), Handbook of Magnetism and Advanced Magnetic Materials, vol. 4, John Wiley and Sons, Chichester, UK, 2007, pp.1–34.

[2] A. Zhukov, V. Zhukova, „Magnetic Properties and Applications of Ferromagnetic microwires with Amorphous and Nanocrystalline Structure (Nova)", Science Publishers Inc, Hauppauge, NY, 2009, p.162.

[3] M. Vázquez, H.Chiriac, A. Zhukov, L. Panina, T. Uchiyama, "On the st ate of the art in magnetic microwires and expected trends for scientific a nd technological studies",in Phys. Status Solidi A 208 (2011), pp. 493–501.

[4] M. Kladivová, J. Ziman, "Properties of a domain wall in a bi-stable magnetic microwire", in Journal of Magnetism and magnetic materials 480 (2019), pp. 193-198.

[5] H.Chiriac, T. A. Ovari, "Amorphous glass covered magnetic wires: preparation, properties, applications", in Prog. Mater. Sci. 40 (1996), pp. 333–407.

[6] S. V. Larin, A. Torcunov, A. Zhukov, J. González, M. Vazquez, L. Panina, "Preparation and properties of glass-coated microwires", J. Magn. Magn. Mater. 249 (2002), pp. 39–45.

[7] J. Horniaková, "Skúmanie vlastností amorfných bistabilných mikrodrôtov pomocou malouhlovej rotácie magnetizácie", diploma thesis, pp. 54.

[8] J. Onufer, J. Ziman, P. Duranka, M. Kladivová, "The influence of annealing on domain wall propagation in bistable amorphous microwire with unidirectional effect", in Physica B: Condensed matter 540 (2018), pp. 58-64.

[9] M. Kladivová, J. Ziman, P. Duranka, "Axial domain wall dimension in a bistable glass-coated microwire", submitted

[10] M. Kladivová, J. Ziman, J. Kecer, P. Duranka, "Study of Axial Dimension of Static Head-to-Head Domain Boundary in Amorphous Glass-Coated Microwire", in ACTA PHYSICA POLONICA A, vol.131 (2017), No. 4, pp. 639-641.

[11] W. J. Carr Jr., „Magnetic domain wall bowing in a perfect metallic crystal", in J. Appl. Phys. 47 (1976) 4176.

[12] M. Kladivová, J. Ziman, „Velocity and profile of the boundary between circular domains in cylindrical ferromagnetic samples", in J. Mag. Mater. 299 (2) (2006), pp. 459-466.

IISMotion - framework for user mobility simulation

[1]*Marcel VOLOŠIN (2nd year),*
Supervisor: [2]*Juraj GAZDA*

[1,2]Dept. of Computers and Informatics, FEI TU of Košice, Slovak Republic

[1]marcel.volosin@tuke.sk, [2]juraj.gazda@tuke.sk

***Abstract*—Simulation of end-users' movement is an essential part of wireless network models that may highly affect conclusions derived from conducted experiments. This paper presents a custom made framework IISMotion for users' movement simulation in a real-world-like environment. Proposed Cuda accelerated Python framework mainly based on the OpenStreetMap database (OSMnx package) and the world's largest Open Database of cell towers OpenCelliD was created to simplify the process of wireless network simulation with users' movement included. It gives developers an ability to freely modify/extend the implementation based on a given task. Numerical results show that IISMotion has the characteristics similar to the commonly used random walk model thus can be considered as a suitable replacement with an additional functionality.**

***Keywords*—mobility modeling, CUDA, heterogeneous networks**

I. Introduction

Rising popularity of wireless networks empowers the effort of engineers and researches worldwide to improve the currently used techniques of spectrum allocation. However, it became obvious that the exponential growth of internet traffic as described in [1] will require not only evolution but also the revolution on the field of wireless networks.

However being technically viable, novelty approaches that can optimize the spectrum usage face the objections from the established operators satisfied with the current state-of-the-art. Proposed solutions therefore forego an extensive analysis to prove not only the technological viability and security concerns [2] but also the profitability that will satisfy the operators. To verify techno-economic characteristics, simulations with various levels of abstraction are often required, depending on the observed indicators. This paper will focus on the essential part of these techno-economic simulations, which is the mobility modeling of end-users [3] using a newly designed framework with a real-world simulation capabilities.

II. IISMotion - framework for real-world mobility simulation

IISMotion [4] is a street random waypoint model with the capabilities to simulate movement of pedestrians and vehicles in environments based on real-world maps thanks to OSMnx framework [5] and OpenStreetMap database [6]. Framework has been given an ability to import real-world locations of base stations originating from OpenCellId database [7] which is considered to be the world's largest open database of cell towers.

Simulation of masses moving in the streets of artificial city requires powerful hardware, therefore model was fully rewritten to fully utilize the advantages of Cuda acceleration which brought a significant improvement in terms of performance. To make the model as lightweight as possible simulation space was also split into a grid with a "patches" of equal size which reduces the number of computations needed to find closest agents to given GPS coordinates. Each entity placed into simulated world is assigned to these patches based on it's coordinates, Search starts on the 0^{th} level and then based on end-user's preferences continues until BTSs are found or even further when desired.

IISMotion framework was designed to support following features:

- simulation of any location with built infrastructure
- possibility to specify map zones with different purposes
- variable number of pedestrians
- variety of movement models including
  - random waypoint ignoring roads, paths, buildings, etc.
  - random waypoint on roads
  - daily routine of user affected by zones
- possibility to include multiple groups of users each with own type of movement and speed
- import of base stations located in given area
- placement of small cell stations in the area (with import and export functionality)
- logging capabilities with adjustable parameters
- Leaflet-based Javascript frontend [8] as seen in Fig. 1

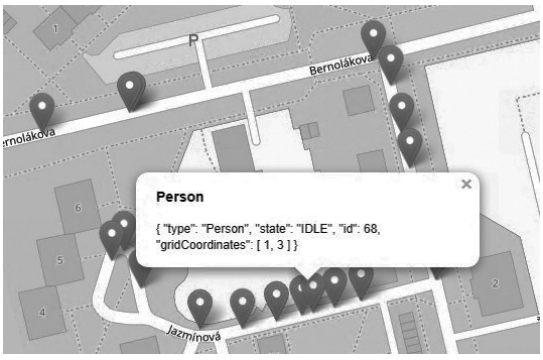

Fig. 1. IISMotion - Live visualization of pedestrians via Leaflet

To mimic the behavior of common end-users the custom behavior model have been designed and implemented that captures the common repetitive nature of peoples' habits. As already mentioned, included feature of zones enables researchers to specify various roles of different environment parts. Current model supports following zones: Entertainment, Housing and Work.

At the initialization phase, each user is assigned the building that will become it's home and other building for work, both for entire simulation. Home is a random building from a random "Housing zone", work from random "Work zone". Multiple zones of same type can be specified, each with a probability of being chosen. Every user is initialized with 8-hour working time starting in the morning at time chosen from normal distribution. User's default routine looks the following way, but can be easily customized:

1) waiting at home until work time
2) leaving home, going to work with a preset speed using roads
3) staying at work
4) leaving work, heading to a random building from "Entertainment" zone, staying there for 2 hours
5) going home, staying there (process is repeated)

We consider the current state-of-art of proposed solution to be suitable for mobility simulation in our models, however we are aware of several areas that may require improvements to reach higher level of realism. IISMotion currently lacks the support for sidewalks, therefore all the simulated movement happens on the road network or freely on the whole area.

A. Numerical results and future

The purpose of this section is to show preliminary results covering the mutual comparison of the well-known random walk model with the IISMotion model, in which the end-users mimic the real mobility traffic patterns. We vary the number of users in the interval $< 100, 700 >$ and observe the measured averaged throughput (Fig. 2). As we can see, the shape of the results for both models is very similar, although we observe some differences. At the end, this differences could have really high impact on planning of RAN infrastructure of the operator, which gives us the conclusion that more sophisticated models (such as IISMotion) are necessary to be included in the RAN planning of the operators in the future.

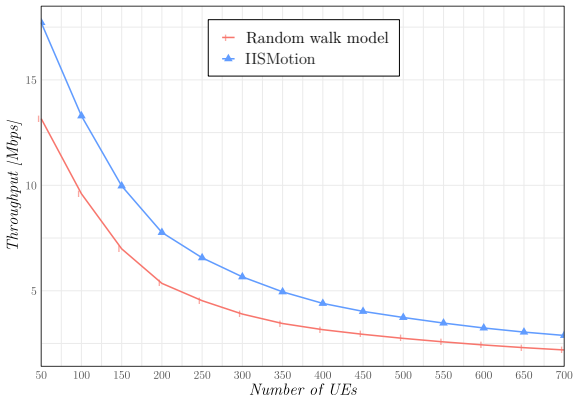

Fig. 2. Performance results: Averaged througput vs. number of users; IISMotion and random walk model

III. Conclusion

Exponential growth of spectrum demand forces the researches to find new ways of spectrum allocation. To verify feasibility and profitability of the new approaches of the spectrum licensing agent-based simulations are commonly used. Mobility modeling is an essential part of these simulations with a major impact on obtained results thus requires sufficient attention in a design phase.

Although being already used for research purposes, IISMotion is expected to be highly improved with a wide set of new features to mimic real-world environment more precisely. One of the most significant improvements will be done via the integration of real data such as from Crawdad [9] or Microsoft [10] for agents' movement destination decisions. Time-varying movement activity of pedestrians inspired by real-world observations with included indoor movement simulation may enable researchers to study the relations between networks and end-users effortlessly. Recent efforts [11], [12], [13] suggest utilization of movable radio access network (RAN) (e.g. unmanned aerial vehicle (UAV)) for optimal dynamic wireless coverage thus support of antenna mounted UAVs is another feature that will be included in an upcoming release to fulfill the needs of wireless network researchers.

Acknowledgment

This work was supported by the Slovak Research and Development Agency, project number APVV-18-0214 and by the Scientific Grant Agency of the Ministry of Education, science, research and sport of the Slovak Republic under the contract: 1/0268/19; Green heterogeneous network topologies with support of UAV mobile stations for 5G+ wireless communication systems.

References

[1] Cisco, "Cisco visual networking index: Global mobile data traffic forecast update, 2016âĂŞ2021," Cisco, Tech. Rep., 02 2017.
[2] L. Vokorokos, A. Baláž, and N. Ádám, "Secure web server system resources utilization," *Acta Polytechnica Hungarica*, vol. 12, no. 2, pp. 5–19, 2015.
[3] D. Karamshuk, C. Boldrini, M. Conti, and A. Passarella, "Human mobility models for opportunistic networks," *IEEE Communications Magazine*, vol. 49, no. 12, pp. 157–165, 2011.
[4] IISLab, "Iismotion - mobility model framework," 2019, [Accessed 02-February-2019]. [Online]. Available: https://bitbucket.org/marcelvolosin/iismotion/
[5] G. Boeing, "Osmnx: New methods for acquiring, constructing, analyzing, and visualizing complex street networks," *Computers, Environment and Urban Systems*, vol. 65, pp. 126–139, 2017.
[6] OpenStreetMap contributors, "Planet dump retrieved from https://planet.osm.org ," https://www.openstreetmap.org, 2017.
[7] U. Labs, "Opencellid: The world's largest open database of cell towers," 2018, [Accessed 18-December-2018]. [Online]. Available: https://en.wikipedia.org/w/index.php?title=OpenCellID&oldid=872929280
[8] P. Liedman, "Leafletrealtime - put realtime data on a leaflet map," 2016, [Accessed 02-February-2019]. [Online]. Available: https://github.com/perliedman/leaflet-realtime
[9] D. College, "Crawdad - community resource for archiving wireless data at dartmouth," [Accessed 02-February-2019]. [Online]. Available: https://crawdad.org/index.html
[10] M. R. Asia, "Geolife gps trajectories - gps trajectory dataset," 2012, [Accessed 02-February-2019]. [Online]. Available: https://www.microsoft.com/en-us/download/details.aspx?id=52367
[11] M. Mozaffari, W. Saad, M. Bennis, and M. Debbah, "Efficient deployment of multiple unmanned aerial vehicles for optimal wireless coverage." *IEEE Communications Letters*, vol. 20, no. 8, pp. 1647–1650, 2016.
[12] Y. Zeng, R. Zhang, and T. J. Lim, "Wireless communications with unmanned aerial vehicles: opportunities and challenges," *arXiv preprint arXiv:1602.03602*, 2016.
[13] M. Alzenad, A. El-Keyi, F. Lagum, and H. Yanikomeroglu, "3-d placement of an unmanned aerial vehicle base station (uav-bs) for energy-efficient maximal coverage," *IEEE Wireless Communications Letters*, vol. 6, no. 4, pp. 434–437, 2017.

Identification Unit Under Test From Test Using Latent Semantic Analysis and Latent Dirichlet Allocation

[1]*Matej MADEJA (3rd year),*
Supervisor: [2]*Jaroslav PORUBÄN*

[1,2]Dept. of Computers and Informatics, FEI TU of Košice, Slovak Republic

[1]matej.madeja@tuke.sk, [2]jaroslav.poruban@tuke.sk

***Abstract*—Tests are an important part of the source code that can help developers understand the production code. While reading the test, the developer subconsciously creates relationships with the source code using naming conventions and lexical analysis. This process unnecessarily employs the developer so automating this process can streamline the development. In this paper we describe the results of automated identification using LSA and LDA natural language approaches for 5 popular Android Github projects. The LSA method reached 13.33% and the LDA nearly 0% success rate. Although the LSA method has proven generally more accurate when used on the source code, the error rate is so high that these approaches do not seem to be suitable for UUT identification.**

***Keywords*—NLP approaches, program comprehension, testing, UUT identification, latent semantics analysis, latent dirichlet allocation.**

I. Introduction

The unit under test (UUT) identification is a general issue in software engineering [1] and most of the time of this identification is associated with at least a partial understanding of the source code and the relations between them. Tests can be considered as an always up-to-date documentation of the production source code [2], so if it is possible to automate and accurately determine UUT, it is possible to shorten the time for the programmer to comprehend the source code.

According to Parizi et al. [3] and Rompaey with Demeyer [4] test and source code have many similarities, e.g. it is possible to create a connection using static call graph, code co-evolution or naming conventions. Perhaps the most common technique that developers subconsciously use to manually identify UUT is the use of naming conventions and lexical analysis (similarity of vocabulary between test and production code). With such identification, the programmer often tries to understand the parts that are not always relevant to him or her. The main task of the programmer is to identify the problem as quickly as possible and implement the solution, so trying to understand the parts that are not important can negatively affect the time and way of the solution. By automating this process we would achieve a more reliable and faster identification that would also be beneficial in the future in the area of automatically generated documentation and creating links between different parts of the code.

II. Using NLP approaches for UUT detection

Natural language processing (NLP) attempts to reduce the barriers in computer-to-human communication [5]. It can therefore be assumed that by using NLP it will be possible to automate this process. The source code consists mainly of structured text in the form of statements but if we do not consider the relationship between words, but only their meaning, it is possible to determine the similarity of different classes and classify them in clusters [6], [7]. The source code can also contain many comments that have form of natural text. Latent Semantic Analysis (LSA) and Latent Dirichlet Allocation (LDA) models are information retrieval (IR) algorithms that expect vectors as input and their input strings are represented as representation called *Vector Space Model*, according to which a particular model can make predictions.

The LSA is an indexing and IR method that uses *Singular Value Decomposition* (SVD) to identify relationships between words in an unstructured text. The model is based on the assumption that words used in the same context have a similar meaning [8]. By extracting terms from the document's body it seeks to create relationships between individual documents. It is important to choose a right number of topics to generate because if too many topics are requested for a short document the algorithm returns also words that should not determine the resulting topic of the document and vice versa.

The LDA model considers each document as a set of topics which characterize it [9]. Each topic consists of a set of words in a certain proportion. Based on the number of topics required the model attempts to rearrange the topics distribution within the documents to achieve the best composition. It is also very important to determine the right number of topics that the algorithm returns. Since both approaches do not take into account the words order they are suitable for source code analysis.

III. Method and results

The complete experiment is described in [10] in detail. The main experiment was conducted on 5 popular Android projects and it was performed by comparing each test class with all existing classes in the project (only Java and Kotlin files considered). After performing NLP analysis for a specific test against each production class the correct UUT should match most. For both mentioned approaches a *bag-of-words*

representation in the form of a dictionary (id + word pair) was used. Creating a corpus of sparse vectors was relatively easy using the functions of python library *gensim*[1].

A. Diversity of document preparation

The results are largely influenced by the preparation of input documents for comparison (governed by the idiom "garbage in, garbage out"). Because the source code contains a lot of content that can negatively influence the analysis, 5 versions of the document preprocessing have been created to see which modifications increase the accuracy of UUT identification:

1) *Full version* - original file version, removed only `\n` chars.
2) *Word split* - all `camelCase` or `snake_case` words has been split. Words out of base conventions, such as `ORMLite`, remained unsplit.
3) *Removed Java keywords* - all Java keywords have been discarded.
4) *Removed comments* - multi- and one-line comments discarded.
5) *Removed imports* - all Java imports removed.

All versions were conducted incrementally, i.e. 4^{th} point also included all previous ones. Another preprocessing of documents that applied to all iterations was the removal of frequently occurring English words using *nltk* library, such as *and*, *a*, *the*, etc. At the same time stemming over the documents has been executed, where inflected or sometimes derived words to their word stem have been reduced, e.g. *cars* to *car*. The last step was to remove words that occurred only once in the corpus of training documents to eliminate their negative impact on results.

B. LSA and LSA success

Altogether we analyzed 2221 production and 168 test classes and in five iterations of document preprocessing a total of 1,093,730 similarity results between the tests and the production source code have been obtained. Firstly all UUT of analyzed projects where identified manually and that an automated ranking using mentioned NLP approaches has been executed. Since we assume that manually identified UUTs are correct it is possible to determine the accuracy of a particular model based on the order of production class in the search result.

As can be seen in the Table I, LSA performed much better than LDA. The accuracy of the LDA model was very low, in the first five results the correct UUT appeared only 2 times. Although the LSA achieved 82 correct UUTs in the first five results for all iterations it is still only 13.33% success rate which is considerably inadequate. From our results, only 5.20% of UUTs were marked correctly (all iterations) and solely by the LSA method. In the results it is necessary to take into account the fact that for the 6 test classes, which tested multiple production classes at once, the most tested class was chosen as the correct UUT.

Word split and *removal of java keywords* (I2 + I3) has the greatest impact on the accuracy of the results. Our expectation was that when comments are removed the results will get worse because there is a potential for sole natural language in the comments. In the Table I it can be seen that removing comments (I4) and imports (I5) had a negligible impact on accuracy. It also shows that the meaning in the code is most often expressed directly in the names of the identifiers, i.e. class, methods and variables names. Using word splitting were obtained the most accurate results, it was the fastest iteration in terms of model training, finding/ranking the best coherence value and search in the index.

[1]https://radimrehurek.com/gensim/

TABLE I
POSITION FREQUENCY FOR FIRST 5 POSITIONS OF ANALYZED MODELS.

Iteration	**Position frequency in the search**											
	LSA						**LDA**					
	1	**2**	**3**	**4**	**5**	Σ	**1**	**2**	**3**	**4**	**5**	Σ
I1		1				1			1			1
I2	4	1	3	5		13						
I3	10	8	2	4	1	25			1			1
I4	9	6	4	1	2	22						
I5	9	6	2	3	1	21						
Σ	32	22	11	13	4		0	0	2	0	0	

IV. FUTURE DIRECTIONS

As can be seen from the results usage of these methods has not been very successful. However, using other programming languages with different syntax or language constructs better results could be achieved. These language attributes could affect how the developer expresses his/her intentions in the source code. It is also expected that using a programming language more similar to a natural language (e.g. *Gherkin*) might consider using contextual NLP approaches. In the future we will also look at comparing the results with other UUT identification techniques, e.g. observation of co-evolution code or helper methods. We will also plan to conduct an experiment looking for a suitable combination of several methods, e.g. in conjunction with approaches based on syntax analysis of the code.

ACKNOWLEDGMENT

This work was supported by project VEGA No. 1/0762/19: Interactive pattern-driven language development.

REFERENCES

[1] M. Madeja, "Towards connections between source code and tests: An overview," in *Proceedings from Conference*, 2019.
[2] S. Demeyer, S. Ducasse, and O. Nierstrasz, *Object-oriented reengineering patterns*. Elsevier, 2002.
[3] R. M. Parizi, S. P. Lee, and M. Dabbagh, "Achievements and challenges in state-of-the-art software traceability between test and code artifacts," *IEEE Transactions on Reliability*, vol. 63, no. 4, pp. 913–926, Dec 2014.
[4] B. V. Rompaey and S. Demeyer, "Establishing traceability links between unit test cases and units under test," in *2009 13th European Conference on Software Maintenance and Reengineering*, March 2009, pp. 209–218.
[5] C. D. Manning, C. D. Manning, and H. Schütze, *Foundations of statistical natural language processing*. MIT press, 1999.
[6] J. I. Maletic and A. Marcus, "Using latent semantic analysis to identify similarities in source code to support program understanding," in *Proceedings 12th IEEE Internationals Conference on Tools with Artificial Intelligence. ICTAI 2000*, Nov 2000, pp. 46–53.
[7] J. I. Maletic and N. Valluri, "Automatic software clustering via latent semantic analysis," in *14th IEEE International Conference on Automated Software Engineering*. IEEE, 1999, pp. 251–254.
[8] S. Deerwester, S. T. Dumais, G. W. Furnas, T. K. Landauer, and R. Harshman, "Indexing by latent semantic analysis," *Journal of the American society for information science*, vol. 41, no. 6, pp. 391–407, 1990.
[9] D. M. Blei, A. Y. Ng, and M. I. Jordan, "Latent dirichlet allocation," *Journal of machine Learning research*, vol. 3, no. Jan, pp. 993–1022, 2003.
[10] M. Madeja and J. Porubän, "Accuracy of unit under test identification using latent semantic analysis and latent dirichlet allocation," 11 2019.

Impact of magnetic and electric field on structure of magnetic fluids

[1]*Maksym KARPETS (1st year)*
Supervisor: [2]*Milan TIMKO*

[1]Dept. of Physics, FEI TU of Košice, Slovak Republic

[1,2]Institute of Experimental Physics SAS, Košice, Slovak Republic

[1]karpets@saske.sk, [2]timko@saske.sk

***Abstract* — The aim of this article is to present a state of the art on impact of magnetic and electric field on structure of magnetic fluids. The experimental results obtained by different authors are reviewed and compared. Additionally, the current solved and unsolved problems are summarized.**

***Keywords* — aggregation, external fields magnetic fluids, magnetic nanoparticles, transformer oil-based ferrofluids.**

I. INTRODUCTION

Magnetic fluids (MF) are liquid dispersions of magnetic nanoparticles (size ~ 10 nm) covered with surfactants [1]. Constituting unique properties they have been studying for diverse applications (Fig. 1). As can be seen from the number of scientific works published in international journals and conferences (Fig. 2), interest in structure of MFs has risen constantly over the last 20 years.

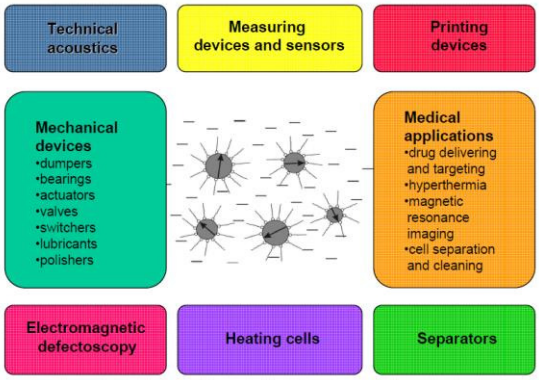

Fig. 1. Magnetic fluids – structure and aplications [2].

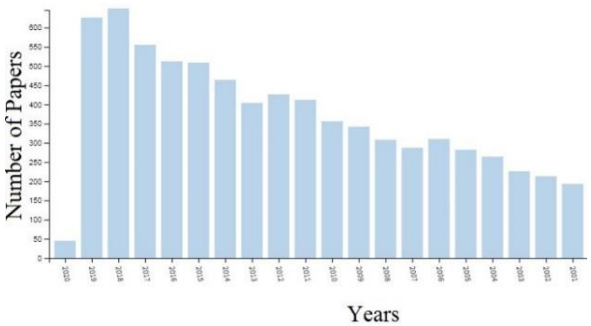

Fig. 2. Numbers of published papers on the subject "structure of magnetic fluids" from 2001 to 2020 (based on Web of Science).

As compared to bulk materials, magnetic nanoparticles possess distinct magnetic properties and attempts have been made to exploit their beneficial properties for technical and biomedical applications.

II. PROPERTIES OF MAGNETIC FLUIDS

There are many parameters of magnetic fluids sensitive to such fields such as density, viscosity, dielectric permeability, magnetic permeability, conductivity, inductivity, heat conductivity, heat capacity, surface tension, ultrasound absorption, optical absorption, refraction index, reflection index [2]. With regards to the potential application of transformer oil (TO)-based MNFs in power transformers, most research studies have focused on three key properties: thermal, dielectric, and viscous. On the other hand, this property is a function of the base liquid, dispersed particles, size distribution, volume fraction, surfactant, and the external magnetic and electric field. One of the fundamental requirements for a ferrofluid is the stability of the magnetic particles against aggregations. Considering the use of magnetite nanoparticle systems for biomedical application one need to understand the structural behavior of the magnetic particles even in electric fields alone. As a first step, this should be studied on a model system like magnetic particles dispersed in isolating liquids (Fig. 3).

The magnetic nanoparticle interactions and subsequent structural reorganization, aggregates, chains and pattern formation have been intensively studied by various experimental methods and theoretical approaches [3], [4]. The magnetic field induced microscopic structures have a substantial impact on macroscopic behavior of ferrofluids. Especially, the effect of the increased viscosity due to the applied magnetic field influences the specific adaptability of ferrofluids applications. Within this context, magnetoviscous effect has been introduced by Odenbach [5], which expresses the measure of the increased dynamic viscosity in relation to the basic viscosity in the absence of a magnetic field.

To a certain extent, the magnetorheological properties of ferrofluids are analogical to those of electrorheological suspensions, which have the capability of responding to an external electric field stimulation [6]. In an effort to combine both, electro and magnetorheological properties in one fluid, electrorheological magnetic fluids were developed [7]. These fluids can be obtained by depositing an electroconductive

substance on the surfaces of magnetic nanoparticles, and coating the surfaces of the resulting particles with a surfactant. In the electrorheological magnetic fluid, the magnetic nanoparticles respond to an external magnetic field, while the electroconductive layer formed on the magnetic particle surfaces responds to an external electric field. As a result, the particles form clusters oriented along the lines of magnetic or electric force. Similarly, electrorheological properties of magnetic fluids can be obtained by mixing a suspension of magnetic particles with a suspension of dielectric particles [8].

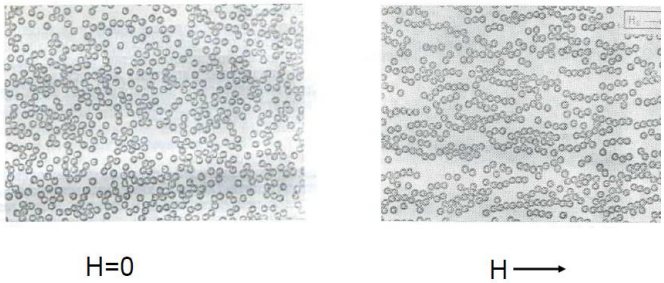

Fig. 3. Modelling of a concentrated ferrofluid with monodisperse Co particles [2].

III. DIELECTRIC SPECTROSCOPY

Study [9] showed that the dielectric response of MF is dependent on the strength and frequency of the electric field. It was also proved [10] that the low frequency relaxation process is slowed down when the inter-electrode gap is increased in units of micrometers and when direct current (DC) bias field is applied to the sample. This effect is related to the formation of aggregates.

In this study, the isothermal dielectric spectroscopy of a transformer oil–based ferrofluid was employed to detect the predicted electric field induced particle cluster formation.

The low-frequency relaxation process was assigned to the electric double layer polarization. It was investigated the role of electrode separation distance at constant electric field intensity on the relaxation maxima. The broadening of the relaxation maximum towards lower frequencies was observed as the response to the increased electrode separation distance. On the basis of the particle size dependent relaxation time, it was associated the broadening with the cluster formation induced by the applied alternating current (AC) electric field. The broader relaxation maximum therefore indicates the increase in the magnetic solid fraction size distribution. A similar indication of the cluster formation was observed when the DC bias voltage was applied (Fig. 4). The observed temporal hysteresis in the relaxation time reflects the particle cluster formation and decay behavior.

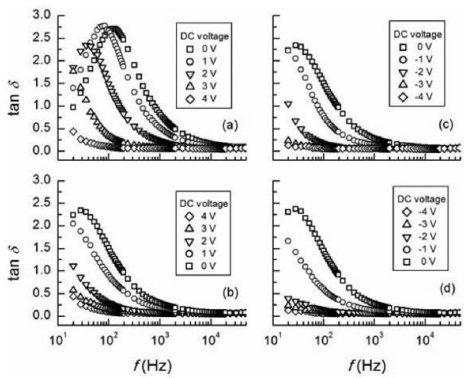

Fig. 4. The dependence of the tan δ loss spectrum on the applied DC bias voltage [10].

IV. SANS EXPERIMENTS

The electric field induced changes in the ferrofluid structure at nanoscale were recently confirmed by situ SANS experiments [11]. Dielectric properties of these systems are dependent on external magnetic field - magneto-dielectric effect. The structure of magnetite nanoparticles and their assemblies as a result of magnetic and Van der Waals interactions were studied by SANS.

It was demonstrated visually observable pattern formation in a transformer oil-based ferrofluid exposed to a DC electric field. The presence of space charge and its motion towards electric field gradients was assumed to be a trigger of the colloidal cloud formation. Electrical forces due to space charge and permittivity variation each play a role in inducing pattern formation and its dynamics. In Fig. 5, an increase in the scattered intensity in the small q region emerges and intensifies with increasing field strength. This is a direct evidence for the particle aggregates in the TOFF induced by the above analyzed electrohydrodynamics and polarization forces between the particles. The dielectric contrast in the TOFF results in the induced electric dipole-dipole interactions and subsequent aggregation. Thus, the scattering curve obtained at 6 kV/cm represents two subsystems of scattering objects in the sample.

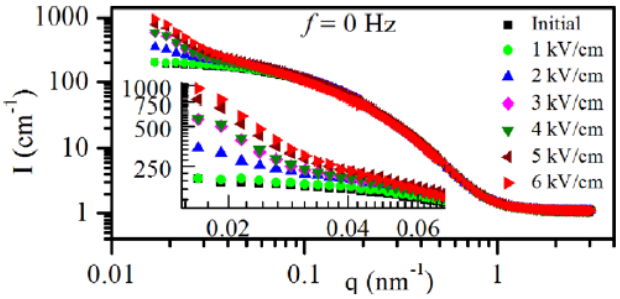

Fig. 5. SANS curves for the ferrofluid exposed to the DC electric field strengths from 0 kV/cm (initial) to 6 kV/cm [11].

V. OPTICAL METHODS

Similar assemblies may be induced even by an electric field itself. However, aggregate formations in MFs under the action of electric field have not been sufficiently investigated yet. Electric interactions are pronounced if the suspended particles are much more polarisable than the surrounding medium [6], e.g. magnetite particles ($\varepsilon > 33.7$) in mineral oil ($\varepsilon \approx 2$). The induced dipole-dipole interactions may lead then to the formation of long chains aligned along the applied field lines. A few studies addressed the influence of electric field on aggregation processes in MF by means of optical methods [12].

It has been shown that magnetic nanoparticles can undergo the electric polarization, resulting in the electric dipole-dipole interaction and aggregation. These aggregates were observed on the macroscopic and nanoscopic scale. The observed electric field influence on the ferrofluid viscosity resembles the well-known magnetoviscous effect.

The macroscopic evidence of the electric field influence on the ferrofluid structure is presented in Fig. 6, which shows the sample appearance in the glass cuvette with two electrodes powered by zero (a) and 5 kV DC voltage (b). It was found [11] that the applied voltage induces the accumulation of the nanoparticles in between the electrodes, forming a visible cloud. Subsequently, a spiky pattern forms from the cloud with the spikes oriented in the field gradient. The initial

particle accumulation can be explained by the induced electric dipole-dipole interaction, subsequent dielectrophoresis and the related electrohydrodynamic flow which pushes the particles towards the electrical equator. On the other hand, the distortion of the cloud is the result of the permittivity and conductivity gradients in the sample with the separated cloud, and the action of an anisotropic electrostatic force on the transition layer between the cloud and its surrounding. The observed macroscopic structural change of the ferrofluid is a reversible phenomenon, independent on the voltage polarity and the orientation of the cuvette with regard to the gravity force.

In a similar way, the magnetic particle assembly was observed in a case, when the electrodes were not in direct contact with the ferrofluid sample. Instead, a submillimeter droplet was placed on a microscope slide and two needle electrodes were attached to the slide from outside the droplet (Fig. 6 (c, d)). Even though the large aggregates were slowly disappearing after interrupting the electric field, one can suppose that the applied electric force acting on the surfactant has a deteriorative consequence on the ferrofluid stability.

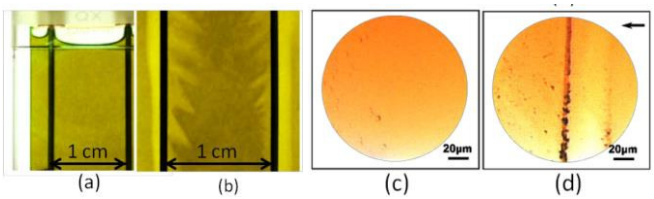

Fig. 6. Ferrofluid with the particle volume fraction Φv = 0.05 % in a glass cuvette with two electrodes under zero electric field (a), and under the action of 5 kV/cm (b). Optical microscopy view focused on a submillimeter droplet of the ferrofluid (Φv = 1 %) in zero electric filed (c), and under the action of 2 kV/mm (d). The arrow indicates the field direction [12].

VI. NEUTRON REFLECTOMETRY

Neutron reflectometry (NR) is one of the most promising methods of studying the structure and physical properties of thin layers of matter [13]. The effect of magnetic nanoparticle assembly formation at a planar interface between a transformer oil-based ferrofluid and single-crystal silicon under non-homogeneous magnetic fields was studied by specular neutron reflectometry (NR) (Fig. 7).

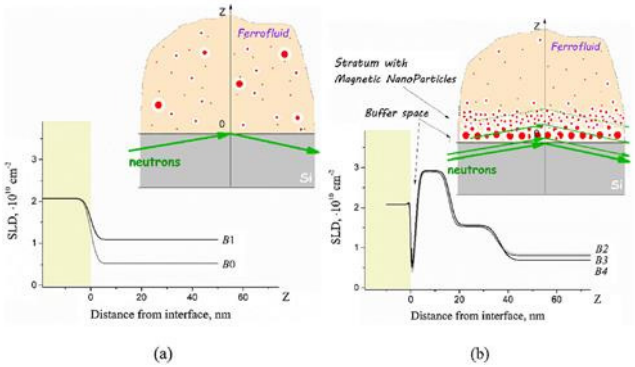

Fig. 7. Scattering length density profiles reconstructed from experimental NR data. B0 refers to the case of background magnetic field (without any externally applied magnets).The cases of B1, B2, B3 and B4 correspond to externally applied magnetic field [14].

The ferrofluid probed represents a stable suspension of dispersed iron oxide nanoparticles (characteristic size about 10 nm) coated with oleic acid in a low-polarity liquid carrier (transformer oil). It was shown that the reflectivity curves are sensitive to the application of a non-homogeneous external magnetic field. In particular, at a low magnetic flux density (<35 mT) they are well described in terms of the simplest model of a strict boundary between two semi-infinite homogeneous media. Nevertheless, slight concentrating of the ferrofluid bulk at the interface was detected. At a high magnetic flux density (35–75 mT), the analysis gives a three-layered structure of in-depth profiles of the scattering length density, thus showing the formation of two effective adsorption layers with different content of magnetic nanoparticles in them [14].

VII. DIELECTRIC PERMITTIVITY STUDY

The insulating and dielectric properties of TO were found to exhibit peculiar enhancement upon the addition of MNPs [15]. A comprehensive mechanism of the increased breakdown field strength is still unknown, however, a few models have been proposed. In the nanoparticle charging model [16], the difference in the dielectric permittivity of the dispersed nanoparticles and the surrounding oil is considered as an essential condition leading to polarization, charge trapping, and subsequent reduction of streamer velocity. Thus, the dielectric permittivity of MNF is a crucial parameter that has been extensively studied [17]. In [18] it was shown that the transformer oil-based magnetic nanofluid can exhibit a DC bias tunable apparent negative permittivity behavior at low frequencies (Fig. 8). This effect is a result of the particle clustering and the interface charge overlap in the applied electric field. Due to the created percolative conductive paths, the nanofluid undergoes transition from capacitive to inductive reactance. This mechanism is feasible at a low-frequency electric field without dynamic perturbations.

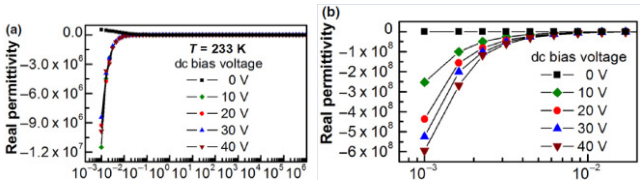

Fig. 8. DC bias voltage influence on the real permittivity spectrum of MNF at 233 K. (a) Whole spectrum with a linear vertical scale. (b) Low-frequency detail on the negative permittivity [18].

VIII. PROBLEMS

Authors have observed that the addition of nanoparticles to the oil improves the dielectric behavior of the fluid increasing its breakdown voltage and the AC pulse and other thermal properties. The application of such liquids could achieve more compact designs of transformers and improve the reliability of the new high voltage transformers for AC or DC.

Although the results reported in good number works are promising, more research is necessary to make nanofluids a feasible industrial solution. Investigations should be carried out to determine aspects such as influence of the applied materials and techniques, the long term stability of the fluids, the thermal and dielectric properties under different conditions or the interaction of the particles with other elements of the transformers. Even though the great progress in the nanofluid synthesis and numerous experimental studies and promising results, we are still encountering barriers restraining the effective application of nanofluids in electrical equipment like power transformers. To boost and support the effective application in the electrical engineering it is necessary, according to [19], to find more effective methods of

nanofluids synthesis and reduce the production costs. Besides that it is demanded to reduce the adverse environmental and human body impact of the nanofluids based on transformer oils.

Another challenge is related to the further investigation of the electric breakdown mechanism in nanofluids and to find a theoretical model, which would satisfy and fully explain the positive effect of nanoparticles in transformer oils on their electric breakdown field strength. To boost the transformer manufacturers and transformer operating companies' interest in utilization of nanofluids, more vivid dissemination and advertising of the cooling and insulating advantages is required. It is worth to mention that currently we can witness a dynamic development and research into novel biodegradable transformer oils.

Two factors restrict further comprehensive analysis of the observed anisotropy effect in MF. First, the high polydispersity of the particles and aggregates extremely complicates the direct application of the structure-factor for modeling 2D scattering from the aggregate phase. Second, the aggregates are not fully oriented, meaning that one cannot determine the average longitude and cross-sectional size characteristics of the aggregates from the standard analysis of the cuts of the 2D scattered intensity parallel and perpendicular to the electric field direction.

Recently, it was carried out a few SANS experiments that could reliably conclude that the electric field induces aggregates formation. This structural behavior depends on the strength and frequency of the applied field. However, as one single SANS measurement took 20 minutes, it was obtained the scattering intensities averaged in the time. Therefore it was missed the information about the quick particle assembly development driven by the applied field. For that purpose SAXS offers the best solution by which we could perform one measurement per 2 seconds.

As the research into electrorheological properties of ferrofluids has not received much attention yet, further and detailed investigation should be conducted in the future. Especially, the electric field induced structural and flow changes should be investigated on ferrofluids for high voltage engineering application. The qualitative and quantitative exploration of the ferrofluid structure and rheology under the external electric fields can shed light on some peculiar dielectric properties of ferrofluids and open a new avenue of ferrofluid research and applications. If the clustering process is sufficiently proved and a static or dynamic cluster structure is understood, its impact on the electric breakdown in ferrofluids should be taken into account.

IX. Conclusion

From the year 2000, interest in nanodielectric fluids applications has increased significantly. Several research groups are working with different materials (both fluid and particle type), focusing their studies on the thermal, dielectric and other properties of these liquids.

The aim of the next works should reveal the time development of magnetic particle assembly driven by an electric field with various intensities and frequencies. Besides getting the complementary information about the induced structure, a further step will be undertaken on investigation of the dynamics of the assembly formation. We believe that such work combined with previous results may shed light on the peculiar dielectric behaviour of ferrofluids based on insulating liquids.

In our investigation we will therefore focus on the apparent magnetic particle cluster formation in external electric and magnetic field studied by *in situ* SAXS, SANS, NR and electrorheology experiments.

References

[1] Odenbach, S. *Colloidal Magnetic Fluids: Basics, Development and Application of ferrofluids;* Springer: Berlin, Germany, 2009; ISBN 9783540853862.

[2] M.V.Avdeev et al. *Structural studies of ferrofluids in bulk and interface by neutron scattering,* presentation

[3] M. V. Avdeev and V. L. Aksenov, "Small-angle neutron scattering in structure research of magnetic fluids," *Phys.-Uspekhi*, vol. 53, no. 10, p. 971, Oct. 2010.

[4] T. Horn, S. Deutschländer, H. Löwen, G. Maret, and P. Keim, "Fluctuations of orientational order and clustering in a two-dimensional colloidal system under quenched disorder," *Phys. Rev. E*, vol. 88, no. 6, p. 062305, Dec. 2013.

[5] S. Odenbach, L. M. Pop, and A. Y. Zubarev, "Rheological properties of magnetic fluids and their microstructural background," *GAMM-Mitteilungen*, vol. 30, no. 1, pp. 195–204, Apr. 2007.

[6] W. Wen, X. Huang, and P. Sheng, "Electrorheological fluids: structures and mechanisms," *Soft Matter*, vol. 4, no. 2, pp. 200–210, Jan. 2008.

[7] T. Fujita and K. Yoshino, "Electrorheological magnetic fluid and process for producing the same." Patent US005507967A, 1996.

[8] T. Fujita, J. Mochizuki, and I. J. Lin, "Viscosity of electrorheological magneto-dielectric fluid under electric and magnetic fields," *J. Magn. Magn. Mater.*, vol. 122, no. 1, pp. 29–33, Apr. 1993.

[9] M. Rajnak et al., "Dielectric response of transformer oil based ferrofluid in low frequency range", J. Appl. Phys., 114, 3, 2013

[10] M. Rajnak, J. Kurimsky, B. Dolnik, P. Kopcansky, N. Tomasovicova, E.A. Taculescu-Moaca, M. Timko, "Dielectric-spectroscopy approach to ferrofluid nanoparticle clustering induced by an external electric field", Phys. Rev. E 2014, 90, 032310.

[11] M. Rajnak, V. I. Petrenko, M. V. Avdeev, O. I. Ivankov, A. Feoktystov, B. Dolnik, J. Kurimsky, P. Kopcansky, and M. Timko, "Direct observation of electric field induced pattern formation and particle aggregation in ferrofluids", Appl. Phys. Lett. 107, 073108 (2015).

[12] M. Rajnak, M. Timko, P. Kopcansky, K. Paulovicova, J. Tothova, J. Kurimsky, B. Dolnik, R. Cimbala, M.V. Avdeev, V.I. Petrenko, A. Feoktystov, "Structure and viscosity of a transformer oil-based ferrofluid under an external electric field", J. Magn. Magn. Mater. 431 (2017) 99–102

[13] M. L. Karpets, T. V. Tropin, L. A. Bulavin, J. W. P. Schmelzer. "Neutron reflectometry for structural studies in thin films of polymer nanocomposites. Modeling", Nuclear Physics and Atomic Energy 19(4):376-382 · December 2018. DOI:10.15407/jnpae2018.04.376

[14] A. Nagornyi, V. I. Petrenko, M. Rajnak, I. V. Gapon, M. V. Avdeev, B. Dolnik, L. A. Bulavin, P. Kopcansky, M. Timko, "Particle Assembling Induced by Non-Homogeneous Magnetic Field at Transformer Oil-Based Ferrofluid/Silicon Crystal Interface by Neutron Reflectometry", Applied Surface Science, 2019. – Vol. 473. – P. 912–917. – Doi.org/10.1016/j.apsusc.2018.12.197.

[15] J. Kurimský, M. Rajnák, R. Cimbala, J. Rajnic, M. Timko, P. Kopcanský, "Effect of magnetic nanoparticles on partial discharges in transformer oil", J. Magn. Magn. Mater. **2019**, 496, 165923.

[16] J.G. Hwang, M. Zahn, F.M. O'Sullivan, L.A.A. Pettersson, O. Hjortstam,R. Liu, "Effects of nanoparticle charging on streamer development in transformer oil-based nanofluids". J. Appl. Phys. 2010, 107, 014310.

[17] I. Malaescu, C.N. Marin, "Dependence on the temperature of the activation energy in the dielectric relaxation processes for ferrofluids in low-frequency field", J. Magn. Magn. Mater. 2002, 252, 68–70.

[18] M. Rajnak et al., "Toward apparent negative permittivity measurement in a magnetic nanofluid with electrically induced clusters", Phys. Rev. Appl. **2019**, 11, 024032.

[19] M. Rafiq et al., *J. Nanomater.*, vol. 2016, 2016, p. e8371560, Jul. 2016.

Implementation of Asymmetric Cryptography Algorithm RSA in Field Programmable Gate Array Environment

[1]*Michal HULIČ (3rd year)*
Supervisor: [2]Liberios VOKOROKOS

[1,2]Dept. of Computers and Informatics, FEI TU of Košice, Slovak Republic

[1]michal.hulic@tuke.sk, [2]liberios.vokorokos@tuke.sk

***Abstract*—This publication is handling the problematics of implementation of selected cryptography algorithms asymmetric category, specifically RSA in asymmetric field. The implementation is focused on representation of computer unit, which is decelerated as hardware accelerator. The solution and the results of systematic tests has the presence at the end of this document. The further steps in this field of research are present in the result chapter.**

***Keywords*—Computer Security, RSA Algorithm, Field Programmable Gate Array**

I. Introduction

This document is summary of previous work in a field of security, with cryptography and hardware architectures which includes RSA algorithm and its application in Field Programmable Gate Array, that acts like a hardware accelerator.

This publication is focused on the previous work with security applications in a field of cryptography solutions [1], classifications of security systems vulnerabilities [2] and cryptography implementations in programmable gate arrays [3], where I started to focus on hardware architectures and finding the vulnerabilities which can affect the whole architecture, steal or change the particular set of data.

The cryptography should be based on unidirectional mathematical function, that secures the process of transformation of message or to encrypted set of data. This transformation named encryption process should be fast and as secure as possible that guarantees that input data in process of encryption will be in best cases computationally impossible to decrypt using mathematical feature of unidirectional functions [11].

This publication is based on the previous scientific work [5] I was working on during the study time before.

The principle of asymmetric ciphers is far more difficult than the symmetric algorithms. The RSA algorithm is widely spared in application for data encryption and for securing digital signatures [4]. The RSA algorithm is one of the most popular encryption algorithms nowadays [9]. The process of computation is presented in chapter III. The key which has less than 1024 bits is now considered as not safe anymore [11].

II. Hardware Environment for Testing and Development

The mentioned cryptography algorithm was implemented on Xilinx Kintex-7 KC705 development board (Fig. 1). The development board provides a hardware environment for developing and evaluating the proposed RSA modules. The key components of the board are XC7K325T2FFG900C FPGA chip, 1 GB DDR3 SODIMM 800 MHz/1600 Mbps memory, USB JTAG connector, SD connector, PCI Express interface, SFP connector, ethernet connector, HDMI connector, I2C bus or GTX receiver and transmitter. The full description of all components of this board is presented in documents [6].

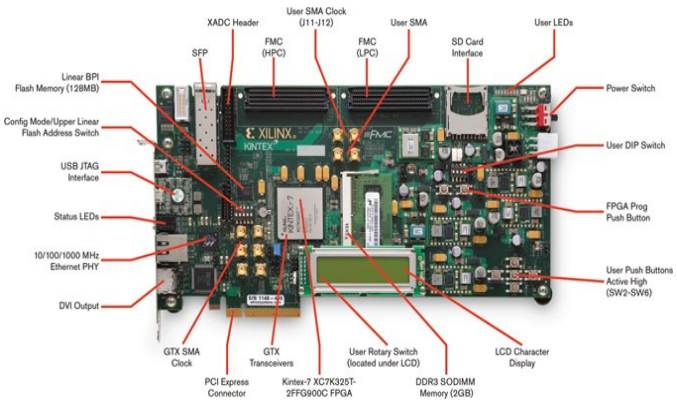

Fig. 1. Programmable Gate Array Development Board Kintex KC705 [6]

III. RSA Algorithm

For RSA algorithm is process of encryption as follows. If person A wants to send a private message M to person B, first person A encrypts the message by public key of person B, and for the person A is possible to decrypt the message using its own private key. The RSA algorithm belongs to group of asymmetric cipher algorithms [10]. RSA (Rivest–Shamir–Adleman) is an algorithm used to encrypt and decrypt messages. It is an asymmetric cryptographic algorithm. Asymmetric means that there are two different keys.

The concept of encrypting a message with one key and not being able to decrypt with the same key is based on one-way functions. Its name suggests the characteristic of a one-way function is that it is not reversible other than with a trial and error approach.

First process is to choose and create private and public key

- *Two big different prime numbers p, q are chosen from random generated numbers*
- *Calculate*

$$n = p \times q \quad (1)$$

- *Calculate*

$$\phi(n) = (p-1)(q-1) \quad (2)$$

- *Next step represent selection of random integer*

$$1 < e < \Phi(n) \text{ whereGCD}(e, \Phi, (n)) = 1 \quad (3)$$

- *Calculate*

$$1 < d < \Phi(n) \text{ where } d = 1 \pmod{\Phi(n)} \quad (4)$$

According the equation (4), as follows the private key exponent is computed.

- Message M need to be selected and encrypted.
- Next step is to find public key, the person N, by using which we are going to encrypt the message M and the (n, e) key is representation of it.
- The message is representation as integer among 0 to n-1. Blocks of messages are used if the message is too large. Each block is also representation as integer as the same range [0, (n1)].
- The final computation called encryption is represented as follows

$$C = M^e \pmod{n} \quad (5)$$

- Using public key (n,e) of person to who we are going to send the encrypted data are send using secure channel.
- Using the private key (n, d) we are going to perform a decryption process which belongs to the first person. The decryption process is computed as follows

$$M = C^d \pmod{n} \quad (6)$$

IV. Tested Results

There were two versions of RSA modules designed. The first version of the proposed RSA module uses spatial parallelism [10], multiple copies of the same hardware components (implementing RSA steps) implemented in the look-up-table (LUT) form (RSA_LUT).

The second solution uses pipelining (RSA_mul16s). The steps of the RSA algorithm were implemented as pipeline stages. The stages are connected one to the next to form a pipe – the message data block enter at one end, progress through the stages, and exit at the other end. The computations in stages are overlapped in execution. Although each message (message blocks) must pass through all stages, a different message (message block) will be in each stage [7].

The RSA modules were designed in Vivado Design Suite - HLx of Editions 2016.3 development software by using C and VHDL languages.

During the testing we had an experience with memory limitation and the final solution is limited to 1024 bits of the key and the message size per one computation cycle using the selected FPGA device on our designed architectural solution.

Time dependency is shown in Tab. 4. We determined that the bigger the message and key length is, the longer it takes to get cipher.

The highest operation clock frequency that we achieved was 254.46 MHz at RSA_LUT module and 152.77 MHz at RSA_mul16s module. The maximal usage of CLB units was at our tested FPGA device at maximum rate of three percentages that represents really low number. Our tested architecture is the demonstration of the higher performance then other compared solutions [4][8][10].

V. Conclusion

The software development tool that was used during the implementation and desing phase was Vivado HLS 2016.3. There were applied two approaches to build RSA computing unit. The first chosen approach was LUT, where RSA_LUT synthesis unit was created. To synthetize RSA_mul16 unit there was Pipeline processing used as second approach. There was given its name based on 16bit logical-arithmetic unit that was used for calculation of the numbers in a field of unsigned numbers. As comparison speed of encryption was created FPGA chip to with rate of management comparing to usage of CPU algorithm. Measured data showed that assumption was fulfilled, and multiple acceleration was present. Also, both RSA modules were compared. The solution of RSA looks up table showed higher working frequency not with higher consumption of CLB. However, this consumption was less than 3%. The final RSA algorithm has implementation in C and VHDL language. The future work will be focused on the security of hardware architectures and prevention of attacks on the hardware architectures.

Acknowledgment

This work was supported by the Faculty of Electrical Engineering and Informatics at the Technical University of Košice under contract No. FEI-2020-70: Behavioral model of component systems based on coalgebras and linear logic."

References

[1] M. Hulič, N. Ádam.: Implementation of Cryptography Algorithms in Field Programmable Gate Array. 2018. In: International Journal of Innovative Science and Research Technology. Vol. 3, no. 7 (2018), p. 521-526. - ISSN 2456-2165

[2] A. Baláž, M. Hulič, M. Kurilec, M. Štancel,: Classification of Security for System Vulnerabilities. 2019. In: 17th International Symposium on Intelligent Systems and Informatics : proceedings. - Budapešť (Hungary) : Institute of Electrical and Electronics Engineers s. 29-34 . - ISBN 978-1-7281-2142-0

[3] M. Hulič. FPGA Implementation of DES cryptography algorithm. 2018. In: SCYR 2018. - Košice : TU, 2018 S. 103-106. - ISBN 978-80-553-2972-7.

[4] A. H. Ansari, A. R. Landge, "RSA algorithm realization on FPGA", International Journal of Advanced Research in Computer Engineering & Technology (IJARCET) Volume 2, Issue 7, July 2013.

[5] M. Hulič.: FPGA Implementation of DES cryptography algorithm. 2018. In: SCYR 2018.

[6] P. Vishwanath, R. C. Joshi, A. K. Saxena, "fpga implementation of des using pipelining concept with skew core key-scheduling". Journal of Theoretical and Applied Information Technology, 2009

[7] L. Vokorokos, E. Chovancová, "Viacjadrová architektúra zameraná na akceleráciu výpočtov, " Acta Informatica Pragensia. Vol. 2, no. 1 (2013), p. 79-90. - ISSN 1805-4951

[8] E. Chovancová, N. Ádám, A. Baláž, E. Pietríková, P.Feciľak, S. Šimoňák, M. Chovanec, "Securing distributed computer systems using an advanced sophisticated hybrid honeypot technology," Computing and Informatics. Roč. 36, č. 1 (2017), s. 113-139. - ISSN 1335-9150.

[9] A. C. Shantilal, "A Faster Hardware Implementation of RSA Algorithm" Department of Electrical & Computer Engineering, Oregon State University, Corvallis, Oregon 97331 USA.

[10] A. Shashank, "FPGA Implementation of RSA Encryption and CRT based Decryption using Parallel Architecture," Journal of Innovation in Electronics and Communication.

[11] W. Stallings, "Cryptography and Network Security Principles and Practices," Prentice Hall. 2005 0-17- 187316-4.

Improving 3D Image Classifiers via Generative Modeling

[1]*Michal VARGA (5th year),*
Supervisor: [2]*Ján JADLOVSKÝ*

[1,2]Dept. of Cybernetics and Artificial Intelligence, FEI TU of Košice, Slovak Republic

[1]michal.varga@tuke.sk, [2]jan.jadlovsky@tuke.sk

***Abstract*—In this paper, we briefly report on our previous and current research activities in the field of generative modeling and 3D image classification. A summary of our research and a proposal for future work is presented. In the past year, we developed a generative enhancement methodology designed to streamline the creation of entirely new deep neural classifier by embedding an existing classifier within a compatible generative architecture. This modification improves the existing classifier's accuracy as well as its viability in domains where large datasets are not available.**

***Keywords*—computer vision, 3D image classification, deep learning, convolutional neural networks, generative modeling, GAN**

I. Introduction

In our research, we focus on the use of generative modeling in 3D image classification. Generative modeling-based classifiers have been successfully utilized to solve various classification problems including the 3D image classification. These models compete alongside non-generative classifiers achieving very similar performance [1]. While some non-generative classifiers differ significantly in structure from those utilizing generative modeling, we see the potential to enhance them with the benefits of the generative approach. Aside from the general pursuit of the highest possible classification accuracy, the motivation for this stems from the issues of the 3D image classification domain itself. While in the 2D domain, this problem is not so prevalent, in 3D, most of the large available datasets are synthetic and the contained classes are usually too generic for specialized problems. The benefit of the generative modeling-based approach is that such classifiers are more tolerant of small datasets.

For this purpose, we developed a generative enhancement methodology which is presented in this paper, alongside the experiments conducted to evaluate its viability and performance benefits. This research builds upon our work from previous years, summarized in [2]. A more extensive paper on this methodology is currently being finalized and will soon be submitted for publishing.

II. Initial status

During the past years, our research has focused on 3D image classification represented in two formats. First, we examined RGB-D images and their classification using 2D convolutional neural networks. The main point of interest we examined was the benefit of additional depth modality in addition to 2D RGB or greyscale images. The results have shown, that the relative improvement of classification accuracy with the depth channel available was up to 10%. [3]

Then, we focused on 3D voxel model classification and the use of generative modeling in classification problems. We developed a data preprocessing pipeline for mesh model voxelization and transformation. This was necessary to use the ModelNet [1] dataset with dense 3D convolutional classifiers. Alongside the preprocessing pipeline, we developed a visualization algorithm to shade and render the voxel grids for easier monitoring and debugging. [4], [2]

Finally, we implemented a Generative Adversarial Network utilizing both data preprocessing and rendering pipelines and trained it successfully on the ModelNet10 dataset. [2]

III. Current Research

Our current research focuses on the use of generative modeling as a tool in classification problems. In the following sections, we present the latest results of our efforts: a generalized generative enhancement methodology for the creation of new generative modeling-based classifiers and an experiment designed to investigate its viability and performance.

A. Generative Enhancement Methodology

We propose a generalized methodology for transforming compatible non-generative classifiers to utilize generative modeling and improve their classification performance and tolerance for small training datasets.

The methodology defines several steps of modification. In the first step, a conditional generator network is created with its output compatible with the classifier input (i.e. same data type, size, number of dimensions or channels, etc.). The generator is conditioned by a class vector, telling it which class of samples to generate.

In another step, the classifier is modified to also perform the discrimination task. This task consists of determining whether the presented sample is real (from the training set) or generated by the generator, therefore fake. This can be achieved, for example, by adding a 'fake' class to the set of output values.

Finally, the training loop is extended to include adversarial optimization of the generator.

B. Experiments and results

We designed an experiment to assess the viability and performance benefit of the proposed methodology. This experiment is based on the evaluation of one of the simplest

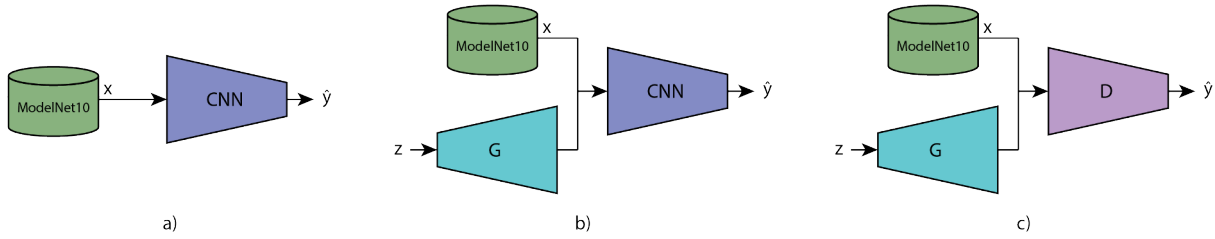

Fig. 1. Top-level architecture diagram showing the structure of the three neural networks used in the experiment. The three models are: (a) plain 3D CNN classifier trained on training dataset examples, (b) same 3D CNN trained on both training dataset examples and generated samples and (c) 3D CGAN.

application cases – a transformation of a 3D convolutional neural network (3D CNN) into a 3D Conditional Generative Adversarial Network (3D CGAN). Three classifier networks have been created for this experiment.

The first network is the 3D CNN itself, which is trained only on the training data from the dataset. The second (augmented 3D CNN) is not structurally different from the first 3D CNN, however, it is also trained using the generated samples from the pre-trained generator from the 3D CGAN network. It is not, however, trained simultaneously with the generator. The third model is the 3D CGAN network. The diagram showing the high-level structure of the three models is shown in Fig. 1.

We compared the classification accuracy and mean average precision (AP) of the three classifiers alongside state-of-the-art generative classifiers in Table I. The results and references to the compared models are available at [5]. While the accuracy of our models does not compete with the state-of-the-art, the main takeaway from these results is that this kind of classifier transformation can significantly improve its performance (89.21% vs. 83.04%) as well as its mean AP.

TABLE I
CLASSIFICATION ACCURACY AND MEAN AVERAGE PRECISION SCORE OF COMPARED 3D IMAGE CLASSIFIERS. EVALUATED ON THE MODELNET10 DATASET. [1]

	Accuracy [%]	Mean AP [%]
Primitive-GAN	92.20	
VIPGAN	94.05	90.69
Achlioptas et al.	95.40	
VRN Ensemble	97.14	
3D-GAN	91.00	
Plain CNN (ours)	83.04	83.75
Augmented CNN (ours)	84.58	86.31
CGAN Classifier (ours)	89.21	89.18

The mechanics of these improvements are not clear, however, they are most likely related to some form of feature knowledge transfer between the generator and classifier during their simultaneous training. One of the possible explanations is simple data augmentation provided by the generator. However, since the performance of the CGAN is higher than that of the augmented CNN, this explanation is not sufficient. The same applies to another theory, that the presence of a generator introduces noise into the classifier and makes it more robust, but the same noise should be present in the augmented CGAN which falls behind in performance.

C. Dataset

The models evaluated in the following experiment have all been trained on and tested using a synthetic 3D model dataset called ModelNet [1]. The dataset comes in two subsets: ModelNet10 and ModelNet40, each containing 10 and 40 classes respectively. Our experiment uses the smaller subset. The models are normalized with relation to the vector of gravity and therefore oriented in the most sensible way. No manual adjustments of the mesh models were performed.

In our preprocessing pipeline [2], the mesh models are voxelized, filled and scaled down to the final size of $32 \times 32 \times 32$. The values are normalized in $[-1, 1]$ range.

IV. CONCLUSION AND FUTURE WORK

The research from the past year has yielded results supporting the viability and potential of the proposed methodology. This shows the possibility of creating entirely new classifiers by transforming existing well-performing non-generative architectures resulting in potentially superior networks.

In our future research, we will further explore other viable candidates for this methodology, including both voxel-based and multi-view 3D image classifiers and evaluate the outcome to further assess the proposed methodology.

Additionally, we will continue our work on the custom rotary table 3D scanner which is currently in the prototype stage. This scanner will be used to acquire 3D scans of physical objects used for the practical real-life model evaluation. The used hardware and software solutions along with related research effort are part of the Technicom project [6].

ACKNOWLEDGMENT

This work has been supported by grant KEGA Implementation of research results in the area of modeling and simulation of cyber-physical systems into the teaching process - development of modern university textbooks – 072TUKE-4/2018.

REFERENCES

[1] Z. Wu, S. Song, A. Khosla, F. Yu, L. Zhang, X. Tang, and J. Xiao, "3d shapenets: A deep representation for volumetric shapes," in *Proceedings of the IEEE Conference on Computer Vision and Pattern Recognition*, 2015, pp. 1912–1920.

[2] M. Varga and J. Jadlovský, "Contribution to 3D Voxel Generative Adversarial Networks," in *SCYR 2019: Proceedings from Conference*, 2019, pp. 56–57.

[3] ——, "Evaluation of Depth Modality in Convolutional Neural Network Classification of RGB-D Images," *Acta Electrotechnica et Informatica*, vol. 18, pp. 26–31, 2018.

[4] ——, "Contribution to Generative Modelling and Classification of 3D Images," in *SCYR 2018: Proceedings from Conference*, 2018.

[5] "Princeton ModelNet," http://modelnet.cs.princeton.edu/.

[6] J. Jadlovský, A. Jadlovská, S. Jadlovská, J. Čerkala, M. Kopčík, J. Čabala, M. Oravec, M. Varga, and D. Vošček, "Research activities of the center of modern control techniques and industrial informatics," in *2016 IEEE 14th International Symposium on Applied Machine Intelligence and Informatics (SAMI)*, Jan. 2016, pp. 279–285.

Intelligent spaces as test platform

[1]*Tomáš TARKANIČ (2nd year),*
Supervisor: [2]*Jaroslav PORUBÄN*

[1,2]Dept. of Computers and Informatics, FEI TU of Košice, Slovak Republic

[1]tomas.tarkanic@tuke.sk, [2]jaroslav.poruban@tuke.sk

***Abstract*—Intelligent or smart spaces are used in many ways. In this paper we present our approach in the use of intelligent spaces. We introduce our will to use smart spaces as test platform. With this planing platform we should be able po observe people, and evaluate some kinds of metrics. Especially we focus on human motion and metrics linked to it. In this paper we also present our progress on the first part of test platform - multi-camera people tracking.**

***Keywords*—intelligent spaces, smart spaces, people observation, multi-camera people tracking**

I. Introduction

There are many places that are called smart or intelligent. We can find houses, offices, building, factories or even cities called smart. One of this kind of places Openlab, is located on the department of Computers and Informatics, TU of Košice. It was build to by playground or test base for projects of student. Also it was meant to be learning/teaching platform [1].

Openlab can be used to simulate smart spaces, so students, teachers or whoever have a will can use it as an universal space of this kind. To be honest Openlab can not simulate every possible smart space, but it is able to transform to many kind of them.

We find out that smart spaces can be used as test base. It mean that we can use Openlab or another intelligent space as platform for measurements. Because of our focus on human centered spaces we decide to explore possibilities of people observation.

II. Intelligent space as test platform

In the following chapter we will describe possibilities of intelligent spaces and specify our focus on people observation. We will describe test base build on the ground of intelligent space.

A. Ways of using smart spaces

According to Belanová [2], are smart or intelligent spaces the ones sensing, understanding of what is happening in them and providing services for human.

Intelligent spaces are used in different ways. As smart homes [3], smart offices [4], smart production lines [5] and also cities becoming smart [6]. But what about concrete usage? Notion smart or intelligent are very often used with the place which should make its usability more comfortable. Another way of application is to help people. Intelligent systems are installed to the retirement homes to help with disasters prevention. Or we can find an examples of fully automated production lines with are build with the goal save a money and make process more precise.

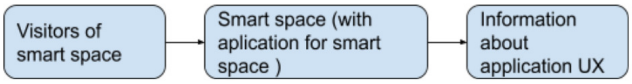

Fig. 1. Goal of test base

The examples mentioned above are definitely not all possible variants of smart spaces applications and usage. But even due to this examples we can divide intelligent spaces on two major types:

- the ones that include persons, or in another words are made it be used by humans and,
- the ones that are manufacturing or not including human to be part of it.

We introduce this dividing because we want to specify our aim at the first kind of intelligent spaces - the one that are made for human.

Intelligent spaces with the aim on human are evolving as the other kinds do. New applications are introduced, new kind of sensors are used. On the figure 1 we can see what we want to achieve. The test base for smart spaces applications, which can be used as tool for user experience testing.

Similarly as the eye tracking and mouse tracking techniques move web testing forward [7][8], we thought that technologies in the smart environment can move forward another kinds of testing.

Why do we thing smart spaces are good to be test base? They contain sensors and actuators [9], which are providing information to us [10], we can use this information for test purpose, in some cases uses do not even have to know that he or she is test participant. Many of smart spaces include in their technical equipment some kind of human tracking technology. Many o them have video cameras installed. We think about the video cameras usage to get some information we can transform to test results.

B. Observation of behavior in intelligent spaces

Most of intelligent spaces include video cameras in the list of hardware equipment. We focus on them.

Video cameras can be used for observation, but there is many things we can observe. One of them is trail. We decide to observe user of smart environment and track their routes. Also we can monitor the times of entering and exit. We can monitor times of stops they made. By doing so we would be able to find:

Fig. 2. Tasks of test base

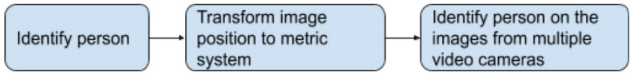

Fig. 3. Video processing structure

- What are the routes of users.
- What are the number of user. (We are planing to implement multi-user observing)
- What are the time users spend in space in average.
- How fast they walk.
- Where and when they stop.

By implementing test base in intelligent space environment, which is mention for tracking people movement we want to find out if measured data can be used to evaluate or improve user experience of application running in the smart space.

C. Test base structure and implementation steps

Openlab as we describe it is suitable place to develop and test test-base for intelligent spaces. This space contain needed sensors - video cameras, which are strategically placed to cover whole place. Its footprint is irregular what make tracking more difficult, but it is better for system designing to by ready for this type of conditions.

To reach the output as we describe in part II-B, we need to specify steps which should be done 2:

1) Firstly we have to get working multi-user, multi-camera tracking.
2) Secondly we have to do research about suitable ways of data storing.
3) Third step is to create algorithm to present data.

About the topic of multi-camera people tracking we can find articles like by Wen [11], where authors introduce method based on a space-time-view hyper-graph, the disadvantage of method is need of previous camera specification.

When we want to store measured data we have to look on the ways to do it. This kind of data match the data type big data by their character. It could be difficult to determinate which data are significant and have to by stored and which should be deleted [12].

Measured data should be presented in the right format and they have to by comparable. Problem with comparison relate mostly to measured route. When we want to tell the end user if two routes are the same we have to implement algorithm to do so, which neglect non significant differences.

III. Test base progress

We describe the steps that need to be accomplished on the way of creating test base used in intelligent spaces 2.

Looking at the first steps we prepare solution for multi-camera people tracking 3.

The set of program were created to accomplish task of people tracking. First part of complex application use YOLO [1] detector to identify person in the camera image. The instance o application have to run for every camera we want to use. Set of data are processed with another application which transform image position to metric system position in real room footprint, this task was fulfilled by using OpenCV Geometric Image Transformations[2]. The last task was to identify the same person on the images from multiple video cameras - task was accomplished by algorithm predicting movement based on distance.

For next work we have to finish another two part of test platform. Data storing problem and data presenting problem.

[1]YOLO detector - https://github.com/pjreddie/darknet/wiki/YOLO:-Real-Time-Object-Detection

[2]Geometric Image Transformations - https://docs.opencv.org/2.4/modules/imgproc/doc/geometric_transformations.html

IV. Conclusion

In this paper we presented our plan to build test platform observing people, on the ground of intelligent spaces. During this year we created first part of platform which detect movement of humans. Our next aim is to complete another part of described platform, data storing and data presenting.

Acknowledgment

This work was supported by project KEGA No. 053TUKE-4/2019: Learning Software Engineering via Continues Challenges and Competitions and VEGA No. 1/0762/19: Interactive pattern-driven language development.

References

[1] J. Porubän, "Challenging the education in the open laboratory," in *2018 16th International Conference on Emerging eLearning Technologies and Applications (ICETA)*. IEEE, 2018, pp. 439–444.
[2] D. BELANOVÁ, M. MACH, P. SINČÁK, and K. YOSHIDA, "The concept of intelligent space with a robot," in *International Symposium on Affective Science and Engineering ISASE2019*. Japan Society of Kansei Engineering, 2019, pp. 1–4.
[3] C. Wilson, T. Hargreaves, and R. Hauxwell-Baldwin, "Benefits and risks of smart home technologies," *Energy Policy*, vol. 103, pp. 72–83, 2017.
[4] K. J. Bakhsh, J. Kabat, R. Bono, S. Tabrizi, and G. Pini, "Smart office; application of a unified analytics center in tunneling construction," in *Tunnels and Underground Cities. Engineering and Innovation Meet Archaeology, Architecture and Art*. CRC Press, 2019, pp. 2279–2287.
[5] Y. Zhang, Y. Cheng, and F. Tao, "Smart production line: common factors and data-driven implementation method," in *ASME 2017 12th International Manufacturing Science and Engineering Conference collocated with the JSME/ASME 2017 6th International Conference on Materials and Processing*. American Society of Mechanical Engineers Digital Collection, 2017.
[6] H. Ahvenniemi, A. Huovila, I. Pinto-Seppä, and M. Airaksinen, "What are the differences between sustainable and smart cities?" *Cities*, vol. 60, pp. 234–245, 2017.
[7] F. Hauser, J. Mottok, and H. Gruber, "Eye tracking metrics in software engineering," in *Proceedings of the 3rd European Conference of Software Engineering Education*, 2018, pp. 39–44.
[8] P. E. Stillman, X. Shen, and M. J. Ferguson, "How mouse-tracking can advance social cognitive theory," *Trends in cognitive sciences*, vol. 22, no. 6, pp. 531–543, 2018.
[9] C. G. García, D. Meana-Llorián, J. M. C. Lovelle *et al.*, "A review about smart objects, sensors, and actuators." *International Journal of Interactive Multimedia & Artificial Intelligence*, vol. 4, no. 3, 2017.
[10] K. K. Patel, S. M. Patel *et al.*, "Internet of things-iot: definition, characteristics, architecture, enabling technologies, application & future challenges," *International journal of engineering science and computing*, vol. 6, no. 5, 2016.
[11] L. Wen, Z. Lei, M.-C. Chang, H. Qi, and S. Lyu, "Multi-camera multi-target tracking with space-time-view hyper-graph," *International Journal of Computer Vision*, vol. 122, no. 2, pp. 313–333, 2017.
[12] A. Yassine, S. Singh, M. S. Hossain, and G. Muhammad, "Iot big data analytics for smart homes with fog and cloud computing," *Future Generation Computer Systems*, vol. 91, pp. 563–573, 2019.

Introduction to the Smart Grids and Smart Metering

[1]*Jozef HUMENÍK (1st year)*
Supervisor: [2]*Jaroslav Džmura*

[1,2]Department of Electric Power Engineering, FEI TU of Kosice, Slovak Republic

[1]jozef.humenik@student.tuke.sk, [2]jaroslav.dzmura@tuke.sk

***Abstract* - This article discusses smart grids and smart metering systems that are an essential part of them. Their history has origins at the beginning of this millennium. In this article is presented from the actual state up to the possibility of development of these areas for the future in the world and particularly in Slovakia. The main asset of this article is to point out the legal aspects of these areas for the territory of the Slovak Republic.**

***Keywords* - Law aspects, Smart Grids, Smart Metering, Smart Meters.**

I. INTRODUCTION

The development of industry in many areas we can see for decades around the world. Electrical power engineering in Slovakia as a country with a high number of qualified experts in this field has no exception.

Smart grids are modernized networks that use information and communication networks and modern technologies for collecting information on electricity generation and consumption. Intelligent networks allow you to increase efficiency automatically (by controlling power flow or shortening peak times), save money (ability to adapt to demand), increase reliability and power generation and distribution. Smart grids include smart electricity meters, intelligent consumers, renewable energy sources and much more. [14]

The term "smart grid" appeared in 2003 in an article by Michael T. Burr. In the article were defined some functionalities and technical definitions of smart grids. One of the main pillars is the use of digital data processing and digital signal transmission, enabling data transmission and easier management of intelligent network information. In the Slovak Republic, smart electricity meters began to appear in 2012. For the purposes of measuring end-user consumption, the distribution companies use more smart metering systems, which are the part of smart grids. Induction electrometers are slowly but surely getting into the background. The Telegestore project was launched in Italy at the beginning of the second millennium. The project used networks with approximately 30 million of Smart Electric Meters. These smart electricity meters were interconnected by means of a digital network using power lines alone. In one case, a wide-band transmission of data over the power line was used, and in the other case, wireless data transmission technologies were used.

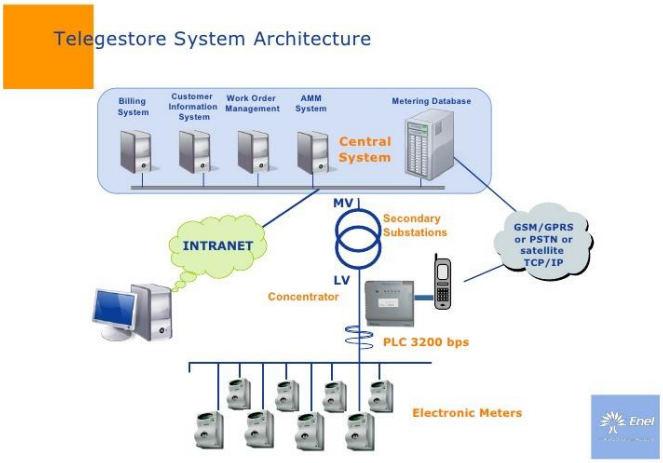

Fig. 1. Telegestore System Architecture [21]

II. THE LAW ASPECTS OF SMART METERING IN THE SLOVAKIA

In this category, we talk about legislation that is valid for the Slovak Republic and is connected to smart grids and smart metering.

A. Decree of the Ministry of Economy of the Slovak Republic No. 358/2013

In 2013, the Ministry of Economy of the Slovak Republic adopted Decree No. 358/2013 laying down the procedure and conditions for the deployment and operation of smart metering systems in electrical power engineering. [3]

Fig. 2. Smart Metering System [26]

The subject matter to this regulation is to establish the criteria and conditions for the deployment of smart metering systems for each end-consumer category of electricity. The required technical parameters (functionalities), data transmission requirements and cooperation between several systems and methods of accessing metering data deadlines for the introduction of smart metering systems for each end-consumer category.

The requirements for categories 1, 2 and 4 are already fulfilled according to the requirements of the applicable legislation. Installation of smart meters in a category No. 3 is still in progress and will end on 31.12.2020.

The above-mentioned decree divides the technical parameters or functionalities of smart metering systems into three categories, namely:

a) basic functionality of the smart metering system,
b) advanced functionality of the smart metering system,
c) special functionality of the smart metering system.

Individual categories slightly differ from each other but the common functionalities are e.g. capability of bidirectional communication between the end-users consumer point and the data centre, continuous off-take and delivery metering with a 15-minute measurement interval and remote reading, recording offtake and delivery to multiple tariffs and associated tariff switching, event registration and failure states of smart meters.

In addition, advanced and special functionality makes it possible to record the quality parameters of the distribution system. The quality parameters obtained by means of intelligent electricity meters are increasingly valuable and are increasingly in demand for the needs of distribution network development, maintaining the required quality parameters of electricity when supplied to end customers, and for the needs of end customers. If the data level (signal) is enough, it is possible to connect the end-consumer within 10 minutes of the request being made by the electricity supplier. In case of insufficient signal to execute the command for the smart meter, the work order for physical connection is issued by an employee of the distribution company.

Regarding the requirements for data transmission and cooperation between individual systems, the communication should be realized in Slovak conditions via the Global System for Mobile Communications (GSM), universal GPRS packet radio service, using the local Ethernet network or indirect communication using concentrators via PLC (Power Line Communication) or WAN protocol. [3]

The use of GSM / GPRS technology is also important in parts of the distribution area, where is not enough level of data services (signal) to enable intelligent electrometers to safely command and perform remote data readings. The remote readings include e.g. load profile 15 min and 10 min, registers and events. Especially in wooded and sparsely populated areas of north-eastern Slovakia and the Spiš region is more difficult to achieve. Inductive and digital electricity meters are mainly used in these areas.

PLC (Power Line Communication) technology is suitable to use especially in densely populated areas, such as urban agglomerations. This technology is important for example in apartment buildings.

In eastern Slovakia, this technology was introduced to the trial operation in 2013, where PRIME and BPL (Broadband Power Lines) technologies were tested. In 2017, new generations of PLC technology began to appear on the world market, which was at a higher technological level than their predecessors. VSD in 2017 tested PRIME (Powerline Intelligent Metering Evolution) and G3-PLC where the test results were much more satisfactory than the last tests, for which technological advances in manufacturing spheres were possible. Whether this technology has the potential for contribution to the sustainable development of intelligent networks not only in Slovakia but also worldwide.

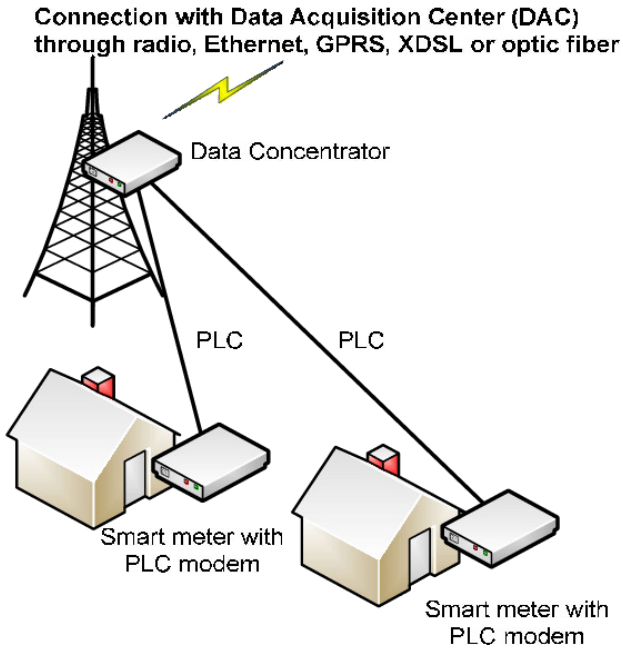

Fig. 3. PLC technology [15]

The Decree specifies the obligation for the distribution network operator to measure at least 80 % of the total volume of distribution points in the distribution area using intelligent metering systems.

In the territories of eastern Slovakia, which is in the report of Východoslovenská distribučná, a.s. consists of about 100,000 offtake points with consumption of more than 4,000 kWh per year. Mostly business entities and households which use electric boilers to heat and utilize electricity to heat domestic hot water. The rest consists of offtake points with an annual consumption of less than 4,000 kWh. Induction and static electricity meters are installed on that consumption metering points.

Based on this decree, OKTE, a.s. (Short-Term Electricity Trader) is obliged to make the measured data available from intelligent metering systems to end-users who request it for meeting the following criteria:

- The applicant is a consumer of electricity at a given point of consumption.

- At a point of consumption with one of three functionalities is installed at the metering point.

B. Energy Act No. 251/2012 of the Collection of Laws

The subject of the amendment to the Energy Act No. 251/2012. It is mainly to establish the rights and obligations of the individual market participants in the energy sector measures aimed at ensuring the security of energy supply (electricity, gas) and the functioning of the internal energy market and statistical supervision of energy in the Slovak Republic. [4]

One of the duties of the distribution system operator is to deduct all types of electricity meters (inductive, digital and smart) at least once a year. Induction meters represent the oldest type of meter, which was produced in single-phase and three-phase versions. In the case of two-tariff measurement an external device, such as a switching clock or a remote-control receiver (HDO) was needed. At the end of 2014, their number in the distribution area of VSD, a.s. was about 400 000 pcs.

Fig. 4. Three-phase electromechanical induction meter [6]

Since 2010, a massive installation of digital electricity meters has started, which has many advantages over its predecessor. These meters do not need external tariff switching devices because they have their own time base and switching relay. At the end of 2014, their number in the distribution area of VSD, a.s. was about 200 000 pcs.

Fig. 5. Three-phase static (digital) meter [7]

In the case of inductive electricity meters, the reading is done physically (manually) at the sampling point and, in the case of digital meters, also physically at the consumption metering point but by means of a manual terminal and optical probe which can make the human factor failure. In some cases, by mutual agreement it is possible to accept the deduction of reports to the end consumer. In practice, this is done in the form of reporting electricity meter status by e-mail, telephone, by self-counting mobile application or by post using a postcard.

In the case of smart electricity meters which represent the latest generation of electricity meters, the deduction is carried out in the form of remote reading by means of the data and collection centre. In this case, the reporting of the states by the end consumer is not accepted. Compared to simple digital electricity meters, they have a larger range of measured quantities as well as several new functionalities.

Fig. 6. Three-phase Smart Meter with special functionality [8]

On the contrary, it is the responsibility of the final electricity consumer to make the supply point available to the employee of the distribution company, which in eastern Slovakia is Východoslovenská distribučná, a.s., in central Slovakia it is Stredoslovenská distribučná, a.s. and in western Slovakia it is Západoslovenská distribučná, a.s. for the purpose of carrying out the deduction of a designated measuring device or checking the technical connection conditions such as checking for the presence of unauthorized sampling or a technical state of the measurement).

One of the obligations of the operator of the regional distribution system is to send the measured data from the consumption metering points where a smart electricity meter is installed to OKTE which collects, manages and makes the measured data available. The transmission system operator, the local distribution system operator and the direct line operator is also obliged to provide the measured data for the individual offtake and handover points of OKTE, which makes the data available for clearing entities, electricity suppliers, the Regulatory Office for Network Industries and the Ministry of Economy of the Slovak Republic.

C. Cybersecurity Act No. 69/2018 of the Collection of Laws

As in any industry the energy sector has no exception, so it is necessary to address the issue of cybersecurity. The requirements under the Cybersecurity Act relate mainly to the security of networks, infrastructure and information systems. Systems for collecting and processing smart metering data also fall into this category. [5]

By adopting this law, many companies have incurred financial expenditures which must invest for securing their data networks, increasing the level of security of their IT infrastructure and of course the data themselves which are often of great value to these companies. In the field of electricity measurement, it is mainly about increasing the security level of

data transmission using verified security certificates and subsequent storage on sufficiently secure storage. They use local disk arrays in their own management and remotely network disks called Cloud storage. [24][25]

III. Conclusion

Smart grids, as the successors of conventional distribution grids are gaining in popularity. Current smart grids are perceived rather as complementary grids supporting conventional distribution grids.

This is evidenced by the implementation of various projects around the world, such as the Telegestore project in Italy or the Smart grid city of Yokohama project in Japan. [11]

An integral part of smart grids is the smart metering systems that have been appearing in Slovakia since 2014 where they gradually began to replace the outdated induction meters. If we want to build an operational and sustainable smart grid, we must focus mainly on the implementation of modern communication technology and measurement systems.

From an economic-legal point of view the close cooperation between the government, distribution companies and the business sector are needed to achieve these objectives. From a cybersecurity perspective it is important to think about securing the networks and protecting sensitive data from unauthorized misuse. Cybersecurity is a challenge that should be raised more frequently when dealing with smart grid projects.

References

[1] NIKMEHR, N., RAVADANEGH, S. N. *Optimal Power Dispatch of Multi-Microgrids at Future Smart Distribution Grids*, IEEE Transactions on Smart Grid, vol. 6, No. 4, 2015, p. 1648–1657.

[2] SHAMSHIRI, M., GAN, C. K., TAN, C. W., *A review of recent development in smart grid and micro-grid laboratories*, IEEE International Power Engineering and Optimization Conference Melaka, Malaysia, 2012, p. 367–372.

[3] Decree of the Ministry of Economy of the Slovak Republic No. 358/2013 of the Collection of Laws, URL: <https://www.slov-lex.sk/pravne-predpisy/SK/ZZ/2013/358/20150801>

[4] Energy Act No. 251/2012 of the Collection of Laws, URL: <https://www.slov-lex.sk/pravne-predpisy/SK/ZZ/2012/251/20200101>

[5] Cyber Security Act No. 69/2018 of the Collection of Laws, URL: <https://www.slov-lex.sk/pravne-predpisy/SK/ZZ/2018/69/20190101>

[6] Figure 4. *Induction electromechanical meter*, URL: <https://www.vsds.sk/edso/domov/technicke-info/meranie-distribucie/elektromery/indukcne>

[7] VSD,a.s. *Digital meter*, URL: <https://www.vsds.sk/edso/domov/technicke-info/meranie-distribucie/elektromery/staticke>

[8] VSD,a.s. *Smart meter*, URL: <https://www.vsds.sk/edso/domov/technicke-info/meranie-distribucie/elektromery/ms>

[9] BARIN, A., CANHA, L.N., ABAIDE, A.R., MAGNAGO, K.F., WOTTRICH, B., MACHADO, R.Q., *Multiple Criteria Analysis for Energy Storage Selection*. Energy and Power Engineering, 2011

[10] TORRITI, Jacopo, *Demand Side Management for the European Supergrid: Occupancy variances of European single-person households*. Energy Policy. 44: 199-206. doi: 10.1016/j.enpol.2012.01.039, 2012

[11] *Yokohama Smart City Project*, [online]. Available at: <https://esci-ksp.org/wp/wp-content/uploads/2012/05/Yokohama-Smart-City-Project-YSCP.pdf>

[12] *Smart Grid Portal: Smart Grid Projects*. EURELECTRIC/JRC, 2014. [online]. Available at: <https://ses.jrc.ec.europa.eu/inventory?field_proj_dev_stage_value=All&field_proj_start_date_value[value][year]=&field_proj_start_date_value2[value][year]=2019&field_proj_countries_involed_tid=&titleproj=&field_proj_application_value>

[13] MOMOH, J., *Smart Grid: Fundamentals of Design and Analysis*, 216, (IEEE P., 2012, ISBN:978-0-470-88939-8

[14] Smart Grid definition by EU Commission, Available at: < https://s3platform.jrc.ec.europa.eu/smart-grids>

[15] VSD,a.s. *PLC technology*, Available at: <https://www.researchgate.net/figure/Heterogeneous-network-with-Power-Line-Communication_fig3_275260763>

[16] ZHAO, Jinquan; HUANG, Wenying; FANG, Zhaoxiong; CHEN, Feng; LI, Kewen; DENG, Yong, *On-Line Voltage Stability Monitoring and Control (VSMC) System in Fujian power grid*. 2007, IEEE Power Engineering Society General Meeting. Proceedings, Power Engineering Society General Meeting, 2007. Tampa, FL, USA: IEEE. p. 1. URL: <doi:10.1109/PES.2007.385975>. Lay summary. ISBN 978-1-4244-1296-9.

[17] CHOWDHURY, S; CROWDHURY, S.P.; CROSSLEY, P. *Microgrids and active distribution networks*. Institution of Engineering and Technology. ISBN 9781849191029.

[18] BIFARETTI, S.; CORDINER, S.; MULONE, V.; ROCCO, V.; ROSSI, J.L.; SPAGNOLO, F. *Grid-connected Microgrids to Support Renewable Energy Sources Penetration*. Energy Procedia. 105: 2910–2915. URL: <doi: 10.1016/j.egypro.2017.03.658.>

[19] KANNBERG, L. D.; KINTNER-MEYER, M. C.; CHASSIN, D. P.; PRATT, R. G.; DESTEESE, J. G.; SCHIENBEIN, L. A.; HAUSER, S. G.; WARWICK, W. M. *GridWise: The Benefits of a Transformed Energy System*. Pacific Northwest National Laboratory under contract with the United States Department of Energy. 2003.

[20] TORRITI, Jacopo. *Peak energy demand and Demand Side Response*

[21] Figure 1. *The Telegestore project in Italy*, URL: <https://www.slideshare.net/enelsharing/smart-metering-and-smart-grids11jul-09.> 2009.

[22] *Smart metering security – Germany leads the way*. Available at: <www.bosch-si.com>. 2017.

[23] FAISALL, M. A.; AUNG, Z.; WILLIAMS, J. R.; SANCHEZ, A. S., *Securing Advanced Metering Infrastructure Using Intrusion Detection System with Data Stream Mining*. 2012.

[24] *FBI: Smart Meter Hacks Likely to Spread — Krebs on Security*. URL: <krebsonsecurity.com>. 2017.

[25] GREVELER, U, Prof. Dr.-Ing; JUSTUS, B., Dr.; LöHR, D., MSc. *Hintergrund und experimentelle Ergebnisse zum Thema*: *Smart Meter und Datenschutz* (in English and German). Fachhochschule Münster of Applied Sciences. 2011.

[26] *Figure 2. Smart Meter System,* URL: <https://www.shutterstock.com/cs/image-vector/smart-metering-system-diagram-vector-244539127>

Investigating the superconducting state and the metallic state properties in perpendicular magnetic field in homogeneous, strongly disordered ultrathin films in the vicinity of Superconductor-Insulator Transition

[1]*Michal KOPČÍK (4th year)*
Supervisor: [2]Pavol SZABÓ

[1,2]Dept. of Low Temperature Physics, Institute of Experimental Physics, Slovak Academy of Sciences

[1]mkopcik@saske.sk, [2]pszabo@saske.sk

After several decades of active research many integral questions regarding Superconductor-Insulator Transition (SIT) as one of the central points of interest of contemporary condensed matter physics remain unanswered. SIT is one of several known realisations of a continuous quantum phase transition. This review summarizes the results of the search for another suitable experimental system that could exhibit the intriguing findings in homogeneously disordered films of molybdenum carbide in the vicinity of the SIT which were presented in my contributions in previous years, as well as the results of the continued efforts to characterize the electronic properties of our MoC films through various methods.

Keywords **— Disordered superconductors, Superconductor-insulator transition, Ultrathin films**

I. Introduction

Superconductor-insulator transition is a type of a continuous quantum phase transition: a phase transition that occurs at zero temperature due to a change in the ground state of the system [1,2,3]. A quantum phase transition is facilitated by quantum fluctuations as opposed to thermal fluctuations associated with regular phase transition. The ground state change occurs as a result of a variation of an external parameter in the Hamiltonian describing the total energy of the system. The most basic examples of such parameters (specifically for the superconductor-insulator transition) are disorder, charge-carrier concentration, external magnetic field and lower dimensionality of the system. This brief review focuses on the results of experiments on homogeneously disordered ultrathin polycrystalline films of molybdenum carbide on an oxidized amorphous silicon substrate prepared by magnetron sputtering. Previous study on molybdenum carbide films [4] showed gradual suppression of superconductivity by reducing the thickness of films. In this case the reduction of the film thickness leads to an increase of disorder expressed via Ioffe-Regel parameter $k_F l$. The thinnest tested sample (3 nm thickness) exhibited homogeneous superconducting phase with transition temperature $T_C = 3.95$ K, thus still relatively distant from the transition to the insulating state. However, theoretical calculations predict $k_F l$ close to unity, which represents the quantum limit for metallic conductivity. Unfortunately, we were unable to produce uniform films with thickness lower than 3 nm. Thinner films exhibited inhomogenities and multi-phase/granular signatures in transport measurements. The situation was repeated in the case of MoN films, where the lowest achieved thickness that preserved homogeneity was ~4 nm, however we were not able to replicate this result again with the same substrate class. This lead to a search for the optimal substrate and sputtering conditions combination to manufacture thinner samples closer to the superconductor-insulator transition.

II. Initial Status

Previously, we demonstrated a presence of unconventional density of states (DOS) above the perpendicular upper critical field $H_{c2}(0)$ in the 4 nm thick molybdenum nitride films by means of tunneling spectroscopy. This kind of logarithmic suppression of DOS at the Fermi energy that persists on the other side of the superconducting transition was observed as a pseudogap in several types of conventional and unconventional superconductors, such as other highly disordered systems in 2D (ultrathin films) and 1D (nanowires) limit as well as high-temperature cuprates. Unlike a pseudogap, this spectral feature is not suppressed in magnetic field. We observed a similar phenomenon in 3 nm MoC thin films, where the tunneling anomaly was actually emphasized in magnetic field. From the shape of $H_{c2}(T)$ temperature dependence and the apparent lack of vortex lattice formation in perpendicular magnetic field we determined that the film entered the Pauli paramagnetic limit region. In conjunction with the observed field dependence of the DOS suppression at the Fermi energy we identified this phenomenon as the low temperature tunneling anomaly in low-dimensional highly disordered systems, also known as the

Altshuler-Aronov effect [5, 6]. This effect is a property of the normal state after the superconductivity gets suppressed by the magnetic field, as opposed to a pseudogap, which is a property of the superconducting state (or more precisely, the result of superconducting fluctuations in the normal state).

III. Tasks Solved

To complete the analysis of the MoC films, we return to the transport data and perform a finite-size scaling to determine the universality class of the transition at zero temperature. This might provide insight into whether the 3 nm film approaches the region, where bosonic excitation effects are necessary to be considered in our purely fermionic treatment of the Altshuler-Aronov anomaly. In the language of continuous quantum phase transitions, the system is characterized by divergence of relevant length scales and universal behavior of physical quantities towards the critical point, which can be expressed in the form of a scaling law

$$\frac{R(B,T)}{R_C} = f\left[(B - B_C)T^{-\frac{1}{\upsilon z}}\right]$$

where R_C is the critical resistance, f is a universal scaling function, B_C is the (upper) critical field, υ is the correlation length exponent and z is the dynamical critical exponent [7]. Magnetoresistance isotherms in the vicinity of the critical point should exhibit a common crossing point, marking the precise values R_C, B_C, and collapse onto each other after rescaling, providing a single pair of υ, z, which determine the universality class of the transition regardless of the microscopic material properties.

Fig. 1 presents a set of sheet resistance $R_\square$ vs perpendicular magnetic field curves measured at temperatures 0.4 - 6 K. Instead of a crossing point which should precisely determine the upper critical field $B_{C2}(0)$ we observe a crossing region between 6.3 and 6.8 T. Similar situation was observed in thin films of indium oxide [8], crystalline lead [9], zirconium chloride and molybdenum disulfide [10], where the crossing field decreases with temperature (this behavior is associated with quantum Griffith phase [11]) as well as in amorphous indium oxide films [12, 13], where the crossing field increases with temperature, which is the case of our MoC sample. Due to the absence of a singular crossing point, no universal values of υ and z are obtainable through finite-size scaling. However, in small temperature intervals the scaling is possible as illustrated in Fig. 2. Considering the uncertainty of arbitrarily defined overlap of scaled curves we extract an approximately linear, proportional dependence of υz on temperature, which, when extrapolated to zero temperature, yields $\upsilon z \approx 0.7$. If we assume $z = 1$ for long-range Coulomb interactions [7], $\upsilon = 2/3$ is a prediction of a (2+1)D model or that of a model without disorder [14, 15], whereas most experiments on strongly disordered 2D systems report $\upsilon \sim 4/3$, as predicted by 2D quantum percolation model [2]. Therefore, we tentatively conclude that the bosonic excitations do not play a crucial role in the field-tuned superconducting transition at low temperatures in the system at the $k_F l$ values approaching unity.

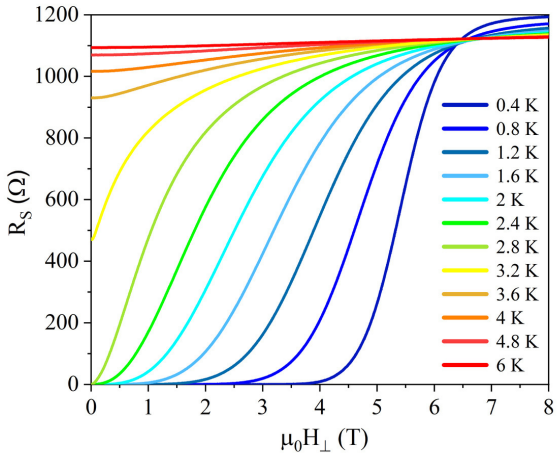

Fig. 1. 3 nm MoC film magnetotransport measurement. Sheet resistance $R_\square$ as a function of temperature for perpendicular magnetic field 0 - 8 T.

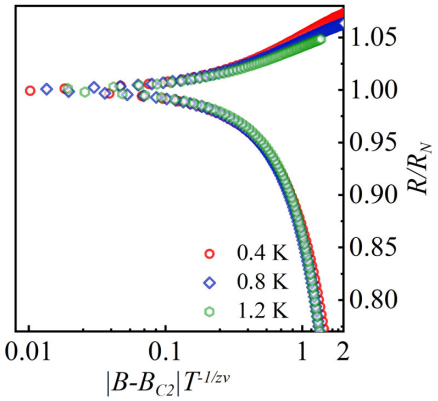

Fig. 2. Finite-size scaling of normalized sheet resistance $R_\square/R_N$ versus the scaling variable $|B - B_{C2}|T^{-1/z\nu}$ for the 3 lowest temperature datasets with the resulting critical exponent product $\upsilon z = 0.92$.

Acknowledgements

This work was supported by the projects APVV-14-0605, VEGA 1/0409/15, VEGA 2/049/16, COST CA16218 Nanocohybri and by the U.S. Steel Košice.

References

[1] V. F. Gantmakher, V. T. Dolgopolov, Phys. Usp. **53**, 1 (2010)
[2] A. M. Goldman, Int. J. Mod. Phys. B **24**, 4081 (2010)
[3] Y. Liu, A. M. Goldman, Mod. Phys. Lett. B **8**, 5 (1994)
[4] P. Szabo, T. Samuely, V. Hašková, J. Kačmarčík, M. Žemlička, M. Grajcar, J. G. Rodrigo, P. Samuely, Phys. Rev. B **93**, 014505 (2016)
[5] B. L. Altshuler, A. G. Aronov, Solid State Communications **30** (1979), 115
[6] B. L. Altshuler, A. G. Aronov, *Electron-Electron Interactions in Disordered Systems*, edited by A. L. Efros, M. Pollak, Elsevier Science Publishers, New York (1985)
[7] S. L. Sondhi, S. M. Girvin, J. P. Carini, D. Shahar, Rev. Mod. Phys. **69**, 315 (1997)
[8] N. A. Lewellyn, I. M. Percher, JJ Nelson, J. Garcia-Barriocanal, I. Volotsenko, A. Frydman, T. Vojta, A. M. Goldman, Phys. Rev. B **99**, 054515 (2019)
[9] Y. Liu, Z. Wang, P. Shan, Y. Tang, C. Liu, C. Chen, Y. Xing, Q. Wang, H. Liu, X. Lin, X. C. Xie, J. Wang, Nat. Comm. **10**, 3633 (2019)
[10] Y. Saito, T. Nojima, Y. Iwasa, Nat. Comm. **9**, 778 (2018)
[11] T. Vojta, J. Phys. A: Math. Gen. **39**, R143 (2006)
[12] A. F. Hebard, M. A. Paalanen, Phys. Rev. Lett. **65**, 927 (1990)
[13] A. Doron, I. Tamir, T. Levinson, F. Gorniaczyk, D. Shahar, Phys. Rev. B **98**, 184515 (2018)
[14] J. Kisker, H. Rieger, Phys. Rev. B **55**, R11981 (1997)
[15] M. C. Cha, S. M. Girvin, Phys. Rev. B **49**, 9794 (1994)

MAS ^{1}H NMR Study of Thermoplastic Corn Starch

[1]*Alojz ŠOLTÝS (4th year)*
Supervisor: [2]Jana TÓTHOVÁ

[1,2]Dept. of Physics, FEI TU of Košice, Slovak Republic

[1]alojz.soltys@tuke.sk, [2]jana.tothova@tuke.sk

***Abstract*— Thermoplastic starches (TPSs) are promising alternatives to conventional biodegradable polymers. Intra- and intermolecular interactions determine properties of TPS which tend to rapidly change over time due to structural relaxation as well as with rising temperature. This paper refers impact of glycerol and urea on thermoplastic corn starch using single-pulse (SP) magic angle spinning (MAS) ^{1}H NMR spectroscopy during ageing as well as temperature dependences of relaxed samples.**

***Keywords*— free water, glycerol, thermoplastic starch, urea**

I. Introduction

Native starch (NS) is a semicrystalline polysaccharide occurring in form of discrete granules made up of two major components. Linear amylose consisting primarily of α-1,4 linkages and highly branched amylopectin with branching points made up of α-1,6 linkages [1].

NS does not behave like a thermoplastic material due to strong inter- and intramolecular hydrogen bonds increasing melting point above temperature of thermic decomposition. In order to process NS as thermoplastic material, these strong hydrogen bonds between hydroxyl groups of starch molecules need to be broken which is done in the presence of plasticizer at a specific temperature and under shear stress in the process called gelatinization [2]. Homogenization of gelatinized starch results in thermoplastic starch (TPS).

Relatively fast structural relaxation of TPS over time, poor mechanical properties and high sensitivity to ambient humidity are the biggest drawbacks of TPSs [4]. Properties of TPS can be also determined by used plasticizer(s) and interactions between them as well as temperature relations of these interactions which is main aim of this paper.

II. Experimental

A. Samples

Native cornstarch Meritena® 100 produced by Brenntag, Slovakia was plasticized by urea and glycerol with a constant weight ratio between starch and plasticizer(s) (Tab. I).

Suspension of native starch, water and preset combination of plasticizers were stirred at the temperature of 70 °C in order to disrupt structure of NS and dried at 100 °C for 5 hours to remove the excess of water. Water in the suspension helps to disrupt starch granules as well as dissolve urea crystallites. TPS was then prepared by kneading of the starch gel in plastograph Barbender PLE 331 for 10 min. at 100 rpm and temperature of 130 °C in order to homogenize the mixture. Afterwards, TPS was pressed into plates at the pressure of 100 kPa and temperature 130 °C for 6 minutes. Samples were then stored in the PE bags in the dark place under the constant temperature of 22 °C.

TABLE I
WEIGHT FRACTIONS OF GLYCEROL AND UREA IN THE SAMPLES RELATIVE TO THE STARCH WEIGHT.

	Urea	Glycerol
U-TPS	0.7	0
UG-TPS	0.35	0.35
G-TPS	0	0.7

B. Nuclear magnetic resonance

The measurements were performed at temperatures varying from 30 to 140 °C on 400 MHz Varian Solid-State NMR spectrometer (VNMRS 400, Palo Alto, CA, USA) equipped with the wide bore magnet using 4 mm ZrO_2 rotors. The duration of ^{1}H π/2 pulse was 2.9 μs, the recycle delay of 10 s and acquisition times of 20 - 80 ms were applied. The chemical shifts were referenced to the TMS using adamantane as an external standard.

Spectral deconvolutions and calculations were done using the Varian VnmrJ 3.2 and Mestrelab Research Mnova 9.0 and OriginPro 8 software packages.

III. Results and Discussion

Fig. 1 shows MAS ^{1}H NMR spectra of U-TPS, G-TPS and UG-TPS measured one day and 52 weeks of storage at temperature of 30 °C. U-TPS spectra consist only of one asymmetrical peak representing superposition of hydrogen nuclei of urea and free water molecules. However, a noticeable broadening of this line over time was observed which can be associated with creating urea-water interactions via hydrogen bonds and so hindering their molecular motion.

Phase separation connected with formation of rigid urea-rich regions over time explains considerable decrease of signal intensity in U-TPS spectrum after 52 weeks of storage.

G-TPS and UG-TPS samples shows significantly better resolution and narrowing of the lines over time in contrast to U-TPS. 52 weeks after sample preparation we can distinguish peaks denoted to glycerol hydrogens directly bound to carbons (3.7 ppm), hydrogens associated to free water molecules (4.8 ppm), glycerol hydroxyl groups (5.3 ppm) and urea hydrogens in the case of UG-TPS (6.0 ppm).

Spectra of G-TPS and UG-TPS measured 1 day after sample preparation show only superposition of signals denoted to free water and glycerol hydroxyl groups as single

peak at 5.1 ppm. Increase of overall intensity of the spectra compared to the intensity of signal denoted to ^{1}H nuclei of glycerol directly bound to carbons is evidence of either water adsorption or phase separation of water molecules over time.

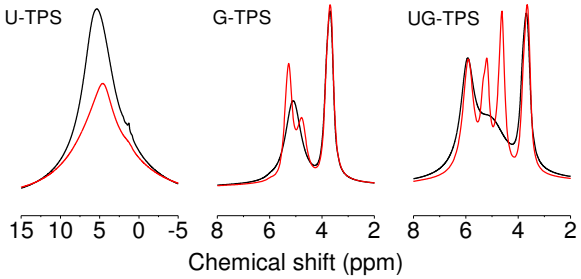

Fig. 1. MAS ^{1}H NMR spectra measured one day (black) and 52 week (red) at 30°C after sample preparation.

MAS ^{1}H NMR spectra measured after 52 weeks of storage did not shown any significant changes, indicating structure stabilization. Such samples were used for measuring temperature dependences of MAS ^{1}H NMR spectra shown in Fig. 2.

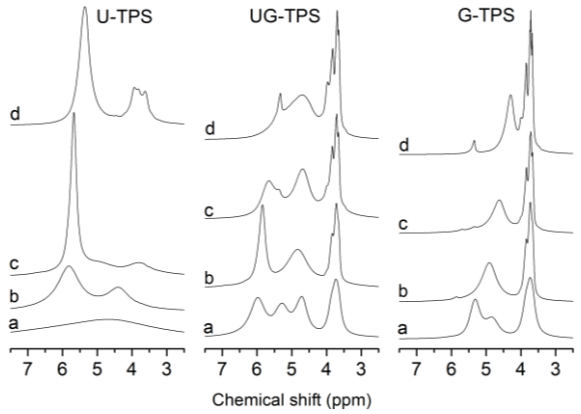

Fig. 2. MAS ^{1}H NMR spectra of U-TPS, G-TPS and UG-TPS measured after storage period of 52 weeks at 30 (a), 60 (b), 100 (c) and 140 °C (d).

Unresolved peak in U-TPS measured at 30 °C split into two peaks at 60 °C. Such rapid increase in resolution cannot be explained only by superposition of signals of water and urea but also by disruption of urea-water complexes. Further increase of temperature leads to position shift of the urea peak and decrease of intensity of the signal of free water due to evaporation. U-TPS spectrum measured at 100 °C shows signal in the region from 3.5 to 4.2 ppm associated with starch macromolecules with noticeable splitting in the spectrum measured at 140 °C.

G-TPS shows significant shift of the peak of hydroxyl groups with increasing temperature. Mentioned signal overlaps peak related to the water at 60 °C and due to evaporation we assume that at 100 and 140 °C only insignificant fraction of intensity belongs to hydrogens of water. Also splitting of the peak at in the region between 3.3 and 4.0 ppm is observed in spectra measured at 60 °C and above as well as a new peak at 5.3 ppm rose up at 140 °C.

UG-TPS spectra have same characteristics as G-TPS except of presence of urea signal, which at 140 °C become a part of asymmetrical signal of hydrogens of urea and hydroxyl groups of glycerol.

Liquid-state ^{1}H NMR spectroscopy of corn starch measured in DMSO-d_6 was published in the past [5-7]. Mobility of starch chains at room temperature is too low to get spectrum of sufficient resolution. However, molecular motion at 140 °C enables us to see some peaks of starch macromolecules as depicted in detail in the Fig. 3.

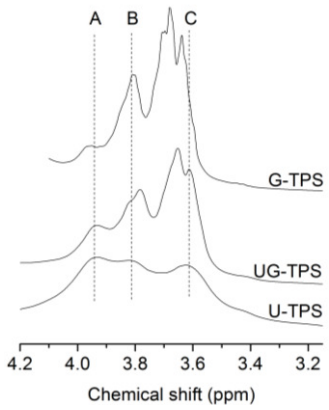

Fig. 3. MAS ^{1}H NMR spectra of U-TPS, G-TPS and UG-TPS measured at 140 °C in the range of 3.15 to 4.2 ppm. Capital letters A-C denote peaks related to the starch macromolecules.

In the spectra we can distinguish peaks at 3.93 and 3.82 ppm (A, B) associated with hydrogens bound to carbons 3, 5 and 6 and peak related to hydrogen bound to carbons 2 and 3 (C). Peaks are superimposed to glycerol signals in the case of G-TPS and UG-TPS which makes spectra more complicated but better resolved than in the U-TPS spectrum [8].

IV. Conclusion

Molecular mobility of urea molecules in U-TPS decrease over time due to formation urea-water complexes. Despite of urea molecules, presence of glycerol in TPS rapidly increases resolution of the spectra. In contrast to U-TPS, narrowing of peaks in G-TPS and UG-TPS was observed with increased storage time.

Rearrangement of urea molecules in U-TPS formed structures with highly restricted molecular motion after 52 weeks of storage.

Molecular mobility of TPS samples above 100 °C is sufficient to see peaks related to starch macromolecules in solid-state ^{1}H NMR spectroscopy.

References

[1] A. Carvalho, Monomers, Polymers and Composites from Renewable Resources, First Edition, Kidlington: Elsevier Ltd., 2008, pp. 321-343.
[2] Y. Zhang, C. Rempel, D. McLaren, Innovation in Food Packaging, Chapter 16, Thermoplastic Starch, 2014, pp. 391-408.
[3] A.-M. Nafchi, M. Moradpour,M. Saeidi,A.-K. Alias, Thermoplastic starches: Properties, challengies, and prospects, in Starch/Stärke, 2013, vol. 65, pp. 61-72.
[4] F. Xie et al, Thermoplastic Starch: Current Development and Future Trends. In: Journal of Renewable Materials 2, 2014, pp. 95 – 106.
[5] M.J. Tizzoti, M.C. Sweedman, D. Tang, Ch. Schaefer, R.G.Gilbert, New 1H NMR spectroscopy for the characterization of native and modified food-grade starches, J. Agric. Food Chem. 59, 2011, pp.6913-6919.
[6] H. Liu, R.Adhikari, Q. Guo, B. Adhikari, Preparation and characterization of glycerol plasticized (high-amylose) starch-chitosan films, J. Food Eng. 113, 2013, pp.588-597.
[7] Y. Li, S, Lin, J. Hu, G. Liu, G. Zhang, Y. Tu, H. Luo, W. Li, Metal ion induced assembly of amylose in aqueous solution, Carbohydr. Polym. 93, 2014, pp.184-189.
[8] A. Šoltýs, V. Hronský, N. Šmídová, D. Olčák, F. Ivanič, I. Chodák, Solid-state 1H and 13C NMR of corn starch plasticized with glycerol and urea, European Polymer Journal 117, 2019, pp. 19-27.

Mechanical properties of organic substrates for face down technology

[1]*Tomáš LENGER (3rd year)*
Supervisor: [2]Alena PIETRIKOVÁ

[1,2]Deptartment of Technologies in Electronics, FEI TU of Košice, Slovak Republic

[1]tomas.lenger@tuke.sk, [2]alena.pietrikova@tuke.sk

***Abstract*—This paper is a summarization of the last year of post gradual study. This paper is focused on lamination of multilayer PCBs. Substrate material with low T_g as well as substrate material with high T_g were used. Mechanical properties of such structures were tested as well. Mechanical testing was realized by 3-point bend test. 3-point bend test seems like the best testing method for evaluation of mechanical properties of multilayer PCBs.**

***Keywords*—embedded components, prepreg, multilayer PCBs,**

I. Introduction

Development of electronics is putting pressure on designers to place more electronic components on the small Printed Circuit Boards (PCBs). Miniaturization of PCBs based on the reducing trace width, isolation gaps, or the dimensions of components packages is reaching its physical limits. Embedding components into substrate opens the door to new opportunities in miniaturization of electronic devices. Embedded components may slightly increase the thickness of PCB but allow marked reduction of PCB area. Furthermore, embedded components can improve electrical properties or reliability of PCBs [1, 2, 3].

Electronic components can be embedded by many technological processes. Embedded components can be created as planar resistor or capacitors, electronic components in Surface Mount Device (SMD) package or even unpackaged chips. There are a few different technologies for embedding components which are using different technological steps [1, 3].

The face down technology is one of the technologies for components embedding. This technology is based on embedding components in SMD package into PCBs. Thickness of PCB depends on thickness of used SMD packages. Required thickness of PCB core can be achieved by implementing PCB laminate of required thickness or by many layers of prepreg [2, 3]. This paper is focused on analysing properties of multilayer PCBs with prepreg based core.

II. Lamination of Multilayer PCBs

This research was focused on mechanical properties of substrate material, which are used for lamination of multilayer PCBs. Laminate materials with low T_g and high T_g as well as prepreg materials with low T_g and high T_g were used for this research. Basic properties of this materials are in Table 1.

TABLE 1
Basic Properties of Used Materials [5, 6]

Type	Glass cloth style	Catalogue thickness of 1 layer (mm)	T_g (°C)	T_d (°C)
DE 104 (laminate)	2116	0.565	135	315
PCL370HR (laminate)	7626	0.565	180	340
DE 104 (prepreg)	2116	0.105	135	315
DE 104 (prepreg)	7626	0.197	135	315
PCL370HR (prepreg)	7626	0.172	180	340

Different conditions of lamination were also used. Lamination of multilayer prepreg materials were done by one step lamination as well as by two step lamination (Fig. 1). One step lamination was done by conditions given by manufacturer of prepreg materials. Two step lamination was divided into two lamination cycles. The first lamination cycle was done by temperature 70 °C and pressure 2 MPa and the second lamination cycle was done by conditions given by manufacturer of prepreg materials.

First step of the two step lamination creates solid structure of prepreg layers which can be manipulated or drilled. This structure allows realization of vias or holes for embedding of components. This approach has big potential for application in components embedding by face down technology.

Number of layers was chosen to achieve approximately the same thickness of embedded samples. Every prepreg material was laminated by one step lamination (samples marked as ”A”) as well as by two step lamination (samples marked as ”B”). Laminate materials and prepreg materials were also laminated to sandwich structures (samples marked as ”M”) which were laminated by two-step lamination (Table 2).

TABLE 2
Types of Samples Used in Experiment

Sample	Material	Layers	T_g (°C)	Thickness (mm)
L1	DE104 (laminate)	1	135	0.56
L2	PCL370HR (laminate)	1	135	0.56
1A	DE104 (prepreg 2116)	10	135	1.21
1B	DE104 (prepreg 2116)	5+5	135	1.16
2A	DE104 (prepreg 7626)	6	135	1.27
2B	DE104 (prepreg 7626)	3+3	135	1.22
3A	PCL370HR (prepreg 7626)	6	180	1.36
3B	PCL370HR (prepreg 7626)	3+3	180	1.32
M1	Combination of L1 and 1B	10+2	135	2.22
M2	Combination of L2 and 3B	6+2	180	2.44

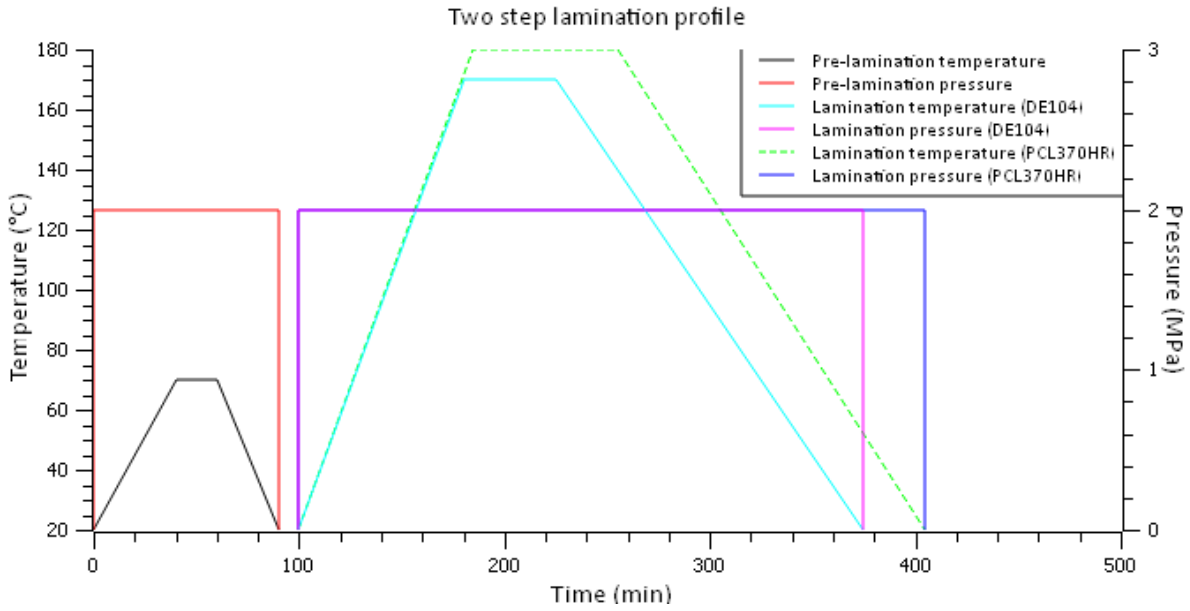

Fig. 1 Lamination profile

III. Mechanical Properties of Multilayer PCBs

Mechanical properties of laminated structures were analyzed by 3-point bend test (Fig. 2). 3-point bend test was realized by Testometric M250-2.5CT. Samples dimensions were 7 mm × 40 mm and thickness of samples varies based on sample type (Table 2). Samples were loaded by constant speed (0.4 mm/min) and applied force was measured.

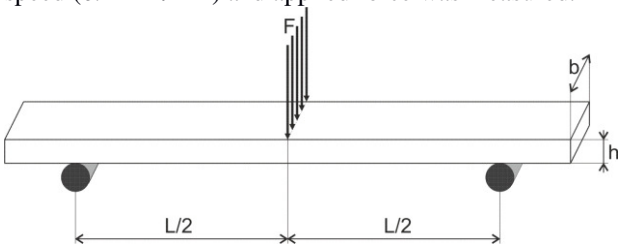

Fig. 2 3-point bend test

Mechanical properties of non-laminated substrates, laminated prepreg materials as well as combination of laminates and prepreg materials (sandwich structures) were analyzed. Mechanical properties were analyzed by flexural strength of samples. Flexural strength is given by [4]:

$$R_{max} = 3F_{max}L/2bh^2 \quad (1)$$

where F_{max} is maximum applied force, L is length between outside points of 3-point bend test b is sample width and h is sample thickness.

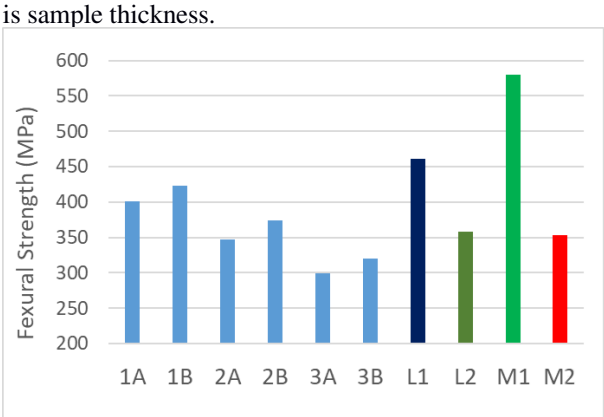

Fig. 3 Flexural strength of various substrate materials

Fig. 3 shows that flexural strength of prepreg materials laminated by two step lamination is even better than flexural strength of same prepreg materials laminated by one step lamination. Fig. 3 also shows that sample based on low T_g material with the thinnest prepreg layer has the best flexural strength of used prepreg materials. Sandwich structure based on low T_g materials has the biggest flexural strength of all used materials.

IV. Conclusion and Future Work

This research was focused on mechanical properties of multilayer PCBs. Mechanical properties were tested by 3-point bend test. This research shows that two step lamination did not have impact on mechanical properties of samples. Furthermore, the sandwich structure shows as promising structure for components embedding by face down technology.

Detailed analysis of mechanical properties of these structures based on organic substrates was accepted for publication in current content journal. Future work will be focused on application of this knowledges and embedding of components in SMD packages into sandwich structures with prepreg based core.

References

[1] Hyunho, K. “Device Embedded Substrate with Embedding Multi Passive Components for Camera Module.” In Pan Pacific Symposium 2015 Proceedings, Kauai, Hawaii, 2015. pp. 242-247. ISBN: 978-1-63439-931-9.

[2] Boettcher, L. et. Al. “Power Electronics Packages with Embedded Components - Recent Trends And Developments.” In SMTA International 2013 Proceedings, Fort Worth, Texas, USA, 2013. s. 337-342. ISBN: 978-1-62993-291-0.

[3] Manesiss, D. et al. “Embedding technologies for heterogeneous integration of components in PCBs-an innovative modularization approach with environmental impact” In 21st European Microelectronics and Packaging Conference and Exhibition, Warsaw, Poland, 2017.

[4] Zweben, C., W. S. Smith, and M. W. Wardle (1979), "Test methods for fibre tensile strength, composite flexural modulus, and properties of fabric-reinforced laminates", Composite Materials: Testing and Design (Fifth Conference), ASTM International.

[5] Isola Group, Isola DE104 Datasheet

[6] Isola Group, Isola PCL370HR Datasheet

Model-Based Augmentation in Semantic Segmentation

[1]*Miroslav JAŠČUR (3rd year),*
Supervisor: [2]*Marek BUNDZEL*

[1,2]Dept. of Cybernetics and Artificial intelligence, FEI TU of Košice, Slovak Republic

[1]miroslav.jascur@tuke.sk, [2]marek.bundzel@tuke.sk

***Abstract*—This article provides overview of the research work that the author conducted in last year. First, we identify the issues regarding semantic segmentation in biomedical imaging. Second, we review state-of-the-art in biomedical image segmentation and strategies that were developed to overcome limited, unlabeled datasets. Finally, we define and evaluate example experiment. Then we describe experiment on small synthesized dataset to verify our hypothesis that random augmentation is not he best tool to augment datasets. Our experiment support the hypothesis that model-based augmentation is a better tool than random augmentation.**

***Keywords*—Deep learning, fully convolutional networks, biomedical imaging, image segmentation, data augmentation.**

I. Introduction

Semantic segmentation is a crucial step in biomedical imaging tasks. While convolutional neural networks remain state-of-the-art solutions for various image processing tasks [1, 2, 3, 4, 5, 6], to achieve state-of-the-art accuracy, it is desirable that they be trained on labeled datasets that are real, varied, and large. While the creation of the aforementioned datasets is a priority, we usually train models with limited number of samples. Furthermore labeling these datasets require a significant amount of effort. Therefore, we identify these problems in biomedical segmentation regarding creation and labeling of datasets.

1) **Limited dataset** – In the medical domain datasets that are large enough to train deep models are rare. We often acquire only tens to hundreds of samples. Ideally, the number of samples would be magnitude higher.
2) **Unlabeled data** – Labeling requires significant expertise, time and money. Especially 3D volumes require advanced software tools to label them. While the number of official labeled datasets is growing, variety of unlabeled datasets are produced every day.
3) **Dataset consistency** – Another issue in biomedical imaging is inconsistency in image acquisition procedures across machines and institutions, which can produce wide variations in resolution, image noise, and tissue appearance [7].

A. State-of-the-art in biomedical image segmentation

Current strategies to overcome these problems in biomedical semantic segmentation have been proposed.

1) **Custom architectures** – A number of architectures are designed for biomedical segmentation: U-Net [8], 3D U-Net [9], V-Net [10]. These fully convolutional neural networks usually contain contractive and expansive layers that are connected at the same level of abstraction, which provides sufficient information flow for pixelwise predictions. This type of architecture provides a powerful building block for biomedical segmentation systems and is considered to be the standard approach to solve this task. Deeper architectures like DeepMedic [11], HighRes3DNet [12] outperform purely contractive-expansive architectures on specific tasks such as brain and lesion segmentation. They contain advanced building blocks of CNNs such as residual connection, atrous spatial pyramid pooling, and dilated/atrous convolution. Furthermore, they re-purpose pretrained convolutional layers originally developed for natural image segmentation. Biomedical segmentation puts attention on specific performance measures (sensitivity/specificity/overlapping regions). We can improve these performance metrics by employing non-traditional loss functions: weighted cross-entropy [8, 9], dice score [10, 13], sensitivity-specificity.
2) **Pre-processing and post-processing** – Semantic segmentation often requires data processing before and after CNN computes pixelwise prediction. Pre-processing steps are usually tied to specific imaging modality: intensity inhomogeneity minimization [14], feature extraction [15]. While the CNN family provides powerful segmentation framework for local pixel prediction, we employ a second, more global, post-processing technique that applies Conditional random field for final pixelwise prediction. The combination of CNN and CRF allows us to achieve state-of-the-art performance, while we train the ensemble either in end-to-end fashion [16, 17], or separately and we apply CRF as a post-processing method [1, 11, 18].
3) **Random and Model-based dataset augmentation** – Random augmentation of biomedical images increases the robustness and precision of the resulting classifier and allows us to to create large volumes of labeled data. Combinations of rotation, scaling, intensity value adjustment, injection of Gaussian noise, shear, and Gaussian blur are commonly used augmentation techniques in biomedical imaging [8, 19, 20]. We can synthesize new samples of data by applying a random coarse n-dimensional deformation field and calculate the new position of pixels through interpolation [9, 10]. While

random augmentation remains the main strategy for generating labeled examples, new model-based augmentation techniques are being developed [21, 22]. Models are usually based around CNNs that can learn spatial transform and then register unlabeled image into labeled image [23, 24].

II. Scientific goal from PhD thesis proposal

Idea: Design learning-based image registration architecture as generative augmentation model.

Hypothesis: Model-based augmentation surpasses random augmentation.

Learning-based registration outperforms classical registration in biomedical image segmentation.Different registration strategies are used, usually based around CNN with supervised or unsupervised learning. These architectures learn spatial and appearance transformation, therefore providing a valuable tool for generating realistic and variable training samples. This process allows us to extract parameters of spatial transformation, and subsequently, we sample and vary these transformations to create more training samples.

However, there is no single evaluation of these learning-based registration models as augmentation models. We propose to evaluate these models with metric, that will reflect capabilities of increasing quality of training dataset. A synthesized dataset can be used to train U-Net in a controlled setting and compare the performance of the classifier with different augmentation models. These model-based augmentations should outperform random ones.

Contribution: Verify if random augmentation is the best tool augment data for encoder-decoder CNNs.

III. Experimental setup

We trained encoder-decoder architecture with same topology (learning parameters) and hyper-parameters. The only varying factor was the augmentation process of the dataset. Topology of the network is vanilla U-net presented in [8]. The learning parameters of the network are optimized using stochastic gradient descent with momentum. Other parameters were initial learning - 0.001, learning rate was decreased to factor of 0.3 every 5 epochs, momentum - 0.9, minibatch size - 10. Training was stopped after 10 epochs, 500 iterations. We used synthetic dataset of generated triangles with added noise of 32x32 pixels for binary classification. This experiment is a proof-of-concept, that the methodology described in Section II is feasible. We used separate hold-out validation with 50/50 split between training and testing dataset.

IV. Experimental results

TABLE I
Comparison of different metrics of the U-Net with various augmentation methods on validation data

	GlobAcc	MeanAcc	MeanIoU	WeightIoU	MeanBF
No aug.	0.9754	0.9450	**0.8627**	0.9735	**0.6863**
Transl.	0.9697	0.9290	0.7713	0.9502	0.5813
Scaling	0.9709	0.9704	0.7878	0.9527	0.5615
Shearing	0.9740	0.9532	0.7977	0.9566	0.6222
Rotation	0.9792	0.9439	0.8233	0.9640	0.6423
Affin. t.	**0.9846**	**0.9730**	0.8598	**0.9875**	0.6564

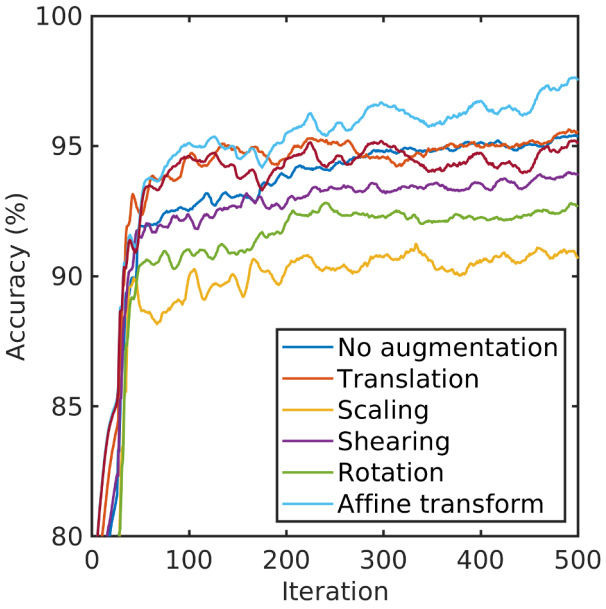

Fig. 1. Training accuracy over 500 iterations with different augmentation methods

In Tab. I we evaluate the performance of U-Net with 5 metrics. Global Accuracy (GlobalAcc) represents ratio of correctly classified pixels to total pixels, regardless of class. Mean Accuracy (MeanAcc) represents ratio of correctly classified pixels in each class to total pixels, averaged over all classes. Average intersection over union (MeanIoU) of all classes. Weighted intersection over union (WeightIoU) Average IoU of all classes, weighted by the number of pixels in the class. Average boundary F1 (MeanBF) score of all images.

U-Net trained on non-augmented data performs above all other augmentation methods in two metrics - average intersection over union and average boundary F1-score. However, our architecture using affine transform as augmentation method performed better in three metrics - global accuracy, average accuracy and weighted area over intersection. Therefore, modelling the transform of the target object in segmentation yielded better results than using random augmentation.

V. Future work

We propose to design learning-based image registration architecture and evaluate its possibilities as augmentation model. We can use these tools in two ways. We can either augment or label the dataset for pixel-wise segmentation CNN. Combination of generative augmentation and encoder-decoder architecture for few-shot segmentation is the final goal the PhD thesis. This deep hybrid model, which would combine an appearance/spatial transform model to create model-based augmentation and CNNs for local pixel segmentation, could be a state-of-the-art model for biomedical imaging

VI. Publications

During 2019, our research group submitted an article[25] in peer reviewed journal - Sensors with 5-year impact factor: 3.302 [26].

References

[1] L.-C. Chen, G. Papandreou, I. Kokkinos, K. Murphy, and A. L. Yuille, "Deeplab: Semantic image segmentation with deep convolutional nets, atrous convolution, and fully connected crfs," *IEEE transactions on pattern analysis and machine intelligence*, vol. 40, no. 4, pp. 834–848, 2018.

[2] J. Long, E. Shelhamer, and T. Darrell, "Fully convolutional networks for semantic segmentation," in *Proceedings of the IEEE conference on computer vision and pattern recognition*, 2015, pp. 3431–3440.

[3] A. Krizhevsky, I. Sutskever, and G. E. Hinton, "Imagenet classification with deep convolutional neural networks," in *Advances in neural information processing systems*, 2012, pp. 1097–1105.

[4] K. Simonyan and A. Zisserman, "Very deep convolutional networks for large-scale image recognition," *arXiv preprint arXiv:1409.1556*, 2014.

[5] S. Ren, K. He, R. Girshick, and J. Sun, "Faster r-cnn: Towards real-time object detection with region proposal networks," in *Advances in neural information processing systems*, 2015, pp. 91–99.

[6] J. Redmon, S. Divvala, R. Girshick, and A. Farhadi, "You only look once: Unified, real-time object detection," in *Proceedings of the IEEE conference on computer vision and pattern recognition*, 2016, pp. 779–788.

[7] K. K. Leung, M. J. Clarkson, J. W. Bartlett, S. Clegg, C. R. Jack Jr, M. W. Weiner, N. C. Fox, S. Ourselin, A. D. N. Initiative *et al.*, "Robust atrophy rate measurement in alzheimer's disease using multi-site serial mri: tissue-specific intensity normalization and parameter selection," *Neuroimage*, vol. 50, no. 2, pp. 516–523, 2010.

[8] O. Ronneberger, P. Fischer, and T. Brox, "U-net: Convolutional networks for biomedical image segmentation," in *International Conference on Medical image computing and computer-assisted intervention*. Springer, 2015, pp. 234–241.

[9] Ö. Çiçek, A. Abdulkadir, S. S. Lienkamp, T. Brox, and O. Ronneberger, "3d u-net: learning dense volumetric segmentation from sparse annotation," in *International conference on medical image computing and computer-assisted intervention*. Springer, 2016, pp. 424–432.

[10] F. Milletari, N. Navab, and S.-A. Ahmadi, "V-net: Fully convolutional neural networks for volumetric medical image segmentation," in *2016 Fourth International Conference on 3D Vision (3DV)*. IEEE, 2016, pp. 565–571.

[11] K. Kamnitsas, C. Ledig, V. F. Newcombe, J. P. Simpson, A. D. Kane, D. K. Menon, D. Rueckert, and B. Glocker, "Efficient multi-scale 3d cnn with fully connected crf for accurate brain lesion segmentation," *Medical image analysis*, vol. 36, pp. 61–78, 2017.

[12] W. Li, G. Wang, L. Fidon, S. Ourselin, M. J. Cardoso, and T. Vercauteren, "On the compactness, efficiency, and representation of 3d convolutional networks: brain parcellation as a pretext task," in *International Conference on Information Processing in Medical Imaging*. Springer, 2017, pp. 348–360.

[13] M. Drozdzal, E. Vorontsov, G. Chartrand, S. Kadoury, and C. Pal, "The importance of skip connections in biomedical image segmentation," in *Deep Learning and Data Labeling for Medical Applications*. Springer, 2016, pp. 179–187.

[14] P. Moeskops, M. A. Viergever, A. M. Mendrik, L. S. de Vries, M. J. Benders, and I. Išgum, "Automatic segmentation of mr brain images with a convolutional neural network," *IEEE transactions on medical imaging*, vol. 35, no. 5, pp. 1252–1261, 2016.

[15] A. Oliveira, S. Pereira, and C. A. Silva, "Retinal vessel segmentation based on fully convolutional neural networks," *Expert Systems with Applications*, vol. 112, pp. 229–242, 2018.

[16] A. G. Schwing and R. Urtasun, "Fully connected deep structured networks," *arXiv preprint arXiv:1503.02351*, 2015.

[17] S. Zheng, S. Jayasumana, B. Romera-Paredes, V. Vineet, Z. Su, D. Du, C. Huang, and P. H. Torr, "Conditional random fields as recurrent neural networks," in *Proceedings of the IEEE international conference on computer vision*, 2015, pp. 1529–1537.

[18] G. Lin, C. Shen, A. Van Den Hengel, and I. Reid, "Efficient piecewise training of deep structured models for semantic segmentation," in *Proceedings of the IEEE Conference on Computer Vision and Pattern Recognition*, 2016, pp. 3194–3203.

[19] Z. Hussain, F. Gimenez, D. Yi, and D. Rubin, "Differential data augmentation techniques for medical imaging classification tasks," in *AMIA Annual Symposium Proceedings*, vol. 2017. American Medical Informatics Association, 2017, p. 979.

[20] H. R. Roth, L. Lu, A. Farag, H.-C. Shin, J. Liu, E. B. Turkbey, and R. M. Summers, "Deeporgan: Multi-level deep convolutional networks for automated pancreas segmentation," in *International conference on medical image computing and computer-assisted intervention*. Springer, 2015, pp. 556–564.

[21] H. Uzunova, M. Wilms, H. Handels, and J. Ehrhardt, "Training cnns for image registration from few samples with model-based data augmentation," in *International Conference on Medical Image Computing and Computer-Assisted Intervention*. Springer, 2017, pp. 223–231.

[22] A. Zhao, G. Balakrishnan, F. Durand, J. V. Guttag, and A. V. Dalca, "Data augmentation using learned transforms for one-shot medical image segmentation," *arXiv preprint arXiv:1902.09383*, 2019.

[23] G. Balakrishnan, A. Zhao, M. R. Sabuncu, J. Guttag, and A. V. Dalca, "An unsupervised learning model for deformable medical image registration," in *Proceedings of the IEEE conference on computer vision and pattern recognition*, 2018, pp. 9252–9260.

[24] P. Weinzaepfel, J. Revaud, Z. Harchaoui, and C. Schmid, "Deepflow: Large displacement optical flow with deep matching," in *Proceedings of the IEEE International Conference on Computer Vision*, 2013, pp. 1385–1392.

[25] N. Ferenčík, M. Jaščur, M. Bundzel, and F. Cavallo, "The rehapiano—detecting, measuring, and analyzing action tremor using strain gauges," *Sensors*, vol. 20, no. 3, p. 663, 2020.

[26] "Sensors | an open access journal from mdpi," https://www.mdpi.com/journal/sensors, (Accessed on 02/11/2020).

Modeling and Control for Walking Robots Using Hybrid Systems

[1]*Lukáš KOSKA (3rd year),*
Supervisor: [2]*Anna JADLOVSKÁ*

[1,2]Dept. of Cybernetics and Artificial Intelligence, FFEI TU of Košice, Slovak Republic

[1]lukas.koska@tuke.sk, [2]anna.jadlovska@tuke.sk

***Abstract*—This paper presents the research work and results which were gained over the last year in the field of modeling and control of hybrid walking systems. Various model configurations have been designed as part of the modeling process, based on the simplest compass gait model. In the field of control, the process of generation and tracking of trajectories was verified for a benchmark underactuated system. The theory of hybrid systems was used to solve research tasks within the experiment ALICE in CERN.**

***Keywords*—hybrid systems, walking models, trajectory generation, detector-control system**

I. Introduction

Human walking stands above all of the other forms of biped locomotion due to the fact that during a major part of the step, the moving body does not occur in the static equilibrium position [1]. For this reason, biped locomotion is one of the most sophisticated forms of movement. One of the most important reasons for studying human locomotion is its effectiveness [2]. The movement of the robot's legs, while passive walking on the inclined plane, is controlled by its own dynamics, powered by the gravitational acceleration [3]. The aim of the control of underactuated walking is to utilize the natural dynamics of the robot, because the control is more efficient and requires less power to the system than the control which tracks the reference trajectory in the fully-actuated system [4]. This paper describes the results obtained in the field of modeling and control of the walking robots during last year.

II. Previous analysis and achieved results

While modeling of walking as such, it is necessary to consider not only the continuous dynamics of the legs but also the discrete events that occur when swing leg impacts the ground. For this reason, it is the most useful to use the concept of the hybrid systems that combine the continuous and discrete dynamics of the model [5].

In the modeling of walking, each discrete state x_d is described by its own continuous dynamics $\boldsymbol{f}_{x_d}(\boldsymbol{x}, u, x_d, u_d, t)$. Lagrange equations are standardly used for deriving the non-linear differential motion equations describing each state. The dynamics of each state can next be expressed using the standard minimal form [6]:

$$\begin{aligned}\boldsymbol{M}(\boldsymbol{\theta}(t))\ddot{\boldsymbol{\theta}}(t) + \boldsymbol{N}(\dot{\boldsymbol{\theta}}(t), \boldsymbol{\theta}(t))\dot{\boldsymbol{\theta}}(t) + \\ + \boldsymbol{P}(\boldsymbol{\theta}(t)) = \boldsymbol{V}(t)\boldsymbol{u}(t)\end{aligned} \quad (1)$$

where $\boldsymbol{\theta}(t)$ represents a vector of generalized coordinates from which it is possible to create a continuous state-space vector as follows: $\boldsymbol{x}(t) = [\boldsymbol{\theta}(t)\, \dot{\boldsymbol{\theta}}(t)]$.

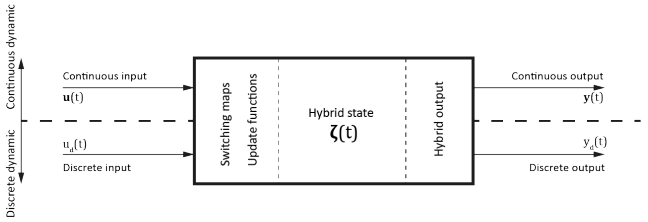

Figure 1. Description of the interaction between continuous and discrete part of the hybrid system [7]

The discrete dynamics is defined by the existence of events specified by the extended hybrid state vector $\boldsymbol{\zeta}(t) = (\boldsymbol{x}(t), \boldsymbol{u}(t), x_d(t), u_d(t))$, where $u(t)$ is a continuous input, $x_d(t)$ discrete state vector and $u_d(t)$ discrete input. The interaction between continuous and discrete part of the hybrid system is shown in Fig. 1.

Several control methods have been developed to be used in control the biped locomotion, most of them use a feedforward control structure, e.g. combining the boundary value problem and optimal control to generate and then track the desired trajectory [6].

Simple benchmark underactuated systems such as cart and pole and acrobot serve to verify control methods for under-actuated robotic walking [8]. A crucial feature that arises in the planned motion of the underactuated robotic walk is periodicity, since the steps are periodically repeated [6][9] .

III. Solved Tasks

This part of the paper summarizes the author's results obtained during last year. **The Compass Gait Model - (CG)**, shown in Fig. 2 represents the basic walking model, which is unactuated and walks down a plane inclined by the angle α. The angle $\theta_{NS}(t)$ in Fig. 2 represents the swing (non-stance) leg and angle $\theta_S(t)$ represents the stance leg. This basic model was extensively studied by Goswami et. al. [2].

The dynamics of the swing and stance legs can be derived using Lagrange equations. The discrete dynamics of the CG model includes only one situation when the swing leg falls on the ground. If the collision condition $s(\boldsymbol{\theta}) : \theta_{NS}(t) + \theta_S(t) + 2\alpha = 0$ is fulfilled, the swing leg becomes stance and stance leg becomes swing leg [11]. Using MATLAB's Symbolic Math

Figure 2. Model of the Compass Gait [10]

Toolbox and Stateflow, we derived and implemented the model of the compass gait system and its derivatives which include knees, feet and torso.

The control law for the bipedal robots can be generated using partial feedback linearization (PFL) method, if the underactuated system is considered. The principle of partial feedback linearization is to add such feedback that ensures that the system behaves like a linear system.

When using PFL principle as a control method, it is necessary to know the reference trajectories. For example, reference trajectories can be obtained by using a model of the passive walk on an inclined plane [10]. The task of PFL method is to control the walking of the robot, not only on the inclined plane, but also on the flat plane ($\alpha = 0$). Linearizing feedback allows to specify the control law in the form:

$$\ddot{\theta}_{NS}(t) = \ddot{\theta}^*_{NS}(t) + K_1(\theta^*_{NS}(t) - \theta_{NS}(t)) + \\ + K_2(\dot{\theta}^*_{NS}(t) - \dot{\theta}_{NS}(t)) \quad (2)$$

In a formula (2), $\ddot{\theta}^*_{NS}(t)$, $\dot{\theta}^*_{NS}(t)$ and $\theta^*_{NS}(t)$ represents the reference acceleration, angular velocity and angle of the swing leg. The control law (2) for an underactuated robotic walking contains two free parameters, K_1 and K_2. These parameters must be set according to the physical parameters of the robot and the reference trajectories. We are currently verifying various approaches how to find these parameters, including one based on evolutionary algorithm.

Since the underactuated walking robots are the part of the more complicated systems, it is preferable to verify the motion planning and control methods firstly on a suitable benchmark underactuated systems such as cart and pole [12]. When using the two-point boundary problem, it is necessary to modify the model of the cart and pole system. The modification consists of replacement the cart with the linear aproximation of the LSM. After the modification, it is possible to use the solution of the two-point boundary problem for the design of the trajectories from the lower stable to the upper unstable equilibrium position of the pendulum, which is dealt with in our most significant paper to date, *Inverted Pendulum With Linear Synchronous Motor Swing Up Using Boundary Value Problem* [6], published in the Acta Polytechnica.

IV. Activities in CERN

The author's research group (Center of Modern Control Techniques and Industrial Informatics) participates in the research project *ALICE experiment at the CERN LHC: The study of strongly interacting matter under extreme conditions* [13], which involves every member of the group. As part of his research activities in CERN, the author attended two business trips over the last year. During these business trips, a framework was designed to create applications in WinCC OA which communicate within the Alfred architecture to control the ALICE's detectors.

V. Future research steps and Conclusion

This article summarizes the author's research activity over the last year. Control of underactuated walking systems is a challenging programming task. For this reason, it will be the subject of further author's research and a subsequent part of his PhD thesis. The parallel aim of the thesis is to design the methodology of generating mathematical models of hybrid walking systems with different configurations which will enable the verification of designed control methods using suitable control structures.

Further research activities of the author will be focused on the design of the intermediate level communication of the *Detector Control System* for ITS subdetector within experiment ALICE in the CERN using a model workplace within the DCAI FEEI TU (http://alice-cern.fei.tuke.sk/).

Acknowledgment

This work has been supported by grant KEGA Implementation of research results in the area of modeling and simulation of cyber-physical systems into the teaching process - development of modern university textbooks – 072TUKE-4/2018 (100%).

References

[1] A. Goswami, B. Thuilot, and B. Espiau, "Compass-like biped robot part i: Stability and bifurcation of passive gaits," Ph.D. dissertation, INRIA, 1996.

[2] A. Goswami, B. Espiau, and A. Keramane, "Limit cycles in a passive compass gait biped and passivity-mimicking control laws," *Autonomous Robots*, vol. 4, no. 3, pp. 273–286, 1997.

[3] L. Koska, "A survey of approaches for modeling and control of effective walking robots," in *SCYR 2018*. TU, 2018, pp. 16–19.

[4] Y. Liu and H. Yu, "A survey of underactuated mechanical systems," vol. 7, no. 7, p. 921–935, 2013.

[5] T. McGeer *et al.*, "Passive dynamic walking," *I. J. Robotic Res.*, vol. 9, no. 2, pp. 62–82, 1990.

[6] L. Koska, S. Jadlovská, D. Vošček, and A. Jadlovská, "Inverted pendulum with linear synchronous motor swing up using boundary value problem," *Acta Polytechnica*, vol. 59, no. 5, pp. 458–466, 2019.

[7] M. Sobotka, "Hybrid dynamical system methods for legged robot locomotion with variable ground contact," Ph.D. dissertation, Technische Universität München, 2007.

[8] S. Jadlovská, L. Koska, and M. Kentoš, "Matlab-based tools for modelling and control of underactuated mechanical systems," *Transactions on Electrical Engineering*, vol. 6, no. 3, 2017.

[9] L. Tedrake, Russel, *Underactuated Robotics: Learning, Planning, and Control for Efficient and Agile Machines*, 2009.

[10] L. Koska, "Contribution to modeling and control for walking robots using hybrid systems," in *SCYR 2019*. TU, 2019, pp. 58–59.

[11] ——, "Modeling, analysis and simulation of the hybrid models of the walking robots," Ph.D. dissertation, Technical University of Košice, 3 2019, dissertation prospectus.

[12] A. Jadlovská, S. Jadlovská, and D. Vošček, "Cyber-physical system implementation into the distributed control system," *IFAC-PapersOnLine*, vol. 49, no. 25, pp. 31–36, 2016.

[13] P. Chochula, L. Jirden, A. Augustinus, G. De Cataldo, C. Torcato, P. Rosinsky, L. Wallet, M. Boccioli, and L. Cardoso, "The alice detector control system," *IEEE Transactions on Nuclear Science*, vol. 57, no. 2, pp. 472–478, 2010.

Modelling and Controlling of Small Hydropower Plants

[1]*Richard OLEXA (1st year)*
Supervisor: [2]Pavol FEDOR

[1,2]Dept. of Electrical Engineering and Mechatronics, FEI Technical University of Košice, Slovak Republic

[1]richard.olexa@tuke.sk, [2]pavol.fedor@tuke.sk

***Abstract* - Research, optimization and practical implementation of a Small Hydropower Plants as a source of clean electricity are one of the actual tasks in the current energetics, which is virtually impossible to solve without powerful computer support due to the strongly nonlinear nature of such systems. The article presents an overview of the most common simulation model schemes of Small Hydropower Plants, whereas explores the sub models of its individual subsystems.**

***Keywords*—Hydraulic turbines, hydropower systems, modelling and controlling hydropower plants, small hydropower plant.**

I. Introduction

Nowadays, it is often heard about the need for recycling and greater environmental protection. However, not only the activists are the ones who speak about this topic, even ordinary people started to pay attention to the polluted air and nature, and therefore being environmental friendly becomes one of the biggest concerns for scientists, researcher, and even for politicians.

The impact of current situation is for example very strong in the automotive industry. More and more electric cars are being produced, bought and moreover, there are already some restrictions for combustion engines vehicles in terms of entering centers of big cities.

As a result of the above-described situation, the car producers have already started transferring their financial resources to the research and development of electric cars. However, did we realize how the "green" electricity is being produced? Fossil fuels are still commonly used to produce electricity, thus we should search for another, more ecofriendly source of energy to replace the old coal power plants.

Because of it, this paper explores the current knowledge in using one of the renewable energy sources – water. Next parts of this paper are dedicated to the brief description of a technology used in hydropower plants, esp. in small hydropower plants (SHP), which potential in Slovakia is still not fully used, plus we introduce some modelling techniques of individual parts of SHP to provide the sufficient simulation model of SHP for our follow-up research in the field of controlling SHP using a universal control scheme.

II. Types of hydropower plants

According to the literature [2],[3],[12], there are many of criteria used to divide the hydropower plants, i.e. according to hydroelectric scheme; amount of generated power; type of the generator; type of the hydraulic turbine; etc. The first two before-mentioned criteria are important in defining and differentiation of small hydropower plants.

A. Hydroelectric scheme – Reservoir Hydropower Plants

The main characteristic of Reservoir Hydropower Plants is a reservoir located in an upland or mountainous area. Usually, the reservoir store a large amount of water and keeps its potential energy available to use throughout the year. Such a construction is used for various purposes, i.e. keeping the grid requirements; controlling the grid frequency; flood protection.

So called Pumped Storage Hydropower Station (PSHS) is one of special forms of this hydroelectric scheme. As a name suggest, the PSHS is able to pump the water between its two reservoirs placed at significantly different vertical levels. Thereby, the PSHS gives the option to keep the grid requirements when needed; e.g. during the peak load, the water is released from the upper reservoir so that the hydropower plant generates the power and contributes to the grid; and on the other hand, at the times of low demand, the water is drawn back from the lower reservoir to the upper one by motors/pumps using the electricity from the grid. It means that PSHS operates on a closed cycle. This way of operation could seem to be inefficient and unprofitable. However, the price difference between the peak load and low demand periods of time makes a price return despite the inefficiency involved. [3]

B. Hydroelectric scheme – Run-of-River Hydropower plants

As the name suggest, the Run-of-River Hydropower Plants (RRHP) are located at rivers, or at the surroundings of rivers. By this type of hydroelectric scheme, there are another two sub-categories; i.e. Pure RRHP and Hybrid RRHP.

The pure ones are characterized by not having any pond as a kind of a small reservoir and hence by using the running water to power the hydraulic turbine directly. Hernandez et.al. [3] term this as a *hydrokinetic power*, which means that the pure RRHP are totally dependent on instantaneous state of the river flow.

On the other side, the hybrid scheme includes a small pond smoothing the short-term flow variation at the turbine. It even

gives the operator an option to increase the amount of power generated during the peak demand time periods of the day.

In some cases, the penstock can be used to enable the pond to be placed at the higher vertical level, and thus to increase the available head. [2],[3]

C. Amount of Power Generated

The exact generated power P_G ranges for each of the following group of the hydropower plants can vary depending on the literature, and therefore combining the sources [2],[3],[14], the list below explores one of the most common definition in terms of the amount of generated power P_G.

1. Micro-Hydropower Plants – P_G up to 100kW
2. Small-Hydropower Plants – with a unit rating P_G between 100kW to 5GW
3. Big Scale Hydropower plants – P_G over 5GW [13]

Assuming all the before-stated criteria and differentiations, this article aims to explore a modelling process of a small scale hydropower plants of the run-of-river hydroelectric scheme with unit rating $P_G = 100kW – 5GW$.

III. Simulation Model of a Small Hydropower Plant

In general, the simulation model of a small hydropower plant (SHP) consists of five main sub-systems, i.e. the *Governor* – representing a turbine control system; the *Servodrive*, that serves as an actuator to regulate the flow of the water throughout the hydraulic turbine via controlling the valves, or guide vanes according to the *Governor* output signal; the simulation model of a *Hydraulic Turbine* – representing the process of conversion of the energy; as well as a block for the *Electric Generator* and another one for the *Grid*. In *Figure 1*, there are all the previous-stated main sub-systems depicted, creating the basic simulation model of SHP.

The vast majority of the scientific papers and literature use a model, wherein all the parameters are being normalized, i.e. their value is between 0 and 1, or in other words between 0 and 100%.

The phenomenon of the water hammer, cavitation and traveling waves are deeply explored in literature [3],[12], while including even the way how to simulate and model their impact on the functionality of hydropower stations and how to reduce it. On the other hand, in case of the SHP, where the length of the penstock, and the height of the water head available are small, the impact of these phenomenon can be neglected.

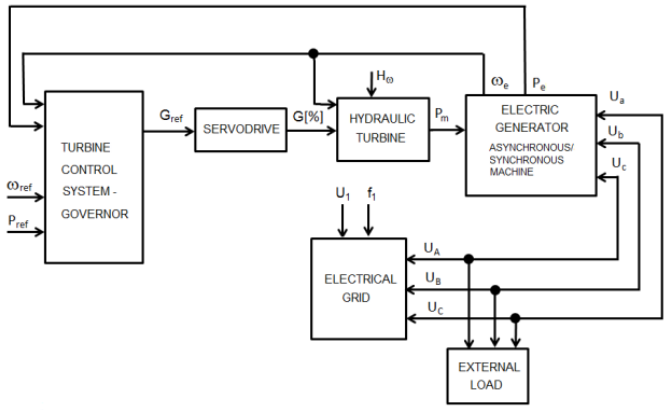

Figure 1 Block diagram of a Small Hydropower Plant [13]

A. Governor – Turbine Control System

Basically, the *Governor*, or the *Turbine Control System* has two main functions, i.e. running up the turbine and reaching the mechanical speed close to the grid frequency considering the number of poles of the electric generator; and after being phased into the grid, i.e. after the synchronization, the Governor controls the power supplied by hydropower plant to the grid.

Usually, PID or PI controllers are being used for controlling such a nonlinear and complex system of hydropower plants. In *Figure 2*, there is block diagram of a PID governor system for controlling the power and the frequency of a controlled hydropower station, where the included variables are: K_P - a proportional gain; K_I – an integral gain; K_D – derivative gain; and α – a permanent droop, that serves to boost the input signal of the controller coming from a power controlling part of the scheme. The function of saturations placed in the *Figure 2* is mainly to give the model of a PID controller an option to keep the output value in the preset range during the operation, and to act as a basic alternative of an anti-reset windup (ARW) protection.

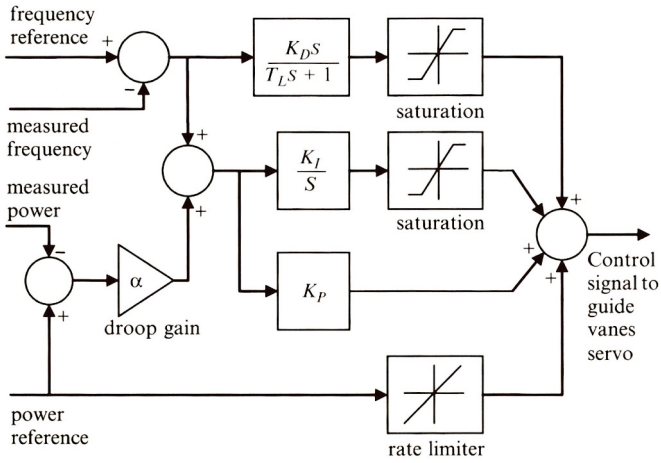

Figure 2 Block diagram of a PID governor for controlling power and frequency [3]

B. Servodrive

The sub-model of the *Servodrive* is often modelled as a second order dynamic system, which state variables are the speed of the guide vane opening and its position. The before-mentioned phenomenon of water hammer and cavitation occurs even in some cases of SHP, esp. when there is a fast change in the position of the servodrive. Therefore, the saturation block is being placed in the simulation model to limit the speed of the servodrive (see *Figure 3*), and thus to ensure the safe operation. Another saturation block is used to set the operation range of the guide vane's position to keep the turbine operating in the most efficient and safest way.

In *Figure 3*, we present our sub-system of the Servodrive, while demonstrating the results obtained via the simulation using Matlab-Simulink software in *Figure 4*.

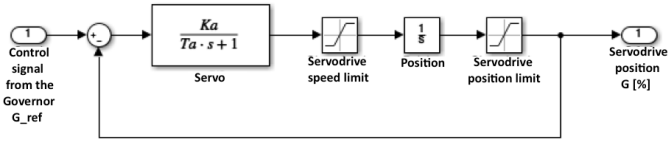

Figure 3 Block diagram of the Servodrive subsystem (parameters Ka and Ta are calculated according to the type of servodrive used in the hydroelectric scheme)

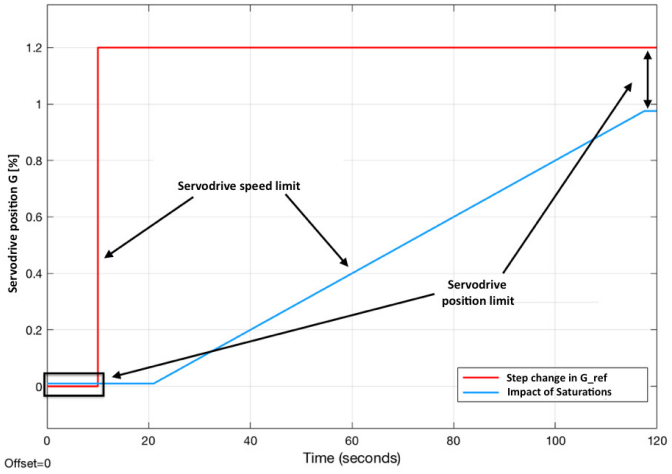

Figure 4 Servodrive position as a reaction to the step change in G_ref = 1.2 at the time t = 10s (Speed limit saturation = 0.01 in both directions; Servodrive position limit saturation = 0.01(lower one) and 0.975(upper one); Ka = 3.33 and Ta = 0.07s)

C. Hydraulic Turbine

The *Hydraulic Turbine* is considered as a heart of the hydropower plant and it is mostly because of its important function in the whole process of electrical energy production, and therefore its accurate model is necessary to achieve realistic and relevant results. The turbine converts a kinetic, or potential energy of the water into a mechanical rotation, that moves the generator's rotor via the common shaft.

For modelling purposes, the proposed subsystem of *Hydraulic Turbine* (see *Figure 5*) does not differ according to the type of the hydraulic turbines. However, the turbine characteristics, or in other words incorporating its efficiency into a model is one of the most important part in proper modelling of the turbine as a part of SHP.

The eq. *(1)* characterize the relation of the actual flow of the water q and other input parameters, i.e. h - a current *water head*; h_l – head losses that are usually neglected in SHP modelling; and so called *Water Time Constant*, which calculation is described by the eq. *(2)*.

$$\frac{dq}{dt} = \frac{(1-h-h_l)}{T_w} \qquad (1)$$

$$T_w = \left(\frac{L}{A}\right)\frac{q_{base}}{h_{base}g} \qquad (2)$$

where: L – the penstock length; A – penstock cross-sectional area; g – gravitational acceleration; h_{base} – the total static head available; and q_{base} – the water flow in case of $G = 1$ (eq. *(3)*).

$$q = G\sqrt{h} \quad \text{, i.e.: } q_{base} = 1\sqrt{h_{base}} \qquad (3)$$

One of the basic ways how to model turbine's efficiency is to use so called variable of *no load flow* q_{nl}, which is considered as a parameter characterizing the constant power losses. The eq. *(4)* describes the relation between the variables.

$$P_m = A_t h(q - q_{nl}) - DG\Delta\omega \qquad (4)$$

where: P_m is mechanical power at the shaft; q represents an actual flow throughout the turbine; D is considered as a *Damping coefficient*; G is the above-mentioned *Guide Vane Opening Position [%]*; and $\Delta\omega$ represents the *speed deviation*. [1],[11]

IEEE Working Committee considers the parameter A_t as a some kind of *Hydraulic Turbine's Gain*, which calculation differs in the scientific papers. The eq. *(5)* serves to calculate the A_t parameter according to the paper [1].

$$A_t = \frac{TURBINE\ POWER\ [MW]}{(GENERATOR\_POWER\ [MVA].h_r(q_r - q_{nl}))} \qquad (5)$$

where the h_r is the rated head needed for the rated flow q_r.

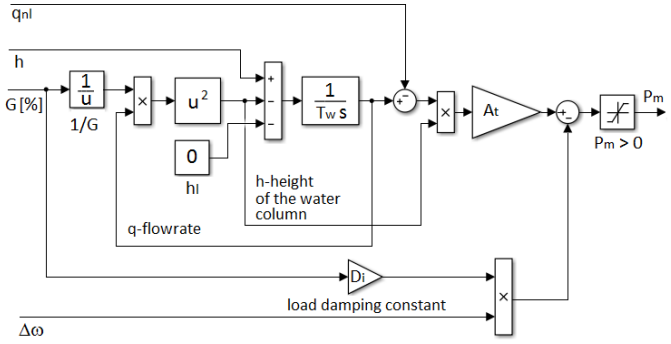

Figure 5 Block diagram of a Hydraulic Turbine Subsystem

Another way how to take into account the turbine efficiency is to calculate its concrete value. Acakpovi; Hagan and Fifatin explore this topic in detail in their scientific paper of *Review of Hydropower Plant Models* [9].

Fuzzy model of Hydraulic Turbine's efficiency

All the previous-mentioned ways of calculating the turbine's efficiency are based on a quite complicated and not always accurate calculations, mainly because of the need of detailed parameters knowledge, or only estimated parameter's values.

The next steps in our research in the field of Modelling a Small Hydropower Plants are and will be in considering other possibilities in terms of universal, but still accurate and fast efficiency calculation. In *Figure 6* and *7* respectively, there is an obvious difference in the maximum possible efficiency of the turbine, caused only by the wearing of the turbine's blades, or its runner, and thus by the change in the blades inner area A_{blades}, which is one of the key values in the calculation defined by [9].

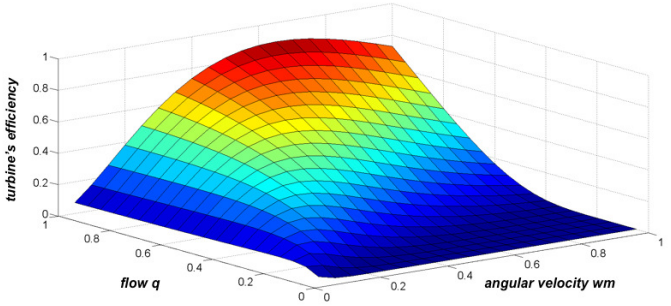

Figure 6 The efficiency of the hydraulic turbine (R_{blades} = 1.9m and A_{blades} = 9m²)

Therefore, so called efficiency "image" of the hydraulic turbine is possible to reach via measuring the water flow q; turbine's mechanical speed $\Delta\omega$ and the turbine's efficiency at the steady state operation points. Thus, such a data could be used in finding a fuzzy inference structure (FIS) of the modelled efficiency describing the measured relations between $[w_m, q] \rightarrow ht$.

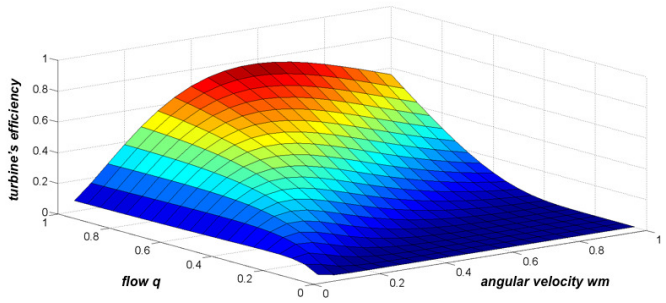

Figure 7 The efficiency of the hydraulic turbine (R_{blades} = 1.9m and A_{blades} = 8m^2)

Based on the database of the before-mentioned measures, a design of a fuzzy model can be done via a standard cluster analysis tools with adaptive approaches resulting in an improved quality of the model and in a reduced development time. One of the basic characteristic of the cluster analysis is the reduction of the number of fuzzy rules, as well as a proper initial setting of a rules parameters.

Using the *Anfisedit* tool included in the *Matlab* software, *Figure 9* shows how parameters obtained from a static fuzzy system could look like, and plus, *Figure 8* depicts the obtained static *Sugeno* type fuzzy system with twelve rules.

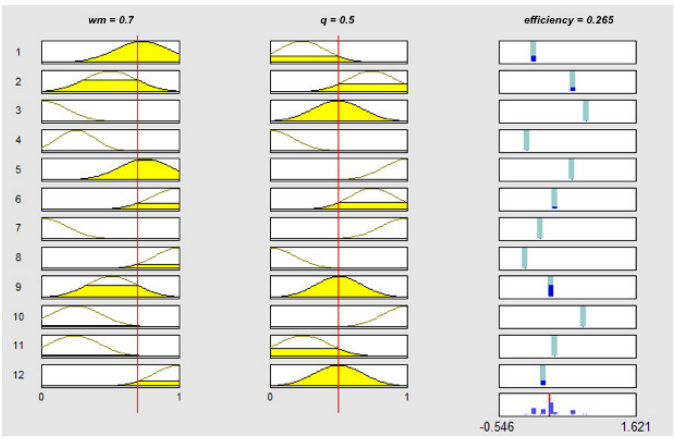

Figure 8 Hydraulic Turbine's Efficiency Fuzzy Model: Sugeno type (12 rules)
(Range of Influence = 0.5; Squash Factor = 1.1; Accept Ratio = 0.45; Reject Ratio = 0.005)

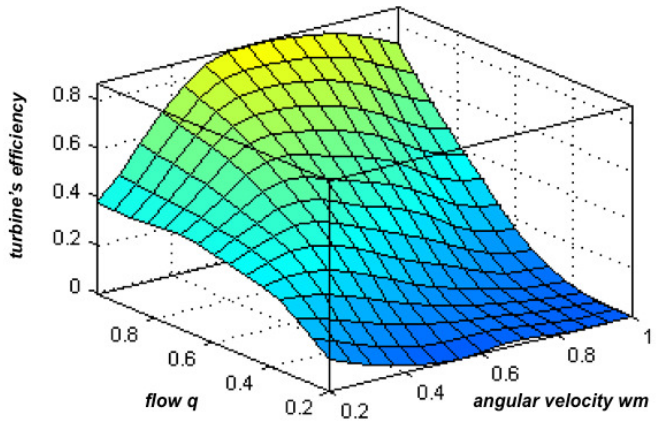

Figure 9 Possible fuzzy representation of the hydraulic turbine's efficiency

D.Electro-Mechanical Subsystem

As the name suggest, it is possible to model the electric generator and the grid in one subsystem. The literature [1],[3],[6],[9],[10],[11] describes most common ways of modelling the electromechanical part of the SHP, while distinguishing between the islanding mode of operation and the operation, when the SHP supplies the national grid system.

ACKNOWLEDGMENT

This work was supported by the Faculty of Electrical Engineering and Informatics, Technical University of Kosice, Slovakia, under the Grant FEI-2020-64, as well as by the APVV project: APVV-16-0206.

REFERENCES

[1] IEEE Working Group., "Hydraulic turbine and turbine control models for system dynamic studies," in IEEE Trans on Power Syst., 1992, 7, pp.167–79.

[2] H.J. Wagner, J. Mathur, Introduction to Hydro Energy Systems: Basics, Technology and Operation. Heidelberg : Springer, 2011. ISBN 978-3-642-20708-2.

[3] G. Munoz-Hernandez, S. Mansoor, D. Jones, Modelling and Controlling Hydropower Plants. 1st Edition. London : Springer London Ltd, 2013. s. 299. ISBN: 978-1-4471-6221-6.

[4] D.G. Ramey, J. W. Skooglund, "Detailed hydro governor representation for system stability studies," in *IEEE Trans on Power Apparatus and Systems*, 1970, 89, pp.106–12.

[5] Y.CH. Choo, K.M. Muttaqui, M. Negnevitsky, "Modelling of Hydraulic Governor Turbine for Control Stabilization," in *ANZIAM Journal*, 2007, 49, pp. C681-C698.

[6] J. Tiwari, et al., "Modelling and Simulation of Hydro Power Plant using MATLAB & WatPro 3.0.," in *Intelligent Systems and Applications*, 2015, 08, pp. 1-8. DOI: 10.5815/ijisa.2015.08.01.

[7] G. Singh, D.S. Chauhan, D. S., "Simulation and Modeling of Hydro Power Plant to Study Time Response during Different Gate States," in *(IJAEST) International Journal of Advanced Engineering Sciences And Technologies*, 2011, Vol. No. 10, Issue No. 1, pp. 042 – 047.

[8] R.A. Naghizadeh, S. Jazebi and B. Vahidi, "Modelling Hydro Power Plants and Tuning Hydro Governors as an Educational Guideline," in *International Review on Modelling and Simulations (I.RE.MO.S)*, 2012, Vol. 5, No. 4., pp.780-1790.

[9] A. Acakpovi, E. B. Hagan and F. X. Fifatin, "Review of Hydropower Plant Models," in *International Journal of Computer Applications*, vol. 18, December 2014, pp. 33-38.

[10] A. A. Usman, A. Abubakar and R. A. Abdulkadir, "Modelling and Simulation of Micro Hydro Power Plant Using Matlab Simulink," in *Proc. 2nd International Conference on Science, Technology and Management*, New Delhi: ICSTM, 2015, pp. 1121-1133.

[11] M. Sattouf, "Simulation Model of Hydro Power Plant Using Matlab/Simulink," in *International Journal of Engineering Research and Applications*, vol. 1, Brno: IJERA, 2014, pp. 295-301. ISSN: 2248-962

[12] J. Giesecke, E. Mosiny, "Wasserkraftanlagen: Planung, Bau und Betrieb". 4., aktualisierte u. erw. Aufl. Berlin: Springer, 2005. ISBN 978-3-540-25505-5

[13] P. Fedor, D. Perduková, R. Olexa, "Modelling a Small Hydropower Plant". In *Proc. Energetika 2019*, Stará Lesná [to be published]

[14] IEEE, "IEEE Guide for Control of Small Hydroelectric Power Plants," In *IEEE Std 1020-1988*, vol., no., pp.1-36, 28 Nov. 1988

[15] C. Jaliu, I. Visa, D. "Diaconescu, Dynamic Model of a Small Hydropower Plan", In *Proc. 12th International Conference on Optimization of Electrical and Electronic Equipment*, 2010.

[16] P. Fedor, D. Perduková, P. Radváni, "Modelovanie Malých Vodných Elektrární". In *Proc. ARTEP 2019: 13. ročník Konferencie odborníkov z univerzít, vysokých škôl a praxe.* Stará Lesná:. s. 001-00

On the processing conditions of rapid annealing method

[1]*Branislav KUNCA (4th year)*
Supervisor: [2]Ivan ŠKORVÁNEK

[1]Department of Physics, Faculty of Electrical Engineering and Informatics, Technical University of Košice

[1,2]Department of Nanomaterials and Applied Magnetism, Institute of Experimental Physics, Slovak Academy of Sciences

[1]kunca@saske.sk, [2]skorvi@saske.sk

***Abstract*—Rapid annealing has been conducted on soft magnetic nanocrystalline $Fe_{80}Nb_3Cu_1Si_6B_{10}$ alloy. Parental as-quenched ribbons were prepared by planar flow casting method. Samples were processed at 500°C using a set of preheated massive copper blocks for 6 – 300s. Reference samples were thermally processed using the conventional annealing method for 3600s. Development of microstructure and magnetic properties has been analyzed in relation to processing conditions.**

***Keywords*—nanocrystalline alloys, rapid annealing, soft magnetic properties, microstructure**

I. Introduction

Development of nanocrystalline structure in ferromagnetic materials offers a possibility to improve their soft magnetic characteristics, making them suitable for various technical applications such as electronic components [1], sensory devices [2] or power apparatus [3]. Specific alloy composition allows formation of nanocrystalline grains with mean diameter between 10 – 30 nm which according to Herzer's Random Anisotropy Model [4] leads to desired suppression of magnetocrystalline anisotropy energy and enhancement of mutual exchange interaction. Conventional isothermal annealing for 30 – 60 minutes at temperatures close to temperature of primary crystallization has become the most common way to ensure formation of desired microstructure [5].

Recently, rapid annealing has been employed as a suitable processing method of soft magnetic materials [6-7]. Combination of high heating rates (10^2 – 10^4 K/s) with short annealing times leads to crystallization process with enhanced nucleation rates and low growth rate. Utilization of pair of preheated Cu blocks showed to be a very promising approach due to the possibility to achieve good thermal stability, high heating rates and at the same time prevent undesirable overheating effects [8]. By these means it is possible to obtain improved soft magnetic properties and nanocrystalline microstructure, unattainable by conventional annealing techniques [9].

In this paper we will discuss processing conditions of rapid annealing method. $Fe_{80}Nb_3Cu_1Si_6B_{10}$ nanocrystalline ribbons were used to demonstrate development of microstructure and magnetic properties after processing at different annealing times. Potential improvements of the experimental setup used at the Department of Nanomaterials and Applied Magnetism, IEP SAS will be discussed.

II. Experimental

Rapidly quenched $Fe_{80}Nb_3Cu_1Si_6B_{10}$ amorphous precursor ribbons were prepared by planar flow casting method. Samples were subsequently submitted to rapid annealing which took place in the air. Specimens were wrapped in the Cu foil packets (thickness ~ 50 μm) to provide its uniform heating and clutched between two massive copper blocks (each approx. 3kg) for 6 – 300s at 500°C, at heating rate estimated to more than 100 K/s, see fig. 1. Separate Cu block held at room temperature was used for cooling of the processed specimen. Time of annealing has been defined as a time elapsed between point of insertion and point of removal of the sample. The copper blocks were heated in the furnace with setpoint temperature stably set for a minimum duration of 15 minutes before processing. Temperature was monitored by thermocouple mounted on the side of the bottom block throughout the whole processing procedure.

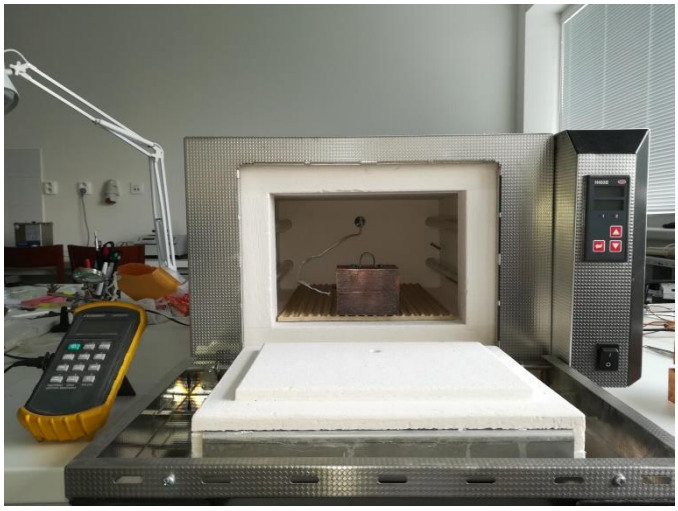

Fig. 1 Experimental setup for rapid annealing of the samples at the Laboratory of Nanomaterials and Applied Magnetism, IEP SAS.

Reference samples were isothermally annealed at the same temperature for 1h under a high vacuum and subsequently cooled to room temperature at a cooling rate 200°C/h.

Microstructure of as – quenched and processed samples has been studied by x - ray diffraction (XRD) with Cu-Kα radiation. Magnetic characteristics were obtained by vibrating sample magnetometer (VSM) and the Forster type B-H loop tracer placed in magnetically shielded room.

III. Results and Discussion

Fig. 2 shows XRD patterns of the as - quenched, conventionally (CA) and rapidly (RA) annealed samples from both TOP and BOTTOM side of the ribbon. Broad peak in the area around 45° typical for amorphous structure has been observed for the as-quenched samples. Small peak detected for the TOP side at 2θ = 82.3° suggests presence small number of Fe nanocrystals with preferred orientation in the (211) direction. Their presence is presumably due to lower cooling rate of the melt during the casting process. On contrary, patterns obtained for conventionally and rapidly annealed samples all show presence of nanocrystalline structure of bcc α-Fe(Si) grains embedded in the residual amorphous matrix.

RA for longer than 30 seconds clearly has negative impact on the microstructure. Detected peaks suggest presence of higher amounts of CuO and small traces of Fe_3O_4. Here lie the boundaries of used equipment as the formation of Fe_3O_4 clearly arose due the fact that the rapid annealing has not been conducted in the vacuum or under protective gas atmosphere. The origin of the CuO is not clear as the original alloy itself contains 1at% of Cu. XRD patterns of the conventionally annealed alloys with similar compositions did not show patterns of CuO oxides and therefore their presence may have arisen from the direct contact of the sample with the Cu envelope. Nevertheless, this claim lacks enough experimental evidence.

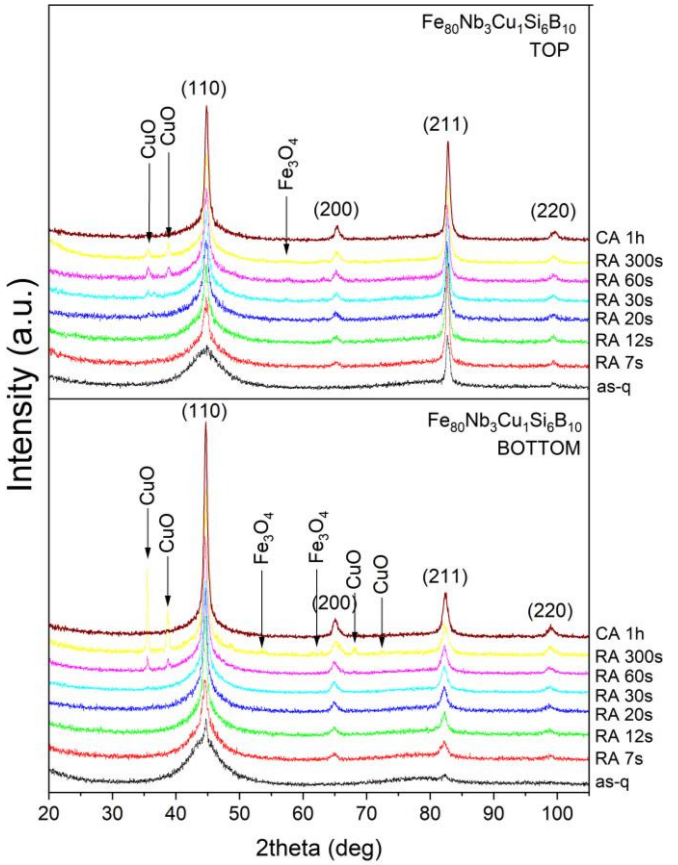

Fig. 2 X-Ray Diffraction patterns from the TOP and BOTTOM side of the as-quenched (as-q) ribbons, as well as rapidly (RA) and conventionally annealed (CA) ribbons at 500°C after various processing times.

Effect of annealing procedures on magnetic properties of the studied alloy has been conducted via measurement of the hysteresis loops (not shown here), which were obtained for 6cm long and 1cm wide samples. Fig. 3 shows development of coercivity (H_c) and saturation magnetization (M_s) with annealing time. Increase of the saturation magnetization and decrease of coercivity of the annealed samples compared to the as-quenched specimen may be attributed to the formation of nanocrystalline structure of the bcc α-Fe(Si) grains. Highest saturation magnetization value of approx. M_s = 155.5 Am^2/kg has been obtained not only after conventional annealing but rapid annealing for 300s (RA_{300}) as well. Coercivities of both samples achieve similar values, slightly smaller for the RA_{300} one. This shows that long term rapid annealing (in the order of minutes) essentially becomes comparable to the conventional annealing process. Positive impacts of high heating rate on the microstructure development are suppressed as growth of the nanocrystals overcomes the anticipated effect of high nucleation rate.

Significant drop of coercivity values was however achieved after short RA processing, up to 30s. H_c values ranged between 6.3 A/m to 6.9 A/m, which is on average 44% lower than in case of CA specimen (9.2 A/m). Saturation magnetization after RA was no lower than 93.5% of M_s obtained after CA. More detailed characterization of these samples may be found in [10].

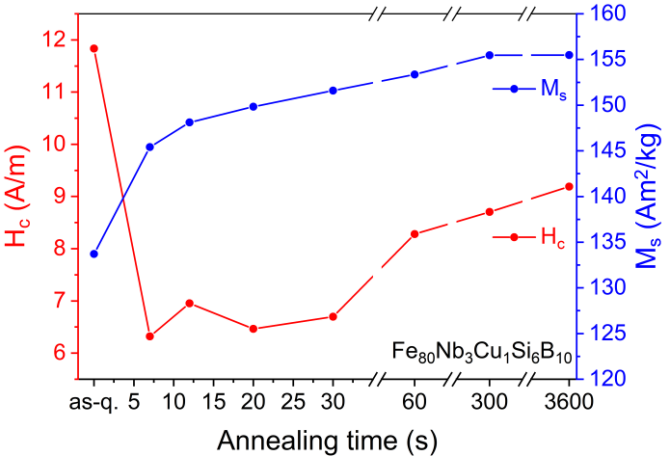

Fig. 3 Evolution of coercivity (H_c) and saturation magnetization (M_s) with annealing time.

IV. Conclusion

Processing conditions of rapid annealing method were investigated. $Fe_{80}Nb_3Cu_1Si_6B_{10}$ ribbons were rapidly annealed at 500°C for 6 - 300s. Microstructure characterization showed presence of nanocrystalline bcc α-Fe(Si) grains for all samples. RA for 60s and longer resulted in formation of Fe_3O_4 and CuO, both presumably as a consequence of thermal processing in air. Short rapid thermal processing has a positive influence on the development of magnetic characteristics. On contrary, comparison of coercivity and saturation magnetization with values obtained for reference sample conventionally annealed for 3600s showed that process of rapid annealing for long duration becomes effectively equivalent to conventional thermal treatment.

Acknowledgment

This work was supported by the projects VEGA 2/0171/19 and JRP SAS-TUBITAK MAGSAT. Authors would like to thank Dr. Peter Švec from Institute of Physics, Slovak

Academy of Sciences, for preparation and microstructure characterization of the samples.

REFERENCES

[1] G.H.Kim, T.H. Noh, G.B. Choi, K.Y. Kim, "Magnetic properties of FeCuNbSiB nanocrystalline alloy powder cores using ball-milled powder" in *Journal of Applied Physics*, vol. **93**, 2003, pp. 7211 – 7213

[2] T. Eggers, D.S. Lama, O. Thiabgoh, J. Marcin, P. Švec, N.T. Huong, I. Škorvánek, M.H. Phan, "Impact of the transverse magnetocrystalline anisotropy of a Co coating layer on the magnetoimpedance response of FeNi-rich nanocrystalline ribbon" in *Journal of Alloys and Compounds* **741**, 2018, pp. 1105 – 1111

[3] K. Byerly, P.R. Ohodnicki, S.R. Moon, A.M. Leary, V. Keylin, M.E. McHenry, S. Simizu, R. Beddingfield, Y. Yu, G. Feichter, R. Noebe, R. Bowman, S. Bhattacharya, "Metal Amorphous Nanocomposite (MANC) Alloy Cores with Spatially Tuned Permeability for Advanced Power Magnetics Applications" in *The Journal of The Minerals, Metals & Materials Society* **70**, 2018, pp. 879-891

[4] G. Herzer, "Grain size dependence of coercivity and permeability in nanocrystalline ferromagnets" in *IEEE Transactions on Magnetics*, vol. **26**, 1990, pp. 1397 – 1402

[5] M.E. McHenry, M.A. Willard, D.E. Laughlin, "Amorphous and nanocrystalline materials for applications as soft magnets" in *Progress in Materials Science*, vol. **44**, 1999, pp. 291 – 433

[6] K. Suzuki, R. Parsons, B. Zang, K. Onodera, H. Kishimoto, T. Shoji, A. Kato, "Nano-crystallization of amorphous alloys by ultra-rapid annealig: An effective approach to magnetic softening", in *Journal of alloys and compounds*, vol. **735**, 2018, pp. 613 - 618

[7] G. Herzer, V. Budinsky, C. Polak, "Magnetic properties of FeCuNbSiB nanocrystallized by flash annealing under high tensile stress", in *Physica Status Solidi B*, vol. **248**, 2011, pp. 2382 – 2388

[8] R. Parsons, B. Zang, K. Onodera, H. Kishimoto, T. Shoji, A. Kato, K. Suzuki, "Copper-free nanocrystalline soft magnetic materials with high saturation magnetization comparable to that of Si steel" in *Applied Physics Letters*, vol. **110**, 2016, no. 012407

[9] B. Zang, R. Parsons, K. Onodera, H. Kishimoto, T.A. Kato, A.C.Y. Liu, K. Suzuki, "Effect of heating rate during primary crystallization on soft magnetic properties of melt-spun Fe-B alloys" in *Scripta Materialia*, vol. **132**, 2017, pp. 68 – 72

[10] B. Kunca, J. Marcin, P. Švec, I. Škorvánek, "Effect of Rapid Annealing on Magnetic Properties of the Nanocrystalline $Fe_{80}Nb_3Cu_1Si_6B_{10}$ Alloy" in *Acta Electrotechnica et Informatica*, vol. **19**, 2019, pp. 33 – 37.

Overview of the Battery Types and their Testing

[1]*Juraj BIĽANSKÝ (1st year),*
Supervisor: [2]*Milan LACKO*

Department of Electrical Engineering and Mechatronics, FEI TU of Košice, Slovak Republic
[1]juraj.bilansky@tuke.sk, [2]milan.lacko@tuke.sk

***Abstract*—This paper provides an overview of the available battery types suitable for electric vehicles and their testing. It describes cyclic testing and variables that need to be measured during testing. According to these results, a custom tester will be proposed soon, which basic block diagram is designed in the further work chapter.**

***Keywords*—battery, state, testing, charging, li-ion, cycle**

I. Introduction

Today, efforts are being made to significantly reduce emissions. Electric vehicles (EV) are coming to the fore because they have lots of advantages like zero emissions, no sound and they are economically and efficiently. The most problematic factor in this vehicle is a battery. It significantly increases the weight of the car and which is the most important battery capacitance reduce range. After discharging, it can't be simply refilled like a classic petrol car, but, it takes several hours to charge.
Information about batteries, which are coming directly from the manufacturer, is usually the result of some standard testing under laboratory conditions. This informations can be quite different from using in real operation, where batteries have to work in more demanding conditions like low and high temperature, step load changes, a fast transition between discharging and charging. All of these factors affect the life cycle of battery. This article discusses about methods, how to best test the battery for real-life use. Later, the measuring system will be designed and made.

II. Comparison of Battery Types for EV

Because we will focus on batteries and their testing, we need to compare different battery types first. Every type has some advantages and disadvantages. After that, we can take one type, which will be best for our purpose. Below in Table 1 is a comparison of basic and most important battery characteristics. There Lead-Acid, Lithium-Ion, Ni-Mh or Ni-Cd. There is also one new type of battery which combine Lithium anode and Nickel-rich cathode. This type is called LICERION. LICERION is lower availability, but you can order it directly from the manufacturer. As you can see lead-acid and Ni-Cd batteries do not meet the main requirement of high power density or Wh/Kg ratio. Ni-Mh battery has lower Wh/Kg ratio like other two batteries and recycling is more demanding too. The best choice is LICERION battery with biggest Wh/Kg ratio, biggest discharging current, very good lifespan and low toxicity. There is one big problem with this battery. Obtaining this battery is very difficult. So we take the second-best choice which is very available options is Li-Ion battery [1], [2], [3].

TABLE I
Comparison of available battery for EV

	LEAD-ACID	LI-ION	NI-MH	LICERION	NI-Cd
Wh/Kg	34-40	100-265	60-120	500	40-60
Wh/€	9	6	?	?	?
Self-discharge	3–20%	<2.5%	<2.9%	?	10%
Cycle durability	<350	<1,200	<2000	<500	<2000
Cell voltage	2	3.3	1.2	?	1.2
Peak current	5C	3C	5C	5C	20 C
Enviromental toxicity	Very High	Low	Medium	Low	Very high

III. Cycle Testing

A. Constant Current Cycle Testing

This is perhaps the most important of the qualification tests. Cells are subjected to repeated charge-discharge cycles to verify that the cells meet or exceed the manufacturer's claimed cycle life. Cycle life is usually defined as the number of charge-discharge cycles a battery can perform before its nominal capacity falls below 80% of its initial rated capacity. These tests are needed to verify that the battery performance is in line with the end product reliability and lifetime expectations and will not result in excessive guarantee or warranty claims.
Temperature, charge/discharge rates and the Depth of Discharge each have a major influence on the cycle life of the cells depending on the purpose of the tests, the temperature and the DOD should be controlled at an agreed reference level in order to have repeatable results which can be compared with a standard. Alternatively, the tests can be used to simulate operating conditions in which the temperature is allowed to rise, or the DOD restricted, to determine how the cycle life will be affected. Similarly cycle life is affected by over charging and over discharging and it is vital to set the correct voltage and current limits if the manufacturer's specification is to be verified [4].

B. Cycle Testing with Programmed Profile

This type of cyclic testing is suitable for battery testing in real condition. Testing conditions like discharging/charging currents, temperatures are preprogrammed in drive profile, so

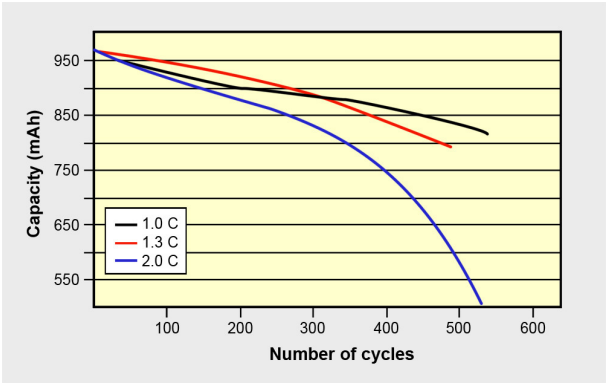

Fig. 1. Lifespan difference between discharging current [5].

the battery is no constantly discharged like in a laboratory. Drive profile should contain an urban cycle, where battery load is vary or suburban cycle where the load is more constant. The profile can also contain home charging or urban fast charging. Testing should result in a better understanding of how the battery is affected by demanding use in the tough conditions the vehicle is and how it affects it's capacity and number of cycles [6].

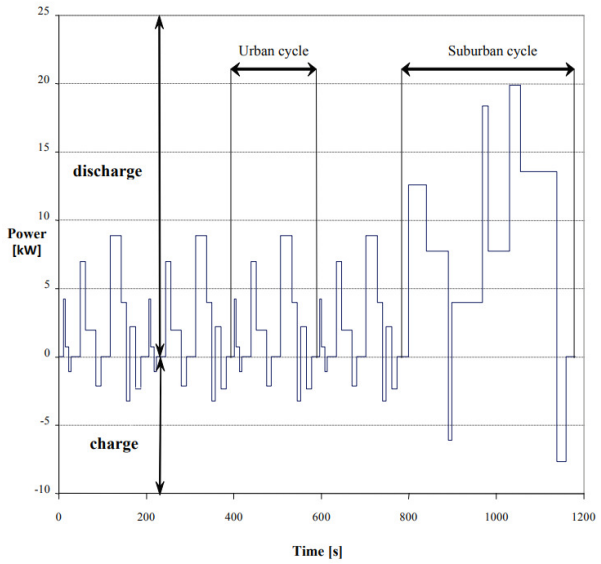

Fig. 2. Preprogramed drive profile [4].

IV. Measuring During Cycle Testing

A. Open Circuit Voltage(OCV)

Measuring a battery's open-circuit voltage is not a reliable measure of its ability to deliver current. As a battery age, its internal resistance builds up. This will reduce the battery's ability to accept and to hold a charge, but the open circuit voltage will still appear normal despite the reduced capacity of the battery. Comparing the actual internal resistance with the resistance of a new battery will provide an indication of any deterioration in battery performance.

B. Current

Measuring current is important for deciding whether the battery is capable of delivering the required current to the load. If not battery is bad or discharged.

C. Battery and Ambience Temperature

Temperature measuring of battery and ambient during tests is important to avoid a situation that battery will operate in a condition where the thermal limits of battery which are defined by the manufacturer are exceeded. Battery temperature measurement also has a safety function which will result in the test ending to prevent ignition when the maximum battery temperature is exceeded [7].

D. Internal Resistance

It is necessary to know the internal resistance of the cell to calculate other states of battery like SOC and SOH. Simple measurement with an ohmmeter is not possible because the current generated by the cell itself interferes with the measurement. To determine the internal resistance, first, it is necessary to measure the open-circuit voltage of the cell. Then a load should be connected across the cell causing a current to flow. This will reduce the cell voltage due to the I.R voltage drop across the cell which corresponds to the cell's internal resistance.

E. Internal Impedance

There is a few methods to measure internal impedance of battery cell:

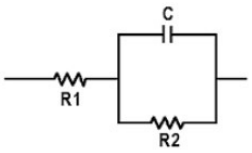

Fig. 3. Impedance inside battery cell[8].

- DC Load Method - it works only for measuring ohmic part of impedance [8]
- AC Conductance - The 1Khz test is another common method. A 1KHz signal excites the battery and Ohm's law calculates the impedance. This method shows different result as DC load method due to parallel capacitance, which is ignored during dc load measuring[8].
- Electrochemical Impedance Spectroscopy (EIS) - Is the most accurate method to determine internal impedance. R1, R2 and C are measured separately, which enables state-of-charge and capacity measurements. The devices used for EIS is Potentiostat or galvanostat[8].

V. Battery States

During a cycle testing is necessary to on-line measuring and evaluating of variables like voltage, current, internal resistance as well as battery and ambience temperature. These variables will be used in evaluating to get an accurate value of states of batteries like the state of charge or state of health.

A. State of Health(SOH)

SOH represents the healthy state of the battery. In other words, SOH indicates how much the battery is corrupted. SOH mainly relates to the ability of a battery to perform a particular discharge or charge. If we want to describe an expression for SOH, we need to define EOL(End Of Life). EOL is defined as state when battery internal resistance is 160% of the same

new battery in the same condition (same temperature, state of charge). Then based on the definition of EOL, we proposed the definition of SOH as:

$$SOH = \frac{R_{EOL} - R_{ACT}}{R_{EOL} - R_{NEW}} \times 100\% \quad (1)$$

in which R_{ACT} is the actual internal resistance of the battery, R_{EOL} is internal battery resistance at End of Life. R_{NEW} is internal battery resistance when the battery is new. All these internal resistance values need to be measured in the same conditions. The range of SOH is 0 - 100%, where 100% means new battery and 0% means bad battery, in EOL, which is not suitable for using and need to be replaced[9].

B. State of Charge(SOC)

SOC gives us information about energy, which is stored inside a battery when a battery is charged or discharged [10]. When the batteries are in use, this information is very important. We need to know when the battery is low or fully charged because we need to protect batteries from undercharging or overcharging to maximize their lifespan. Currently, several types of research have been conducted to determine the state of charge as accurately as possible:

1) Open Circuit Voltage: This method is based on measuring open-circuit battery voltage. The results are not so accurate, because there are many factors like temperature or battery age, which affect the measuring precision. If we want to measure more accurate, we need to compensate for these factors. As you can see in Fig.4 this method is good especially for lead-acid batteries, because open circuit voltage is more dependent on the state of charge like in lithium-ion batteries[11].

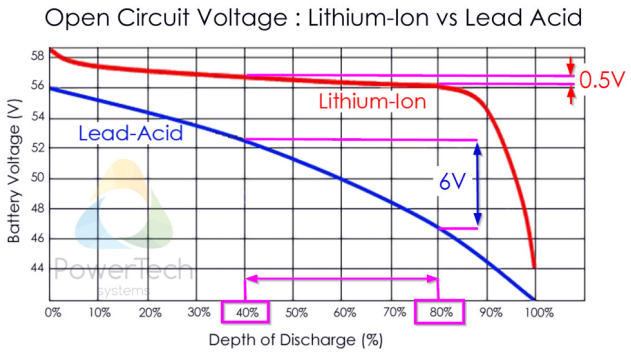

Fig. 4. Difference between discharge characteristics and OCV-SOC dependence of lead-acid and lithium-ion batteries.

2) Coulomb Counting: Measurement of current in and out from battery cell has been utilized for the basis of remaining battery capacity measurement [12]. Current that getting in and out from battery cell makes the change on the electrical charge left in the battery time by time. This method is known as Coulomb counting which can provide high accuracy but still requires compensation from an operational condition such as open-circuit voltage (OCV) estimation method. Current measurement method probably causes a few power losses in the current circuit and also slightly increasing the battery's temperature. Basically, this method is less accurate for weak and strong current because it has relatively high disturbances [13].

3) Internal Resistance: During the cell charge-discharge cycles the composition of the active chemicals in the cell changes as the chemicals are converted between the charged and discharged states, and this will be reflected in changes to the cell impedance. Thus measurements of cell internal impedance can also be used to determine SOC however these are not widely used due to difficulties in measuring the impedance while the cell is active as well as difficulties in interpreting the data since the impedance is also temperature-dependent [14].

4) New Methods: There is also a newly developed method which combines more measuring method to the one measuring cycle to maximize accuracy. SOC can be also determined by using Fuzzy prediction or Kalman Filter [15], [16], [17].

VI. Available Solutions

There are several manufacturers which are focusing on battery testing equipment. They have a wide portfolio from small testers for battery cells to big testers for whole battery modules or packs.

A. Arbin Instrument

Company which is specialising just for battery testing. Their portfolio is wide, from small battery cells to whole battery packs for cars.

Fig. 5. Airbin Instrument battery cells and capacitors tester.

- Electrochemistry, Battery and Supercapacitor Testing
- Coulombic Efficiency (HPCE) Measurements
- Life Cycle Testing
- EIS (electrochemical impedance spectroscopy)
- EIS Electric Vehicle (EV) Cell Testing (DRIVE PROFILE (DRIVE CYCLE) and temperature simulations)
- 24-bit Measuring Resolution and <25ppm or <100ppm precision
- Data Logging Rate: 2000 points per second, per system
- TCP/IP Connection
- Up to 96 battery cells or capacitors at once

B. Chroma

- Battery and Supercapacitor Testing
- Flexible sampling recording (Δt, ΔV, ΔI, ΔQ, ΔE)
- Life Cycle Testing
- High precision output and measurement up to 0.015% of full scale
- Built-in EDLC capacitance and DCR test function
- V / I sampling rate: 50 KHz (Δt:20 μS)
- Dynamic waveform simulation
- TCP/IP Connection
- Up to 48 battery cells or capacitors at once

Fig. 6. Chroma battery cells and capacitors tester.

VII. Further Work

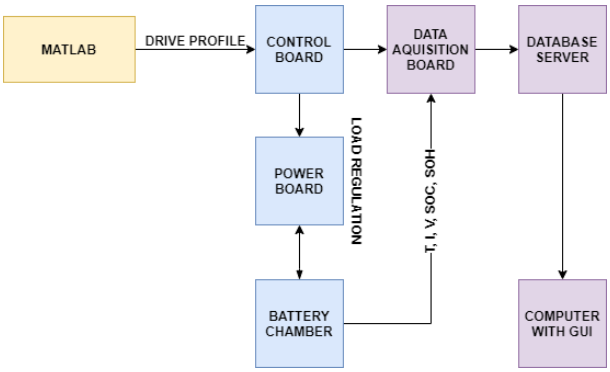

Fig. 7. Block diagram of measuring system which is developed.

After creating an overview of the batteries, measurement methods, and states that we can evaluate, we can start designing our solution. The solution will be proposed according to the block diagram below. 6 blocks can be seen in the diagram and these are colour-coded into 3 units:

1) Simulation part(orange)
2) Control and Power part(blue)
3) Evaluation part(purple)

A. Simulation

In the MATLAB program, a simulation model will be created, which will contain a time-varying testing profile of battery loading. After that this profile will be exported and loaded into the Control Board.

B. Control and Power Part

The control board should be based on a faster dual or more core processor. In case of sufficient power CPU, the evaluation part can be integrated into the Control Board. The board will control the inverter, which will act on the batteries as an electronic load, the value of load will vary according to the pre-programmed drive profile. The battery chamber will contain measurement slots for 8 battery li-ion cells.

C. Evalution Part

The part that will result in measuring variables during tests and then calculating battery states such as charge and battery life. State of health will also be tested in the laboratory. Measurement data and battery states will be written to the database server so that the results can be stored and viewed easily.

VIII. Conclusion

The article is an overview of the basic types of batteries and their testing methods. Future research will focus on cyclic test methods with a programmable profile. A tester will be designed and built for this method. Preliminary design and description of blocks can be seen in the further work chapter. The method can be improved by adding temperature changes around the battery to create conditions that are even more similar to the real.

References

[1] J. P. Aditya and M. Ferdowsi, "Comparison of nimh and li-ion batteries in automotive applications," in *2008 IEEE Vehicle Power and Propulsion Conference*. IEEE, 2008, pp. 1–6.

[2] V. Alminauskas and W. Johnson, "Comparison of" aa" nickel metal hydride cells with" aa" ni-cd cells," in *IECEC 96. Proceedings of the 31st Intersociety Energy Conversion Engineering Conference*, vol. 2. IEEE, 1996, pp. 1144–1147.

[3] S. Power. Licerion® high energy density, lithium-metal rechargeable batteries. [Online]. Available: https://sionpower.com/products/

[4] J. Li, C. Ying, Y. Sun, and J. Sun, "A new design of battery constant current discharge system," in *2011 2nd International Conference on Artificial Intelligence, Management Science and Electronic Commerce (AIMSEC)*. IEEE, 2011, pp. 6509–6512.

[5] Battery and energy technologies. [Online]. Available: https://www.mpoweruk.com/life.htm

[6] F. Vellucci, V. Sglavo, G. Pede, E. Pasca, V. Malvaldi, and S. Scalari, "Life cycles test on a lithium battery system," in *IECON 2014-40th Annual Conference of the IEEE Industrial Electronics Society*. IEEE, 2014, pp. 3129–3134.

[7] R. Hulett, J. Kulick, J. Gorman, S. Aggarwal, P. Balma, W. Bartley, T. Burse, C. Chaplin, W. Diab, J.-P. Faure *et al.*, "Ieee-sa standards board meeting minutes 29 march 2012 ieee operations center, piscataway, new jersey, usa 9: 00 am–11: 45 am," 2012.

[8] Batteryuniversity. [Online]. Available: https://batteryuniversity.com/learn/article/how_to_measure_internal_resistance

[9] D. Haifeng, W. Xuezhe, and S. Zechang, "A new soh prediction concept for the power lithium-ion battery used on hevs," in *2009 IEEE vehicle power and propulsion conference*. IEEE, 2009, pp. 1649–1653.

[10] S. Yuan, H. Wu, and C. Yin, "State of charge estimation using the extended kalman filter for battery management systems based on the arx battery model," *Energies*, vol. 6, no. 1, pp. 444–470, 2013.

[11] S. Susanna, B. R. Dewangga, O. Wahyungoro, and A. I. Cahyadi, "Comparison of simple battery model and thevenin battery model for soc estimation based on ocv method," in *2019 International Conference on Information and Communications Technology (ICOIACT)*. IEEE, 2019, pp. 738–743.

[12] I.-S. Kim, "Nonlinear state of charge estimator for hybrid electric vehicle battery," *IEEE Transactions on Power Electronics*, vol. 23, no. 4, pp. 2027–2034, 2008.

[13] E. Leksono, I. N. Haq, M. Iqbal, F. N. Soelami, and I. Merthayasa, "State of charge (soc) estimation on lifepo 4 battery module using coulomb counting methods with modified peukert," in *2013 Joint International Conference on Rural Information & Communication Technology and Electric-Vehicle Technology (rICT & ICeV-T)*. IEEE, 2013, pp. 1–4.

[14] X. Wei, B. Zhu, and W. Xu, "Internal resistance identification in vehicle power lithium-ion battery and application in lifetime evaluation," in *2009 International Conference on Measuring Technology and Mechatronics Automation*, vol. 3. IEEE, 2009, pp. 388–392.

[15] A. Zenati, P. Desprez, and H. Razik, "Estimation of the soc and the soh of li-ion batteries, by combining impedance measurements with the fuzzy logic inference," in *IECON 2010-36th Annual Conference on IEEE Industrial Electronics Society*. IEEE, 2010, pp. 1773–1778.

[16] P. A. Topan, M. N. Ramadan, G. Fathoni, A. I. Cahyadi, and O. Wahyunggoro, "State of charge (soc) and state of health (soh) estimation on lithium polymer battery via kalman filter," in *2016 2nd International Conference on Science and Technology-Computer (ICST)*. IEEE, 2016, pp. 93–96.

[17] A. Eddahech, O. Briat, and J.-M. Vinassa, "Real-time soc and soh estimation for ev li-ion cell using online parameters identification," in *2012 IEEE Energy Conversion Congress and Exposition (ECCE)*. IEEE, 2012, pp. 4501–4505.

Pathological Speech Processing: Review

[1]*Máté HIREŠ (1st year),*
Supervisor: [2]*Peter DROTÁR*

[1,2]Department of Computers and Informatics, FEI TU of Košice, Slovak Republic

[1]mate.hires@tuke.sk, [2]peter.drotar@tuke.sk

***Abstract*—This paper describes an investigation of voice pathology detection. This is a preliminary study in the field of automatic detection of voice disorders. We compare some of the available voice databases, which contains both healthy and pathological voice recordings. We also compare some methods, which use neural networks for the detection and achieved significant results. Finally we discuss the presented methods and their results in term of their accuracy.**

***Keywords*—voice pathology, speech disorders, machine learning, signal processing, deep learning.**

I. Introduction

The human voice can have a radical effect on the health condition of an individual. It can be radically affected by neoplasm, vocal palsy and other phonotraumatic diseases. Automatic detection of these pathological voice disorders is a very challenging and significant medical classification problem. Voice pathology includes evaluation and treatment of voice production related diseases, which are affecting fluency, intonation, phonation and breathing. Since the computer-aided analysis and diagnosis of human voice can be an effective and low-cost tool for patients around the world, voice pathology has congested specific interest amongst machine learning and signal processing scientists. The current activity of the detection of voice disorders includes a special procedure called *laryngeal endoscopy* [1], [2]. This is a very complicated and expensive procedure and it also requires an expert to perform the evaluation. To detect voice disorders without intrusion, we can analyze the voice directly.

Many scientists work on the automatic detection of voice disorders, exactly in the last few years. Van der Merwe [3] provides a foundation and accentuates the necessity of the research related to voice disorder detection. Kent [4] discusses the connection between voice production and its dysfunctions. Some studies found specific speech dysfunctions within some particular population groups [5], [6].

Thanks to the amount of available data and the advancement in the computational power, a lot of appropriate Deep Learning models are provided for speech processing. Hence, we are allowed to use complex model architectures. We can teach convolutional layers [7] to detect various features that could help us to differentiate pathological and healthy voice. Some Interspeech challenges [8], [9] also attracted interest in the application of Machine Learning and signal processing techniques for voice pathology detection.

A lot of available datasets contain recordings, which are recorded in more different environments, thus it makes hard to find common features in the samples. The Saarbruecken Voice Database (SVD) [10] could be an ideal set of data to start the research in this area, since all of its recordings are sampled at 50 kHz with 16-bit resolution.

II. Related work

Deep learning models got popular from the introduction of the deep Boltzman machine in 2006 [11]. From this time using these models, researchers and scientist have achieved significant results in many fields, such as medical analysis [2], [12], [13], computer vision [14], cybersecurity [15], etc. There are a lot of research articles in the field of voice pathology detection, where the researchers used SVD for their work [16], [17], [18], [19], [20]. They yielded certain features from the voice recordings. These features contains mel-frequency cepstral coefficients, energy, entropy, harmonics-to-noise ratio, normalized noise energy, multidimensional voice program parameters, etc. Hence, multiple classifiers have been used. Most of the researchers used traditional methods like Support Vector Machine classifier (SVM), Dimensionality Reduction Method (DRM), glottal source excitation, Gaussian mixture models, k-means clustering. Deep Neural Network (DNN) methods were also significantly useful. Notable results were achieved for example with the Far Eastern Memorial Hospital (FEMH) dataset using transfer learning techniques [21]. It consists of transferring the knowledge from a small dataset to another previously trained model, which was trained on a similar domain [22].

Voices are mostly affected by cancer, nodules, polyps, cysts, laryngitis, vocal tremors, spasmodic dysphonia, vocal fold paralysis and sulcus diseases [1]. The results of the voice pathology detection depends on the data used. Dankovičová et al. differentiated healthy and dysfunctional voice samples with the accuracy of over 70% using traditional methods [23]. Kasuya et al. effectively identified glottic cancer, vocal cord polyp and other nerve paralysis diseases [24]. Fang et al. identified polyp, cyst, nodules, neoplasm, and other diseases as well by using deep learning models [1]. They achieved over 90% accuracy in female and over 94% accuracy in male subjects. Dibazar et al. connected pitch dynamics, Mel-frequency spectral coefficients and Hidden Markov Model classifier (HMM) to identify some voice disorders. Working with data from the Massachusets Eye and Ear Infirmary (MEEI) they implemented a model, which resulted with the accuracy of over 99% [25]. Souissi et al. achieved over 86% accuracy using 2000 recordings [17]. Al-nasheri et al. pushed the accuracy of 99% [18]. Hemmerling at al. achieved the highest accuracy of 100%, who detected the disorders

for women and men separately [19]. However, since these results were achieved on specific datasets, the high accuracy can be questionable.

III. Datasets

A. The Saarbruecken Voice Database (SVD)

The SVD is a collection of voice recordings from more than 2000 patients [10]. One recording session contains the following recordings:

- Recording of the vowels [i, a, u] produced at normal, high and low pitch,
- Recordings of the vowels [i, a, u] with rising-falling pitch,
- Recording of the sentence ”Guten Morgen, wie geht es Ihnen?” ("Good morning, how are you?").

This is a total of 13 files per session. The signals for each case are stored in separate files. All the samples are recorded at 50 kHz with 16 bit resolution. This dataset contains 71 different pathologies including organic and functional.

B. The Far Eastern Memorial Hospital database (FEMH)

This dataset includes 60 normal voice samples and 402 samples of common voice disorders, including vocal nodules, polyps, andcysts, glottic neoplasm, vocal atrophy, laryngeal dystonia, unilateral vocal paralysis and sulcus vocalis. It contains 3-second long voice samples of patients sustaining the vowel sound /a/ [1]. These samples were recorded using a high-quality microphone with a digital amplifier under a background noise level between 40 and 45 dBA. The sampling rate was 44,100 Hz with a 16-bit resolution.

C. The Massachusetts Eye and Infirmary Voice Disorders Database (MEEI)

The MEEI Voice Disorders Database was delivered in 1994 at the MEEI Voice and Speech Lab and partly at Kay Elemetrics Corp. [26]. It contains over 1400 samples of recordings of:

- sustained of vowel /a/, from which 53 is normal and 657 pathological,
- continuous speech, from which 53 is normal and 661 pathological.

All the samples have 16 bit resolution, but as a disadvantage, the samples are recorded in two different environments. The frequency for normal samples is 50 kHZ, while the frequency of the pathological samples is either 25 or 50 kHz. (53 normal and 657 pathological files) and continuous speech (53 normal and 661 pathological).

D. The Arabic Voice Pathology Database (AVPD)

The AVDP dataset was developed at the Communication and Swallowing Disorders Unit of King Abdul Aziz University Hospital, Riyadh, Saudi Arabia [27]. The idea behind the creation of this dataset is to overcome the environmental problems of the MEEI dataset, which could lead to non-accurate results. The dataset contains:

- voice samples of successive speech tasks,
- sustained phonation of the vowels /a/, /e/ and /o/,
- counting from 0-10,
- a standardized Arabic passage,
- reading of three common words.

The sample frequency of all collected samples in AVPD is 50 kHz.

E. New Spanish Speech corpus database

This database contains speech recordings of 50 people with Parkinson’s disease and 50 healthy recordings with 25 male and 25 female on each category. The participants are Colombians, speaking native Spanish. This database is balanced in terms of age and gender as well. The average age of the participants is approximately 60 in each category and subcategory. The recordings were sampled at 44100 Hz with 16 bits of resolution.
The participants had to perform different tasks to analyze some aspects of their voice. The tasks can be grouped into the following aspects: (i) phonation, (ii) articulation, (iii) prosody. Detailed description of each task is described in [28].

IV. Methodology

A. DNN Architecture

The following Deep Neural Network (DNN) architecture was presented by Harar et al. [20]. They used two stacks of convolutional layers so their model can transform the input into a set of more abstract repeating patterns, that could be important for the decrease of the network cost. Between each stack there is a max pooling layer to reduce the dimension of the input vector. Moreover, they wrapped all the convolution and pooling layers in a TimeDistributed layer to keep the time axis unchanged. The resulting matrices are then reshaped to be connected to a recurrent Long-Short-Term-Memory (LSTM) layer. This LSTM layer is set so it can remember the changes in time. At last, there is a stack of 3 fully connected layers, which ends with a 2 neuron Softmax layer for the final classification. One of the neurons are for the healthy and one for the pathological class.

The detailed DNN architecture with its input and output parameters is shown in Fig. 1.

B. CNN Architecture

Convolutional Neural Networks (CNN) are variants of the standard neural network. They are not using fully connected hidden layers. They have a special network architecture, which consists of alternating convolution and pooling layers, most of them are hidden. In the following text we will discuss the CNN architecture used by Wu at al. in [29].
The weights are shared among all the units, where each unit is calculated as

$$h_m^k = \sigma(\sum_{l=1}^{I}\sum_{n=1}^{N_W} v_{l,n+m-1} w_{l,n}^k + w_0^k), \qquad (1)$$

where $v_{l,m}$ is the m-th unit of the l-th input layer V and $h_{k,m}$ is the m-th unit of the k-th convolutional layer H. N_W is the size of all the weights, where $w_{l,n}^k$ is the n-th unit of the given weight. The feature extraction is an automatic process by the shared-weights.
A pooling layer is fundamental for dimensional reduction to decrease the complexity of the computations. To build such

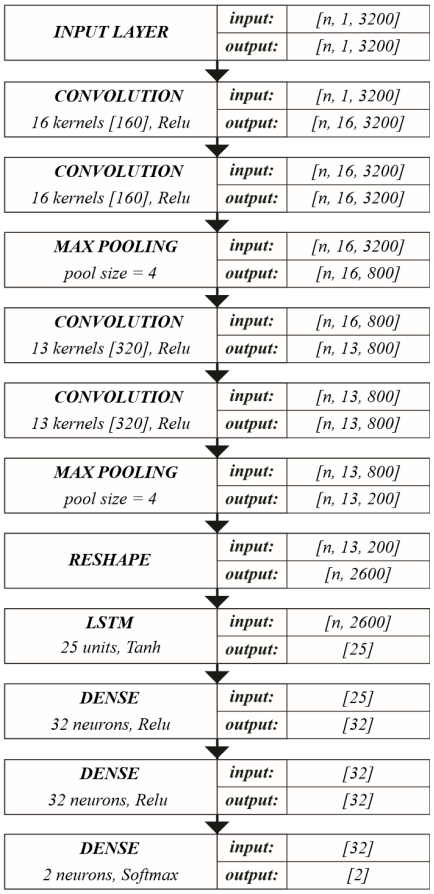

Fig. 1. The detailed DNN architecture by Harar et al. [20]

a pooling layer, maximization function is used. The pooling layer is defined as follows:

$$p_m^k = \max_{n=1}^{G} h_{l,(m-1)\times s+n}, \tag{2}$$

where G is the size of the pooling window using maximization function. The value s is a step, when the pooling window shifts among the convolutional layer.

They used 10 hidden layers. After the first layer, which has the shape of 8^*3 with the step 1, each following layer was convolved with 8 filters with the shape 8^*3^*8 and the step 1. They set 4^*4 pooling windows and a RELU activation function. Next, they formed the feature map into a fully connected layer to train the model classification. To overcome the over-fitting problems, L2-regularization is used.

C. Feature Extraction Procedure

The following model was created by Banerjee et al. for feature extraction [13].

Firstly, there is a 25ms segment size and a 10ms shift size used to extract the features for each patient. This model extracts three types of features for each segment:

- Prosodic features,
- Vocal-Tract features,
- Excitation features.

These three types produce overall 54 features for each segment. Next, there are 162 features formed by taking the first and second time derivates for each segment. Finally there is a concatenation of 15 consecutive feature vectors to create a final vector of size 2430, which serve for diagnosis. The detailed description of the features is shown in Table I.

TABLE I
DESCRIPTION OF SPEECH FRAME FEATURES [13]

Feature Type	N. of Features
Prosodic features	
Short-time energy, Average power, Average magnitude, Zero crossings, Mean, Standard deviation, Median, Max, Min, Range, Dynamic range, Interquartile range	12
Vocal-tract features	
MFCC (Mel Frequency Cepstrum Coefficients)	39
Teager Energy Operator	1
Excitation features	
Jitter	1
Shimmer	1
Total number of raw features per frame	54
First order time derivative of raw features	54
Second order time derivative of raw features	54
Total number of features per frame	162

D. Deep Belief Network

Once the features are extracted, the training of a deep belief network can be done. As an example method we have chosen the transfer learning approach by Islam et al. [21]. They trained their Deep Belief Network (DBN) on the TIMIT dataset [30]. The classification is performed in two steps, pre-training and fine-tuning. In the first step, the DBN learns the input feature in an unsupervised manner in different layers. A stack of layers are learned using the restricted Boltzman machine algorithm. The states are notable only in the visible layer. The DBN learns the hidden features via the following energy function:

$$E(v,h) = -\sum_{i \in input} b_i v_i - \sum_{j \in f\,ea} b_j h_j - \sum_{i,j} v_i h_j w_{ij}, \tag{3}$$

where v_i and h_j represents the binary states of input i and feature j, respectively. Attributes b_i and b_j are the biases for input i and feature j and w_{ij} is the weight between them. In the second, fine-tuning step the truth is attached on the topmost layer with the pre-trained weights. The fine-tuning is a supervised procedure, thus a soft-max layer is added on top of the learned weight so the weights could be fine-tuned for the phoneme cases. The model uses stochastic gradient descent algorithm for weight optimization. To determine the probability of the visible vector, the following function is used:

$$p(v) = \sum_{h \in H} p(v,h) = \frac{\sum_h exp(-E(v,h))}{\sum_{u,g} exp(-E(u,g))}, \tag{4}$$

where H is the set of all possible binary hidden vectors in the DBN.

E. Transfer Learning

Transfer learning is proved to be notably useful within all the deep learning methods. This technique is useful especially when there is limited training data. It consists of transferring the knowledge from a small dataset to another previously trained model, which was trained on a similar domain [22].

Once the model is trained, transfer learning approach can be applied on different layers of the trained model. The following transfer learning approach is modelled by Islam et al. [21] following the DBN modelling (see previous subsection) and it contains the following steps:

1) Training of a DBN model using all the samples from the TIMIT dataset for 39 phoneme classes, see Table I.
2) The FEMH training dataset is added to the trained DBN model to find the representation in a given layer.
3) An SVM classifier model is trained with a linear kernel and grid optimization for the new representation of the FEMH data, an SVM to find the optimal parameters.
4) The trained SVM model predicts the unlabelled testing data in the FEMH dataset.
5) Repeating the whole procedure for all the layers of the DBN model.

V. Discussion

In this paper we have discussed the process of voice pathology detection. We showed some notable results achieved using some machine learning techniques. We also observed some auxiliary methods used in machine learning algorithms. Since the deep learning and transfer learning approaches tent to be more precise in comparison with the traditional voice recognition methods, we can consider more investigation in voice detection using deep learning techniques to achieve more accurate results. Convolutional neural network showed up to be very effective in extracting important features from the spectograms of voice recordings, which helps in diagnosis. Deep belief network is useful for making the system more robust by initializing the weights. In the future work we will further analyze and experiment with optimizing as well as upgrading the existing algorithms or combining the used methods, respectively so we can achieve better performance. Transfer learning and CNN based feature extraction could potentially provide an additional approach to the automatic voice pathology detection problem.

Acknowledgment

This work was supported by the Slovak Research and Development Agency under contract No. APVV-16-0211.

References

[1] S.-H. Fang, Y. Tsao, M.-J. Hsiao, J.-Y. Chen, Y.-H. Lai, F.-C. Lin, and C.-T. Wang, "Detection of Pathological Voice Using Cepstrum Vectors: A Deep Learning Approach," *Journal of Voice*, vol. 33, no. 5, pp. 634–641, 2019.

[2] S. R. Schwartz, S. M. Cohen, S. H. Dailey, R. M. Rosenfeld, E. S. Deutsch, M. B. Gillespie, E. Granieri, E. R. Hapner, C. E. Kimball, H. J. Krouse *et al.*, "Clinical practice guideline: hoarseness (dysphonia)," *Otolaryngology–Head and Neck Surgery*, vol. 141, no. 1_suppl, pp. 1–31, 2009.

[3] M. R. McNeil, D. Robin, and R. Schmidt, *Clinical management of sensorimotor speech disorders*. Thieme New York, 1997.

[4] R. D. Kent, "Research on speech motor control and its disorders: A review and prospective," *Journal of Communication disorders*, vol. 33, no. 5, pp. 391–428, 2000.

[5] L. E. DeLisi, "Speech disorder in schizophrenia: review of the literature and exploration of its relation to the uniquely human capacity for language," *Schizophrenia bulletin*, vol. 27, no. 3, pp. 481–496, 2001.

[6] P. Lieberman, E. Kako, J. Friedman, G. Tajchman, L. S. Feldman, and E. B. Jiminez, "Speech production, syntax comprehension, and cognitive deficits in parkinson's disease," *Brain and language*, vol. 43, no. 2, pp. 169–189, 1992.

[7] Y. LeCun, L. Bottou, Y. Bengio, and P. Haffner, "Gradient-based learning applied to document recognition," *Proceedings of the IEEE*, vol. 86, no. 11, pp. 2278–2324, 1998.

[8] B. Schuller, S. Steidl, A. Batliner, E. Nöth, A. Vinciarelli, F. Burkhardt, R. v. Son, F. Weninger, F. Eyben, T. Bocklet *et al.*, "The interspeech 2012 speaker trait challenge," in *Thirteenth Annual Conference of the International Speech Communication Association*, 2012.

[9] J. Kim, N. Kumar, A. Tsiartas, M. Li, and S. S. Narayanan, "Automatic intelligibility classification of sentence-level pathological speech," *Computer speech & language*, vol. 29, no. 1, pp. 132–144, 2015.

[10] B. Woldert-Jokisz, "Saarbruecken voice database," 2007.

[11] G. E. Hinton, S. Osindero, and Y.-W. Teh, "A fast learning algorithm for deep belief nets," *Neural computation*, vol. 18, no. 7, pp. 1527–1554, 2006.

[12] A. Krizhevsky, I. Sutskever, and G. E. Hinton, "Imagenet classification with deep convolutional neural networks," in *Advances in neural information processing systems*, 2012, pp. 1097–1105.

[13] D. Banerjee, K. Islam, K. Xue, G. Mei, L. Xiao, G. Zhang, R. Xu, C. Lei, S. Ji, and J. Li, "A deep transfer learning approach for improved post-traumatic stress disorder diagnosis," *Knowledge and Information Systems*, vol. 60, no. 3, pp. 1693–1724, 2019.

[14] P. Liu, S. Han, Z. Meng, and Y. Tong, "Facial expression recognition via a boosted deep belief network," in *Proceedings of the IEEE conference on computer vision and pattern recognition*, 2014, pp. 1805–1812.

[15] M. M. U. Chowdhury, F. Hammond, G. Konowicz, C. Xin, H. Wu, and J. Li, "A few-shot deep learning approach for improved intrusion detection," in *2017 IEEE 8th Annual Ubiquitous Computing, Electronics and Mobile Communication Conference (UEMCON)*. IEEE, 2017, pp. 456–462.

[16] D. Martínez, E. Lleida, A. Ortega, A. Miguel, and J. Villalba, "Voice pathology detection on the Saarbrücken voice database with calibration and fusion of scores using multifocal toolkit," in *Advances in Speech and Language Technologies for Iberian Languages*. Springer, 2012, pp. 99–109.

[17] N. Souissi and A. Cherif, "Dimensionality reduction for voice disorders identification system based on mel frequency cepstral coefficients and support vector machine," in *2015 7th international conference on modelling, identification and control (ICMIC)*. IEEE, 2015, pp. 1–6.

[18] A. Al-nasheri, G. Muhammad, M. Alsulaiman, and Z. Ali, "Investigation of voice pathology detection and classification on different frequency regions using correlation functions," *Journal of Voice*, vol. 31, no. 1, pp. 3–15, 2017.

[19] D. Hemmerling, A. Skalski, and J. Gajda, "Voice data mining for laryngeal pathology assessment," *Computers in biology and medicine*, vol. 69, pp. 270–276, 2016.

[20] P. Harar, J. B. Alonso-Hernandezy, J. Mekyska, Z. Galaz, R. Burget, and Z. Smekal, "Voice pathology detection using deep learning: a preliminary study," in *2017 international conference and workshop on bioinspired intelligence (IWOBI)*. IEEE, 2017, pp. 1–4.

[21] K. A. Islam, D. Perez, and J. Li, "A transfer learning approach for the 2018 FEMH Voice Data Challenge," in *2018 IEEE International Conference on Big Data (Big Data)*. IEEE, 2018, pp. 5252–5257.

[22] S. J. Pan and Q. Yang, "A survey on transfer learning," *IEEE Transactions on knowledge and data engineering*, vol. 22, no. 10, pp. 1345–1359, 2009.

[23] Z. Dankovičová, D. Sovák, P. Drotár, and L. Vokorokos, "Machine Learning Approach to Dysphonia Detection," *Applied Sciences*, vol. 8, no. 10, p. 1927, 2018.

[24] H. Kasuya, S. Ogawa, Y. Kikuchi, and S. Ebihara, "An acoustic analysis of pathological voice and its application to the evaluation of laryngeal pathology," *Speech communication*, vol. 5, no. 2, pp. 171–181, 1986.

[25] A. A. Dibazar, S. Narayanan, and T. W. Berger, "Feature analysis for automatic detection of pathological speech," in *Proceedings of the Second Joint 24th Annual Conference and the Annual Fall Meeting of the Biomedical Engineering Society][Engineering in Medicine and Biology*, vol. 1. IEEE, 2002, pp. 182–183.

[26] M. Eye and E. Infirmary, "Voice disorders database, version. 1.03 (cd-rom)," *Lincoln Park, NJ: Kay Elemetrics Corporation*, 1994.

[27] T. A. Mesallam, M. Farahat, K. H. Malki, M. Alsulaiman, Z. Ali, A. Al-Nasheri, and G. Muhammad, "Development of the Arabic voice pathology database and its evaluation by using speech features and machine learning algorithms," *Journal of healthcare engineering*, vol. 2017, 2017.

[28] J. R. Orozco-Arroyave, J. D. Arias-Londoño, J. F. Vargas-Bonilla, M. C. Gonzalez-Rátiva, and E. Nöth, "New Spanish speech corpus database for the analysis of people suffering from parkinson's disease." in *LREC*, 2014, pp. 342–347.

[29] H. Wu, J. Soraghan, A. Lowit, and G. Di Caterina, "A deep learning method for pathological voice detection using convolutional deep belief networks," *Interspeech 2018*, 2018.

[30] J. S. Garofolo, L. F. Lamel, W. M. Fisher, J. G. Fiscus, and D. S. Pallett, "DARPA TIMIT acoustic-phonetic continous speech corpus CD-ROM. NIST speech disc 1-1.1," *NASA STI/Recon technical report n*, vol. 93, 1993.

Research of superconductivity in strongly disordered systems by scanning tunneling microscopy

[1]*Marek KUZMIAK (1st year),*
Supervisor: [2]*Pavol SZABÓ*

[1]Dept. of Physics, FEI TU of Košice, Slovak Republic
[1,2]Centre of Low Temperature Physics, Institute of Experimental Physics Slovak Academy of Sciences, Slovak Republic

[1]marek.kuzmiak@tuke.sk, [2]pszabo@saske.sk

***Abstract*—My research group is dealing with the experimental study of superconducting materials with competing orders. My colleagues are studying the coexitence of superconductivity with magnetism and the influence of charge density waves and multiband Fermi level to the superconducting characteristics. The subject of my PhD work is the study of the influence of low dimensionality and nano-size effects for the superconducting properties in ultra-thin films. During the first year of my thesis I am studying the physical properties of superconductors and strongly disordered systems, the influence of applied magnetic field for the basic superconducting parameters and acquainting with Low Temperature Scanning Tunneling Microscopy (STM) measurements. In this paper I am presenting the actual state of my studies.**

***Keywords*—Superconductivity, Disordered system, SIT, Scanning tunneling microscopy.**

I. Introduction

This paper is dealing with the basic physical properties of strongly disordered superconducting materials. After short introduction, the characteristic properties of superconductors, as the zero resistance and the ideal diamagnetism are presented. I discuss the influence of disorder for the superconducting state and show possible mechanisms of the superconductor-insulator transition (SIT). I show the basic differences between the bosonic and the fermionic way of the SIT. At the end, the Low Temperature Scanning Tunneling Microscopy is presented as an ideal experimental method for the study of local superconducting properties in strongly disordered superconductors.

II. Superconductivity

On 10 July 1908, the great Dutch physicist Heike Kamerlingh Onnes opened a new chapter in low temperature physics. He was able to reach first liquefied helium ^4He in the world. By the way, the boiling point of helium ^4He is $4.22\ K$ at normal atmospheric pressure. In addition, when we pump vapours of helium ^4He, we can reach a temperature around $1\ K$ too.

After some time, Heike Kamerlingh Onnes observed the behavior of various metals such as mercury, lead and tin, while he was cooling them in liquid helium ^4He. For example, he measured the electrical resistance of these various metals. One day, he discovered that at about $4.2\ K$ the electrical resistance of his mercury sample fell abruptly to zero. We can show it in Figure 1. He said that the electrical resistance of his mercury

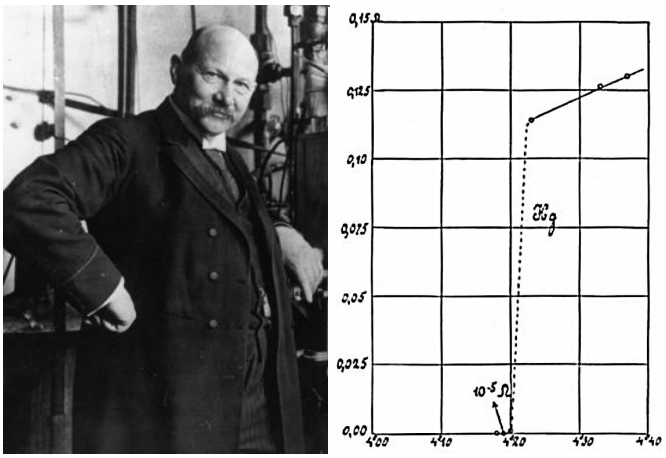

Fig. 1. Heike Kamerlingh Onnes and his a historic measured plot for mercury. The historic plot shows resistance (measure in Ω) versus temperature (measure in K). The experiment shows the superconducting transition at $4.20\ K$. Within $0.01\ K$, the electrical resistance jumped from unmeasurably small (less than 10^{-6}) to $0.1\ \Omega$.

sample was immeasurable. This interesting behaviour was naturally called superconductivity. A critical temperature T_C is characteristic of all superconducting materials. It's the temperature which the sample had when it transitioned from normal to superconducting state. On 28 April 1911, Heike Kamerlingh Onnes presented his discovery to the Royal Netherlands Academy of Art and Sciences. This day is officially called like the Day of Birth of Superconductivity [1], [2].

An important discovery in this area were made by the great German physicists Meissner and Ochsenfeld. In their article [3], they describe the so-called Meissner effect. This effect shows the difference of behaviour between a perfect conductor and a classical superconductor in the presence of magnetic field. As we can see in Figure 2, when cooling down the classical superconductor in the presence of applied magnetic field, the magnetic field is excluded from entering the superconductor after crossing the critical temperature T_C. The perfect conductor would tend to trap in the flux of magnetic field instead. The superconductor levitation in the presence of an external magnetic field is a possible consequence of this phenomenon. This is because the superconductor has the opposite magnetization M as an applied magnetic field H. It follows that $M = -H$. The magnetic induction B inside

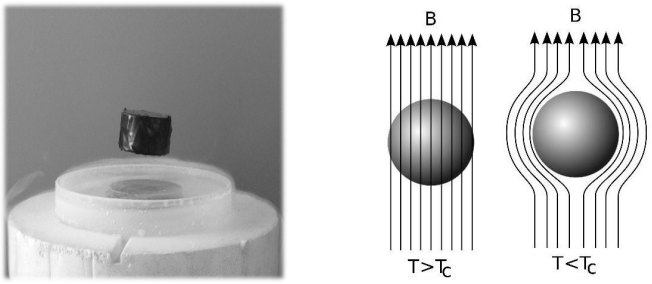

Fig. 2. The levitation of the magnet over superconductor and the graphical approximation of Meissner effect. Magnetic field lines are represented as arrows. These arrows are excluded from a superconductor when it's below its critical temperature T_C.

the superconductor is expressed in the equation

$$B = \mu_0(H + M) = 0 \ . \tag{1}$$

We can also say that they have discovered perfect diamagnetism. We know it from the equation of susceptibility χ which expresses the sensitivity of the material to the external magnetic field

$$\chi = \frac{M}{H} = \frac{-H}{H} = -1 \ . \tag{2}$$

In summary we can say that the zero electrical resistance and the perfect diamagnetism are basic properties of superconductors [4], [5], [6].

III. Disordered system

The solid state physics teaches us [7] that in classical metals the behaviour of free electrons is described by the Drude-Sommerfeld model. This model says that some electrons can move in a stationary and positively charged ion lattice because they aren't attached to atoms in any way. This electron scattering occurs in pure metals primarily due to thermal vibrations of the atomic lattice. We know about other types of electron scattering when a disorder is included in the system. The disorder can be introduced into the system with chemical or physical doping, introducing a defect in the atomic lattice, etc. When we are focusing to 2D materials, the electrical conductivity σ can be defined by the well known Drude formula

$$\sigma = \frac{ne^2\tau_{zr}}{m} \ , \tag{3}$$

where n is the density of charge carriers, e is the electron charge, m is the electron mass and τ_{zr} is the time period between two collisions. The electron-electron interactions are neglected in this case. The Pauli exclusion principle says that two or more identical fermions can't occupy the same quantum state within a quantum system simultaneously. Fermi energy E_F is the highest occupied quantum state in such the quantum system. In addition to Fermi energy E_F, we also introduce Fermi wave number k_F, Fermi velocity v_F, Fermi wavelength λ_F and a charge carrier density for a two-dimensional system n_{2D} with these expressions

$$k_F = \sqrt{\frac{2mE_F}{\hbar^2}} \ , \tag{4}$$

$$v_F = \frac{\hbar k_F}{m} = \frac{l_{zr}}{\tau_{zr}} \ , \tag{5}$$

$$\lambda_F = \frac{2\pi}{k_F} \ , \tag{6}$$

$$n_{2D} = \frac{k_F^2}{2\pi} \ , \tag{7}$$

where $\hbar$ is a reduced Planck constant, π a Archimedes' constant and l_{zr} is a mean free path, which is the average distance between two collisions. When we use these expressions in the Drude formula (3), we get the equation

$$\sigma_{2D} = \frac{k_F^2}{2\pi}\frac{e^2\tau_{zr}}{m} = \frac{k_F v_F e^2 \tau_{zr}}{2\pi\hbar} = \frac{e^2}{h}k_F l_{zr} \ , \tag{8}$$

where h is a Planck constant [8]. The system is in metallic state if $k_F l_{zr} \gg 1$. If the disorder of the system increases, the mean free path l_{zr} decreases proportionately. If the mean free path l_{zr} is gradually reduced to a value comparable to the interatomic distance $a \approx 1/k_F$, the electrons are strongly localised and the system becomes insulating. At this point, a metal-insulator transition occurs. The so-called Ioffe-Rogel criterion [9] applies, when $k_F l_{zr} \approx 1$. By applying this criterion to equation (8), we can express the maximum possible value of a specific electrical resistance in metallic state

$$R_{2D} = \frac{1}{\sigma_{2D}} = \frac{h}{e^2} \cong 25,8128 \ \text{k}\Omega \ . \tag{9}$$

In superconductors, the charge carriers are Cooper pairs whose charge is twice as high. By applying this criterion to equation (8), we can express the value of quantum resistance of the electron pair

$$R_{2DS} = \frac{h}{(2e)^2} \cong 6,4532 \ \text{k}\Omega \ . \tag{10}$$

The microscopic explanation of the electron localisation is generally called Anderson localisation [10]. The electron-electron interaction in such system was first described by Altshuler and Aronov [11]. Then they theoretically showed that it leads to logarithmic decrease of the electron density of states.

If the disorder is included in the superconducting system, the superconductor-insulator transition (SIT) can be observed. After the disorder increases, electrical resistance increases and the critical temperature T_C decreases. Then we can see a gradual transition from a state with zero electrical resistance (superconductor) to a state with measurable electrical resistance (insulator). We can see a demonstration of SIT in Figure 3. The disorder can be introduced with physical or chemical doping, applying a magnetic field, reducing a size of the sample (e.g. thickness) to the coherence length level or reduction of charge carrier density [12], [13].

The theoretical physics considers SIT to be a quantum phase transition. Compared to a classical phase transition, it can occur at absolute zero temperature. The quantum wave functions of electrons are localised, when the material is in its insulating state, as opposed to its superconducting state. Real experiments are executed at final temperatures, where the thermal excitations affect the resultant behaviour of the sample. A possible overview of the SIT was elaborated in article [14] by Gantmakher and Dolgopolov. They write about several theoretically predicted mechanisms of SIT. We can see three basic theoretically predicted mechanisms described by their phase diagrams in Figure 4. The Figure 4 a) shows the so-called fermionic scenario, when it happens a continuous transition from the insulating to the metallic and then to the superconducting state. The Figure 4 b) shows the so-called bosonic scenario for low temperatures, when it happens a directly transition from the superconducting

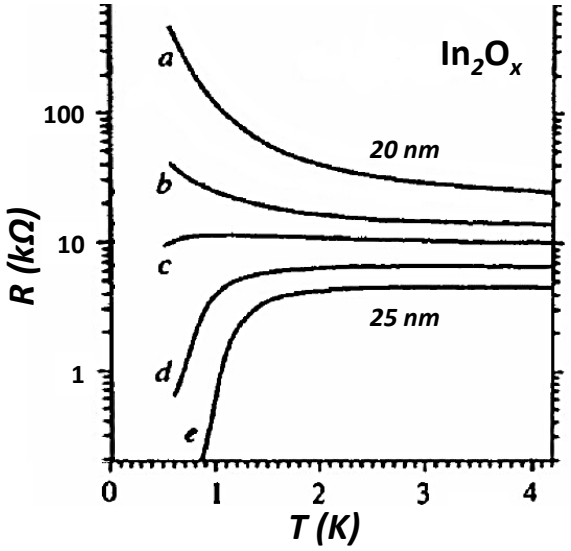

Fig. 3. SIT of In_2O_x thin films. The plot shows resistance (measure in Ω) versus temperature (measure in K). We can see characteristics for thin films $(20 - 25\ nm)$ in a zero magnetic field.

to the insulating state by localisation of the Cooper pairs. The Figure 4 c) shows phase diagram of transition, which was proposed by Larkin [15]. The transition from metallic to insulating state is impossible at the temperature range where the sample is superconducting.

Today's world research community is trying to find out which theoretical mechanism of SIT is correct.

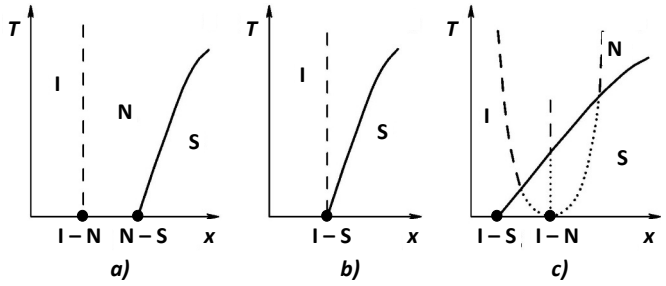

Fig. 4. Phase diagrams of SIT, where T is temperature, x is control parameter, I is insulator, N is metal and S is superconductor. Quantum transitions are represented by the dots on the x-axis. Thermodynamic transitions are represented by the solid lines. Boundaries between the regions are represented by the dashed lines. Virtual boundaries are represented by the dotted lines.

Moreover, in recent years it has been said that the bosonic scenario is a universal SIT scenario. The bosonic mechanism SIT is shown in Figure 5 a). The bosonic scenario was observed in disordered TiN [16], NbN [17] and InO [18] samples. A typical behavior of this quantum transition is:

1) Together with increasing disorder the superconducting critical temperature T_C decreases faster than superconducting energy gap Δ. At the same time the coupling strength parameter $\frac{2\Delta(0)}{k_B T_C}$ increases and Cooper pair islands may locally persist even on the insulating side of the transition [16], [18].
2) Spatial inhomogeneity of the Δ parameter was observed around SIT in the range coherent length ξ [16], [17], [18].
3) Tunneling spectra measured above T_C show the presence of a pseudogap. It's a possible result of incoherent clusters of Cooper pairs in normal state [16], [17], [18].

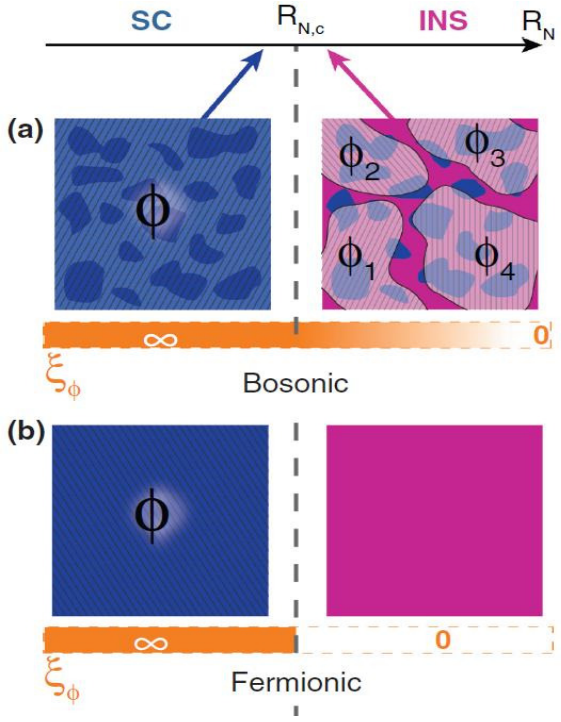

Fig. 5. Illustrations of disorder-driven SITs involving the emergence of inhomogeneities that lead to Cooper pair islanding (bosonic SIT) and pair breaking in homogeneous films (fermionic SIT). The superconducting (SC) to insulating (INS) film transitions occur with increasing normal state sheet resistance R_N, at a critical value R_{Nc}. Blue regions are paired, and pink regions are unpaired. The orange bar depicts the expected Cooper pair phase coherence length ξ_ϕ, which sets the size of the phase coherent regions in the bosonic insulator. The parallel stripes represent the phase angle of the superconducting wave function, denoted as ϕ [20].

4) In the thin films with the highest disorder, superconducting vortices were not seen. Inability to observe the vortex lattice close to the critical point is another hint towards gradual loss of long-range coherence [16], [17].

Although a lot of researchers think that the bosonic scenario is a universal SIT scenario, our scientific group has shown, that the SIT in highly disordered MoC thin films is realized through the fermionic scenario [19]. The fermionic mechanism SIT is shown in Figure 5 b). A typical behavior of this quantum transition is:

1) Together with increasing disorder the superconducting critical temperature T_C decreases proportionally with the decrease of the energy gap Δ. Than the coupling strength parameter $\frac{2\Delta(0)}{k_B T_C}$ remains constant and the gap apparently vanishes at the critical point.
2) A homogeneous superconductivity is observed around the SIT.
3) A pseudogap wasn't observed in measurements above the critical temperature T_C.

IV. Scanning Tunneling Microscopy

The scanning tunneling microscopy (STM) was invented in 1981 by Gerd Binning and Heinrich Roher [21] in IBM laboratory in Zurich. They won a Nobel Prize in Physics in 1986 for their invention. Scanning a surface of a conducting sample with atomic resolution, atomic manipulation and direct measurement of local density of states are the main possibilities that STM allows. Moreover, there is an option of doing a map of tunneling spectra with the help of combining

microscopy and spectroscopy option of STM. In this case in each point of a topography a tunneling spectrum is measured as well and effectively a map of local density of states is obtained along with the topography.

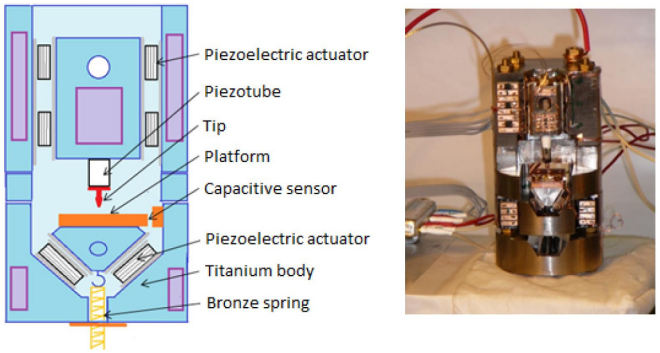

Fig. 6. Schematic illustration and photo of the head of our home made STM.

Our group has a home made STM. The STM is built in a Pan Slider design, which is known for its very high rigidity and is mainly used in vacuum and cryogenic environments. A scheme and a photo of the STM are shown in Figure 6. The movement in our STM is realized via a piezoelectric actuator. The scanning is performed using the tip. The tip is usually made of cut bulk gold wire and for this reason besides the sample there is also a bulk gold on the platform. This serves for the sharpening of the tip by controlled collision method, where the tip is repeatedly pushed into the sample of the same material and retracted. This happens until one atom remains on the tip.

Cooling of our system is secured by the commercial JANIS ^{3}He refrigerator. Structure of this refrigerator is shown in Figure 7. Head of our STM is thermally connected to the ^{3}He pot, which allows us to cool the sample down to 300 mK. This is the temperature of liquid ^{3}He, which is being pumped by a sorption pump with active charcoal

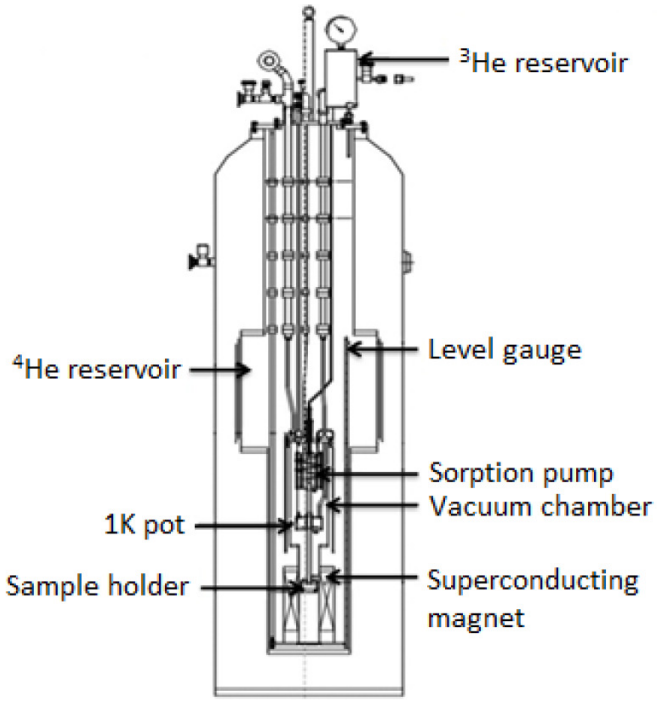

Fig. 7. Structure of the commercial JANIS refrigerator, model HE-3-SSV.

inside. Head of our STM is placed in the superconducting magnet, which allows us to apply magnetic field up to 8 Tesla.

In summary we can also say, that the STM is a very useful device for the study of local superconducting properties in the strongly disordered systems.

V. Conclusion

The experimental study of SIT is very interesting not only from the view of basic research but also from the view of applications. In the age of microelectronics and endless miniaturization of the electronic circuits it is very important to know the applicability of the used materials. In my thesis I will try to shed some light to the problem of nano size effects in metals and some superconducting materials. After the first year of basic studies of superconductivity and STM methods I will continue in thin film preparing and performing real physical experiments.

Acknowledgment

This work was supported by the Ministry of Education, Science, Research and Sport of the Slovak Republic and the Slovak Academy of Sciences under contracts No. VEGA 1/0409/15, VEGA 2/049/16, APVV-14-0605, COST CA16218 Nanocohybri and by the U.S. Steel Košice.

References

[1] D. van Delft and P. Kes, "The discovery of superconductivity," *Physics Today*, vol. 63, pp. 38–43, September 2010.
[2] M. Tinkham, *Introduction to superconductivity (2nd ed.)*. McGraw Hill Book Co., NY, USA: University Science Books, 2004.
[3] W. Meissner and R. Ochsenfeld, "Ein neuer Effekt bei Eintritt der Supraleitfähigkeit," *Naturwissenschaften*, vol. 21, pp. 787–788, November 1933.
[4] P. Samuely and col., *Kryofyzika a nanoelektronika*. Košice: ÚEF SAV, 2011.
[5] P. Valko, *Supravodivost'*. Zlín: Kniha Zlín, 2011.
[6] S. Takácz and L. Cesnak, *Supravodivost'*. Bratislava: Alfa, 1979.
[7] N. D. Ashcroft and N. D. Mermin, *Solid State Physics*. Brooks Cole, NY, USA: University Science Books, 1976.
[8] C. Kittel, *Introduction to Solid State Phzsics*. John Wiley Sons, Inc., NY, USA: University Science Books, 2004.
[9] A. F. Ioffe and A. R. Regel, "Non-crystalline, amorphous and liquid electronic semiconductors," *Progress in Semiconductors*, vol. 4, pp. 237–291, 1960.
[10] P. W. Anderson, "Absence of Diffusion in Certain Random Lattices," *Physical Review*, vol. 109, pp. 1492–1505, March 1958.
[11] B. L. Altshuler and A. G. Aronov, "Electron-electron Interactions in Disordered Systems," *Elsevier*, vol. 10, pp. 1–153, 1985.
[12] D. B. Haviland and col., "Onset of Superconductivity in the two-dimensional limit," *Physical Review Letters*, vol. 62, pp. 2180–2183, May 1989.
[13] A. M. Goldman, "Superconductor-insulator transitions," *International Journal of Modern Physics B*, vol. 24, pp. 4081–4101, 2010.
[14] V. F. Gantmakher and V. T. Dolgopolov, "Superconductor-insulator quantum phase transition," *Physics Uspekhi*, vol. 53, pp. 1–49, April 2010.
[15] A. I. Larkin, "Superconductor-insulator transitions in films and bulk materials," *Annalen der Physik*, vol. 8, pp. 785–794, November 1999.
[16] B. Sacepe and col., "Disorder-Induced Inhomogeneities of the Superconducting State Close to the Superconductor-Insulator Transition," *Physical Review Letters*, vol. 101, p. 157006, October 2008.
[17] M. Chand and col., "Phase diagram of the strongly disordered s-wave superconductor NbN close to the metal-insulator transition," *Physical Review B*, vol. 85, p. 014508, January 2012.
[18] B. Sacepe and col., "Localization of preformed Cooper pairs in disordered superconductors," *Nature Physics*, vol. 7, pp. 239–244, 2011.
[19] P. Szabó and col., "Fermionic scenario for the destruction of superconductivity in ultrathin MoC films evidenced by STM measurements," *Physical Review B*, vol. 93, p. 014505, January 2016.
[20] S. M. Hollen and col., "Collapse of the Cooper pair phase coherence length at a superconductor-to-insulator transition," *Physical Review B*, vol. 87, p. 054512, February 2013.
[21] G. Binning and H. Rohrer, "Scanning tunneling microscopy," *Surface Science*, vol. 152–153, pp. 17–26, April 1985.

Review of Online Supervised Learning Method

[1]*Andrinandrasana David Rasamoelina (1st year),*
Supervisor: [2]*Peter Sinčak*

[1,2]Dept. of Cybernetics and Artificial Intelligence, FEI TU of Košice, Slovak Republic

[1]andrijdavid@tuke.sk, [2]peter.sincak@tuke.sk

***Abstract*—Traditional machine learning algorithms works in a batch learning or offline learning manner. It works considerably on a variety of problems. However, this does not hold when we have a stream of data and we have to update our model in real time. Online learning techniques overcome this challenge. In this work we provide a review of best known online supervised learning method.**

***Keywords*—Online Learning, Machine Learning, Optimization.**

I. Introduction

Most of the time, traditional machine learning algorithms works in a batch learning or offline learning manner. As in batch learning our model is trained by some specific learning algorithm using the entire training set and afterwards the model is deployed for inference without the seldom of performing any update. Such learning methods suffer from expensive retraining cost when dealing with new training data, and thus are poorly scalable for real-world applications. However in this era of big data, traditional methods become more restricted, especially when we have access to live data feeds/stream. Therefore elaborating new technic and method for online learning becomes a primary importance.

Online learning is a subfield of machine learning that includes an important family of learning techniques which are devised to learn models incrementally from data in a sequential manner. This method overcomes the drawbacks of traditional batch learning and permits the update of the model intently, instantly and efficiently when new training data instances arrive. Therefore, online learning algorithms are far more efficient and scalable for large-scale machine learning tasks in real-world where data are not only large, but also arrives at a high velocity.

As in offline learning algorithm, we have multiple types of online learning depending on the task. First, online supervised learning where full feedback information is available [1]; then online learning with limited feedback [2], and finally online unsupervised learning [3] where no feedback is available.

In this study we will only focus on online supervised learning.

II. Related Work

Wang et al. [1] proposes a new method for online supervised learning for Spiking Neural Network [4] with adaptive structure. Li et al. [5] proposes a collaborative online multitask learning method, which learns a global model over the entire data of multiple tasks. Cesa-Bianchi and Lugosi [6], Shalev-Shwartz et al. [7] gives an interesting overview of online learning and online convex optimization. Woeginger and Fiat [8], Bottou [9], Rakhlin and Tewari [10], Blum [11] provide a tutorial and notes on online learning algorithm. Furao et al. [12] proposes an enhanced self-organizing incremental neural network and improves upon [13].

III. Theory

Spam email detection can be considered as an online binary classification problem [14, 15, 16]. This problem can be expressed as follows: consider a sequence of instances/objects represented in a vector space, $\mathbf{x}_t \in \mathbb{R}^d$, where t denotes the t-th round and d is the dimensionality, and $y_t \in \{+1, -1\}$ denote the true class label. On the t-th round, an instance $\mathbf{x}_t$ is received by the learner, which then employs a binary classifier $\mathbf{w}_t$ to make a prediction on $\mathbf{x}_t$, e.g., $\hat{y}_t = \text{sign}(\mathbf{w}_t^\top \mathbf{x}_t)$ that outputs $\hat{y}_t = +1$ if $\mathbf{w}_t^\top \mathbf{x}_t \geq 0$ and $\hat{y}_t = -1$ otherwise. After the prediction step, the learner receives the ground true label y_t and can properly measure the loss, e.g., using the hinge-loss $\ell_t(\mathbf{w}_t) = \max\left(0, 1 - y_t \mathbf{w}_t^\top \mathbf{x}_t\right)$ [17]. Whenever the loss is nonzero, the learner updates the prediction model from $\mathbf{w}_t$ to $\mathbf{w}_{t+1}$ by applying some strategy on the training example $(\mathbf{x}_t, y_t)$. This procedure is summarized in Algorithm 1.

Algorithm 1: Online Binary Classification Algorithm.

```
Initialize the predictor w_1;
for t = 1, 2, ..., T do
    Receive instance: x_t ∈ R^d;
    Predict ŷ_t = sign(w_t^⊤ x_t) as the label of x_t;
    Receive the ground truth: y_t ∈ {−1, +1};
    Loss: ℓ_t(w_t) which is a convex loss function on both
    w_t^⊤ x_t and y_t;
    Update the prediction model w_t to w_{t+1};
end for
```

By using this algorithm over a sequence of T rounds, the number of mistakes made by the online learner can be calculated as $M_T = \sum_{t=1}^{T} \mathbb{I}(\hat{y}_t \neq y_t)$.

As for classical learning algorithms, the goal of an online learning task is to minimize the regrets against the best fixed model in hindsight, defined as:

$$R_T = \sum_{t=1}^{T} \ell_t(\mathbf{w}_t) - \min_{\mathbf{w}} \sum_{t=1}^{T} \ell_t(\mathbf{w}) \tag{1}$$

Where the second term is the loss of the optimal model $\mathbf{w}^*$. This loss can only be known in retrospection after seeing all the instances alongside their corresponding labels.

From the theoretical perspective of regret minimization, if an online algorithm guarantees that its regret is sublinear as a function of T, i.e., $R_T = o(T)$, it implies that

$\lim_{T\to\infty} R(T)/T = 0$. Which means that on average the learner performs almost as well as the best fixed model in hindsight.

A. Convex Optimization

Many online learning problems can essentially be formulated as an online convex optimization task [18, 19]. In the following part, we introduce some basics of online convex optimization task.

An online convex optimization task typically consists of two major elements: a convex set $\mathcal{S}$ and a convex cost function $\ell_t(\cdot)$. At each time step t, the online algorithm decides to choose a weight vector $\mathbf{w}_t \in \mathcal{S}$; after that, it suffers a loss $\ell_t(\mathbf{w}_t)$, which is computed based on a convex cost function $\ell_t(\cdot)$ defined over $\mathcal{S}$. The goal of the online algorithm is to choose a sequence of decisions $\mathbf{w}_1, \mathbf{w}_2, \ldots$ such that the regret in hindsight can be minimized.

More properly, an online algorithm aims to obtain a low regret R_T after T rounds, where the regret R_T is defined as:

$$R_T = \sum_{t=1}^{T} \ell_t(\mathbf{w}_t) - \inf_{\mathbf{w}^* \in \mathcal{S}} \sum_{t=1}^{T} \ell_t(\mathbf{w}^*), \tag{2}$$

where $\mathbf{w}^*$ is the solution that minimizes the convex objective function $\sum_{t=1}^{T} \ell_t(\mathbf{w})$ over $\mathcal{S}$.

e.g., considering an online binary classification task for training online Support Vector Machines (SVM) [20] from a sequence of labeled instances $(\mathbf{x}_t, y_t), t = 1, \ldots, T$, where $\mathbf{x}_t \in \mathcal{R}^d$ and $y_t \times \{+1, -1\}$. The loss function can be defined as $\ell(\cdot)$ as $\ell_t(\mathbf{w}_t) = \max(0, 1 - y_t \mathbf{w}^\top \mathbf{x})$ and the convex set S as $\{\forall \mathbf{w} \in \mathcal{R}^d | \|\mathbf{w}\| \leq C\}$ for some constant parameter C. A variety of algorithms exists to solve this problem.

Readers are forwarded to the books Shalev-Shwartz [2], Hazan et al. [18] for an in depth treatment of this subject.

IV. Online Supervised Learning

Methods of online supervised learning can be categorized in two: first and second order method. First-order learning leverage the model's first-order information during learning process. I.e only exploit the first order derivative information of the gradient for the online optimization tasks. However unlike the first-order online learning algorithms, second-order online learning algorithms exploit both first-order and second-order information in order to accelerate the optimization convergence. Despite improved learning performance, second-order online learning algorithms often fall short in higher computational complexity. In this study we only focus on first-order learning algorithm which is described in the next section.

A. Perceptron

Perceptron [21, 22, 23] is the oldest algorithm for online learning. Algorithm 2 presents the Perceptron algorithm for online binary classification.

In theory, by assuming the data is separable with some margin γ, the Perceptron algorithm makes at most $\left(\frac{R}{\gamma}\right)^2$ mistakes, where the margin γ is defined as $\gamma = \min_{t\in[T]} |\mathbf{x}_t \cdot \mathbf{w}^*|$ and R is a constant such that $\forall t \in [T], \|\mathbf{x}_t\| \leq R$. The larger the margin γ is, the tighter the mistake bound will be.

Several versions of the Perceptron algorithms have been proposed in literature. One simple variation is the **normalized perceptron** algorithm, which only differs in the updating rule as follows:

$$\mathbf{w}_{t+1} = \mathbf{w}_t + y_t \frac{\mathbf{x}_t}{\|\mathbf{x}_t\|}$$

The mistake bound of the **normalized perceptron** algorithm can be improved from $\left(\frac{R}{\gamma}\right)^2$ to $\left(\frac{1}{\gamma}\right)^2$ for the separable case due to the normalization effect.

Algorithm 2: Perceptron

INIT: $\mathbf{w}_1 = 0$
for $t = 1, 2, \ldots, T$ **do**
  Given an incoming instance $\mathbf{x}_t$, predict
  $\hat{y}_t = f_t(\mathbf{x}_t) = sign(\mathbf{w}_t \cdot \mathbf{x}_t)$;
  Receive the true class label $y_t \in \{+1, -1\}$;
  if $\hat{y}_t \neq y_t$ **then**
    $\mathbf{w}_{t+1} \leftarrow \mathbf{w}_t + y_t \mathbf{x}_t$;
  end if
end for

B. Winnow

Unlike the Perceptron algorithm which uses additive updates, Winnow [24] makes use of multiplicative updates rules. The problem setting is slightly different from the Perceptron: $\mathcal{X} = \{0, 1\}^d$ and $y \in \{0, 1\}$. The goal is to learn a **monotone disjunction classifier** $f(x_1, \ldots, x_n) = x_{i_1} \vee \ldots \vee x_{i_k}$ where $i_k \in 1, \ldots, d$. The separating hyperplane for this classifier is given by $x_{i_1} + \ldots + x_{i_k}$. Algorithm 3 illustrate the Winnow algorithm.

Algorithm 3: Winnow

INIT: $\mathbf{w}_1 = \mathbf{1}^d$, constant $\alpha > 1$ (e.g.,$\alpha = 2$)
for $t = 1, 2, \ldots, T$ **do**
  Given an instance $\mathbf{x}_t$, predict $\hat{y}_t = \mathbb{I}_{\mathbf{w}_t \cdot \mathbf{x}_t \geq \theta}$ (outputs 1 if statement holds and 0 otherwise);
  Receive the true class label $y_t \in \{1, 0\}$;
  if $\hat{y}_t = 1, y_t = 0$ **then**
    set $w_i = 0$ for all $x_{t,i} = 1$ ("elimination" or "demotion"),
  end if
  if $\hat{y}_t = 0, y_t = 1$ **then**
    set $w_i = \alpha w_i$ for all $x_{t,i} = 1$ ("promotion").
  end if
end for

The Winnow algorithm has a mistake bound of $\alpha k(\log_\alpha \theta + 1) + n/\theta$ where $\alpha > 1$ and $\theta \geq 1/\alpha$ where the target function is a k-literal monotone disjunction.

C. Passive-Aggressive Online Learning (PA)

This is methods follows the principle of margin-based learning [25]. Specifically, given an instance $\mathbf{x}_t$ at round t, PA formulates the updating optimization as follows:

$$\mathbf{w}_{t+1} = \arg\min_{\mathbf{w}\in\mathbb{R}^d} \frac{1}{2}||\mathbf{w} - \mathbf{w}_t||^2 \qquad s.t. \;\; \ell_t(\mathbf{w}) = 0 \tag{3}$$

where $\ell_t(\mathbf{w}) = \max(0, 1 - y_t \mathbf{w} \cdot \mathbf{x}_t)$ is the hinge loss. The above resulting update is passive whenever the hinge loss is zero, i.e., $\mathbf{w}_{t+1} = \mathbf{w}_t$ whenever $\ell = 0$. In contrast,

whenever the loss is nonzero, the approach will force $\mathbf{w}_{t+1}$ aggressively to satisfy the constraint regardless of any step-size; the algorithm is therefore named after this behaviour as **Passive-Aggressive** [25, 26]. Specifically, it aims to keep the updated classifier $\mathbf{w}_{t+1}$ to stay close to the previous classifier (passiveness) and ensure every incoming instance to be classified correctly by the updated classifier (aggressiveness). This algorithm assumes that the training data is always separable, which may not be true for noisy training data in real-world applications. To overcome this limitation, two variants of PA relax the assumption as:

$$\begin{aligned} &\text{PA}-\text{I}: \mathbf{w}_{t+1} = \arg\min_{\mathbf{w}\in\mathbb{R}^d} \frac{1}{2}||\mathbf{w}-\mathbf{w}_t||^2 + C\xi \\ &\text{subject to} \quad \ell_t(\mathbf{w}) \leq \xi \quad \text{and} \quad \xi \geq 0 \\ &\text{PA}-\text{II}: \mathbf{w}_{t+1} = \arg\min_{\mathbf{w}\in\mathbb{R}^d} \frac{1}{2}||\mathbf{w}-\mathbf{w}_t||^2 + C\xi^2 \\ &\text{subject to} \quad \ell_t(\mathbf{w}) \leq \xi \end{aligned} \tag{4}$$

where C is a positive parameter to balance the trade-off between *passiveness* and *aggressiveness*. By solving the three optimization tasks, we can derive the closed-form updating rules of three PA algorithms:

$$\mathbf{w}_{t+1} = \mathbf{w}_t + \tau_t y_t \mathbf{x}_t, \quad \tau_t = \begin{cases} \ell_t/||\mathbf{x}_t||^2 & \text{(PA)} \\ \min\{C, \ell_t/||\mathbf{x}_t||^2\} & \text{(PA-I)} \\ \frac{\ell_t}{||\mathbf{x}_t||^2 + \frac{1}{2C}} & \text{(PA-II)} \end{cases}$$

It is important to note a significant difference between Passive-Aggressive and Perceptron algorithms. As perceptron only changes the weight if there is an error in the classification. Nonetheless, when the loss is nonzero even if the classification is correct, PA algorithms actively make an update. In theory [25], PA algorithms have comparable error limits, but empirically PA algorithms often outperform Perceptron considerably. The PA algorithms are outlined in Algorithm 4.

Algorithm 4: Passive Aggressive Algorithms

INIT: $\mathbf{w}_1$, Aggressiveness Parameter C;
for $t = 1, 2, \ldots, T$ **do**
  Receive $\mathbf{x}_t \in \mathbb{R}^d$, predict $\hat{y}_t$ using $\mathbf{w}_t$;
  Suffer loss $\ell_t(\mathbf{w}_t)$;
  Set $\tau = \begin{cases} \ell_t/||\mathbf{x}_t||^2 & \text{(PA)} \\ \min\{C, \ell_t/||\mathbf{x}_t||^2\} & \text{(PA-I)} \\ \frac{\ell_t}{||\mathbf{x}_t||^2 + \frac{1}{2C}} & \text{(PA-II)} \end{cases}$
  Update $\mathbf{w}_{t+1} = \mathbf{w}_t + \tau_t y_t \mathbf{x}_t$;
end for

D. Online Gradient Descent (OGD)

Many online learning problems can be formulated as an online convex optimization task, which can be solved by applying the OGD algorithm. Let's consider the online binary classification using the hinge loss as an example, $\ell_t(\mathbf{w}) = \max(0, 1 - y_t \mathbf{w} \cdot \mathbf{x}_t)$. By applying the OGD algorithm, we can derive the updating rule as follows:

$$\mathbf{w}_{t+1} = \mathbf{w}_t + \eta_t y_t \mathbf{x}_t \tag{5}$$

where η_t is the learning rate. The OGD algorithm is outlined in Algorithm 5, where any generic convex loss function can be used. $\Pi_{\mathcal{S}}$ is the projection function to constrain the updated model to lie in the feasible domain.

Algorithm 5: Online Gradient Descent

INIT: $\mathbf{w}_1$, convex set $\mathcal{S}$, step size η_t;
for $t = 1, 2, \ldots, T$ **do**
  Receive $\mathbf{x}_t \in \mathbb{R}^d$, predict $\hat{y}_t$ using $\mathbf{w}_t$;
  Suffer loss $\ell_t(\mathbf{w}_t)$;
  Update $\mathbf{w}_{t+1} = \Pi_{\mathcal{S}}(\mathbf{w}_t - \eta_t \nabla \ell_t(\mathbf{w}_t))$
end for

OGD and PA share similar updating rules but differ in the way that OGD often employs some predefined learning rate scheme while PA selects the optimal learning rate of τt at each round but is subject to a predefined cost parameter of C. In literature, different OGD variants have been proposed to improve either theoretical bounds or practical issues, such as adaptive OGD [27], and mini-batch OGD [28, 29, 30], amongst others.

E. Mini-batch Online Gradient Descent

Mini-batch is a method where the incremental update is performed on an average of the subgradients with respect to several instances or one mini-batch at a time. The algorithm runs as follows:

Algorithm 6: Mini-Batch Online Gradient Descent

INIT: $\mathbf{w}_0 = 0$;
for $t = 0, 1, 2, \ldots, T$ **do**
  Receive b incoming instances $\mathbf{x}_{tb+1}, ...\mathbf{x}_{tb+b}$,
  $\hat{y}_{tb+i} = f_t(\mathbf{x}_{tb+i}) = \text{sign}(\mathbf{w}_t \cdot \mathbf{x}_{tb+i})$ for $i \in 1, ..., b$;
  Receive the ground truth $y_{tb+i} \in \{+1, -1\}$;
  Suffer loss for the t-th batch
  $\mathcal{L}_t(\mathbf{w}_t) = \frac{1}{b}\sum_{i=1}^{b} \ell(\mathbf{w}_t, \mathbf{x}_{tb+i})$;
  Update $\mathbf{w}_{t+1} = \Pi_{\mathcal{S}}(\mathbf{w}_t - \eta_t \nabla \mathcal{L}_t(\mathbf{w}_t))$;
end for

Multiple alogorithms from literature use mini-batch settings. E.g Pegasos [31] algorithm follows the above standard online gradient descent method and proved that when the loss function is the L2 regularized hinge loss [32], the expected regret is $O(ln(T)/(\lambda T))$, where λ is the parameter for the regularizer. Cotter et al. [33] improves the performance of previous algorithms by adopting accelerated gradient methods. Recently, Li et al. [34], Dekel et al. [28] considered the mini-batch methods in distributed setting.

F. Averaged Gradient Algorithms

The convergence rate of OGD algorithm is $O(\sqrt{T})$ for convex loss function and $O(1/T)$ for smooth and strongly convex loss function. Evidently, there is a great gap in the convergence rate between OGD and Full Gradient Descent, where the gradient is calculated with regards to all instances in the dataset and the convergence rates are $O(1/T)$ and $O(\rho^T)$ $(\rho < 1)$ respectively. This disparity is due to the variance of the gradient calculated only from one instance. Some algorithms were proposed to reduce the variance. However, these methods are usually online algorithms in batch setting, i.e., the instances are processed for more than once.

*1) **Stochastic Average Gradient (SAG)** [35]:* solves the last problem using the gradient averaging strategy. The goal is to minimize the following function: $P(\mathbf{w}) = \sum_{i=1}^{n} \ell_i(\mathbf{w})$ where n is the total number of training instances. During the t-th iteration, the algorithm randomly chooses one instance i_t to update the gradient. For the other instances, the algorithm uses the stored gradient that was calculated during the last time i_t. The classifier is updated as follows:

$$\mathbf{w}_{t+1} = \mathbf{w}_t - \frac{\eta_t}{n} \sum_{i=1}^{n} \mathbf{g}_i^t, \quad \text{where} \quad \mathbf{g}_i^t = \begin{cases} \nabla \ell_i(\mathbf{w}_t) & i = i_t \\ \mathbf{g}_i^{t-1} & i \neq i_t \end{cases}$$

Assuming that the loss function is smooth, this algorithm is proven to have a convergence of $O(\sqrt{n}/T)$ for convex loss function and $O(\rho^T/n)$ for strongly convex function.

*2) **Stochastic Variance Reduced Gradient (SVRG)** [36]:* algorithm shares similar idea as SAG algorithm in reducing the variance of stochastic gradient. The algorithm works as follows: Every m iterations, the algorithm get an estimated $\mathbf{w}$ as $\widetilde{\mathbf{w}}$. The gradient at $\widetilde{\mathbf{w}}$ is calculated as:

$$\nabla P(\widetilde{\mathbf{w}}) = \frac{1}{n} \sum_{i=1}^{n} \nabla \ell_t(\widetilde{\mathbf{w}})$$

During one iteration, the update rule is

$$\mathbf{w}_t = \mathbf{w}_{t-1} - \eta_t(\nabla \ell_i(\mathbf{w}_{t-1}) - \nabla \ell_{i_t}(\widetilde{\mathbf{w}}) + \nabla P(\widetilde{\mathbf{w}}))$$

Therefore the gradient used in this update is an unbiased estimation of $\nabla P(w_{t-1})$. After m iterations, the $\widetilde{\mathbf{w}}$ is set to current $\mathbf{w}_t$ or a randomly chosen vector from the last m classifiers. Under the condition of strongly convex and smooth, this algorithm converges at the rate of $O(\rho^T)$.

G. Other first-order algorithms

In literature, other first-order online learning algorithms exists. E.g Approximate Large Margin Algorithms (ALMA) [37] which is a large margin variant of the p-norm Perceptron algorithm, the metaGrad algorithm [38] who tries to adapt the learning rate automatically for faster convergence, and the Relaxed Online Maximum Margin Algorithm (ROMMA) [39]. Many of these algorithms often follow the principle of large margin learning.

V. Conclusion

This work presented a review of online supervised learning method. We have mainly focused on this category because it is a natural extension of traditional offline learning. Therefore the methods presented in this work could be applied into real-world problems where batch-learning algorithm suffers from limitations due to the problem definition itself (e.g., live data stream). The other type of online learning method is left for another work.

References

[1] J. Wang, A. Belatreche, L. Maguire, and T. M. Mcginnity, "An online supervised learning method for spiking neural networks with adaptive structure," *Neurocomputing*, vol. 144, pp. 526–536, 2014.

[2] S. Shalev-Shwartz, *Online learning and online convex optimization*. Now Publishers, 2012.

[3] A. Banerjee and S. Basu, "Topic models over text streams: A study of batch and online unsupervised learning," in *Proceedings of the 2007 SIAM International Conference on Data Mining*. SIAM, 2007, pp. 431–436.

[4] Jianguo Xin and M. J. Embrechts, "Supervised learning with spiking neural networks," in *IJCNN'01. International Joint Conference on Neural Networks. Proceedings (Cat. No.01CH37222)*, vol. 3, July 2001, pp. 1772–1777 vol.3.

[5] G. Li, S. C. Hoi, K. Chang, W. Liu, and R. Jain, "Collaborative online multitask learning," *IEEE Transactions on Knowledge and Data Engineering*, vol. 26, no. 8, pp. 1866–1876, 2013.

[6] N. Cesa-Bianchi and G. Lugosi, *Prediction, learning, and games*. Cambridge University Press, 2006.

[7] S. Shalev-Shwartz *et al.*, "Online learning and online convex optimization," *Foundations and Trends® in Machine Learning*, vol. 4, no. 2, pp. 107–194, 2012.

[8] G. J. Woeginger and A. Fiat, *Online Algorithms: The State of the Art*. Springer, 1998.

[9] L. Bottou, "Online learning and stochastic approximations," *On-line learning in neural networks*, vol. 17, no. 9, p. 142, 1998.

[10] A. Rakhlin and A. Tewari, "Lecture notes on online learning," *Draft, April*, 2009.

[11] A. Blum, "On-line algorithms in machine learning," in *Online algorithms*. Springer, 1998, pp. 306–325.

[12] S. Furao, T. Ogura, and O. Hasegawa, "An enhanced self-organizing incremental neural network for online unsupervised learning," *Neural Networks*, vol. 20, no. 8, pp. 893–903, 2007.

[13] S. Furao and O. Hasegawa, "An incremental network for on-line unsupervised classification and topology learning," *Neural networks*, vol. 19, no. 1, pp. 90–106, 2006.

[14] D. Sculley and G. M. Wachman, "Relaxed online svms for spam filtering," in *Proceedings of the 30th annual international ACM SIGIR conference on Research and development in information retrieval*, 2007, pp. 415–422.

[15] V. R. Carvalho and W. W. Cohen, "Single-pass online learning: Performance, voting schemes and online feature selection," in *Proceedings of the 12th ACM SIGKDD international conference on Knowledge discovery and data mining*, 2006, pp. 548–553.

[16] D. Sculley, "Advances in online learning-based spam filtering," Ph.D. dissertation, Tufts University, 2008.

[17] L. Rosasco, E. D. Vito, A. Caponnetto, M. Piana, and A. Verri, "Are loss functions all the same?" *Neural Computation*, vol. 16, no. 5, pp. 1063–1076, 2004.

[18] E. Hazan *et al.*, "Introduction to online convex optimization," *Foundations and Trends® in Optimization*, vol. 2, no. 3-4, pp. 157–325, 2016.

[19] N. N. Schraudolph, J. Yu, and S. Günter, "A stochastic quasi-newton method for online convex optimization," in *Artificial intelligence and statistics*, 2007, pp. 436–443.

[20] C. Bahlmann, B. Haasdonk, and H. Burkhardt, "Online handwriting recognition with support vector machines-a kernel approach," in *Proceedings Eighth International Workshop on Frontiers in Handwriting Recognition*. IEEE, 2002, pp. 49–54.

[21] F. Rosenblatt, "The perceptron: a probabilistic model for information storage and organization in the brain."

Psychological review, vol. 65, no. 6, p. 386, 1958.

[22] S. Agmon, "The relaxation method for linear inequalities," *Canadian Journal of Mathematics*, vol. 6, pp. 382–392, 1954.

[23] A. B. Novikoff, "On convergence proofs for perceptrons," STANFORD RESEARCH INST MENLO PARK CA, Tech. Rep., 1963.

[24] N. Littlestone, "Learning quickly when irrelevant attributes abound: A new linear-threshold algorithm," *Machine learning*, vol. 2, no. 4, pp. 285–318, 1988.

[25] K. Crammer, O. Dekel, J. Keshet, S. Shalev-Shwartz, and Y. Singer, "Online passive-aggressive algorithms," *Journal of Machine Learning Research*, vol. 7, no. Mar, pp. 551–585, 2006.

[26] S. Shalev-Shwartz, K. Crammer, O. Dekel, and Y. Singer, "Online passive-aggressive algorithms," in *Advances in neural information processing systems*, 2004, pp. 1229–1236.

[27] E. Hazan, A. Rakhlin, and P. L. Bartlett, "Adaptive online gradient descent," in *Advances in Neural Information Processing Systems*, 2008, pp. 65–72.

[28] O. Dekel, R. Gilad-Bachrach, O. Shamir, and L. Xiao, "Optimal distributed online prediction using mini-batches," *Journal of Machine Learning Research*, vol. 13, no. Jan, pp. 165–202, 2012.

[29] M. Biehl and H. Schwarze, "Learning by online gradient descent," *Journal of Physics A*, vol. 28, pp. 643–656, 1995.

[30] D. Soudry, D. Di Castro, A. Gal, A. Kolodny, and S. Kvatinsky, "Memristor-based multilayer neural networks with online gradient descent training," *IEEE transactions on neural networks and learning systems*, vol. 26, no. 10, pp. 2408–2421, 2015.

[31] S. Shalev-Shwartz, Y. Singer, N. Srebro, and A. Cotter, "Pegasos: Primal estimated sub-gradient solver for svm," *Mathematical programming*, vol. 127, no. 1, pp. 3–30, 2011.

[32] R. C. Moore and J. DeNero, "L1 and l2 regularization for multiclass hinge loss models," in *Symposium on Machine Learning in Speech and Natural Language Processing*, 2011. [Online]. Available: http://www.ttic.edu/sigml/symposium2011/papers/Moore+DeNero_Regularization.pdf

[33] A. Cotter, O. Shamir, N. Srebro, and K. Sridharan, "Better mini-batch algorithms via accelerated gradient methods," in *Advances in neural information processing systems*, 2011, pp. 1647–1655.

[34] M. Li, T. Zhang, Y. Chen, and A. J. Smola, "Efficient mini-batch training for stochastic optimization," in *Proceedings of the 20th ACM SIGKDD international conference on Knowledge discovery and data mining*, 2014, pp. 661–670.

[35] M. Schmidt, N. Le Roux, and F. Bach, "Minimizing finite sums with the stochastic average gradient," *Mathematical Programming*, vol. 162, no. 1-2, pp. 83–112, 2017.

[36] R. Johnson and T. Zhang, "Accelerating stochastic gradient descent using predictive variance reduction," in *Advances in neural information processing systems*, 2013, pp. 315–323.

[37] C. Gentile, "A new approximate maximal margin classification algorithm," *Journal of Machine Learning Research*, vol. 2, no. Dec, pp. 213–242, 2001.

[38] T. van Erven and W. M. Koolen, "Metagrad: Multiple learning rates in online learning," in *Advances in Neural Information Processing Systems*, 2016, pp. 3666–3674.

[39] Y. Li and P. M. Long, "The relaxed online maximum margin algorithm," in *Advances in neural information processing systems*, 2000, pp. 498–504.

Rules adaptation in the decision-making process

[1]*Ľudmila PUSZTOVÁ (3rd year)*
Supervisor: [2]František BABIČ

[1,2]Department of Cybernetics and Artificial Intelligence, FEI TU of Košice, Slovak Republic

[1]ludmila.pusztova.2@tuke.sk, [2]frantisek.babic@tuke.sk

***Abstract*— The purpose of this paper is to present the case-based reasoning (CBR) method and the progress of our proposed approach to improving the adaptation phase in this method. The rules adaptation, especially in the medical diagnostics process, is one of the most critical problems in the successful implementation of CBR technology in decision systems. Adaptation is often a challenging issue because it is traditionally done manually by experts in the relevant field. The presented approach will be verified and evaluated in the medical diagnosis process.**

***Keywords*—Case-based reasoning, Rule adaptation, Medical diagnosis**

I. Introduction

The term case-based reasoning [1] consists of three words that need a short explanation. A "case" is actually an experience of a solved problem situation. It can be represented as in many different ways. A case base is a collection of such cases. The term "based" means that the reasoning is based on cases; that is, cases are the first source for reasoning. The term most characteristic of the approach is "reasoning." It means that the approach is intending to conclude using cases, given a problem to be solved. The CBR method is a method used to solve a problem based on previous problems with a known solution.

In Figure 1, we can see the CBR cycle consists of successive steps [2], specifically selecting and retrieving the most similar cases (RETRIEVE), reusing and controlling of proposed solution (ADAPT), and storing the learned case (RETAIN).

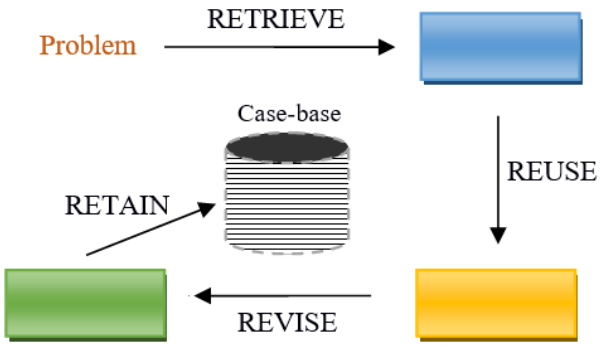

Fig. 1 Case-based reasoning cycle

In general, at the beginning of the entire CBR cycle is initially selected similar cases from the knowledge base. Individual cases must be compared to find those that are most similar to the new one. When a similar case is found, a new case is tested. If the selected rule proves to be the most appropriate, it is applied to solve a new case and then is stored in the case base and immediately available for further use. Otherwise, the existing solution needs to be revised to reflect the new case.

II. The initial status of the research task

Although this method is relatively successful in the medical field [3], it has some existing limitations. The most critical operation of the CBR method is the adaptation step, which is often left out of the process. For this reason, the existence of systems supporting all steps of the CBR method is much lower. This fact is also confirmed by a study [4], in which of 76 examined systems, 51 completely avoids automatic adaptation, so work only as retrieval systems. Some authors tried to solve the adaptation problem by using computational techniques (genetic algorithm or artificial networks) [5] or by creating a hybrid CBR system that integrates case-based reasoning and rule-based reasoning [6]. These facts led us to solve this issue, especially in the application of this method to medical records.

III. Results of the previous work

In previous research [7][8], we have been focusing on how to improve the adaptation phase of the CBR mechanism in the medical domain. Based on the findings and our experiences with medical diagnostics, we proposed a new solution to solve this challenge. We presented our solution at the international conference International IFIP Cross Domain (CD) Conference for Machine Learning & Knowledge Extraction (MAKE) 2019, where we received some recommendations for updating our approach. Figure 2 presents graphically the main part of our solution.

The assumption of starting the RETRIEVE step in our approach is a list of decision rules generated by suitable algorithms. The new case is comparing with decision rules stored in case base by an inference mechanism. This mechanism can find: (1) identical case to the new one, and relevant rule can be applied, (2) very different case to the new ones, where is needed the input from experts, (3) partly similar cases that can be adapted related to the new conditions under the supervision of the expert. If the third state occurs, the cycle will continue, but firstly is need to investigate the differences: 1) if the cases differ only in one condition - the expert will consider possible adjusting of it and 2) if the cases differ in multiple parameters - we identify a list of different parameters;

calculate a difference for this parameters with existing cases; expert will help us to allocate weights by importance for particular differences; the parameters with high weights will be adapting to the most similar case, and the target class will be determined (REUSE-REVISE-RETAIN).

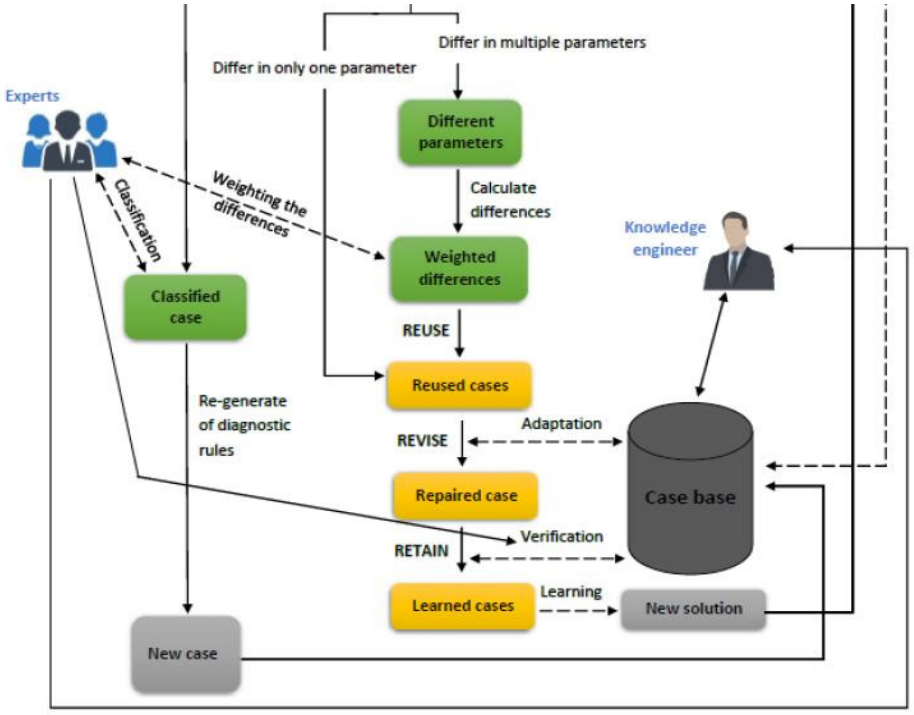

Fig. 2 Our approach for rule adaptation

In our research group, I participated in creating a decision support system, which has been designed and implemented also on the CBR principles. In this approach, we mainly focused on the RETRIEVE step, which enables its user to find the most similar historical cases to a new case and suggest the most probable result. The system also provides useful visualizations to the expert, who is responsible for the final decision for the new case. This system was testing on anonymized medical data about real patients with cardiovascular disease. The main benefit of this system is to help the doctors to determine diagnosis faster and more precisely and assist them in deciding whether the current patient needs more examinations. This approach will be presented at the international conference Medical Informatics Europe in Geneva in April 2020.

IV. ACTUAL STATE

We focus on the practical application of the proposed approach shown in Figure 2, which we will consequently verify on real patients with cardiovascular disease. We gradually have been creating respective modules.

The first module generates decision sub-rules by appropriate machine learning algorithms. After the initial reading of the available data in the form of a table, it is possible to find out the necessary information about the loaded dataset in both text and graphical form. Subsequently, by selecting the algorithm for generating the decision tree, it is possible to test the created model and determine the accuracy of the model on the test set. From the created decision tree, it is possible to generate a set of sub-rules. Of course, one case may be covered by one or more sub-rules, including the logical operator "AND." The set of sub-rules can be download in the form of a table. In this way, a knowledge base is created containing a list of sub-rules. The number of sub-rules depends on the size of the input dataset entering the 1st module.

The second module already represents the decision support system, in which the user has an input dataset through the user interface. This module has loaded the table of sub-rules generated in module 1. To write a new case, the user must enter all the values of the available attributes of the new case in sequence. Each new case in the system will be represented as a single table row composed of specific attribute values separated by a separator. Subsequently, the new case is comparing with the sub-rules stored in the knowledge base. Comparing will result in a list of the most similar sub-rules and their percentage match with the new case. If the inference mechanism finds an identical sub-rule to the new case, the target value is the same as for the existing one. If the inference mechanism does not find any suitable sub-rule, it is necessary to classify the new case by an expert or to re-generate the rules in module 1. This process will be verified and evaluated in the medical diagnosis process.

ACKNOWLEDGMENT

The work was partially supported by The Slovak Research and Development Agency under grants no. APVV-16-0213 and APVV-17-0550.

REFERENCES

[1] K.Feng, A. Xu, P. Wu, D. He *et al.,* "Case-based reasoning model based on attribute weights optimized by genetic algorithm for predicting end temperature of molten steel in RH," in *Journal of Iron and Steel Research International*, 2019, vol.26, pp. 585-592.

[2] S. Begum, M.U.Ahmed, P.Funk *et al.,* "Case-Based Reasoning Systems in the Health Sciences: A Survey of Recent Trends and Developments," in *Transactions on Systems Man and Cybernetics Part C (Applications and Reviews).* IEEE,2011, vol 41, no.4, pp. 421-434.

[3] R.T.Macura and K.Macura, "Case-based reasoning: opportunities and applications in health care," in *Artificial Intelligence in Medicine*, 1997, vol. 9, no. 1, pp. 1-4.

[4] N.Choudhury and S. Begum, "A Survey on Case-based Reasoning in Medicine," in *International Journal of Advanced Computer Science and Applications*, 2016, vol.7, no.8, pp.136-144.

[5] Z.S. Zubi and R.A. Saad, "Using Some Data Mining Techniques for Early Diagnosis of Lung Cancer," in *Recent Researches in Artificial Intelligence, Knowledge Engineering and Data Base*. Tripoli: Libya, 2011, pp. 32-7.

[6] D.A. Sharaf-elDeen and I.F. Moawad, "A Breast Cancer Diagnosis System using Hybrid Case-based Approach," in *International Journal of Computer Applications*, 2013, vol 72, pp. 14-9.

[7] Ľ.Pusztová, "Knowledge models from data sources," in *19th Scientific Conference of Young Researchers*, 2019, pp.105-106

[8] Ľ.Pusztová, F.Babič, J.Paralič and Z.Paraličová, "How to Improve the Adaptation Phase of the CBR in the Medical Domain," in *Machine Learning and Knowledge Extraction*, International Cross-Domain Conference for Machine Learning and Knowledge Extraction, Springer,2019, vol. 11713, pp.168-177.

SMART household control with unifying graphical user interface by Microsoft HoloLens

[1]*Martin Sivý (3rd year)*
Supervisor: [2]Branislav SOBOTA

[1,2]Dept. of Computers and Informatics, FEI TU of Košice, Slovak Republic

[1]martin.sivy@tuke.sk, [2]branislav.sobota@tuke.sk

***Abstract*— Software solutions, applications, and interfaces implemented for SMART devices gained a lot of popularity over the last years. Variety of different devices and appliances can be SMART such as televisions, fridges, washing machines and other white goods, electrical sockets, lights, air conditioners and many others. Every SMART device has its own specific user interface designed by the manufacturer. Interfaces among different manufacturers and devices can be vastly different. There is a lack of solutions on the market that would unify all of these different interfaces into one that could simplify the user experience. This paper proposes a solution for unification of SMART interfaces that would enable the control of different devices with the use of one interface. It describes development of this universal solution, both server and client side, with the use of head mounted device Microsoft HoloLens. It will provide services and functionality for user control of a wide range of SMART components and unite all interfaces into one application solution. Proposed method can reduce production cost of SMART devices if all interfaces would be represented by one device such as HoloLens, Oculus, mobile device or other.**

***Keywords*—virtual reality, smart environment, user interface**

I. Introduction

SMART solutions are becoming more popular nowadays. A lot of companies devote themselves to production of such devices and they also create user applications and interfaces that support the control of their products. Every company creates its own applications, interfaces and standards to enable the user control of their appliances. This is beneficial for the company, because it can compete with its rivals, but not very pleasant for the end user. In order to control all appliances and devices he owns, user needs to have installed all of the different applications for example on his smart phone. He has to memorize how to use them and if he owns devices from different companies, these applications could have different user interfaces. In this scenario, one unified user interface used to control all of them would be preferable. Demand of users for smart devices with an easy user interface is rapidly growing. One study [1] examined the opinion of mainstream users about the SMART household appliances and their future. Based on this research, preferred SMART product features were identified. Researchers examined benefits of these features and their use cases. They also divided users into categories and compared their expectations of what SMART household appliances should be capable of. They discovered that the most important need of an average user is the ability to control his SMART environment remotely and intuitively. The SMART environment also has to be accessible to all users in a suitable way and has to be adapted to children, adults and seniors. The goal of this paper is to create data generic interface for communication of SMART appliances and backend server-side application that can integrate any new SMART device easily regardless of its manufacturer brand.

II. Backend server-side application for controlling SMART household

The main part of this work is the server-side application. This application controls all SMART devices and handles user input from frontend devices such as HoloLens or other data helmets and smartphones. The main advantage of this approach is the elimination of multiple different manufacturer's applications or for variety of devices, and the ability to schedule the behavior of various appliances in advance, so that the user doesn't need to have the helmet or phone by his side later. The server continuously monitors the state of the appliances and the execution of their scheduled tasks. Other benefit of such system is the ability to prototype the appliances as the HoloLens can simulate their state in the virtual reality without the need to physically own them in the SMART household. User can also use this feature to design his ideal household and choose the location or position of devices in advance to the purchase. Simulated appliances can be represented by a 3D model. More information about user interfaces using virtual reality is provided in [5].

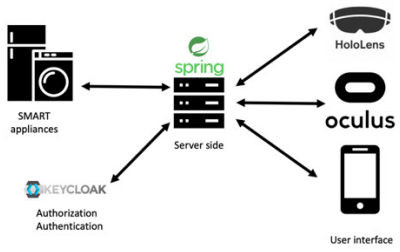

Fig. 1 Architectural design of proposed solution

The architecture of proposed solution is shown in Fig. 1. The manufacturer can create unified interfaces with the use of dynamic 2D controller that consist of predefined structures such as labels, buttons, checkboxes, radio buttons, images and other. These are the building blocks of simple unified user experience. The setup of these structures used for controlling the specific device are stored in a map structure, along with the

style and positioning that will be used for the visualization, as seen in Fig. 2.

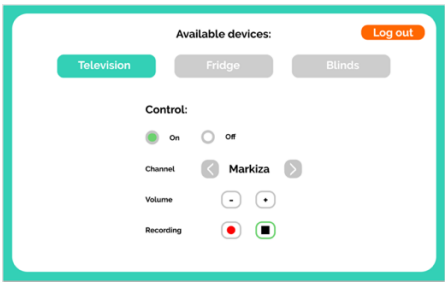

Fig. 2 User interface for smartphone, listing all available devices

III. Authorization

Access to device control and user privileges in system of SMART devices and resources needs to be managed in a secure way. Keycloak [4] was used in proposed solution to manage access privileges of end users. Keycloak can easily add authentication to server application and secure services with minimal effort when properly set. All requests to server-side application must have authorization token. Application has to communicate with Keycloak service and ask for permission to perform actions in household based on user identity and roles in the system. Access to perform any action can be easily denied. We can use this to limit the ability of children to perform changes in the system or to turn on appliances that would be dangerous for them. These roles and permissions are created by the owner of the household in admin area when creating an account. Owner is also responsible for registering new SMART appliances in household.

IV. Universal control of household appliances using unifying interface

Most of current applications for controlling SMART devices are device or manufacturer specific. User has to download multiple applications to control one household which could be considered redundant or complicated. Switching between different applications to setup the whole household is not convenient. This problem is solved by proposed solution with the use of unified interface using head mounted device HoloLens that uses virtual reality. However, this solution produces another problem that needs to be addressed. HoloLens, since it uses virtual reality, needs to be able to recognize and correctly identify SMART appliances in the room that it's mapping with cameras. A lot of research has been done in the field of object recognition in space. HoloLens has to recognize specific devices in the room and identify how to operate them. Some research papers [2] recognize appliances from camera image, other [3] use the user's proximity to the devices into account when selecting the device to be controlled. It is also necessary to design a user interface in such a way that it satisfies user's needs, provides rich virtual reality experience and is user-friendly.

The HoloLens was used to create an intelligent user interface for SMART device control. HoloLens can recognize rooms in which it has been used previously and can recollect where the devices are located. Depending on device's location, HoloLens can identify what specific appliance it is and ask the server-side application for up-to-date information about its state as well as for permission to control the device and change its state. For other head mounted devices that have difficulties with recognizing SMART devices in space, printed QR codes placed directly on devices could be used. QR code would be a unique identifier of the device used in request similar to the system using HoloLens with the same response containing device state. Only the device recognition would be implemented differently if needed based on head mounted device capabilities. QR code would be scanned and stored during registration of new appliance in the household by the owner.

Another problem of using head mounted device to control SMART household appliances is that the user has to be physically in the room standing next to the device in order to control it. Smartphone application could be used to control appliances remotely at any time. However, for smartphone that is not capable of orientation in 3D space, and its device controlling function is slightly different, another similar interface can be created with manual registering of appliances. QR codes can be used to simplify the registering process as well.

V. Conclusion and Future Research

The current state of SMART household environment interfaces uses a variety of systems based on manufacturer. Every manufacturer wants to enforce its own solution. In order to reduce many different interfaces and applications needed to control one household, unified user interface and application is proposed. Users need one application that can control all appliances at once. Without this unified approach they have to use different applications and switch between them when they want to control multiple appliances at the same time. The current state of work provides simplified user interface for interaction with household devices. Virtual reality platform can be of great help when designing natural interface that is intuitive. It is possible to customize it based on user's needs and habits at almost zero costs. It won't specific, it could be used by any company for any device. Standards will be developed to provide the companies with consistent interface design that will be easy and intuitive to be used. Potential of this work lies not only in the unification of SMART devices but also in IoT solutions.

Future work and research will be focused on creating intelligent user interfaces using the available technologies in our laboratory LIRKIS, with the use of HoloLens and Oculus Quest taking future or different head mounted displays into account. Proposed approach will be tested an evaluated experimentally and will be created incrementally in order to achieve intuitive and easy to use interface for environment of simulated smart household appliances.

Acknowledgment

This work has been supported by the APVV grant no. APVV-16-0202 "Enhancing cognition and motor rehabilitation using mixed reality".

References

[1] Coskun, Aykut, Gül Kaner, and İdil Bostan. Is smart home a necessity or a fantasy for the mainstream user? A study on users' expectations of smart household appliances. In: International Journal of Design 12.1 2018.

[2] de Freitas, Adrian A., et al. Snap-to-it: A user-inspired platform for opportunistic device interactions. In: Proceedings of the 2016 CHI Conference on Human Factors in Computing Systems. 2016.

[3] Ledo D, Greenberg S, Marquardt N, Boring S. Proxemicaware controls: designing remote controls for ubiquitous computing ecologies. In: Proceedings of the 2015 international conference on human–computer interaction, 2015.

[4] Christie, Marcus A., et al. Using keycloak for gateway authentication and authorization. 2017.

[5] Sivý M, Hudák M. Uniformed Intelligent user interface for Smart Home using Virtual Reality. In: Poster 2019 : proceedings of the international student scientific conference. – Prague, p. 1-5-ISBN 978-80-01-06581-5

Semantic model for description of data mining processes

[1]*Juliana IVANČÁKOVÁ (3rd year)*
Supervisor: [2]Peter BUTKA, [2]Peter BEDNÁR

[1, 2, 3]Department of Cybernetics and Artificial Intelligence, FEI TU of Košice, Slovak Republic

[1]juliana.ivancakova@tuke.sk, [2]peter.butka@tuke.sk, [3]peter.bednar@tuke.sk

***Abstract*— The aim of the work, which is presented in this article, is to create a system that will enable automatic generation of scripts for data mining process tasks. This paper focuses on the semantic model describing the process in data analytics. Semantic Web and ontologies such as DSO, EXPO, LABORS, and OntoDM are discussed in the introduction. Since the goal is to generate scripts for data mining tasks automatically, the CRISP-DM methodology is briefly described. The creation of automatic script generation is translated from a semantic graph to code in the Python environment. During the evaluation, this code is compared with the real code of algorithms typical for data analysis.**

***Keywords*— data mining, DSO, OntoDM, ontology, semantic model**

I. Introduction

Over the past decades, a great deal of research has been carried out not only in the areas of clinical research, medicine but also in the natural sciences and many other sectors. Today's modern era, full of information and data, is flooding the world with "Big Data," thanks to significant technological advances. This leads to an exponential increase in data generation, and therefore data minig processes require sufficient resources to analyze and retrieve data [1]. The article in the next chapter gives the reader a theoretical basis for the issue. The third chapter describes how to create a semantic model that allows you to automatically derive a process model and then automatically generate a Python script. The final part is focused on testing and evaluation.

II. Semantic web and ontologies

The Semantic Web seeks to improve the current web so that computers can process, interpret, and interconnect information presented on the web to help people find the knowledge they need to provide a common framework that enables not only data sharing but also reuse within applications, businesses, and communities. The Semantic Web aims to solve the most problematic issues related to the choice of modeling techniques. The vision of the Semantic Web is realized by a basic set of technologies such as. RDF, RDFS, OWL. One of the Semantic Web technologies [2] is also the ontologies that help to interpret the heterogeneity of big data by linking data concepts to classes of ontological data. Ontologies organize domain concepts in a hierarchy through logical relationships between them. Therefore, semantic mapping using dictionaries, lexicons, and topic mapping links data concepts with ontological classes. Nowadays, the term ontology is becoming more and more popular, especially in the field of information sciences. Currently, several specific ontologies describe medical as well as other experiments. Ontology in the field of medicine, OBI [3], explains the concepts of medical terminology and the relationships between them, thus enabling the sharing of medical knowledge and providing a standard for the representation of biological and biomedical examinations. EXPO [4] ontologies represent a proposal for the formalization of scientific experiments, and an extension of this proposal is ontology LABORS.

A. Ontologies for data mining processes

The basic element of data science is the formal description of experiments for efficient analysis, annotation, and sharing of results. Ontologies describing data-analytical processes include basic information subjects for data mining and knowledge discovery in databases representation. OntoDM [5] defines concepts for describing scenarios and data flow workflows. Its hallmark is that it uses BFO [6] as a higher-level ontology and template, a set of formally defined relationships from relational ontology, and reuses OBI classes and connections. It ensures compatibility and interconnection with other ontologies.

B. Data Science Ontology (DSO)

DSO [7] is a knowledge base on data science with a focus on computer programming. In addition to cataloging and organizing data science concepts, it provides the ontology of semantic annotation of commonly used software libraries such as pandas and scikit-learning. Annotations map the types and functions of libraries to universal concepts of the ontology. The purpose of DSO is to enable:

- semantic queries for data analysis,
- comparison of semantic similarity between data analyses,
- automated statistical meta-analysis,
- meta-learning for machine learning.

DSO defines basic concepts from ontology, such as task types, algorithms, their settings, preprocessing operations. DSO has various kinds of DM tasks, such as classification, regression, clustering, anomaly detection, association analysis, and the like.

III. Semantic model for data mining processes

A semantic model was created that should allow the formal description of data-analytical processes, ensure replicability of data-analytical processes, and automatically generate scripts for a given task of discovering knowledge in databases. The

definition of the model is based on the DSO ontology, which was gradually extended according to a procedure that included the following steps:

1. Creating a case study base - description of content case studies, task and data description, and scripts to solve a given task that was created manually by a data analyst in Python programming language.
2. Mapping concepts to code fragments - individual script code commands have been annotated with concepts from DSO ontology.
3. Mapping generalization - code fragments that have been annotated by the same DSO concept and that performed the same operations over data or models were generalized to a parameterizable template that serves to automatically generate a code snippet for the operation defined by the DSO concept.
4. Creating generalized models for data-analytical processes - for various types of tasks such as classification, regression, clustering, etc. we have created generalized process semantic graphs composed of DSO concepts that link the operations needed to solve the tasks.

The resulting model allows for a given task to automatically derive a process model that applies to the task and automatically generates a script to implement this process in Python.

IV. TESTING

Testing was performed on selected case studies of data analysis applications. For selected tasks, a semantic graph was derived, which was automatically converted into a script in Python programming language and compared with code created manually by a data analyst. Testing was evaluated by various code comparison metrics such as:

- the total number of lines of code,
- the number of matching features,
- the number of modified features,
- the number of features added,
- and the total code coverage.

In addition to evaluating the code coverage, the accuracy of the learned models was also tested and there were no significant differences in the quality of the learned models between the generated and original code.

A. Analysis evaluation

The model was applied to 2 selected data files. One of them contained data on lending for cars. The aim was to classify whether new customers would buy car insurance. The weather was predicted for the second dataset. In both cases, the classification task was solved. The files had nominal and numeric attributes and contained missing values.

TABLE 1
COMPARING OF RESULTS (1. DATASET VS. 2. DATASET)

	Number of lines code	Total number of functions	Number of the same functions	Number of modified functions	Number of added functions	Total code coverage (%)
1.	239/183*	47/35*	9	12	14	74
2.	79/147*	19/24*	2	12	3	92

**compared code/our code*

V. CONCLUSION

The goal was to create a model for automatic script generation that describes the processes of semantic models for data analytics tasks. In the first analysis, our model achieved code coverage of 74% while adding several features that our model couldn't list. In the second analysis, our model made significantly better code coverage of up to 92%. The repeated launch of our model has achieved favorable results with a deviation of +/- 1.43%.

ACKNOWLEDGMENT

The research presented in this paper was financially supported by the grant APVV-16-0213.

REFERENCES

[1] Inmon, W. H. & Linstedt, D.: Data Architecture: a Primer for the Data Scientist 49–55 (Morgan Kaufmann, 2015).
[2] Hitzler, P., Krotzsch, M. & Rudolph, S.: Foundations of Semantic Web Technologies. (CRC Press, 2009).
[3] Schober, D., Kusnierczyk, W., Lewis, S.E., Lomax, J.: Towards naming conventions for use in controlled vocabulary and ontology engineering. In: Proceedings of BioOntologies SIG, ISMB 2007, pp. 29.
[4] Soldatova, L.N. and King, R.D., An ontology of scientific experiments. Journal of The Royal Society Interface 3, 795–803, 2006.
[5] Panov, P., Džeroski, S., and Soldatova, L.N. (2010). Representing Entities in the OntoDM Data Mining Ontology. In Inductive Databases and Constraint-Based Data Mining, S. Džeroski, B. Goethals, and P. Panov, eds. (New York, NY: Springer New York), pp. 27–58.
[6] Smith, B., Ceusters, W., Klagges, B., Köhler, J., Kumar, A., Lomax, J., Mungall, C., Neuhaus, F., Rector, A.L. and Rosse, C., Relations in biomedical ontologies. Genome Biology 6, r46., 2005.
[7] Patterson E., Baldini I., Mojsilovic A., Varshney K. What is the Data Science Ontology? [online] [cit. 29.01.2020] <https://www.datascienceontology.org/help.>
[8] Antoniou, G., Van Harmelen, F., A semantic Web primer. 2nd ed. Cambridge, Mass: MIT Press; 2008. 264 s. (Cooperative information systems).
[9] Trnka, A., Využitie dolovania dát v zdravotníctve. In: Slovak Journal of Health Sciences. Roč. 2010, č. 1-2, s. 19-24. ISSN 1338-161X.
[10] Larose, D., Discovering Knowledge in Data: An Introduction to Data Mining, John Wiley, 2005, 222 s. ISBN 0-471-66657-2.

Simulation of Multilayered Network Routing Concept for Upcoming 5G Networks

[1]*Dávid HRABČÁK(4th year),*
Supervisor: [2]*L'ubomír DOBOŠ*

[1,2]Dept. of Electronics and Multimedia Communications, FEI TU of Košice, Slovak Republic

[1]david.hrabcak@tuke.sk, [2]lubomir.dobos@tuke.sk

***Abstract*—In this paper, the simulation results of Multilayered Network Routing Concept for Upcoming 5G Networks will be presented. The aim of Multilayered Network Routing composed in this research is to provide a resilient way to deal with the disrupted infrastructure of upcoming 5G networks. A new era of networks with the phenomenon, that is known as the Internet of Things (IoT) brings smart homes, smart cities and new critical applications and services. Those services include public health, public safety and many more. In order to provide constant functioning of those services even in disrupted infrastructure, the Multilayered Network Routing Concept was proposed. The simulations provided in this paper shows, that proposed concept is capable of providing such a role in upcoming 5G networks.**

***Keywords*—Mobile Ad-Hoc Networks, Wireless Sensor Networks, DRONET, Multilayered networks, Concept, Routing ,Simulations**

I. Introduction

The upcoming trend in the research of modern networks is pointed out towards new fifth generation of networks, also known as 5G. With the Internet of Things (IoT), new internet will become more and more complex, smart and pervasive. In the future, this connection leads as into smart homes, smart cities and smart applications, that will affect our daily life. Such applications and services include industrial automation, public health and information systems, city management, energy efficiency, and public safety.

The connection of those abilities and services will be crucial in upcoming 5G networks. However, one of the urgent goals is to provide uninterrupted operations of critical services such as public safety and health service in scenarios, when fixed network infrastructure is disrupted. This scenario includes natural disasters (earthquakes, fires, floods, hurricanes), human errors (nuclear, chemical, biological, radiological exposures or railway and car accidents) and malicious criminal actions (terrorist or cyber-attacks)[3].

The solution to these problems is the Multilayered Network model, proposed in previous research as a routing concept. It is composed of three layers of different networks, that included Wireless Sensor Networks (WSN), Mobile Ad-Hoc Networks (MANET) and the network of unmanned aerial vehicles (UAVs) known as DRONET. In this model, the WSN provides the data collection and act as an IoT network. Since communication among WSN sensors is limited due to constrained resources, the role of speed delivery of critical data is held by MANET. If the disrupted area is big so the neither MANET or WSN nodes are unable to deliver critical data, the DRONET will provide backbone network, that is possible to deliver critical data over long distances. In this paper, the simulations results of such scenario prove, that Multilayered Network model is capable to provide a mentioned role in the upcoming 5G networks.

II. Structure of proposed Multilayered Network

The Concept of Multilayered Network model was previously proposed in research [2]. It is composed of three layers, that accommodate three different types of wireless networks. The first WSN network layer is supposed to replace the role of the IoT network in disrupted network infrastructure scenarios. It is build to collect data measured in the given environment and provide them to the cloud data centres. In disrupted scenarios, when access point (AP) to the cloud is not available, critical data could be delivered through the second MANET layer to the different part of the network, where AP is functional. The advantage of this solution are higher data rates, longer radio ranges and mobility of MANET nodes over WSN nodes. As the mobility of MANET nodes could be an advantage in order to bring data closer to the goal, it also could be a disadvantage. Mobility could cause the MANET network to split into disconnected islands without AP connectivity. This problem is solved by DRONET backbone networks, that is capable to deliver data over long distances with high data rates to functional AP. The described scenario above is depicted on Fig 1.

III. Technical a routing description of layers in Multilayered Network model

In this section, all layers of Multilayered Network model will be described in order to provide technical and routing recommendations needed to set up simulations.

A. The WSN layer

The first layer consists of low energy wireless sensors, that are able to operate in a multi-hop ad-hoc manner. However, the sensors of the WSN network are resource-constrained devices. Therefore, sensors operate at low data rates in order to be energy efficient. The best suitable technology that also preserves MESH routing is IEEE 802.15.4 ZigBee at the link layer. This communication technology sensors to communicate over distances up to about 10 meters and with maximum transfer data rates of 250 Kbps, or lower [3]. In order to provide interlayer communication, the wireless sensors of the

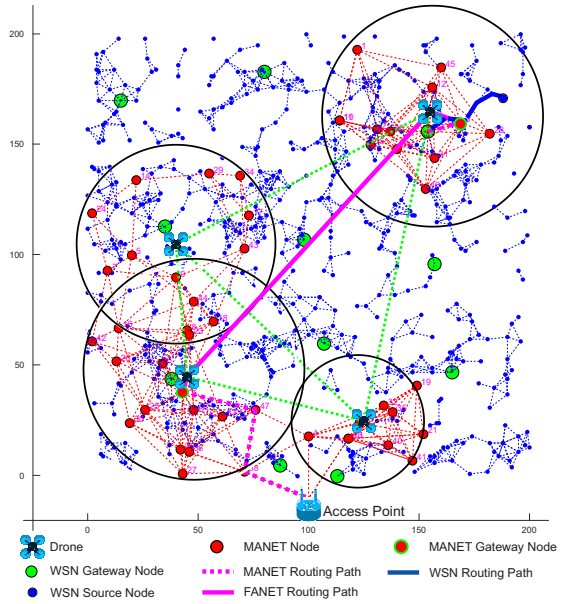

Fig. 1. The Simulation of Multilayered Network Routing

WSN network need to be divided into two types. The first type is an ordinary sensor, that is responsible for data collection and distribution. The second is the gateway sensor, which is only a WSN sensor, that is allowed to send critical data to higher layers. The WSN gateway sensor also accommodates two protocol stacks, because it need to implement second IEEE 802.11 Wi-Fi interface in order to be able to communicate with MANET devices [5]. Therefore, this solution corresponds to the tree or sink topology architectures, where data are routed from ordinary sensors to gateways. Therefore, the recommended routing protocols are Based-Cluster [7] and RLP Weight [4]. That routing protocols also support 6LoWPAN protocol, that is used between the routing layer and MAC layer [6]. 6LoWPAN protocol is responsible for translating IEEE 802.15.4 ZigBee frames into IPv6 packets, that allows WSN sensors to send data to the internet.

B. The MANET layer

Second MANET layer is composed of wireless mobile devices such as cell phones, PDAs or laptops. Those devices are not strictly energy-constrained and provide higher data rates and longer radio ranges. The communication technology in this layer is IEEE 802.11 Wi-Fi, where standard such as 802.11n is able to provide data rate range from 54 Mbps to 600 Mbps with radio range up to 252 meters in outdoor. Since the MANET layer also accommodates IPv6 addressing, the recommended routing protocols are IPv6 enabled DSR [8]. The MANET layer also introduces the gateway system, but the gateways are elected by clustering based on DRONET observation explained in the next section.

C. The DRONET layer

The third layer is composed of UAVs, also known as drones. This layer accommodates two communication technologies, IEEE 802.11 Wi-Fi and IEEE 802.16 WiMAX. Wi-Fi communication is needed for communication and discovery purposes of MANET nodes and WiMAX is used for communication with other drones, since it can provide 10 km radio range [11]. DRONET is also responsible for MANET network clustering based on topology and GPS positions retrieved from discovered nodes. With clustering such as Particle Swarm Optimization algorithm (PSO) [9], Cluster Heads (CH) of each cluster are selected and those CHs will become MANET gateways. Recommended routing protocols are AODV or OLSR [10].

IV. Simulations

The simulations were designed based on the criteria described above. The simulation scenario includes 500 by 500 meters area, 2000 WSN nodes, and 100 MANET nodes. The aim of simulations was to show advantage of using multiple layers over one WSn layer in terms of data delivery time, number of hops and data rates. The results are summarized in Tab I.

TABLE I
The Results of Multilayered Network Model Simulations

	WSN network	Multilayered Network model
Avegare data rates [Mbps]	0,031	62,630
Number ofh ops	11	5
Time of delivery [s]	39,05	5,47

V. Conclusion

Based on simulations is possible to see, that Multilayered Network model provides higher data rates, lower number of hops and shorter delivery time against comparison with WSN network alone. Based on this simulation is possible to say that with the achieved results, the Multilayered Network model is capable to provide resilient way to operate in 5G.

Acknowledgment

This work has been performed partially in the framework of the Ministry of Education of Slovak Republic under research projects VEGA 1/0492/18, KEGA 046TUKE-4/2018 and APVV-17-0208.

References

[1] D. Hrabcak & L. Dobos, "The Concept of Multilayered Network Routing in Upcoming 5G Networks ," Scientific Conference of Young Researchers of the Faculty of Electrical Engineering and Informatics Technical University of Košice. - Košice (Slovensko), pp.160-161. 2019

[2] M. Erdelj & E. Natalizio, "UAV-assisted disaster management: Applications and open issues," Int. J. Advanced Networking and Applications, 10(03), 3833-3842, 2018.

[3] "IEEE Standard for Local and metropolitan area networks–Part 15.4: Low-Rate Wireless Personal Area Networks (LR-WPANs)," in IEEE Std 802.15.4-2011 (Revision of IEEE Std 802.15.4-2006), pp.1-314, 2011.

[4] L. B. Saad & B. Tourancheau (2011, February) "Sinks mobility strategy in IPv6-based WSNs for network lifetime improvement," In 2011 4th IFIP International Conference on New Technologies, Mobility and Security (pp. 1-5). IEEE.

[5] M. Gast, "802.11 wireless networks: the definitive guide," O'Reilly Media Inc Pub (2005): 656, 2005.

[6] N. Kushalnagar, G. Montenegro & C. Schumacher, "IPv6 over low-power wireless personal area networks (6LoWPANs): overview, assumptions, problem statement, and goals," (No. RFC 4919), 2007.

[7] X.Wang, S. Zhong & R. Zhou (2012)," A mobility support scheme for 6LoWPAN," Computer Communications, 35(3), 392-404.

[8] Q. Liu & H. Qin, " Implementation and Improvement of DSR in Ipv6," Procedia Engineering, 29, 716-720, 2012.

[9] V. Loscri, E. Natalizio & N. Mitton, "Performance evaluation of novel distributed coverage techniques for swarms of flying robot," In Wireless Communications and Networking Conference (WCNC), 2014 IEEE (pp. 3278-3283), 2014.

[10] K. Daniel & C. Wietfeld, "Using public network infrastructures for UAV remote sensing in civilian security operations," DORTMUND UNIV (GERMANY FR), 2011.

[11] A. Ghosh, D. R. Wolter, J. G. Andrews & R. Chen, "Broadband wireless access with WiMax/802.16: current performance benchmarks and future potential," IEEE communications magazine, 43(2), 129-136, 2015.

Smart channel resource management for wireless networks

[1]*Dominik NEZNÍK (4th year),*
Supervisor: [2]*L'UBOMÍR DOBOŠ*

[1,2]Dept. of Electronics and Multimedia Communications, FEI TU of Košice, Slovak Republic

[1]dominik.neznik@tuke.sk, [2]lubomir.dobos@tuke.sk

***Abstract*—The article describes how combination of game theory and fuzzy logic can be used as method for radio resource management in wireless, sensor, smart or other types of networks. Smart or intelligent method improves channel management due to fact that it uses the advantages of both methods (game theory and fuzzy logic).**

***Keywords*—fuzzy logic, game theory, channel selection, sensor networks, smart selection, wireless networks.**

I. Introduction

Wireless networks, multi layer networks or any type of networks need to communicate. Communication is related with frequency of channel and technology of connection. Channel management in network is related with spectrum sensing, where devices can obtain information about devices in radio range. Every type of communication in networks is related to select the right channel. Radio resource management study available channels to select the best one based on input parameters. This era is about network connection, be online and use smart devices. Today in some cities are 5G networks (next generation of communication technology) to test operation, speed and interference. We can use radio resource management in different area of communication. Drones can help with communications, when no base station is near or is damaged. Also these drones need to select right channel based on spectrum sensing and data collection from surrounding. Drone as base stations can be used in areas with no mobile connection to provide access to the Internet.

II. Previous work

Research was oriented to implement fuzzy logic method and game theory in wireless networks to manage and assign suitable channels to each wireless devices in network. Based on spectrum sensing we can choose parameters to describe quality of available channels. Exist a lot of parameters to describe the quality of channel. We decide to choose some of them and call them priority parameters. We use three parameters to describe channel quality. Number of these priority parameters increase time and complexity of algorithm. Article [1] described how we implement fuzzy logic to channel selection, also what type of rules, membership functions and priority parameters we used. Another article [2] described game theory as method for channel selection and input parameters for simulations.

III. Progress in the research area

We aim our research to combine game theory and fuzzy logic and create intelligent (smart) method for channel selection between devices in wireless networks. Game theory based on type of game improve or decrease the gain for each device. Main difference is if device want to cooperate or non-cooperate to improve only gain for itself. Our research use prisoner dilemma as type of game to improve rank of channel quality. Priority of channel selection is speed (time for calculation), due to fact, that mobile devices can move. Players with their strategy and also with mutual cooperation can improve channel selection [3].
Our purpose why we use game theory in smart method is to evaluate the quality of channels multiple times and try to find better value of channel quality value. Also implement strategy, where each device cooperate with others and share informations. These two parameters can improve the value of channel quality in fuzzy logic. Fuzzy logic is able to rank each channel, but we also need to perform a cooperation of devices and strategy to increase quality of network and improve output of smart method.

TABLE I
Parameters of Simulations

Parameters names	***Values***
Simulated area [m]	500 x 500
Radio range of node [m]	100
Nodes [quantity]	40
Regular deployment	–
Game iteration	20
Strategy	cooperation

IV. Simulation and results

This section describes how we implement smart method in wireless network with simulation program Matlab. Based on simulations we can say if this method improve or decrease channel selection and distribution in wireless networks. Parameters of simulations is shown in Tab. I. Input parameters for fuzzy logic is traffic, radio signal strength and SIR. Each parameter is defined by membership function. Game theory is represented by iterations and strategy for each device in network. Fig. 1 shows path from source to destination device. This path is selected based on dijkstra algorithm for shortest path between nodes 1 and 40. Each time of iteration is different values of input parameters due to other devices channel selection. When we start the simulation we need to have

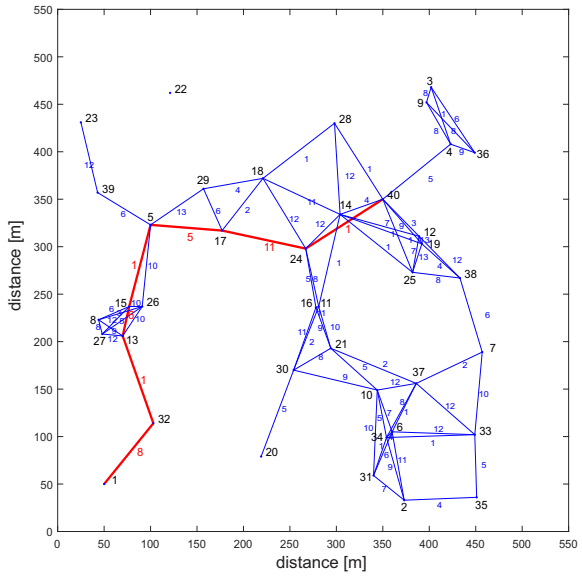

Fig. 1. Selected path based on dijkstra algorithm.

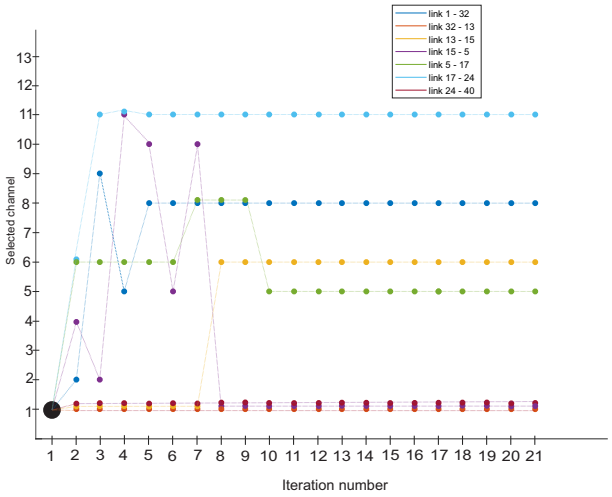

Fig. 2. Channels links for devices in selected path.

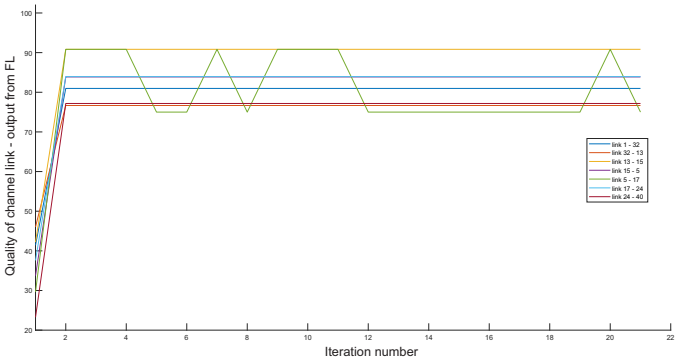

Fig. 3. Quality of links on selected path from source to destination.

channel for link between two devices so we allocate channel 1, when they are in radio range. Then at the second iteration we use fuzzy logic with input parameters such as traffic, SIR and RSS. Membership functions of each parameters and rules for them define the output of fuzzy logic. This output is a number from interval 0 to 100. Higher number means more suitable to select. Node select the channels with the highest value of output for each devices in radio range. Fig. 2 shows allocated channel on path from source to destination device. Final channel allocation is at last iteration. Second iterations based on output from fuzzy logic change channel if deficiency of output value of channel in actual iteration and output of the same channel at previous iteration is higher as threshold, then devices change the channels. Threshold value as deficiency of outputs is set to 20. If deficiency is lower as threshold the channel is unchanged. When we compare channel between nodes 1 and 32 on fig. 1 we can see, that on this area are only these two devices. It means minimum or no interference from devices connected to device 13. On the other hand channel between nodes 15 and 5, there are devices in radio range and it means more interference from others. As we can see on fig. 3 each channel between two nodes unchanged value from first to fourth iteration. They have constant quality value of channel. Device needs to change channel to obtain the same value of quality. Link between devices 24 and 40 don't change value because there are no better channel to improve quality of link. Output from fuzzy logic describe quality of channel. Higher value means more suitable channel. We can see how nodes in radio range influence quality of channel between two nodes.

V. Conclusion

Smart channel allocation is suitable to be used in radio resource management to improve quality of links in network. Different type of game influence result of channel rank due to different strategy of game with same input parameters. Application of radio resource management is suitable to implement in various types of wireless networks (sensors, drones) and improve quality of links between devices.

Acknowledgment

This work has been performed partially in the framework of the Ministry of Education of Slovak Republic under research projects VEGA 1/0492/18, KEGA 046TUKE-4/2018 and APVV-17-0208.

References

[1] NEZNIK, D., DOBOS, L., Fuzzy logic based channel ranking for CR-MANET, *Radioelektronika 2018: 28th International conference. Prague, Czech Republic: Institute of Electrical and Electronics Engineers, ISBN 978-1-5386-2485-2*, pp. 1 – 5, 2018.

[2] NEZNIK, D., DOBOS, L., Game theory for wireless networks, *SCYR 2019, Košice: TU*, pp. 89 – 90, 2019.

[3] MYERSON, R. B., Game Theory: Analysis of Conflict, First Harvard University Press paperback edition, 1997.

[4] NEZNIK, D., DOBOS, L., Channel ranking in wireless network with CR, *SCYR 2018, Košice: TU*, pp. 51 – 52, 2018.

[5] TRESTIAN, R., ORMOND, O., MUNTEAN, G.-M., Game theory-based network selection: Solutions and challenges. IEEE Communications surveys & tutorials, vol. 14, no. 4, pp. 1212–1231, 2012.

[6] FELEGYHAZI, M., HUBAUX, J.-P., Game theory in wireless networks: A tutorial. 2006.

[7] MARDEN, J. R., SHAMMA, J. S., Game Theory and Control. Annual Review of Control, Robotics, and Autonomous Systems, no. 0, 2018.

[8] BENSLAMA, M., BOUCENNA, M. L., and BATATIA, H., Ad hoc networks telecommunications and game theory. John Wiley & Sons, 2015.

[9] MUNOZ-GARCIA, F.; TORO-GONZALEZ, D.; *Strategy and Game Theory: Practice Exercises with Answers*, Springer; 2nd ed. 2019 edition, ISBN: 978-3-030-11902-0.

[10] HOSSAIN, E.; RASTI, M.; BAO LE, L.; *Radio Resource Management in Wireless Networks* An Engineering Approach, Cambridge University Press 2017, ISBN: 978-1-107-10249.

Smart grids and their impact on the distribution system

[1]*Maksym Oliinyk (2nd year)*
Supervisor: [2]Jaroslav Džmura

[1,2]Dept. of Electric Power Engineering, FEI TU of Košice, Slovak Republic

[1]maksym.oliinyk@tuke.sk, [2]jaroslav.dzmura@tuke.sk

***Abstract*—the concept of smart grids is used to refer to a group of technologies that work together to create a next-generation network. The use of individual components of a smart grid can not only reduce efficiency, but also disrupt the normal functioning of the distribution network. For this reason, a complete solution is needed, which will include individual elements, communication, and monitoring and control systems.**

***Keywords*— smart grid, electric vehicle charging, microgrid, renewable energy sources.**

I. Introduction

The energy system based on the Smart Grid concept is a single energy-information complex where managed objects must allow remote control. Systems for assessing the situation and emergency automation - to reduce excessive requirements for reserves of power and information capacities. [1] The appearance of such a system is an opportunity, due to new technologies and a new control system, to radically change the principles of functioning of the electric network. As part of the transition from classical networks to new generation networks, the European Union has identified the following important areas of development [2]:

1. Intelligent network management.
2. Demand Management (DSM).
3. Integrated production and storage (DG&S).
4. Electric transport.
5. Broad integration of renewable energy sources.

Although the theoretical upgrade of the network is simple, the deployment of an intelligent network is a complex technical process. Consequently, the success of a smart network will require a comprehensive multidisciplinary understanding of the various technologies whose activities must be coordinated to ensure its successful, efficient and safe operation. In regions where the implementation of smart grids has already been partially implemented, economic benefits are shown. Such solutions for the modernization of the electric network reduce energy bills for consumers; the installation of batteries improved uninterrupted power supply for critical loads, improved energy quality and reduced the number of accidents [1].

In my research for the first year, I focused on how various technologies have an impact on modern networks, as well as on methods for solving them. Therefore, besides the problem of inconsistency in the production of electric energy, there are other features of the functioning of renewable energy sources that affect the functioning of the energy system, which were investigated in several scientific articles. Some of them are listed below:

1. The installation of a large number of renewable energy sources, has led to such a thing as a negative price for electricity. It is increasingly found in countries with large installed capacity of renewable energy sources. Therefore, in Germany for the first week of February, the price went into the negative zone 4 times fig.1 [3].

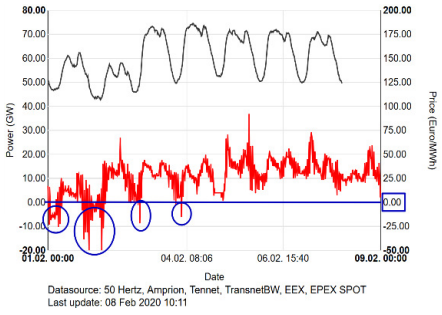

Fig. 1. Price changes in Germany due to high generation in renewable energy sources [3]

2. Installation of a large number of renewable energy sources with insufficient battery capacity in low voltage networks causes an increase in electric power losses during transmission because of the so-called reverse power flow fig. 2[4].

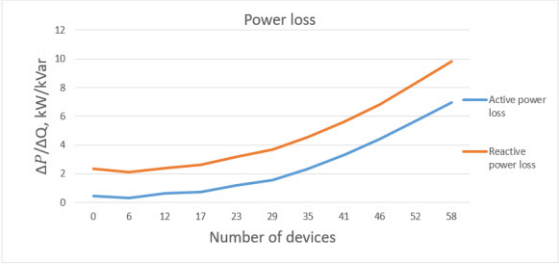

Fig. 2. Changes of active and reactive power loss [4]

3. Installation of a large number of renewable energy sources in low voltage networks causes an increase in voltage in individual sections of the network, sometimes exceeding the permissible limits fig3 [5].

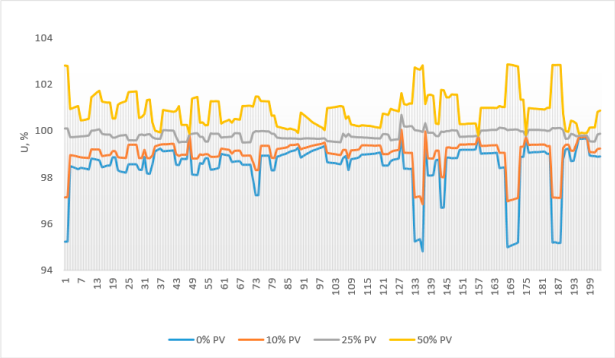

Fig. 3. Change in voltage in network sections with an increase in solar panels [5]

4. The installation of a large number of renewable energy sources in low voltage networks causes an increase in short circuit currents fig 4. [4].

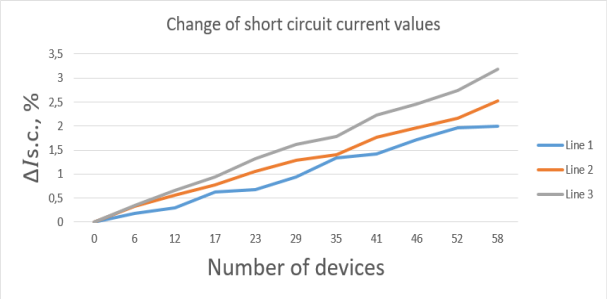

Fig. 4. Changes in short-circuit currents depending on the number of connected photovoltaics [4].

In recent years, there has been a clear trend in the automotive industry towards a shift from classic cars with an internal combustion engine to electric cars. That is, in the coming years, more and more cars with zero emissions of harmful substances will begin to appear on the roads, which, according to forecasts, should eventually completely displace classic cars [6]. Several scientific articles have investigated how widespread use of electric vehicles will impact the functioning of classic networks. From the conclusions of the studies, the following conclusions can be drawn [7]:

1. Modern networks are technically able to withstand the use of electrical machines up to 35% of the total [7].

2. When using electric machines for 15% of the total, it increases losses in the electric network by 100%, and when using 35%, the losses increase by 330% [7].

Most of the above problems can be solved by installing energy storage systems of different capacities. In addition to improving the physical performance of the network (reducing currents in lines, reducing power losses during transmission, keeping voltage within acceptable limits) fig 5[7].

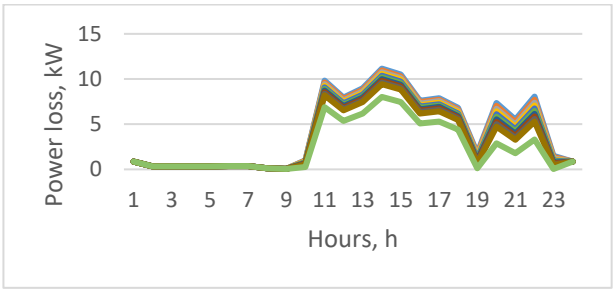

Fig. 5. The dependence of active power losses when using storage systems with a capacity of 10-100 and 180 kW [7]

It is possible to use negative electricity prices for so-called price arbitration (when prices are near zero or in the negative zone to buy electricity and store in batteries, and sell during peak hours, when the cost is maximum). With lower battery costs, this will open up additional opportunities for distribution companies.

At the moment, we can conclude that for the full operation of networks based on the concept of Smart Networks, an integrated approach to the use of a group of technologies is required, as well as the creation of a management system for them. In my further studies, I plan to focus on various control systems. Which can be grouped into several groups:

- management on the consumer side,
- charge management for electric vehicles,
- management of electric energy storage systems,
- voltage control using solar panel systems (inverter + solar panels)

ACKNOWLEDGMENT

This work was supported by the Scientific Grant Agency of the Ministry of Education of Slovak Republic and the Slovak Academy of Sciences by the projects VEGA No. 1/0372/18.

REFERENCES

[1] N. Nikmehr, S. N. Ravadanegh, "Optimal power dispatch of multimicrogrids at future smart distribution grids," IEEE Transactions on Smart Grid, 2015, pp. 1648–1657.

[2] Anna Mengolini, "Smart grid projects outlook 2017", Luxembourg, 2017, ISSN 1018-5593 Available on internet: <https://ses.jrc.ec.europa.eu/sites/ses.jrc.ec.europa.eu/files/u24/2017/sgp_outlook_2017-online.pdf>

[3] Prices on electricity in Germany, Available on internet: < https://energy-charts.de/index.htm>

[4] Zsolt Čonka, Maksym Oliinyk, ...[et all], „The Impact of a Low-voltage Smart Grid on the Distribution System", in EPE 2019 : Proceedings of the 20th International Scientific Conference on Electric Power Engineering. - Ostrava (Česko) : Vysoká škola báňská – Technická univerzita Ostrava s. 1-5 [USB-key]. - ISBN 978-1-7281-1333-3

[5] Maksym Oliinyk, Michal Kolcun, Michal Ivančák, „Inteligentné siete", in Electrical Engineering and Informatics 9 : proceedings of the Faculty of Electrical Engineering and Informatics of the Technical University of Košice. - Košice : FEI TU, 2018 S. 283-288. - ISBN 978-80-553-2713-6

[6] Global EV Outlook 2019, Available on internet: <https://webstore.iea.org/global-ev-outlook-2019>

[7] Maksym Oliinyk, Jaroslav Džmura, "Power loss in smart grids" in: Elektroenergetika 2019: Proceedings of the 10th International Scientific Symposium on Electrical Power Engineering. - Košice (Slovensko) : Technická univerzita v Košiciach 541-545 [CD-ROM]. - ISBN 978-80-553-3324-3

Specification of Surface Finish for Modern PCB

[1]*Daniel DZIVÝ (1st year)*
Supervisor: [2]*Alena PIETRIKOVÁ*

[1,2]Dept. of Technologies in Electronics, FEI TU of Košice, Slovak Republic

[1]daniel.dzivy@tuke.sk, [2]alena.pietrikova@tuke.sk

***Abstract*—This paper presents use of PCB surface finishes and its impact in electronics. Work offers an actual research of the most common surface finishes in electronics, its advantages and disadvantages as well as testing of its properties. Paper also analyzes the need of surface finishes, which has the same purpose, but various usage as well as analyzes its application process and used materials. The comparison of various surface finishes is leading to survey its structure, storage conditions, major faults that leads to uncertainty as well as possibilities of usage in electronics, aimed for fine pitches, solderability testing and measuring the resistance of solder joint for different PCB surface finishes.**

***Keywords*—surface finish, reliability, solderability, wettability.**

I. Introduction

The miniaturization of electronic components is leading to reduction of dimensions of its solder pads as well as increasing requirements of reliability of solder joints. Surface finish is one of the most important materials that is chosen before the manufacturing. It is necessary for covering the copper pads because it reacts with oxygen, that getting worse the solderability of solder pads as well as reliability of solder joints. The main purposes of PCB surface finishes are:

- prevent of oxidation of copper solder pads or other forms of corrosion,
- maintain good solderability and wettability of copper pads that guarantee good solder joint,
- to prevent short circuits through the soldering process,
- create background for wire bonding technologies,
- create barrier for dissolving the copper through the fabrication process,
- make functional interface,
- suppress growth of tin whiskers,
- long term reliability.

For the miniaturization purpose, which is major in electronics, it is important for surface finish be very thin, perfect flat and homogenous on the whole surface of PCB. It is important to analyze these demanding specifications due to repeated reflow process.

On the surface of solder pads, the oxide layer arises by reaction of oxygen with copper, so the main purpose of PCB surface finish is to prevent oxidation of copper soldering pads. There are many surface finishes sharing the market, but none of them covers all requirements. Each surface finish has advantages as well as disadvantages that makes it attractive for certain applications.

For consider, which finish is better, there are several testing methods that could be done. Quality properties of certain surface finishes should be measured and validated, so purpose of finish can be set before manufacturing process [1], [2], [3].

II. Materials of Surface Finishes

In general, PCB surface finishes are divided into metallic (Cu, Sn, HASL, Au, Ag, Ni+Au, …) and nonmetallic (OSP, solder mask, …). Fig. 1 shows usage of PCB surface finishes from years 2003 before restriction of hazardous substances and after year 2007 [1], [2].

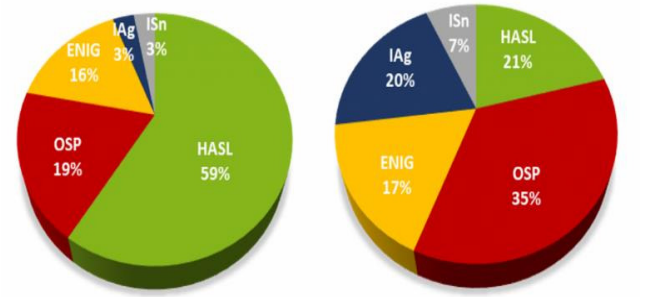

Fig. 1 Global usage of PCB surface finishes for year 2003 (left) and for year 2007 (right) [4].

Galvanic deposition of copper belongs to metallic surface finishes. It is used for temporary treatment, and its function is to raise electrical conductivity. Silver and Tin are cost effective surface finishes, that are good for fine pitches and silver for aluminum wire bonding technology. There are issues with wasting the chemicals as well as with hazardous exhalants made at coating process. Tin is used for maintenance good solderability of copper pads, but there is issue with whiskers (long thin strings) that are made because of fast cooling due to internal stress. HASL (Hot Air Solder Levelling) is method of dipping PCB into molted solder, SnPb or SnAgCu, that is levelled with hot air blowing on PCB. Before dip, the flux must be added. Despite of thermal shock and high energy waste, this is the most popular PCB surface finish. Gold or nickel are added onto already treated PCBs. Its purpose is to make functional interface like connectors or interconnections between chips with advantage of low transition resistivity [1], [3], [5], [6], [21].

Metallic surface finishes are coated overall copped coating, or only on soldering pads, that are allocated with solder mask. There are several methods how to deposit finishes: [5].

- dipping – HASL, OSP,
- galvanic – copper, tin,
- chemical – silver, tin, nickel, gold,
- screen printing – solder mask,
- spraying – OSP.

TABLE 1
BASIC PROPERTIES OF THE MOST COMMON PCB SURFACE FINISHES [1], [2], [3], [6].

Surface finish	OSP	HASL	ImAg	ImSn	ENIG
Relative Cost	1	1.5	1.5	1.1	3
Thickness in µm	0.1-0.156	1.5-45	0.08-0.25	0.6-1.2	Ni: 3-5 Au: 0.05-0.2
Storage time (months)	3	18	12	6	24
Planar	yes	no	yes	yes	yes
Temperature of fabrication in °C	40	240-270	50	70	80
Wave soldering	yes	yes	yes	no	yes
Times of reflows	2	6	6	2	6
Wire bondable	no	no	yes	no	yes
ICT	no	yes	yes	yes	yes

Tab. 1 shows the main properties of surface finishes, that are known for manufacturer, as well as for customer and it is useful for considering, which PCB surface finish is the best for his purpose.

III. SURFACE FINISHES DEFECTS

Nowadays, we have such a very good quality PCB fabrication process, but it doesn't mean that is perfect and without mistakes. Every surface finish has its several disadvantages that are its issues through the fabrication. Only few defects are mentioned, but there are more problems linked with manufacturing process.

One of the most common issue is planarity of the HASL coating. Due to its inaccurate fabrication process of levelling the excess solder, on the soldering pads are made bumps with various thickness. This issue is problematic for BGA components with fine pitches that is inconceivable use HASL for this type of application. As we can see in Fig. 2, on pads, the coating was uneven and did not cover the whole pad with the evidence of non-wetting or de-wetting. We can consider, that solder had not wetted the copper substrate. This can cause issue in the soldering process with solder wetting [1], [7], [8].

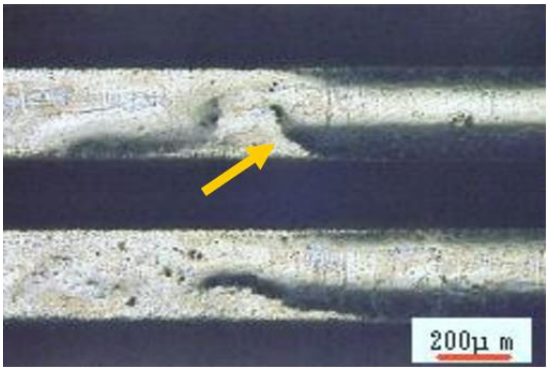

Fig. 2 Detail of PCB soldering pad with HASL surface finish [8].

Another issue that is made in the soldering process is voiding among the solder and surface finish due to thermal cycling. This issue was discovered mostly with ImAg surface finish, and silver plating process was optimized. Immersion silver coating has major problem that is creep corrosion. Creep corrosion arises by dissolving the silver in the environment with high humidity of sulfur. Creep corrosion effect is shown in Fig. 3 [6], [9], [10].


Fig. 3 Detail of Creep corrosion effect of silver coating [9].

As mentioned on the beginning, surface finish has to prevent short circuits. But immersion tin surface finish has issue with whiskers. Whisker, as mentioned above, is thin conductive string that is made by the impact of physical interfacial pressure after the plating process. Whisker can grow almost few millimeters long and 5 µm thick. As we can see in Fig. 4, there is issue with short circuit due to whiskers [11].

Fig. 4 Detailed view of tin whisker [12].

Even the most expensive PCB surface finish has its fabrication issue. Black solder pad belongs to presence of phosphorus in electro-less nickel plating. It is important to understand the reaction mechanism, when solder reacts with ENIG plating. During the soldering process, solder is melted on the top of the pad, and gold layer dissolves into the solder, so the solder joint is created by the nickel and tin. Reaction of nickel atoms with tin enhance the crystallization of amorphous Ni-P into the P-rich nickel layer [2], [13].

IV. Materials Used For Surface Finishes

Choosing the right material is difficult due to environmental issues. The most used SnPb HASL become restricted for basic application, due to RoHS, because lead was declared as a hazardous substance. Since then, customers and manufacturers started using other lead-free surface finishes as well as research in electronics started finding the optimal solution for certain application. The other trend is placement of component with fine pitches, that SnPb HASL cannot offer reliable joint due to various thickness. Other environmental problem is emission of exhalants that arises by manufacturing processes [6], [13].

A. Immersion Silver

As mentioned above, problems with exhalants is exceptional for immersion processes, where nitric acid HNO_3 is the base of the solution. However, immersion silver is thin planar layer of silver with thickness of 0.08-0.25 μm. Dip in nitric acid saturated with silver proceed simple displacement reaction, where silver ions are displacing the copper ions along the surface [6], [13], [14].

B. Immersion Tin

Immersion tin is another low-cost metallic planar surface finish. In contrast with silver, the base material for tin immerse can be methane, sulfonic acid, sulfate of chloride. Process of the coating is similar to silver, based on the displacement reaction. Difference between finishes is thickness, that for tin is more than two times thicker [6], [13].

C. ENIG

Another chemical based finish is ENIG, that is applied through the deposition of an initial layer of nickel followed by thin layer of gold that was chosen for protection of nickel for preventing corrosion as well as to preserve solderability. Manufacturing process consist of catalyst, acid dip, electroless nickel immersion and gold immersion. Catalyst consist of palladium salt in an acidic solution $Pd(NH_3)$, where palladium atoms displaces copper atoms on the surface. Acid dip, based on weak sulfuric or hydrochloric acid, removes any residual catalyst from non-copper surfaces, to prohibit plating on the solder mask or other areas of the PCB. The following high temperature acidic bath is used to plate nickel (3-5 μm) onto catalyst covered surface. This solution contains nickel ions as well as phosphorous, that is co-deposited with nickel. Last step is dip in solution with contamination of pure gold, where displacement reaction occurs. Thickness of gold is 0.05-0.2 μm [6], [13].

D. HASL

Hot air solder levelling surface finish was the most popular option in PCB surface finishing technology before the lead-free era. Even though it doesn't require chemical bath, it has long shelf life and relatively low cost compared to ENIG. However, also in this process, there are some energy wasting issues, due to keep the solder melted. Another energy wasteful process is levelling the excessive solder with hot air knives. Before lead-free era, material used for HASL surface finish was eutectic Sn37Pb63. Nowadays, it was replaced with the commonly used SAC305. Before dipping into melted solder, the flux has to be added on the PCB, as well as micro etching must be done before the application [6], [13], [15].

E. OSP

Organic solderable preservative is an anti-oxidant film applied on copper surface. Surface finish is nearly invisible due to transparency and thickness (0.1-0.5 μm). OSP consists of benzimidazole or phenylimidazole dissolved in water and acid. Main coating is deposited by dipping into OSP solution for 1-3 minutes. Protective layer chemically bonds to the copper, that preserves the solderability of the copper pads. After the dip, the excessive film is levelled with the air knife [6], [13].

V. Measurement of Surface Finishes Properties

Before we decide, which surface finish is better, there are several testing methods for measuring its properties for comparing. Some surface finishes had problems with thick layer of brittle IMC, short creep rupture lifetime insufficient wetting, inadequate solderability, which means low reliability of the solder joints. However, electrical tests can be also done for qualitative as well as quantitative testing [15].

A. Wettability testing

Comparing the wettability among the various surface finishes brings us the answer for question, which surface finish has better wettability. Meniscograph is measuring instrument to determine wetting force. As we can see in Fig. 5, test is realized by dipping the substrate with the certain surface finish into the melted solder, and wetting force (mN) is measured. This test is also called wetting balance test and presents quantitative and qualitative results [15], [16].

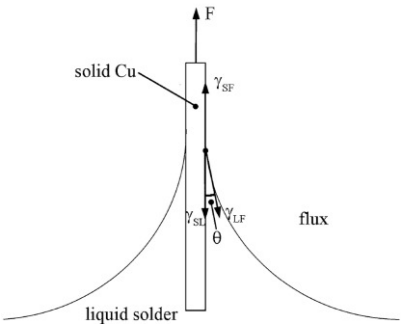

Fig. 5 Schematic cut of the wetting balance test [17].

Another quantitative test for wettability can be done by statistical method of reflow performance. The wetting pattern (Fig. 8, sector 2) includes 12 parallel lines in vertical and horizontal directions. On the top of the surface finish, there are printed 15 solder paste bricks 0.4 mm long with pitch 0.1-0.4 mm between them. When ideal wetting occurs, whole line is covered with the solder. Wetting percentage can be calculated by ratio of number of gaps after reflowing / number of gaps before reflowing multiplied by 100% [18].

B. Measuring the electrical resistivity

Measuring the electrical resistivity of the solder joint with various surface finishes can tell us, which can be more conductive and how surface finish affects the whole circuit. Electrical resistivity of solder joint is measured as electrical voltage drop on the solder joint with electrical current flow. For measuring, Kelvin´s method will be used (Fig. 6). Measured solder joint is connected to DC current generator with constant value of current. By using voltmeter, voltage drop on solder joint is measured and consequential electric resistivity will be calculated by ratio of the voltage (V)/current (A) [1], [19], [20].

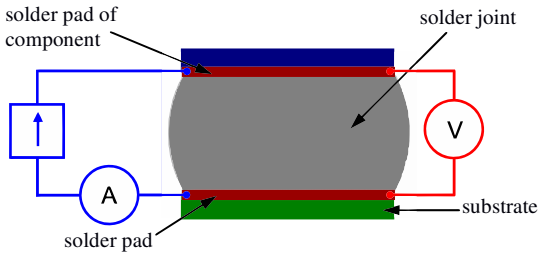

Fig. 6 Principle of Kelvin´s method for analyze electrical resistivity.

C. Voiding test

In this type of test, void area is measured using the percentage evaluation of voids towards solder. As we can see in Fig. 7, red color indicates voids and black color solder. Voiding percentage is then evaluated by ratio of voids to solder multiplied by 100%. Lower voiding area indicates better voiding performance. Ideal value for voiding is 0% [18].

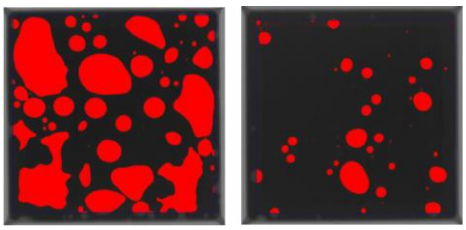

Fig. 7 Image of voiding test from combination of immersion tin (left) and immersion silver (right) with solder paste SAC 305 [18].

For testing purposes, we made testing pattern (Fig. 8), that can be used for measuring properties of surface finishes. Pattern consists of 5 sectors. Sector 1 is used for measuring the electrical resistivity. For measuring the wettability is used sector 2 as well as sector 5, and voiding can be measured in sector 3. Sector 4 is for measuring other properties such as roughness, thickness or planarity.

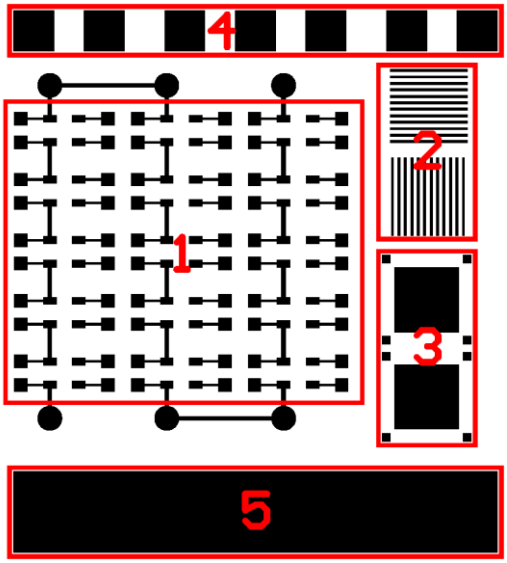

Fig. 8 Universal testing pattern for PCB finishes.

VI. Conclusion

This paper brings the comparison of the most common PCB surface finishes, their advantages, disadvantages as well as its properties such as thickness, relative cost or temperature of fabrication. Furthermore, process of manufacturing is also described and necessary technological procedures during the coating for each surface finish, used materials are mentioned.

Work also offers view of PCB surface finish quantitative and qualitative testing of its electrical and mechanical properties. Various surface finishes have different properties, which have to be evaluated and according to results, customer can decide which surface finish will be better for his application.

Due to these measurements, in this paper is described testing pattern, on which we can measure wettability, voiding, roughness, resistivity of solder joint, planarity and thickness. For future work, this pattern will be manufactured and applied in testing procedure.

Surface finishes are very important in manufacturing process and selecting the right material can be difficult. On the one hand, we need good wettability, and on the other hand, we need planarity and small thickness. If we can develop new surface finish that is combination of these two features, we can use this surface finish for fine pitch components in consideration of miniaturization.

My future work will be focused for developing new type of surface finish for needs of miniaturization also developing new testing methods for comparing the quality between various surface finishes (new type of surface finish, new treatment of surface finishes).

References

[1] A. Pietriková, J. Durišin, P. Mach, "Diagnostika a Optimalizácia Použitia Ekologických Materiálov pre Vodivé Spájanie v Elektronike," Technical university of Kosice, 2010.
[2] R. Schueller, "Considerations for Selecting a Printed Circuit Board Surface Finish," DfR Solutions, Minneapolis, MN, USA, 2013.
[3] C. Myers, "PCB Surface Finishes," 2013.
[4] C. Zheng, "Choosing a Surface Finish for Fine-pitch Components," Seeed technology, Shenzen, China, 2019.
[5] J. Nable, "PCB Surface Finishes: A General Review," Hong Kong, 2016.
[6] Implementing Cleaner Printed Wiring Board Technologies: Surface Finishes, U.S.EPA, Washington, USA, 2000.
[7] Y. Yang, "Failure Analysis for Bad Wetting on HASL PCB," in *18th International Conference on Electronic Packaging*, 2017, pp. 126–129.
[8] K. W. Sweatman, "Hot Air Solder Levelling in the Lead-free Era," 2006.
[9] M. Weeks, D. J. Zueck, "Sulfur Corrosion of Printed Circuit Board Surface Finishes in Three Different Sulfur-rich Environments," SMTAI, 2015, pp. 384–398.
[10] P. Savolainen, R. Schueller, "Creep Corrosion of Electronic Assemblies in Harsh Environments," DfR Solutions, 2007.
[11] R. J. Hanson, "Electronics Surface Finish Overview," *SMTA Upper Midwest Expo*, 2015.
[12] Ch. Wickramasinghe, "Evidence for iron whiskers in the Universe," *Current Issues in* Cosmology, 2006, pp. 152–161.
[13] K. J. Puttlitz, K. A. Stalter, "Handbook of Lead-Free Solder Technology for Microelectronic Assemblies," New York, USA, 2004, ISBN: 0-8247-4870-0.
[14] T. I. Török, "Nanoscale Characterization of Thin Immersion Silver Coatings on Copper Substrates," 2015.
[15] Ch. W. Wayne, K. Sweatman, "Study of Pb-free HASL PCB Surface Appearance Impact on 2nd Level Interconnect Solderability," *IEEE 14th Electronics Packaging Technology Conference*, 2012, pp. 676–680.
[16] A. Sewiorek, A. Kudyba, N. Sobczak, M. Homa, Z. Huber, Z. Adamek, J. Wojewoda-Budka, "Effects of PCB Substrate Surface Finish and Flux on Solderability of Lead-Free SAC305 Alloy," *Journal of Materials Engineering and Performance vol. 22*, 2013, pp. 2247–2251.
[17] F. Wang, "Wettability, Interfacia Behavior and Joint Properties of Sn – 15Bi Solder," *Journal of Electronic Materials vol. 48*, 2019.
[18] T. Lentz, "How Does Surface Finish Affect Solder Paste Performance?" SMTA International, USA, 2018.
[19] Ľ. Andráš, Ľ. Antoška, "Princípy Merania Malých/Veľkých Odporov z Hľadiska Potreby Revízneho Technika," *XXVI. Odborný Seminár*, 2018.
[20] J. Ďurišin, "Vlastnosti Spojov na Báze Bezolovnatého Spájkovania," dissertation thesis, Košice, 2009.
[21] Y. M. Cheung, "Revisit of Wirebonding on Immersion Silfer-Finish Board," 2000.

Spiral technical coil simulation and parameter verification

[1]*Peter HRABOVSKÝ (2nd year)*
Supervisor: [2]Ján MOLNÁR

[1,2]Department of Theoretical and Industrial Electrical Engineering, FEI TU of Košice, Slovak Republic

[1]peter.hrabovsky@tuke.sk, [2]jan.molnar@tuke.sk

***Abstract*—The introduction of the paper briefly describes the current situation in the field of 3D printing of conductive materials. Next part of the article is devoted to simulation of spiral technical coil in the COMSOL Multiphysics program. The design of a spiral technical coil test sample is described in the third part of the paper. The conclusion of the article is devoted to verification of measured, calculated and simulated data.**

***Keywords*—3D printing, COMSOL Multiphysics, conductive materials, simulation, spiral technical coil, verification.**

I. Introduction

Today, we encounter a large number of electrical equipment every day. They help us to fulfill our work tasks, meet everyday needs and make our lives easier in different ways. One of these devices is a 3D printer. In recent decades, 3D printing has evolved from a sophisticated process that requires expensive machines (used only by larger companies) to a significant number of relatively inexpensive open-source projects, allowing a much wider audience to use this technology. Today, an ordinary person can buy a 3D printer, create an object in CAD software, or download it from an Internet database, and materialize the model in the comfort of their own home with their own and inexpensive 3D printer. With the advent of new print materials, opportunities to print unprecedented objects increase. Developments in the field of electrically conductive printing materials with admixtures of graphene, carbon or copper open up a wide range of applications in industrial electrical engineering. It allows the printing of sensors and simpler circuits, it can change the entire standard of electronic devices that are now capable of working in three-dimensional space instead of conventional PCB. Given that the coil is an essential part of any electronic device, this study is focused on its design and implementation using 3D printing. The various results achieved so far will also be described.

II. Simulation of Spiral Coil using by COMSOL Multiphysics

The properties of any electrical element can identify directly by measuring or using appropriate software. For the measurement itself, it is necessary to have a measuring element available. Otherwise, it is necessary to solve the problem with the help of computer technology using software simulation tools such as COMSOL Multiphysics. In this chapter, we will discuss the design of a coil and identification its properties using computational techniques.

After designing the spiral coil in the graphical software environment, it is necessary to set a various parameter as the material used for the winding of the coil (earned from the measuring of electrical conductivity of special conductive 3D printing filament [1]) and the type of environment (air) and more others conditions.

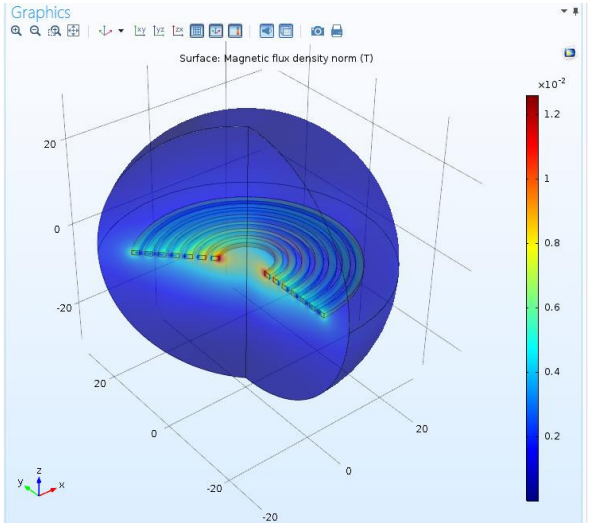

Fig. 1 Density of magnetic flux in 3D space

In Fig. 1 we can be seen that the largest magnetic flux density is in the center of the coil and decreases with increasing coil radius. The spool shown in the Fig. 1 has the following parameters: Outer diameter (d_{out}) - 50.27 mm, Inner diameter (d_{in}) – 11.096 mm, the space between two turns (s) - 1.07 mm, wire width (w) - 1.6 mm, wire thickness (h) - 1 mm, number of coil turns (N) - 9.

The inductance of the coil can be determined from the total energy of the magnetic field generated by the current passing through the turns of the coil using equation (1). The current through the winding of coil during the simulation was 1A.

$$L = \frac{2W_m}{I^2} \tag{1}$$

By solving the equation (1) we get the inductance value of spiral coil: L = 1.44 µH. This value of the inductance will then be verified using the measurement and calculation with special formula in the next section of this article.

III. Realization and Parameter Verification of 3D Printed Spiral Coil

A. The design, 3D model of spiral coil using by CAD software.

To verify the simulation results, we modeled a spiral planar coil in CAD software called Fusion360. On the Fig. 2 we can see the 3D model of the spiral planar coil. The coil dimensions were given in the previous chapter.

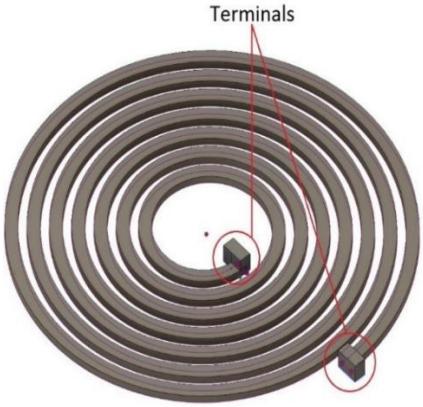

Fig. 2 The 3D model of spiral coil designed in CAD software

B. The process of producing a spiral coil using by 3D printer.

The CAD model was then cut into individual horizontal layers with the help of CAM software and printed with a 3D printer. The spiral coil 3D printing process itself is shown in Fig. 3. The 3D FDM printer with 0.8 mm diameter nozzle (manufacturer's recommended nozzle diameter) was used. A special conductive metal-polymer material called Electrify from Multi3D was used to print the spiral coil.

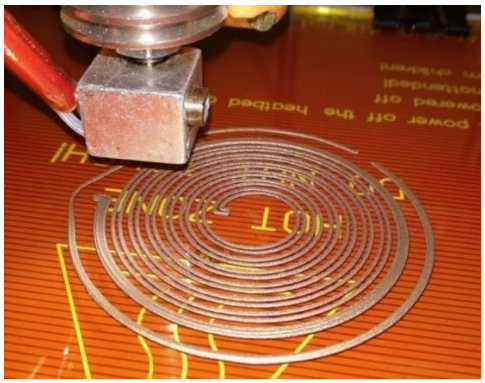

Fig. 3 The process of printing spiral coil using by 3D FDM printer

C. Verification parameters of printed spiral coil.

On Fig. 4 we can see measuring inductance of spiral coil using by programmable LCR bridge HM8118.

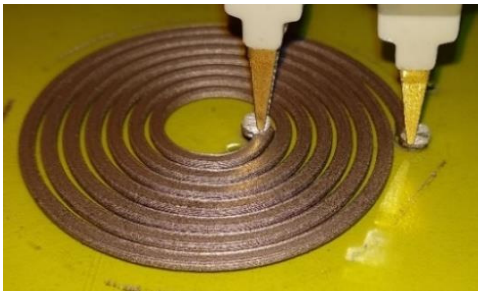

Fig. 4 Measuring inductance of spiral coil using by LCR bridge

Measuring the coil in the frequency range 10 kHz to 100 kHz was measured inductance values in the range 1.6127 µH to 1.9131 µH. Using the coil simulation in the COMSOL Multiphysics simulation program, we obtained an inductance value of 1.44 µH at a frequency of 10 kHz. The difference in inductance between the measured value and the value obtained by the simulation was 0.1727 µH. This difference may be due to a greater number of adverse effects. One reason may be material, from the catalogue values given by the manufacturer do not match the actual material values (from publication [1]). Another cause is, of course, the inaccuracy of the 3D printer used and others adverse effects.

We can also say that the analytical calculation according to formula (2) gives the result:

$$L = \frac{\mu_0 \cdot N^2 \cdot d_{avg} \cdot C_1}{2}\left[\left(\ln\frac{C_2}{g}\right) + C_3 g + C_4 g^2\right], \quad (2)$$

$$L = 1.3513 \cdot 10^{-6} H = 1.3513\,\mu H$$

Where d_{avg} is the average coil radius determined by the equation (3).

$$d_{avg} = \frac{d_{out} + d_{in}}{2} \quad (3)$$

And where ρ is the fill ratio determined by equation (4).

$$\rho = \frac{d_{out} - d_{in}}{d_{out} + d_{in}} \quad (4)$$

Where $C_1 - C_2$ are constants obtained from this publication [2][3][4], with $C_1 = 1$, $C_2 = 2.46$, $C_3 = 0$, $C_4 = 0.2$, $\mu_0 = 4\pi 10^{-7}$ H.m^{-1}, and N is the number of coil turns. All others parameters of equations (3) and (4) have been listed in chapter II.

Solving the analytical calculation of the equation (2), we determined value of the coil inductance to 1.3513 µH. This result obtained by analytical calculation is also considered to be approximate.

IV. Conclusion

In view of the facts described in this article, it is necessary to research this problem in more details. In the coming period, the research will focus on examining and addressing the following topics: Plating of a conductive Electrifi material with a copper layer. Use of tin as a conductive material for printing winding of coil. Design and production of plastic form for winding of coil and following the casting of the winding using a suitable liquid metal. Creating a database of coils of various shapes and dimensions. Simulation of coil property depending on different shapes, dimensions and materials used. Creating an application to select the suitable coil based on customer requirements.

The ultimate goal of the work should be a system that can facilitate the selection of a technical coil with appropriate parameters according to customer requirements.

References

[1] P. Hrabovský, J. Molnár. "Measuring the electrical resistance of a conductive material for a 3D printer" In: *Journal of Industrial Electrical Engineering.* vol. 3, no. 1, pp. 52-58, 2019.

[2] Kouril, Lukas, et al. "Coil optimization with aid of flat coil optimizer." *Proceedings of the 5th WSEAS congress on Applied Computing conference, and Proceedings of the 1st international conference on Biologically Inspired Computation. World Scientific and Engineering Academy and Society (WSEAS)*. 2012.

[3] Zhao, Jonsenser. "A new calculation for designing multilayer planar spiral inductors." *EDN (Electrical Design News)* 55.14 (2010): 37.

[4] Mohan, Sunderarajan S., et al. "Simple accurate expressions for planar spiral inductances." *IEEE Journal of solid-state circuits* 34.10 (1999): 1419-1424.

The contribution of machine learning algorithms and its categorization

[1]*Jakub PALŠA (1st year),*
Supervisor: [2]*Liberios VOKOROKOS*

[1,2]Dept. of Computer and Informatics, FEI TU of Košice, Slovak Republic

[1]jakub.palsa@tuke.sk, [2]liberios.vokorokos@tuke.sk

***Abstract*—This article analyzes basic machine learning information. The introduction briefly describes the meaning and essence of development. The most important part of this article is the categorization of machine learning and the assignment of the most used algorithms in the recent period. In conclusion, the comparison and the benefit of the algorithms are described using the obtained information.**

***Keywords*—machine learning, supervised learning, unsupervised learning, semi-supervised learning, reinforcement learning, algorithms.**

I. Introduction

As the philosopher Polonayi noted, "We can know more than we can tell [4]". Understanding speech, cycling and face recognition are tasks that people know how to do, but our ability to think about how we do these tasks is bad. Polanyi's paradox created a set of tasks that could be automated by computer programming [5]. However, machine learning algorithms make it possible to train computer systems to be more capable and accurate than those that can be manually programmed by humans. Manually programming new computer programs is labor-intensive. Therefore, this process is replaced by a more automated process of the existing machine learning algorithm.

Machine learning is a subdivision of artificial intelligence in that it devotes itself to techniques and algorithms, which allows the computer system "to learn". Learning should be understood as making some changes to the internal state of the system, which will make it more efficient to adapt to changes in the surrounding environment. This means that based on the information the system learns, it can respond adequately to different input values [3].

Deep or machine learning has made significant advances in resolving, which for many years have resisted the best attempts of the artificial intelligence community. It is considered very good in detecting structures in high dimensional data and is therefore used in many areas such as business, science and government [6].

II. Techniques and Machine Learning Algorithms

Machine learning algorithms use methods of statistical analysis, in-depth data analysis and elements of mathematical statistics. For a better understanding, the essence of a computer is accuracy, which implies that it still works only with accurate data. Machine learning gives the computer an estimate, which is also based on accuracy and calculations, and which has a high role in machine learning applications [2].

Machine learning techniques apply to several kinds of problems. Examples include language and written text recognition, recognition of illegal use credit cards, face recognition, speech recognition, gaming, and many more [1].

Somebody can ask, "Why should machines learn?" There are many reasons why machine learning is important to us. In addition to achieving machine learning helps us understand how humans and animals learn, there are also important technical reasons [3]:

- Often, people produce machines that do not work as intended in the environments in which they are used. This is because some features of the working environment may not be known at the time of the design of the machine. Therefore, machine learning can be used directly in the workplace to improve machines.
- For certain tasks, the data may be too large to be clearly processed. Machines can learn this information gradually and capture more data than humans.
- As time passes, the environment also changes. Machines that could adapt to the changing environment would reduce the need for a frequent redesign of the environment.
- There is a constant stream of events in the world that is caused by people. The design of the systems is constantly changing to match new knowledge. However, machine learning methods could track these changes and adapt automatically to these changes.

III. Categorization of machine learning

To select a suitable machine learning algorithm, it is necessary to identify the general category of the problem. Each algorithm has its advantages and disadvantages. The decision to choose the right algorithm depends on the data obtained. Years of research have developed a large number of machine learning algorithms for different data. Some work well with the text, others work better with numeric data or continuous values. Algorithms are divided into three basic groups, according to the type of task they can perform, namely:

- regression [7],
- clustering [8],
- classification [9].

By obtaining results it is possible to choose from several algorithms. This procedure is often used in practice despite higher time demands. Substantial categorization of algorithms includes the following division:

A. Supervised learning

Supervised learning creates a mathematical model from a dataset that contains inputs and required outputs, also known as control signals. Data is defined as trained data and consists of training sets. In a mathematical model, training algorithms are represented by a vector or file, and the trained data is represented by a matrix [10]. Through iterative optimization of the objective function, trained algorithms learn the function that is used to predict the output associated with new inputs. With optimal function, it is possible to determine the algorithm's correct outputs for inputs that were not part of the training data. If the algorithm improves the accuracy of its outputs or predictions over time, we can say that it has learned to perform this task [11].

The success of the algorithm is determined by a process called cross-validation, which is performed only in classifications. This means that the algorithm must classify the object according to the input data. Subsequently, the dataset (a set of trained data from which the function learns patterns and connections in the data) is divided into two subsets - training and testing. Where training is used to learn a program and test to measure its success. After the function training is completed, the test subset is inserted into the program as an input and its output is compared to the correct output in the test subset of the dataset.

Supervised learning are most commonly used. In this model, it is necessary to teach the algorithm to what result to work out. It works on a similar principle as when a child learns to recognize different things by remembering a picture from a book. The teacher's learning algorithm is trained by a set of data that has a predefined output.

B. Unsupervised learning

Unsupervised learning algorithms deal with a set of data that contains only inputs and look for structure in the data, such as clustering or grouping data points. Therefore, algorithms learn from test data that has not been classified, labeled, or categorized. Algorithms identify common features in the data and respond based on the presence or absence of such common features in any new data[12].

The division of unsupervised learning can be divided into two groups, namely clustering, and association. The task of clustering is to connect data into groups that have something in common. And the association's task is to find association rules that describe groups of data and the relationships between them.

Unsupervised learning must work towards a result without much human help. An example of teaching without a teacher is when a child learns to recognize things only based on the characteristic (color, shape, ...) of the thing and not based on the title. The child will look for similarities between the images and divide them into groups, assigning each group its new label.

C. Semi-supervised learning

The combination of the two previous approaches creates a third approach. In this approach, a large number of input data X is available, but only a part of them also have output data Y [20]. Many problems fall into this type of machine learning. The reason for the missing output values is the time demand, cost or need of experts in the field. This approach makes it possible to use non-teacher learning techniques to determine the relationship between data and teacher learning techniques to predict data without output values. The values thus obtained can be further used to better train the model.

D. Reinforcement learning

Reinforcement learning is a type of machine learning, where agents learn how to behave by observing the actions and their results [21]. The information is provided as feedback behind the machine's action in a dynamic environment. Based on the action taken and the feedback, the machine will learn how to behave in certain situations. This kind of machine learning has found use especially in computer games, where machines are used as opponents in multi-player games. The strength and success of this approach are demonstrated by OpenAI Five (a system of five neural networks) who defeated DOTA's top 2 players around the world in DOTA [22]. Feedback learning has also found application in other areas such as:

- self-driving cars,
- robots,
- advertising and marketing.

IV. Machine learning algorithms

Several machine learning algorithms have been developed using experiments and research. Each algorithm has its advantages and disadvantages and it is not possible to compare and evaluate the best one. This chapter describes the best-known models.

A. Random Forest

The first algorithm for random decision forests was developed using the Tin Kam Ho method [13] using the random subspace method, a method of introducing the classification proposed by Eugen Kleinberg's "stochastic discrimination" method.

Random Forest is a combined learning method for regression and classification. It is a file tool to build decision trees that requires a subset of observations and a subset of variables. It creates a larger number of such trees and connects them together as shown in FIG. 1, to obtain a more accurate and stable forecast [15]. The algorithm uses random data to determine the distribution that best describes it. The result is a set of trees, each tree containing its own rules, which implies that it has a different output. The result is determined by the choice where, out of the set of results for which the largest number of trees have âĂIJvotedâĂİ, is considered the most likely [14].

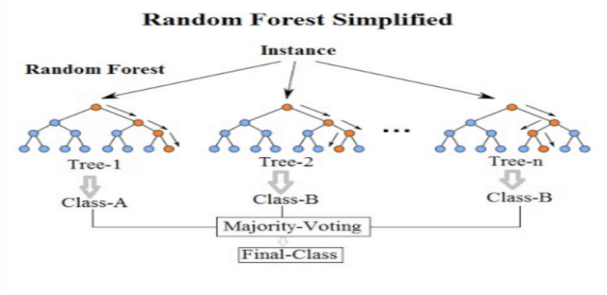

Fig. 1. Random forest algorithm - tree joining

B. Support Vector Machines

Supported Vector Machines (SVM) is a machine learning method with a teacher that is mainly used for classification and regression analysis. The goal of the supported vectors method is to find a plane that divides the space of the symptom in such a way that the trained data belonging to other classes lie in opposite semi-spaces, see Fig. 2. The optimum plane is such that the value of the minimum distance of the point from the plane is as large as possible [16].

In the SVM algorithm, each data item is plotted as a point in the N-dimensional space, where N is the number of containing elements and the value of each element is the value of a particular coordinate [14].

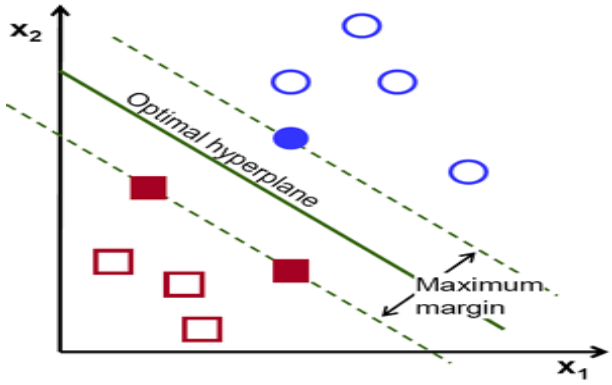

Fig. 2. Support vector machines algorithm

C. Artificial Neural Networks

Artificial neural networks are inspired by the principle of functioning of the nervous system, whose basic building components are nerve cells - neurons. The neural network arises from the interconnection of individual neurons. The connection is made by outputting pulses of the neuron, which are applied to the inputs of other neurons. The basic network topology consists of an input layer, one or more hidden layers and an output layer. The backpropagation algorithm used to teach the network is based on comparing the real network output with the expected value and then adapting the weights and thresholds of certain neurons from the output layer to the input layer.

Each algorithmic learning cycle consists of two transitions [17]:

- **Transition forward** - a signal is applied to the input layer and spreads through the individual layers up to the output layer. On the output layer, the output signal is compared with the expected values of the output vector.
- **Transition backward** - the difference between the output signal and the expected values yields an error function that penetrates backward of the last layer in the reverse direction. Subsequently, weights of neurons in all layers are adjusted against the gradient of the error function.

An example of the functioning of an artificial neural network algorithm can be seen in Figure 3.

D. K-means algorithm

It is a type of unsupervised algorithm that solves the clustering problem. Clustering is similar to classifications, but unlike it classifies elements into classes without names.

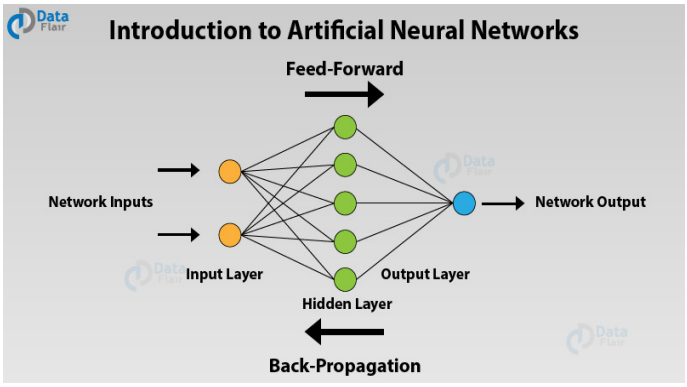

Fig. 3. Example of artificial neural network [3]

The k-means algorithm works in two steps: assignment and optimization [18]. The assignment adds several centorids to the noise space, which are the points defining the clusters. Centorids are placed in random positions and their number should be the same as the number of bursts. Centorids can move in the individual steps of the algorithm, but the data points must remain stationary. The second step is optimization. When optimized, the centorids move to the center of the area in which the points of their category are located and assigned the closest points. The centroid's position is recalculated to form the center of its cluster, repeating this process until the centoride's position has stabilized. Subsequently, the centorides are removed from the space and marked clusters are formed whose point properties are the same [14]. An example of the K-means algorithm is shown in FIG. 4

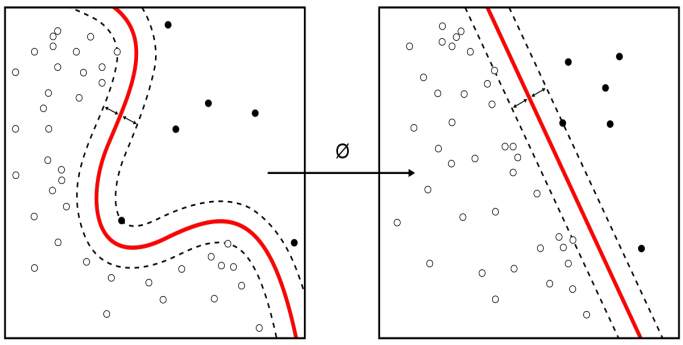

Fig. 4. Example of K-means algorithm

V. The benefits of machine learning algorithms based on the information obtained

These algorithms are the most widely used machine learning algorithms at present. Each algorithm has its own elements of learning that have different specializations in certain areas of systemic activities.

Machine learning algorithms and machine learning, in general, are a matter of developing the technologies of the future. Using machine learning algorithms, we can accelerate complex processes in different areas of human life and avoid unnecessary, often-occurring, human errors. Algorithms can help in difficult decision-making situations, thus saving time for people to perform skilled human activities that can often save human life.

VI. Conclusion

The aim of the research was to get acquainted with the logic and importance of machine learning. The thesis describes techniques and algorithms that are necessary for machine learning. The main goal was to compare the currently used algorithms, which are divided into four basic categories of machine learning. After the correct classification, the benefits of these algorithms were highlighted based on the information obtained.

References

[1] T. G. Dietterich, "Machine-Learning Research", AIMag, vol. 18, no. 4, p. 97, Dec. 1997.

[2] S. Sra, S. Nowozin, Stephen J. Wright, "Optimization for Machine Learning," Cambridge, (2012).

[3] Nils J. Nilsson, "Introduction to MAchine Learning (textbook)," Stanford University, (1998).

[4] D. Autor, "Polonayis Paradox And The Shape Of Employment Growth (National bureau of economic research)," Cambridge: Massachusetts Avenue, 2014.

[5] E. Brynjolfsson, T. Mitchell, "What can machine learning do? Workforce implications," Cambridge, 2017.

[6] Y. LeCun, Y. Bengio, G. Hinton, "Deep learning" Nature 521, 436 444, (2015).

[7] Segal, M. R. Machine Learning Benchmarks and Random Forest Regression. UCSF: Center for Bioinformatics and Molecular Biostatistics, University of California: San Francisco, (2014).

[8] A. McGregor, M. Hall, P. Lorier, J. Brunskill, "Flow Clustering Using Machine Learning Techniques," Lecture Notes in Computer Science, vol 3015.(2004).

[9] R. Bost, R.A. Popa, S. Tu, S. Goldwasser, "Machine learning classification over encrypted datam," (2015).

[10] S.J. Russell, P. Norvig, "Artificial intelligence: a modern approach (book style)," Malaysia; Pearson Education Limited, (2016).

[11] S. R. Michalski, G.Jaime Carbonell, M. Tom Mitchell, "Machine Learning: An Artificial Intelligence Approach (chapter in the book)," California (1983), pp. 6-18.

[12] V. Roman, "Unsupervised Machine Learning: Clustering Analysis (article)," (2019).

[13] Tin Kam Ho, "Random decision forests," Proceedings of 3rd International Conference on Document Analysis and Recognition, Montreal, Quebec, Canada, 1995, pp. 278-282 vol.1.

[14] S. Ray, "Commonly used Machine Learning Algorithms (with Python and R Codes)," (2017).

[15] T. S. Stava, "Tuning the parameters of your Random Forest model," (2015)

[16] T. Hastie, R. Tibshirani, Jerome Friedman, "The Elements of Statistical Learning: Data Mining, Inference, and Prediction (book style)," USA: Stanford University, (2009), pp. 417-438.

[17] J. Svitek, "Poznávanie, umelá inteligencia a strojové učenie," (2018). url: https://www.efocus.sk/kategoria/ict-technologie/clanok/poznavanie-umela-inteligencia-a-strojove-ucenie

[18] K. Alsabti, S. Ranka, V. Singh, "An efficient k-means clustering algorithm". Electrical Engineering and Computer Science, (1997).

[19] C. L. Ramsey, John J. Grefenstette, "Case-Based Initialization of Genetic Algorithms," Naval Research Laboratory, Washington, DC 20375-5337, (1993).

[20] Z. XIAOJIN. âĂIJSemi-Supervised Learning TutorialâĂİ. In: Department of Computer Sciences University of Wisconsin, Madison, USA. 2007.

[21] V. KURAMA. Reinforcement Learning with Python. (cit. 03. 12. 2018) url: https://towardsdatascience.com/reinforcement-learning-with-python-8ef0242a2fa2.

[22] V. SAVOV. The OpenAI Dota 2 bots just defeated a team of former pros. (cit. 08. 12. 2018) url: https://www.theverge.com/2018/8/6/17655086/dota2-openai- botsprofessional-gaming-ai.

The impact of FACTS facilities during short-circuit in power system

[1]*Vladimír KOHAN (1st year)*
Supervisor: [2]Michal KOLCUN

[1,2]Dept. of Electric Power Engineering, FEI TU of Košice, Slovak Republic

[1]vladimir.kohan@tuke.sk, [2]michal.kolcun@tuke.sk

Abstract — **The present article is focused to impact of FACTS systems and their utilization for improvement of transient stability during set short-circuit. This article consists of simulations of SVC, STATCOM, TCSC and UPFC systems of a practical representation in NEPLAN software. This paper is focuses on implementing FACTS devices and is compared to different types of controllers. The modeling of the elements in the NEPLAN program shows the regulator's response to voltage and active and reactive power at the short-circuit. The final chapter is dedicated on the recommendation of the practice use of FACTS devices in power transmission system that can help to operate the power flow, stabilize voltage oscillations and improve the transient phenomena.**

Keywords: FACTS, transient phenomenon, controller, short-circuit, dynamic stability

I. INTRODUCTION

The operation of each FACTS system is different, and therefore, when it is installed, it will be determined in advance what type of controller is to be dealt with in order to provide the most optimal solution to the individual problems in a given line or node, whether global or local. In almost any case, any version that is suitably set up for a given network greatly improves the quality of either transmission or transients and the stability of electricity.

This scheme examined transient phenomena (dynamic stability) adjusted to 3-phase short-circuit and subsequently observed power system oscillation using flexible devices with and without the use of it.

The application of FACTS systems is mainly limited by the investment costs due to power semiconductor devices and the overall complexity of the technology structure. However, due to their high reliability and efficiency, the return on these devices exceeds the costs associated with their purchase and installation [1], [15].

Using the NEPLAN computational program, a simple diagram (Figure 1.) was constructed to observe transient events with the implementation of FACTS systems and to compare their response and ability to regulate voltages and power flows with the best possible ability to maintain system stability. In the given scheme, disturbances are defined, where the line "LINE23" is disconnected at 0.2 s from both nodes and in the node "BUS3" at a time of 0.1 s a three-phase short-circuit with a duration of 0.1 s is set (thus up to 0.2 s).

In the following subchapters, the individual effects of the controllers will be graphically presented, starting with a system where the generator is not using flexible systems (only the wake-up controller is used) and then compared with individual FACTS devices (SVC, TCSC, STATCOM with UPFC - in this order). Each of the waveforms shows the time on the x axis (from 0s to 5s) and the y-axis shows the bus voltages and active and reactive power on the generator in proportional units. All elements of the FACTS system will connect to a node called "BUS4".

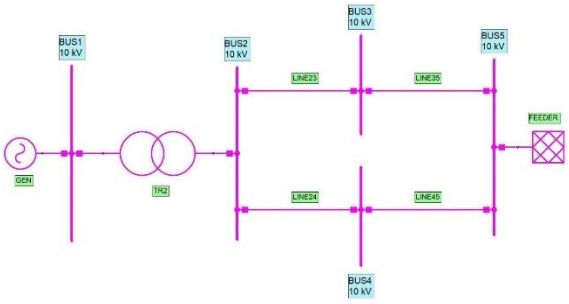

Figure 1. Fundamental scheme

The scheme consists of a generator, a transformer, a series-parallel line and a feeder. All of these elements are enough to keep track of dynamic influences, stability, and voltage fluctuations in a variety of unwanted phenomena in the system. In our case, disconnecting the line and applying a three-phase short circuit in the node can be observed in the oscillations of the voltage and power, thereby evaluating why it is necessary and advantageous to use the control FACTS devices [3],[9].

II. SIMPLIFIED MODEL OF SIMULATION OF DYNAMIC PHENOMENA WITHOUT AND WITH USING EXCITER IN NEPLAN PROGRAMME

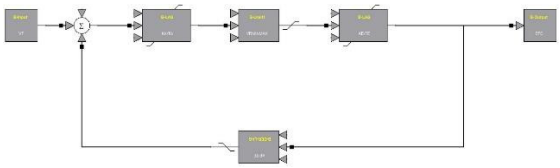

Figure 2. Controller exciter

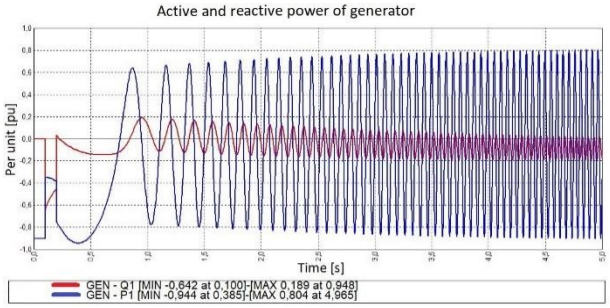

Figure 3. Without exciter P, Q

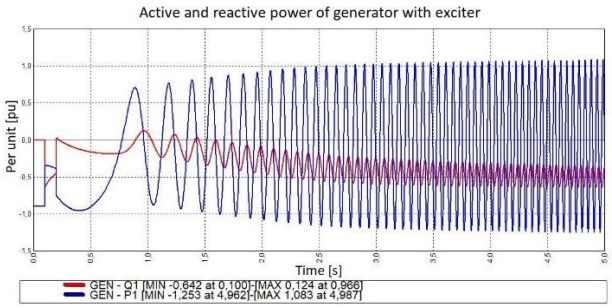

Figure 4. With Exciter P, Q

Figure 3. and Figure 4. shows the active (blue wave) and reactive (red wave) waveforms of the generator without and using the exciter controller. From the waveforms it can be seen that with the set failure, the generator has grown to the point that it has not been able to stabilize itself to a constant power value. The generator has dropped out of synchronism while the amplitude of the oscillation increases with increasing time - generator shutdown is required (power supply stabilization). The exciter response can also be noted by the fact that the reactive power oscillation has stabilized at a lower value (without amplitude change) compared to the non-exciter generator [5],[6].

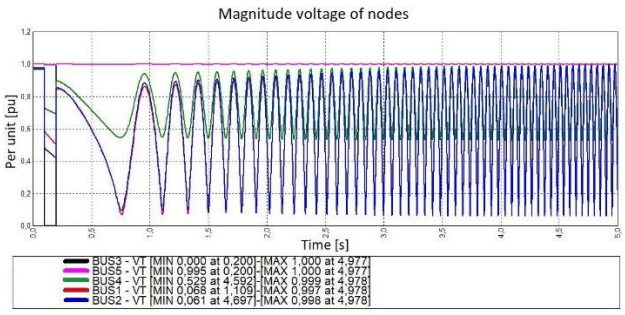

Figure 5.Voltage without exciter

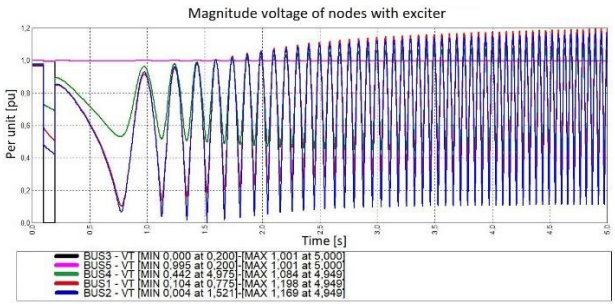

Figure 6. Voltage with exciter

Disconnection of the line "LINE23" and the formation of a three-phase short-circuit on the bus "BUS3" due to large currents and interaction of the entire system oscillated the voltage as shown in Figure 5. and Figure 6. As a result of the exciter controller, the voltage fluctuations at the "BUS1" generator outlet were shifted (similar to reactive power) above 1 p.j. and similarly they could not stabilize. The voltages "BUS5" have almost constant value throughout the monitored time. This is due to the fact that "FEEDER" is considered to be a so-called. a hard network - a network capable of delivering any amount of power without much voltage change (used to calculate and simulate waveforms for NEPLAN). Thus, we can conclude that the driver cannot stabilize and compensate for the serious failure and is not sufficient to stabilize and regulate the dynamic events in the system [4], [22].

III. DYNAMIC MODEL OF SVC CONTROLLER

The main purpose of the SVC regulator is to increase the transmission capacity of the power system. This can be achieved if voltage is provided (by stabilizing it) and by increasing system stability boundaries. In order to stabilize the voltage at the receiving end of the transmission line and to contribute to the improvement of transient stability, the SVC essentially functions as a voltage regulator. While reactive power changes to reduce and quickly damp oscillations during voltage fluctuations, and especially after major bus failures [10], [19], [20].

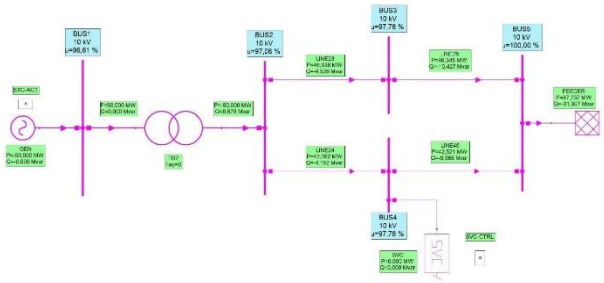

Figure 7. Model with SVC

The FACTS system technology, called SVC, is placed in the model in the "BUS4" node, with each FACTS element having its own controller, which controls the individual parameters for power transmission based on inputs and outputs. It is a modern trend that SVC controllers have also been widely used to control offtake in industry or household to improve a power factor [7].

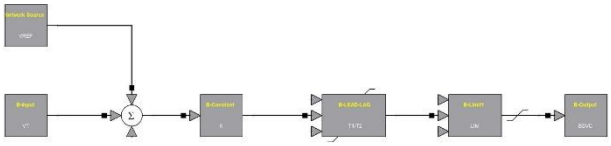

Figure 8. Controller of SVC system

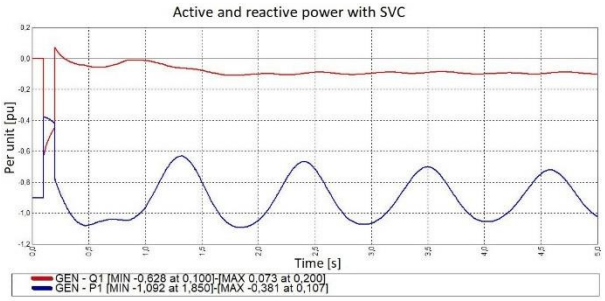

Figure 9. Active and reactive power with using of SVC system

In Figure 9. we can observe the response and influence of the controller and SVC system on generator performance compared to its use or using other FACTS systems (listed in other subchapters). The reactive power the SVC was able to stabilize to an almost constant value while the active power settled at low oscillations, which no longer set a constant value with the controller.

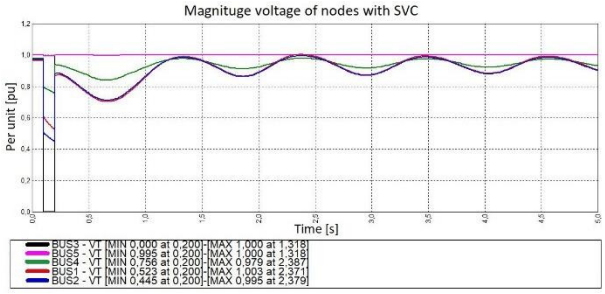

Figure 10. Magnitude voltage with using of SVC system

The SVC system greatly influenced the voltage fluctuations in all system nodes except the "BUS3" fault and the "BUS5" hard network node. Voltage fluctuations were managed by SVC to much lower values, which the network can handle much better, thereby delaying system disruption, disconnecting power supplies, or preventing generator outage from synchronism [17].

IV. DYNAMIC MODEL OF TCSC CONTROLLER

For studies of dynamic stability and oscillation events, a TCSC device may be represented by a variable reactance that is modeled as a variable reactance at a base frequency due to failure and during frequency variation - the frequency remains constant.

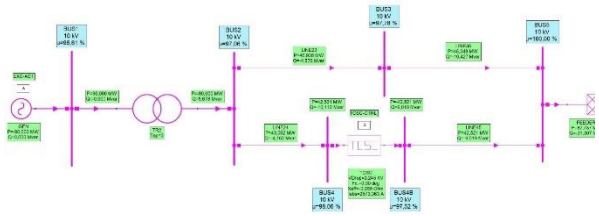

Figure 11. Model with TCSC device

Each of the FACTS devices is designed for the purpose of controlling or controlling the parameters in the system. Thus, the regulator may have entered different input values (voltage, current, power, etc.), which it monitors during operation and thereby controls the output value by means of the members included in the diagram, which may also differ from other regulators (susceptance - change of admittance, inductance - impedance change and others) [18].

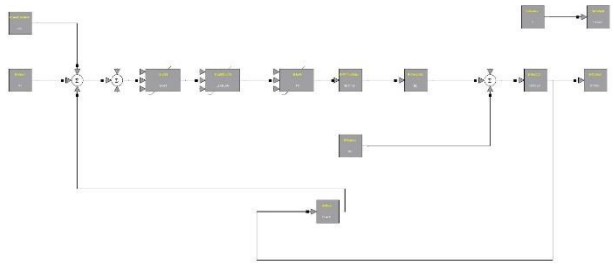

Figure 12. Controller of TCSC system

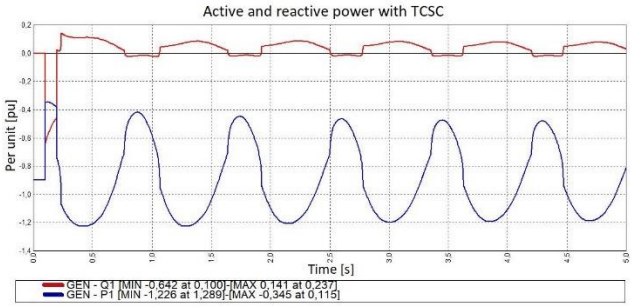

Figure 13. Active and reactive power with using of TCSC

On the curves of active and reactive power of the generator of Figure 13. we can also observe a marked improvement in performance oscillation compared to a non-FACTS-based scheme. Compared to the SVC system, the module thus failed to stabilize TCSC reactive power without oscillations. From the graph (red waveform) we can see when the regulator has turned the controller on and off to achieve the best possible power transmission operation by the power system [11].

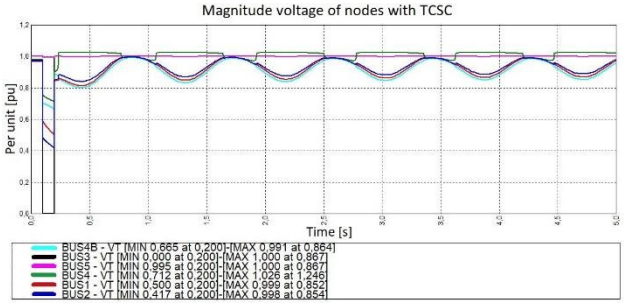

Figure 14. Magnitude voltage with using of TCSC system

Switching on the TSCS module also affected the voltage that the controller was able to settle for minimal fluctuation to ensure its subsequent amplification amplitude as was the case without using a FACTS device. When switching the semiconductor elements in the TCSC, the voltage variation in the "BUS4" node was changed step by step when the oscillations and voltage oscillations were changed due to the impedance change (see Figure 14) [12].

V. DYNAMIC MODEL OF STATCOM CONTROLLER

Dynamic models of STATCOM devices are based on dynamic SVC systems, the difference being that each of them is constrained by a different value. STATCOM is restricted by current (between IC max and IL max) while SVC is limited by susceptance (between BC and BL) [23].

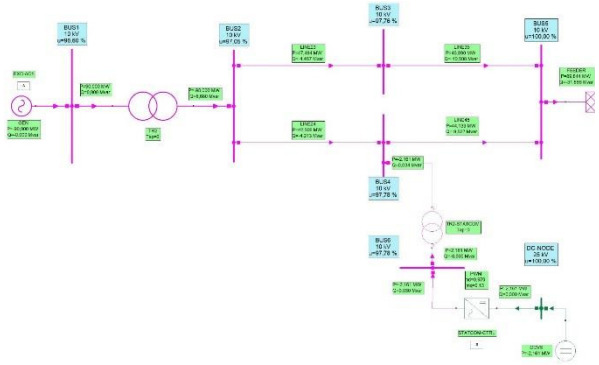

Figure 15. Model with STATCOM device

Each FACTS system has its own controller structure and is, in a way, unique in design and control of given parameters in a system or compensated area. The same technology of a given type of FACTS system can have many designs with a different controller control principle. It means different concurrency of input and output information - another mathematical model of the controller diagram. While the output of them is always connected and it is connected to the switching and switching control pulses of semiconductor components [14].

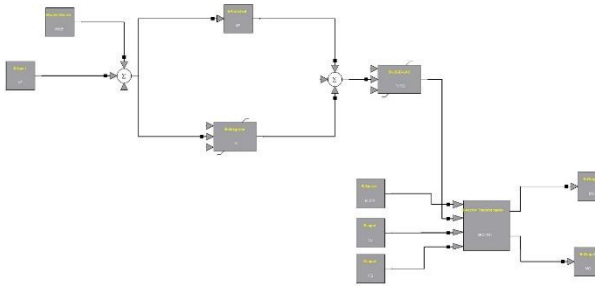

Figure 16. Controller of STATCOM system

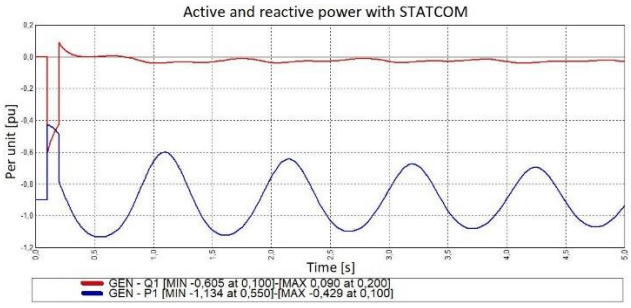

Figure 17. Active and reactive power with using of STATCOM system

As with previous simulations of FACTS controllers used to improve system stability and dynamics, STATCOM technology is able to similarly regulate and reduce voltage and active and reactive power oscillations even when using other equipment designs. From the graphs shown in Figure 17. and Figure 18. we can observe the influence of the STATCOM controller system, which has stabilized the reactive power to almost constant value, and the active power has substantially reduced the amplitude of the oscillations and limited their rapid step changes as opposed to without the FACTS controllers [16].

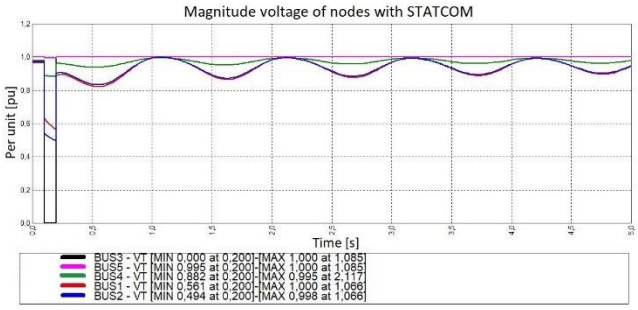

Figure 18. Magnitude voltage with using of STATCOM system

VI. DYNAMIC MODEL OF UPFC CONTROLLER

The UPFC is a combination of serial and parallel controlled compensation. The UPFC system may appear to be interconnected two known as devices, namely STATCOM and SSSC interconnected via VSC converters with a DC link. This device can independently control both active and reactive power transmitted by the transmission line.

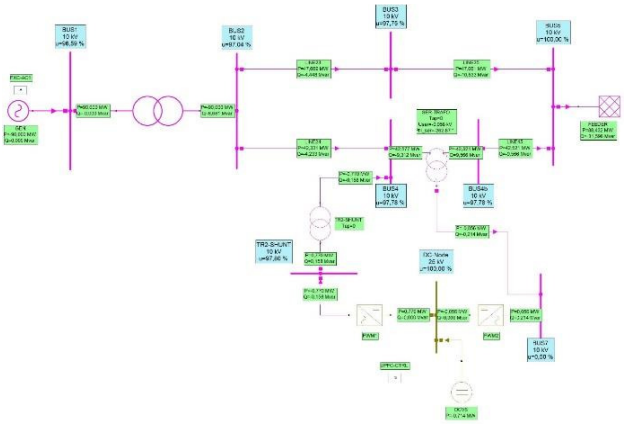

Figure 19. Model with UPFC device

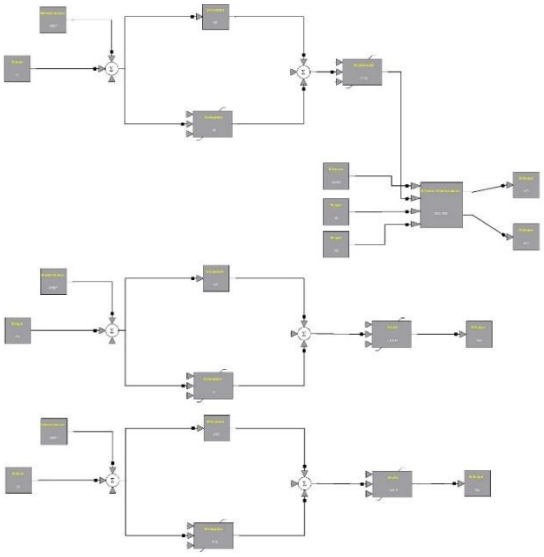

Figure 20. Controller of UPFC system

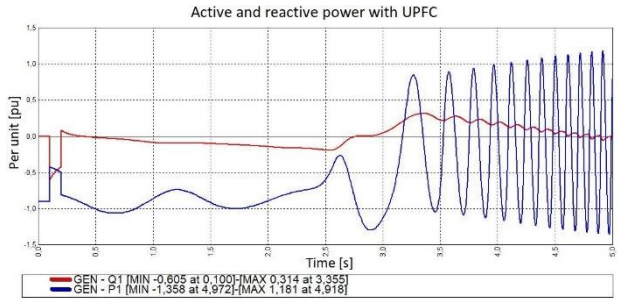

Figure 21. Active and reactive power with using of UPFC system

In Figure 21. and Figure 22. we can see the response of the UPFC system controller, which failed to compensate for the failure, stabilize or mitigate the effects of oscillation of power, voltage, and other system parameters. By approximately 2.9 seconds when the first greater active power oscillation was generated, the controller was unable to stabilize this oscillation. As a result, the amplitude of power and voltage increased with increasing time and would oscillate until the local area in the network or the entire system was broken down. In this case, we can say that the synchronous generator has dropped out of synchronism and the UPFC controller has failed to improve the power transmission in the system.

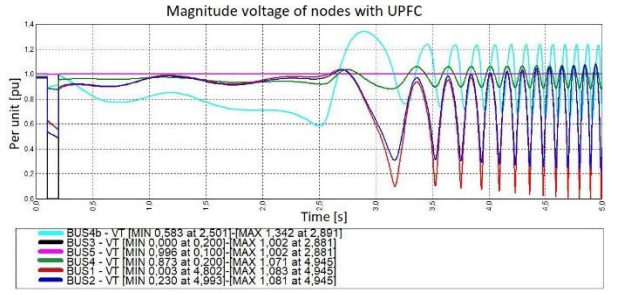

Figure 22. Magnitude voltage with using of UPFC system

CONCLUSION

From the individual developments and research on the impact of FACTS devices in this model, we can evaluate that in the vast majority of these devices are able to greatly ensure the improvement and reliability of the power system. Each device has its own controller and its design and location is suitable for various applications that need to be solved for their installation. This is an analysis for the purpose of applying the device to the system, and which of the electricity quality indicators need to be improved or optimized at a given location. It can be a power factor improvement, reactive power compensation, node voltage stability, increased transmission capacities, and especially the fastest possible dynamic events in various failures, resulting in rapid assistance for synchronous generators and preventing their outage from synchronism. Through FACTS systems, we can manage power flows, ensure continuous production, transmission and supply of electricity, and thus strengthen the whole system as a whole, thereby avoiding blackouts or even a major problem such as the aforementioned "Blackout" systems [13], [21], [24].

Due to the rapidly evolving demand for electricity, it can be stated that FACTS systems will be largely implemented in different locations, whether transmission or distribution systems. However, before they are put into practice, an analysis is needed to address what equipment is best suited to the issue and to which part of the network to use the selected system to make it as reliable as possible to optimize electricity transmission [1], [2], [8], [25].

ACKNOWLEDGEMENT

This work was supported by the Scientific Grant Agency of the Ministry of Education of Slovak Republic and the Slovak Academy of Sciences by the projects VEGA No. 1/0372/18.

REFERENCES

[1] EREMIA, M. – LIU, CH. CH. – EDRIS, A. A. 2016. Advanced Solutions in Power Systems; HVDC, FACTS, and Artificial Intelligence, 1. ed. New Jersey: Wiley-IEEE Press, 2016. 271-717 p. ISBN 978-1-119-03569-5.

[2] MATHUR, R.M., VARMA, R. K. 2002. Thyristor-Based FACTS Controllers for Electrical Transmission System. New York: Wiley-IEEE Press, 2002. 1-493 p. ISBN 978-0-471-20643 1.

[3] HINGORANI, N. G. – GYUGYI, L. 2000. Understanding FACTS; Conceps and Technology of Flexible AC Transmission Systems. New York: IEEE Press, 2000. 1-425 p.ISBN 0-7803-3455-8.

[4] Goňo, M., Kyncl, M., Goňo, R., Kłosok-Bazan, I.: Experience with the production of electricity from biogas at sewage treatment plant in the Czech Republic, Przeglad Elektrotechniczny, Volume 89, Issue 11, 2013, Pages 12-15

[5] EREMIA, M. – SHAHIDEHPOUR, M. 2013. Handbook of Electrical Power System Dynamics; Modeling, Stability, and Control. New Jersey: IEEE Press, 2013. 291-724 p. ISBN 978-1-118-49717-3.

[6] GÖNEN, T. 2014. Electrical Power Transmission System Engineering; Analysis and Design. 3. ed. Boca Raton: CRC Press, 2014. 140-176 p. ISBN 978-1-4822-3222-6.

[7] PADIYAR, K. R. 2011. HVDC Power Transmission System. 2. ed. Kent: New Academic Science Ltd., 2011. 155-170 p. ISBN 978-1-906574-77-2.

[8] J. Kurimsky, R. Cimbala, and I. Kolcunova, "Multi-scale decomposition for partial discharge analysis," Prz. Elektrotechniczny, vol. 84, no. 9, pp. 191–195, 2008.

[9] KIM, CH. – SOOD, V. K. – JANG, G. LIM, S. – LEE, S. 2009. HVDC TRANSMISSION, Power Conversion Applications in Power System. Singapur: Wiley-IEEE Press, 2009. 1-357 p. ISBN 978-0-470-82295-1.

[10] Mikita, M., Kolcun, M., Špes, M., Vojtek, M., Ivančák, M. Impact of electrical power load time management at sizing and cost of hybrid renewable power system (2017) Polish Journal of Management Studies, 15, pp. 154-162. DOI: 10.17512/pjms.2017.15.1.15

[11] ZHU, J. 2015. Optimization of Power System Operation. 2. ed. New Jersey: Wiley-IEEE Press, 2015. 13-576 p. ISBN: 978-1-118-85415-0

[12] OTTER, J. 1988. Výkonová Elektronika pre elektrické pohony. Bratislava: Alfa, 1988. 23-391 s. ISBN 063-571-88.

[13] KVASNICA, P – JEVČÁK, M. 1982. Prechodné Javy v Elektrizačných Sústavách; Príklady. Košice: Rektorát Vysokej školy technickej v Košiciach, 1982. 5-182 s. ISBN 85-625-82.

[14] VIŠNYI, Ľ. 1978. Statické Meniče Elektrickej Energie. Bratislava: Alfa, 1978. 5-148 s. ISBN 63-705-78.

[15] SAUER, P. W. – PAI M. A. 1998. Power System Dynamics and Stability. New Jersey: Prentice-Hall, 1998. 5-335 p. ISBN 0-13-678830-0.

[16] GRIGSBY, L. L. 2012. The Electric Power Engineering Handbook; Power System Stability and Control. 3. ed. Boca Raton: CRC Press, 2012. 1-450 p. ISBN 978-1-4398-8320-4.

[17] Martinek, Z., Hromadka, A., Hammerbauer, J.: Reliability characteristics of power plants, ADVANCES IN ELECTRICAL AND ELECTRONIC ENGINEERING, Vol. 15, Issue: 1, Pg. 34-45, 2017

[18] Gono, R., Rusek, S., Kratky, M., Slivka, M.: Component reliability parameters of distribution network, (2015) Proceedings

of the 8th International Scientific Symposium on Electrical Power Engineering, ELEKTROENERGETIKA 2015, pp. 364-367.

[19] Fedor P., Perduková D.: Fuzzy Model Based Optimal Continuous Line Controller. In: Proc. of the 8th Int. Scientific Symposium on Electrical Power Engineering ELEKTROENERGETIKA 2015. Stará Lesná, 2015, pp. 404-407. ISBN 978-80-553-2187-5

[20] Kolcun, M., Rusek, K. Analysis of prices for electricity at the Polish power exchange [Analiza cen energii elektrycznej na towarowej giełdzie energii] (2018) Polish Journal of Management Studies, 17, pp. 155-164. DOI: 10.17512/pjms.2018.17.1.13

[21] DOKIC, D. L. – BLANUŠA B. 2015. Power Electronics; Converters and Regulators.

[22] 3. ed. Switzerland: Springer Internatioanl Publishing, 2015. 4-592 p. ISBN 978-86-7466-492-6.

[23] TRZYNADLOWSKI, A. M. 2015. Power Electronic Converters and Systems; Frontiers and applications. Croydon: CPI Group, 2015. 1-617 p. ISBN 978-1-84919-826-4.

[24] HOLMES, D. G. – LIPO, T. A. 2003. Pulse Width Modulation for Converters. Danvers: IEEE Press, 2003. 3-668 p. ISBN 0-471-20514-0.

[25] JIJUN, Y. – HAIQING, X. – JIANKUN, L. – GANG, CH. – QUN, L. – PENG, L. 2017. Unified Power Flow Controller Technology and Application. Ninjing: Academic Press, 2017. 19-41 p. ISBN 978-0-12-813485-6.

The impact of using distributed generation in smart networks

[1]*Daniel PÁL (2nd year)*
Supervisor: [2]Ľubomír BEŇA

[1,2]Dept. of Electric Power Engineering, FEI TU of Košice, Slovak Republic

[1]daniel.pal@tuke.sk, [2]lubomir.bena@tuke.sk

***Abstract* — As the share of renewable energy sources increases, the classic centralized scheme is transformed into decentralized electricity generation. Thanks to renewable energy is now economically profitable to produce electricity directly at the point of consumption. Despite the advantages offered by renewable distributed generation technologies, the incorrect integration of distributed generation into existing distribution networks may give rise to several economic and technical challenges. Optimal planning of distributed production is therefore of paramount importance to ensure that the power of the distribution network can meet the expected energy quality, voltage stability, reduced energy loss, reliability and profitability.**

***Keywords* — distributed generation, renewable energy sources, SMART Grid.**

I. INTRODUCTION

At present, the so-called centralized generation of electricity is most often used. Centralized production is a form of power generation, in which electricity is produced in large power plants, which are located at large distances from end users. The amount of electricity produced is based on statistics, which is based on electricity consumption in the past. After power generation, the power supply voltage transformed to a higher voltage level, in order to reduce transmission losses by lines. Voltage in the vicinity of consumers is transformed back to a lower voltage [1][2]. This can be seen in the Fig. 1 below.

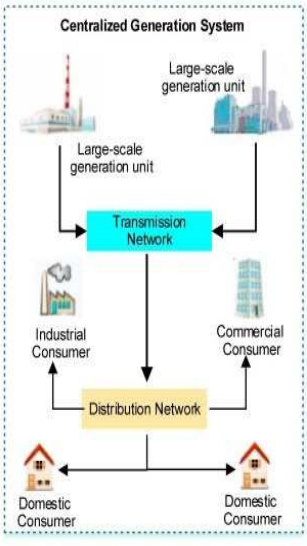

Fig. 1 Centralized generation system [3]

II. SMART GRID

In increasing the share of renewable energy sources is a classic centralized schema changes for decentralized production of electricity. Thanks to renewable energy sources it is currently economically profitable to produce electricity directly at the point of consumption. In the case of excess energy, it is also possible to store it for use when needed. New sources and new technologies are therefore increasingly appearing in the electricity grid. There is a need for new communication between such components. The electricity grid is transformed into a smart grid (SMART GRID). Smart Grid is shown in the Fig. 2.

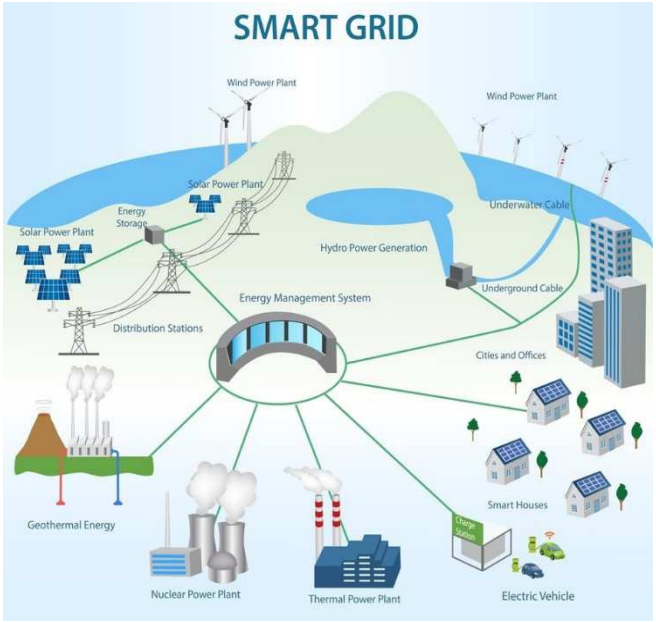

Fig. 2 SMART Grid [4]

The topic of smart grids is nowadays becoming increasingly topical, since electricity is needed to use most effectively. Energy must be transferred from production to the point of consumption with the least possible losses.

There are various methods how to reduce power losses in the networks. For example:

- usage of distributed generations,
- network reconfiguration.

In this article the first method will be described in more detail.

III. DISTRIBUTED GENERATION

Distributed generation refers to a variety of technologies that generate electricity at or near where it will be used. In applying distributed generation are commonly used renewable energy sources. Renewable energy sources are combined with heat and power plants. It is much easier to build small power plants than large power plants. It can be seen in the Fig. 1, that the electricity is produced with centralized method, but in the distributed generation it is produced with decentralized method, so the production is much more distributed in the networks [5][6]. This is shown in the Fig. 3.

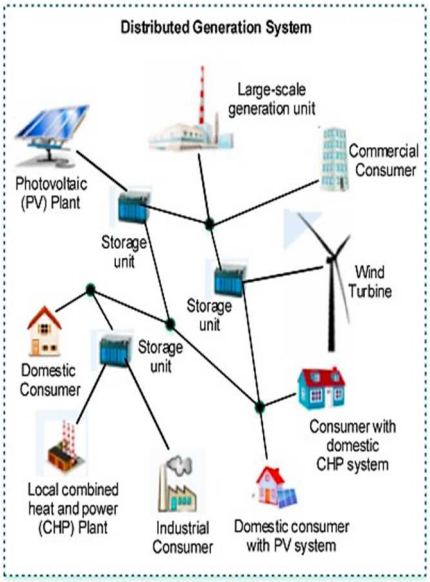

Fig. 3 Distributed generation system [3]

Typical distributed generation performance values are as follows:

- Hydro power plants
  - Small → 0.025 (MW) - 1 (MW)
  - Large → 1 (MW) - 100 (MW)
- Wind turbines → 200 (W) - 3 (MW)
- Solar power plants → 20 (W) - 100 (kW)
- Geothermal plants → 5 (MW) - 100 (MW)
- Biomass → 0.1 (MW) - 20 (MW),
- Battery → 0.5 (MW) - 5 (MW) [5][6].

The benefits of using distributed generations:

- reduction of power losses,
- improvement on electricity quality,
- improvement on system reliability,
- reduction of greenhouses gases emission,
- an emergency supply of power,
- reduction of peak power requirements,
- offsets to investments in generation, transmission, or distribution facilities that would otherwise be recovered through rates,
- provision of ancillary services, including reactive power [5][6][7].

Before application distributed generation, it is necessary to examine the network where to connect the new power plant to get the benefits described above. These cases may arise:

1. Determination of the optimal power (P, Q) of the power plant if the connection point is predetermined - for example, renovating an old power plant, or there is a place for photovoltaics because the best conditions are there. In this case, only the power of the plant can be changed.
2. Determination of the optimum connection point if the power output of the plant is predetermined - in this case the power is given - e.g. we want to connect batteries, biomass to the network, and only we can change where it is connected to the network.

To reduce the loss beyond the size of the installed power value, the method has some effect on what type of generator is used. The generator can:

1. Produce only active power – (P+),
2. Produce only reactive power – (Q+),
3. Produce active and reactive power – (P+), (Q+),
4. Produce active power but take reactive power – (P+), (Q-) [8].

IV. FUTURE RESEARCH

Further research focuses on setting up a computer program designed to calculate network losses based on input parameters. The loss-based program should determine the location of the distributed generations with optimization algorithm in order to reduce the losses and increase network stability.

ACKNOWLEDGMENT

This work was supported by the Scientific Grant Agency of the Ministry of Education of Slovak Republic and the Slovak Academy of Sciences by the projects VEGA No. 1/0372/18.

REFERENCES

[1] Electricity is delivered to consumers through a complex network. [online]. Available at: https://www.eia.gov/energyexplained/electricity/delivery-to-consumers.php. Accessed on January 27, 2020.

[2] H. Farhangi: The path of the smart grid. In: *IEEE Power and Energy Magazine*. Vol. 8, no. 1, pp. 18-28, January-February 2010. ISSN 1558-4216.

[3] A. Ehsan, Q. Yang: "Optimal integration and planning of renewable distributed generation in the power distribution networks: A review of analytical techniques". In: Applied Energy. Elsevier Ltd. 2018, Volume 210, pp. 44-59. ISSN: 0306-2619.

[4] How Secure Is Our Smart Grid? [online]. Available at: https://www.govtech.com/blogs/lohrmann-on-cybersecurity/how-secure-is-our-smartgrid.html. Accessed on February 2, 2020.

[5] L. I. Dulă, M. Abrudean, D. Bică: „Optimal Location of a Distributed Generator for Power Losses Improvement". In: Procedia Technology. Elsevier Ltd. 2016, Volume 22, pp. 734-739. ISSN: 2212-0173.

[6] Dulău LI, Abrudean M and Bică D.: Automation of a Distributed Generation System, 49th Universities' Power Engineering Conference (UPEC), IEEE Xplore, pp. 1-5, 2014. ISBN: 978-1-4799-6557-1.

[7] Distributed Generation: What are the benefits? [online]. Available at: https://alcse.org/distributed-generation-benefits/. Accessed on February 3, 2020.

[8] P. Mehta, P. Bhatt, V. Pandya: „Optimal selection of distributed generating units and its placement for voltage stability enhancement and energy loss minimization". In: Ain Shams Engineering Journal. 2018, Volume 9, Issue 2. pp. 187-201. ISSN: 2090-4479.

Thermal simulation of CNC milling machine actuators

[1]*Branislav FECKO (2nd year)*
Supervisor: [2]Tibor VINCE

[1,2]Department of Theoretical and Industrial Electrical Engineering, FEI TU of Košice, Slovak Republic

[1]branislav.fecko@tuke.sk, [2]tibor.vince@tuke.sk

***Abstract* — The paper describes an actuators thermal model simulations of CNC milling machine. After defining individual heat sources in CNC milling machine we started to create models of part of CNC machine with heat losses simulation. The publication is specifically aimed at investigating the thermal conditions of a DC motor with a permanent magnet and a hybrid stepper motor.**

***Keywords* — actuator, CNC milling machine, copper losses, DC motor, eddy current, hysteresis losses, Simulink, stepper motor, thermal model**

I. Introduction

The DC motors and stepper motors are often used in practice. In our case, the DC motor is used as spindle in CNC milling machine and stepper motors provide moves of CNC machines axis. We need create thermal model of engine to calculate the heat generated by the engines. The largest amount of the heat in the DC motor is generated by current passing through the motor winding. Since the current value depends on the load, it is necessary to know the operation of the DC motor at different loads. The goal is to develop an accurate model of the DC motor which will be used to predict the value of the supply current. The heat in the stepper motor is generated by copper losses and iron losses. More detailed analysis was created in the article [1]. This paper is focused to research to copper losses and their influence to heating of engines. In the last part of paper the motor thermal models are verified by the measured values.

II. Thermal Model

To create a thermal simulation of a CNC milling machine, a precise thermal model of the drives is required. In the following subchapters we will illustrate simulations of individual engines created in the Simulink. The model of electric motors was extends its thermal conditions, considering the thermal capacities, the thermal conductivity of the components, the heat transfer between the individual parts of the structure, and the location of the losses incurred. By simulating the thermal model, the results of heating the engines under certain operating conditions were obtained.

Simulink model of DC motor with permanent magnets

In the first part we created basic simulation of DC motor. The simulation was published in Article [2]. In Fig. 1 we can see the connection of all the Simulink blocks witch we used in the simulation. The block DC motor is powered by a controlled DC voltage source. Next we have a voltmeter and an ammeter plugged in to determine the values of the power quantities and the probes that plot their waveforms. Simulation simulates engine without load. Block Load Torque presents the load generated by the fan. That is part of the engine and torque that needs to be done to spin the encoder.

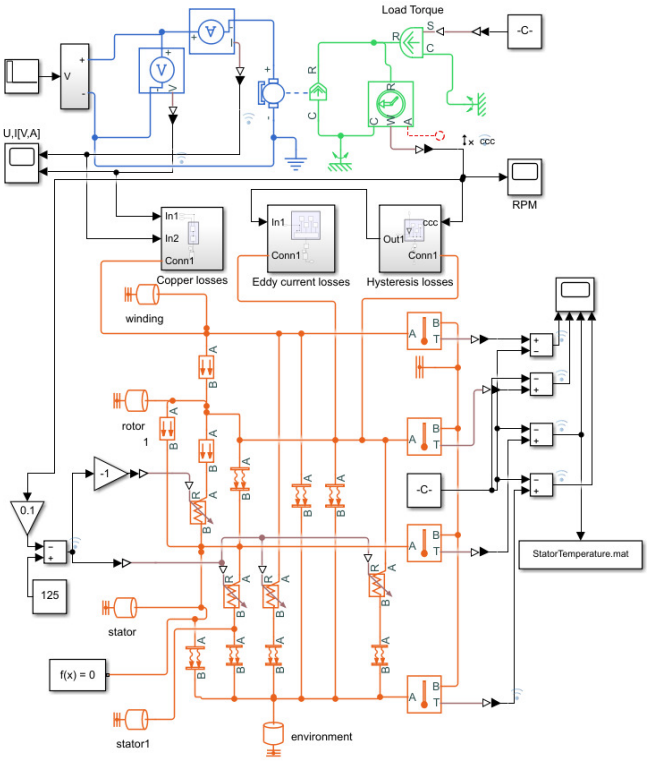

Fig. 1 Thermal simulation of DC motor in Simulink

To create a simulation of the thermal model of a DC motor it was necessary to analyze in detail the properties of the motor part materials. The heat transfer between its parts and to correctly determine the heat sources and their location. The created simulation was compared with the measured values.

Simulink model of Hybrid Stepper motor

The thermal simulation of the stepper motor consists of the power supply of the motor, the stepper motor, the module used for generating losses, the thermal capacities of the individual parts of the motor and their transmission between them. The thermal simulation is shown in Fig. 2.

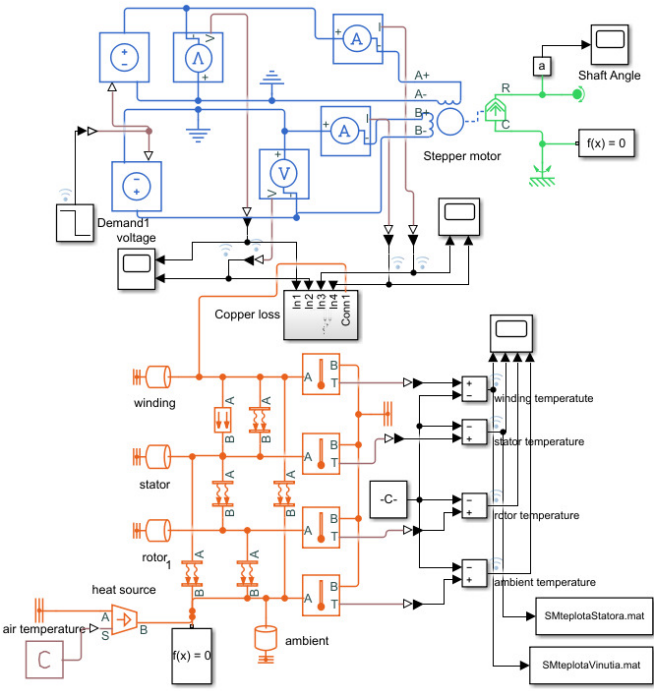

Fig. 2 Thermal simulation of stepper motor in Simulink

The electrical part of the simulation is made of blue and the simulation of the thermal conditions of the engine is drawn in orange. For the simulation the components of the thermal mass representing the parts of the engine and the components of the heat and convection were used. The heat source was used to model copper losses that were placed directly on the motor winding. The thermal simulation describes the state at a constant current of 1.7 A in both motor phases.

The simulation was used to verify the individual thermal conditions of the engine, such as heat transfer between components and surroundings. During the simulation, both motor windings were excited continuously, in this state the rotor does not move and current flows through the windings. The simulated state is suitable for verifying the accuracy of Joule losses calculation due to the non-creation of other types of rotor movement losses.

III. Verification of Simulated Date

We have created a thermal model to simulate the temperature of individual engine components. To verify the simulation, it was necessary to compare the accuracy of the model by real motor measuring. The conditions of simulation and measurements was same. The results of comparing the simulation and measurement of real device are as follows.

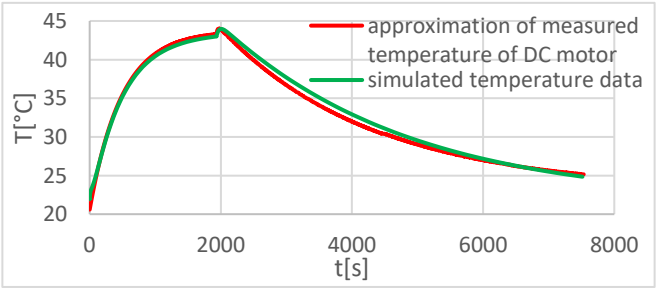

Fig. 3 Comparison of measured and simulated data of DC motor

The following graphs show a simulation of the stepper motor temperature.

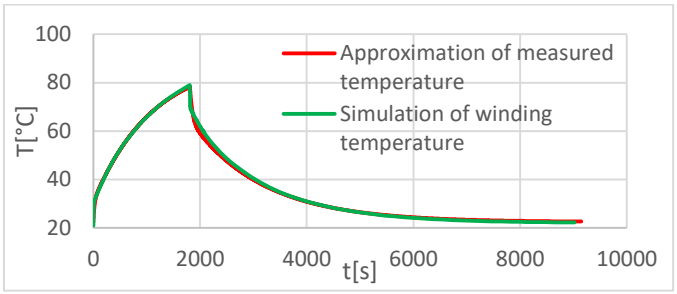

Fig. 4 Comparison of measured and simulated temperatures of the stepper motor winding

The design of the stepper motor made it possible to measure the winding temperature and the rotor temperature separately. Therefore, for stepper motor we have two temperature comparison graphs of stator and winding temperature.

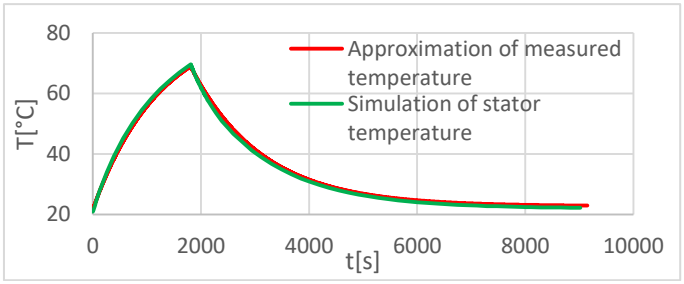

Fig. 5 Comparison of measured and simulated temperatures of the stator part of the stepper motor

IV. Conclusion and Next Steps

By comparing the simulated data, we can say that the simulation created is sufficiently accurate for further use in modeling the complete thermal model of the CNC milling machine. My next step will be to extend the model of stepper motor to simulate the iron losses and subsequently to create models to extend the state of different engine load. After completing the thermal models of the engines, it will be necessary to create the model of the entire CNC milling machine. Which will be consist from the conversion of the production process into the heat generated by the CNC machine.

References

[1] Fecko B., Vince T.: Electromagnetic losses in stepper motors. Vol. 2, Issue 3 (2018) Journal of Industrial Electrical Engineering, Vol.2 (2018), Issue 3, pp: 30-33, ISSN 2454-0900

[2] Fecko B., Vince T.: Simulink simulation of DC motors. Vol. 3, Issue 1 (2019) Journal of Industrial Electrical Engineering, Vol.2 (2018), Issue 4, pp: 44-47, ISSN 2454-0900

[3] Fecko B., Vince T.: Losses in DC motors. Vol. 2, Issue 4 (2018) Journal of Industrial Electrical Engineering, Vol.2 (2018), Issue 4, pp: 44-47, ISSN 2454-0900

[4] HAITAO, Zhao; JIANGUO, Yang; JINHUA, Shen. Simulation of thermal behavior of a CNC machine tool spindle. International Journal of Machine Tools and Manufacture, 2007, 47.6: 1003-1010.

[5] MathWorks: Simulink documentation [online] [20.03.2019.]. Available online: https://ch.mathworks.com/help-/simulink/

[6] V. Hrabovcová, P. Rafajdus, M. Franko, P.Hudák.: Meranie a modelovanie elektrických strojov. Vydala Žilinská univerzita v Žiline/EDIS-vydavateľstvo ŽU. 2014. ISBN 978-80-554-0852-1

[7] MORAR, Alexandru. The modelling and simulation of bipolar hybrid stepping motor by Matlab/Simulink. Procedia Technology, 2015, 19: 576-583.

Towards a Real Time Personalized Facial Emotion Recognition framework

[1]*Fouzia Adjailia (2nd year),*
Supervisor: [2]*Peter Sinčák*

[1,2]Dep. Cybernetics and Artificial Intelligence, FEI TU of Košice, Slovak Republic

[1]fouzia.adjailia@tuke.sk, [2]peter.sincak@tuke.sk

***Abstract*—Emotion and the ability to understand them are considered a channel of non-verbal communication. It is an important factor to achieve a smooth and yet robust interaction between machines and humans. In this research we proposed a framework that enables us to recognize the true emotions of the employees by showing them stimulus to provoke their real and true emotions.**

***Keywords*—facial emotion recognition, virtual avatar, human-robot interaction.**

I. Introduction

Vision is an important non-verbal communication channel, as a result, computer vision has attracted much attention from researchers. Research on the human face is very popular in image analysis and computer vision because the applications of automatic facial information analysis are numerous and span several fields, ranging from Human-Computer Interaction (emotion recognition) to law enforcement (face recognition).

Facial expression is an effective communication channel that helps to understand the inner state of the mind of human beings, Human face plays a critical role in recognizing the emotional state of the person based on expressions regardless of the person's origin or cultural background. These expressions are a result of a complex muscle structure. An observational study made by Paul Ekman [1] to find whether humans show a similar appearance of emotions. He made this study on a tribe in New Guinea and it showed that facial expressions are the same as civilized people, Finally he proved that we show a universal expressions that help to recognize emotions.

Cloud computing has recently emerged as a paradigm that shifts the hosting and delivering of services over the internet. this paradigm has attracted the business owners since it facilitates the use of requirement for used to provisioning and help it to start even from the small [2].

Cloud computing is a distributed computing paradigm that enables access to virtualized resources including computers, networks, storage, development platforms or applications [3].

II. Analysis and design

We begin, in this section, by presenting the proposed system requirement analysis that motivated its design, functional and non-functional requirement are dealt with also which will allow us to generate use cases after gathering and validating the set of functional requirements

A. Requirement analysis

Capturing the requirements of the system is the first phase in the development, which defines what the system should do or provide for the user. To identify and define the requirements of the system more clearly, the system has to be considered like a black box, the actor can be usually a human user as well as external I/O devices.

1) Functional Requirements:: Some of the primary functions under-developed that the initial proposed version are described as below.

- Facial detection and recognition.
- Facial emotion recognition.
- Virtual avatar.
- Chatbot.
- Recommendation system.

2) Non-Functional Requirements::

- **Cloud based:** The system must deployed in the cloud.
- **Usability:** The system must be easy to use and simple.
- **Performance:** The system must be reliable.
- **Aware:** The system must be aware of its environment.

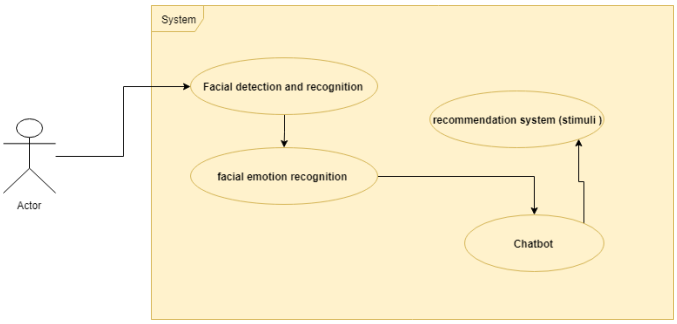

Fig. 1. Use case diagram of our proposed system

3) Use case: We were careful to consider all of these requirements in designing our System. We are now ready to present the architecture itself and its design methodology.

B. Design

The proposed experiment consists of an interface that includes an avatar to make it more adopted by users, the avatar has the ability to build a conversation with the users via a chatbot in order to maintain a long term conversation during which the emotions are being recognised. the system also provides facial recognition to make the study more efficient. once the

emotions are recognised by our system which is deployed in the cloud, a form of stimuli is given for the user, in order to improve their emotional stat. as well as a feedback in order to improve the preferences of every user figure 4.

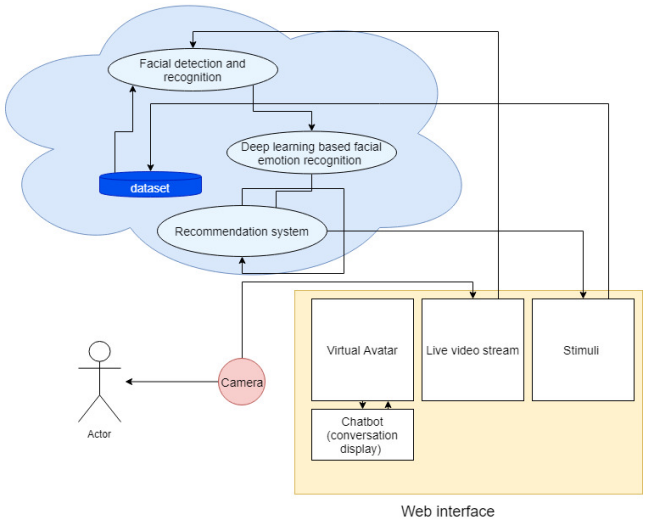

Fig. 2. Proposed design

III. Prototype implementation

The core of our proposed system is to implement a real time facial emotion recognition system that surpass the stat of the art using deep learning approaches. since the system in cloud based, connection must be guaranteed, Camera is also must be provided to capture the images of users in real time to analyse it in the cloud, a feedback is given in form of conversation based on avatar see figure 3

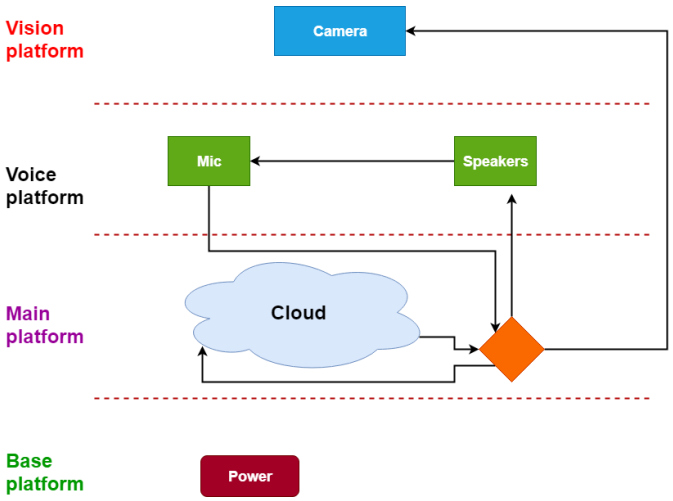

Fig. 3. Prototype implementation

IV. Discussion

In the first part, the images of the employees were taken and been trained for facial recognition, the frames are extracted from the Kinect camera-sensor-captured video. The system, when a face is being detected, and recognized, s stimulus will be showed to the employees in order to provoke their emotions where a capture of face will be stored in the dataset.

For second part, we will guarantee the employees the access to their data for labeling,

After the images will be labeled, a model will be trained using Convolutional neural networks.

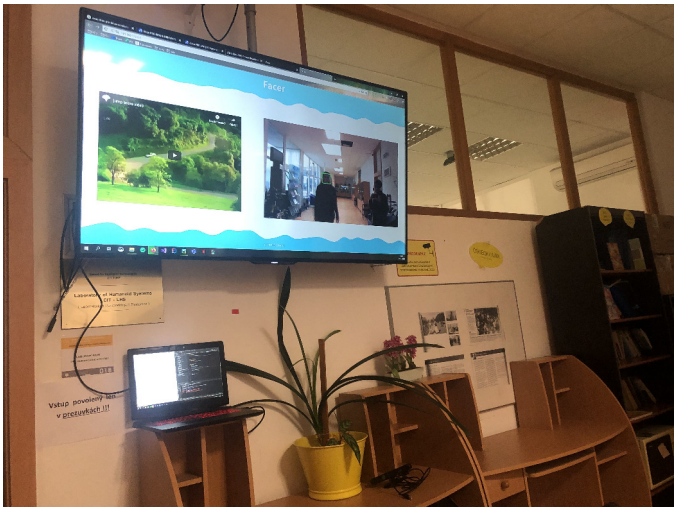

Fig. 4. implementation

V. Conclusion

We proposeded a framework that works as a link between the three areas, a setup of deep learning based facial emotion recognition system that is deployed in the cloud, we aim to build an interaction with the users using virtual robots and to crowd-source the data needed for a better results by showing stimuli to the users to recognise their true emotions.

Acknowledgment

This research work was supported by APVV project 015-0730 “Cloud Based Human Robot Interaction” and FEI grant “Increasing Server Performance for Deep Learning” for the year 2020.

References

[1] P. Ekman, “Universal facial expressions of emotions,” *California mental health research digest*, vol. 8, no. 4, pp. 151–158, 1970.
[2] Q. Zhang, L. Cheng, and R. Boutaba, “Cloud computing: state-of-the-art and research challenges,” *Journal of internet services and applications*, vol. 1, no. 1, pp. 7–18, 2010.
[3] P. Mell, T. Grance *et al.*, “The nist definition of cloud computing,” 2011.

Transfer Learning and Feature Extraction from Convolutional Neural Network to boost the Explainable Classifier's performance

[1]*Patrik Sabol (4nd year),*
Supervisor: [2]*Peter Sinčák*

[1,2]Dept. of Cybernetics and Artifical Intelligence, FEI TU of Košice, Slovak Republic

[1]patrik.sabol@tuke.sk, [2]peter.sincak@tuke.sk

***Abstract*—In this paper, we proposed deep CNN models for the classification of histopathology images, which were later used for feature extraction in order to boost performance of the explainable classifier, called Cumulative Fuzzy Class Membership Criterion (CFCMC). First, we utilized eight well-known CNN (Convolutional Neural Network) models, pre-trained on ImageNet dataset, which were fine-tuned for classification into eight types of tissue on histopathological images of the colorectal cancer. Moreover, we proposed light versions of three pre-trained models, which were trained from scratch to show the usefulness of the transfer learning techniques. The results show that pre-trained models perform better than the ones trained from scratch. Furthermore, features extracted from deep CNN models significantly boosted performance of the CFCMC classifier.**

***Keywords*—cancer detection, explainable classifier, explainable AI, image classification, transfer learning, feature extraction**

I. Introduction

In machine learning, there are many powerful classification algorithms with the ability to classify data with high accuracy. However, the central problem of many of such classifiers is that they are regarded as black-box models (e.g. deep learning), because even if the underlying mathematical principles are understandable they lack transparencies in rationalizing their decisions and explaining the data in a human-friendly form. On the other hand, white-box models (e.g. decision trees) provide very interpretable output but at a cost of losing performance (accuracy). In machine learning, this is known as the trade-off between the transparency and the accuracy [1].

In our research, we developed explainable classifier, Cumulative Fuzzy Class membership Criterion [2], whose explainable ability come out directly from its structure [3]. Explainability of the classifier is based on semantic extraction by post-processing of the CFCMC structure giving auxiliary output about data structures, resulting in explanatory mechanism that explains the complexity of the particular data in the form of semantics. Moreover, it provides the value that describes the possibility of the input sample to be misclassified to the one particular class. Therefore, our approach should speed up the decision process of the expert, and hence it is suitable for supporting decision-making of the experts.

In our further research, the first mean of the explanation for breast cancer detection was introduced in [4]. Furthermore, we have studied the usefulness of the proposed classifier for decision-making of the pathologists during examination of histopathological samples of the colorectal cancer data.

However, during this study, we have found out that the proposed classifier performs poorly on raw image data. Therefore, we decided to employ deep CNN (Convolutional Neural Network) as a feature extractor.

II. Experiments

The focus of the experiments is to find the architecture of the CNN with the best performance as a feature extractor for the explainable classifier CFCMC. Moreover, we examine the usefulness of utilization of the pre-trained CNN models on colorectal cancer data against the ones trained from scratch.

A. Histopathological data description

We used publicly available dataset released in [5] by *Kather et al.*. It consists of H&E tissue slides, which were cut into 5000 small tiles of the size 150x150 pixels, each of them annotated with one of eight tissue classes. The data are class-balanced, each of the class consists of 625 tiles.

B. Experimental setup

In our experiments, we utilized eight well-known CNN models, pre-trained on ImageNet [6] dataset, specifically, *AlexNet* [7], *VGG-16* [8], *Inception-v3* [9], *ResNet-50* [10], *Xception* [11], *DenseNet121* [12], *Inception-ResNet-V2* [13] and *EfficientNet0* [14]. For all of them, the fully connected layers were cut and replaced with dense layer with 1024 neurons with ReLU activation functions and 8 neurons with softmax activation function.

Moreover, we created three lighter models that were trained from scratch, specifically *VGG-like* model with 12 convolutional layers and 2 fully-connected layers, *Inception-like* model with 3 inception layers and *ResNet20* model with the depth 20.

All models were trained using Adam [15] optimizer to minimize cross-entropy for 100 epochs with learning rate set to value 0.0001.

Finally, to train explainable CFCMC classifier, we extracted features from last dense layer of all CNN models. Experimental setup for the CFCMC algorithm is as follows: number of clusters for each of the classes was set to 1. Value of the threshold θ was set to value $\theta = 0.01$. For optimization of the CFCMC, MATLAB implementation of the genetic algorithm

	CNN model	CFCMC model
Raw image	—	59.35(3.43)
AlexNet	91.43(2.42)	85.32(3.26)
VGG-16	93.61(1.75)	92.42(2.02)
Inception-v3	92.76(1.44)	90.79(2.04)
ResNet-50	**93.80(1.08)**	91.28(1.64)
Xception	93.58(1.25)	**92.78(1.74)**
DenseNet121	92.76(1.29)	92.06(1.75)
Inception-ResNetV2	92.76(1.02)	91.44(1.95)
EfficientNet0	90.97(1.39)	85.84(5.83)
VGG-like	80.88(1.14)	80.21(2.14)
Inception-like	85.25(2.82)	83.97(3.04)
ResNet20	90.14(1.24)	84.01(5.02)

TABLE I
PERFORMANCE RESULTS OF DIFFERENT CNN MODELS AND CORRESPONDING CFCMC MODELS

was used with population size of 50 individuals. Mutation rate was set to 0.2. Arithmetic crossover and adaptive feasible mutation operators were used for reproduction. Stochastic uniform selection was used to choose parents for next generation. Algorithm stops at 30^{th} generation.

C. Experimental results

Table I provides performance results of difference CNN models and corresponding CFCMC models. Classification results are evaluated 10-folds cross validation test.

From Table I it can be observed that pre-trained and fine-tuned models outperforms the ones trained from scratch. Moreover, it can be seen that features extracted from CNN models significantly boost performance of the explainable CFCMC models.

III. CONCLUSION

In this paper, we have trained 11 deep CNN models on histopathological images of colorectal cancer image data. Thanks to transfer learning techniques, we have fine-tuned 8 deep CNN architectures, which were pre-trained on well-known ImageNet dataset. Moreover, we created three lighter models that were trained from scratch. Results show that fine-tuned pre-trained models outperformes the ones trained from scratch.

Furthermore, we have extracted features from all CNN models that were used to train models of the explainable CFCMC classifier. Result show that these features significantly boost classification performance of the CFCMC classifier, which was the primary goal of this research.

ACKNOWLEDGMENT

This research work was supported by APVV project 015-0730 "Cloud Based Human Robot Interaction".

REFERENCES

[1] Guido Bologna and Yoichi Hayashi. Characterization of symbolic rules embedded in deep dimlp networks: a challenge to transparency of deep learning. *Journal of Artificial Intelligence and Soft Computing Research*, 7(4):265–286, 2017.

[2] P. Sabol, P. Sinčák, J. Buša, and P. Hartono. Cumulative fuzzy class membership criterion decision-based classifier. In *2017 IEEE International Conference on Systems, Man, and Cybernetics (SMC)*, pages 334–339, Oct 2017.

[3] Patrik Sabol, Peter Sinčák, Jan Magyar, and Pitoyo Hartono. Semantically explainable fuzzy classifier. *International Journal of Pattern Recognition and Artificial Intelligence*, 33(12):2051006, 2019.

[4] Patrik Sabol, Peter Sinčák, Kana Ogawa, and Pitoyo Hartono. Explainable classifier supporting decision-making for breast cancer diagnosis from histopathological images. In *2019 International Joint Conference on Neural Networks (IJCNN)*, pages 1–8. IEEE, 2019.

[5] Jakob Nikolas Kather, Cleo-Aron Weis, Francesco Bianconi, Susanne M Melchers, Lothar R Schad, Timo Gaiser, Alexander Marx, and Frank Gerrit Zöllner. Multi-class texture analysis in colorectal cancer histology. *Scientific reports*, 6:27988, 2016.

[6] Jia Deng, Wei Dong, Richard Socher, Li-Jia Li, Kai Li, and Li Fei-Fei. Imagenet: A large-scale hierarchical image database. In *2009 IEEE conference on computer vision and pattern recognition*, pages 248–255. Ieee, 2009.

[7] Alex Krizhevsky, Ilya Sutskever, and Geoffrey E Hinton. Imagenet classification with deep convolutional neural networks. In *Advances in neural information processing systems*, pages 1097–1105, 2012.

[8] Karen Simonyan and Andrew Zisserman. Very deep convolutional networks for large-scale image recognition. *arXiv preprint arXiv:1409.1556*, 2014.

[9] Christian Szegedy, Vincent Vanhoucke, Sergey Ioffe, Jon Shlens, and Zbigniew Wojna. Rethinking the inception architecture for computer vision. In *Proceedings of the IEEE conference on computer vision and pattern recognition*, pages 2818–2826, 2016.

[10] Kaiming He, Xiangyu Zhang, Shaoqing Ren, and Jian Sun. Deep residual learning for image recognition. In *Proceedings of the IEEE conference on computer vision and pattern recognition*, pages 770–778, 2016.

[11] François Chollet. Xception: Deep learning with depthwise separable convolutions. In *Proceedings of the IEEE conference on computer vision and pattern recognition*, pages 1251–1258, 2017.

[12] Gao Huang, Zhuang Liu, Laurens Van Der Maaten, and Kilian Q Weinberger. Densely connected convolutional networks. In *Proceedings of the IEEE conference on computer vision and pattern recognition*, pages 4700–4708, 2017.

[13] Christian Szegedy, Sergey Ioffe, Vincent Vanhoucke, and Alexander A Alemi. Inception-v4, inception-resnet and the impact of residual connections on learning. In *Thirty-first AAAI conference on artificial intelligence*, 2017.

[14] Mingxing Tan and Quoc V Le. Efficientnet: Rethinking model scaling for convolutional neural networks. *arXiv preprint arXiv:1905.11946*, 2019.

[15] Diederik P Kingma and Jimmy Ba. Adam: A method for stochastic optimization. *arXiv preprint arXiv:1412.6980*, 2014.

Transfer learning in deep convolutional networks for biomedical images

[1]*Matej GAZDA (1st year),*
Supervisor: [2]*Ján PLAVKA*

[1,2]Department of Mathematics and Theoretical Informatics, FEI TU of Košice, Slovak Republic

[1]matej.gazda@tuke.sk

***Abstract*—This paper provides an overview of applications of transfer learning used in deep convolutional neural networks. It focuses on support of decision making for medical personnel in tasks, such as skin cancer detection, Parkinson disease evaluation and bone age assessment.**

***Keywords*—deep learning, convolutional neural networks, biomedical engineering, data analysis**

I. Introduction

The concept of neural networks has been known for decades. Convolutional Neural Networks (CNNs) were introduced by [1] in 1980; however, the most significant breakthrough happened after ILSVRC competition in 2012 thanks to efficient hardware utilization, deep architectures, and new activation functions such as rectified linear unit (ReLU). Since then, neural networks play a crucial role in a large variety of tasks ranging from object detection, facial recognition [2] to natural language processing. The most significant advantage of neural networks lies in its deep architecture that can extract features on different levels of abstraction. In comparison with traditional machine learning, there is no need for laborious feature engineering.

One vivid area of research is the application of neural networks in the medical domain. Deep learning was used in [3] to predict the time that a patient should be in the intensive care unit after heart surgery, thus reducing the cost and waiting time for other patients. Authors of [4] utilized deep learning for the detection of mitosis in breast histology images. Study [5] created a deep learning model that achieves performance on par with professional doctors at the task of detecting skin cancer.

Despite its proven efficiency, usage of deep learning in biomedical tasks has several problems. Firstly, neural networks need a high number of labeled observations, which can be troublesome because labeling the observations correctly has to be done by experts. Secondly, most of the existing biomedical datasets have a low number of observations, and extending them can lead to different problems.

The aim of this paper is to describe transfer learning (TL) in deep convolutional neural networks, which is used to increase the efficiency of training on small datasets. Transfer learning is a process where information gathered on one problem is utilized on a problem in a different domain. Regardless of the progress in TL and success in several papers [5] [6], rules for choosing variables are still not known.

II. Related work

A. Melanoma detection

Malignant melanoma is the most severe type of skin cancer that develops in the cells called melanocytes, which color the skin. In 2012 approximately 100 000 new cases were identified in Europe, which accounts for 3% of all new cases of cancer that year. It is estimated that the deaths summed up for 1% of all cancer deaths in the same year [7]. The probability of curing the illness increases if detected early. However, many cases are still missed by domain experts.

Both handcrafted and deep learning techniques were proposed for computer-aided evaluation of skin lesions [6] [5]. [5] used GoogleNet Inception v3 architecture with weights pretrained on the ImageNet dataset, with a target dataset of the size of 129405 images (example Fig. 1). They proved that CNN could diagnose melanoma with accuracy matching professional dermatologists.

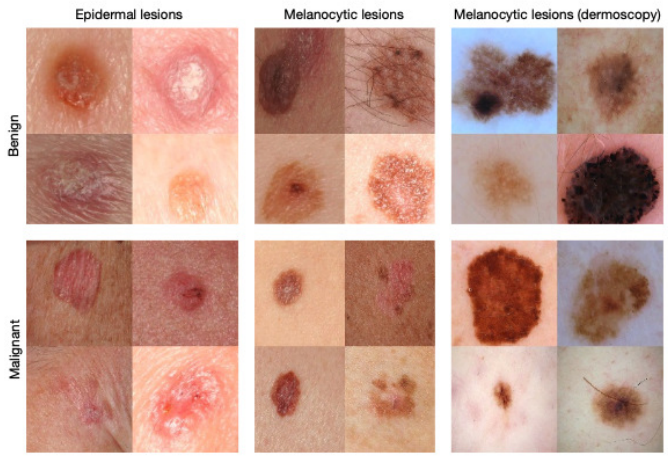

Fig. 1. Malignant and benign example images from [5] dataset.

Hagerty et al. [8] used fusion of handcrafted features and deep learning. Transfer learning was performed via ResNet-50 network and achieved 87% accuracy. In the case of the fusion technique, they improved accuracy to as much as 94%.

Detection of Melanoma is still a very actual problem, as many circumstances may be remarkably improved. Among other things, algorithms for hair removal from images and segmentation of colored and healthy skin are still being developed.

B. Parkinson disease evaluation

Parkinson's disease (PD) is a neurological disorder of the central nervous system affecting mainly motoric functions. The disease progresses slowly, starting with shaking, slowness of movement, and various psychiatric manifestations. According to [9], professionals diagnose patients of PD with accuracy in the range from 75% to 92%.

Numerous approaches were proposed to provide a decision support system to help medical personnel correctly evaluate the patients. Three basic approaches exist. The first approach is to analyze features extracted from signals from handwriting captured by specialized device, such as x and y coordinates, speed, and pressure recorded [10]. The second approach is to apply speech processing to detect voice impairments, such as slowness, monotone, and softness. The third approach based on CNN is based purely on an analysis of an image of a handwritten digit, letter, syllabus, or Archimedean spiral. The third approach seems to be the way forward because it does not need to have any specialized device nor laborious feature engineering.

Previous research in this field evaluated their proposition against two datasets called HandPD [11] and PaHaW [10]. Both datasets provide a balanced ratio of patients suffering from PD and healthy controls. HandPD consists of four repetitions of Archimedean spiral and meander drawings from 66 observations. PaHaW consists of nine tasks: *Archimedean spiral*, letter *l*, syllabus *le*, words *les*, *lektorka*, *porovnat* and*nepopadnout* and sentence *Tramvaj uz dnes nepojede*. The distinction between HandPD spiral and PaHaW spiral is that in HandPD subject was following a preprinted line (see Fig. 2 and Fig. 5).

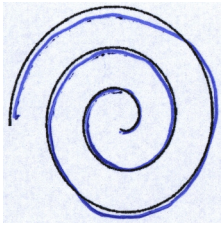

Fig. 2. Example of Archimedean spiral from HandPD dataset [10]

Authors of [12] used AlexNet [13] architecture with transfer learning (both fine-tuning and feature extraction approaches) from ImageNet and MNIST database and evaluated it on PaHaW dataset. [12] reported as much as 98% accuracy; however, the results cannot be taken as conclusive because training accuracy was reported, and data-leakage was present.

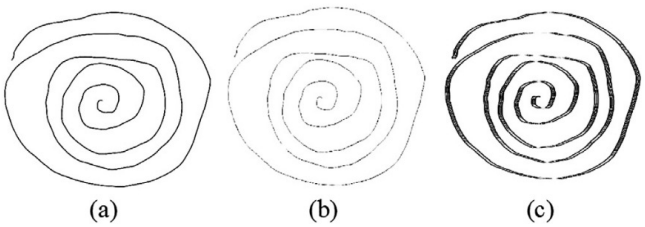

Fig. 3. Example of PaHaW Archimedean spiral a) raw data, b) Median filter residual image, c) edge data [14]

AlexNet network and ImageNet datasets were utilized in [14] and verified this approach on PaHaW [10] dataset. To further increase the performance, a fusion of CNNs trained on images transformed by nonlinear functions such as Median filter residual data and edge data was proposed (see Fig. 3). Features were extracted from the penultimate layer and passed to SVM classifier. Through the fusion of CNNs, they acquired as much as 83% accuracy.

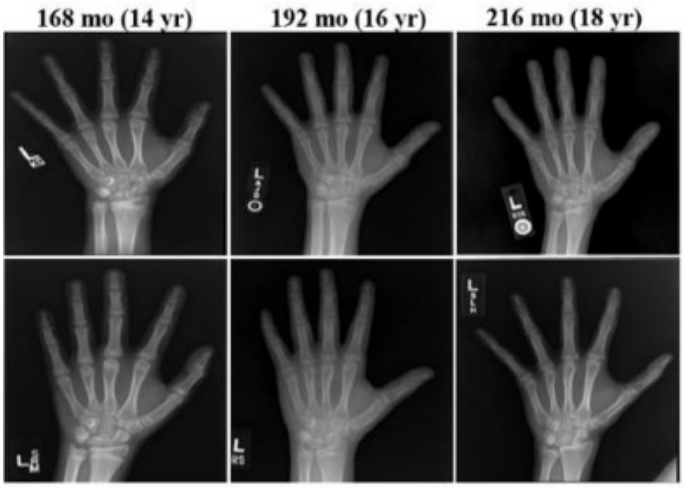

Fig. 4. Left-hand radiology images of subjects ranging from 14 to 18 years

C. Bone Age Assessment

Skeletal bone assessment is a common examination used in pediatric radiology for diagnostic and therapeutic investigation of endocrinology abnormalities [15]. Generally, the examination is started by taking radiological image of the left hand and then evaluate it using either Greulich & Pyle (G&P) method or Tanner-Whitehouse (TW) method. An x-ray image is a perfect match for CNN. Pediatric bone age assessment works rely upon two key datasets; RSNA [16] and private SCH. RSMA consists of 12480 X-ray images and SCH of 12390 images.

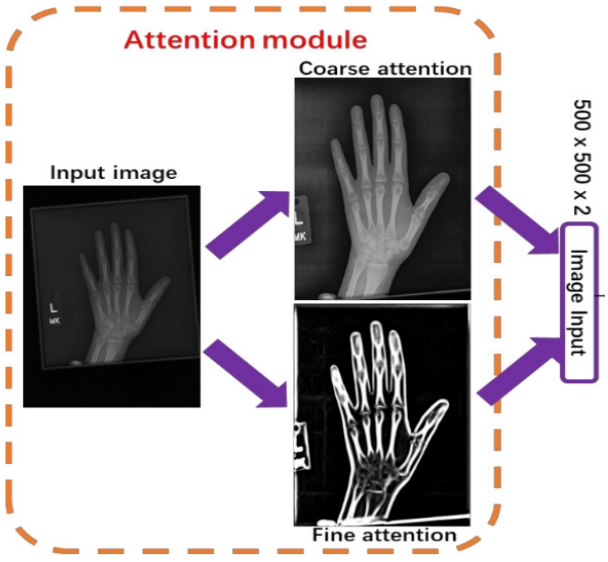

Fig. 5. Attention module [17]

Authors of [17] proposed a decision support system to complete the bone assessment. The system was created of two parts, the first was the attention module, and the second was

Regression CNN. The attention module can be considered as a data augmentation technique, as it created from one input image images with coarse/fine attention maps. The second part was a regression CNN, with Inception-V3 as a base network. With this system, they achieved mean absolute error (MAE) of 5.3 ± 5.5 months on SCH dataset and 5.2 ± 5.1 months on the RSNA dataset.

III. Convolutional Neural Network

CNNs are a special type of neural network specialized in tasks, where the input is in the form of arrays such as time-series or images. The architecture consists of an input layer, multiple convolutional blocks, and an output layer. In addition to that, some popular network architectures such as VGG (see Table I) [18] or AlexNet [13] (see Table II) include few fully connected layers right in front of the output layer. Convolutional blocks consist of convolutional layers, pooling functions such as max-pooling or min-pooling, and finally, the nonlinear activation functions such as ReLU or tanh.

Similarly to other types of neural networks, optimization is performed by minimizing the cost function by the back-propagation algorithm. The cost function can be typically expressed as an expectation of error across the data-generating distribution p_{data} [19].

$$J(\boldsymbol{\theta}) = \mathbb{E}_{(\mathbf{x},y)\sim p_{data}} L(f(\mathbf{x};\boldsymbol{\theta}), y) \tag{1}$$

where L is a loss function, such as binary or categorical crossentropy, f is a function that predicts the output, x is the input and y is the corresponding label.

A. Neural Network optimization

Neural Network optimization is performed by lowering cost function $J(\boldsymbol{\theta})$. Lowering is done by modifying the parameters $\boldsymbol{\theta}$ in the direction of antigradient. The antigradient g may be calculated based on one sample, on a mini-batch of size B, and the entire training dataset. The most deep learning models use mini-batch gradient descent. Minibatches are sampled from the data-generation distribution p_{data} in form of input $\{x^{(1)}, x^{(2)}, x^{(3)}, ..., x^{(B)}\}$ with corresponding labels $\{y^{(1)}, y^{(2)}, y^{(3)}, ..., y^{(B)}\}$ [19].

Antigradient based on mini batch can be calculated as

$$\hat{\mathbf{g}} = \frac{1}{B} \nabla_\theta \sum_i L(f(\mathbf{x}^{(i)};\boldsymbol{\theta}), y^{(i)}). \tag{2}$$

Modifying $\boldsymbol{\theta}$ in the direction of antigradient $\hat{g}$ performs method called stochastic gradient descent (SGD). Many variations of SGD methods exists, such as Adadelta [20] or Adagrad [21].

B. Data augmentation

Data augmentation is a process of creating new images with preserved labels by slightly modifying the original images. Data augmentation is used on the training dataset to enlarge it artificially and reduce the chance of overfitting. During this process, one must be careful that the original image and all images transformed from that one should be a part of only set. On Fig. 6 are two plots. The first plot shows the desired training and testing accuracy over ten epochs. The second plot shows the results of training, in which overfitting happened. Model is overfit in case that its predictions correspond exactly to the training data and fails to generalize on data that it hasn't seen.

TABLE I
VGG16 architecture

Layer	Size	Kernel Size	Stride
Input layer	$224 \times 224 \times 3$	-	-
Convolutional	$224 \times 224 \times 64$	3×3	1
Convolutional	$224 \times 224 \times 64$	3×3	1
Max Pooling	$224 \times 224 \times 64$	2×2	2
Convolutional	$112 \times 112 \times 128$	3×3	1
Convolutional	$112 \times 112 \times 128$	3×3	1
MaxPooling	$112 \times 112 \times 128$	2×2	2
Convolutional	$56 \times 56 \times 128$	3×3	1
Convolutional	$56 \times 56 \times 256$	3×3	1
Convolutional	$56 \times 56 \times 256$	3×3	1
MaxPooling	$56 \times 56 \times 256$	2×2	2
Convolutional	$28 \times 28 \times 256$	3×3	1
Convolutional	$28 \times 28 \times 512$	3×3	1
Convolutional	$28 \times 28 \times 512$	3×3	1
MaxPooling	$28 \times 28 \times 512$	2×2	2
Convolutional	$14 \times 14 \times 512$	3×3	1
Convolutional	$14 \times 14 \times 512$	3×3	1
Convolutional	$14 \times 14 \times 512$	3×3	1
MaxPooling	$14 \times 14 \times 512$	2×2	2
Dense Layers	2048		
Dense Layers	2048		
Output layer	1000		

TABLE II
AlexNet architecture

Layer	Size	Kernel Size	Stride
Input layer	$227 \times 227 \times 3$	-	-
Convolutional	$227 \times 227 \times 3$	11×11	4
Max Pooling	$55 \times 55 \times 96$	3×3	2
Convolutional	$27 \times 27 \times 96$	5×5	2
MaxPooling	$27 \times 27 \times 256$	3×3	2
Convolutional	$13 \times 13 \times 256$	3×3	1
Convolutional	$13 \times 13 \times 384$	3×3	1
Convolutional	$13 \times 13 \times 384$	3×3	1
MaxPooling	$13 \times 13 \times 256$	3×3	2
Dense Layers	4096		
Dense Layers	4096		
Dense Layers	4096		
Output layer	1000		

The most basic transformations used for data augmentation are flipping the image horizontally or vertically, rotating the image by any angle, shifting, or cropping the image.

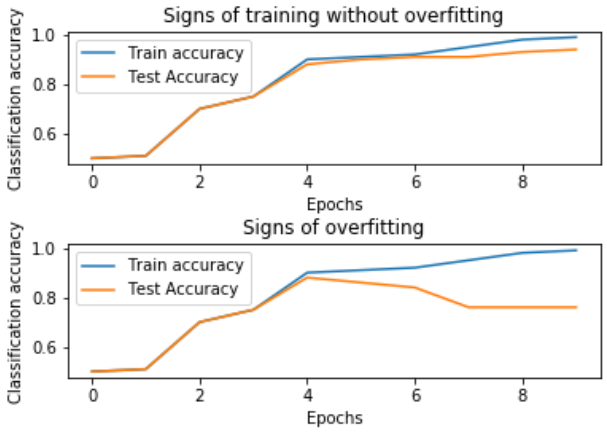

Fig. 6. Example of desired training and training with overfit

Perez et al. [22] used Generative Adversarial Nets (GANs) to augment data by transferring the styles from images to

different phase of day, like night or day and also different seasons like winter or summer.

IV. Transfer Learning

Transfer learning is a process in which knowledge gained during learning on one task is utilized on another. Generally, lower layers of CNNs tends to learn more abstract features, such as color blobs or Gabor filters [23]. As this behaviour applies to all the natural image datasets, it is reasonable to think that such layers can be shared across multiple tasks. On the other hand, the upper layers learn more task-specific features, which may not help during the training on different datasets.

The two most common approaches are called feature extraction and finetuning. During the feature extraction, all the layers are frozen, except for the last fully-connected layer, which has to be replaced to match the number of labels of target datasets. Finetuning approach is based on freezing layers of one part of the network and retrain the unfrozen layers.

The major problem of finetuning is that no general rules are known. The optimal number of frozen layers varies regarding to network architecture, the similarity of original and target datasets, the number of observations, and a couple of other variables. The only way to find the optimal number of frozen layers is by running extensive experiments.

Study [23] provided a quantification of the transferability of features from CNN layers. Transferability can give an insight whether the features are more specific to the original dataset or they are more general; therefore they can be used for transfer learning. They also discussed the difficulties with optimization in case that the network is split into two parts, leaving the first part frozen and train only the second network. This may negatively impact the convergence of the training. They also claim that random weights at higher layers can be better than pretrained weights from very distinct tasks.

Research in [24] derived another measurement of transferability based on entropy. Based on the their own transferability measurement they provided framework for choosing the best source dataset for transfer learning.

V. Conclusion

We have demonstrated the importance of deep learning in biomedicine, especially in diagnosis of serious illnesses. We also explained transfer learning, its advantages and also mentioned the problems that haven't been solved. Atop of that we also briefly explained how CNNs work and described how data augmentation can impact its training.

Acknowledgment

This work was supported by the grant TUKE FEI-2020-69 and by the Slovak Research and Development Agency under contract No. APVV-16-0211 and No. APVV-18-0214.

References

[1] K. Fukushima, "Neocognitron: A self-organizing neural network model for a mechanism of pattern recognition unaffected by shift in position," *Biological cybernetics*, vol. 36, no. 4, pp. 193–202, 1980.

[2] Z.-Q. Zhao, D.-S. Huang, and B.-Y. Sun, "Human face recognition based on multi-features using neural networks committee," *Pattern recognition letters*, vol. 25, no. 12, pp. 1351–1358, 2004.

[3] J. V. Tu and M. R. Guerriere, "Use of a neural network as a predictive instrument for length of stay in the intensive care unit following cardiac surgery." in *Proceedings of the Annual Symposium on Computer Application in Medical Care*. American Medical Informatics Association, 1992, p. 666.

[4] D. C. Cireşan, A. Giusti, L. M. Gambardella, and J. Schmidhuber, "Mitosis detection in breast cancer histology images with deep neural networks," in *International conference on medical image computing and computer-assisted intervention*. Springer, 2013, pp. 411–418.

[5] A. Esteva, B. Kuprel, R. A. Novoa, J. Ko, S. M. Swetter, H. M. Blau, and S. Thrun, "Dermatologist-level classification of skin cancer with deep neural networks," *Nature*, vol. 542, no. 7639, pp. 115–118, 2017.

[6] S. Pathan, K. G. Prabhu, and P. Siddalingaswamy, "Techniques and algorithms for computer aided diagnosis of pigmented skin lesionsâĂŤa review," *Biomedical Signal Processing and Control*, vol. 39, pp. 237–262, 2018.

[7] "Encr | european network of cancer registries," https://encr.eu/, (Accessed on 02/06/2020).

[8] J. R. Hagerty, R. J. Stanley, H. A. Almubarak, N. Lama, R. Kasmi, P. Guo, R. J. Drugge, H. S. Rabinovitz, M. Oliviero, and W. V. Stoecker, "Deep learning and handcrafted method fusion: higher diagnostic accuracy for melanoma dermoscopy images," *IEEE journal of biomedical and health informatics*, vol. 23, no. 4, pp. 1385–1391, 2019.

[9] A. Schrag, Y. Ben-Shlomo, and N. Quinn, "How valid is the clinical diagnosis of parkinson's disease in the community?" *Journal of Neurology, Neurosurgery & Psychiatry*, vol. 73, no. 5, pp. 529–534, 2002.

[10] P. Drotár, J. Mekyska, I. Rektorová, L. Masarová, Z. Smékal, and M. Faundez-Zanuy, "Decision support framework for parkinsonâĂŹs disease based on novel handwriting markers," *IEEE Transactions on Neural Systems and Rehabilitation Engineering*, vol. 23, no. 3, pp. 508–516, 2014.

[11] C. R. Pereira, D. R. Pereira, F. A. Silva, J. P. Masieiro, S. A. T. Weber, C. Hook, and J. P. Papa, "A new computer vision-based approach to aid the diagnosis of parkinson's disease," *Computer Methods and Programs in Biomedicine*, vol. 136, pp. 79–88, 2016.

[12] A. Naseer, M. Rani, S. Naz, M. I. Razzak, M. Imran, and G. Xu, "Refining parkinsonâĂŹs neurological disorder identification through deep transfer learning," *Neural Computing and Applications*, vol. 32, no. 3, pp. 839–854, 2020.

[13] A. Krizhevsky, I. Sutskever, and G. E. Hinton, "Imagenet classification with deep convolutional neural networks," in *Advances in neural information processing systems*, 2012, pp. 1097–1105.

[14] M. Moetesum, I. Siddiqi, N. Vincent, and F. Cloppet, "Assessing visual attributes of handwriting for prediction of neurological disordersâĂŤa case study on parkinsonâĂŹs disease," *Pattern Recognition Letters*, vol. 121, pp. 19–27, 2019.

[15] A. Albanese and R. Stanhope, "Investigation of delayed puberty," *Clinical endocrinology*, vol. 43, no. 1, pp. 105–110, 1995.

[16] S. S. Halabi, L. M. Prevedello, J. Kalpathy-Cramer, A. B. Mamonov, A. Bilbily, M. Cicero, I. Pan, L. A. Pereira, R. T. Sousa, N. Abdala *et al.*, "The rsna pediatric bone age machine learning challenge," *Radiology*, vol. 290, no. 2, pp. 498–503, 2019.

[17] X. Ren, T. Li, X. Yang, S. Wang, S. Ahmad, L. Xiang, S. R. Stone, L. Li, Y. Zhan, D. Shen *et al.*, "Regression convolutional neural network for automated pediatric bone age assessment from hand radiograph," *IEEE journal of biomedical and health informatics*, vol. 23, no. 5, pp. 2030–2038, 2018.

[18] K. Simonyan and A. Zisserman, "Very deep convolutional networks for large-scale image recognition," *arXiv preprint arXiv:1409.1556*, 2014.

[19] I. Goodfellow, Y. Bengio, and A. Courville, "Deep learning book," *MIT Press*, vol. 521, no. 7553, p. 800, 2016.

[20] M. D. Zeiler, "Adadelta: an adaptive learning rate method," *arXiv preprint arXiv:1212.5701*, 2012.

[21] J. Duchi, E. Hazan, and Y. Singer, "Adaptive subgradient methods for online learning and stochastic optimization," *Journal of machine learning research*, vol. 12, no. Jul, pp. 2121–2159, 2011.

[22] L. Perez and J. Wang, "The effectiveness of data augmentation in image classification using deep learning," *arXiv preprint arXiv:1712.04621*, 2017.

[23] J. Yosinski, J. Clune, Y. Bengio, and H. Lipson, "How transferable are features in deep neural networks?" in *Advances in neural information processing systems*, 2014, pp. 3320–3328.

[24] M. J. Afridi, A. Ross, and E. M. Shapiro, "On automated source selection for transfer learning in convolutional neural networks," *Pattern recognition*, vol. 73, pp. 65–75, 2018.

Translation of Natural Language Sentences into Logic Constructions

[1]*Zuzana BILANOVÁ (4th year),*
Supervisor: [2]*Liberios VOKOROKOS*

[1,2]Dept. of Computers and Informatics, FEI TU of Košice, Slovak Republic

[1]zuzana.bilanova@tuke.sk, [2]liberios.vokorokos@tuke.sk

***Abstract*—This paper describes a new logic system that allows formalizing the meaning of natural language sentences and revealing semantic ambiguities. This logic system is based on transparent intensional logic and predicate linear logic. The combination of these logic made it possible to create a unique system with high expressive power. Its potential in computer science is demonstrated by the implementation of a semantic machine that automatically generates semantic representations of natural language sentences.**

***Keywords*—natural language semantics processing, predicate linear logic, semantic machine, transparent intensional logic**

I. Introduction

The meaning of the natural language expressions should be revealed by their analysis, because the grammatical structure of the expression is usually different from its logical structure. It is a common problem in natural language processing that understanding an expression differs from how it was thought. The misinterpretations of the premise and subsequent errors of reasoning and argumentation occur. Logical analysis of the natural language [1] deals with explaining the meanings of expressions in the natural language.

The structure of the paper is as follows.
Section I is devoted to a short overview of newly proposed logic system that would allow formalizing the meaning of natural language sentences.
Section II describes the implementation of its semantic machine - type analysis and construction synthesis levels.
Section III presents conclusions that summarize the adequacy of the described solution.

II. Source-oriented transparent intensional logic

Source-oriented transparent intensional (SOTIL) logic is created by linking two logic systems - transparent intensional logic and predicate linear logic. The goal of this fusion is to create a new, extremely expressive logic system that allows the logical analysis of natural language.

Pavel Tichý [2], the autor of transparent intensional logic (TIL), specified ramified theory of types where the basic type level contains the simplest natural language entities. The object base B in TIL contains set of truth values o, set of individuals ι, set of time points τ, set of possible worlds ω.

The hierarchy of types in TIL allows to construct objects above the object base B as a function above that base. (α-)intentions are objects of type $(\alpha_{\tau\omega})$ that representing functions from possible worlds at time points to objects of type α.

In TIL, the meaning of expression is expressed by using abstract algorithm-structured procedures called constructions. Constructions may be:

- variables (x) - construct object dependent on its valuation,
- trivialization $({}^0X)$ - constructs object X without any change,
- closure $(\lambda x_1, ..., x_n X)$ - constructs the function,
- composition $([XY_1, ..., Y_n])$ - constructs the result of an application of function to arguments.

The disadvantage of TIL is the absence of a proof calculus, which is why it could not be fully automated yet. We decided to choose a logic system that would increase the expressive power of TIL. Such a system could be predicate linear logic.

Predicate linear logic [3] was formulated by Jean-Yves Girard in 1987 as a formalism describing problems with an explicitly determined amount of resources. It is a non-classical logic of actions and resources, and also it is a generalization of propositional, predicate and intuitionist logic.

Syntax of the predicate linear formulas φ and terms t can be expressed by following production rule in Backus-Naur form:

$$\begin{aligned}&\varphi ::= 1 \mid 0 \mid \bot \mid \top \mid P(t, ..., t) \mid \varphi \otimes \varphi \mid \varphi \& \varphi \mid \varphi \oplus \varphi \mid \\ &\varphi \parr \varphi \mid \varphi \multimap \varphi \mid \varphi^{\bot} \mid !\varphi \mid ?\varphi \mid (\forall x)\varphi \mid (\exists x)\varphi, \\ &t ::= x \mid c \mid f(t, ..., t),\end{aligned} \tag{1}$$

where '$1, 0, \bot, \top$' are logical constants, '$P(t, ..., t)$' is predicate, '$\otimes, \parr$' are multiplicative logical connectives, '$\oplus, \&$' are additive logical connectives, '$\multimap$' is linear implication, '$(.)^{\bot}$' is negation, '!, ?' are modal operators, '$\forall, \exists$' are quantifiers, 'x' is variable, 'c' is constant and '$f(t, ..., t)$' is the application of a functional symbol to a term 't'.

The advantages of PLL: PLL constants can capture not only the truth but also the meaning of the expressions in the form of predicate linear formulas, PLL has four logical connectives, because of which it is an extremely expressive system, PLL operators describe dependent and independent choice of individual, PLL can describe the consumption of resources, what is a special way to capture changing world conditions, PLL can be automated due to a fully-defined deduction calculus.

More about SOTIL syntax, semantics, and sequent calculus is in [4].

III. SOTIL SEMANTIC MACHINE

Analysis of natural language expressions has two-levels. In the first one, syntactic analysis is performed using a Stanford CoreNLP parser [5], which was carefully selected after comparison with competing parsers. The second step is the semantic analysis of expressions. Our implementation of SOTIL semantic machine works in three successive steps (illustrated in Figure 1):

1) type analysis - to each word of the sentence is assigned adequate type,
2) construction creation - formalization of the meaning of an analyzed sentence,
3) type control - a voluntary step to prove if the earlier steps were correctly done.

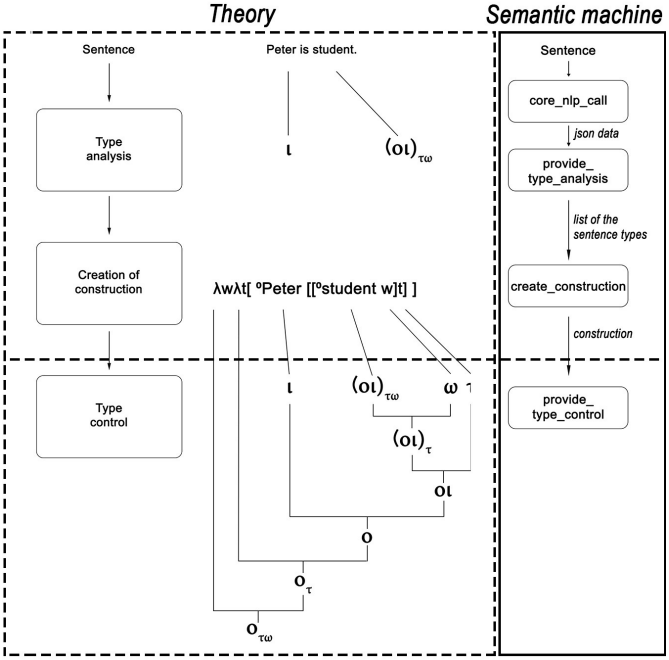

Figure 1. Three-step analysis in SOTIL - theory and implementation[6].

The output of SOTIL semantic machine is a sentence represented by SOTIL construction.

A. Type analysis

The analyzed types extend basic SOTIL types o, ι, ω, τ. E.g. the attribute type $(\iota\iota)_{\tau\omega}$ is identified as follows: it is necessary to find a dependency *case*, where an individual is a dependent element and the indicator *'s* describes an independent element. Another option is to find the dependency *nmod:poss* - the dependent element is the individual and the independent element is the attribute that is owned by the individual (shown in Figure 2).[1]

Within the type analysis, other nine types were identified in a similar way.

B. Construction creation

After all types are identified, the construction of sentence is made. Each word is in specific relation to the other words of the sentence. Sometimes more lexical units represent one type. In sentence "The number of cars and motorbikes is growing."

[1]The meaning of mentioned dependencies is explained at [7]

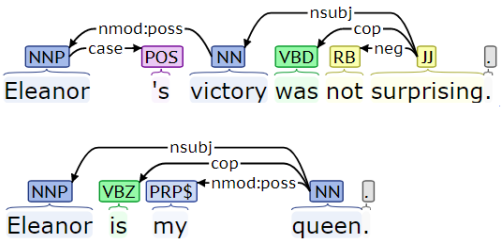

Figure 2. Attribute type of SOTIL.

objects *number*, *of*, *cars* are originally incorrectly analyzed as independent words. In reality, they have together value type. In the final construction, our algorithm put them together as one object - *number_of_cars*.

$$\lambda w \lambda t[[[[^0\text{growing } w]t]^0\text{number\_of\_cars}] \otimes [[[^0\text{growing } w]t]^0\text{number\_of\_motorbikes}]] \quad (2)$$

In a similar way, SOTIL performs automated translation from natural language into logical constructions that represent its meaning.

IV. CONCLUSION

The benefit of the presented research is the creation of a new logical system SOTIL. Its great expressive power makes it possible to formalize the meaning of natural language and removes semantic ambiguities.

The SOTIL semantic machine is the basis of future research in which its outputs will be used in an inference machine. The SOTIL inference machine enables computer processing of natural deduction over the knowledge base of natural language.

ACKNOWLEDGMENT

This work was supported by the following projects:

- Faculty of Electrical Engineering and Informatics at the Technical University of Košice under contract No. FEI-2020-70: Behavioral model of component systems based on coalgebras and linear logic.
- Slovak Research and Development Agency under the contract No. SK-AT-2017-0012: Semantics technologies for computer science education.

This support is very gratefully acknowledged.

REFERENCES

[1] L. T. F. Gamut, "Logic, language, and meaning, volume 2: Intensional logic and logical grammar," *University of Chicago Press*, 1990.
[2] P. Tichý, "The foundations of frege's logic," *De Gruyter, Berlin and New York*, 1988.
[3] E. Demeterová, Z. Bilanová, D. Mihályi, and V. Novitzká, "Lygon - a programming language for linear logic," *Electrical Engineering and Informatics 5 : Proceedings of the Faculty of Electrical Engineering and Informatics of the Technical University of Košice. - Košice : TU*, pp. 45–48, 2014.
[4] Z. Bilanová, "Logická analýza prirodzeného jazyka prostredníctvom transparentnej intenzionálnej logiky a lineárnej logiky," *Doctoral thesis*, p. 125, 2020.
[5] C. D. Manning, M. Surdeanu, J. Bauer, J. Finkel, S. Bethard, and D. McClosky, "The stanford corenlp natural language processing toolkit," *Association for Computational Linguistics (ACL) System Demonstrations*, pp. 55–60, 2014.
[6] B. Bednár, Z. Bilanová, and A. Pekár, "The automated translation of natural language sentences into intensional logic at the type analysis and construction synthesis levels," *Acta Electrotechnica et Informatica*, vol. 19, pp. 3–7, 2019.
[7] M. C. de Marneffe and C. D. Manning, "Stanford typed dependencies manual," *https://www.bibsonomy.org/bibtex/2487e67b81281e38900ec97bd2915ec45/butonic*, 2018.

Tremor Detection Using Strain Gauges

[1]*Norbert FERENČÍK (4^{th} year),*
Supervisor: [2]*Marek BUNDZEL*

[1,2]Dept. of Cybernetics and Artificial intelligence, FEI TU of Košice, Slovak Republic

[1]norbert.ferencik@tuke.sk, [2]marek.bundzel@tuke.sk

***Abstract*—This article describes the use of the strain gauges for tremor tracking and detection. The Rehapiano is a versatile tremor detector that measures the tremor of all ten fingers. The patient is accompanied by a virtual nurse during the exercise. Thanks to the virtual nurse, Rehapiano does not need another rehabilitation technician or doctor. The results of the exercise are processed and evaluated using Fourier transform. The patient's amplitude and frequency is a major indicator of current health status. The results of such measurements are used as a quantifier of disease development or ascertaining the patient's response to the treatment provided.**

***Keywords*—Tremor, virtual nurse, fourier transform, amplitude, frequency.**

I. Introduction

The project RehaPiano - REHAbalitation PlAtform inNOvation is dedicated to creating a software and hardware platform that diagnoses and trains the current movement and functional properties of the human upper musculoskeletal system. This device is mobile and modular, with the ability to diagnose fine motor. I have been working on Rehapiano for the last two years of my Ph.D. studies. With my solution, the patient can use the device to record the force of a finger pressing with the help of pressure sensors and also to record the response time of the patient to the stimulus. In the case of the fingers on the hand, we try to make sensing of the strength of each finger separate so that the maximum pressure on the sensors exerted by each finger is detected. Rehapiano can be used not only by patients for rehabilitation but also by people who want to improve fine motor skills. The Rehapiano device can be seen in Figure 1.

Fig. 1. Device Rehapiano, which includes 10 strain gauges and a keyboard. A monitor is included, but not shown.

II. Tremor

Tremor is characterized in medicine as an involuntary rhythmic and periodic movement of body parts. All body parts may be affected, including the head, chin, and soft palate [1]. Muscle contractions during a tremor have a regular frequency [2]. Tremor results from a pathological plaque in the brain that activates the nerves and shakes the corresponding part of the body. The formation of such a deposit is essential genetically in the essential tremor; In Parkinson's disease, shaking causes dopamine deficiency in certain parts of the brain [3, 4, 5, 6].

For the differential diagnosis of tremor, it is important to distinguish when shaking occurs. Shaking at rest is most powerful when there is no physical activity. It may accompany drug intoxication, addictive substance or Parkinson's disease. Static shaking occurs when the body or body part is actively held against gravity. Intentional shaking, on the other hand, occurs mainly in targeted movements. Tremor can be divided into more than 20 groups [7]. The basic phenomenological division [8] is based on the circumstances of the occurrence of the form of tremor - depending on whether the tremor occurs at rest (resting) or during active innervation (action), static load (postural), or during movement of the affected part body (kinetic and intense). Further shaking is possible according to body location, frequency (slow to 4 Hz, medium 5-7 Hz, fast over 7 Hz) or amplitude (fine - deviations up to 1 cm, medium 1-2 cm, coarse over 2 cm). Tremor can be a manifestation of a variety of physiological and pathological conditions, appearing as an isolated symptom or as part of characteristic syndromes [9, 10]. The graphical distribution of tremors can be seen in Figure 2.

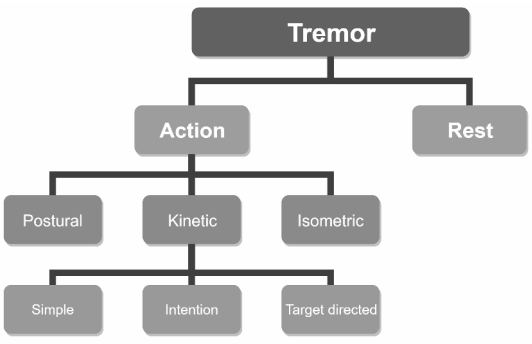

Fig. 2. Tremor, according to its etiology, is categorized as rest tremor or action tremor, the latter being further subdivided into action postural and action kinetic tremor.

III. Methods

We made a subject estimation convention. The Rehapiano is appropriate for estimating activity tremor produced during deliberate muscle contraction. Each subject was provoked to apply force with a given finger. The sufficiency of this power is shown utilizing vertical green bars (see Figure 3). By inducing targeted muscle withdrawal, the tremor may show and the target red line of the power at 40Hz frequency. The measurement protocol can be modified by changing the required sequence of fingers, time, and force to be maintained. However, we used the same protocol parameters for all subjects. The example in Figure 3 shows the measurement of the subject patient's left hand with the middle finger. The subject does not see the target value.

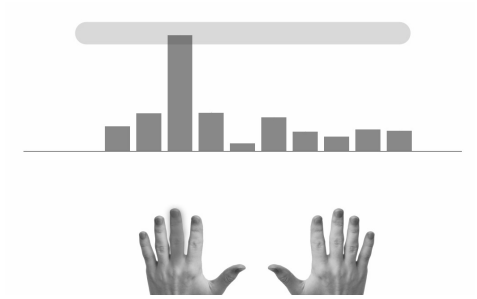

Fig. 3. Example of finger force measurement.

IV. Data evaluation

In this article, I will give just one example of exercise evaluation. In the graph of Figure 4 I compare the exercise of a healthy subject and a patient with Parkinson's disease. At the top of the graph, we can see the exercise of a healthy patient. The middle finger (see Figure 3) reached the desired value (in this case 300 grams). He was asked by the virtual nurse to stay in the red area for 3 seconds. Green is the time area in which the virtual nurse measurement was performed. As can be seen, the strength of the subject developed over time was stable.

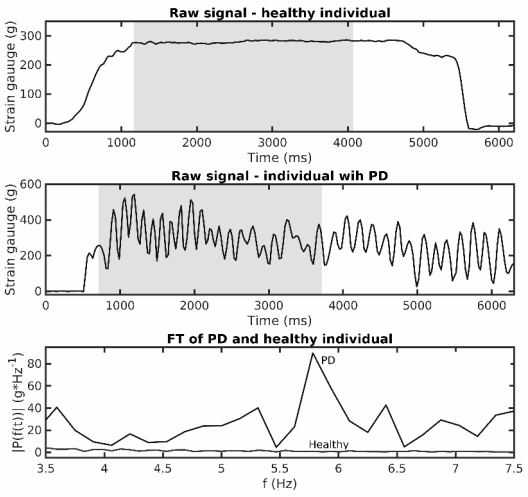

Fig. 4. Example of an exercise. Top - healthy patient, middle - patient with Parkinson's disease, bottom - fourier transformation of healthy and patient with Parkinson's disease.

The middle graph shows the measurement of a patient with Parkinson's disease (patient data not necessary for evaluation) at an early stage. From the graph, it can be seen that the patient has reached the desired value, but the tremor has manifested itself in the path and oscillation around the desired value. The bottom graph is an exercise evaluation in the form of tremorial cause quantification data. The red curve is a Fourier transform of healthy patient data. It is clear from the graph that the frequency change did not occur. Blue is represented by the Fourier transformation of Parkinson's patient data. The chart shows a tremor with a frequency of 5.5Hz to 6.3Hz. On the left axis, we can see the amplitude.

V. Conclusion

The results of the measurements are intended to diagnose the patient's disease. An example is to monitor the patient based on the medications used for a selected period time. Based on the data obtained, the doctor can monitor the development of the condition and the effect of the treatment on the patient. It should be noted that no research on tremorial causes has been conducted in patients with Parkinson's disease using strain gauges to date. The next step in Rehapiano's tremor research is the creation of a computer game, during which the patient is motivated to exercise by gaming activity.

VI. Publications

During 2019, our research group submitted an article[3] in peer reviewed journal - Sensors with 5-year impact factor: 3.302.

References

[1] T. D. Sanger, D. Chen, D. L. Fehlings, M. Hallett, A. E. Lang, J. W. Mink, H. S. Singer, K. Alter, H. Ben-Pazi, E. E. Butler *et al.*, "Definition and classification of hyperkinetic movements in childhood," *Movement Disorders*, vol. 25, no. 11, pp. 1538–1549, 2010.

[2] R. J. Elble, "Tremor," in *Neuro-geriatrics*. Springer, 2017, pp. 311–326.

[3] N. Ferenčík, M. Jaščur, M. Bundzel, and F. Cavallo, "The rehapiano—detecting, measuring, and analyzing action tremor using strain gauges," *Sensors*, vol. 20, no. 3, p. 663, 2020.

[4] S. Smaga, "Tremor," *American family physician*, vol. 68, no. 8, pp. 1545–1552, 2003.

[5] E. D. Louis, "Essential tremor," *New England Journal of Medicine*, vol. 345, no. 12, pp. 887–891, 2001.

[6] R. J. Elble, "Physiologic and essential tremor," *Neurology*, vol. 36, no. 2, pp. 225–225, 1986.

[7] J. Jankovic, F. Cardoso, R. G. Grossman, and W. J. Hamilton, "Outcome after stereotactic thalamotomy for parkinsonian, essential, and other types of tremor," *Neurosurgery*, vol. 37, no. 4, pp. 680–687, 1995.

[8] M. Hallett, "Tremor: pathophysiology," *Parkinsonism & related disorders*, vol. 20, pp. S118–S122, 2014.

[9] R. Erro, I. Rubio-Agusti, T. A. Saifee, C. Cordivari, C. Ganos, A. Batla, and K. P. Bhatia, "Rest and other types of tremor in adult-onset primary dystonia," *J Neurol Neurosurg Psychiatry*, vol. 85, no. 9, pp. 965–968, 2014.

[10] T. Brown, P. Rack, and H. Ross, "Different types of tremor in the human thumb." *The Journal of physiology*, vol. 332, no. 1, pp. 113–123, 1982.

Understanding the naturalness of a social human-robot interaction

[1]*Lukáš HRUŠKA (2nd year),*
Supervisor: [2]*Peter SINČÁK*

[1,2]Dept. of cybernetics and artificial intelligence, FEI TU of Košice, Slovak Republic

[1]lukas.hruska@tuke.sk, [2]peter.sincak@tuke.sk

***Abstract*—With the development of artificial intelligence is comming the age where the man and machine are interacting on a daily basis. This is going to be reflected in the social interaction as well. Robots are being developed with a singular purpose: to provide people company. However, it is proving to be a challenging task to actually understand peoples' expectations and social norms from the point of artificial intelligence to the degree, where it would be able to behave in such fashion, that we would interact with it in the same manner we do with other people.**

***Keywords*—android robot, emotion analysis, natural human-robot interaction, social robotics**

I. Introduction

Recent years have seen ever increasing rate of the development of the artificial intelligence. It is to be expected, that these advances would not be wholly confined to the immaterial digital world. By giving the algorithm a physical body, we allow it to interact with our world and in turn with us. However, this social interaction has to conform to peoples' expectations. Studies [1] have shown that people tend to respond socially and to apply social rules to technology. "Unlike usual computer programs, robots do have physical 'body' which allows them to interact with their environment and in turn with people as well. The robot's ability to move and act autonomously gives it unique aspect in the interaction"[2]. Other examples point out the novelty factor of the interaction and waning interest over time, such as office assistant [3] and school classroom [4] robots being completely forgotten after several months. Moreover, people have a tendency to attribute intentionality to technology, especially robots. The development of systems capable of, at least partially, fulfilling those expectations is very tedious task, therefore, most of the social interaction is based on, so called, Wizard of Oz systems, such as [5] [6] [7]. In this case, we can safely assume, that the operator, as a human being, is an expert in social interaction. However, if we move a step further down the road, how can we tell, the ongoing interaction is felt as natural and not forced?

II. Body

Erica, as presented by [8], is an autonomous android system capable of conversational interaction, featuring advanced sensing and speech synthesis technologies, and arguably the most human-like android built to date.

As a part of the experiment, the android is sitting in a cubicle in the main hall of the institute and is available for conversations during the normal office hours. Anyone interested may come in for a talk. However, the system controlling the robot is based on manually created decision trees, without any form of machine learning whatsoever. Our task is to create an automatic system, that would assess the naturalness of a conversation. The system is logging the whole interaction including the robot's state and state of the person using several kinects, cameras and microphone arrays.

Fig. 1. Person (left) engaged in the social interaction with the android robot (right).

The whole experiment consisted of 19 participants, 9 male, 10 female, all of them were students, aged 18-24 (mean 20.58).

Our task was to collect suitable data, to analyze it and design a classifier, that would be able to assess the perceived naturalness of the interaction.

First, we tried to run a cloud-based emotion analysis from face recognition using Microsoft's face API 2.Unfortunately, it is difficult to detect any emotion on Japanese person's face. Out of the 8 emotions supported by this API, only 1 had been detected - happiness. The rest was completely missing, with the exception of a fallback - neutral emotion, which dominated graphs. This points out either that the classifier used is faulty or people are truly not showing negative emotions, hiding behind their poker-faces.

Second part was based on analyzing the sentiment from the interaction 3. This proved far more successful and according to our Japanese colleagues, the output was reliable.

Finally we have asked participants to fill in questionnaires I, with mixed results from people. Some felt, the interaction was

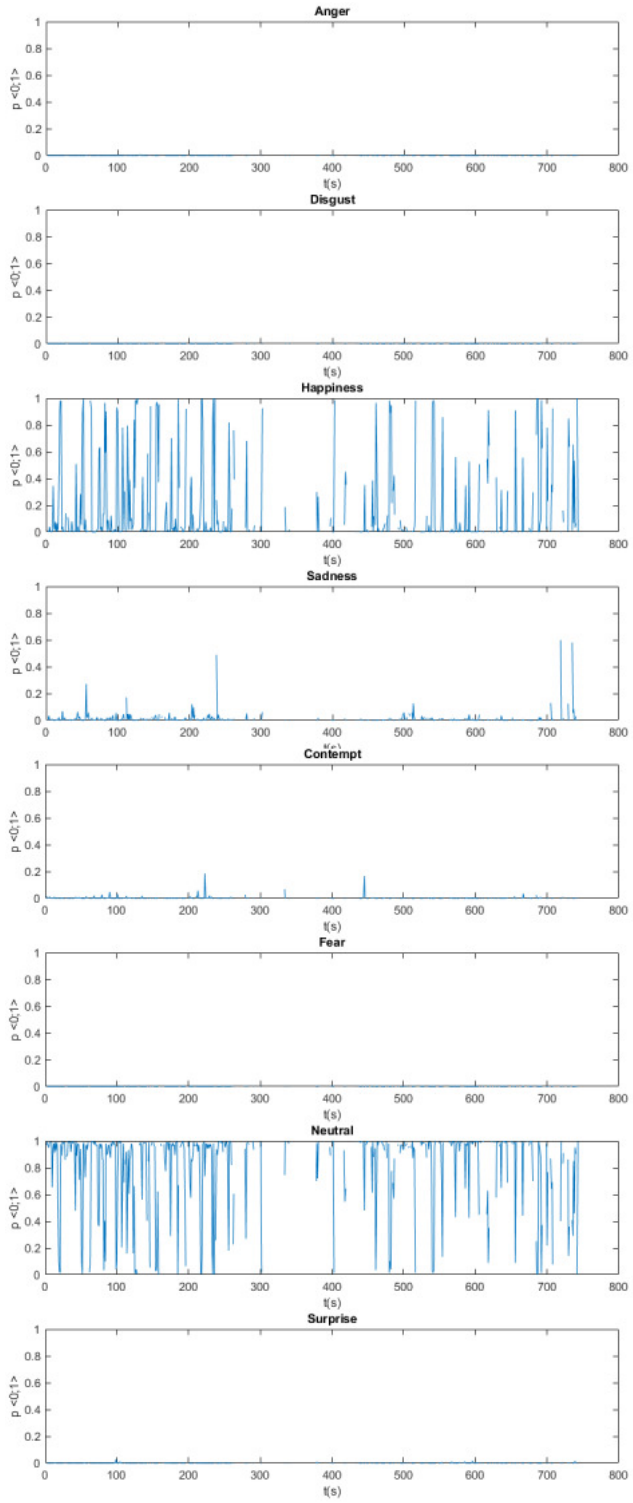

Fig. 2. Results of the emotion analysis: only happiness and neutral emotions are detected. Probability of remaining emotions remains insignificant. X axis shows time [s] and Y axis shows probability of the emotion in the given time <0, 1>. Note: the graph has been smoothed using 5 samples sliding window average

natural, whereas others had their reservations, some tied to the way Erica spoke/behaved, some to its design (this phenomenon has been described by [9]).

To directly define, what makes a conversation natural, due to the very subjectivity of the task, is a monumental undertaking. However, we are currently looking into describing it indirectly with the premise: “A natural conversation in one, that is not unnatural”. Although, it is not wholly accurate, it is more likely to detect patterns in behaviour, implicating discomfort, as well as higher delays in response times (although this can be caused by genuine thinking) and looking around instead of focusing on the robot.

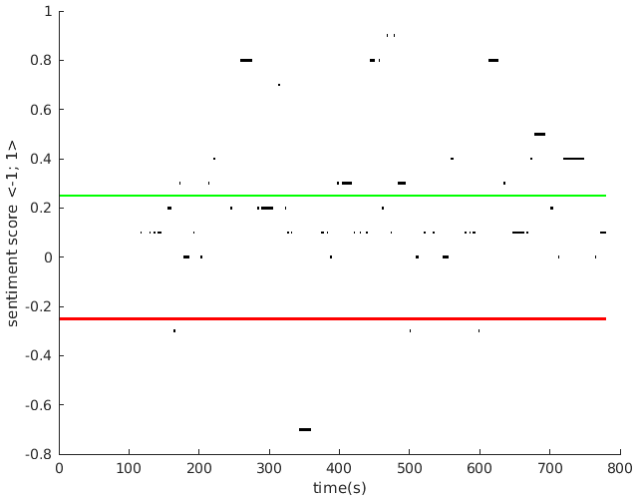

Fig. 3. Results of the sentiment analysis of the person from a single interaction, green and red line denote separation between positive <1;0.25>, neutral (0.25; -0.25) and negative sentiment <-0.25;-1>.

question	mean	mode
became close to the android	4.53	5
the android likes me	4	4
had a natural conversation	4.16	5
want to talk to the android again	5.26	6
want to communicate on a regular basis	3.95	5
resembling a real human in appearance	4.80	6
resembling a real conversation topics	4.6	4
responses were mechanical	4.16	5
felt the android’s intention	4.21	5

TABLE I
SELECTED RESPONSES FROM THE QUESTIONNAIRE: VALUES ARE IN RANGE FROM 1 (WORST) TO 7 (BEST).

III. Conclusion

People have their own personalities when it comes to social interaction. This study is proving, that the robot has to live up to peoples’ expectations. Moreover, uncanny valley plays a big part. As observed in other experiments with humanoid (not android) robots, such as Nao, people were significantly more accepting, likely due to novelty and lower expectations, whereas in the case of Erica’s human-like appearance, they were expecting human-like behaviour as well. This research is still ongoing, especially the process of designing the actual classifier.

Acknowledgment

I would like to thank to my professor, Peter Sinčák for his experience and guidance during the research. Moreover, I would like to thank to doctor Takashi Minato and the rest of the team in ATR for the opportunity to participate in their research. The opportunity was made available through Erasmus+ mobility for higher education 2019.

References

[1] J. Sung, R. E. Grinter, and H. I. Christensen, “" pimp my roomba" designing for personalization,” in *Proceedings of the SIGCHI Conference on Human Factors in Computing Systems*, 2009, pp. 193–196.

[2] J. E. Young, J. Sung, A. Voida, E. Sharlin, T. Igarashi, H. I. Christensen, and R. E. Grinter, "Evaluating human-robot interaction," *International Journal of Social Robotics*, vol. 3, no. 1, pp. 53–67, 2011.
[3] H. Huttenrauch and K. S. Eklundh, "Fetch-and-carry with cero: Observations from a long-term user study with a service robot," in *Proceedings. 11th IEEE International Workshop on Robot and Human Interactive Communication*. IEEE, 2002, pp. 158–163.
[4] T. Kanda, R. Sato, N. Saiwaki, and H. Ishiguro, "A two-month field trial in an elementary school for long-term human–robot interaction," *IEEE Transactions on robotics*, vol. 23, no. 5, pp. 962–971, 2007.
[5] G. Hoffman, "Openwoz: A runtime-configurable wizard-of-oz framework for human-robot interaction," in *2016 AAAI Spring Symposium Series*, 2016.
[6] R. Toris, D. Kent, and S. Chernova, "The robot management system: A framework for conducting human-robot interaction studies through crowdsourcing," *Journal of Human-Robot Interaction*, vol. 3, no. 2, pp. 25–49, 2014.
[7] L. Hruška, G. Magyar, and P. Sinčák, "Teleoperation platform for cloud robotics," *Proceedings of the Faculty of Electrical Engineering and Informatics of the Technical University of Košice: Electrical Engineering and Informatics 7*, pp. 671–676, 2016.
[8] D. F. Glas, T. Minato, C. T. Ishi, T. Kawahara, and H. Ishiguro, "Erica: The erato intelligent conversational android," in *2016 25th IEEE International Symposium on Robot and Human Interactive Communication (RO-MAN)*. IEEE, 2016, pp. 22–29.
[9] M. Mori *et al.*, "The uncanny valley," *Energy*, vol. 7, no. 4, pp. 33–35, 1970.

Unsupervised HetNet small cell placement optimization (April 2020)

[1]*Eugen ŠLAPAK (2nd year),*
Supervisor: [2]*Juraj GAZDA*

[1,2]Dept. of Computers and Informatics, FEI TU of Košice, Slovak Republic

[1]eugen.slapak@tuke.sk, [2]juraj.gazda@tuke.sk

***Abstract*—This work describes wireless heterogeneous network (HetNet) small cell placement automation using machine learning approaches, with the aim of removing the need for supervision of HetNet design domain expert.**

Apart from description of finished previous work with self-organizing map (SOM), new street graph simulation scenario comparing performance of mini-batch K-Means clustering with two variations of SOM is introduced. The work concludes with a brief mention of ongoing and future efforts of reinforcement learning applied to real-time cell placement reconfiguration instead of a static placement.

***Keywords*—small cell placement, heterogeneous network, unsupervised learning**

I. Introduction

Upcoming 5G networks will employ multiple types of base transceiver stations. Apart from so called macrocells - conventional radio cells covering large areas, smaller transceivers - so called small cells, will be added. The purpose of such radio access network (RAN) densification by deployment of new smaller cell types is better wireless spectrum reuse, as smaller cells can use different frequency than macrocells to avoid co-channel interference, and by covering small area also avoid mutual interference.

Deployment of new type of cells requires decision on their placement. RAN coverage problem is NP-hard [1], so heuristic approaches are required, to efficiently search for its solution.

Traditionally cell placement relied on simple regular hexagonal placement of macrocell base stations and later on stochastic geometry, with research [2] showing that stochastic geometry models indeed bring network properties closer to those of real-world RANs, when expressed in terms of coverage probability.

This means, that cell placement based on stochastic geometry can be used as a baseline that approximates the real world RAN small cell placement for comparison to new proposed approaches. More specifically, new cell placement approaches can be compared to stochastic one, in terms of multiple RAN key performance indicators (KPIs), like coverage probability, average throughput or fairness (as defined by Raj Jain in [3]).

II. Previous research

Author‘s research published in [4] successfully demonstrated advantages of SOM over stochastic binomial point process (BPP), in terms of all KPIs mentioned in introduction. This work focused on application of SOM neural network, by training it on simulated user location data, generated by "hourglass" simulation scenario (named "hourglass" due to the arrangement Bézier trajectories), plotted in Fig. 2.

Weight vectors of individual neurons, representing spatial location of small cells, were changed during the SOM‘s training resulting in unsupervised small cell placement.

III. SOM and mini-batch K-Means in street graph scenario

The objective of the K-Means clustering algorithm is to minimize the function in Eq. 1

$$J(C) = \sum_{k=1}^{K} \sum_{x_i \in C_k} \|x_i - \mu_k\|^2, \tag{1}$$

where $C = \{c_k\}, k = 1..K$ is the set of all clusters, $X = \{x_i\}, i = 1..n$ is the set of all training samples and μ_k is the mean of cluster c_k.

Mini-batch variant of K-Means clustering was chosen for evaluation, because it enables computationally efficient training on user locations in individual discrete simulation time instances. Each time-step generates one batch.

Method of SOM neuron weight update can be briefly described by Eq. 2 [5]:

$$W_v(s+1) = W_v(s) + \theta(u, v, s) \cdot \alpha(s) \cdot (D(t) - W_v(s)). \tag{2}$$

Where s is the training iteration step. W_v is the weight vector of SOM neuron v. θ represents neighbourhood function, that returns 0 if the distance of the best matching unit neuron u and one of the other neurons that comprise SOM, denoted as v, is greater than the neighbourhood radius, or 1 if their distance is lower than this radius value.

All investigated algorithms have constraint on the maximum number of user-to-cell associations - users become associated with the next closest neuron or the next closest centroid of one, for which such association capacity is exhausted.

With neighbourhood radius set to 0 during the whole duration of SOM training, SOM‘s algorithm is equivalent to K-Means clustering.

Evaluation of mini-batch K-Means clustering algorithm in a scenario with 100 users moving deterministically and 100 users moving according to Lévy flight mobility model as in Fig. 1 showed similar improvements of KPIs as those demonstrated by SOM (more closely described in author‘s publication [6]). Prompting further research into differences

in performance between these algorithms, but also between regular SOM presented in Eq. 2 and SOM that uses signal to interference plus noise (SINR) metric for user-to-cell distance computation, in a more advanced simulation scenario.

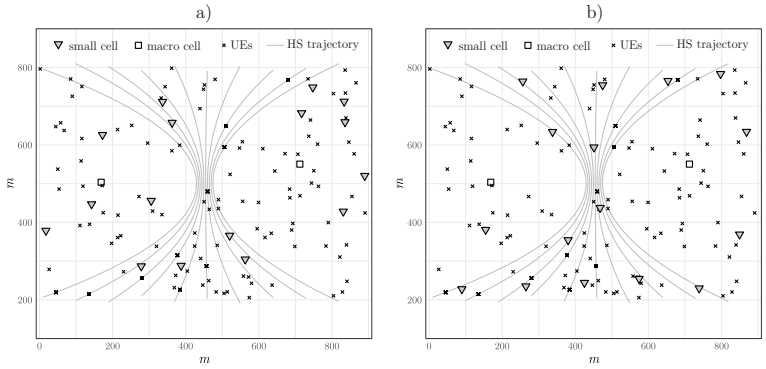

Fig. 1. Comparison of small cell placement by BPP and mini-batch K-Means clustering (right), for 16 small cells in an "hourglass" simulation scenario.

New realistic scenario uses street graph extracted from OpenStreetMap data and users moving along the graph edges. Users move towards the randomly generated waypoints located on the graph. Real-world macrocell placement is determined from OpenCellId project data (crowd sourced location of transceivers) and their height is inferred from building heights, as visible in 3D renderings of scenario in Fig. 2.

Results comparing improvements achieved with individual investigated placement methods are available in Fig. 3

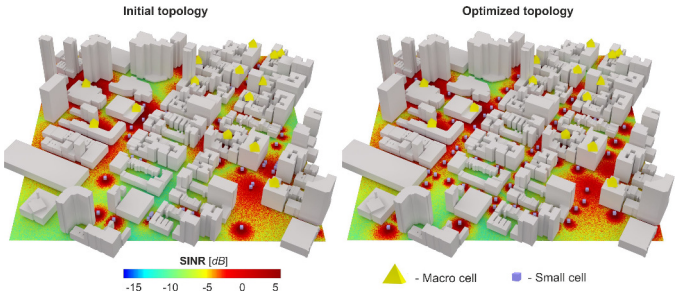

Fig. 2. Initial (left) and optimized (right) placement with cells aligned along the streets and placed via training that takes into account average user density.

With increasing number of small cells to be placed, SOM with euclidean metric had the clean advantage in placement performance in terms of average throughput KPI.

Research measuring performance of small cell placement in street graph scenario was published in [7].

IV. Future Research Direction

Current and future research will focus on real-time placement of drone-mounted small cells, that is able to quickly and flexibly meet the user demand. Reinforcement learning, more specifically its popular variant deep Q-learning, first introduced by DeepMind in [8], was chosen as an ideal artificially intelligent approach for this task, as it deals with real-time interaction of agent with its changing environment with ability to learn in a vast state space thanks to usage of neural network instead of traditional Q-table as its approximator.

As single agent will not be that useful by itself, swarm of drones will be trained using approaches introduced in [9] and [10], where only a single agent is learning and neural network

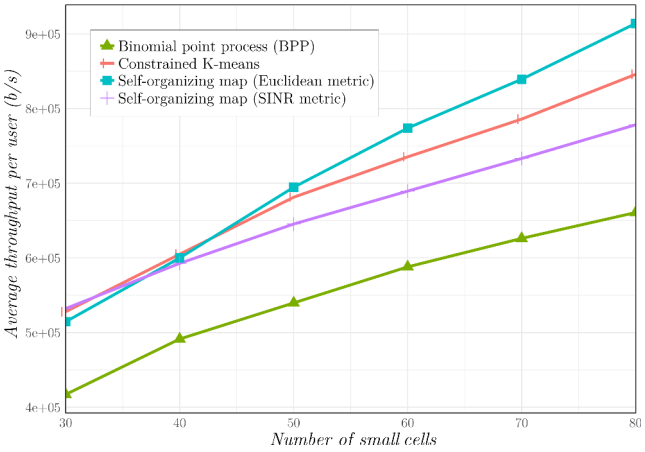

Fig. 3. Average throughput per user for different small cell counts and cell placement algorithms.

which determines Q-values of all other agents is fixed during some time period to let the learning agent learn how to interact with non-learning agents. After some time period, new policy (choice of actions in individual possible world states) acquired by learning agent is passed to all other non-learning agents in simulation. This process is repeated multiple times and training eventually converges to unchanging efficient policy used by all participating agents.

Acknowledgment

Research presented in this work was financially supported by the Slovak APVV grant APVV-15-0055 and APVV-18-0214.

References

[1] S. P. Mendes, G. Molina, M. A. Vega-Rodríguez, J. A. Gómez-Pulido, Y. Sáez, G. Miranda, C. Segura, E. Alba, P. Isasi, C. León *et al.*, "Benchmarking a wide spectrum of metaheuristic techniques for the radio network design problem," *IEEE Transactions on Evolutionary Computation*, vol. 13, no. 5, pp. 1133–1150, 2009.

[2] C.-H. Lee, C.-Y. Shih, and Y.-S. Chen, "Stochastic geometry based models for modeling cellular networks in urban areas," *Wireless Networks*, vol. 19, no. 6, p. 1063–1072, 2012.

[3] R. Jain, D. M. Chiu, and H. WR, "A quantitative measure of fairness and discrimination for resource allocation in shared computer systems," *CoRR*, vol. cs.NI/9809099, 01 1998.

[4] J. Gazda, E. Šlapak, G. Bugár, D. Horváth, T. Maksymyuk, and M. Jo, "Unsupervised learning algorithm for intelligent coverage planning and performance optimization of multitier heterogeneous network," *IEEE Access*, vol. 6, pp. 39 807–39 819, 2018.

[5] T. Kohonen, "Self-organized formation of topologically correct feature maps," *Biological cybernetics*, vol. 43, no. 1, pp. 59–69, 1982.

[6] E. Slapak, J. Gazda, G. Bugár, M. Volosin, D. Horváth, and T. Maksymyuk, "Hetnet spatial topology design using mini-batch k-means clustering," *2019 IEEE 15th International Conference on the Experience of Designing and Application of CAD Systems (CADSM)*, pp. 1–4, 2019.

[7] T. Maksymyuk, E. Šlapak, G. Bugar, D. Horváth, and J. Gazda, "Intelligent framework for radio access network design," *Wireless Networks*, pp. 1–16, 2019.

[8] V. Mnih, K. Kavukcuoglu, D. Silver, A. A. Rusu, J. Veness, M. G. Bellemare, A. Graves, M. Riedmiller, A. K. Fidjeland, G. Ostrovski *et al.*, "Human-level control through deep reinforcement learning," *Nature*, vol. 518, no. 7540, pp. 529–533, 2015.

[9] M. Egorov, "Multi-agent deep reinforcement learning," *CS231n: Convolutional Neural Networks for Visual Recognition*, 2016.

[10] J. K. Gupta, M. Egorov, and M. Kochenderfer, "Cooperative multi-agent control using deep reinforcement learning," in *International Conference on Autonomous Agents and Multiagent Systems*. Springer, 2017, pp. 66–83.

Usage of battery energy storage in power systems in ancillary services

[1]*Jakub URBANSKÝ (3rd year)*
Supervisor: [2]Ľubomír BEŇA

[1,2]Dept. of Electric Power Engineering, FEI TU of Košice, Slovak Republic

[1]jakub.urbansky@tuke.sk, [2]lubomir.bena@tuke.sk

***Abstract*—— this paper deals with utilization of battery energy storage in power systems. Energy storage systems play a significant role in proper integration of renewable energy resources in maintaining reliable and modern power system. They can reduce power fluctuation, enhance electric system flexibility, and enables the storage and dispatching of the electricity produced by variable renewable energy sources. Battery energy system seems to be necessary addition for future of the power system.**

***Keywords*— renewable energy sources, battery energy storage systems, ancillary services, accumulation**

I. INTRODUCTION

The electric power system, as any part of the industry, is undergoing a constant development. In the recent years has tendency to incline more toward so called "green sources" or in other words renewable energy sources (RES), mainly from environmental reasons. The Renewable Energy Directive enact goal for European Union to achieve its 20% renewables target by year 2020 [1] and 27% by year 2030 [2].

Electric power systems needs to preserve stable balance between production and consumption of electric energy [3]. Penetration of RES such as, photovoltaics and wind energy has brought new issues for the stable operation of power system, due to their unpredictable electricity production character [4]. Recent development in field of RES. mainly in photovoltaic, and emission free transport brought increased interest in energy storage. Due to unpredictable electricity generation from RES, energy storage plays important role in maintaining stable and secure operation of power grid, system flexibility and enables the storage of electricity in time of their increased production. On other hand, at time of insufficient production it can dispatch stored energy for their immediate usage. [5]

Energy storage can be utilized in power systems as stable source of ancillary services to provide reliable operation of power grid [4]. My dissertation thesis will be focused on collaboration of renewable energy sources with battery energy storage systems (BESS).

II. BATTERY ENERGY STORAGE SYSTEMS

BESS can be defined as an integration of battery cells, connected in series or in parallel to reach desired voltage and capacity, with purpose to form large electric energy storage device. It stores direct current (DC) energy. It is connected to the power grid via power electronic converters. It can provide negative (with charging) or positive (with discharging) regulation power to the grid. [7].

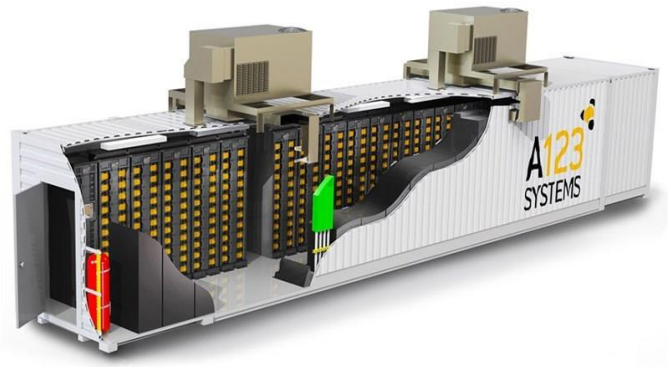

Fig. 1. An example of a battery energy storage system

Basic composition of BESS was presented by [8], the main components are:

- battery,
- power converter,
- transformer,
- controller,
- battery management system.

Manufacturers of BESS tends to ship them in form of containers, as they provide flexibility for the system design and transportability (Fig. 1.) The battery is connected to the power converter. When batteries are discharging power converter acts as inverter. When batteries are being charged power converter acts as rectifier. Converter is connected to transformer, which transfers voltage to higher value and vice versa. Battery management system, which is connected to battery and controller, monitors each cell and maintains them. Controller has the logic necessary to manage proper BESS function by the defined algorithm.[9]

Application of the BESS in power systems

The installed power capacity of grid BESS (Fig. 2.) is currently around 2.5 GW globally [8].

Utility side application such as frequency regulation, spinning reserve, voltage support, peak power shaving (arbitrage), load leveling, island grid, black start support. [9]

Customer side applications such as peak shaving, load shifting, off-grid supply. [9]

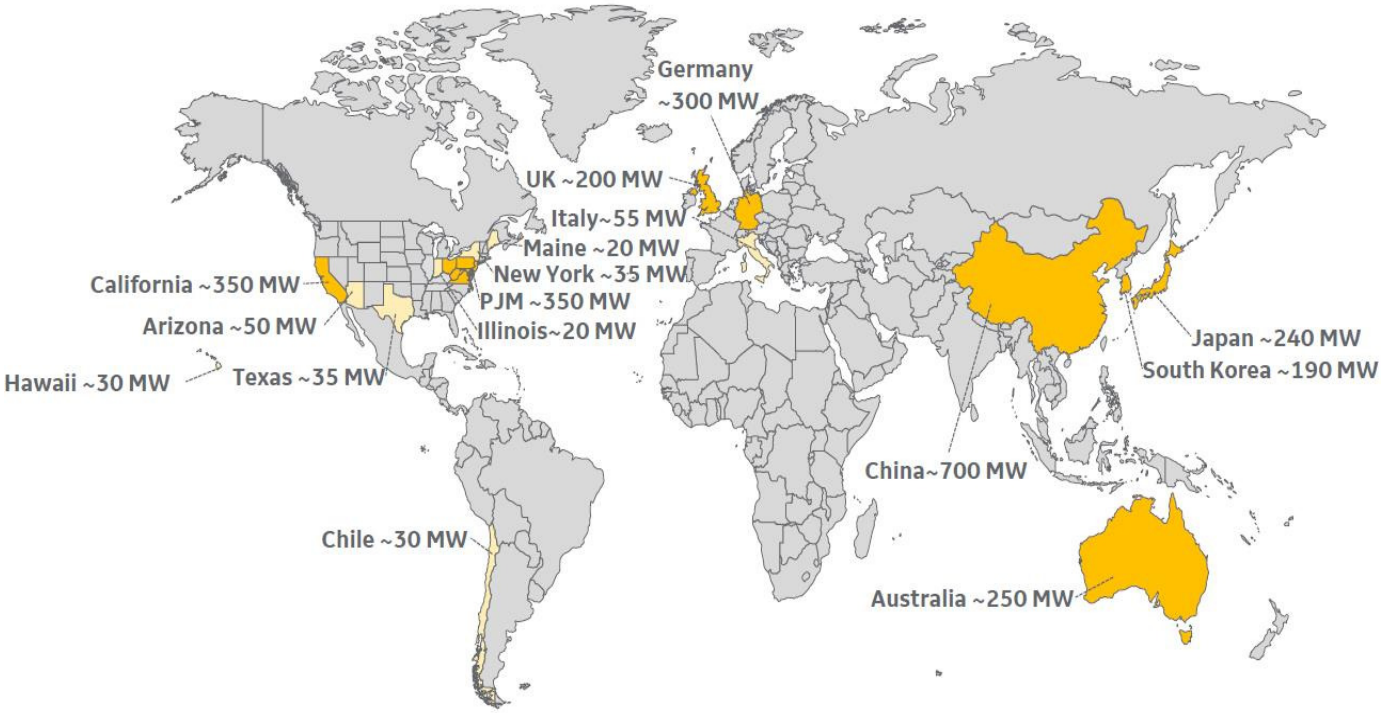

Fig. 2. The installed power capacity of grid BESS globally [8]

III. Publications

To this date, I am author or co-author of 38 publications:

- ADE (1),
- ADF (6)
- AED (11),
- AFA (3),
- AFC (11),
- AFD (6).

Of which 6 are indexed in Scopus database and 2 are indexed in Web of Science. Partial results of my research are published in articles of which I am author or co-author.

IV. Thesis of Dissertation Work

1. Analysis of current requirements of Slovak republic power system for possibility connection of RES and energy storage systems
2. Analysis of current requirements of Slovak republic electric power system on ancillary services.
3. Identification and description of BESS suitable for providing ancillary services.
4. Identifying the optimal combination of RES and BESS for providing ancillary services.
5. On selected examples, evaluate the economic efficiency of RES in collaboration with BESS for providing ancillary services.
6. Analysis of the achieved results and making recommendations for future direction of the research.

Acknowledgment

This work was supported by the Scientific Grant Agency of the Ministry of Education of Slovak Republic and the Slovak Academy of Sciences by the projects VEGA No. 1/0372/18.

References

[1] European Commission: Renewable energy directive[Online]. Available at: <https://ec.europa.eu/energy/en/topics/renewable-energy/renewable-energy-directive> Accessed on February 7, 2020

[2] European Commission: 2030 Energy Strategy [Online]. Available at: < https://ec.europa.eu/energy/en/topics/energy-strategy-and-energy-union/2030-energy-strategy> Accessed on February 7, 2020

[3] M. Kolcun, V. Griger, Ľ. Beňa, J. Rusnák, "Prevádzka elektrizačnej sústavy", Technická univerzita v Košiciach 2007: ch. 1. ISBN 978-80-8073-837-2

[4] M. Merlo, D. Falabretti, "Battery Energy Storage Systems for Ancillary Services Provision," POLITECNICO DI MILANO, Scuola di Ingegneria Industriale e dell'Informazione, Dipartimento di Energia
Corso di Laurea Magistrale in Ingegneria Energetica 2017

[5] M. Vojtek, M. Kolcun, "Research of energy storages utilization in electric power system," SCYR 2018, pp. 218-2019

[6] S. Ould Amrouche et. al., "Overview of energy storage in renewable energy systems," International Journal of Hydrogen Energy, Vol. 41, Issue 45, 7 December 2016, pp. 20914-20927

[7] B. Xu, "Degradation-limiting Optimization of Battery Energy Storage System Operations," Master Thesis, EEH Power Systems Laboratory, ETH Zurich, Switzerland, 2013

[8] General Electric Company: Battery Energy storage systems (BESS): ancillary services and beyond [Online]. Available at: < https://tinyurl.com/svsqr9p> Accessed on February 7, 2020

[9] J. Huvilinna, "Value of Battery Energy Storage at Ancillary Service Market," Master Thesis, Aalto University , School of Electrical Engineering, Finland, 2015

Author's index

SCYR 2020
Nonconference Proceedings of Young Researchers

Published: Faculty of Electrical Engineering and Informatics
Technical University of Košice
Edition I, 212 pages
Number of CD Proceedings: 50 pieces

Editors: prof. Ing. Alena Pietriková, CSc.
Ing. Emília Pietriková, PhD.

ISBN 978-80-553-3538-4